The NPC Pathway and Persistence of Intracellular Pathogens

Yuzhe Weng

A thesis presented for the degree of
Doctor of Philosophy

Michaelmas 2023



Department of Pharmacology

Linacre College

University of Oxford

Abstract

Intracellular pathogens have the ability to survive and replicate within host cells, resulting in their long-term cellular and systemic persistence. A pivotal strategy for achieving this persistence is through the prevention of phagosome-lysosome fusion. Studies by Fineran *et al.* have established a mechanistic link between *Mycobacterium tuberculosis* (*Mtb*) infection and Niemann-Pick disease type C (NPC), a rare lysosomal storage disorder. *Mtb* infection involves the shedding of microbial lipids that inhibit NPC1 in host cells. Our study has confirmed that the lipid-mediated inhibition of NPC1 is widespread in clinically relevant global human *Mtb* strains. However, we observed no such inhibition with lipid extracts from *Mycobacterium canettii*, an ancestral species of modern human *Mtb* strains. These findings imply that the evolution of NPC1 inhibition conferred greater virulence of *Mtb* strains. Analysis of sphingolipids revealed that *Mtb* H37Rv lipid extract manipulates sphingosine metabolism. By analysing the activity of fractionated *Mtb* H37Rv lipid and commercially obtained purified *Mtb* lipid components, we have identified several candidates, including SL-1 and PIMs, that may be involved in the inhibition of the NPC pathway. In addition, we have identified *Salmonella enterica* serovar Typhimurium (*S.* Typhimurium), another intracellular pathogen, which inhibits the host cell NPC pathway and induces NPC cellular phenotypes. We have found that NPC1 inhibition is independent of the effector protein secreted during infection, and that lipid extract from *S.* Typhimurium can induce comparable NPC cellular phenotypes to live infection models. Our study therefore shows for the first time the involvement of the NPC pathway in the persistence of multiple intracellular pathogens.

Acknowledgement

Firstly, I would like to thank my supervisor, Frances Platt, for her patience, professional academic guidance and warm encouragements throughout the past four years, which helped me develop confidence and build a healthy mindset in research. I want to give a very special thanks to Nick Platt for his detailed supervision, not only academically but also for broadening my view of the world. Many thanks to Nick and Fran for their prompt and detailed feedback on the thesis manuscript, and for tolerating my grammatical errors.

I really appreciate the help and support from every past and current member of Platt Lab and the creation of a warm, supportive and family-like environment. I appreciate everyone's support through the hard times during the COVID-19 pandemic. Many thanks to Dawn, who provided expertise and guidance on lab work and set me up with good practice for lab work. Thanks to David, Danielle, Kerri, and Allie for their professional guidance in HPLC works. Thanks to Maria for the guidance in confocal microscopy and western blot works and the warm Christmas dinner. Special thanks to Dave for being a fabulous office neighbour and broadening my knowledge about the UK, Claire for always bringing joy to the lab and for amazing baking skills, Qiao for always supporting me emotionally, Hsin for his warm encouragements, Reuben for his kindness for helping with everything, Rosalie (Yixuan) for being the first student that I supervised, Marya for her American views and Rebecca, Hannah and Puravi for creating a nice DPhil student atmosphere.

I would like to thank all collaborators involved in this study. Special thanks to Dr Gerald Larrouy-Maumus at Imperial College London for providing the raw materials in mycobacterial lipid study and extensive knowledge in mycobacterial lipid biochemistry, Dr Brian Robertson at Imperial College London for supplying raw materials for this study, and Dr Teresa Thurston at Imperial College London for providing essential materials and guidance for the *Salmonella* studies and for reviewing the thesis manuscript. Many thanks to members in the laboratory of Professor Sarah Spiegel at Virginia Commonwealth University for helping with sphingolipid LC-MS lipidomic analysis and Professor Mary Jackson at Colorado State University for providing mutant *Mtb* lipid extracts. I would also like to thank Dr Emily Eden from UCL for the support in the membrane contact site studies.

Thanks to all my friends who have been helping and supporting me through the years. Last but not least, I want to express my gratitude to my parents for supporting me through my studies and I truly appreciate the love and support from both of them throughout the past four years.

List of abbreviations

ABCA1	ATP-binding cassette transporter A1
ACAT	acetyl-CoA transferase
AG	arabinogalactan
ASM	acid sphingomyelinase
ASMD	acid sphingomyelinase deficiency
ATP	adenosine triphosphatase
BCG	Bacillus Calmette–Guérin
BMDM	bone marrow-derived macrophage
BSA	Bovine serum albumin
C1P	ceramide-1-phosphate
CDase	ceramidase
CerS	ceramide synthase
CERT	ceramide transport protein
CFP	culture filtration protein
CFU	colony forming unit
$CHCl_3$	chloroform
CK	ceramide kinase
CL	cardiolipin
COPD	chronic obstructive pulmonary diseases
CtxB	cholera toxin subunit B
DAG	diacylglycerol
DAT	diacyltrehalose
DHS1P	Dihydrosphingosine 1-phosphate
EE	early endosome
ER	endoplasmic reticulum
ERT	enzyme replacement therapy
ESAT	early secreted antigenic target
ESCRT	endosomal sorting complex required for transport system
ESX	early secretory antigenic target secretion system
FAMES	fatty acid methyl esters

FAS	fatty acid synthase
GCS	glucosylceramide synthase
GD	Gaucher disease
GlcCer	glucosylceramide
GlcSph	glucosylsphingosine
GMM	glucose monomycolate
GPI	glycosylphosphatidylinositol
GPL	glycopeptidolipids
GSL	glycosphingolipid
h	hour
HIV	human immunodeficiency virus
HOPS	homotypic fusion and sorting
HP-β-CD	2-Hydroxypropyl-β-cyclodextrin
IFN-γ	interferon-γ
IGRA	interferon-γ release assay
IL	interleukin
LA	lipid A
LacCer	lactosylceramide
LAM	lipoarabinomannan
LAMP	lysosomal associate membrane protein
LC	liquid chromatography
LD	lipid droplet
LDL	low-density lipoprotein
LE	late endosome
LM	lipomannan
LOS	lipooligosaccharide
LPS	lipopolysaccharide
LSD	lysosomal storage diseases
LTBI	latent TB infection
M6P	mannose-6 phosphate
MA	mycolic acid
MAC	*Mycobacterium avium* complex
mAGP	mycolylarabinogalactan-peptidoglycan

MALDI-ToF	matrix-assisted laser desorption/ionisation-time of flight
MAME	mycolic acid methyl ester
ManLAM	mannose-capped lipoarabinomannan
MDR	multi-drug resistance
MeOH	methanol
MΦ	macrophage
MFI	mean fluorescent intensity
MHC	major histocompatibility complex
min	minute
MmpL	mycobacterial membrane protein large
MS	mass spectrometry
Mtb	*Mycobacterium tuberculosis*
MTBC	*Mycobacterium tuberculosis* complex
MTOC	microtubule organising centre
mTORC1	mammalian target of rapamycin complex 1
NAADP	nicotinic acid adenine dinucleotide phosphate
*N*B-DNJ	*N*-butyl-deoxynojirimycin
NLRP3	NOD-, LRR- and pyrin domain-containing protein 3
NOS	nitrogen oxidative species
NP-HPLC	normal phase high-performance lipid chromatography
NPA	Niemann-Pick disease type A
NPB	Niemann-Pick disease type B
NPC	Niemann-Pick disease type C
NTD	N-terminal domain
NTM	non-tubercular mycobacterium
NTS	non-typhoid *Salmonella*
PAMP	pathogen-associated molecular pathway
PAT	polyacyltrehalose
PC	phosphatidylcholine
PDIM	phthiocerol dimycocerosates
PE	phosphatidylethanolamine
PG	peptidoglycan
PGL	phenolic glycolipid

pi	post infection
PI	propidium iodide
PIM	phosphatidylinositol mannoside
PPARγ	proliferator-activated receptor γ
PT	phosphotidyltrehalose
rEGCase	recombinant endoglycoceramidase
RP-HPLC	reverse phase high-performance lipid chromatography
RT	room temperature
s	second
S1P	sphingosine-1-phosphate
SCV	salmonella-containing vacuole
SIF	*Salmonella*-induced filament
SK	sphingosine kinase
SL	sulpholipid
SM	sphingomyelin
SMase	sphingomyelinase
SMS	sphingomyelin synthase
SphK	sphingosine kinase
SPI	*Salmonella* pathogenicity island
SPPase	S1P phosphatase
SPT	serine palmitoyl transferase
SRT	substrate reduction therapy
SSD	sterol sensing domain
STARD3	StAR Related Lipid Transfer Domain Containing 3
T3SS	type 3 secretion system
TAG	triacylglycerol
TB	tuberculosis
TDM	trehalose dimycolate
TFEB	transcription factor EB
TL	total lipid
TLR	toll-like receptor
TMM	trehalose monomycolate
TNF-α	tumour necrosis factor-α

TPC	two-pore channel
TRPML	transient receptor potential receptors mucolipins
TST	tubercular skin test
WT	wild-type

Content

Abstract ..... **i**

Acknowledgement ..... **ii**

List of abbreviations ..... **iv**

List of Figures ..... **xxi**

List of Tables ..... **xxviii**

Chapter 1. Introduction **1**

1.1. Lysosomal storage diseases (LSDs) **3**

1.2. Niemann-Pick diseases **4**

1.2.1. Niemann-Pick disease type A and type B 4

1.2.2. Niemann-Pick disease type C 5

1.2.3. NPC clinical symptoms 5

1.2.4. NPC cellular phenotypes 6

1.2.4.1. NPC1 and NPC2 7

1.2.4.2. The pathological cascade in NPC 9

1.2.5. NPC therapies 18

1.3. NPC pathway and intracellular pathogens **18**

1.4. Tuberculosis **19**

1.4.1. Phylogeny of mycobacteria 21

1.4.2. *Mtb* cellular pathogenesis 24

1.4.2.1. Formation of granuloma 24

1.4.2.2. Foamy macrophages 26

1.4.3. Intracellular persistence 27

1.4.3.1. *Mtb* effector proteins 27

1.4.3.2. *Mtb* lipids 28

1.5. NPC and mycobacteria 31

Lay summary of the work 36

Chapter 2. Inhibition of the Niemann-Pick C1 protein is a conserved feature of multiple strains of *Mycobacterium tuberculosis* 38

2.1. Introduction 39

2.2. Material and Methods 42

2.2.1. Cells 42

2.2.2. Mycobacterial culture and cell wall lipid extraction 42

2.2.3. Lipid solubilisation and addition to cell culture 44

2.2.4. LysoTracker™ staining for flow cytometry (FACS) analysis 44

2.2.5. Pro-IL1β staining for FACS analysis 45

2.2.6. LysoTracker™ live cell staining for confocal microscopy 45

2.2.7. Cell lysate preparation and protein quantification prior to Western Blotting 46

2.2.8. Western blotting 46

2.2.9. qPCR 48

2.2.10. Immunofluorescence staining 48

2.2.11. Filipin staining of cholesterol 49

2.2.12. Amplex Red assay determination of cholesterol. 49

2.2.13. Cholera toxin subunit B (CtxB) staining 50

2.2.14. Analysis and quantification of GSLs by normal phase high-performance liquid chromatography (NP-HPLC) 50

2.2.15. Thin-layer chromatography (TLC) of extractible lipids and matrix-assisted laser desorption/ionisation-time of flight (MALDI-ToF mass spectrometry (MS)) lipid fingerprints. 52

2.2.16. Statistical analysis 53

2.3. Results 54
2.3.1. Cell wall total lipid (TL) extract of *Mtb* H37Rv increases LysoTracker™ staining intensity in RAW 264.7 MΦ. 54
2.3.2. *Mtb* H37Rv TL extract significantly increases LysoTracker™ staining intensity in murine bone marrow-derived MΦ (BMDMΦ)…….. 57
2.3.3. *Mtb* H37Rv TL extract causes a significant reduction in the frequency of pro-IL1β positive RAW 264.7 MΦ that had been stimulated by LA. 58
2.3.4. TL extracts of *Mtb* clinical isolates, but not *M. canettii*, increase LysoTracker™ staining intensity of RAW 264.7 MΦ. ...60
2.3.5. TL extract of *M. canettii* decreases LysoTracker™ staining intensity of RAW 264.7 MΦ. 63
2.3.6. TL extracts of representative *Mtb* clinical strains, but not with *M. canettii,* increase the diameter and frequency of LysoTracker™ positive compartments in RAW 264.7 MΦ. 64
2.3.7. Optimisation of LAMP-1 immunostaining for confocal microscopy in RAW 264.7 MΦ. 68
2.3.8. LAMP-1 immunostaining confirmed expansion of LE/Lys volume following incubation with TL extracts of representative *Mtb* clinical strains but not *M. canettii* in RAW 264.7 MΦ. 70
2.3.9. Optimisation of LAMP-1 Western blotting 74
2.3.10. Expression of LAMP-1 is not altered in *Mtb* H37Rv TL-treated RAW 264.7 MΦ. 75
2.3.11. *Mtb* H37Rv TL extract increases Npc1, but not Npc2 expression in RAW 264.7 MΦ. 77
2.3.12. Expression of *Npc1* and *Npc2* transcripts are increased in *Mtb* H37Rv TL-treated RAW 264.7 MΦ. 79

2.3.13. TL extracts of representative *Mtb* clinical strains, but not *M. canettii* induce partial redistribution of intracellular cholesterol to the endo-lysosomal system of RAW 264.7 MΦ. 80

2.3.14. TL extracts of *Mtb* clinical strains and *M. canettii* do not affect cholesterol levels in RAW 264.7 MΦ. 84

2.3.15. Optimisation of GM1 ganglioside labelling and trafficking in RAW 264.7 MΦ. 85

2.3.16. Exposure to lipids from representative *Mtb* strains but not *M. canettii* perturb GM1 ganglioside intracellular trafficking in RAW 264.7 MΦ. 87

2.3.17. GSL species accumulate in RAW 264.7 MΦ incubated with lipid extracts of strains representative of different *Mtb* lineages but not with *M. canettii* lipid. 90

2.3.18. Lipid composition of clinical strains representative of different *Mtb* lineages. 96

2.4. Discussion 102

Chapter 3. Other Mycobacteria and the NPC pathway 111

3.1. Introduction 112

3.2. Material and methods 119

3.2.1. Cells 119

3.2.2. Mycobacterial culture and cell wall lipid extraction 119

3.2.3. Lipid solubilisation and addition to cell culture 119

3.2.4. LysoTracker™ staining for FACS analysis 119

3.2.5. Immunofluorescence staining 119

3.2.6. Filipin staining of cholesterol 120

3.2.7. Amplex Red assay determination of cholesterol 120

3.2.8. CtxB staining 120

3.2.9. Analysis and quantification of GSLs by NP-HPLC 120

3.2.10. Statistical analysis 120

3.3. Results 121

3.3.1. TL extracts of *M. abscessus*, *M. avium* and *M. bovis*, but not *M. leprae* or *M. smegmatis*, increase LysoTracker™ staining intensity of RAW 264.7 MΦ. 121

3.3.2. TL extracts of *M. abscessus*, *M. avium*, *M. bovis* and *M. leprae*, but not *M. smegmatis*, induce expansion of LE/Lys in RAW 264.7 MΦ. 123

3.3.3. TL extracts of *M. abscessus*, *M. bovis* and *M. leprae*, but not *M. avium* and *M. smegmatis,* induce cholesterol accumulation in the endo-lysosomal system of RAW 264.7 MΦ. 125

3.3.4. TL extracts of *M. abscessus*, *M. bovis*, *M. leprae* or *M. avium* do not affect cholesterol content of RAW 264.7 MΦ, but significantly increased by *M. smegmatis* extract. 128

3.3.5. TL extracts of *M. abscessus*, *M. bovis*, *M. leprae*, *M. avium* and *M. smegmatis* perturb GM1 ganglioside intracellular trafficking in RAW 264.7 MΦ. 129

3.3.6. Levels of identified GSL species are changed significantly in RAW 264.7 MΦ treated with TL extracts of specific mycobacteria….. 131

3.4. Discussion 136

Chapter 4. *Mtb* cell wall lipids and sphingosine metabolism 144

4.1. Introduction 145

4.2. Material and methods 152

4.2.1. Cells 152

4.2.2. Mycobacterial culture and cell wall lipid extraction. 152

4.2.3. Lipid solubilisation and addition to cell culture. 152

4.2.4. Cell lysate preparation for sphingolipids lipidomic analysis…….. 152

4.2.5. Determination of sphingosine and sphinganine by reverse-phase high-performance liquid chromatography (RP-HPLC)…152

4.2.6. Sphingoid-base lipid analysis by liquid chromatography-mass spectrometry (LC-MS). 154

4.2.7. BODIPY-LacCer trafficking by confocal microscopy 154

4.2.8. Western blotting 155

4.2.9. Statistical analysis....156

4.3. Results....157

4.3.1. Optimisation of RP-HPLC analysis of sphingosine and sphinganine. 157

4.3.2. Optimisation of the extraction of sphingosine and sphinganine from cell lysates.....159

4.3.3. U18666A induces a sustained increase in sphingosine but a transient increase in sphinganine, whereas *Mtb* H37Rv TL extract induces a transient increase of both sphingosine and sphinganine in RAW 264.7 MΦ. 161

4.3.4. *Mtb* H37Rv TL extract induces S1P and dihydro-S1P (DHS1P) accumulation in RAW 264.7 MΦ. 164

4.3.5. *Mtb* H37Rv TL extract induces ceramide and monohexosylceramide accumulation in RAW 264.7 MΦ. 166

4.3.6. *Mtb* H37Rv TL extract induces SM accumulation in RAW 264.7 MΦ.....168

4.3.7. Optimisation of BODIPY-LacCer trafficking in RAW 264.7 MΦ. 169

4.3.8. *Mtb* H37Rv TL extract induces BODIPY-LacCer accumulation in lysosomes in RAW 264.7 MΦ.....171

4.3.9. U18666A does not alter SphK1 or SphK2 protein expression in RAW 264.7 MΦ.....172

4.3.10. *Mtb* H37Rv TL increases SphK2, but not SphK1 in RAW 264.7 MΦ.....174

4.4. Discussion....176

Chapter 5. Inhibition of the NPC Pathway by Lipid Components from *Mtb* 182

5.1. Introduction 184
5.2. Material and Methods 192
5.2.1. Cells 192
5.2.2. Mycobacterial culture and lipid extract 192
5.2.3. *Mtb* lipid fractionation 193
5.2.4. Lipid solubilisation and addition to cell culture 193
5.2.5. MALDI-ToF analysis of lipid composition. 194
5.2.6. TLC for PIM profile 194
5.2.7. LysoTracker™ staining for FACS analysis....194
5.2.8. Immunofluorescent staining 194
5.2.9. Filipin staining of free cholesterol. 194
5.2.10. CtxB staining 194
5.2.11. Sphingosine and sphinganine levels by RP-HPLC. 195
5.2.12. GSL levels determined by NP-HPLC. 195
5.2.13. Statistical analysis 195
5.3. Results 196
5.3.1. Fractionated *Mtb* H37Rv TL extract significantly increases LysoTracker™ staining intensity of RAW 264.7 MΦ. 196
5.3.2. Fractionated *Mtb* H37Rv TL extract inhibits pro-IL1β synthesis in RAW 264.7 MΦ. 198
5.3.3. MALDI-ToF MS analysis of the lipid compositions in fractions 13, 14 and 15 of *Mtb* TL extract. 199
5.3.4. Lipid components of the *Mtb* cell wall increase the relative volume of the acidic compartment in RAW 264.7 MΦ. 201

5.3.5. Lipid components of the *Mtb* cell wall induced a reduction in the frequency of pro-IL1β positive RAW 264.7 MΦ that had been stimulated by LA. 203

5.3.6. Lipid components of the *Mtb* cell wall cause dose-dependent inhibition in pro-IL1β synthesis in RAW 264.7 MΦ. 205

5.3.7. MALDI-ToF MS analysis of the composition of *Mtb* lipids, SL-1, TDM, $PIM_{1,2}$ and PIM_6. 208

5.3.8. SL-1, TDM, $PIM_{1,2}$ and PIM_6 of *Mtb* cell wall increase the size of LE/Lys in RAW 264.7 MΦ visualised by LAMP-1 immunostaining. 209

5.3.9. SL-1, TDM, $PIM_{1,2}$ and PIM_6 induce cholesterol accumulation in RAW 264.7 MΦ. 211

5.3.10. SL-1, TDM, $PIM_{1,2}$ and PIM_6 perturb GM1 ganglioside intracellular trafficking in RAW 264.7 MΦ. 215

5.3.11. Exposure to PIM_6 significantly increases Npc1 and Npc2 expression, whereas SL-1 only increases Npc2 expression in RAW 264.7 MΦ. 217

5.3.12. PIM_6 enhances transcriptions of *Npc1* and *Npc2* in RAW 264.7 MΦ. 219

5.3.13. SL-1 increases the level of sphingosine level, and PIM_6 increases the level of sphinganine level in RAW 264.7 MΦ. 221

5.3.14. SL-1 and $PIM_{1,2}$ induce GSL accumulation in RAW 264.7 MΦ… 222

5.3.15. MALDI-ToF MS of TL extracts of *Mtb* H37Rv and *ΔpimE Mtb* H37Rv. 225

5.3.16. TL extract of *Mtb* H37Rv and *ΔpimE Mtb* H37Rv increase LysoTracker™ staining intensity of RAW 264.7 MΦ. 227

5.3.17. TL extracts of *Mtb* H37Rv and *ΔpimE Mtb* H37Rv induce cholesterol re-distribution in RAW 264.7 MΦ. 229

5.3.18. TL extracts of *Mtb* H37Rv and *ΔpimE Mtb* H37Rv significantly increase the expression of Npc1 but not Npc2 in RAW 264.7 MΦ….. 230

5.3.19. TL extracts of *Mtb* H37Rv and *ΔpimE Mtb* H37Rv significantly increase the transcription of Npc1 but not Npc2 in RAW 264.7 MΦ…. 232

5.4. Discussion.....234

Chapter 6. *Salmonella* and the NPC pathway 243

6.1. Introduction 244

6.2. Material and methods 256

6.2.1. Cells 256

6.2.2. *S.* Typhimurium strains and infection assays 256

6.2.3. *S.* Typhimurium TL extract. 257

6.2.4. Lipid solubilisation and addition to cells. 257

6.2.5. Filipin staining for free cholesterol.....257

6.2.6. LAMP-1 immunostaining for confocal analysis. 258

6.2.7. AmplexRed assay determination of total cholesterol. 258

6.2.8. CtxB staining for intracellular GM1 ganglioside distribution…… 258

6.2.9. RP-HPLC measurement of sphingosine and sphinganine levels. 258

6.2.10. NP-HPLC measurement of GSL levels. 258

6.2.11. Western blotting 259

6.2.12. qPCR.....259

6.2.13. Immunofluorescent staining of Npc1 for confocal microscopy…. 259

6.2.14. BODIPY-LacCer trafficking.....260

6.2.15. Statistical analysis.....260

6.3. Results 261
6.3.1. Optimisation of the post-infection (pi) period of *S.* Typhimurium infection in RAW 264.7 MΦ.....261
6.3.2. Infection with WT and *ΔssaV S.* Typhimurium increases the size of LAMP-1 positive compartments in RAW 264.7 MΦ. 263
6.3.3. Infection with WT, *ΔssaV, ΔsifA, ΔsseJ* or *ΔsifAsseJ S.* Typhimurium induces endo-lysosomal cholesterol accumulation in RAW 264.7 MΦ. 267
6.3.4. Infection with WT, *ΔssaV* and *ΔsseJ*, but not in *ΔsifA* or *ΔsifAsseJ S.* Typhimurium increases the cholesterol content of RAW 264.7 MΦ. 272
6.3.5. Perturbed intracellular trafficking of GM1 ganglioside in RAW 264.7 MΦ infected with WT, *ΔssaV, ΔsifA, ΔsseJ* or *ΔsifAsseJ S.* Typhimurium. 273
6.3.6. Infection with WT, *ΔssaV, ΔsifA, ΔsseJ* and *ΔsifAsseJ S.* Typhimurium causes sphingosine and sphinganine accumulation in RAW 264.7 MΦ.....277
6.3.7. GSLs accumulate in RAW 264.7 MΦ infected with WT, *ΔssaV, ΔsifA, ΔsseJ* or *ΔsifAsseJ S.* Typhimurium. 279
6.3.8. RAW 264.7 MΦ infection with WT, *ΔssaV, ΔsifA, ΔsseJ* or *ΔsifAsseJ S.* Typhimurium does not affect Npc1 expression but significantly increases the expression of Npc2.....282
6.3.9. Expression of *Npc1* and *Npc2* genes are decreased in WT, *ΔssaV, ΔsifA* or *ΔsseJ S.* Typhimurium-infected RAW 264.7 MΦ but are increased with *ΔsifAsseJ S.* Typhimurium infection. 284
6.3.10. Npc1 is recruited to SCV in RAW 264.7 MΦ infected with WT or *ΔssaV S.* Typhimurium. 285
6.3.11. *S.* Typhimurium TL extract increases LysoTracker™ staining intensity of RAW 264.7 MΦ. 290

6.3.12. Confocal microscopy of LysoTracker™ staining confirms expansion of the acidic compartment in RAW 264.7 MΦ treated with *S.* Typhimurium TL extract. 292

6.3.13. *S.* Typhimurium and *Mtb* H37Rv TL extracts increase LysoTracker™ staining intensity of WT but not CHO$^{Npc1-/-}$ cells…….. 293

6.3.14. LPS significantly increases LysoTracker™ staining intensity of RAW 264.7 MΦ but not WT CHO cells. 295

6.3.15. *Mtb* H37Rv and *S.* Typhimurium TL extracts significantly increase LysoTracker™ staining intensity of WT and *Tlr4*$^{-/-}$ murine bone marrow-derived MΦ (iBMDMΦ). 298

6.3.16. LAMP-1 immunostaining confirms expansion of LE/Lys volume in RAW 264.7 MΦ treated with *S.* Typhimurium TL extract…. 300

6.3.17. *S.* Typhimurium TL extract induces partial cholesterol redistribution to the endo-lysosomal system of RAW 264.7 MΦ……. 302

6.3.18. *S.* Typhimurium TL extract does not affect the total cholesterol level content of RAW 264.7 MΦ. 304

6.3.19. *S.* Typhimurium TL extract perturbs GM1 ganglioside trafficking in RAW 264.7 MΦ. 305

6.3.20. *S.* Typhimurium TL extract perturbs BODIPY-LacCer trafficking in RAW 264.7 MΦ. 306

6.3.21. *S.* Typhimurium TL extract significantly increases Npc2 but not Npc1 protein levels in RAW 264.7 MΦ. 309

6.3.22. *S.* Typhimurium TL extract enhances expression of *Npc1* and *Npc2* genes in RAW 264.7 MΦ. 311

6.3.23. *S.* Typhimurium TL extract induces transient sphingosine and sphinganine accumulation in RAW 264.7 MΦ. 312

6.3.24. *S.* Typhimurium TL extract enhances SphK2 protein in RAW 264.7 MΦ.....313

6.3.25. *S.* Typhimurium TL extract induces GSL accumulation in RAW 264.7 MΦ.....314

6.4. Discussion.....318

Chapter 7. Conclusion and Future Studies.....329

Bibliography 338

Appendix 1.....383

Appendix 2.....384

Appendix 3.....386

List of Figures

Figure 1. Functions of lysosomes. 3
Figure 1.2.3. Schematic representation of the main forms of Niemann-Pick disease type C... 6
Figure 1.2.4.1. Structures of Ncr1 (yeast orthologue of NPC1) and NPC2...8
Figure 1.2.4.2.1. The pathogenic cascade in NPC....10
Figure 1.2.4.2.2. NPC pathway in lipid metabolism....11
Figure 1.2.4.2.3. Endocytic trafficking and endo-lysosomal Ca^{2+} signalling...14
Figure 1.2.4.2.4. Simplified scheme of GSL biosynthesis. 17
Figure 1.4.1.1. Schematic of phylogenetic relationship of specific mycobacterial species. 22
Figure 1.4.1.2. Schematic of the phylogeny of Mycobacteria tuberculosis. 23
Figure 1.4.2.1. Progression of the human tubercular granuloma. 25
Figure 1.5. Schematic of proposed lipid-mediated inhibition of the NPC pathway by pathogenic mycobacteria. 33
Table 1.5. Summary of cellular phenotypes induced by BCG or M. smegmatis infection and MAMES/FAMES or TDM treatment. 34
Figure 2.3.1.1. FACS gating strategy for analysis of LysoTracker™ staining of RAW 264.7 MΦ.……....55
Figure 2.3.1.2. Mtb H37Rv TL extract from two independent sources significantly increases LysoTracker™ staining intensity of RAW 264.7 MΦ.....56
Figure 2.3.2. Mtb H37Rv TL extract from two independent sources significantly increases LysoTracker™ staining intensity in murine BMDMΦs. ..58
Figure 2.3.3. Treatment with Mtb H37Rv TL extract results in a dose-dependent reduction in the frequency of pro-IL1β positive RAW 264.7 MΦ stimulated with LA. 59
Figure 2.3.4. Mycobacterial lipids that can significantly increase LysoTracker™ staining intensity of RAW 264.7 MΦ are widely distributed across Mtb clinical strain but not M. canettii. 62
Figure 2.3.5. TL extract of M. canettii induces a dose-dependent decrease of LysoTracker™ staining intensity of RAW 264.7 MΦ.....63

Figure 2.3.6.1. U18666A increases the frequency and size of LE/Lys in RAW 264.7 MΦ.....65
Figure 2.3.9. Optimisation of denaturation temperature of RAW 264.7 MΦ lysate for LAMP-1 western blotting. 74
Figure 2.3.11. Exposure to Mtb H37Rv significantly increases the expression of Npc1 in RAW 264.7 MΦ. 78
Figure 2.3.12. Mtb H37Rv TL significantly enhances transcription of Npc1 and Npc2 genes in RAW 264.7 MΦ. 80
Figure 2.3.13.2. Mtb lipids induced a partial redistribution of cholesterol to intracellular puncta in RAW 264.7 MΦ. 83
Figure 2.3.16.1. U18666A affects GM1 ganglioside trafficking in RAW 264.7 MΦ.....88
Figure 2.3.16.2. TL extracts of representative Mtb clinical strains, but not M. canettii affect GM1 ganglioside trafficking in RAW 264.7 MΦ. 90
Figure 2.3.17.1. U18666A causes GSL accumulation in RAW 264.7 MΦ.....91
Figure 2.3.18.1. TLCs of lipids from Mtb clinical isolates. 97
Figure 2.3.18.2. MALDI lipid fingerprinting of mycobacteria.....101
Figure 2.4. Schematic of proposed lipid-mediated inhibition of NPC pathway during pathogenic mycobacteria infection. 109
Figure 3.3.1. TL extracts of M. abscessus, M. avium and M. bovis, but not M. leprae and M. smegmatis, significantly increase LysoTracker™ staining intensity of RAW 264.7 MΦ. 122
Figure 3.3.2. TL extract of M. abscessus, M. avium, M. bovis and M. leprae, but to a much lesser extent M. smegmatis, induce significant expansion of LE/Lys in RAW 264.7 MΦ visualised by LAMP-1 immunostaining.....124
Figure 3.3.3. TL extracts of M. abscessus, M. avium, M. bovis, M. leprae and M. smegmatis induce a partial redistribution of cholesterol to intracellular puncta in RAW 264.7 MΦ. 127
Figure 3.3.4. TL extracts of M. abscessus, M. bovis, M. leprae or M. avium do not affect cholesterol content, while M. smegmatis significantly increased it in RAW 264.7 MΦ... 128
Figure 3.3.6. Levels of identified GSL species are changed significantly in RAW 264.7 MΦ treated with TL extracts of specific mycobacteria. 134

Figure 4.1.1. The sphingolipid metabolism pathway. 147
Figure 4.1.2. Structure of sphingosine and sphinganine..... 148
Figure 4.1.3. Structure of sphingosine-1-phosphate. 149
Figure 4.3.1.1. Representative RP-HPLC profiles for C18 sphingosine, C18 sphinganine and C20 sphingosine. 157
Figure 4.3.1.2. Linear correlation between the quantification of sphingosine and sphinganine in RAW 264.7 MΦ and protein input as determined by RP-HPLC..... 158
Figure 4.3.2. Optimisation of the extraction of sphingosine and sphinganine from RAW 264.7 MΦ. 160
Figure 4.3.3. Mtb H37Rv TL extract induces a transient increase in sphingosine and sphinganine in RAW 264.7 MΦ. 163
Figure 4.3.4. Mtb H37Rv TL extract induces sphingosine, sphinganine, S1P and DHS1P accumulation in RAW 264.7 MΦ. 165
Figure 4.3.5. Mtb H37Rv TL extract treatment induces ceramide and monohexosylceramide accumulation in RAW 264.7 MΦ. 167
Figure 4.3.6. Mtb H37Rv TL extract induced SM accumulation in RAW 264.7 MΦ..... 169
Figure 4.3.7. Optimisation of BODIPY-LacCer trafficking in RAW 264.7 MΦ..... 170
Figure 4.3.8. Mtb H37Rv TL extract induces BODIPY-LacCer lysosomal accumulation in RAW 264.7 MΦ. 172
Figure 4.3.9. U18666A treatment does not alter SphK1 and SphK2 protein levels in RAW 264.7 MΦ. 173
Figure 4.3.10. Mtb H37Rv TL extract does not alter SphK1 but increases SphK2 expression in RAW 264.7 MΦ. 175
Figure 5.1.1. Schematic of the Mtb cell envelope. 185
Figure 5.1.2. Structure of mycolic acid, TDM and sulfolipid-1 from Mtb cell wall..... 188
Figure 5.1.3. Structure (A) and the biosynthesis pathway (B) of PIM. 190
Figure 5.3.1. Fractionated Mtb H37Rv and M. smegmatis TL extracts significantly increase LysoTracker™ staining intensity of RAW264.7 MΦ. 197

Figure 5.3.2. LA-dependent pro-IL1β synthesis in RAW 264.7 MΦ inhibited by selected Mtb H37Rv cell wall lipid fractions. 199
Figure 5.3.3. MALDI-ToF MS of Mtb H37Rv lipid fractions 13, 14, and 15..... 201
Figure 5.3.4. Lipid components from Mtb cell wall increase LysoTracker™ MFI in RAW 264.7 MΦ. 202
Figure 5.3.5. Lipid components from Mtb cell wall induced an reduction in the frequency of pro-IL1β positive RAW 264.7 MΦ that has been stimulated by LA..... 204
Figure 5.3.6. Lipid components of the Mtb cell wall induce dose-dependent inhibition of pro-IL1β in RAW 264.7 MΦ. 206
Figure 5.3.7. MS profile of SL-1, TDM, $PIM_{1,2}$ and PIM_6. 208
Figure 5.3.8. Expansion of lysosomal compartment in RAW 264.7 MΦ in response to SL-1, TDM, $PIM_{1,2}$ and PIM_6 visualised by anti-LAMP-1 staining..... 210
Figure 5.3.9.1. SL-1, TDM, $PIM_{1,2}$ and PIM_6 induce redistribution of cholesterol to intracellular puncta in RAW 264.7 MΦ. 212
Figure 5.3.10. SL-1, TDM, $PIM_{1,2}$ and PIM_6 perturb GM1 ganglioside trafficking in RAW 264.7 MΦ. 216
Figure 5.3.11. Exposure to PIM_6 significantly increases the expression of Npc1 and Npc2 in RAW 264.7 MΦ. 218
Figure 5.3.12. PIM_6 enhances the transcription of Npc1 and Npc2 in RAW 264.7 MΦ..... 220
Figure 5.3.13. SL-1 increases sphingosine, and PIM_6 increases sphinganine content of RAW 264.7 MΦ. 221
Figure 5.3.14. SL-1 and $PIM_{1,2}$ induce GSL accumulation in RAW 264.7 MΦ..... 224
Figure 5.3.15.1. MALDI-ToF MS profile of TL extracts from H37Rv (A) and ΔpimE Mtb H37Rv (B). 226
Figure 5.3.15.2. TLC profile of PIMs of WT and ΔpimE Mtb H37Rv lipid extract..... 227
Figure 5.3.16. TL extracts of Mtb H37Rv and ΔpimE Mtb H37Rv significantly increase LysoTracker™ staining intensity of RAW 264.7 MΦ. 228

Figure 5.3.17. TL extracts of Mtb H37Rv and ΔpimE Mtb H37Rv induce re-distribution of cholesterol in RAW 264.7 MΦ.....230
Figure 5.3.19. TL extracts of Mtb H37Rv and ΔpimE Mtb H37Rv increase Npc1 and Npc2 transcription in RAW 264.7 MΦ. 233
Figure 5.4. Structure of SL-1, TDM, PIM_2 and PIM_6. 237
Figure 6.1.1. Schematic of the structure of S. Typhimurium. 246
Figure 6.1.2. Pathogenesis of S. Typhimurium. 248
Figure 6.1.3. The intracellular life cycle of S. Typhimurium. 251
Figure 6.1.4. Proposed interaction of Salmonella effector proteins with NPC1 between Salmonella-containing vacuole and ER membrane.....254
Figure 6.3.1. WT S. Typhimurium infection induces a partial redistribution of cholesterol to intracellular puncta in RAW 264.7 MΦ.....262
Figure 6.3.2. Expansion of LAMP-1 positive compartments in RAW 264.7 MΦ infected with WT or ΔssaV S. Typhimurium. 266
Figure 6.3.3. WT, ΔssaV, ΔsifA, ΔsseJ or ΔsifAsseJ S. Typhimurium infection induces a partial redistribution of cholesterol to intracellular puncta in RAW 264.7 MΦ.....271
Figure 6.3.4. WT, ΔssaV and ΔsseJ, but not ΔsifA or ΔsifAsseJ S. Typhimurium infection increases cholesterol in RAW 264.7 MΦ.....272
Figure 6.3.5. WT, ΔssaV, ΔsifA, ΔsseJ or ΔsifAsseJ S. Typhimurium infection perturb GM1 ganglioside trafficking in RAW 264.7 MΦ.....277
Figure 6.3.6. Infection with WT, ΔssaV, ΔsifA, ΔsseJ or ΔsifAsseJ S. Typhimurium causes sphingosine and sphinganine accumulation in RAW 264.7 MΦ.....278
Figure 6.3.7. WT, ΔssaV, ΔsifA, ΔsseJ or ΔsifAsseJ S. Typhimurium infection cause GSL accumulation in RAW 264.7 MΦ. 280
Figure 6.3.8. Infection with WT, ΔssaV, ΔsifA, ΔsseJ or ΔsifAsseJ S. Typhimurium infections do not alter Npc1 expression but increase that of Npc2 in RAW 264.7 MΦ.. 283
Figure 6.3.9. Gene expression of Npc1 and Npc2 in RAW 264.7 MΦ is reduced by infection with WT, ΔssaV, ΔsifA or ΔsseJ S. Typhimurium but increased by infection with ΔsifAsseJ.....285

Figure 6.3.10. Co-localisation of S. Typhimurium, Npc1 and LAMP-1 in RAW 264.7 MΦ infected with WT or ΔssaV S. Typhimurium.....289
Figure 6.3.11. S. Typhimurium TL extract significantly increases LysoTracker™ staining intensity but reduces cell viability of RAW 264.7 MΦ.291
Figure 6.3.12. Increased lysosomal frequency and size in RAW 264.7 MΦ treated with S. Typhimurium TL extracts visualised with LysoTracker™ Green DND-26..... 293
Figure 6.3.13. S. Typhimurium and Mtb H37Rv TL extracts increase LysoTracker™ staining intensity in WT but not in CHO$^{Npc1-/-}$ cells. 295
Figure 6.3.14. LPS increases LysoTracker™ staining intensity in RAW 264.7 MΦ but not in WT CHO cells. 297
Figure 6.3.15. Mtb H37Rv and S. Typhimurium TL extracts significantly increase LysoTracker™ staining intensity in WT and Tlr4$^{-/-}$ murine iBMDMΦ.299
Figure 6.3.16. Expansion of the LE/Lys compartment in RAW 264.7 MΦ in response to treatment with S. Typhimurium TL extract visualised by anti-LAMP-1 immunostaining. 301
Figure 6.3.17. S. Typhimurium TL extract induces a partial redistribution of cholesterol to intracellular puncta in RAW 264.7 MΦ.....303
Figure 6.3.18. S. Typhimurium TL extract treatment does not change the amount of cholesterol in RAW 264.7 MΦ. 304
Figure 6.3.19. S. Typhimurium TL extract perturbs GM1 ganglioside trafficking in RAW 264.7 MΦ. 306
Figure 6.3.20. S. Typhimurium TL extract perturbs BODIPY-LacCer trafficking in RAW 264.7 MΦ. 308
Figure 6.3.21. S. Typhimurium TL extract increases the amount of Npc2 but not Npc1 protein in RAW 264.7 MΦ. 310
Figure 6.3.22. S. Typhimurium TL extract enhances the expression of Npc1 and Npc2 genes in RAW 264.7 MΦ. 311
Figure 6.3.23. S. Typhimurium TL extract induces transient sphingosine and sphinganine accumulation in RAW 264.7 MΦ.....312
Figure 6.3.25. S. Typhimurium TL causes GSL accumulation in RAW 264.7 MΦ.....316

Figure 7. Some selected human pathogens able to resist Acanthamoeba phagocytosis in the phylogenetic tree of prokaryotes...331
Appendix figure 1. TL extract of B. pseudomallei increases LysoTracker™ staining intensity of WT and CHO$^{Npc1-/-}$ cells. 385
Appendix figure 2. Gene expression levels in U18666A or Mtb H37Rv TL-treated RAW 264.7 MΦ. 387

List of Tables

Table 1.4.1. Summary of the Mycobacterium genus.....21

Table 2.2.2. Genotypes of the selected Mtb clinical isolates strains used in this study……. 43

Table 2.3.17. Summary of the relative accumulation of total and specific GSL species in RAW 264.7 MΦ treated with U18666A or TL extracts of representative Mtb clinical strains or M. canettii. 95

Table 2.4. Summary of NPC cellular phenotypes induced by TL extracts of representative Mtb clinical strains and M. canettii in RAW 264.7 MΦ.....103

Table 3.3.6. Summary of changes to identified GSL species are changed significantly in RAW 264.7 MΦ treated with TL extracts of specific mycobacteria……... 135

Table 3.4. Summary of NPC cellular phenotypes induced by TL extracts of M. abscessus, M. avium, M. bovis, M. leprae, M. smegmatis and Mtb H37Rv in RAW 264.7 MΦ……..…..136

Table 5.2.2. Mtb H37Rv purified lipids obtained from BEI Resources and the solvents used for solubilisation. 192

Table 5.3.6. Summary of dose-dependent inhibition of pro-IL1β synthesis by lipid components from Mtb cell wall in RAW 264.7 MΦ.....207

Table 5.3.14. Summary of the fold change and statistical analysis of GSLs in RAW 264.7 MΦ treated with lipid component from the Mtb cell wall.....225

Table 5.4. Summary of NPC phenotypes induced by SL-1, TDM, $PIM_{1,2}$ and PIM_6……... 237

Table 6.3.7. Summary table of fold change and statistical significance of GSL content of RAW 264.7 MΦ infected with WT, ΔssaV, ΔsifA, ΔsseJ and ΔsifAsseJ S. Typhimurium. 281

Table 6.3.25. Summary of the fold change and statistical analysis of GSLs in RAW 264.7 MΦ treated with S. Typhimurium TL extract.....317

Table 6.4.1. Summary of functions of effector proteins from SPI-2.....320

Table 6.4.2. Summary of NPC cellular phenotypes induced by S. Typhimurium infection and TL extract of S. Typhimurium in RAW 264.7 MΦ…….....321

Table 7. Summary of alteration in NPC1 and NPC2 levels in RAW 264.7 MΦ treated with bacterial lipid(s) or bacterial infection. 334

Chapter 1. Introduction

Lysosome

Lysosomes are dynamic organelles that are primarily known for their involvement in the catabolism and recycling of extracellular and intracellular macromolecules via the activities of multiple acid hydrolases [1]. However, it is now recognised that their roles are far more complex and have a much greater influence on cellular homeostasis than previously appreciated (Fig 1.) [2]. Indeed, lysosomes are important signalling hubs and are central to the regulation of metabolism and growth through nutrient sensing and interactions with other organelles (Fig 1.) [3]. The acidic compartment is a key intracellular store of calcium (Ca^{2+}), which is mobilised by nicotinic acid adenine dinucleotide phosphate (NAADP) in response to particular stimuli [4]. Relevant to the studies described in this thesis, the lysosome is also important for host defence against pathogens, including bacteria, viruses and parasites [5]. Here we describe investigations of how intracellular pathogens manipulate a specific lysosomal pathway to promote their intracellular survival.

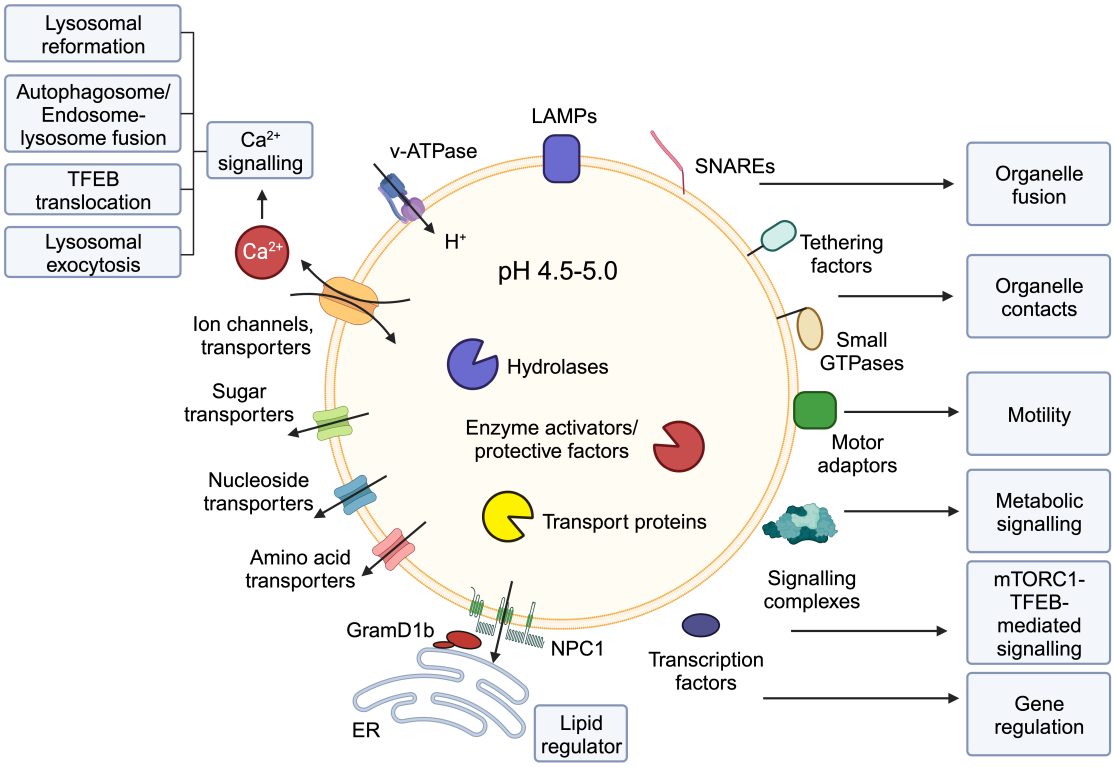


Figure 1. Functions of lysosomes.

ER, endoplasmic reticulum. Adapted from [2].

1.1. Lysosomal storage diseases (LSDs)

LSDs are a group of rare metabolic disorders caused by inherited mutations in genes encoding proteins involved in lysosomal function leading to the accumulation of undegraded substrates. More than 70 individual LSDs have been identified [6, 7]. Based upon the nature of the stored substrates, LSDs have been subclassified into, for example the sphingolipidoses (sphingoid accumulation), mucopolysaccharidoses (mucopolysaccharide accumulation) and the neuronal ceroid lipofuscinoses (lipofuscin accumulation) [8]. The combined incidence rate of LSDs is believed to be around 1 in 5,500 live births but is likely to be an underestimate [6]. However, individual LSDs are rare, ranging from 1 in 50,000 to 250,000 live births [6]. The prevalence of LSDs can

vary according to geography and ethnicity. For example, Gaucher disease (GD) caused by *GBA* mutation is the most common LSD, with an overall prevalence of 1 in 50,000 live births [9], but in the Ashkenazi Jewish population occurs at 1 in 1000 live births [10]. Treatments for LSDs are limited and are mostly managed by symptomatic and supportive therapies. However, enzyme replacement therapy (ERT), enzyme enhancement chaperone therapy and substrate reduction therapy (SRT) are available for some LSDs [6].

1.2. Niemann-Pick diseases

First identified by Albert Niemann and Ludwig Pick in the 1920s in a child with nervous system impairment, the eponym “Niemann-Pick diseases” has been used to describe a group of lysosomal disorders featuring hepatosplenomegaly and sphingomyelin (SM) storage [11]. Four subgroups A to D of Niemann-Pick disease have been identified, and each has different pathologies. Type D was originally referred to as the ‘Nova Scotia’ isolate [12] and subsequently renamed as Niemann-Pick disease type C (NPC) [13].

1.2.1. Niemann-Pick disease type A and type B

Niemann-Pick disease type A (NPA) and type B (NPB) are caused by autosomal recessive mutations in the *SMPD1* gene, which regulates the expression of acid sphingomyelinase (ASM) [14]. NPA and NPB are collectively known as acid sphingomyelinase deficiency (ASMD) [14]. NPA patients exhibit hepatosplenomegaly and rapid progressive neurodegeneration, and most fail to survive beyond the first year of life [15]. NPB patients exhibit

hepatosplenomegaly and compromised pulmonary function without central nervous system (CNS) impairment and live into adulthood with variable life expectancy [16-18]. NPA and NPB exhibit foam cell formation in the liver, spleen, lymph nodes, lung airways and bone marrow, which is characterised by lipid accumulation (especially SM) [15, 19, 20]. Enzyme replacement therapy, by administration of recombinant human ASM intravenously in NPB patients, is very beneficial. For example, chronic fatigue is attenuated, tissue lipid accumulation is reduced and lung function is improved without causing significant adverse effects [21]. There is also a very significant reduction in spleen and liver volumes [21].

1.2.2. Niemann-Pick disease type C

NPC is an inherited autosomal recessive disease caused by mutations in NPC1 (about 95% of clinical cases) or NPC2 (5% of clinical cases) proteins. The prevalence of NPC is estimated to be at 1 in 120,000 live births [11, 22]. The age of disease onset varies greatly ranging from neonatal to adulthood. The mean age of survival based on natural history studies in untreated patients is 11 years [23].

1.2.3. NPC clinical symptoms

NPC is an LSD involving visceral and neurological manifestations. Clinical presentation of NPC is very variable, and although the majority of cases occur within infancy and childhood, adult-onset disease has been identified [11].

Neurological and visceral manifestations and the disease progression in NPC are summarised in Figure 1.2.3.

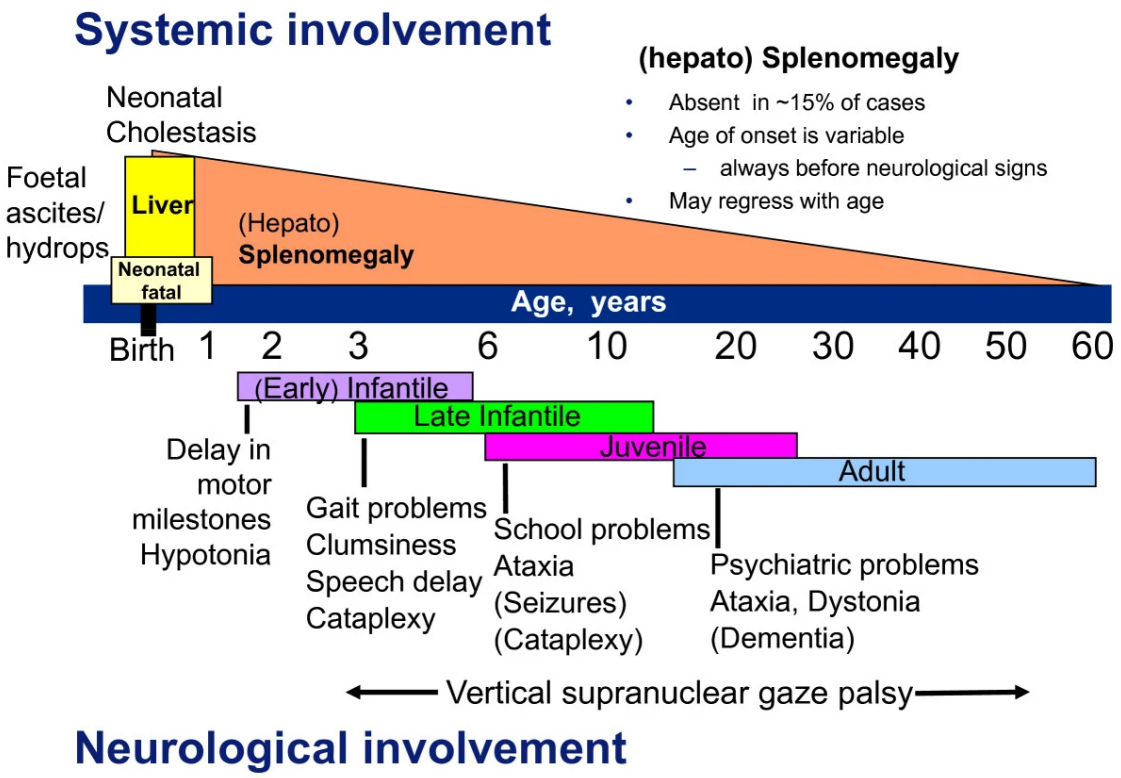


Figure 1.2.3. Schematic representation of the main forms of Niemann-Pick disease type C.

Adapted from [11].

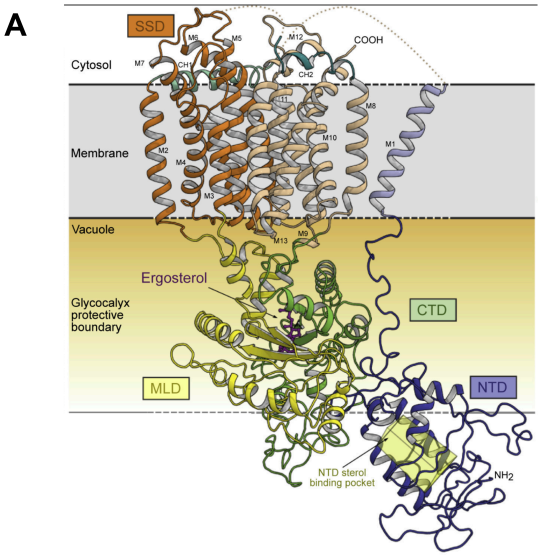
1.2.4. NPC cellular phenotypes

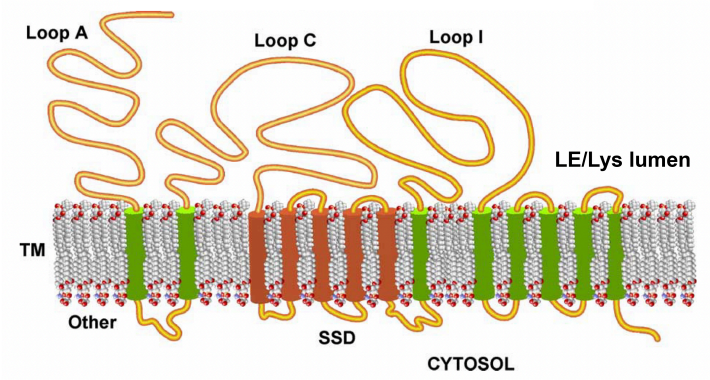
Accumulation of various lipid species occurs in NPC tissues, including unesterified cholesterol (free cholesterol) and sphingolipids, which result from impaired vesicle trafficking in the endocytic system [24]. Clinically, the accumulation of unesterified cholesterol in late endosomes/lysosomes (LE/Lys) in patient fibroblasts detected by the 'filipin test' has historically been the basis for the NPC clinical diagnostic test [25]. Amongst the lipid accumulation observed in LSDs, lysosomal sphingosine accumulation and reduced lysosomal Ca^{2+} are

unique phenotypes [26]. How NPC1 and NPC2 proteins regulate these phenotypes will be discussed in detail below.

1.2.4.1. NPC1 and NPC2

NPC disease is caused by mutations in either the *NPC1* or *NPC2* genes. As mutations in two independent proteins cause the same clinical disease, it is proposed that NPC1 and NPC2 function together in the same cellar pathway, often referred to as the NPC pathway. NPC1 is a transmembrane protein (1278 amino acids) located on the limiting membrane of the LE/Lys (Fig 1.2.4.1.A.), while NPC2 is a small soluble mannose-6-phosphorylated glycoprotein that resides in the lysosomal lumen (Fig 1.2.4.1.B.) [27-29].





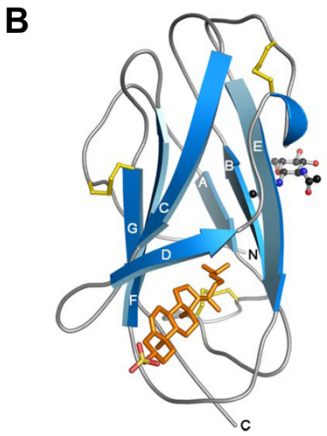


Figure 1.2.4.1. Structures of Ncr1 (yeast orthologue of NPC1) and NPC2.

Panel A. Predicted crystal structure of Ncr1 (upper panel) and topology of NPC1 protein (lower panel). NTD, N-terminal domain; CTD, C-terminal domain; MLD, middle luminal domain; LE/Lys, late endosome/lysosome; TM, transmembrane domains; SSD, sterol-sensing domains. Panel B. Ribbon presentation of NPC2 protein structure. Cholesterol sulphate (oxygen in red, carbon in gold, sulphur in yellow) is shown to bind to the lumen of NPC2 protein. The glycosylation point at Asn-39 is shown as a ball-and-stick representation. Adapted from [28, 29].

The NPC1 protein consists of 13 transmembrane domains, a sterol sensing domain (SSD) on the cytosolic side, three large loops on the LE/Lys lumen side and a C-terminal cytoplasmic tail (Fig 1.2.4.1.A.) [29]. Over 400 mutations that span the protein have been identified in NPC patients [29], and most affected individuals are compound heterozygotes carrying two different *NPC1* mutations on the two alleles. It has been hypothesised that NPC2 binds cholesterol on vesicles in the LE/Lys lumen [28], which it then transfers to the NPC1 protein, facilitating its transport out of the lysosome [30]. Loops C and I of NPC1 protein

form a tunnel connecting the N-terminal domain (Loop A) and the SSD to enable cholesterol egress from the LE/Lys lumen to cytosol at acidic pH [30-33]. However, there is considerable evidence that is incompatible with this model. Critically, NPC1 has been demonstrated to regulate membrane contact sites between endocytic organelles and the endoplasmic reticulum (ER), and artificial tethering of the membrane contact sites rescues cholesterol accumulation and other phenotypes in NPC1-deficient cells [34]. Despite this, the precise roles of NPC1 and NPC2 in lipid trafficking remain unclear.

1.2.4.2. The pathological cascade in NPC

The complex nature of the cellular and biochemical phenotypes that characterise NPC cells has meant that it has not been straightforward to identify the pathological mechanisms that lead to disease in cells with established disease, for example, in mutant patient fibroblasts. In order to address this challenge, Lloyd-Evans and colleagues used pharmacological inhibition of NPC1 activity to determine the temporal sequences of events that are downstream of NPC1 loss of function [26]. They determined that sphingosine accumulated in the lysosome within 10min of pharmacological NPC1 inhibition in RAW 264.7 macrophage (MΦ) by U18666A, which is an amphipathic steroid that binds to the SSD domain of NPC1, and that resulted in a reduction in the lysosomal Ca^{2+} content of the lysosome within a similar time frame [26, 35]. In contrast, GSL and cholesterol did not accumulate significantly until 2h and over 4h respectively [26]. Furthermore, exogenous sphingosine addition was the only stored lipid that could induce disease phenotypes in healthy cells [26]. Raising of cytosolic Ca^{2+} was able to compensate for insufficient release of lysosomal Ca^{2+} and provided

benefit in mouse models of NPC disease *in vivo* [26]. A cartoon of the proposed pathogenic cascade in NPC is shown in Fig 1.2.4.2.1.

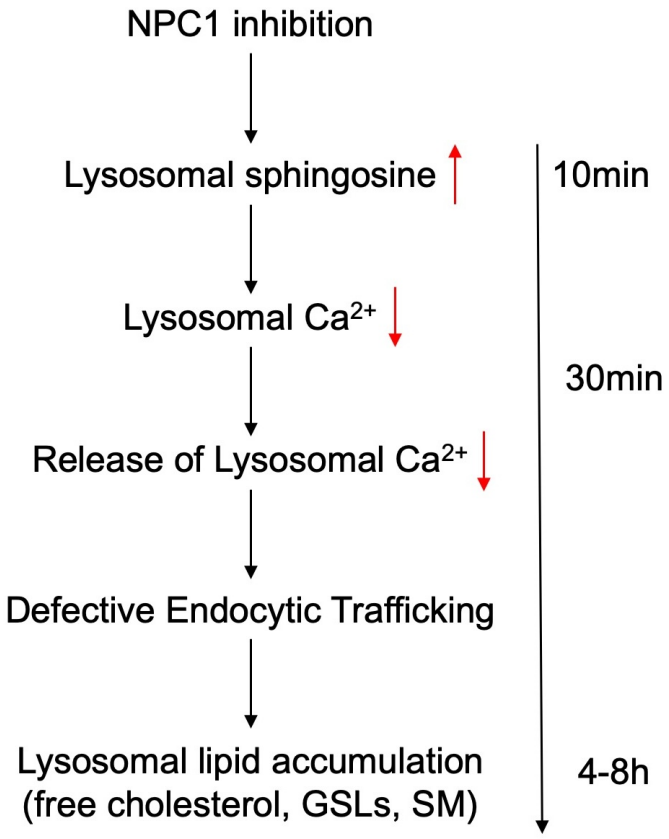


Figure 1.2.4.2.1. The pathogenic cascade in NPC.

The sequence of biochemical and cell biological events that underlie the pathogenesis of NPC disease. The times indicated are those reported in RAW 264.7 MΦ after Npc1 inhibition with U18666A. Adapted from [26].

The role of the NPC pathway in lipid metabolism in healthy and NPC disease cells is summarised in Fig 1.2.4.2.2. [36]. Each of the components of the pathway will be discussed in detail in the following sections.

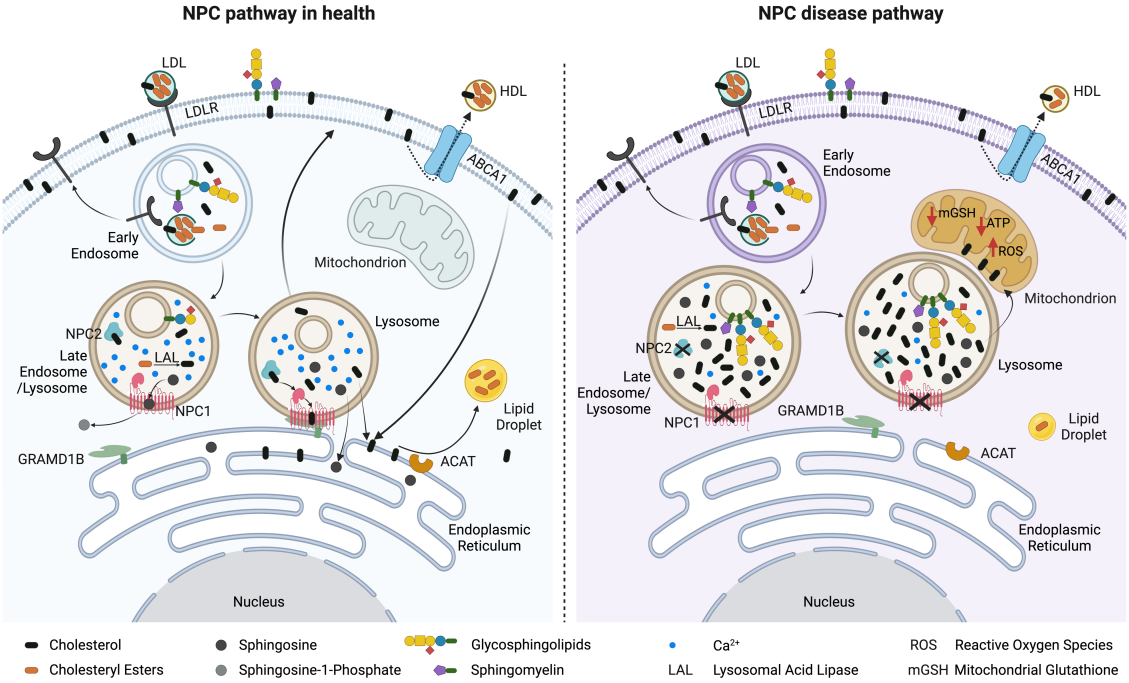


Figure 1.2.4.2.2. NPC pathway in lipid metabolism.

The left panel illustrates the lipid metabolism in healthy cells, whilst the right panel illustrates lipid accumulation in NPC disease cells. LDL, low-density lipoprotein; ACAT, acetyl-CoA transferase. Adapted from [36].

Lysosomal sphingosine accumulation

Sphingosine and sphinganine accumulate in NPC patient fibroblast and in *Npc1*$^{-/-}$ mouse tissue [37, 38]. Sphingosine-1-phosphate (S1P), which is a downstream product from sphingosine generated in lysosomes by sphingosine kinases (SphKs), is reduced in NPC patient fibroblast due to reduced SphK activity [37]. Sphingosine is protonated in acidic organelles and therefore requires a transporter to remove it from the lysosome to be phosphorylated [26, 39]. Lipid-

protein interaction study shows that NPC1 protein possesses a binding pocket for sphingosine [39]. More recently, direct interactions between NPC1 and sphingosine have been confirmed through the use of a multifunctional lipid probe [40], consistent with its potential role as a sphingosine transporter.

Lysosomal Ca^{2+}

Endosomes and lysosomes are important intracellular stores of Ca^{2+} and hence are signalling organelles. Although physically small in comparison to the ER, the luminal Ca^{2+} concentration is comparable to the ER, which is between 400 to 600μM [41]. Endo-lysosomal Ca^{2+} are taken up by endocytosis and rapidly released from the acidic compartments [42]. Lysosomal Ca^{2+} homeostasis is regulated by multiple pathways, all of which influence organelle cation content. Lysosomal membrane potential and the control of acidic pH via the uptake of H^+ ion is mediated via the vacuolar ATPase (V-ATPase) together with H^+ exchangers; re-filling of the store by Ca^{2+} pumps and coupled exchangers; luminal Ca^{2+} buffers and Ca^{2+} release mechanisms such as mucolipins (TRPMLs) and two-pore channels (TPCs), are all critical (Figure 1.2.4.2.3.) [4, 43-45]. Ca^{2+} released from ER by inositol triphosphate receptor ($InsP_3R$) are influx to LE/Lys lumen by the H^+/Ca^{2+} exchanger on the LE/Lys membrane [43, 44]. Mobilisation of Ca^{2+} release from the lysosome via TPCs is triggered by the unique second messenger NAADP [46, 47]. TPCs exist in different isoforms with overlapping distribution within the endo-lysosomal system. TPC1 is present primarily in the early endosomes (EEs), whilst TPC2 is located in the LE/Lys [48]. TPC3 is mainly found in recycling endosomes and suppresses Ca^{2+} release [4, 49]. On the other

hand, TRPML1 is expressed on the LE/Lys membrane and TRPML2/3 is expressed on both EEs and LE/Lys; both can regulate the release of Ca^{2+} [50].

In NPC1 deficient cells, there is a significant decrease in LE/Lys lumen Ca^{2+}, but levels in mitochondria and ER are not altered [26]. NPC disease is the first human disease found to have reduced lysosomal Ca^{2+} levels. The drop reduces the electrochemical driving force for Ca^{2+} release and may lower the sensitivity of TPCs to NAADP [51]. The importance of the loss of lysosomal Ca^{2+} homeostasis in NPC pathogenesis was confirmed using two experimental approaches; chelation of luminal Ca^{2+} induced NPC cellular phenotypes and elevating cytosolic Ca^{2+} using a weak SERCA antagonist curcumin could compensate for the insufficient release of lysosomal Ca^{2+} [26].

Endocytic trafficking

Whilst the full range of biological processes that are influenced by lysosomal Ca^{2+} has not been determined, it is known that it plays important roles in the functioning of the endo-lysosomal pathway [52]. The endocytic vesicle trafficking is regulated by Ca^{2+} release from endo-lysosomal compartments via local release and signalling rather than global Ca^{2+} released from ER (Figure 1.2.4.2.3.) [53].

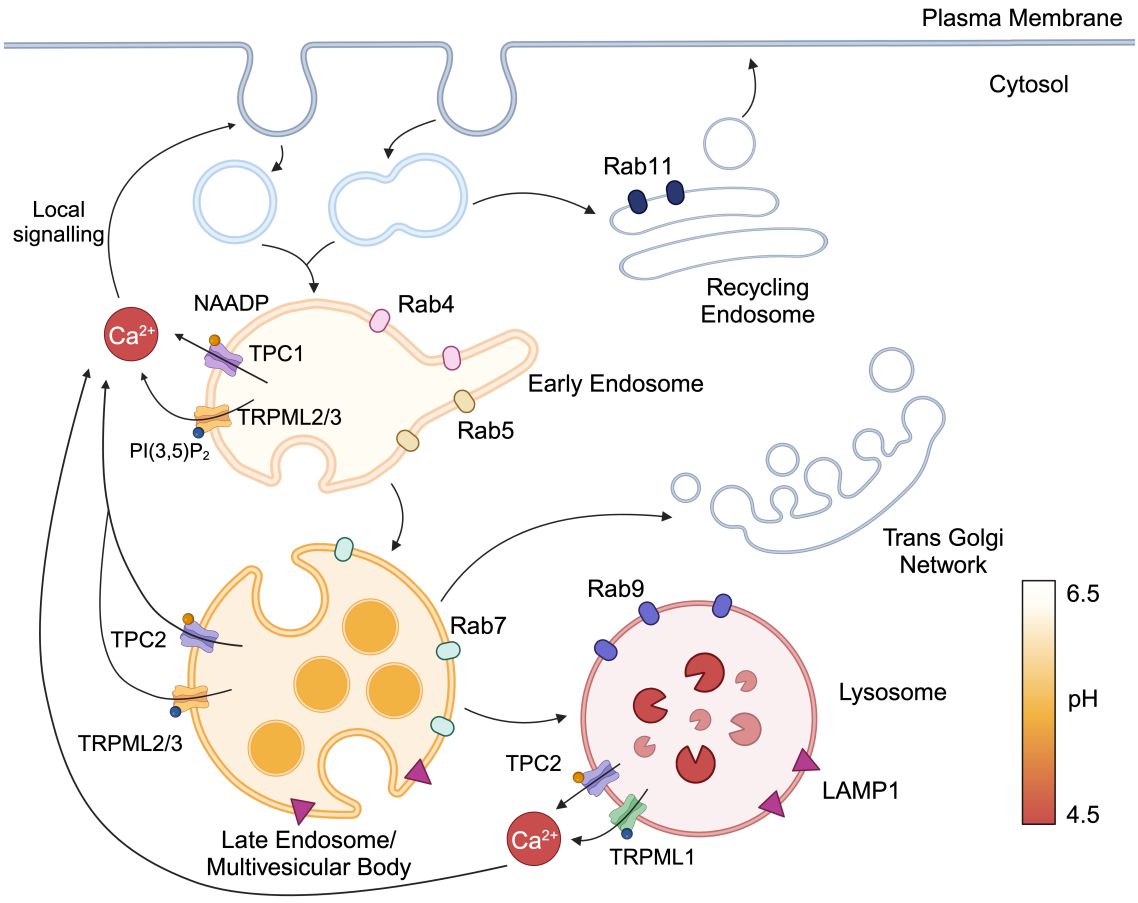


Figure 1.2.4.2.3. Endocytic trafficking and endo-lysosomal Ca^{2+} signalling.
Adapted from [54].

The process of endocytosis starts with the internalisation of molecules in EEs, which are a major sorting hub for endocytic cargos. Internalised molecules, especially membrane receptors, will be recycled and trafficked back to the plasma membrane via recycling endosomes, while the others are trafficked into LEs or multivesicular bodies and then fuse with lysosomes for degradation or go to the *trans*-Golgi network via retromers [55]. EEs, LEs and lysosomes are marked with specific Rab-GTPases (Rab4/5 for EEs; Rab7 for LEs; Rab9 for lysosomes), which are required for vesicle motility, docking and fusion [56-58]. SNARE proteins work collectively with Rab5 for vesicle docking and fusion on

EEs [58, 59], which requires the release of lysosomal luminal Ca^{2+} after the formation of *trans*-SNARE complexes [60]. Fusion events between LEs and lysosomes enable the passage of luminal contents through the pathway and delivery to the terminal compartment, which is directed by the endosomal sorting complex required for transport (ESCRT) system [61, 62].

The low Ca^{2+} content in NPC lysosomes is consistent with endocytic trafficking defects [63, 64] and failure of organelle fusion with the lysosome [65, 66], which is characteristic of NPC disease and results in the accumulation of multiple lipid species.

Lipid storage

The defect in endo-lysosomal trafficking in NPC cells results in the accumulation of lipids, such as unesterified cholesterol and sphingolipids [24]. Accumulation of lysosomal cholesterol, GSLs and SM in RAW 264.7 MΦ is observed within 4 to 8h of pharmacological inhibition of NPC1 (Fig 1.2.4.2.1) [26].

Cholesterol homeostasis is tightly controlled in mammalian cells [67]. Cholesterol is internalised primarily as low-density lipoprotein (LDL) particles via clathrin-dependent uptake [68] but can also be generated from acetyl-CoA by *de novo* biosynthesis [69]. In brief, cholesterol is transported and re-cycled between different cellular membranes to achieve appropriate distribution; to the plasma membrane of which it is an essential component; to the ER, where levels are sensed and the rate of biosynthesis adjusted accordingly and stored in lipid droplets or is removed by efflux [70]. Several pathways have been proposed that

enable cholesterol to reach the plasma membrane or the ER [71]. Following endocytosis, cholesteryl esters are delivered to endosomes and then to the LE/Lys where they are hydrolysed by acidic lipases to yield unesterified cholesterol (Fig 1.2.4.2.2.) [30, 67, 68]. Free cholesterol can exit the LE/Lys for delivery to ER for esterification by acetyl-CoA transferase [72] or storage and to the plasma membrane from which it can be effluxed by the ATP-binding cassette transporter A1 (ABCA1) [70], whose function is associated with the activities of NPC1 and NPC2 (Fig 1.2.4.2.2.) [73, 74]. Substantial evidence supports bidirectional transport between endosome/LE/Lys and ER via membrane contact sites and the involvement of sterol-binding proteins, including ORP1L and StAR Related Lipid Transfer Domain Containing 3 (STARD3) [75, 76].

NPC1 has been shown to be critical for the formation of contact sites between the lysosome and the ER through interactions with GramD1b to regulate cholesterol egress and artificial tethering in NPC1-deficient cells rescues lysosomal lipid accumulation (Fig 1.2.4.2.2.) [34]. Interestingly, in the absence of NPC1, contacts between lysosomes and mitochondria mediated by STARD3 are increased, which is consistent with the enhanced delivery of cholesterol to mitochondria in *NPC1*$^{-/-}$ cells (Fig 1.2.4.2.2.) [77].

GSLs and other sphingolipids accumulate in LE/Lys in NPC due to endocytic trafficking defects [78]. GSLs compose a hydrophobic ceramide moiety linked to a hydrophilic glycan head group [79]. The simplest of these are galactosylceramide (GalCer) found primarily in myelin and glucosylceramide (GlcCer) which is the precursor for most GSLs, including neural GSLs and

gangliosides (Fig 1.2.4.2.4.) [80]. The addition of a Galβ1-4 residue to GlcCer creates lactosylceramide (LacCer), which is the structural basis for Globo-, Lacto-, Neolacto- and Ganglio-series of GSLs (Fig 1.2.4.2.4.) [80]. Accumulation of GSLs is characteristic of several sphingolipid LSDs, including Gaucher disease (GlcCer storage), Tay-Sachs (GM2 ganglioside accumulation), Fabry disease (Gb3 storage), Sandoff disease (GM2 ganglioside accumulation) and GM1 gangliosidosis (GM1 accumulation) [81]. In NPC disease, all GSLs showed accumulation in both patient fibroblast and mouse models, with LacCer, GlcCer, GM2 and GM3 as the most abundant species [78]. Impaired cholesterol transport also contributes to GSL storage and miss-trafficking in NPC1-deficient cells [82, 83].

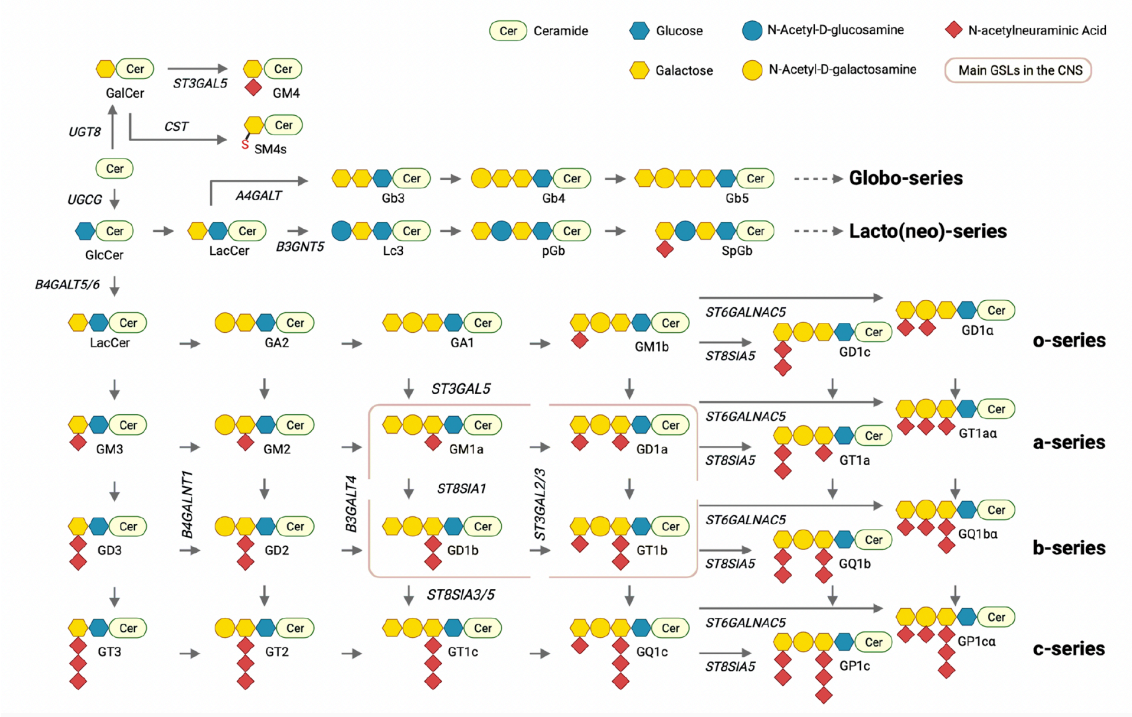


Figure 1.2.4.2.4. Simplified scheme of GSL biosynthesis.

Major gangliosides expressed in the central nervous system in the adult mammalian brain are boxed in pink. Adapted from [84].

1.2.5. NPC therapies

The only approved therapy (world-wide except the USA where it is prescribed off-label) for NPC is substrate reduction therapy (SRT) using the imino sugar drug miglustat (*N*-butyldeoxynojirimycin), which is an inhibitor of GlcCer biosynthesis [85]. The concept of SRT is to reduce the rate of glycosphingolipid (GSL) biosynthesis to offset its storage s glycosphingolipids are stored in NPC along with other lipids [86]. A long-term survival study of patients receiving miglustat concluded that the drug doubled life expectancy with the mean survival being 22 years of ages as opposed to age 11 in untreated patients [87]. Other drugs to treat NPC, such as 2-Hydroxypropyl-β-cyclodextrin (HP-β-CD), which facilitates the removal of unesterified cholesterol, and arimoclomol, which induces the expression of heat shock protein 70 to improve lysosomal functions, have undergone recent clinical trials but neither received approval from the Federal Drug Administration [88, 89]. Gene therapy has shown great promise in animal models of the disease but has not yet been trialled in individuals affected by NPC [89].

1.3. NPC pathway and intracellular pathogens

A number of studies have shown that NPC1 and NPC2 are important for microbial pathogenesis. Perhaps the best example is the requirement of NPC1 as the receptor for Ebola virus [90, 91]. NPC1 and Ca^{2+} release from lysosomes via TPCs are necessary for the virus to be able to escape from the lysosome and genetically deficient cells are resistant to infection [92]. Loss of NPC1 also reduces infection by Bluetongue virus and SARS-COV-2 [93, 94]. In contrast, human immunodeficiency virus (HIV) suppresses NPC1 and NPC2 to modulate

cholesterol trafficking in host cells [95]. Previous studies from Fineran *et al.* showed a mechanistic link between NPC disease and *Mycobacterium tuberculosis* (*Mtb*) infection [96].

1.4. Tuberculosis

Tuberculosis (TB) is caused by infection with the obligate human pathogen *Mtb* and remains a significant global health challenge. According to the World Health Organisation (WHO), 1.6 million deaths were caused by TB in 2021, making TB the 13th leading cause of death and the second with respect to fatal infections after COVID-19 [97]. Around 10 million new TB infections are reported annually and occur in almost all countries and across all age groups [97]. TB has a higher prevalence in low and lower-middle-income countries, such as regions in Southeast Asia, South Africa and the Western Pacific [97-99]. Individuals suffering from malnutrition or compromised immunity, such as due to HIV infection, are more susceptible to TB [100].

TB disease progression and management

Mtb typically causes a pulmonary infection, which presents as a spectrum from asymptomatic to a life-threatening disease. *Mtb* bacilli enter individuals via aerosol transmission and primarily target the lung. Initial *Mtb* infection may be eliminated from the bronchial airways by innate or adaptive immunity [100]. When not cleared, *Mtb* bacilli can persist for a long period of time without displaying clinical symptoms. This condition is referred to as latent TB infection (LTBI), and affected patients can be diagnosed by interferon-γ (IFN-γ) release assay (IGRA) and tubercular skin test (TST), but is more problematic in immunocompromised

individuals [101, 102]. LTBI is the most common clinical subtype, with 25% of patients being asymptomatic, and up to 50% not having a prolonged cough [103]. Whilst LTBI can be lifelong, between 5% to 15% of patients develop reactivation [101, 104]. A nine-month course of self-administered isoniazid (INH9) reduces the rate of reactivation by 90% [105, 106]. From LTBI to subclinical and active TB, the patients transform from an asymptomatic, non-transmissible to a transmissible state with common symptoms such as cough, fever and weight loss [100, 107]. Pulmonary damage caused by active TB is typically identified by computed tomography (CT) and magnetic resonance imaging (MRI) [100]. The current preventative approach to TB is to immunise with the Bacille Calmette-Guérin (BCG) vaccine, which comprises attenuated *Mycobacterium bovis* (*M. bovis*) that was developed by Calmette and Guérin and first administered in 1921 [108]. However, the effectiveness of BCG vaccines is variable and is more protective for children rather than adults against active TB but shows decreasing protection after 10 to 15 years [109-111]. The standard drug treatment is a combination of isoniazid, rifampicin, pyrazinamide and ethambutol [112]. However, the emergence of multidrug-resistant *Mtb* strains has significantly impacted efficacy, and the need to develop new drugs is urgent. Various combination drug treatments are undergoing phase three trials and may become important for the control of multi-drug resistant *Mtb* if successful [113]. The past and current clinical trials of *Mtb* drug treatment are summarised by Perrin *et al.* with clinical trial numbers [113].

1.4.1. Phylogeny of mycobacteria

TB is caused by a group of closely related mycobacteria known as the *Mycobacterium tuberculosis* complex (MTBC). Associations with humans can be traced back three million years to East Africa, and the ancestor to more modern *Mtb* strains evolved around 20,000 to 15,000 years ago [114, 115]. The genus *Mycobacterium* in phylum *Actinomycetota* is composed of approximately two hundred species. Broadly, it can be divided into TB-causing and non-tuberculous mycobacteria (NTM), together with *Mycobacterium leprae* (*M. leprae*), which is genetically distinct [116]. Mycobacteria can also be classified into fast-growing (those that require two to five days to form a colony) and slow-growing species, which require more than seven days (Table 1.4.1) [117, 118]. Species from MTBC and *M. leprae* are slow-growing mycobacteria (Table 1.4.1) [118]. The majority of NTM are rapidly growing mycobacteria and are abundant in the environment, such as in soil and sources of water, but only a small number are pathogenic in humans and/or animals (Table 1.4.1) [119].

	Non-tuberculous mycobacteria	
Slow-growing mycobacteria		Fast-growing mycobacteria
M. tuberculosis complex	*M. avium* complex • *M. avium* • *M. intracellulare* • *M. chimaera*	*M. chelonae-abscessus* complex • *M. abscessus* subsp. *abscessus* • *M. abscessus* subsp. *bolletii* • *M. abscessus* subsp. *massiliense* • *M. chelonae*
M. leprae	*M. haemophilum*	*M. fortuitum*
	M. xenopi	*M. smegmatis*
	M. kansasii	*M. vaccae*
	M. simiae	
	M. marinum	
	M. ulcerans	
	M. terrae complex	
	M. gordonae	

True pathogens
Opportunistic pathogens
Saprophytes

Table 1.4.1. Summary of the Mycobacterium genus.

Adapted from [118].

The phylogeny of mycobacteria is primarily based upon comparative analyses of ribosomal genes such as 16s rRNA sequences, together with house-keeping genes that include *hdp65*, *gyrB*, *rpoB*, *gyrA* and *dnaN* nucleotides [120-122]. In brief, the phylogenetic tree based upon 1941 core proteins suggests the existence of five distinct monophyletic groups within the genus *Mycobacterium*, one of which, the *Tuberculosis-Simiae* clade, includes all of the major human pathogens [122]. In Fig 1.4.1.1., a mycobacterial phylogenetic tree based on the relatedness of the iron-regulated protein HupB, a nucleotide-associated protein that is essential for *Mtb* growth, is presented [123, 124].

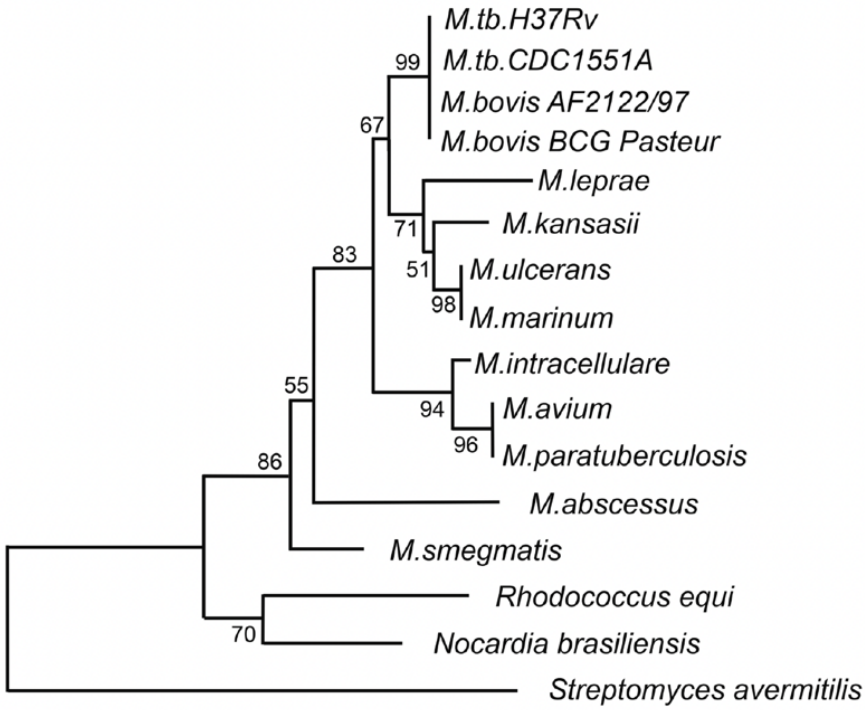


Figure 1.4.1.1. Schematic of phylogenetic relationship of specific mycobacterial species.

Phylogenetic tree of mycobacteria based upon the relatedness of the iron-regulated protein, HupB [123].

Phylogeny of *Mycobacteria tuberculosis*

The phylogeny of a global collection of *Mtb* strains is based on 212 single nucleotide polymorphisms (SNP) [125], which identify five major *Mtb* lineages (lineages 1, 2, 3, 4, 7) and two of *Mycobacterium africanum* strains (lineages 5, 6) (Fig 1.4.1.2.). So-called 'Modern' lineages (lineages 2, 3, 4) differ from the 'ancestral' lineages (lineages 1, 7) by the deletion of the *TbD1* gene [126, 127]. Genome-based studies suggest that MTBC likely evolved from a pool of recombinogenic mycobacterial strains that resembled current *M. canettii* strains [128].

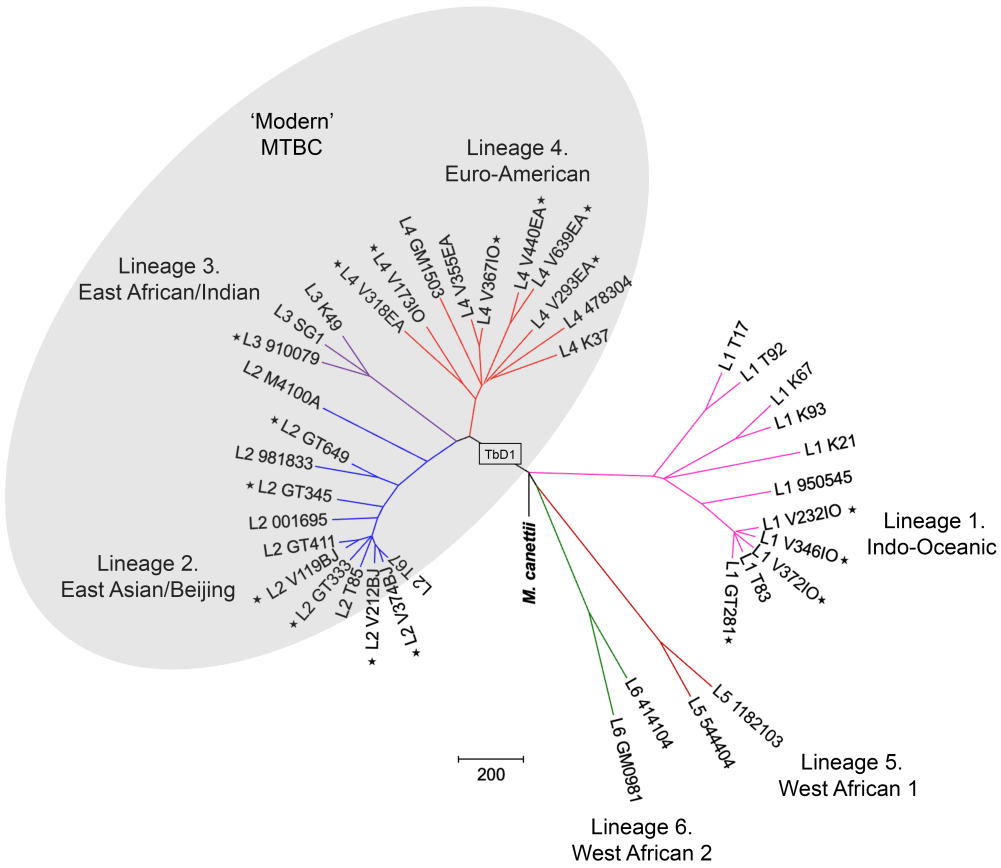


Figure 1.4.1.2. Schematic of the phylogeny of Mycobacteria tuberculosis.

'Modern' clades of MTBC are shaded in grey. Strains marked with stars are tested in Chapter 2. Adapted from [127].

1.4.2. *Mtb* cellular pathogenesis

Mtb is an obligate intracellular pathogen and has successfully evolved several survival strategies, which facilitate persistence at both the level of the cell and systemically. For example, the formation of granuloma in the lung serves as a replication centre for *Mtb* bacilli, whilst perhaps the most significant intracellular survival strategy is the prevention of fusion between *Mtb*-containing phagosomes and the host cell lysosome. These strategies will be discussed in detail in the following sections.

1.4.2.1. Formation of granuloma

The formation of granuloma in lung tissue is characteristic of active TB infection and the granuloma environment promotes the survival, replication and release of *Mtb* bacilli from the airway (Fig. 1.4.2.1). Upon entering the host respiratory tract, *Mtb* bacilli are phagocytosed by alveolar MΦ [129]. Infected cells then release pro-inflammatory cytokines to recruit mononuclear immune cells from the blood to the site of infection, which generates the early granuloma [130]. This structure has a core of infected cells surrounded by foamy MΦ and other mononuclear phagocytes, which in turn are surrounded by lymphocytes [131]. As the granuloma matures, a fibrous collagenous cuff is formed that delineates the periphery of the structure [129]. At the final stage, the infected MΦ in the centre undergoes necrosis to form a caseating core and replicating bacilli are released into the airway [129].

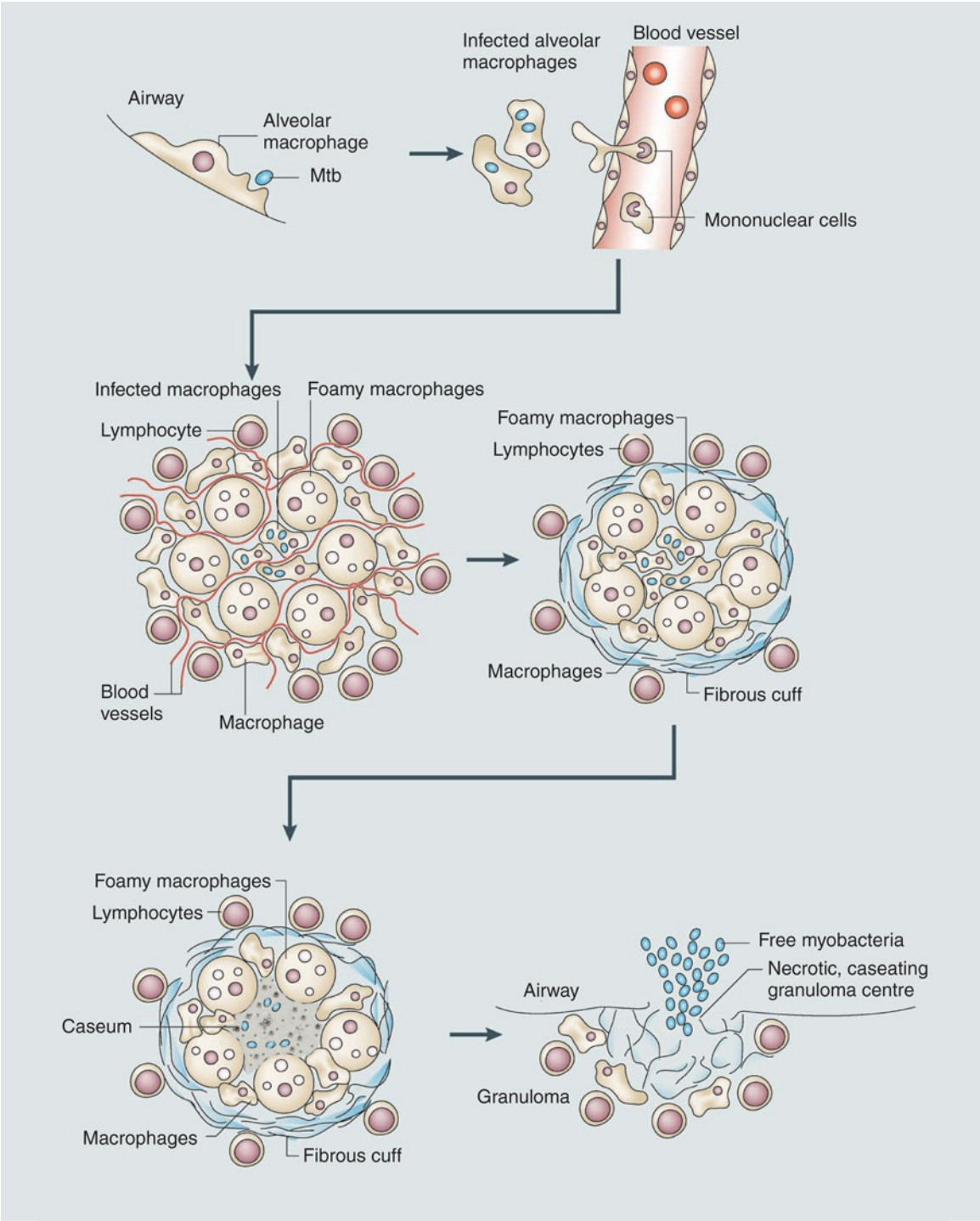


Figure 1.4.2.1. Progression of the human tubercular granuloma.

Adapted from [129].

1.4.2.2. Foamy macrophages

One feature of granuloma is the accumulation of foamy MΦ (Fig. 1.4.2.1.) [132]. The foam cell is characterised by dysregulated lipid metabolism, which results in lipid accumulation [129]. Apart from *Mtb* infection, the foam cell phenotype is also present in other bacterial infections such as *Salmonella enterica* Serovar Typhimurium (*S.* Typhimurium) and *Nocardia brasiliensis*, and other metabolomic and autoimmune diseases, including NPC, atherosclerosis and multiple sclerosis [133-136]. The main cause of foam MΦ formation during *Mtb* infection is the excessive influx of oxidised LDL (oxLDL), which results mainly in triglyceride accumulation in lipid droplets [137, 138]. *Mtb* interacts with the host MΦ lipid-sensing nuclear receptors peroxisome proliferator-activated receptor γ (PPARγ) and testicular receptor 4 (TR4), creating a niche for oxLDL binding to CD36 on the MΦ plasma membrane [139]. OxLDL contains oxidised products, including fatty acids, oxidised proteins and lipid-derived products, which facilitate the persistence and survival of intracellular bacilli by inducing lysosomal dysfunction and lysosomal free cholesterol accumulation [140, 141]. Cholesterol is required for several aspects of *Mtb* infection. Bacilli access and utilise cholesterol as a carbon source for growth [142] and to facilitate survival during the non-replicating persistent state [143, 144]. Plasma membrane cholesterol is necessary for the phagocytosis of *Mtb* [145], whilst *in vivo* studies indicate a role for cholesterol in dormancy and reactivation [146].

1.4.3. Intracellular persistence

Mtb has evolved multiple mechanisms to evade the host immune response and perturb lysosomal function as a means to achieve intracellular survival and persistence. Proteins and lipids secreted or shed by *Mtb* bacilli make important contributions to these mechanisms.

1.4.3.1. *Mtb* effector proteins

Mtb encodes five type VII secretion systems (T7SS), which are early secretory antigenic target secretion systems (ESX) 1 to 5 [147]. T7SS is a hexamer embedded in the inner plasma membrane of the mycobacteria [148]. The functions of ESX1, 3 and 5 are better understood than ESX2 and 4.

ESX1, which is necessary for virulence, is responsible for the secretion of proteins encoded in the region of deletion 1 (RD1), whose expression is restricted in modern pathogenic *Mtb* strains (Fig 1.4.1.2.) [149]. For example, the attenuated *M. bovis* vaccine strain, BCG, is defective in ESX1 [150]. The most studied protein from ESX1 is the early secreted antigenic target (ESAT)-6 (also known as EsxA). ESAT-6, together with culture filtration protein (CFP)-10 (also called EsxB), form a dimer, which forms pores on the phagosome membrane, plasma membrane and organelle membrane to promote *Mtb* pathogenesis [151]. However, this was later proved to be a detergent-mediated artefact [152]. The ESAT-6/CFP-10 complex also manipulates the host immune response depending on the stage of infection [153, 154]. Antigen presentation is affected as a result of the interaction between the ESAT-6/CFP-10 complex and β-2-microglobulin (β2M), which regulates major histocompatibility complex I (MHC-I)

antigen presentation on MΦ [155]. In addition, the ESAT-6/CFP-10 complex induces interferon-gamma (IFN-γ) and tumour necrosis factor-alpha (TNF-α) production by T cells [156]. ESX1 is also required for MyD88/interleukin (IL) pathway-dependent activation of NOD-, LRR- and pyrin domain-containing protein 3 inflammasome (NLRP3) and the spread of *Mtb* into the lung cavity [157]. The ESAT-6/CFP-10 complex manipulates phagosome maturation and inhibits autophagic clearance of mycobacteria in host MΦ [158, 159].

ESX3 impacts the survival of *Mtb* through the regulation of iron availability and prevention of phagosome maturation [160]. EsxG and EsxH secreted from ESX3 function in a way akin to the ESAT-6/CFP-10 complex from ESX1 and form a dimer [161]. They disrupt the ESCRT complex on the host cell ER and impair the endocytic trafficking and maturation of the *Mtb*-containing phagosome [162].

ESX5 primarily affects the host immune response. During *Mtb* infection, ESX5 effector proteins induce IL-1β secretion and NLRP3 inflammasome activation [163, 164]. IL-1β production is necessary to control the *Mtb* infection *in vivo* [165], and it is tightly regulated depending on the virulence of the mycobacteria [166, 167].

1.4.3.2. *Mtb* lipids

Mycobacterial cell wall lipids play a key role in TB pathogenesis and intracellular persistence. Unlike other Gram-positive bacteria, the mycobacterial envelope is composed of an inner membrane and an outer membrane connected by a peptidoglycan and arabinogalactan layer, with a capsule composed of mannan-

containing long-chain lipids anchoring the outer membrane [168]. The bioactivities of *Mtb* cell wall lipids have been extensively studied with respect to host-pathogen interactions. Specific lipid species affect the host immune response, enhance phagocytosis, prevent compartment acidification, block phagosome-lysosome fusion and inhibit autophagy [169]. The complex lipid composition and structure of the cell wall are described in greater detail in Chapter 5.

Synthesis of membrane lipids

Fatty acids, glycerol lipids, phospholipids and prenol lipids are the main lipid species in mycobacterial membranes [170]. *Mtb* has two distinct enzyme systems, fatty acid synthase (FAS) I and II, which are responsible for the production of membrane phospholipids and outer membrane glycolipids [170]. FAS I is responsible for *de novo* synthesis of acyl-CoA from acetyl-CoA and malonyl-CoA in the cytosol [171]. FAS II system catalyses elongation of the species generated by FAS I. An important product resulting from the activities of FAS I and II is mycolic acid (MA), which is the main component of the *Mtb* outer membrane [171]. MA is further elongated to become trehalose monomycolate (TMM) and transported by mycobacterial membrane protein Large 3 (MmpL3) located on the inner membrane to the outer membrane to form trehalose dimycolate (TDM) [172, 173]. Glycolipids and phospholipids are synthesised near the *Mtb* inner membrane. The main functional phospholipids species are cardiolipin (CL) and members of the phosphoinositol (PI) family [170]. The PI synthetic pathway will be described in Chapter 5.

Release of *Mtb* lipids

Cell wall lipids are released either passively or actively. Passive lipid release includes the shedding of membrane lipids through close contact between bacilli and the phagosome/plasma membrane and in the case of *Mycobacterium avium*, the phagosome membrane is required to avoid phagosome-lysosome fusion [174]. Electron microscopy has revealed the shedding of phosphatidylinositol mannosides (PIMs) and lipoarabinomannan (LAM) by *Mtb* within phagosomes [175]. Active release of membrane lipids involves the formation of vesicles on mycobacterial membranes, which will be spread and taken up by uninfected neighbouring cells to modulate immune responses [176]. The 'bystander cell effect' is also mediated by lipids shed from *Mtb* bacilli, resulting in neighbouring uninfected cells exhibiting the phenotypes observed in infected cells, such as lipid droplet accumulation and inflammatory activation [129, 175, 177, 178].

Mtb lipids and immune regulation

Lipid components of the mycobacterial cell wall influence immune response during the early and late stages of infection [179]. *Mtb* cell wall lipids, such as phthiocerol dimycocerosates (PDIM) of the outer membrane, act as pathogen-associated molecular patterns (PAMPs) during initial infection [180]. Lipomannan (LM) and LAM are recognised by Toll-Like Receptor (TLR) 2 on MΦ and initiate pro-inflammatory responses and granuloma formation [181, 182]. PIMs interact with TLR2/4 and cause proinflammatory cytokine production [183]. TDM binds to C-type lectins to induce TNF-α production, which is essential for lung granuloma formation [184]. TDM on intracellular *Mtb* inhibits antigen presentation by the MΦ [185].

Roles of *Mtb* lipids in intracellular persistence

Mtb cell wall lipids are involved in *Mtb* intracellular survival strategies, including inhibition of phagosome and LE/Lys acidification, block of phagosome-lysosome fusion and prevention of autophagy and autophagosome formation. There is evidence that both PDIM and the terpene nucleotide, 1-tuberculosinyladenosine (1-TbAd), can inhibit compartment acidification [180, 186, 187]. Multiple lipid species have been shown to impede fusion. One example of this is phagosomes containing PIM-coated latex beads that avoid fusion with the lysosome [188]. LAM modulates the SM/cholesterol ratio on phagosomes to influence vesicle fusion [189]. TDM, otherwise known as cord factor, can affect both acidification and phagosome-lysosome fusion [190, 191]. Additional mechanisms that favour intracellular survival are also dependent upon envelope lipids. For example, PDIM facilitates the escape of bacilli from phagosome to cytosol, promotes MΦ death and prevents the production of reactive nitrogen species [186, 192].

1.5. NPC and mycobacteria

Although NPC and TB are two distinct and apparently unrelated diseases, there are several published reports suggesting possible links. A clinical case report proposed *NPC1* as a susceptibility gene for *Mtb* infection because a child who developed BCG-itis after vaccination was subsequently diagnosed with NPC [193]. MicroRNA-25 (miRNA-25) is significantly upregulated by *Mtb* or BCG infection and targets NPC1 to promote mycobacterial survival, whereas miRNA-25 deficient mice display enhanced resistance [194]. NPC2 has been proposed as a biomarker for the diagnosis of TB as a result of evidence of increased mRNA

in a patient cohort [195]. A clinical study showed that vitamin A-triggered antimicrobial activity against *Mtb* required the expression of NPC2 [196].

A study by Fineran *et al.* has proposed a mechanistic link between NPC and TB with the hypothesis that pathogenic mycobacteria target the NPC pathway by shedding lipid(s) that inhibit NPC1 to induce host cellular phenotypes that promote intracellular survival [96]. Briefly, the authors demonstrated phenotypic convergence of NPC cells and cells infected with *Mtb* or BCG in both murine and human MΦ. In the absence of a direct assay for NPC1 activity, they analysed phenotypes indicative of the loss of NPC1 activity as seen in either genetically deficient cells or cells treated with the pharmacological inhibitor U18666A. The shared phenotypes include reduced lysosomal luminal Ca^{2+} concentration, storage of cholesterol, GSL, SM and sphingosine, altered ganglioside trafficking and enhanced NPC1 expression (Table 1.5.) [96]. *Mtb* lipids could induce the same phenotypes observed with infection, and overexpression of NPC1 impaired their ability to induce NPC phenotypes [96]. *Mycobacterium smegmatis* (*M. smegmatis*), a non-persistent environmental mycobacterium, was unable to induce NPC phenotypes in wild-type host cells, whereas cells lacking NPC1 protein were unable to clear *M. smegmatis* [96]. Curcumin, a weak SERCA antagonist, which can compensate for the deficiency in lysosomal Ca^{2+} release from lysosomes by increasing cytosolic Ca^{2+} levels, was able to significantly reduce mycobacterial burden in MΦ *in vitro* and zebrafish *in vivo* [96]. NPC phenotypes were induced not only in infected cells but also in neighbouring non-infected cells, suggesting that lipids are shed by mycobacteria and reach the

LE/Lys and also escape from the infected cell, are endocytosed by neighbouring uninfected cells where they inhibit NPC1 (Fig 1.5.) [96].

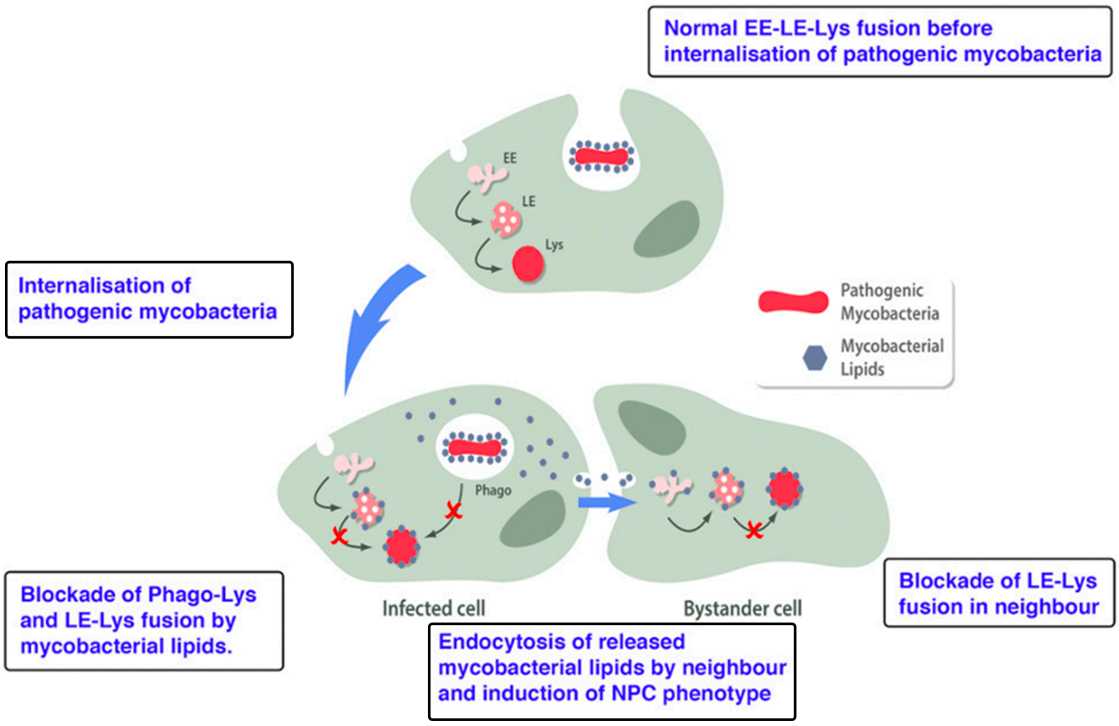


Figure 1.5. Schematic of proposed lipid-mediated inhibition of the NPC pathway by pathogenic mycobacteria.

Following internalisation by phagocytosis, mycobacteria residing in the phagosome shed cell wall lipids, which reach the LE/Lys of the host cell, where they inhibit the NPC1 protein. This causes a reduction in LE/Lys Ca^{2+} levels and blocks phagosome-lysosome fusion. Lipids released by infected cells are endocytosed by neighbouring cells and induce NPC phenotypes, including blockade of late endosome-lysosome fusion. EE, early endosome; LE, late endosome; Lys, lysosome; Phago, phagosome. Adapted from [96].

NPC cellular phenotypes	Mycobacterial infection		Mycobacterial lipid treatment	
	BCG	*M. smegmatis*	MAMES/FAMES	TDM
Lysosomal Ca^{2+} content	↓	-	Not evaluated	↓
Lysosomal Ca^{2+} release	↓	-	Not evaluated	↓
LysoTracker™ intensity	↑	-	Not evaluated	↑
Sphingosine accumulation	Yes	No	Yes	Yes
Cholesterol accumulation	Yes	No	Yes	Yes
GSL accumulation	Yes	No	Not evaluated	Not evaluated
Lysosomal GM1 ganglioside accumulation	Yes	No	Yes	Yes
Lysosomal SM accumulation	Yes	No	Yes	Not evaluated
NPC1 protein level	↑	Not evaluated	Not evaluated	Not evaluated
NPC2 protein level	-	Not evaluated	Not evaluated	Not evaluated

Table 1.5. Summary of cellular phenotypes induced by BCG or M. smegmatis infection and MAMES/FAMES or TDM treatment.

↓, decreased; ↑, increased; -, not altered; MAMES/FAMES, mycolic acid methyl esters/fatty acid methyl esters; TDM, trehalose dimycolatye. Summarised from Fineran *et al.* [96].

Aims

In this study, we hypothesised that the inhibition of the host NPC pathway is a shared mechanism among various bacterial intracellular pathogens, which benefits their intracellular pathogenesis in host cells.

Therefore, in this thesis, we aimed to:

- Determine whether mycobacterial lipid-mediated NPC1 inhibition is widespread amongst human clinical *Mtb* strains and other pathogenic species of mycobacteria.
- Investigate how *Mtb* cell wall lipids manipulate host cell sphingolipid metabolism.
- Identify the active lipid species from the *Mtb* cell wall that inhibit the NPC pathway.
- Investigate if other intracellular pathogens, such as *Salmonella*, also target the NPC pathway to enhance their intracellular survival.

Lay summary of the work

Some of the most significant infectious microbes that affect human health reside within the cells of the host rather than exist extracellularly. In order to survive, they manipulate the machinery of the host cell and do so to prevent their delivery to a part of the cell, the lysosome, in which they would be destroyed.

Previous studies have suggested a mechanistic link between Niemann-Pick disease type C (NPC), a rare, inherited disease, and tuberculosis (TB), a common infectious condition caused by *Mycobacterium tuberculosis* (*Mtb*). In both, the functioning of the lysosome is perturbed, and material that normally would end up in the lysosome is unable to reach it. Unexpectedly, the two diseases share multiple phenotypes. It was confirmed that *Mtb* lipids alone are able to induce the phenotypes that characterise the genetic disease in which the NPC1 protein is non-functional.

In this thesis, we examined the distribution of activity amongst lipid extracts of multiple clinically relevant strains and lineages of *Mtb*, as well as other related pathogenic mycobacteria that cause disease in animals. By screening for induction of NPC cellular phenotypes, we showed the lipid-mediated inhibition of NPC1 protein by *Mtb* is widespread amongst modern clinical strains and other non-tubercular pathogenic mycobacteria but absent from a species that is believed to resemble the ancestral one from which *Mtb* evolved. In addition, we showed that specific glycolipid species isolated from the mycobacterial cell wall were able to induce many of the NPC phenotypes. We also demonstrated that

Mtb lipid treatment resulted in changes to the metabolism of a specific class of lipids, sphingolipids, that mimic those that occur in NPC.

Finally, we hypothesised that inhibition of the host NPC pathway might be a strategy adopted by other intracellular pathogens to facilitate their survival. In support of this proposal, we showed that the phylogenetically distinct microbe *Salmonella* is able to induce NPC cellular phenotypes via a lipid-dependent mechanism.

We conclude the NPC pathway is targeted by multiple intracellular pathogens and may be the target of a host-targeted anti-microbial therapeutic strategy that would not be subject to the emergence of resistance.

Chapter 2. Inhibition of the Niemann-Pick C1 protein is a conserved feature of multiple strains of *Mycobacterium tuberculosis*

2.1. Introduction

Mtb is the causative agent of the human TB [197]. One of the key strategies for intracellular survival and persistence of *Mtb* is preventing the fusion of *Mtb*-containing phagosomes with host cell lysosomes to avoid degradation [169]. Whilst several lipids have been shown to be capable of blocking fusion (described in Chapter 1), our understanding of the mechanisms that are responsible remains incomplete.

A mechanistic link between NPC and pathogenic mycobacteria

Fineran *et al.* previously reported the unexpected phenotypic similarities in cellular phenotypes between NPC cells and foamy MΦ infected with *Mtb* and BCG [96]. In brief, all the cellular phenotypes that define NPC, including a reduction in the lysosomal Ca^{2+} levels, prevention of phagosome-lysosome fusion and accumulation of specific lipid species (including cholesterol, SM, sphingosine and GSL) within the endo-lysosomal system were observed in cells infected with *Mtb* or BCG but not *M. smegmatis* [96]. The induction of NPC phenotypes in non-infected cells was consistent with the hypothesis that pathogenic mycobacteria shed lipid(s) which are taken up by neighbouring cells that inhibit NPC1 (Fig 1.5.) [175, 198, 199]. Critically, all of the NPC cellular phenotypes were induced not only in infected or lipid-treated murine RAW 264.7 MΦ but also in human monocyte-derived MΦ, thereby confirming relevance to human disease.

Limitations of *Mtb* H37Rv strain as an experimental model

Previously, Fineran and colleagues utilised *Mtb* H37Rv and BCG in their studies [96]. *Mtb* H37Rv is a widely used laboratory-adapted strain that has been used extensively for investigating *Mtb* phylogeny, molecular epidemiology and the detection of drug-resistant mutations [200]. The *Mtb* H37 strain was originally isolated from a patient with pulmonary TB in 1905 [201], and further delineated into 'virulent' (Rv) and 'avirulent' (Ra) strains in 1934 [202]. In 1998, the genome sequence of H37Rv was established to be the *Mtb* reference sequence [203]. However, H37Rv displays limitations, particularly with respect to virulence in animal and cell infection models. For example, caseous necrosis and the formation of multinucleated giant cells does not occur with H37Rv infection in mice [204], and the replication rate of *Mtb* H37Rv in human monocyte-derived MΦ is slower than that of patient isolates [205]. Virulence, immunopathology and transmissibility vary between different clinical isolates of *Mtb*, meaning infection with H37Rv cannot fully reproduce all of the features of clinical disease [206]. Therefore, to confirm the relevance of lipid-mediated inhibition of NPC1, it was important to determine whether clinically relevant strains also induce NPC phenotypes. We therefore obtained lipids extracts from *Mtb* strains illustrated in Fig 1.4.1.2. representing lineage 1, 2, 3 and 4.

Aims

This chapter is based on the published paper ‘Inhibition of the Niemann-Pick C1 protein is a conserved feature of multiple strains of pathogenic mycobacteria’ [207]. In this chapter, we aim to:

- Determine the ability of lipid extracts from multiple strains of human tubercular mycobacteria to inhibit NPC1.
- Investigate if this ability is relevant to the evolution of human tubercular mycobacteria.

2.2. Material and Methods

2.2.1. Cells

RAW 264.7 MΦ were obtained from ATCC (American Tissue Culture Collection). RAW 264.7 MΦ were cultured in RPMI-1640 media supplemented with 10% Foetal Bovine Serum (FBS) (v/v) (Sigma, F7524), 1% glutamine (v/v) (Gibco, 25030-024) and 1% penicillin/streptomycin (v/v) (P/S) (Sigma-Aldrich, P0781) (R10) at 37ºC with 5% CO_2. Cells were passaged routinely for no more than 20 passages to maintain viability (>90%). Bone marrow cells were collected from the femurs of BALB/c mice and differentiated into bone marrow-derived MΦ (BMDMΦ) using macrophage colony-stimulating factor (M-CSF) containing L-929 cell supernatant (prepared by Dr Nick Platt) [208].

2.2.2. Mycobacterial culture and cell wall lipid extraction

Mtb strains were cultured in Sauton's medium by Dr Gerald Larrouy-Maumus at Imperial College, London. *Mtb* clinical strains consisted of 16 clinical strains of *Mtb* collected in Vietnam: 4 Indo-Oceanic (Lineages 1), 6 Beijing (Lineage 2) and 6 Euro-American (Lineage 4) to reflect the genotypic diversity. Strains tested in this study are summarised in Table 2.2.2. The following reagents were obtained through BEI Resources, NIAID, NIH: *Mtb*, Strain, CDC1551, total lipids, NR-14838; *Mtb*, Strain East African Indian 91_0079, NR-44098; *Mtb* Strain H37Rv, total lipids, NR-14837; *Mycobacterium canettii* total lipids, NR-40334.

Strain	Spoligotype[I]	ST number[II]	Lineage category[III]	Lineage number[IV]	Lineage geographical location[V]
232	EA14_VNM	ST139	Ancient	1	IO
346	EA14_VNM	ST140	Ancient	1	IO
372	EA14_VNM	ST141	Ancient	1	IO
281	ZERO	ST405	Ancient	1	IO
374	BEIJING	ST1	Modern	2	BJ
212	BEIJING	ST2	Modern	2	BJ
333	BEIJING	ST3	Modern	2	BJ
119	BEIJING	ST4	Modern	2	BJ
345	BEIJING LIKE	Unclassified	Modern	2	BJ
649	BEIJING LIKE	ST269	Modern	2	BJ
318	T1	ST53	Modern	4	EA
173	H1	ST62	Modern	4	EA
367	ZERO	ST405	Ancient	1	IO
440	H3	ST946	Modern	4	EA
639	H3	ST50	Modern	4	EA
293	T1	ST53	Modern	4	EA

Table 2.2.2. Genotypes of the selected Mtb clinical isolates strains used in this study.

I and II indicate the classification in accordance with the international spoligotyping database [209]. III indicates the classification based on the evolutionary phylogenetic tree [210]. IV indicates the classification in accordance with sequence alignment [211]. V indicates the BJ (East Asian/Beijing), IO (Indo-Oceanic) and EA (Euro-American) classification.

Lipid extracts from *Mtb* were prepared by Dr Gerald Larrouy-Maumus at Imperial College, London. Heat-killed (98^{o}C for 2h) mycobacteria were first washed 3 times with Dulbecco's phosphate-buffered saline (PBS) (Gibco, 14190-094). The pellets were then extracted with chloroform ($CHCl_3$): methanol (MeOH) 1:2 (v/v) for 12 h at room temperature, followed by $CHCl_3$: MeOH 1:1 (v/v) extraction and a subsequent $CHCl_3$: MeOH 2:1 (v/v) extraction for 3h at room temperature. Pooled extracts were concentrated and evaporated to dryness.

2.2.3. Lipid solubilisation and addition to cell culture

Dried *Mtb* lipids were re-constituted in dimethyl sulfoxide (DMSO) (Sigma, D2650) at a concentration of 20mg/ml by heating to 60^{o}C and sonicated for 10min in an ultrasonic water bath (Fisherbrand, FB11026). The DMSO stock was further diluted to 200µg/ml in pre-warmed R10 (60^{o}C), sonicated for 3min, cooled to room temperature and immediately added to the cell culture. RAW 264.7 MΦ were seeded in a 96-well plates at 5 x 10^4 cells/well and allowed to adhere overnight before treatment. Lipids in R10, U18666A (Merck, 662015, at a final concentration of 2µg/ml as positive control) and DMSO only (vehicle control, at a concentration equivalent to that in diluted lipids) were added and plates were incubated at 37^{o}C with 5% CO_2 for 48h or as specified in the results section.

2.2.4. LysoTracker^{TM} staining for flow cytometry (FACS) analysis

After treatment, cells were transferred into a 96-well U bottom plates (GreinerOne) and washed with PBS twice and pelleted at 377xg for 5min. Cells were then stained with 200nM LysoTracker^{TM} Green DND-26 (ThermoFisher, L7526) in PBS at room temperature for 10min in the dark. After staining, cells were pelleted, washed, and resuspended in 200µl of PBS and kept on ice prior to analysis. Dead cells were identified by the addition of 5ug/ml propidium iodide (PI) (Sigma, P4864) immediately before running on a BD FACS-Canto II Flow Cytometer (Beckton Dickinson). Compensation was set up using unstained, untreated cells, PI-stained freeze-thawed cells and LysoTracker^{TM}-stained U18666A-treated cells. A minimum of 10,000 viable cell events were collected for each sample using the DIVA software v0.1 (Beckton Dickinson), and the data were analysed using FlowJo software (Version10, FlowJo, LLC).

2.2.5. Pro-IL1β staining for FACS analysis

After treatment with *Mtb* lipid extracts, all media containing mycobacterial lipids or drugs was removed, and cells were stimulated with 50ng/ml kdo2-lipid A (LA) (Adipogen, AG-CU1-0001) for 6h in a 37^{o}C incubator. Cells were harvested, transferred into U-bottom 96-well plates, and pelleted by centrifugation at 377xg for 5min. Cells were washed with PBS twice and fixed with Fixation Buffer (Biolegend, 420801) for 30 min on ice. Cells were centrifuged as above, washed with PBS and permeabilised with Intracellular Staining Permeabilisation Wash Buffer (Biolegend, 421002) for 10min on ice. Cells were then blocked with purified rat anti-mouse CD16/CD32 (Fc block, 421002) antibody (0.5µg diluted in 50µl of permeabilisation buffer) (BD Biosciences) for 20min on ice and then stained with 50µl of fluorescein-conjugated anti-pro-IL1β antibody (0.5mg/ml, rat monoclonal, FITC, Invitrogen, 11-7114-82) for 30 min on ice. Cells were washed twice with permeabilisation buffer, pelleted, resuspended in PBS and put on ice prior to FACS analysis. Samples were run on FACS-Canto II Flow Cytometer (Beckton Dickinson), and data were collected and analysed as described above.

2.2.6. LysoTracker^{TM} live cell staining for confocal microscopy

LysoTracker^{TM} live cell imaging was performed using Cellview Cell Culture Slides (Greiner, 543979). Approximately 1.4 x 10^4 cells were seeded into each well and incubated at 37^{o}C overnight. After treatment, cells were washed with PBS and stained with 200nM LysoTracker^{TM} Deep Red (ThermoFisher, L12492) for 10 min in the dark at room temperature. Cells were then washed and stained with 200nM Hoetsch 33342 nucleus stain (ThermoFisher, H1399) for 5 min, washed again and mounted in PBS and imaged within 1h. Images were captured using a x60

oil-immersion (Type F immersion oil, Leica) objective with the excitation and emission wavelength appropriated for LysoTracker™ Red. Hoechst 33342 nuclear staining was imaged with excitation at 405 nm and emission at 480 nm wavelength. Images were acquired on a Leica-SP8 confocal microscope using LAS X software. Confocal images were analysed using ImageJ Fiji (NIH, USA). The lysosomal diameter was determined for a minimum of 100 lysosomes from at least three random fields.

2.2.7. Cell lysate preparation and protein quantification prior to Western Blotting

Cells were harvested, pelleted and lysed with RIPA buffer (ThermoFisher, 89901) containing cOmplete™ EDTA-free protease inhibitor cocktail (Merck, 11836170001) on ice for 30 min with vortexing every 10min and centrifuged at 10,000xg at 4°C for 30 min. The supernatant was collected, and the protein concentration of the supernatant was determined by bicinchoninic acid (BCA) assay (Sigma, B9643) according to the manufacturer's instructions. Absorbance at 540nm was measured in a CLARIOstar plate reader (BMG Labtech), and protein concentrations were calculated with CLARIOstar software (BMG Labtech) using values obtained from dilutions of bovine serum albumin (BSA) (Sigma, P5619).

2.2.8. Western blotting

Cell lysates were diluted with RIPA buffer containing protease inhibitor cocktail to 2mg/ml and mixed with SDS Blue loading buffer (BioLabs, B7703S) and dithiothreitol (DTT, BioLabs, B7705S) and heated at 95°C or 50°C for 10 min.

20µg of protein was loaded onto NuPAGE™ 4-12% Bis-Tris Gels (ThermoFisher, NP0336BOX) and run in NuPAGE™ MOPS SDS running buffer (ThermoFisher, NP0001) at 180 Volt, 3 Amps, 300 Watts (BioRad). Novex™ Sharp Pre-stained protein standard (ThermoFisher, LC5800) was included to indicate the relative mobility of proteins. Gels were transferred to Immuno-Blot® PVDF membrane (Bio-Rad, 10026933) using BIORAD transblot turbo transfer system (Bio-Rad) and blocked with 5% (w/v) skimmed milk (Sigma, 70166) in PBS containing 0.1% Tween 20 (v/v) (Sigma, P5927) for 1h at room temperature or overnight at 4°C. Membranes were incubated with primary antibody (rabbit monoclonal, anti-mouse-LAMP1 antibody, 1:1000, Abcam, ab208943; rabbit polyclonal anti-mouse-Npc1 antibody, 1:1000, Novus, NB400-148; rabbit polyclonal anti-mouse-Npc2 antibody, 1:1000, Atlas Antibodies, HPA00835) diluted in 2.5% (w/v) skimmed milk in PBS containing 0.1% Tween 20 and 10mM sodium azide (Sigma, S8032) overnight at 4°C. The membrane was washed with PBS containing 0.1% Tween 20 (three times for 20min) and incubated with horseradish peroxidase (HRP)-conjugated anti-rabbit secondary antibody (mouse monoclonal, 1:5000, Sigma, A1949-1VL) diluted in 2.5% skimmed milk in PBS containing 0.1% Tween 20 for 1h at room temperature. The membrane was washed with PBS containing 0.1% Tween 20 as before and developed with SuperSignal™ West Femto substrate (ThermoFisher, 34094) or Pierce™ ECL western blotting substrate (ThermoFisher, 32106). Membranes were re-probed with peroxidase-conjugated anti-β-actin antibody AC-15, 1:10,000 (mouse monoclonal, Sigma, A3845) to evaluate the equivalence of protein loading. Images were obtained using ChemiDoc XRS system (BioRad) and processed and analysed with ImageLab software (BioRad).

2.2.9. qPCR

RNA was isolated using Monarch total RNA MiniPrep kit (BioLabs, T2010S) according to the manufacturer's protocol. cDNA was synthesised using iScript™ cDNA synthesis kit (BIO-RAD, 1708891). Reaction mixes containing cDNA template, PowerUp™ SYBER™ Green Master Mix (ThermoFisher, A25742) and specific primers were run on a CFX96 Real-Time PCR system (BIO-RAD). Assays specific for relative expression of murine β-actin were used to normalise for input.

2.2.10. Immunofluorescence staining

RAW 264.7 MΦ were seeded into a 24-well plate on coverslips at a density of 1 x 10^6 cells/well. Lipid treatment was performed as described in 2.2.3. After treatment, RAW 264.7 MΦ were washed with PBS and fixed with 4% paraformaldehyde (PFA) (w/v) (TAAB, P001) for 15min at room temperature. Cells were permeabilised with 0.1% saponin (w/v, Sigma, S4521) in PBS for 15min at room temperature, washed with PBS, and blocked with 5% goat serum (v/v) in PBS for 45min at room temperature. Cells were then incubated with a primary rat anti-mouse-LAMP-1 antibody (rat monoclonal, clone 1D4B, 1:500, Abcam, ab25245) diluted in PBS containing 10% goat serum (v/v) and 0.1% saponin overnight at 4°C. Cells were then washed three times with PBS containing 0.1% saponin and stained with fluorescein-conjugated anti-rat IgG secondary antibody Alexa Flour™ 488 (donkey polyclonal, 1:1000, Invitrogen, A21208) for 45 min at room temperature. Cells were stained with DAPI (4′,6-diamidino-2-phenylindole, ThermoFisher, 10236276001) (1:20.000 dilution) to visualise nuclei and mounted with Prolong Gold Antifade (ThermoFisher,

P36930). Imaging was carried out on a Leica-SP8 confocal microscope. Images were analysed using ImageJ Fiji (NIH, USA).

2.2.11. Filipin staining of cholesterol

For labelling of free cholesterol, cells were fixed with 4% PFA (w/v) for 15min at room temperature and washed with PBS and incubated with 1.5mg/ml glycine (Sigma, G8898) in PBS for 10 min to quench aldehyde groups. Filipin complex from *Streptomyces filipinensis* (Sigma, F9765) was dissolved in DMSO to a concentration of 5mg/ml immediately before use. Cells were then stained with a filipin working solution of PBS containing 0.05mg/ml filipin complex, 10% FBS (v/v) and 0.2% Triton x100 (v/v, Sigma, X100) for 2h under room temperature. Cells were washed with PBS and stained with PI (1:3000) prepared in PBS to visualise nuclei and mounted with Prolong Gold Antifade. Imaging was carried out on a Leica-SP8 confocal microscope. Images for cholesterol distribution were obtained using x40 or x60 oil-immersion objective with 405nm laser for excitation with 0.75% UV. Images were analysed using ImageJ Fiji (NIH, USA).

2.2.12. Amplex Red assay determination of cholesterol.

Cells were lysed in glass tubes in 0.1ml ddH_2O and freeze/thawed three times. 2ml $CHCl_3$: MeOH 2:1 (v/v) was added to each sample and sonicated for 5min in an ultrasonic water bath at room temperature and mixed for 2h on a mechanical roller. 0.4ml MeOH was added to samples, centrifuged for 10min at 1500xg, and the supernatant was saved. 0.8ml CH_3Cl and 0.73ml ddH_2O were added to obtain a final composition of $CHCl_3$: MeOH: ddH_2O 8:4:3 (v/v/v). Lysates were mixed and centrifuged as above, the upper phase was removed, and the lower phase

was washed three times with $CHCl_3$: MeOH: ddH_2O 3:48:47 (v/v/v) and dried under N_2 flow. Total cholesterol in the samples was determined using Amplex Red Cholesterol Assay Kit (Sigma, A12216) according to the manufacturer's protocol.

2.2.13. Cholera toxin subunit B (CtxB) staining

After treatment with lipid or drug, RAW 264.7 MΦ were washed with cold Hanks' Balanced Salt Solution (HBSS) (Lonza, 10-527F) and incubated with 0.5ug/ml Cholera Toxin Subunit B (CtxB), Alexa Fluor™ 488 (ThermoFisher, C34775) in cold HBSS for 30 min on ice. Cells were washed with HBSS, replaced with fresh R10 media and chased for 1h at 37°C. Cells were then washed with HBSS containing 1% goat serum (v/v) and fixed with 4% PFA (w/v) for 15 min at room temperature. Nuclei were stained with DAPI and mounted with Prolong Gold Antifade. Imaging was carried out on a Leica-SP8 confocal microscope with excitation and emission wavelength in the Alexa 488 setting. Images were captured using a ×60 oil-immersion (Type F immersion oil, Leica). Images were analysed using ImageJ Fiji (NIH, USA).

2.2.14. Analysis and quantification of GSLs by normal phase high-performance liquid chromatography (NP-HPLC)

After treatment, cells were washed with cold PBS and harvested. Cell pellets were then lysed with 50µl ddH_2O and freeze/thawed three times with vortexing. Protein concentrations were determined by BCA assay (Sigma) according to the manufacturer's instructions.

GSLs were analysed as described previously [212, 213]. Lipids from aqueous cell homogenates (0.2mg protein equivalent lysate in 0.2ml) were extracted with $CHCl_3$: MeOH 1:2 (v/v) overnight at 4°C. The GSLs were further purified on solid-phase C18 columns (Telos, 210-100M-001T) and eluted with 2ml of $CHCl_3$: MeOH 98:2 (v/v), 2ml of $CHCl_3$: MeOH 1:3 (v/v) and 1ml MeOH. After elution, the GSL fractions were dried under a stream of N_2 at 42°C and digested with recombinant endoglycoceramidase (rEGCase I, GenScript) to release ceramide-linked glucosylceramide-derived GSL oligosaccharides. The liberated free glycans were then fluorescently labelled at 80^{o}C for 60min with anthranilic acid (2AA, Sigma, A89855) and sodium cyanoborohydride (Sigma, 156159). To remove excess 2AA labelling, labelled glycans were purified using DPA-6S SPE columns (Supelco, 52624U). Purified 2AA-labelled oligosaccharides were separated and quantified by normal-phase high-performance liquid chromatography (NP-HPLC) as previously described [212]. The NP-HPLC system consisted of a Waters Alliance 2695 separations module and an in-line Waters 2475 multi λ-fluorescence detector set at Ex λ360 nm and Em λ425 nm. The solid phase used was a 4.6 x 250 mm TSK gel-Amide 80 column (Tosoh Bioscience). Glucose unit values (Gus) were determined using a 2AA-labelled glucose homopolymer ladder (Ludger). To calculate molar quantities from integrated peaks in the chromatogram, 2.5pmol 2AA-labelled chitotriose (Ludger) was injected as a calibration standard with each sample set.

2.2.15. Thin-layer chromatography (TLC) of extractible lipids and matrix-assisted laser desorption/ionisation-time of flight (MALDI-ToF mass spectrometry (MS)) lipid fingerprints.

TLC and MALDI lipid analyses were performed by Dr Gerald Larrouy-Maumus, Imperial College, London. Heat-killed mycobacteria were first washed 3 times with PBS. The pellets were $CHCl_3$: MeOH 1:2 (v/v) extracted for 12h at room temperature, followed by one $CHCl_3$: MeOH 1:1 (v/v) extraction and one $CHCl_3$: MeOH 2:1 (v/v) extraction for 3h at room temperature. Pooled extracts were concentrated and evaporated to dryness. Total lipids extracted were normalised to the dried weight of the lipid extract. The dried lipid extracts were resuspended in $CHCl_3$ at a final concentration of 20mg/ml. 5µl, equivalent to 100µg, were loaded on TLC. TLCs were run in four different solvent systems: Petroleum Ether: Diethyl Ether 95:5 (v/v); $CHCl_3$: MeOH 9:1 (v/v); $CHCl_3$: MeOH 8:2 (v/v) and $CHCl_3$: MeOH: H_2O 60:25:4 (v/v/v). Then, TLCs were sprayed with a solution of 5% phosphomolybdic acid in 100% ethanol and heated at 200°C for 2min in order to reveal the lipids. All experiments were performed in triplicate for statistical confidence.

For lipid MALDI-ToF fingerprinting, 0.5µg of total lipid extract was loaded and immediately overlaid with 0.5µl of a 2,5-dihydroxybenzoic acid (DHB) matrix used at a final concentration of 10mg/ml in $CHCl_3$: MeOH 9:1 (v/v). Bacterial total lipid extracts and matrix were mixed directly on the target by pipetting, and the mix was dried gently under a stream of air. MALDI-ToF MS analysis was performed on a 4800 Proteomics Analyzer (Applied Biosystems) using the reflectron mode. Samples were analysed by operating at 20kV in the positive and negative ion

modes using an extraction delay time set at 20 nanoseconds. Data were obtained using Data Explorer version 4.9 (build 115) Applied Biosystems.

2.2.16. Statistical analysis

Independent experiments were undertaken in their entirety and performed using different batches of cells and treatments and were performed at different times. Aliquots of cells and reagents were allocated randomly between experimental and control groups. The normality of data was assessed using the Shapiro-Wilk normality test. Appropriate statistical tests were selected based on the nature of the variables and the number of replicates for each data set, which are indicated for each investigation. A null hypothesis was assumed, which permitted the calculation of probability values as a measure of statistically significant relationships. Statistical analyses were performed on data sets with $n>2$. The p values were determined with a 95% confidence interval. Analysis and statistical significance of all data sets were determined using GraphPad Prism 10. For confocal microscopy data, images from random fields were acquired. When possible, the investigator was blinded to sample identification, and the data were also scored by a second investigator who was not familiar with the experimental setup.

2.3. Results

2.3.1. Cell wall total lipid (TL) extract of *Mtb* H37Rv increases LysoTracker™ staining intensity in RAW 264.7 MΦ.

The volume of the acidic compartment (late endosome/lysosome - LE/Lys) is significantly expanded in NPC1-deficient cells and RAW 264.7 MΦ treated with the cation amphiphile U18666A [214]. Therefore, an increase in relative LE/Lys volume was used as the primary indication of the loss of NPC1 activity. We used the pH-sensitive fluorescent probe, LysoTracker™, which selectively accumulates in acidic compartments to determine the relative volume of LE/Lys in mycobacterial TL-treated and control MΦ. Analyses were made by FACS. To verify that the ability of *Mtb* H37Rv TL extracts to increase the acidic compartment volume was not an inadvertent artefact of the preparation of lipid extracts, we compared TL extracts obtained from two independent sources: BEI Resources (annotated as BEI) and from our collaborator, Dr Gerald Larrouy-Maumus at Imperial College, London (annotated as ICL).

The gating strategy employed to identify the different cell populations was as follows; cell viability and dead cells were excluded based upon positive PI staining (Fig 2.3.1.1.B.); live (PI negative) single cells were identified according to forward scatter area (FSC-A) verses forward scatter height parameters (FSC-H) (Fig 2.3.1.1.C.), and the mean fluorescent intensity (MFI) of LysoTracker™ stained single, live cells was determined.

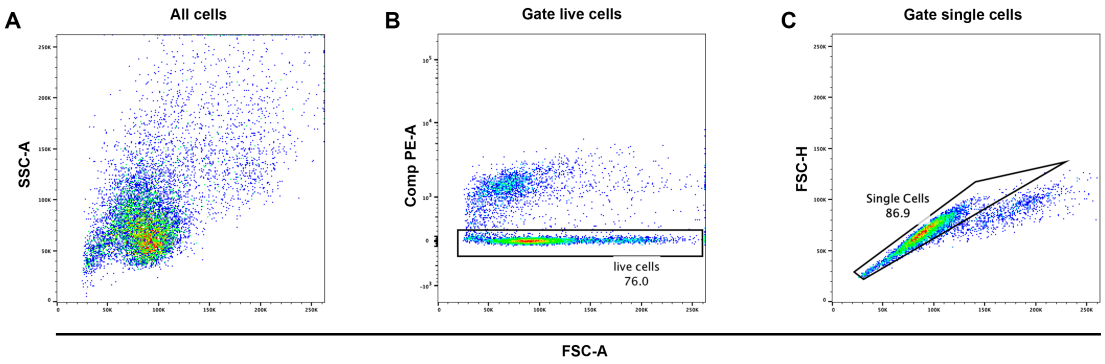


Figure 2.3.1.1. FACS gating strategy for analysis of LysoTracker™ staining of RAW 264.7 MΦ.

Representative dot plots of RAW 264.7 MΦ gated for live cells (PI negative, Panel B) and singlets (Panel C).

LysoTracker™ staining intensity of RAW 264.7 MΦ was significantly increased after incubation with each of the *Mtb* H37Rv TL (Fig 2.3.1.2.A.), and there was no significant difference between the lipid extracts (Fig 2.3.1.2.A.). We also examined whether the storage of TL extracts in different solvents affected the activity. There was a significant increase in LysoTracker™ staining intensity of RAW 264.7 MΦ treated with 50µg/ml and 100µg/ml *Mtb* H37Rv TL extract diluted from DMSO or R10 stock (Fig 2.3.1.2.B.). There was a small but significant difference in staining intensity when extracts were used at 50µg/ml, but no significant differences were detected at the higher concentration (Fig 2.3.1.2.B.).

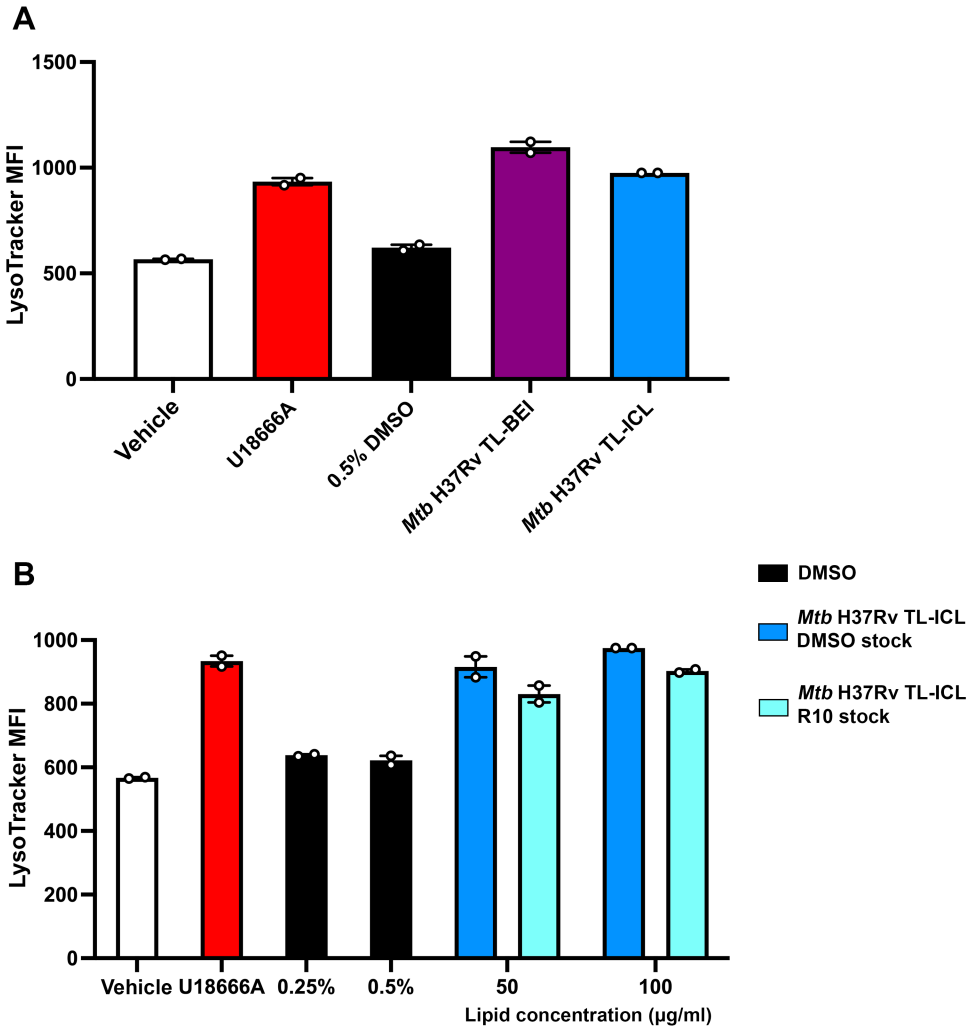


Figure 2.3.1.2. Mtb H37Rv TL extract from two independent sources significantly increases LysoTracker™ staining intensity of RAW 264.7 MΦ.

RAW 264.7 MΦ were treated with TL extract of *Mtb* H37Rv (100µg/ml for 48h), stained with LysoTracker™ Green DND-26 and analysed by FACS. DMSO and U18666A (2µg/ml for 48h) treatments were vehicle and positive controls respectively. Panel A. Quantification of LysoTracker™ staining intensity in treated RAW 264.7 MΦ. Data are mean ± SEM, n=2. Panel B. Quantification of LysoTracker™ staining intensity in RAW 264.7 MΦ treated with *Mtb* H37Rv TL extract from BEI Resources or ICL stored in R10 media or freshly made. MFI, mean fluorescence intensity. Data are mean ± SEM, n=2. Data are representative of 3 independent experiments.

2.3.2. *Mtb* H37Rv TL extract significantly increases LysoTracker™ staining intensity in murine bone marrow-derived MΦ (BMDMΦ).

To confirm the activities of *Mtb* H37Rv TL extract in increasing LysoTracker™ staining intensity were not limited to RAW 264.7 MΦ, which is an immortalised murine cell line, we made comparable treatments of primary murine bone marrow-derived MΦ (BMDMΦ). LysoTracker™ staining intensity was significantly increased for wild-type (WT) BMDMΦ treated with 100µg/ml *Mtb* H37Rv TL for 48h but not when incubated with 10µg/ml lipid (Fig 2.3.2.). The LysoTracker™ staining intensity of cells treated with the higher concentration of lipid was equivalent to or greater than WT cells incubated with U18666A or untreated *Npc1*$^{-/-}$ BMDMΦ (****p<0.0001, Fig 2.3.2.).

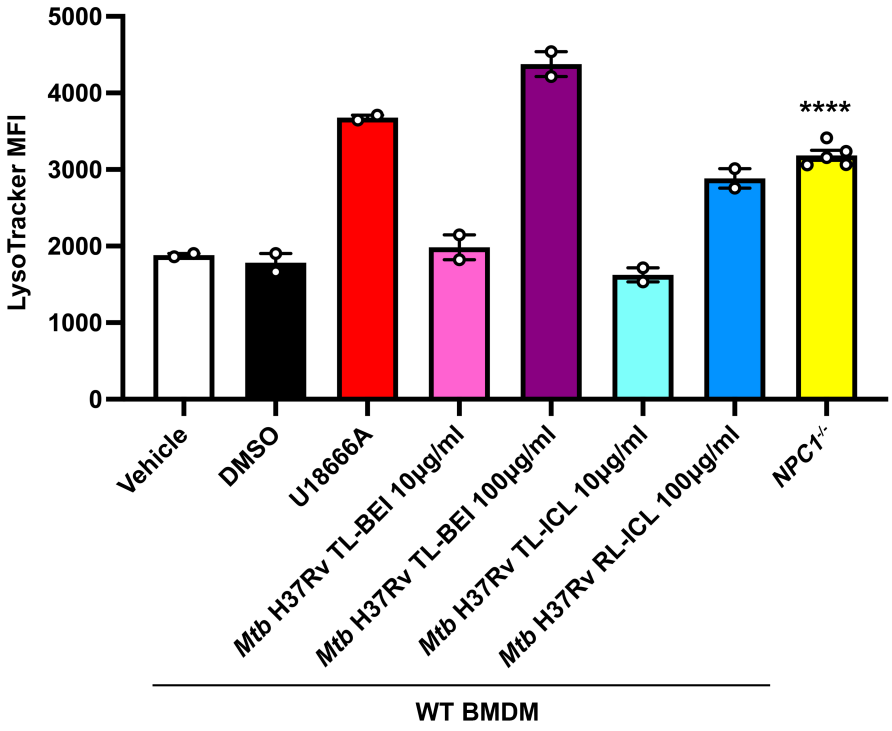


Figure 2.3.2. Mtb H37Rv TL extract from two independent sources significantly increases LysoTracker™ staining intensity in murine BMDMΦs.

Wild-type (WT) murine BMDMΦs were treated with 10μg/ml or 100μg/ml *Mtb* H37Rv TL extract from BEI Resources or ICL for 48h. Untreated *Npc1*$^{-/-}$ BMDMΦs were the positive control. DMSO and U18666A (2μg/ml for 48h) treatments were vehicle and positive controls respectively. MFI, mean fluorescence intensity. Data are mean ± SEM, n=2. Statistical analysis, Welch's t-test. ****p<0.0001. Statistical comparisons of *Npc1*$^{-/-}$ is relative to vehicle control. Data are representative of 2 independent experiments.

2.3.3. *Mtb* H37Rv TL extract causes a significant reduction in the frequency of pro-IL1β positive RAW 264.7 MΦ that had been stimulated by LA.

Unpublished studies have found that there is impaired production of pro-IL1β in *Npc1*$^{-/-}$ peritoneal MΦ or U18666A-treated RAW 264.7 MΦ after priming with LPS, which were generated by Dawn Shepherd [215]. We investigated whether treatment with *Mtb* H37Rv TL prior to priming had a similar effect on synthesis of the cytokine precursor. The gating strategy for identifying pro-IL1β positive cells is shown in Fig 2.3.3.A. We observed a dose-dependent decrease in the frequency of pro-IL1β positive RAW 264.7 MΦ that had been exposed to *Mtb* H37Rv TL before stimulation with lipid A (LA) (****p<0.0001, Fig 2.3.3.B.). The decrease resulting from exposure to the highest concentration of *Mtb* H37Rv TL was comparable to that caused by U18666A (****p<0.0001, Fig 2.3.3.B.).

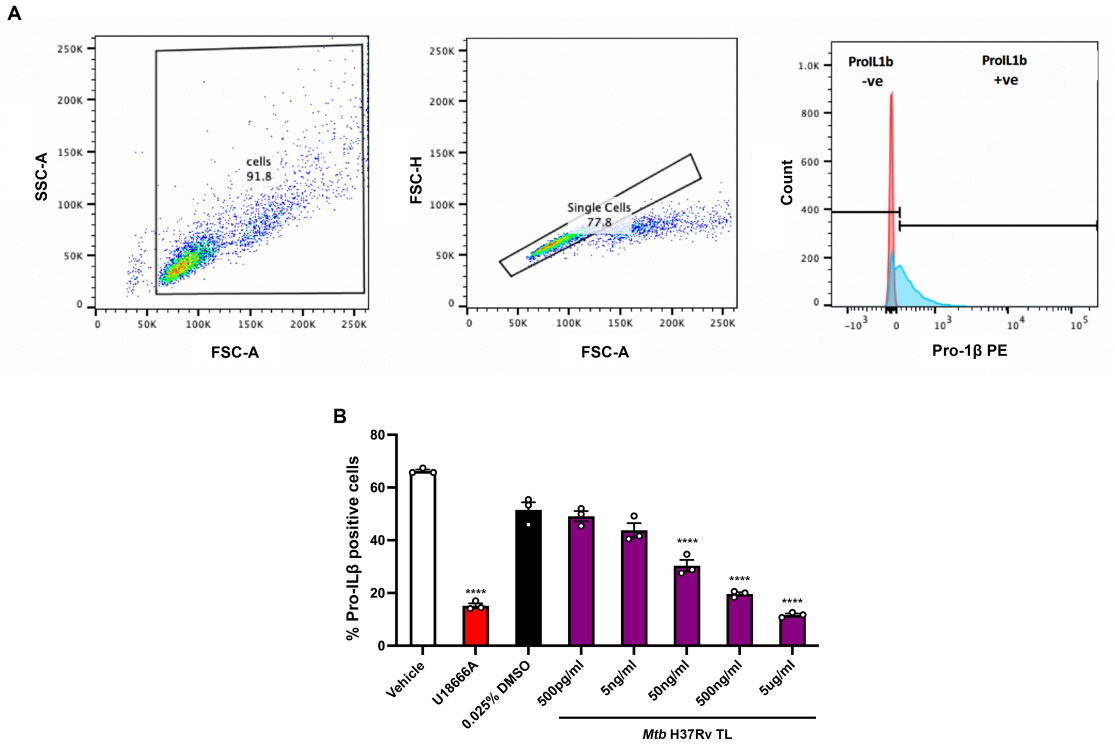


Figure 2.3.3. Treatment with Mtb H37Rv TL extract results in a dose-dependent reduction in the frequency of pro-IL1β positive RAW 264.7 MΦ stimulated with LA.

RAW 264.7 MΦ were treated with TL extract of *Mtb* H37Rv (500pg/ml to 5μg/ml for 48h), and then stimulated with lipid A (50ng/ml for 6h) to trigger pro-IL1β production. Panel A. Representative dot plots of RAW 264.7 MΦ either untreated (red) or incubated with *Mtb* H37Rv TL extract (blue), stimulated with lipid A and stained for pro-IL1β expression. Panel B. Quantification of the frequency of pro-IL1β positive RAW 264.7 MΦ. Data are mean ± SEM, n=3. Statistical analysis, 2-way ANOVA with Sidak multiple comparisons. ****p<0.0001, otherwise not significant. Statistical comparison of U18666A treatment is relative to vehicle control. Statistical comparisons of lipid treatments are relative to DMSO controls. Data are representative of 2 independent experiments. Data were generated by Dawn Shepherd.

2.3.4. TL extracts of *Mtb* clinical isolates, but not *M. canettii*, increase LysoTracker™ staining intensity of RAW 264.7 MΦ.

The above results confirmed that *Mtb* H37Rv TL extract was able to increase the relative LE/Lys volume in RAW 264.7 MΦ and BMDMΦ as seen by LysoTracker™ staining and inhibit pro-IL1β production in RAW 264.7 MΦ. We then investigated whether cell wall lipid extracts of *Mtb* clinical isolates representative of different lineages were also capable of inducing NPC cellular phenotypes.

TL extracts of *Mtb* strains listed in Table 2.2.2. were generated using the same protocol as was used for *Mtb* H37Rv and applied to RAW 264.7 MΦ (100μg/ml for 48h). TL extracts of all mycobacteria strains tested induced a significant increase in LysoTracker™ staining intensity, with the exception of strains 232 and 346 from lineage 1 and strain 212 from lineage 2 (****p<0.0001 for strains 281 and 372 from lineage 1; ****p<0.0001 for strains 119, 333, 345, 649, p=0.0008 for strain 374 from lineage 2; ****p<0.0001 for all strains from lineage 4, Fig 2.3.4.A.). Treatment with *M. canettii* TL extract resulted in a significant decrease in LysoTracker™ staining intensity in comparison to vehicle-treated controls (p=0.0059, Fig 2.3.4.A.). LysoTracker™ staining intensity of RAW 264.7 MΦ exposed to lipid extract of *Mtb* strains 119, 173, 293, 367, 440, 369 and H37Rv was enhanced to a level that was not significantly different from that of cells treated with the NPC1 pharmacological inhibitor, U18666A (Fig 2.3.4.A.).

In order to determine whether the lack of a significant increase in LysoTracker™ staining intensity following incubation with extracts of the *Mtb* strains 232, 364 and 212 might be due to the treatment of cells with a sub-threshold lipid

concentration, we increased the dose to 200µg/ml and incubated for 48h. We also tested the activity of the TL extract of strain 91_0079 from lineage 3 at the same final concentration. With a higher dose, a significant increase in LysoTracker™ staining intensity was observed in RAW 264.7 MΦ (p=0.0006 for strain 232; p=0.0451 for strain 346; p=0.0062 for strain 212; ****p<0.0001 for strains 374, 91_0079 and H37Rv, Fig 2.3.4.B.). However, despite increasing the final concentration to 200µg/ml, we did not detect a significant increase in LysoTracker™ staining intensity with *M. canettii* TL (Fig 2.3.4.B.). When analysed collectively, there was a significant increase in LysoTracker™ staining intensity after treatment with lipid extracts from each of the *Mtb* lineages (p=0.0380 for lineage 1; p=0.0058 for lineage 2; p=0.0003 for lineage 4, Fig 2.3.4.C.).

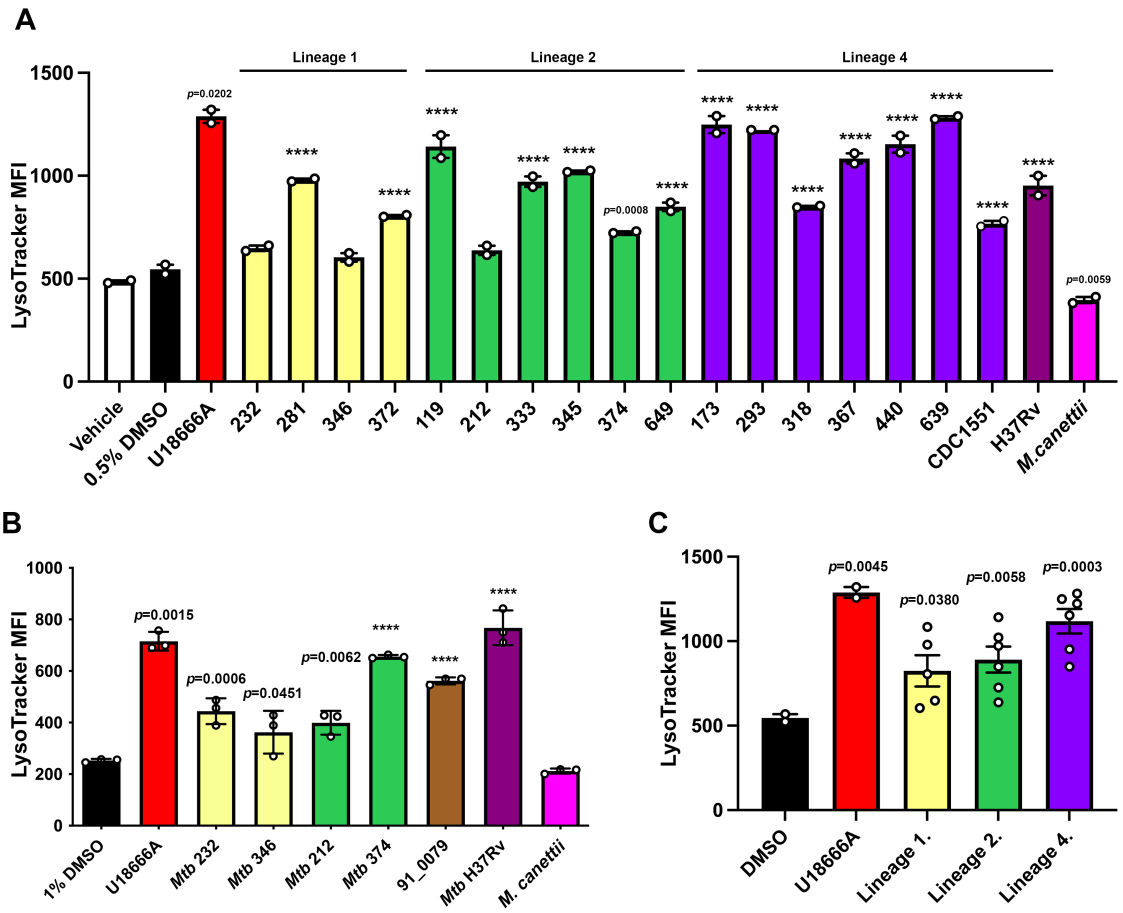


Figure 2.3.4. Mycobacterial lipids that can significantly increase LysoTracker™ staining intensity of RAW 264.7 MΦ are widely distributed across Mtb clinical strain but not M. canettii.

DMSO and U18666A (2μg/ml for 48h) treatments were vehicle and positive controls respectively. Panel A. Quantification of LysoTracker™ staining intensity of RAW 264.7 MΦ were treated with TL extract of *Mtb* strains from lineages 1, 2 and 4, or *M. canettii* (100μg/ml for 48h). Data are mean ± SEM, n=2. Statistical analysis, one-way ANOVA with Dunnett multiple comparisons. ****$p<0.0001$, other p values as indicated, otherwise not significant. Statistical comparison of U18666A treatment is relative to vehicle control. Statistical comparisons of lipid treatments are relative to DMSO controls. Panel B. Quantification of LysoTracker™ staining intensity of RAW 264.7 MΦ treated with TL extract of selected strains from lineages 1, 2 and 3 (91_0079) (200μg/ml for 48h). Data are mean ± SEM, n=3. Statistical analysis, one-way ANOVA with Dunnett multiple comparisons. ****$p<0.0001$, other p values as indicated, otherwise not significant. Statistical comparison of U18666A treatment is relative to vehicle control. Statistical comparisons of lipid treatments are relative to DMSO controls. Panel C. Summary of LysoTracker™ staining intensities from lineages 1, 2 and 4. MFI, mean fluorescence intensity. Data are mean ± SEM, n=2 for vehicle and U18666A-treated, n>6 for lineages 1, 2 and 4. Statistical analysis, Welch's t-test. p values as indicated. Statistical comparison of U18666A treatment is relative to vehicle control. Statistical comparisons of lipid treatments are relative to DMSO controls. Data are representative of 2 independent experiments.

2.3.5. TL extract of *M. canettii* decreases LysoTracker™ staining intensity of RAW 264.7 MΦ.

In light of the unexpected decrease in LysoTracker™ staining intensity of *M. canettii* TL extract-treated RAW 264.7 MΦ, we investigated for a possible dose-dependent effect of the lipid extract and made comparisons with equivalent doses of *Mtb* H37Rv TL extract. *Mtb* H37Rv TL induced a significant dose-dependent increase in LysoTracker™ staining intensity of RAW 264.7 MΦ in comparison to vehicle (Fig 2.3.5.), whereas the *M. canettii* TL extract resulted in a significant decrease in staining intensity at the highest concentration tested (Fig 2.3.5.).

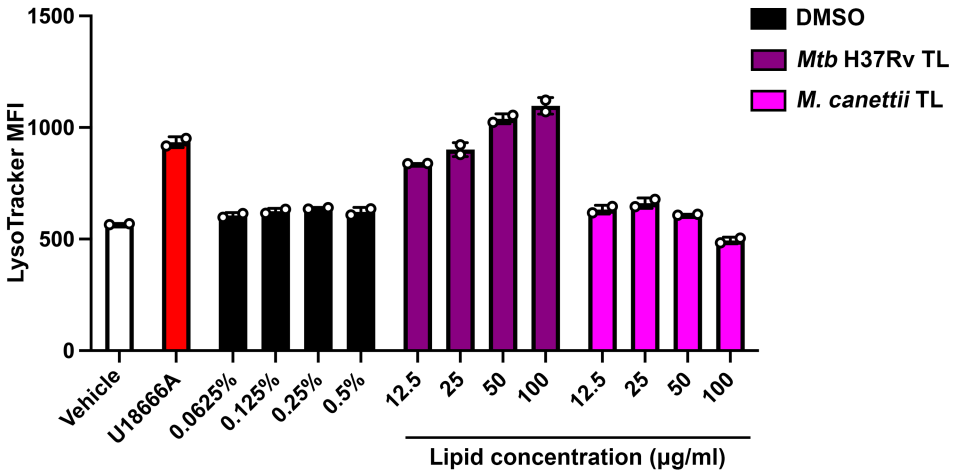


Figure 2.3.5. TL extract of M. canettii induces a dose-dependent decrease of LysoTracker™ staining intensity of RAW 264.7 MΦ.

RAW 264.7 MΦ were treated with *Mtb* H37Rv or *M. canettii* TL extract at concentrations of 12.5 to 100µg/ml for 48h. DMSO and U18666A (2µg/ml for 48h) were vehicle and positive controls. MFI, mean fluorescence intensity. Data are mean ± SEM, n=2. Data are representative of 3 independent experiments.

2.3.6. TL extracts of representative *Mtb* clinical strains, but not with *M. canettii,* increase the diameter and frequency of LysoTracker™ positive compartments in RAW 264.7 MΦ.

The increase in the relative volume of the acidic compartment as revealed by FACS analysis of LysoTracker™ stained cells could represent an increase in either the frequency or size of LE/Lys or a combination of the two. To discriminate between these possibilities, we undertook confocal microscopy of lipid-treated RAW 264.7 MΦ that were stained with LysoTracker™ Deep Red. Cells that had been treated with *Mtb* lipid extracts representative of each lineage (lineage 1, strain 281; lineage 2, strain 333; lineage 4, strain 639 and H37Rv) along with *M. canettii* at the concentration of 100μg/ml for 48h were analysed. Exposure to U18666A was used as a positive control and resulted in a statistically significant increase in both mean diameter (****p<0.0001, Fig 2.3.6.1.A.C.D.) and the abundance (p=0.0362, Fig 2.3.6.1.B.) of LysoTracker™ positive puncta. There was also a significant increase in both parameters in cells treated with lipid extracts of each of the strains that are representative of the three *Mtb* lineages (frequency, p=0.0016 for strain 281; p=0.0012 for strain 333; ****p<0.0001 for strains 639 and H37Rv, Fig 2.3.6.2.A.B; mean diameter, ****p<0.0001, Fig 2.3.6.2.C.D,). However, there was no significant increase in either diameter or frequency in cells incubated with *M. canettii* TL (Fig 2.3.6.2.).

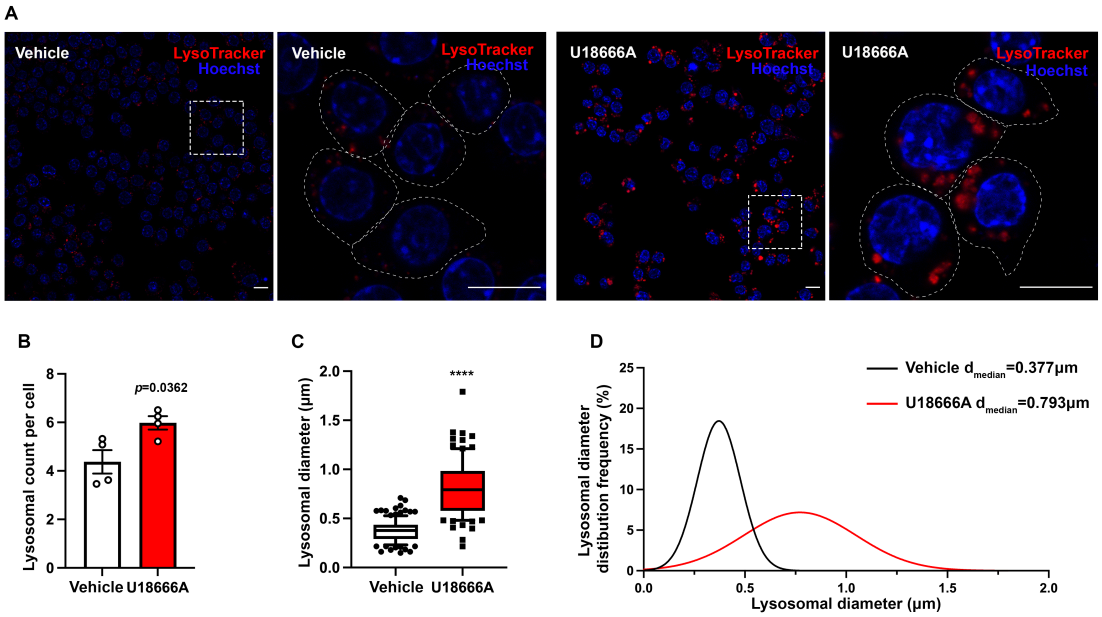


Figure 2.3.6.1. U18666A increases the frequency and size of LE/Lys in RAW 264.7 MΦ.

Cells were treated with U18666A (2µg/ml for 48h) and stained with LysoTracker™ Deep Red for confocal microscopy analysis. Panel A. Representative confocal microscopy images. LysoTracker™ Deep Red, red; Hoechst, blue. Scale bar represents 10µm. For each pair, the right image is a higher magnification of the region outlined in the left image. Panel B. Number of lysosomes per cell per optical plane in treated RAW 264.7 MΦ. Data are mean ± SEM, n=4. Statistical analysis, Welch's t-test. *p* values as indicated. Statistical comparison of U18666A treatment is relative to vehicle control. Panel C. Mean lysosomal diameter (µm) in treated RAW 264.7 MΦ. Box and whisker plot, box contains 90% of events. n>80 from at least 3 individual cells. Statistical analysis, Welch's t-test. ****p<0.0001. Statistical comparison of U18666A treatment is relative to vehicle control. Panel C. Histogram of lysosomal diameter distribution frequency. Bin width, 0.05µm. Vehicle: min: 0.149µm, max: 0.709µm, centre: 0.377µm; U18666A: min: 0.216µm, max: 1.791µm, centre: 0793µm. Statistical analysis, Gaussian distribution. Data are representative of 2 independent experiments.

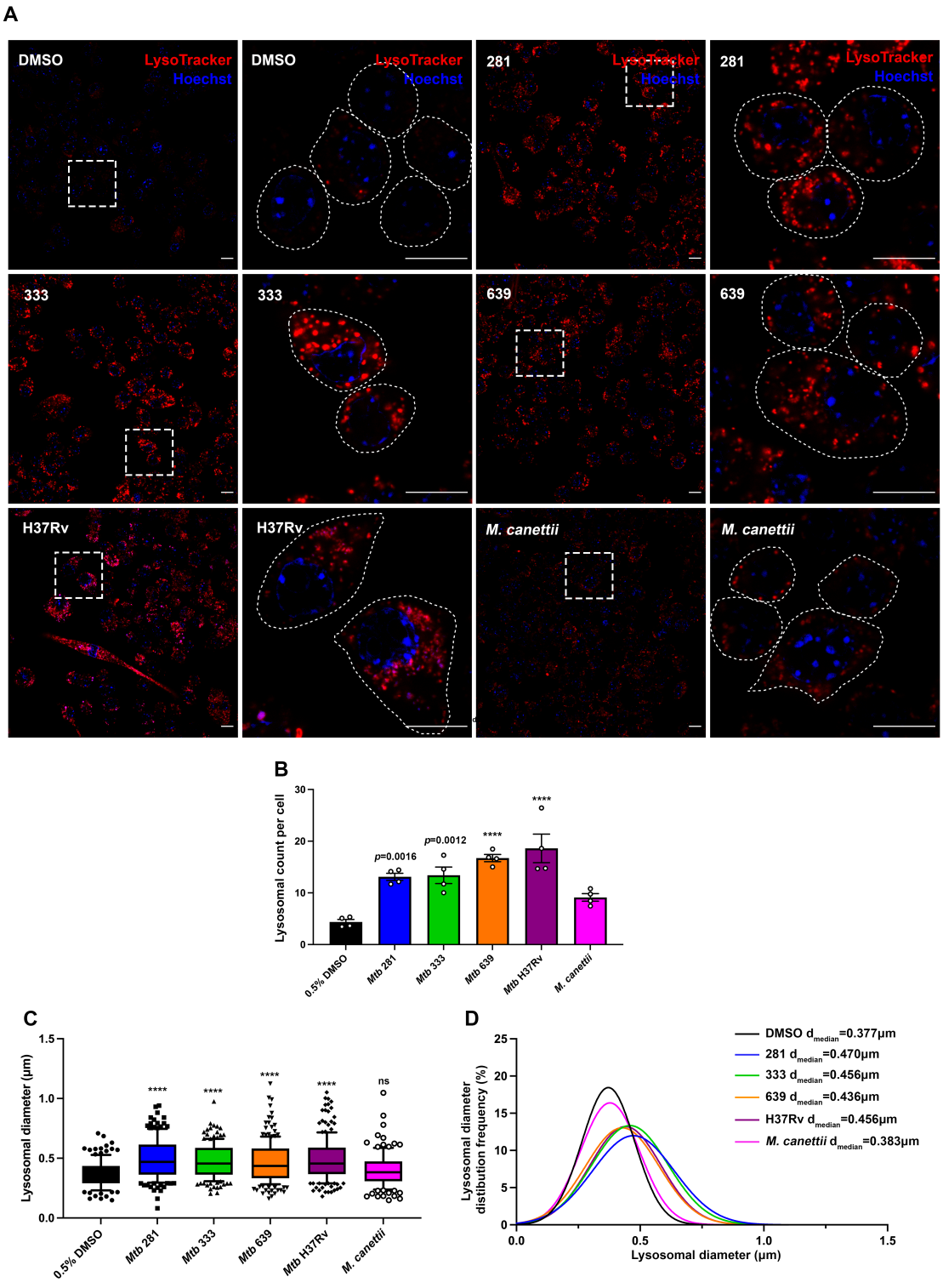

A
DMSO
LysoTracker
Hoechst
281
333
639
H37Rv
M. canettii
B
Lysosomal count per cell
p=0.0016
p=0.0012
****
0.5% DMSO
Mtb 281
Mtb 333
Mtb 639
Mtb H37Rv
M. canettii
C
Lysosomal diameter (μm)
ns
D
Lysosomal diameter distribution frequency (%)
Lysosomal diameter (μm)
DMSO d median =0.377μm
281 d median =0.470μm
333 d median =0.456μm
639 d median =0.436μm
H37Rv d median =0.456μm
M. canettii d median =0.383μm

Figure 2.3.6.2. Expansion of the lysosomal compartment in RAW 264.7 MΦ in response to treatment with TL extracts of representative Mtb clinical strains, but not M. canettii, visualised with LysoTracker™ Deep Red staining.

Cells were treated with TL extract from *Mtb* clinical strains or *M. canettii* (100μg/ml for 48h) and stained with LysoTracker™ Deep Red for confocal microscopy analysis. DMSO was the vehicle control. Panel A. Representative confocal microscopy images of treated RAW 264.7 MΦ. LysoTracker™ Deep Red, red; Hoechst, blue. Scale bar represents 10μm. For each pair, the right image is a higher magnification of the region outlined in the left image. Panel B. Number of lysosomes per cell per optical plane in treated RAW 264.7 MΦ. Data are mean ± SEM, n=4. Statistical analysis, Welch's t-test. ****p<0.0001, other p values as indicated, otherwise not significant. Statistical comparisons of lipid treatments are relative to DMSO controls. Panel C. Mean lysosomal diameter (μm) in treated RAW 264.7 MΦ. Box and whisker plot, box contains 90% of events. n>120 from at least 3 individual cells. Statistical analysis, one-way ANOVA with Kruskal-Wallis multiple comparisons. ****p<0.0001. Statistical comparisons of lipid treatments are relative to DMSO controls. Panel D. Histogram of lysosomal diameter distribution frequency. Bin width, 0.05μm. DMSO: min: 0.149μm, max: 0.709μm, centre: 0.377μm; 281: min: 0.081μm, max: 0.941μm, centre: 0.470μm; 333: min: 0.204μm, max: 0.975μm, centre: 0.456μm; 639: min: 0.161μm, max: 1.124μm, centre: 0.436μm; H37Rv: min: 0.180μm, max: 1.052μm, centre: 0.456μm; *M. canettii*: min: 0.149μm, max: 1.047μm, centre: 0.383μm. Statistical analysis, Gaussian distribution. Data are representative of 2 independent experiments.

2.3.7. Optimisation of LAMP-1 immunostaining for confocal microscopy in RAW 264.7 MΦ.

To further validate the expansion of LE/Lys compartments following incubation with *Mtb* TL extract, we imaged treated RAW 264.7 MΦ that has been stained with anti-LAMP-1 antibody by confocal microscopy. This first necessitated the optimisation of the staining protocol. We determined conditions for cell permeabilisation and primary antibody concentration. Permeabilisation of RAW 264.7 MΦ with PBS containing 0.1% saponin (w/v) for 15min at room temperature prior to incubation with anti-LAMP-1 antibody significantly improved the resolution and detection of lysosomal puncta as compared to non-permeabilised cells (Fig 2.3.7.1.). Comparison of RAW 264.7 MΦ stained with 2.5μg/ml (1:1000 dilution) or 5μg/ml (1:500 dilution) anti-LAMP-1antibody revealed improved definition with the higher concentration of the reagent (Fig 2.3.7.2.). These conditions were used therefore, in all subsequent investigations.

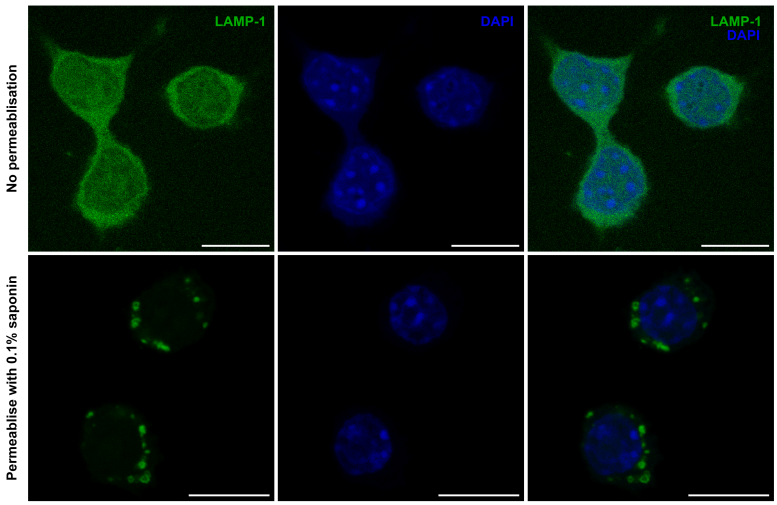


Figure 2.3.7.1. Optimisation of LAMP-1 of RAW 264.7 MΦ for confocal microscopy: permeabilisation.

RAW 264.7 MΦ were fixed and either not permeabilised (upper panels) or permeabilised (lower panels) before anti-LAMP-1 antibody staining. LAMP-1, green; DAPI, blue. Scale bar represents 10μm.

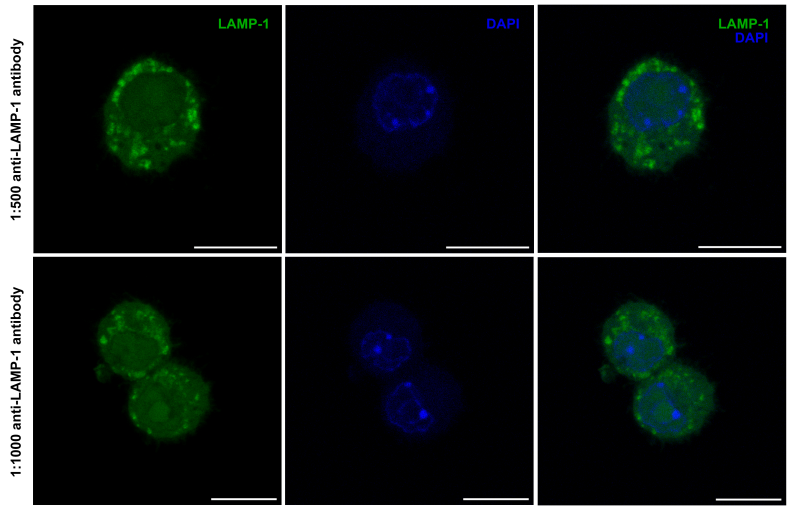


Figure 2.3.7.2. Optimisation of anti-LAMP-1 immunostaining in RAW 264.7 MΦ for confocal microscopy: primary antibody concentration.

Representative confocal images of RAW 264.7 MΦ fixed, permeabilised and stained with anti-LAMP-1 antibody at a dilution of 1:500 (upper panels) or 1:1000 (lower panels) and examined by confocal microscopy. LAMP-1, green; DAPI, blue. Scale bar represents 10μm.

2.3.8. LAMP-1 immunostaining confirmed expansion of LE/Lys volume following incubation with TL extracts of representative *Mtb* clinical strains but not *M. canettii* in RAW 264.7 MΦ.

We determined the size of the LE/Lys compartments in RAW 264.7 MΦ treated with TL extract of *Mtb* clinical strains by staining for LAMP-1 expression and examination by confocal microscopy (Fig 2.3.8.1.A., Fig 2.3.8.2.A.). U18666A treatment significantly increased LE/Lys diameter (a 2.16-fold increase compared with vehicle control) (****p<0.0001, Fig 2.3.8.1.B.). There was a statistically significant increase in the mean diameter and the size distribution of LAMP-1 positive compartments in RAW 264.7 MΦ treated with TL extracts of human tubercular mycobacteria (****p<0.0001, Fig 2.3.8.2.B.C.), but there was no statistical increase in LE/Lys diameters in *M. canettii* TL-treated cells and only a minor shift in the size distribution (Fig 2.3.8.2.B.C.).

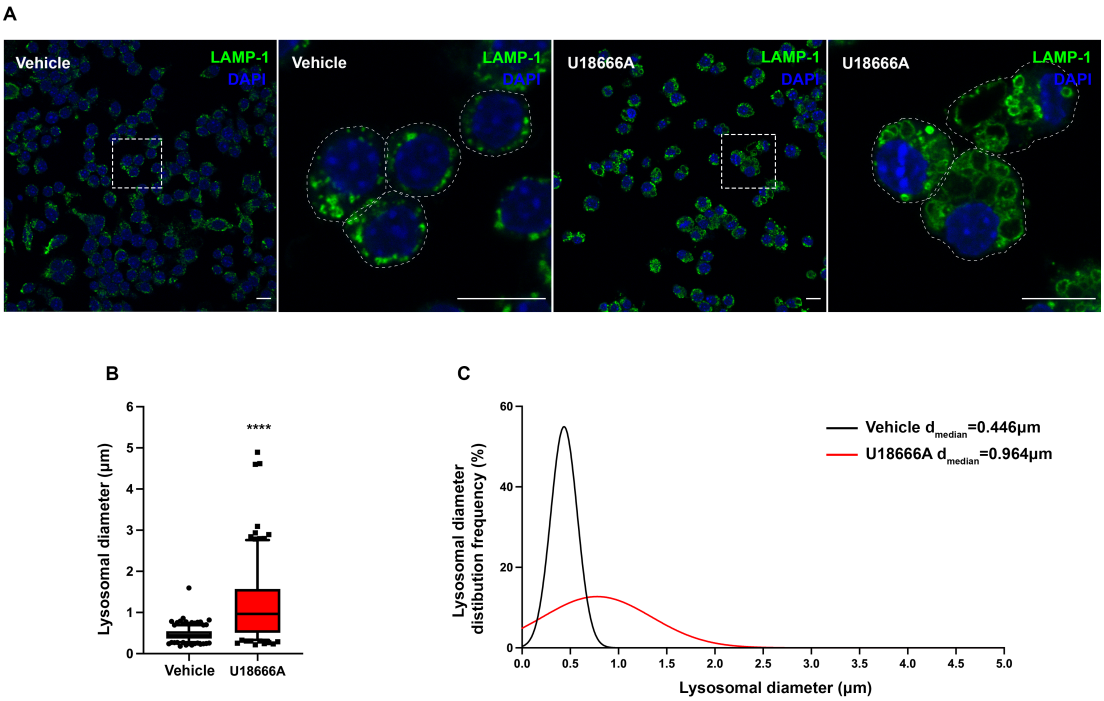


Figure 2.3.8.1. U18666A treatment increases the size of LE/Lys in RAW 264.7 MΦ visualised by LAMP-1 immunostaining.

Cells were treated with U1866A (2µg/ml for 48h). Panel A. Representative confocal microscopy images in treated cells. LAMP-1, green; DAPI, blue. For each pair, the right image is a higher magnification of the region outlined in the left image. White dotted lines indicate the cell outline. Scale bar represents 10µm. Panel B. Mean lysosomal diameter (µm) in treated RAW 264.7 MΦ. Box and whisker plot, box contains 90% of events. n>100 from at least 3 individual cells. Statistical analysis, Mann-Whitney test. ****p<0.0001. Statistical comparison of U18666A treatment is relative to vehicle control. Panel C. Histogram of lysosomal diameter distribution frequency in treated RAW 264.7 MΦ. Bin width, 0.2µm. Vehicle: min: 0.180µm, max: 1.60µm, centre: 0.446µm; U18666A: min: 0.216µm, max: 4.89µm, centre: 0.964µm. Statistical analysis, Gaussian distribution. Data are representative of 2 independent experiments.

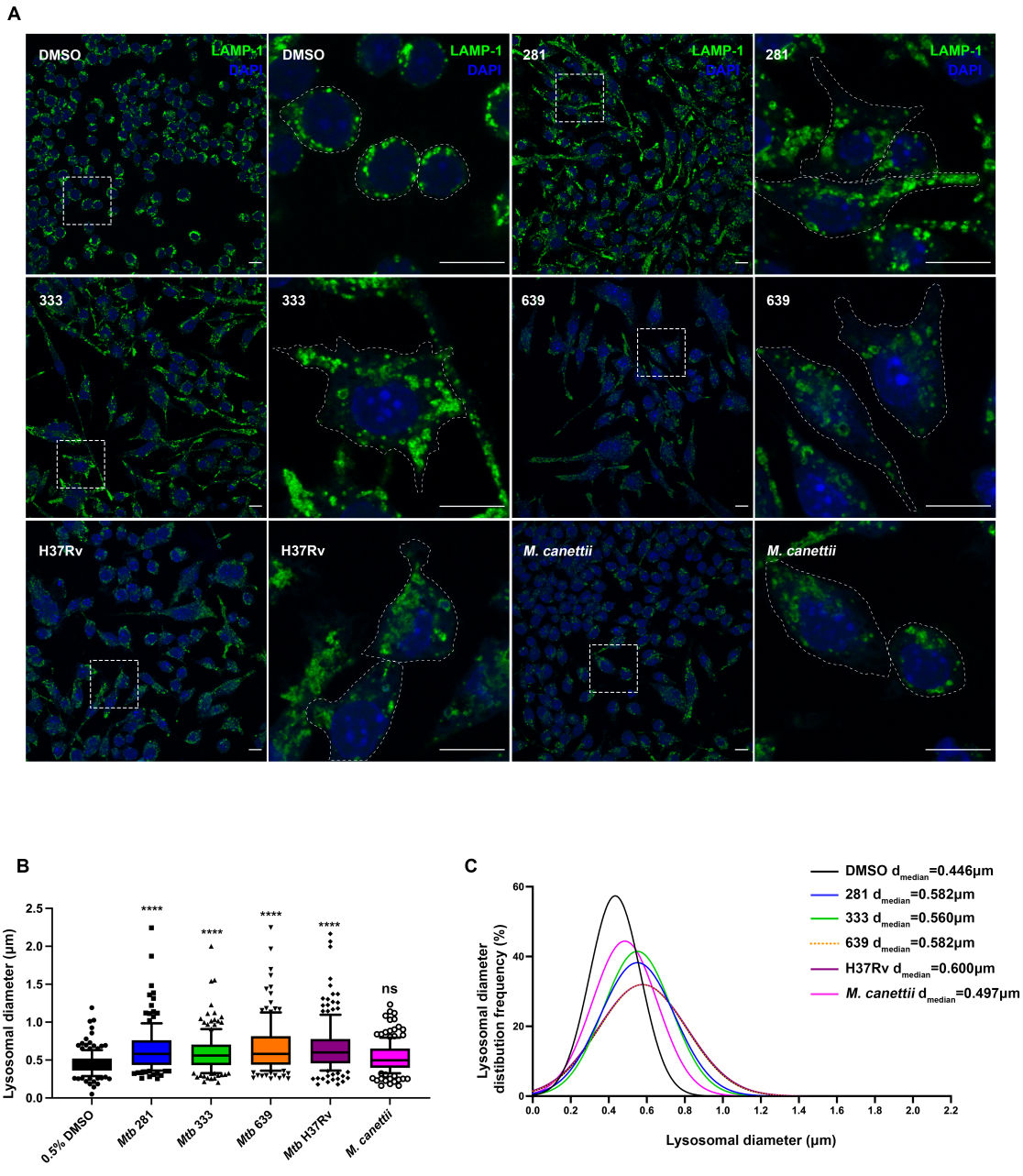

A
DMSO
LAMP-1
DAPI
281
333
639
H37Rv
M. canettii
B
Lysosomal diameter (μm)
****
ns
0.5% DMSO
Mtb 281
Mtb 333
Mtb 639
Mtb H37Rv
M. canettii
C
Lysosomal diameter distibution frequency (%)
Lysosomal diameter (μm)
DMSO d median=0.446μm
281 d median=0.582μm
333 d median=0.560μm
639 d median=0.582μm
H37Rv d median=0.600μm
M. canettii d median=0.497μm

Figure 2.3.8.2. TL of Mtb clinical strains, but not M. canettii increase the size of LE/Lys in RAW 264.7 MΦ visualised by LAMP-1 immunostaining.

Cells were treated with TL extract of *Mtb* clinical strains (100μg/ml for 48h). DMSO (0.5% for 48h) was the vehicle control. Panel A. Representative confocal microscopy images in treated RAW 264.7 MΦ. LAMP-1, green; DAPI, blue. Scale bar represents 10μm. For each pair, the right image is a higher magnification of the region outlined in the left image. White dotted lines indicate the cell outline. Panel B. Mean lysosomal diameter (μm) in treated RAW 264.7 MΦ. Box and whisker plot, box contains 90% of events. n>130 from at least 3 individual cells. Statistical analysis, Mann-Whitney test. ****p<0.0001, otherwise not significant. Statistical comparisons of lipid treatments are relative to DMSO controls. Panel C. Histogram of lysosomal diameter distribution frequency in treated RAW 264.7 MΦ. Bin width, 0.2μm. DMSO: min: 0.051μm, max: 1.19μm, centre: 0.446μm; 281: min: 0.255μm, max: 2.240μm, centre: 0.582μm; 333: min: 0.204μm, max: 2.000μm, centre: 0.560μm; 639: min: 0.253μm, max: 2.250μm, centre: 0.582μm; H37Rv: min: 0.180μm, max: 2.17μm, centre: 0.600μm; *M. canettii*: min: 0.161μm, max: 1.23μm, centre: 0.497μm. Statistical analysis, Gaussian distribution. Data are representative of 2 independent experiments.

2.3.9. Optimisation of LAMP-1 Western blotting

We observed enhanced LAMP-1 immunoreactivity in RAW 264.7 MΦ treated with *Mtb* H37Rv TL extract (Fig 2.3.8.2.A.), which could reflect an increase in the amount of the specific protein or redistribution of LAMP-1 within an enlarged organelle. In order to discriminate between these two possibilities, we undertook western blotting of LAMP-1 protein expression in lipid-treated or control cells.

In order to ensure quantitative detection of LAMP-1 protein, we optimised western blotting for the protein. First, we compared heat denaturation of the lysate at 50ºC or 90ºC for 10min prior to SDS-PAGE separation. Heating to 50ºC resulted in enhanced clarity (Fig 2.3.9.A.) and intensity (Fig 2.3.9.B.) of immunoreactivity as compared to samples heated to 95ºC.

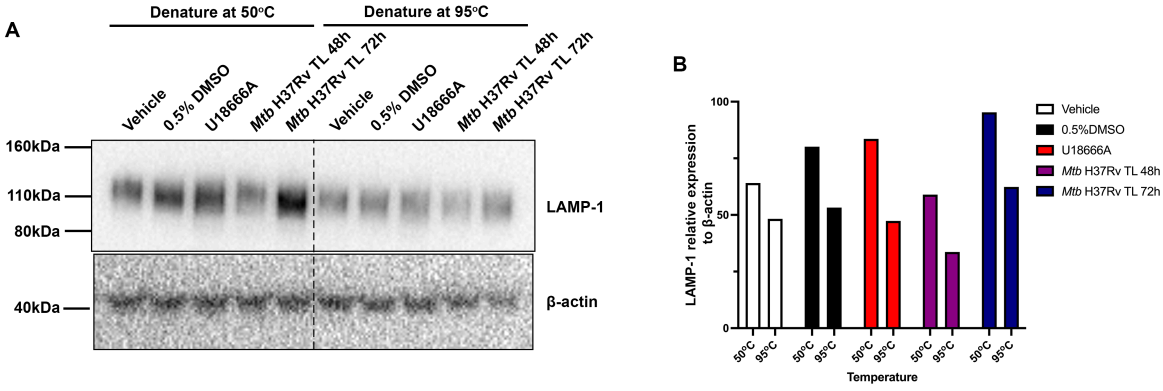


Figure 2.3.9. Optimisation of denaturation temperature of RAW 264.7 MΦ lysate for LAMP-1 western blotting.

Protein extracts were denatured at either 50ºC or 95ºC for 10min and then separated on SDS-PAGE, blotted to membrane and probed with anti-LAMP-1 antibody. Panel A. Representative western blot images. Specific protein band representing LAMP-1 is indicated. Expression of β-actin was used as evidence of equivalent lysate loading. Panel B. Quantification of the intensity of LAMP-1 band normalised to β-actin. Single data points are shown in the graph.

2.3.10. Expression of LAMP-1 is not altered in *Mtb* H37Rv TL-treated RAW 264.7 MΦ.

To assess LAMP-1 protein expression levels in vehicle-treated and *Mtb* H37Rv TL extract-treated RAW 264.7 MΦ, lysates were prepared from cells incubated with 100μg/ml TL extract, DMSO or U18666A (2μg/ml) for 48h. The level of LAMP-1 was not significantly changed in U18666A or *Mtb* H37Rv-treated RAW 264.7 MΦ (Fig 2.3.10.A.B.). However, whilst transcription of LAMP-1 was also not significantly changed in *Mtb* H37Rv TL-treated RAW 264.7 MΦ, it was significantly increased in U18666A-treated RAW 264.7 MΦ (p=0.0064, Fig 2.3.10.C.).

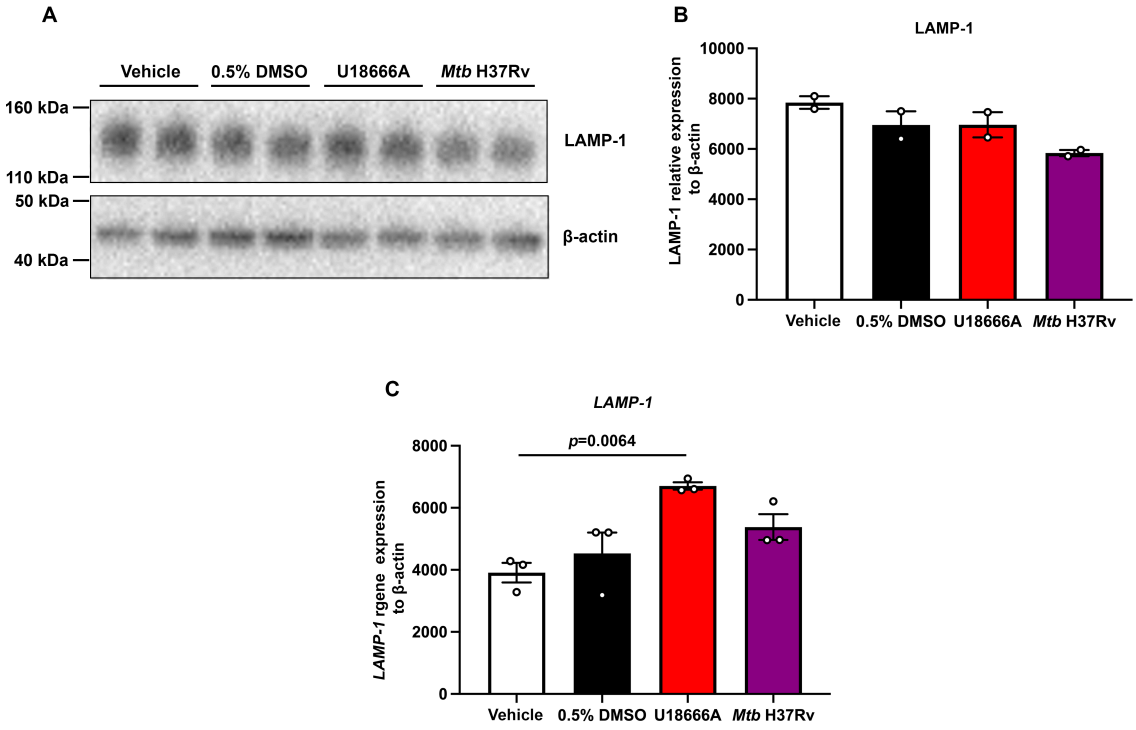
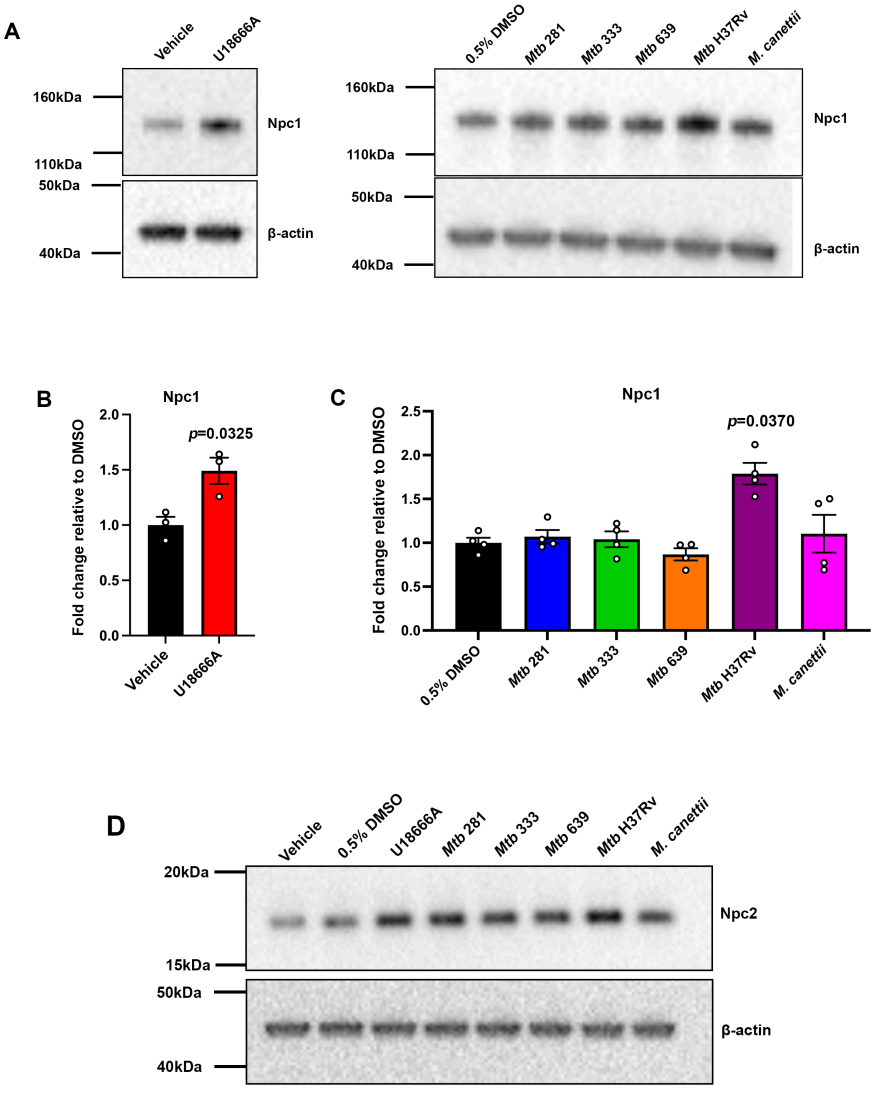


Figure 2.3.10. LAMP-1 protein expression or gene transcription in RAW 264.7 MΦ are not altered by Mtb H37Rv TL treatment.

Cells were treated with *Mtb* H37Rv TL extract (100µg/ml for 48h). DMSO and U18666A (2µg/ml for 48h) treatments were vehicle and positive controls respectively. Panel A. Representative western blot images of LAMP-1 and β-actin in treated RAW 264.7 MΦ. β-actin was used for normalisation of protein loading. Panel B. Quantification of LAMP-1 protein levels in treated RAW 264.7 MΦ normalised to β-actin. Data are mean ± SEM, n=2. Panel C. LAMP-1 gene expression treated RAW 264.7 MΦ determined by qPCR. Data are mean ± SEM, n=3. Statistical analysis, Welch's t-test. *p* values as indicated, otherwise not significant. Statistical comparison of U18666A treatment is relative to vehicle control. Statistical comparison of lipid treatment is relative to DMSO control. Data are representative of 2 independent experiments.

2.3.11. *Mtb* H37Rv TL extract increases Npc1, but not Npc2 expression in RAW 264.7 MΦ.

To evaluate whether *Mtb* clinical strains affect Npc1 and Npc2 protein expression, we measured the levels of the two proteins by western blotting. Probing blots of RAW 264.7 MΦ lysates treated with vehicle, U18666A or mycobacterial TL extracts revealed that U18666A induced a significant increase in Npc1 (p=0.0325, Fig 2.3.11.A.B.), as did *Mtb* H37Rv TL extract (p=0.0370, Fig 2.3.11.A.C.), but other TL extracts had no significant effect. U18666A treatment induced a significant increase in Npc2 expression (p=0.0015), but no apparent changes were observed in response to treatment with TL extracts (Fig 2.3.11.D.E.).



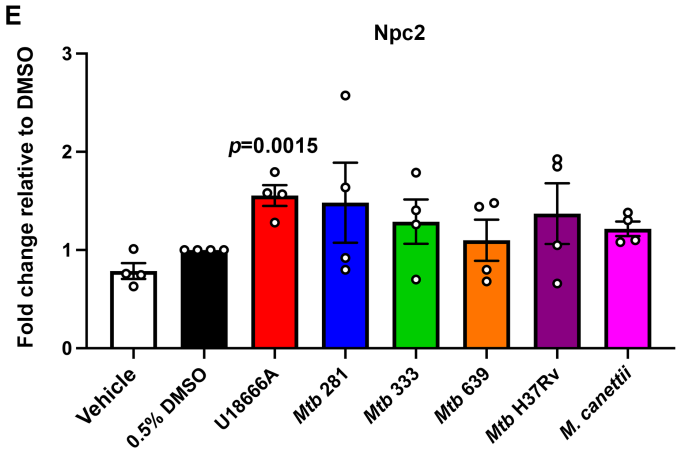


Figure 2.3.11. Exposure to Mtb H37Rv significantly increases the expression of Npc1 in RAW 264.7 MΦ.

Cells were treated with TL extract of *Mtb* clinical strains (100µg/ml for 48h). DMSO and U18666A (2µg/ml for 48h) treatments were vehicle and positive controls respectively. β-actin expression was used to normalised protein loading. Panel A. Representative Npc1 protein western blot images of lysates of treated RAW 264.7 MΦ. Panel B.C. Quantification of relative Npc1 protein expression normalised to β-actin. Data are normalised to fold change compared to DMSO control. Data are mean ± SEM, n=3. Statistical analysis, Welch's t-test. *p* values as indicated, otherwise not significant. Statistical comparison of U18666A treatment is relative to vehicle control. Statistical comparisons of lipid treatments are relative to DMSO controls. Panel D. Representative Npc2 protein western blot image in treated RAW 264.7 MΦ. Panel E. Quantification of relative Npc2 protein expression normalised to β-actin. Data are normalised to fold change compared to DMSO control. Data are mean ± SEM, n=4. Statistical analysis, Welch's t-test. *p* values as indicated, otherwise not significant. Statistical comparison of U18666A treatment is relative to vehicle control. Statistical comparisons of lipid treatments are relative to DMSO controls. Data are representative of 4 independent experiments.

2.3.12. Expression of *Npc1* and *Npc2* transcripts are increased in *Mtb* H37Rv TL-treated RAW 264.7 MΦ.

We investigated whether transcription of *Npc1* and *Npc2* genes in RAW 264.7 MΦ treated with *Mtb* H37Rv TL was changed. Q-PCR confirmed that *Npc1* gene expression was significantly increased at 48h and 72h of treatment with *Mtb* H37Rv TL (Fig 2.3.12.A.). Although expression of *Npc1* was enhanced by U18666A at 48h (Fig 2.3.12.A.), there was no effect on *Npc2* at the same time point (Fig 2.3.12.B.), and *Npc2* was significantly increased only at 72h with *Mtb* H37Rv TL extract (Fig 2.3.12.B.).

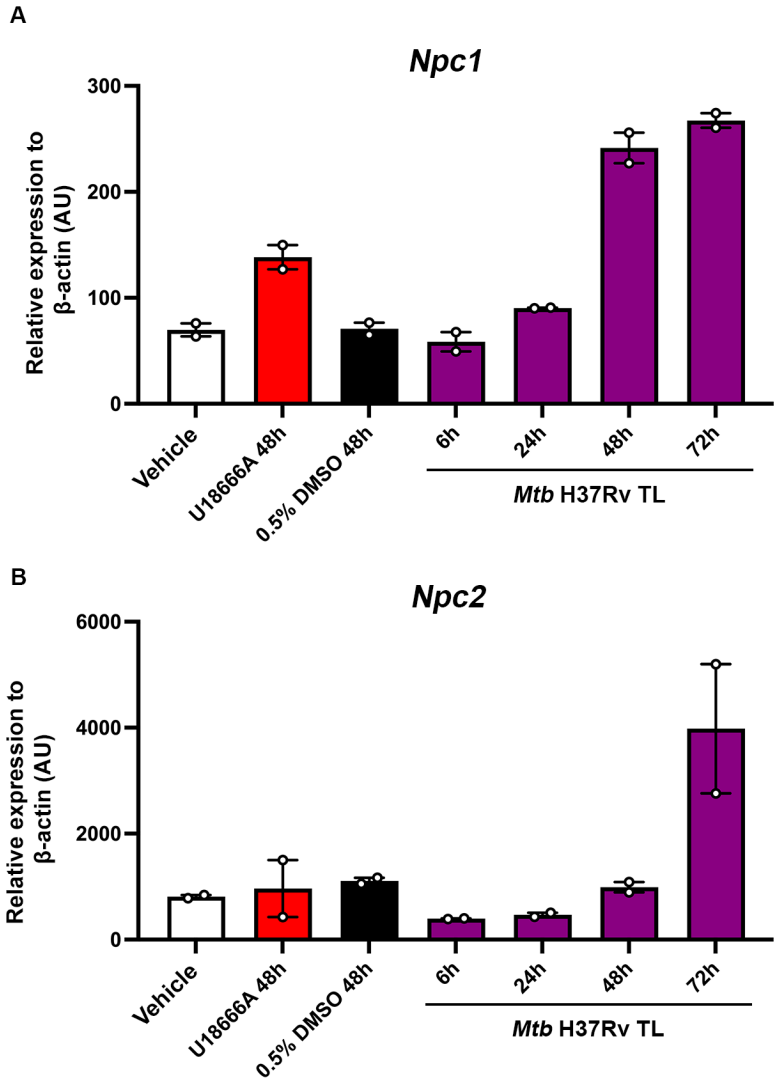


Figure 2.3.12. Mtb H37Rv TL significantly enhances transcription of Npc1 and Npc2 genes in RAW 264.7 MΦ.

Cells were treated with TL extract of *Mtb* H37Rv (100µg/ml for 6h to 72h). DMSO and U18666A (2µg/ml for 48h) treatments were vehicle and positive controls respectively. Gene expression level was normalised to *β-actin* expression. Panel A. Quantification of *Npc1* transcription in treated cells by qPCR. Panel B. Quantification of *Npc2* transcription in treated cells by qPCR. Data are mean ± SEM, n=2. Data are representative of 3 independent experiments.

2.3.13. TL extracts of representative *Mtb* clinical strains, but not *M. canettii* induce partial redistribution of intracellular cholesterol to the endo-lysosomal system of RAW 264.7 MΦ.

To study whether Npc1 activity is inhibited by TL extracts of H37Rv, representative *Mtb* clinical strains and *M. canettii*, we analysed for the induction of specific NPC cellular phenotypes in RAW 264.7 MΦ after incubation with lipid. Accumulation of cholesterol in the endo-lysosomal system revealed by filipin staining is a prominent NPC clinical phenotype [216]. RAW 264.7 MΦ were therefore incubated with mycobacterial lipid extracts, stained with filipin and examined by confocal microscopy. In U18666A-treated RAW 264.7 MΦ, intracellular redistribution of free cholesterol was visible as lysosomal filipin-positive puncta (red arrows, Fig 2.3.13.1.A.), and to quantify, we determined the frequency of cells displaying lysosomal puncta. Treatment with U18666A (****p<0.0001, Fig 2.3.13.1.B.), as well as extracts of all of the representative *Mtb* clinical strains resulted in a significant increase in the frequency of filipin-positive cells (p=0.0049 for strain 281; p=0.0273 for strain 333; p=0.0210 for strain 639; p=0.0162 for strain H37Rv, Fig 2.3.13.2.A.B.). In contrast, relatively few puncta

were detected in RAW 264.7 MΦ treated with TL extract of *M. canettii* and were not significantly greater in number than vehicle control cells (Fig 2.3.13.2.A.B.).

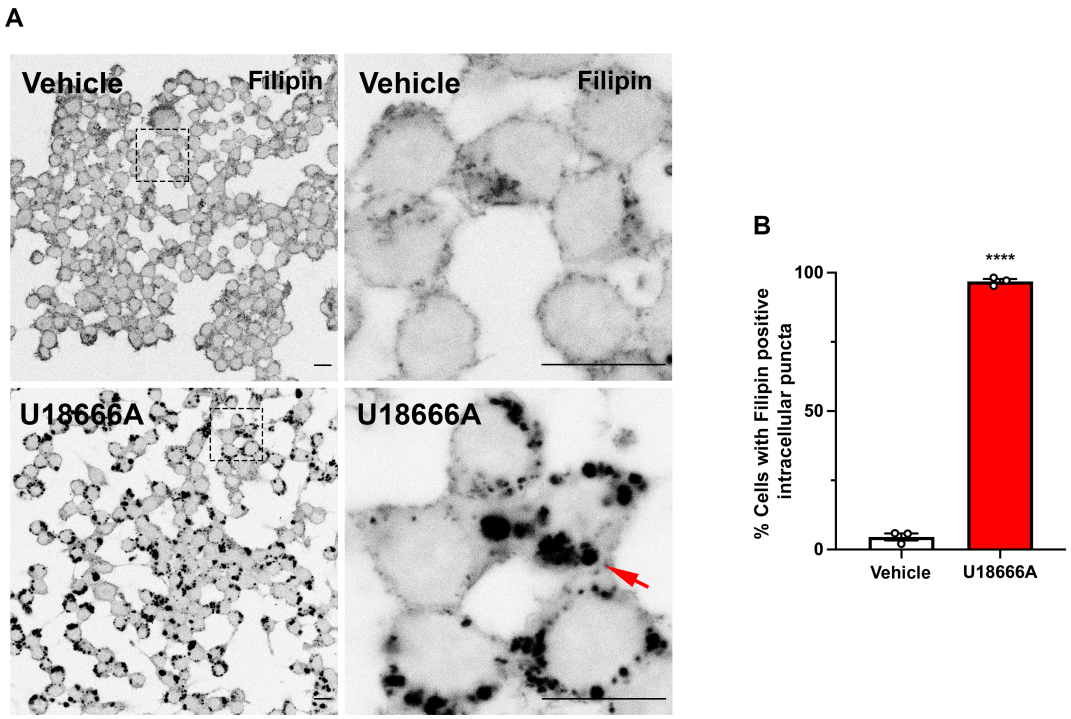
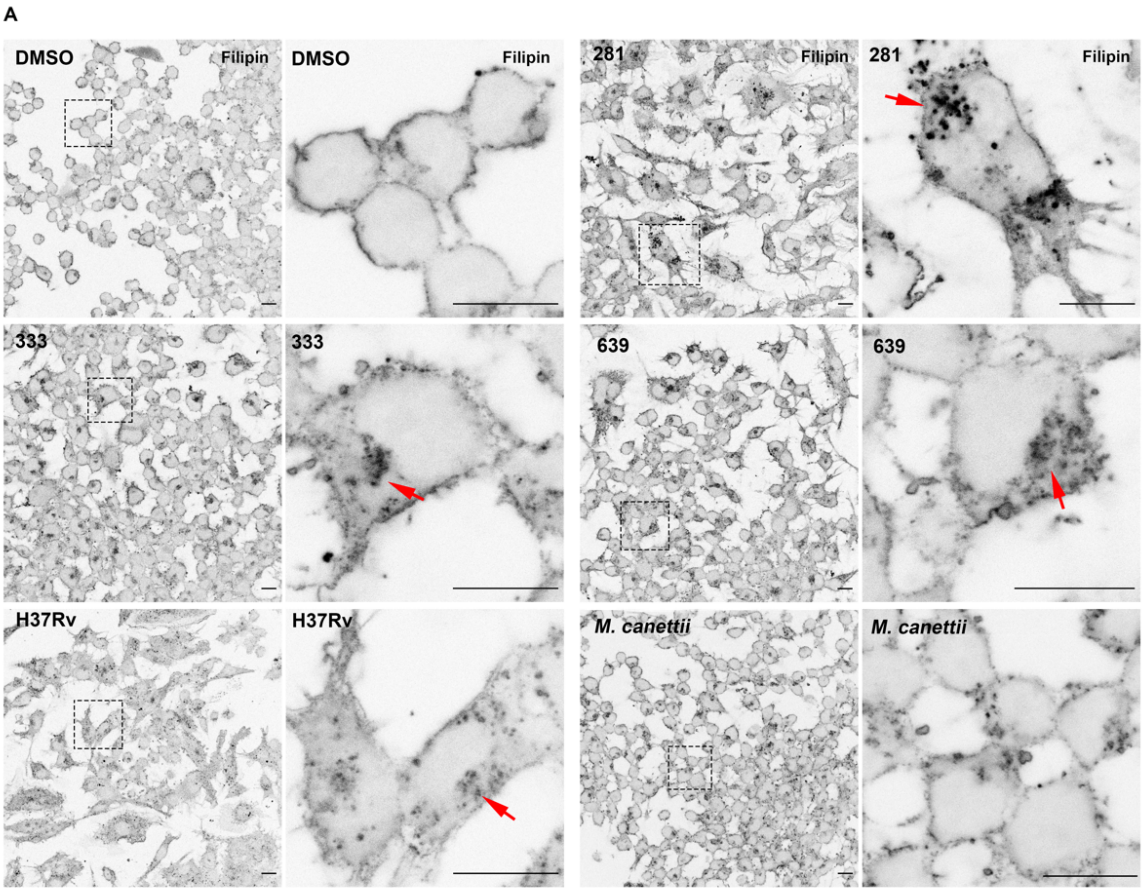


Figure 2.3.13.1. U18666A induces a partial redistribution of cholesterol to intracellular puncta in RAW 264.7 MΦ.

Cells were treated with U18666A (2µg/ml for 48h). Panel A. Representative confocal microscopy images of vehicle or U18666A-treated RAW 264.7 MΦ stained with filipin. Filipin, black. Scale bar represents 10µm. For each pair, the right image is a higher magnification of the region outlined in the left image. Red arrows indicate filipin-positive puncta. Panel B. Frequency of cells with intracellular filipin-positive puncta. Data are mean ± SEM, n=3. Statistical analysis, Welch's t-test. ****p<0.0001. Statistical comparison of U18666A treatment is relative to vehicle control. Data are representative of 2 independent experiments.


A
DMSO
Filipin
DMSO
Filipin
281
Filipin
281
Filipin
333
333
639
639
H37Rv
H37Rv
M. canettii
M. canettii

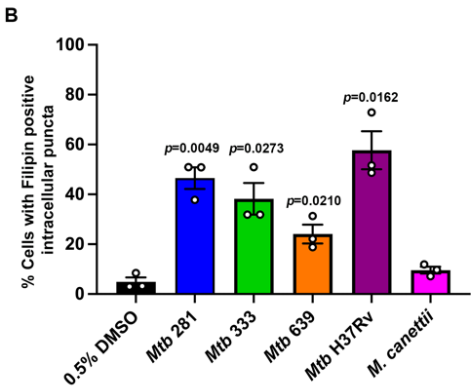

B
% Cells with Filipin positive intracellular puncta
100
80
60
40
20
0
p=0.0049
p=0.0273
p=0.0210
p=0.0162
0.5% DMSO
Mtb 281
Mtb 333
Mtb 639
Mtb H37Rv
M. canettii

Figure 2.3.13.2. Mtb lipids induced a partial redistribution of cholesterol to intracellular puncta in RAW 264.7 MΦ.

Cells were treated with TL extracts of *Mtb* clinical strains or *M. canettii* (100µg/ml for 48h). DMSO (0.5% for 48h) was used as vehicle control for lipid treatment. Panel A. Representative confocal microscopy images of treated RAW 264.7 MΦ. Filipin, black. Scale bar represents 10µm. For each pair, the right image is a higher magnification of the region outlined in the left image. Red arrows indicate filipin-positive puncta. Panel B. Frequency of cells with intracellular filipin-positive puncta. Data are mean ± SEM, n=3. Statistical analysis, Welch's t-test. *p* values as indicated, otherwise not significant. Statistical comparisons of lipid treatments are relative to DMSO controls. Data are representative of 2 independent experiments.

2.3.14. TL extracts of *Mtb* clinical strains and *M. canettii* do not affect cholesterol levels in RAW 264.7 MΦ.

Total cholesterol content of RAW 264.7 MΦ incubated with U18666A or TL extracts of *Mtb* clinical strains or *M. canettii* was determined biochemically using the Amplex Red assay. There was a significant increase in cholesterol content in U18666A-treated RAW 264.7 MΦ (p=0.0360, Fig 2.3.14.A.) but not in cells incubated with lipid extracts of the representative *Mtb* strains or *M. canettii* (Fig 2.3.14.B.).

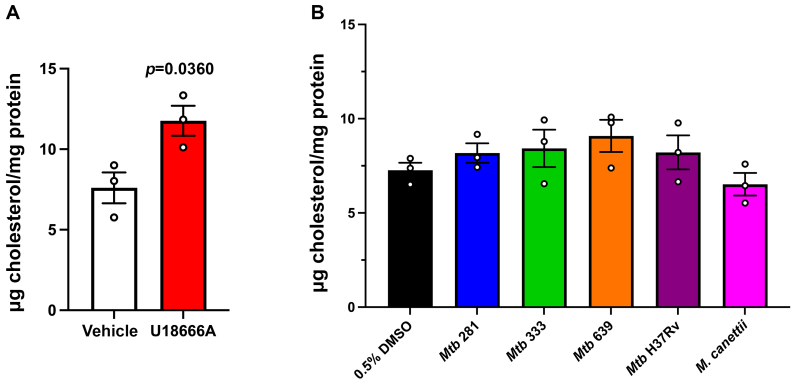


Figure 2.3.14. TL extracts of Mtb clinical strains do not affect the cholesterol content of RAW 264.7 MΦ.

Cells were treated with TL extract of *Mtb* clinical strains or *M. canettii* (100µg/ml for 48h). DMSO and U18666A (2µg/ml for 48h) treatments were vehicle and positive controls respectively. Panel A. Total cholesterol content (µg/mg protein) in vehicle and U18666A-treated RAW 264.7 MΦ. Data are mean ± SEM, n=3. Statistical analysis, Welch's t-test. p values as indicated. Statistical comparison of U18666A treatment is relative to vehicle control. Panel B. Total cholesterol content (µg/mg protein) of RAW 264.7 MΦ treated with TL extracts of *Mtb* clinical strains or *M. canettii*. Data are mean ± SEM, n=3. Statistical analysis, Welch's t-test. No statistically significant difference. Statistical comparisons of lipid treatments are relative to DMSO controls. Data are representative of 2 independent experiments.

2.3.15. Optimisation of GM1 ganglioside labelling and trafficking in RAW 264.7 MΦ.

In NPC1-deficient cells, the recycling of GSL species is perturbed, resulting in the miss-trafficking of GSLs from their normal recycling pathway via the Golgi to the lysosome [217]. This distribution can be visualised by pulse-chase tracking of GM1 ganglioside labelled with fluorescent cholera toxin B subunit (CtxB) [218]. Cells were incubated with AlexaFluor™ 488-conjugated CtxB for 30 min, washed, fresh medium added and incubated for up to 150min at 37°C and inspected by confocal microscopy. U18666A treatment, which inhibits Npc1 activity [35] resulted in the appearance of lysosome-located CtxB at all time points (red arrows), whereas in vehicle-treated cells, puncta in lysosomes was only obvious at extended incubation periods of 90min and beyond (red arrows, Fig 2.3.15.). At incubation times of 60min and 75min, GM1 ganglioside in vehicle-treated cells was primarily restricted to the Golgi apparatus (white arrows, Fig 2.3.15.). Based upon the differential localisation of GM1 puncta in control and U18666A treated cells, a chase period of 60min was chosen for all subsequent studies that involved labelling with CtxB (Fig 2.3.15.).

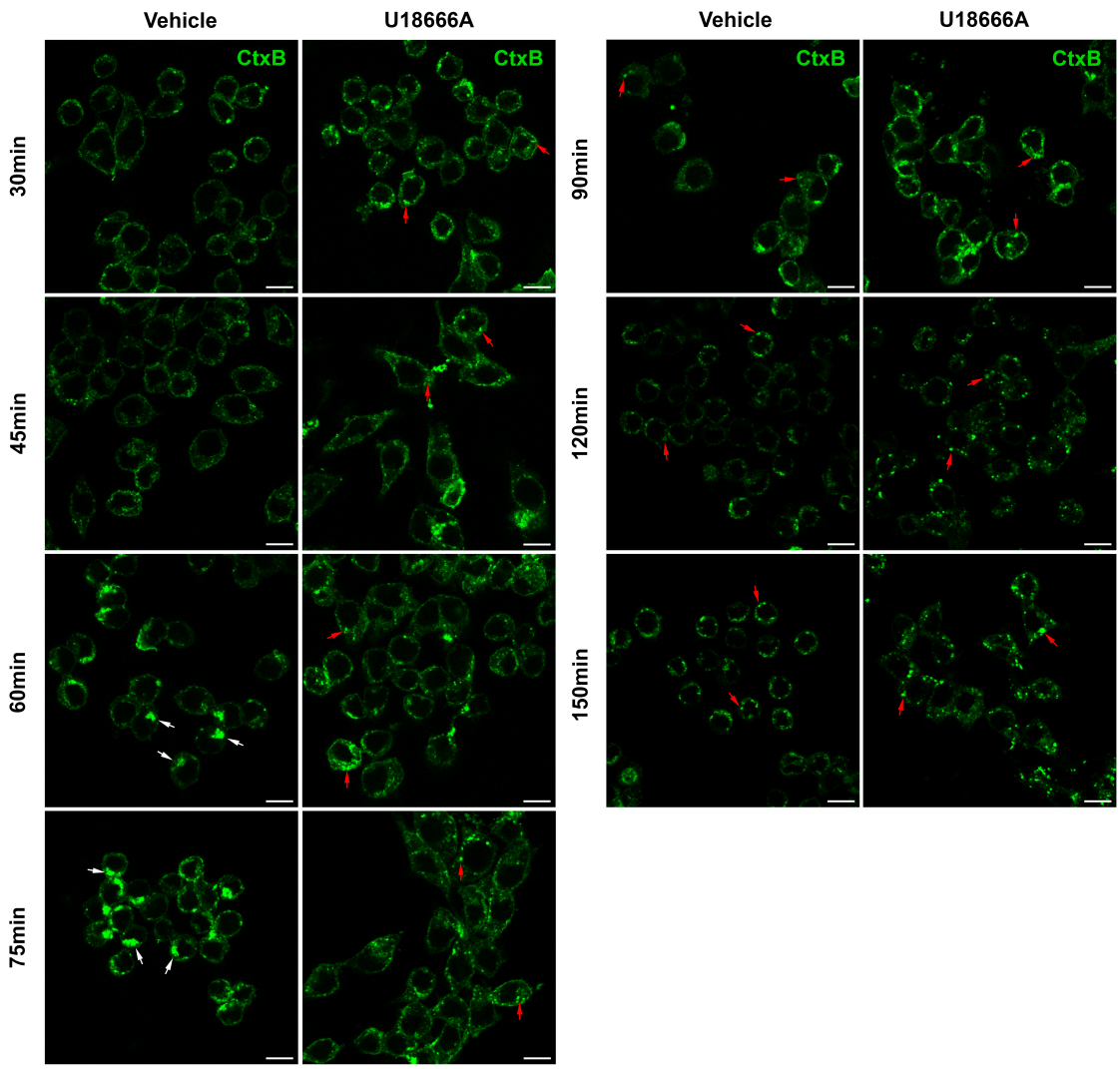


Figure 2.3.15. Optimisation of CtxB labelling of GM1 ganglioside in RAW 264.7 MΦ.

Cells were either treated with vehicle or U18666A (2μg/ml for 48h), labelled with AlexaFluor™ 488-conjugated CtxB for 30 min and then chased for up to 150min. Representative confocal images of vehicle or U18666A-treated RAW 264.7 MΦ. White arrows indicate Golgi distribution; red arrows indicate lysosomal distribution. CtxB, green. Scale bar represents 10μm.

2.3.16. Exposure to lipids from representative *Mtb* strains but not *M. canettii* perturb GM1 ganglioside intracellular trafficking in RAW 264.7 MΦ.

Pulse-chase labelling with fluorescently tagged CtxB revealed that U18666A treatment of RAW 264.7 MΦ resulted in the redistribution of GM1 ganglioside away from recycling through the Golgi apparatus to the endo-lysosomal compartment (red arrows), whereas in vehicle-treated cells, it was restricted to the Golgi apparatus (white arrows, Fig 2.3.16.1.A.). The frequency of U18666A-treated RAW 264.7 MΦ with lysosomal localisation of GM1 was significantly increased compared to vehicle control (****p<0.0001, Fig 2.3.16.1.B.). Examination revealed lysosomal CtxB fluorescent puncta in RAW 264.7 MΦ treated with TL extracts of representative *Mtb* strains (red arrows) with the exception of *M. canettii* (white arrows) TL-treated cells, in which GM1 ganglioside was confined to the Golgi apparatus compared to the DMSO vehicle control (Fig 2.3.16.2.A.). The frequency of cells with lysosomal localisation of GM1 ganglioside was significantly increased in *Mtb* clinical strain TL-treated RAW 264.7 MΦ (p=0.0004 for strains 281; p=0.0002 for strain 333; ****p<0.0001 for strains 639 and H37Rv, Fig 2.3.16.2.B.), but not in *M. canettii* extract-treated cells, which were not different from the control.

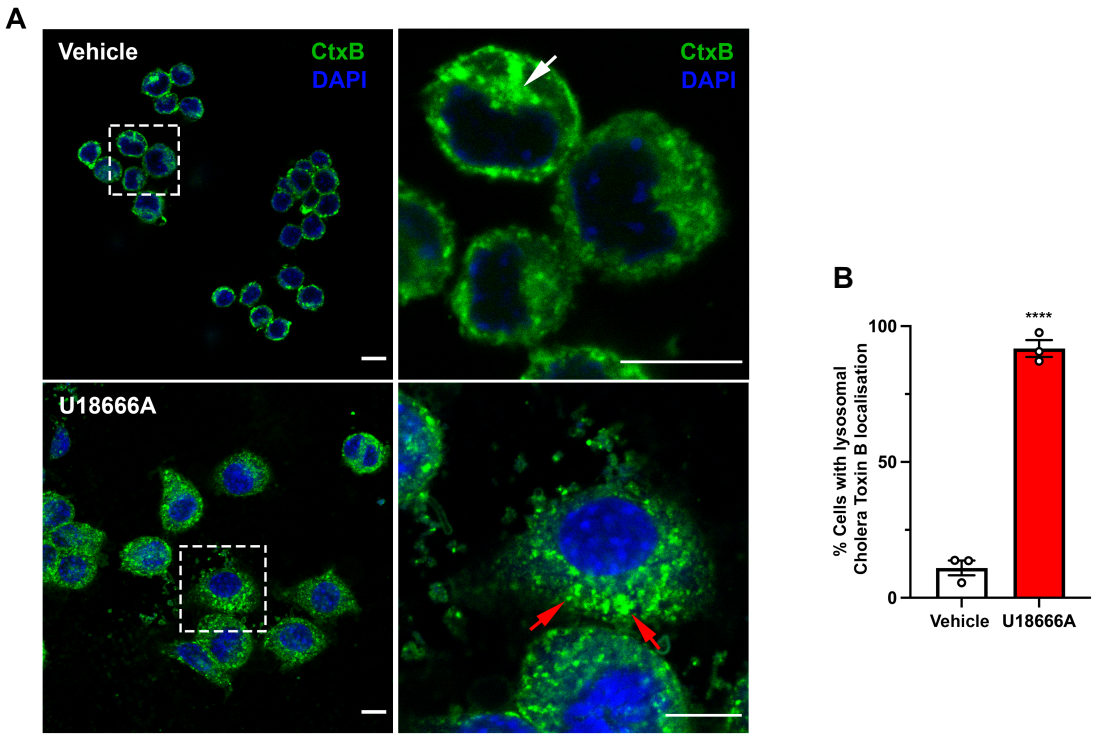


Figure 2.3.16.1. U18666A affects GM1 ganglioside trafficking in RAW 264.7 MΦ.

Cells were treated with U18666A (2µg/ml for 48h). Panel A. Representative confocal microscopy images of treated cells. CtxB, green; DAPI, blue. Scale bar represents 10µm. White arrows indicate Golgi distribution; red arrows indicate lysosomal distribution. For each pair, the right image is a higher magnification of the region outlined in the left image. Panel B. Frequency of cells with lysosomal GM1 distribution. Data are mean ± SEM, n=3, each representing a minimum of 100 cells in randomly selected fields. Statistical analysis, Welch's t-test. ****p<0.0001. Statistical comparison of U18666A treatment is relative to vehicle control. Data are representative of 2 independent experiments.

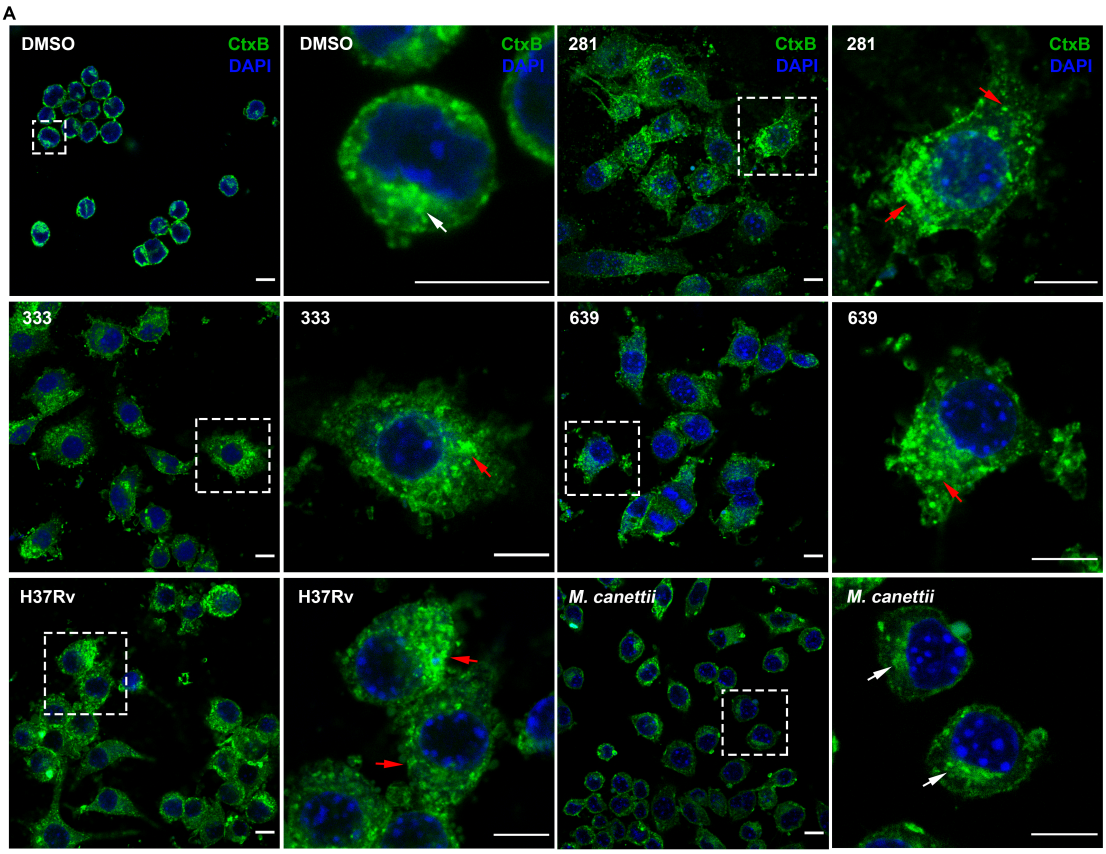

A
DMSO
CtxB
DAPI
DMSO
CtxB
DAPI
281
CtxB
DAPI
281
CtxB
DAPI
333
333
639
639
H37Rv
H37Rv
M. canettii
M. canettii
B
% Cells with lysosomal Cholera Toxin B localisation
100
80
60
40
20
0
p=0.0004
p=0.0002
****
****
0.5% DMSO
Mtb 281
Mtb 333
Mtb 639
Mtb H37Rv
M. canettii

Figure 2.3.16.2. TL extracts of representative Mtb clinical strains, but not M. canettii affect GM1 ganglioside trafficking in RAW 264.7 MΦ.

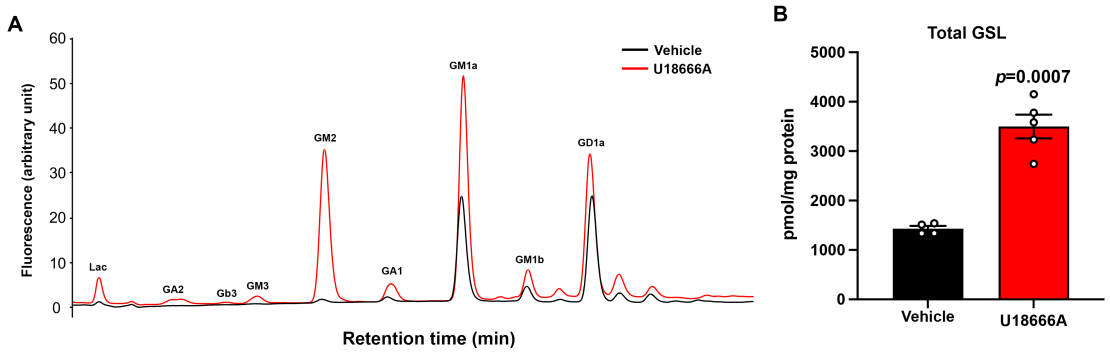
Cells were treated with TL extract of *Mtb* clinical strains or *M. canettii* (100µg/ml for 48h). DMSO (0.5% for 48h) was the vehicle control. Panel A. Representative confocal microscopy images of GM1 ganglioside distribution. CtxB, green; DAPI, blue. Scale bar represents 10µm. White arrows indicate Golgi distribution; red arrows indicate lysosomal distribution. For each pair, the right image is a higher magnification of the region outlined in the left image. Panel B. Frequency of cells with lysosomal GM1 distribution. Data are mean ± SEM, n=3, each representing a minimum of 100 cells randomly selected fields. Statistical analysis, Welch's t-test. ****$p<0.0001$, other p values as indicated, otherwise not significant. Statistical comparisons of lipid treatments are relative to DMSO controls. Data are representative of 2 independent experiments.

2.3.17. GSL species accumulate in RAW 264.7 MΦ incubated with lipid extracts of strains representative of different *Mtb* lineages but not with *M. canettii* lipid.

Impaired lipid transport and catabolism cause the accumulation of multiple GSLs in NPC cells [6, 81]. We therefore investigated whether GSLs accumulated in RAW 264.7 MΦ treated with TL extracts of representative clinical *Mtb* strains and *M. canettii* and determined their abundance by NP-HPLC.

Representative HPLC profiles of GSLs of the vehicle and U18666A-treated RAW 264.7 MΦ are shown in Fig 2.3.17.1.A. U18666A significantly increased the

amount of total GSLs (p=0.0007, Fig 2.3.17.1.B.) and individual GSL species (****p<0.0001 for Lac, GA2, GM3, GM2, GA1; p=0.0004 for Gb3; p=0.0011 for GM1a; p=0.0038 for GM1b) but not GD1a (Fig 2.3.17.1.C.).



C

		Lac	GA2	Gb3	GM3	GM2	GA1	GM1a	GM1b	GD1a
% Area	Vehicle	1.16%	0.46%	0.14%	0.34%	1.69%	1.83%	42.44%	6.15%	45.79%
	U18666A	2.99%	1.55%	0.21%	1.43%	26.88%	3.67%	35.26%	4.38%	23.62%
Fold increase to vehicle	U18666A	**** 6.72±0.35	**** 7.46±0.37	p=0.0005 3.19±0.27	**** 8.77±0.63	**** 41.35±2.82	**** 4.96±0.33	p=0.0003 2.13±0.15	p=0.0018 1.81±0.14	ns 1.27±0.10

Figure 2.3.17.1. U18666A causes GSL accumulation in RAW 264.7 MΦ.

Cells were treated with U18666A (2μg/ml for 48h). Panel A. Representative HPLC profiles of GSLs in vehicle or U18666A-treated RAW 264.7 MΦ. Panel B. Quantification of total GSLs in RAW 264.7 MΦ treated with vehicle or U18666A. Data are mean ± SEM, n=5. Statistical analysis, Welch's t-test. p values as indicated. Panel C. Summary table of quantification of the abundance of specific GSL species in RAW 264.7 MΦ treated with U18666A relative to vehicle control. Data are mean ± SEM, n=5. Statistical analysis, Welch's t-test. ****p<0.0001, other p values as indicated. Statistical comparison of U18666A treatment is relative to vehicle control. Data are representative of 2 independent experiments.

Overlaid representative HPLC profiles of GSLs from DMSO and mycobacterial TL-treated RAW 264.7 MΦ are shown in Fig 2.3.17.2.A. With the exception of *M. canettii* TL, which significantly reduced total GSLs in treated RAW 264.7 MΦ (p=0.0048, Fig 2.3.17.2.B.), extracts of each of the representative *Mtb* clinical strains significantly increased total GSLs (p=0.0002 for strain 281; p=0.0042 for strain 381; p=0.0008 for strain 639; p=0.0048 for H37Rv, Fig 2.3.17.2.B.). The most abundant lipid species GM1a, GM1b and GD1a were significantly increased by all *Mtb* strains but not *M. canettii*, in response to which they were either not significantly different (GM1a) or were significantly reduced (p=0.0043 for GM1b; p=0.0016 for GD1a, Fig 2.3.17.2.B.). As summarised in Table 2.3.17., strain 281 from *Mtb* lineage 1 significantly increased eight of the individual lipid species, strain 333 from lineage 2 increased five lipid species, and lineage 4 strains 639 and H37Rv increased four and seven distinct lipid species respectively. *M. canettii* TL extract only significantly enhanced two minor lipid species (p=0.0084 for GM2; p=0.0117 for GA1), albeit to a relatively small extent (both GSLs were increased by ~1.2-fold by *M. canettii* extract whereas GM2 was increased >2.0-fold and GA1 >1.8-fold by *Mtb* lipids), did not alter the level of three individual lipids (GA2, Gb3, and GM1a) and significantly reduced the level of four lipids (Lac, GM3, GM1b and GD1a, Table 2.3.17.), which was not observed with any of the *Mtb* strains.

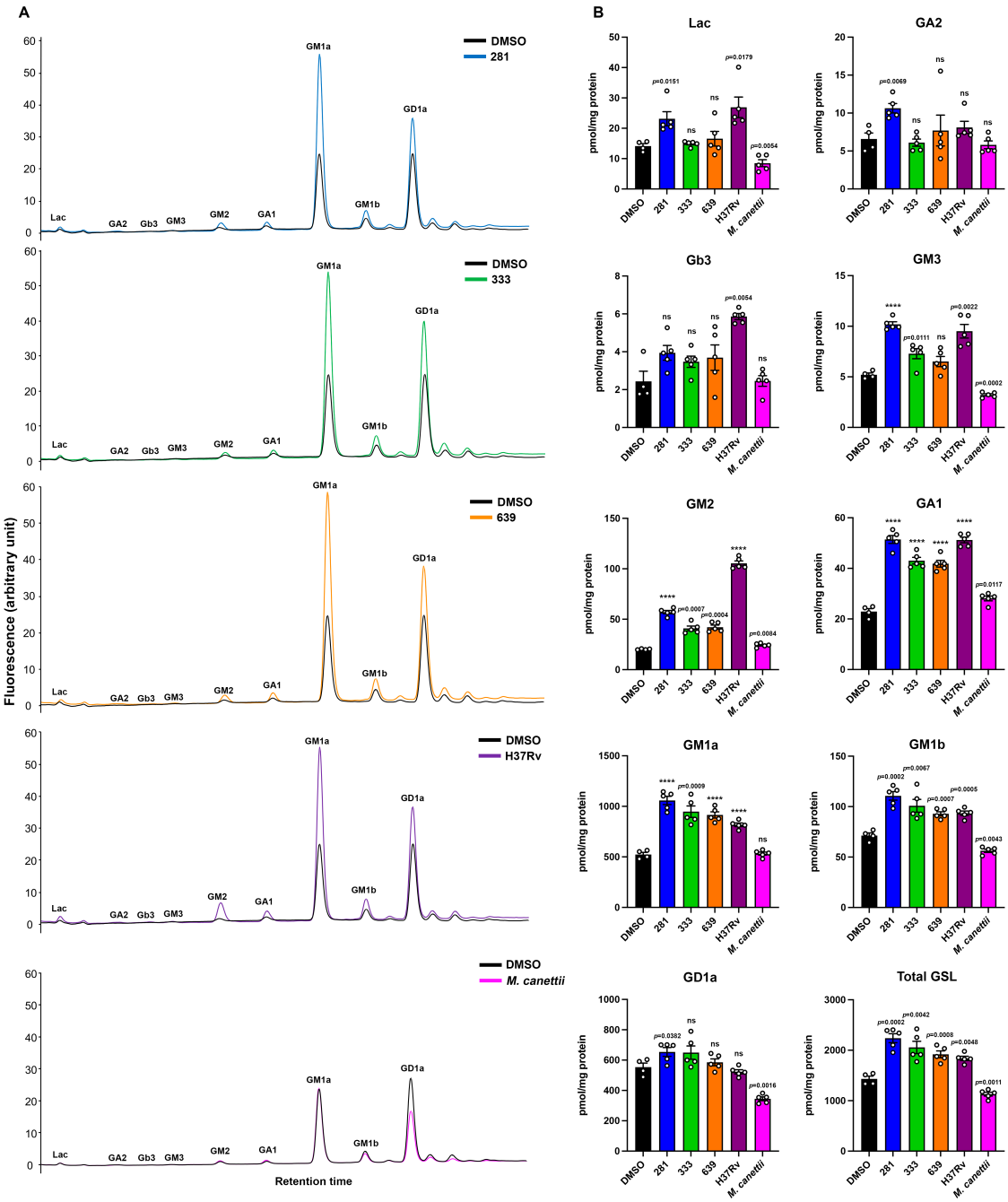

A
B
DMSO
281
333
639
H37Rv
M. canettii
Lac
GA2
Gb3
GM3
GM2
GA1
GM1b
GM1a
GD1a
Fluorescence (arbitrary unit)
Retention time
pmol/mg protein
Total GSL
ns

Figure 2.3.17.2. Mtb lipids extracts, but not M. canettii extract, induce GSLs accumulation in RAW 264.7 MΦ.

Cells were treated with TL extract of *Mtb* clinical strains or *M. canettii* (100μg/ml for 48h). DMSO (0.5% for 48h) was the vehicle control. Panel A. Representative HPLC profiles for GSLs in extracts of vehicle and mycobacterial lipid-treated RAW 264.7 MΦ. Panel B. Quantification of individual GSL species in treated RAW 264.7 MΦ. Data are mean ± SEM, n=5. Statistical analysis, Welch's t-test. ****p<0.0001, other p values as indicated, otherwise not significant. Statistical comparisons of lipid treatments are relative to DMSO controls. Data are representative of 2 independent experiments.

GSL species	U18666A	281	333	639	H37Rv	*M. canettii*
Lac	**** 6.72±0.35	*p*=0.0151 1.64±0.16	ns 1.05±0.03	ns 1.17±0.17	*p*=0.0179 1.90±0.24	*p*=0.0054 0.60±0.08
GA2	**** 7.46±0.37	*p*=0.0069 1.62±0.10	ns 0.93±0.07	ns 1.17±0.31	ns 1.23±0.12	ns 0.88±0.08
Gb3	*p*=0.0005 3.19±0.27	ns 1.62±0.16	ns 1.42±0.12	ns 1.51±0.28	*p*=0.0054 2.40±0.07	ns 1.01±0.12
GM3	**** 8.77±0.63	**** 1.96±0.05	*p*=0.0111 1.40±0.10	ns 1.52±0.10	*p*=0.0022 1.83±0.13	*p*=0.0002 0.62±0.02
GM2	**** 41.35±2.82	**** 2.82±0.08	*p*=0.0007 2.02±0.11	*p*=0.0004 2.08±0.10	**** 5.21±0.12	*p*=0.0084 1.20±0.04
GA1	**** 4.96±0.33	**** 2.24±0.07	**** 1.88±0.06	**** 1.82±0.06	**** 2.23±0.05	*p*=0.0117 1.23±0.04
GM1a	*p*=0.0003 2.13±0.15	**** 2.02±0.08	*p*=0.0009 1.81±0.11	**** 1.75±0.06	**** 1.56±0.03	ns 1.02±0.03
GM1b	*p*=0.0018 1.81±0.14	*p*=0.0002 1.55±0.06	*p*=0.0067 1.41±0.09	*p*=0.0007 1.30±0.03	*p*=0.0005 1.31±0.03	*p*=0.0043 0.79±0.02
GD1a	ns 1.27±0.10	*p*=0.0382 1.18±0.05	ns 1.17±0.08	ns 1.06±0.04	ns 0.95±0.03	*p*=0.0016 0.62±0.02
Total GSL	*p*=0.0007 2.44±0.17	*p*=0.0002 1.56±0.06	*p*=0.0042 1.44±0.09	*p*=0.0008 1.34±0.05	*p*=0.0048 1.28±0.03	*p*=0.0011 0.79±0.03

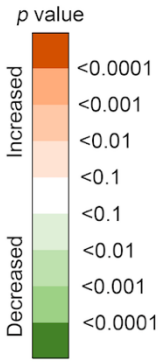


Table 2.3.17. Summary of the relative accumulation of total and specific GSL species in RAW 264.7 MΦ treated with U18666A or TL extracts of representative Mtb clinical strains or M. canettii.

Data represent mean ± SEM fold change in lipid abundance relative to DMSO-treated control cells, a minimum of n=4 to 5 samples per treatment. Statistical analysis, Welch's t-test. ****p<0.0001, other p values as indicated, otherwise not significant. Statistical comparison of U18666A treatment is relative to vehicle control. Statistical comparisons of lipid treatments are relative to DMSO controls. Spectrum of colours indicated significantly increased (red) or decreased (green) levels.

2.3.18. Lipid composition of clinical strains representative of different *Mtb* lineages.

Lipid compositions of lipid extract of clinical *Mtb* strains were analysed by Dr Gerald Larrouy-Maumus at Imperial College, London. Using a combination of different solvent conditions and thin layer chromatography (TLC), together with MALDI-ToF MS in the positive and negative ion mode, lipid preparations from each of the *Mtb* clinical strains were analysed. As shown in Fig. 2.3.18.1., TLC of extractible lipids from the strains produced qualitatively comparable profiles, with no obvious differences in composition.

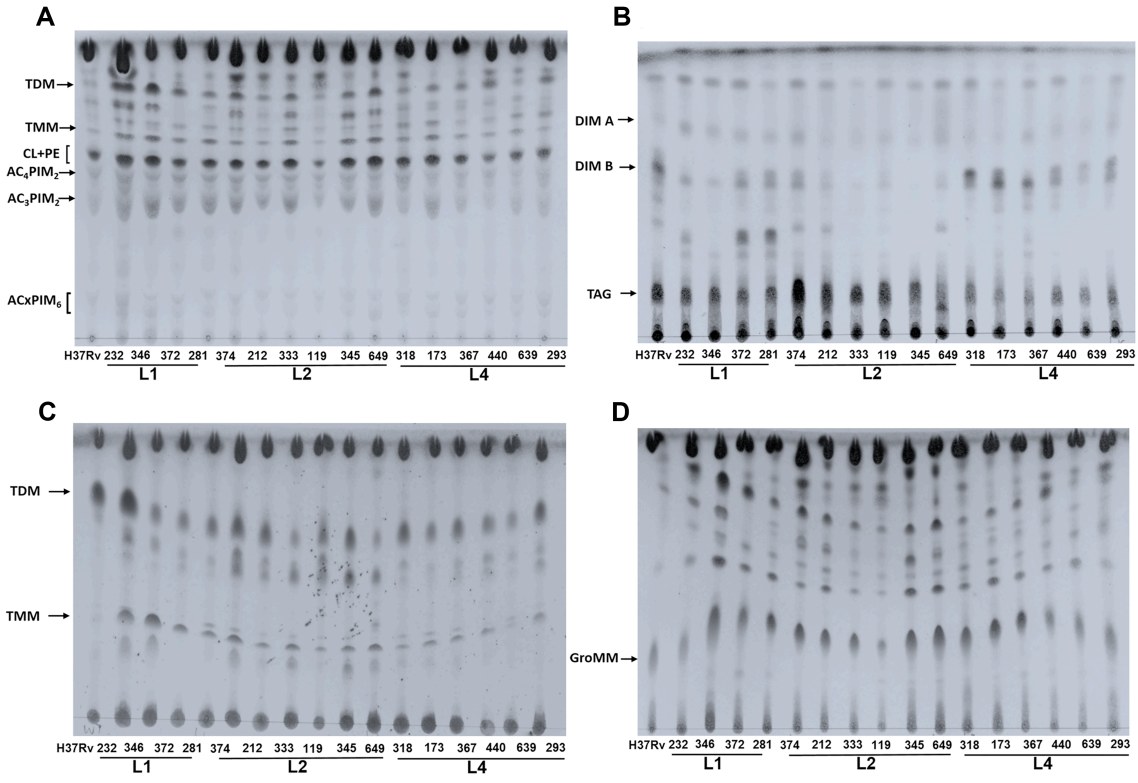
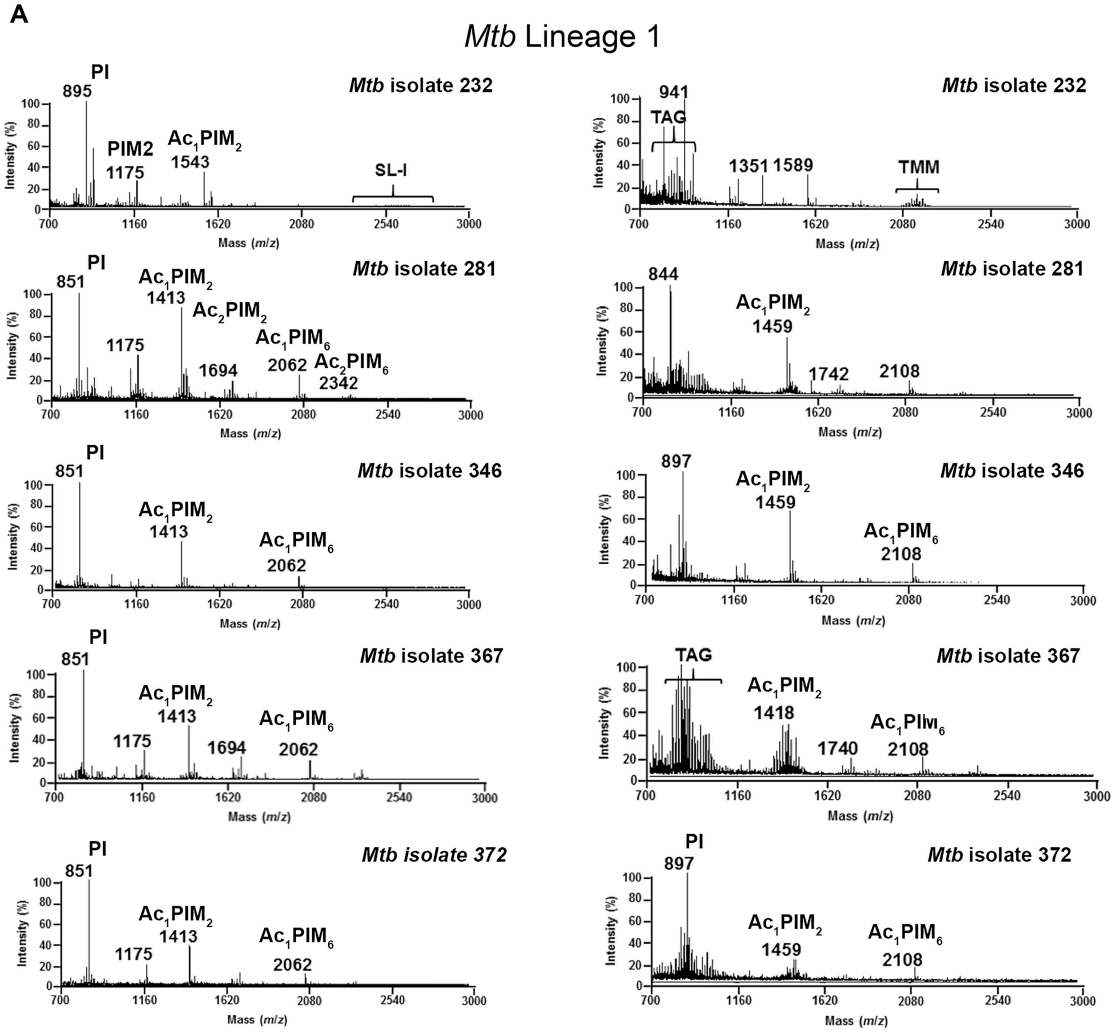


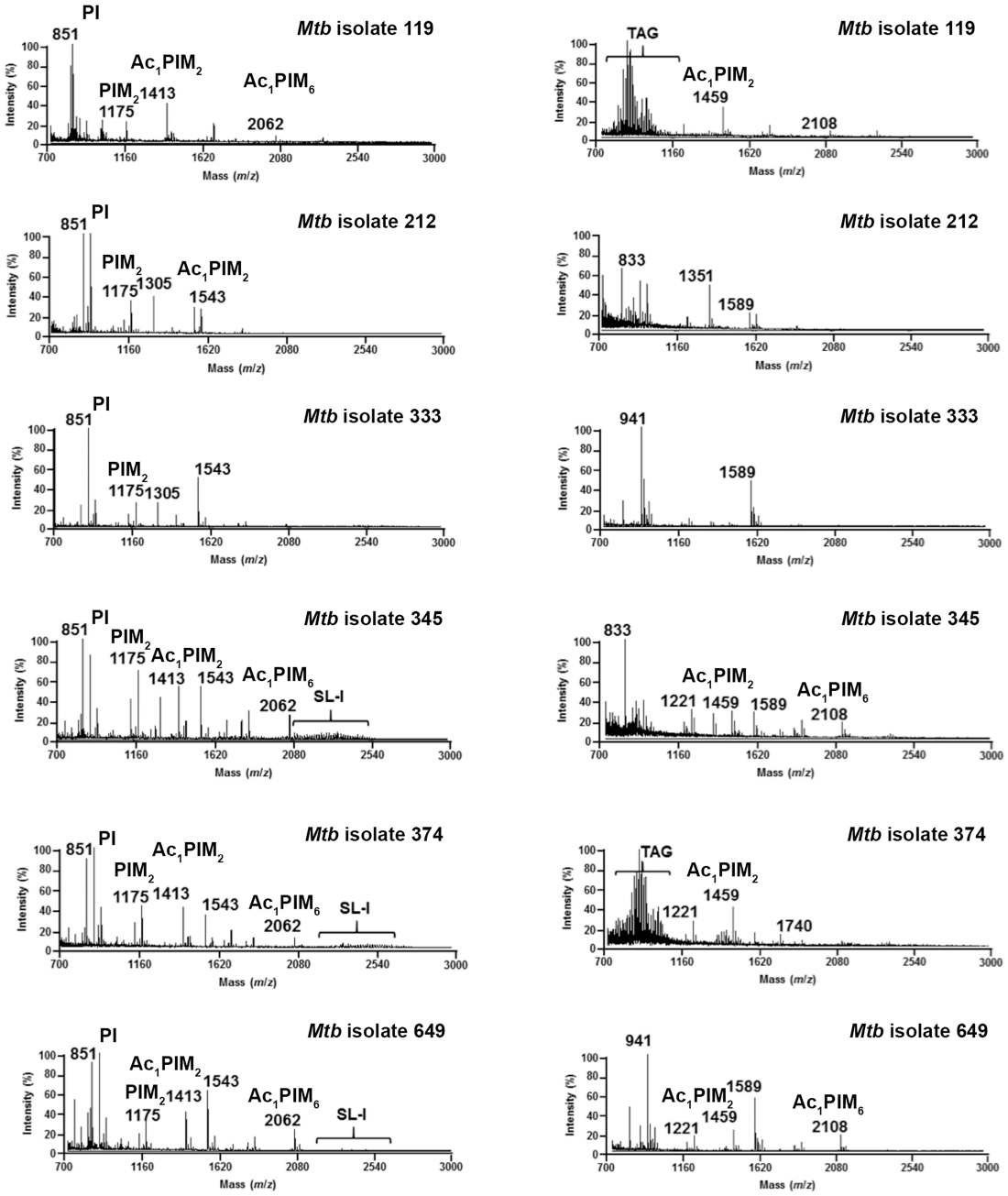
Figure 2.3.18.1. TLCs of lipids from Mtb clinical isolates.

TLCs were run in four different solvent systems. Petroleum Ether: Diethyl Ether 95:5 (v/v) (Panel A); $CHCl_3$: MeOH 9:1 (v/v) (Panel B); $CHCl_3$: MeOH 8:2 (v/v) (Panel C) and $CHCl_3$: MeOH: H_2O 60:25:4 (v/v/v) (Panel D). The migration of specific lipid species is indicated. TDM, trehalose dimycolate; TMM, trehalose monomycolate; CL, cardiolipin; PE, phosphatidyl-ethanolamine; Ac_4PIM_2, tetra-acyl-phosphatidyl-*myo*-inositol-dimannosides; Ac_3PIM_2, tri-acyl-phosphatidylinositol dimannosidase; DIM A, phthiocerol dimycocerosates, DIM B, phthiodiolone dimycocerosates; TAG, triacylglycerol; GroMM, glycerol monomycolate. Data are representative of 2 independent experiments. These data were generated by Dr Gerald Larrouy-Maumus at Imperial College, London.

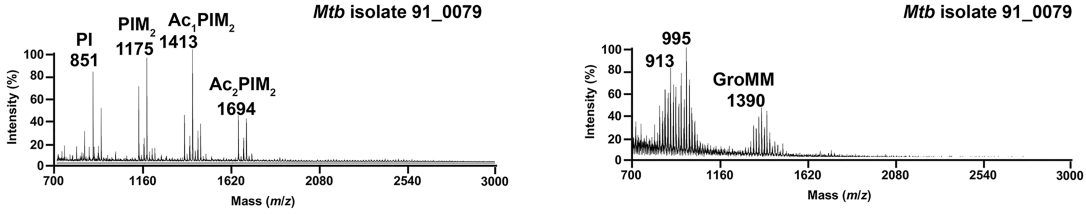
Similarly, in the analysis by MALDI in the negative ion mode, the mass spectra of the mycobacterial strains displayed similar patterns mainly assigned to phosphatidyl-*myo*-inositolmannosides and sulpholipids (SL) in the *Mtb* strains (Fig 2.3.19.2.A.). Analysis by MALDI in the positive ion mode revealed a range of lipids, glycolipids, and species-specific lipids (Fig 2.3.18.2.B.).



B *Mtb* Lineage 2



C *Mtb* Lineage 3



Negative ion mode

Positive ion mode

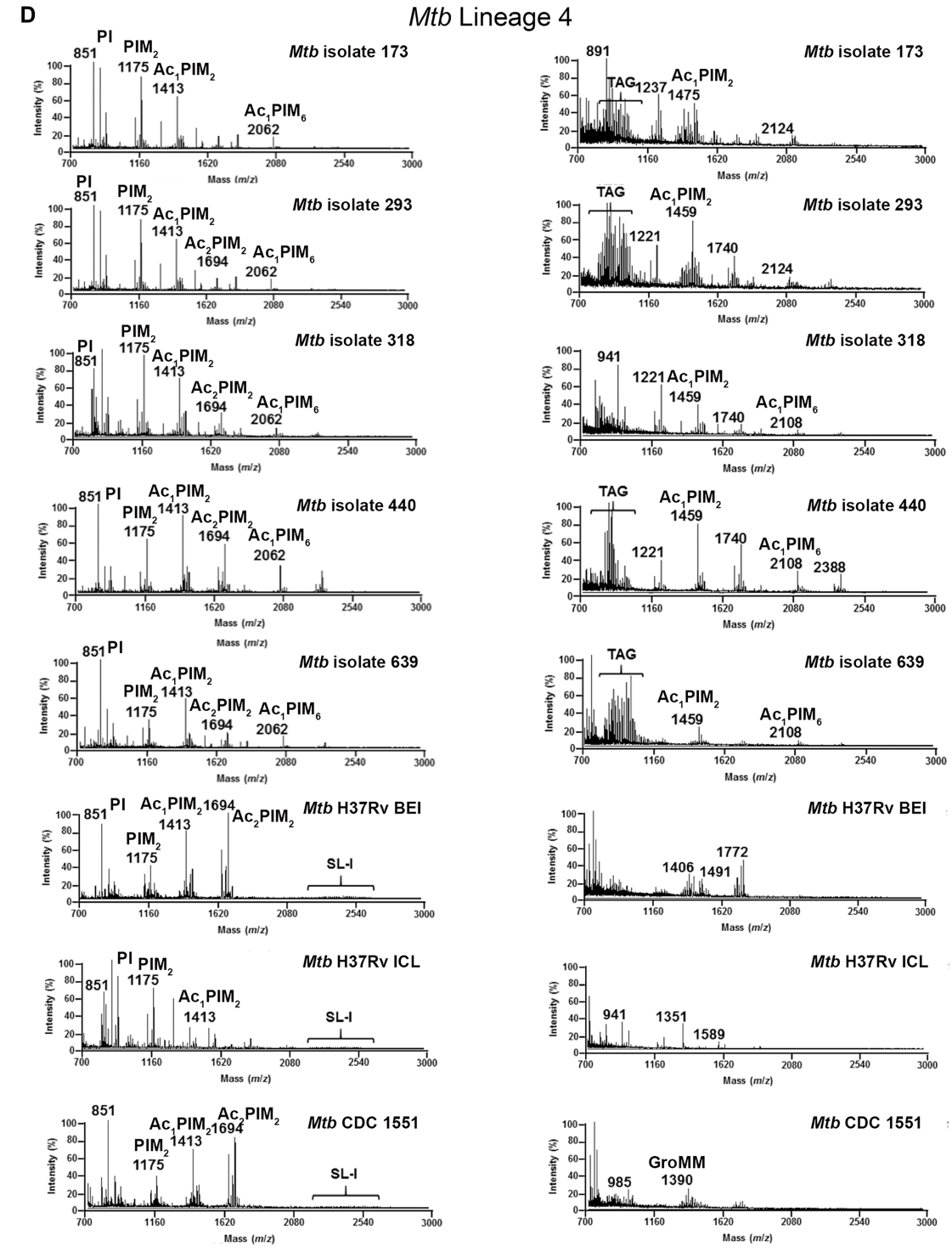

D
Mtb Lineage 4
Mtb isolate 173
Mtb isolate 293
Mtb isolate 318
Mtb isolate 440
Mtb isolate 639
Mtb H37Rv BEI
Mtb H37Rv ICL
Mtb CDC 1551
PI
PIM2
Ac1PIM2
Ac2PIM2
Ac1PIM6
TAG
SL-I
GroMM
PGL
E
M. canettii
Intensity (%)
Mass (m/z)
Negative ion mode
Positive ion mode

Figure 2.3.18.2. MALDI lipid fingerprinting of mycobacteria.

MALDI-ToF mass spectrometry of mycobacterial lipids in negative ion mode (left-hand panels) and positive ion mode (right-hand panels). Panel A, *Mtb* lineage 1; Panel B, *Mtb* lineage 2; Panel C, *Mtb* lineage 3; Panel D, *Mtb* lineage 4; Panel E, *M. canettii*. TAG, Triacylglycerol; SL-1, sulpholipid-1; PI, phosphatidylinositol; PIM_2, di-acyl-phosphatidyl-myo-inositol-dimannosides; Ac_1PIM_2, tri-acylphosphatidyl-*myo*-inositol-dimannosides; Ac_2PIM_2, tretra-acyl-phosphatidyl-*myo*-inositol-dimannosides; Ac_1PIM_6, tri-acyl-phosphatidyl-*myo*-inositol-hexamannosides; Ac_2PIM_2, tretra-acyl-phosphatidyl-myoinositol- hexamannosides; GroMM, glycerol monolycolate; PGL, phenol glycolipid. Molecular masses are indicated. Data are representative of 2 independent experiments. These data were generated by Dr Gerald Larrouy-Maumus at Imperial College, London.

2.4. Discussion

The unexpected phenotypic convergence of NPC cells and cells infected with pathogenic mycobacteria was revealed in a study conducted by Fineran and colleagues [96]. The authors provided extensive evidence of phenocopying between genetically *Npc1*-deficient and mycobacterium-infected cells and provided evidence that lipid-mediated inhibition of Npc1 by *Mtb* induces cell biological changes that facilitate intracellular survival of the pathogen. The proposed mechanism suggested cell wall lipid(s) are shed by the ingested pathogen and reach the LE/Lys, where they inhibit the activity of Npc1. Second, the specific lipid(s) escapes the infected cell and is endocytosed by neighbouring, non-infected cells, where it inhibits the NPC pathway and thereby mediates a bystander cell effect.

A prerequisite of this hypothesis is that inhibitory lipid(s) are widely distributed amongst *Mtb* strains that cause TB and correlate with the ability to survive intracellularly. In the original investigation, studies were limited to the strain H37Rv, which is the most widely used strain for laboratory experimentation and is the accepted *Mtb* reference sequence. However, laboratory stocks of the strain have diverged and evolved genetic changes that impact upon virulence and transmission, meaning its use as a pathogenic model is problematic for generalising conclusions for clinical strains [200]. To address this issue, we investigated whether Npc1 inhibitory activity could be detected in clinically-relevant *Mtb* strains representative of the major geographical lineages that cause TB globally. Lipid extracts of these strains were therefore screened for their ability to induce NPC cellular phenotypes (summarised in Table 2.4.)

NPC Phenotype	Strain 281 lineage 1	Strain 333 lineage 2	Strain 639 lineage 4	Strain H37Rv lineage 4	*M. canettii*
LE/Lys expansion by FACS	Yes	Yes	Yes	Yes	No
LE/Lys expansion by LAMP-1 immunostaining	Yes	Yes	Yes	Yes	No
Increased Npc1/Npc2 protein level	No	No	No	Yes	No
Filipin-positive lysosomal puncta	Yes	Yes	Yes	Yes	No
Increased Total Cholesterol	No	No	No	No	No
GM1 mis-trafficking	Yes	Yes	Yes	Yes	No
Total GSL storage	Yes	Yes	Yes	Yes	No

Table 2.4. Summary of NPC cellular phenotypes induced by TL extracts of representative Mtb clinical strains and M. canettii in RAW 264.7 MΦ.

We confirmed in the previous data [96] that a lipid extract of H37Rv was able to induce expansion of the acidic compartment, demonstrating the robustness of the original finding. Secondly, the extracts had comparable effects on both RAW 264.7 MΦ and primary murine BMDMΦ, showing that induction of the NPC phenotype was not restricted to an immortalised cell line. Genomic phylogeny studies have identified seven prominent lineages of human-adapted mycobacteria that have differential geographic distribution [127]. We therefore sampled multiple strains representative of geographical lineages: Lineage I, East Africa, Philippines and the rim of the Indian Ocean; Lineages 2, East Asia; Lineage 3, East African/Indian and Lineages 4, modern *Mtb* complex of Europe, American and Africa [219]. Cell wall lipid extracts were prepared from twenty strains, encompassing genetic diversity within the lineages. We used FACS

analysis of LysoTracker™ staining intensity as our primary assay since it allowed for relatively high throughput and generated quantitative, statistically-validated data. When tested at a concentration of 100μg/ml, sixteen of the *Mtb* strains induced significant expansion of the acidic compartment as indicated by significantly enhanced staining intensity. Four strains were negative, two were from lineage 1 and two from lineage 2 but were positive when re-tested at a concentration of 200μg/ml lipid. It is possible that the differential potencies reflected lower amounts of the specific NPC1 inhibitory lipid(s) in these strains, but it could also be the consequence of differential recovery during extraction or relative pathogenicity of the strains [220-222]. It will be difficult to distinguish between these possibilities until the identification of the bioactive lipid(s) has been determined (which will be discussed further in Chapter 5). It was notable that six strains, 119, 173, 293, 367, 440 and H37Rv, were capable of expanding relative lysosomal volume to an extent not different from that caused by the pharmacological NPC1 inhibitor, U18666A, which directly binds to and inhibits NPC1 [35].

Probably the most significant result with respect to the relationship between the ability to inhibit Npc1 and *Mtb* ancestry was the finding that *M. canettii* extract did not enhance LysoTracker™ staining intensity in RAW 264.7 MΦ. The MTBC comprises a group of related mycobacteria that can cause tuberculosis in humans or animals [223]. *M. canettii* is a smooth tubercle bacillus (SmTB), which is considered to resemble one of the most recent common ancestors of MTBC [224]. TB cases caused by *M. canettii* infection are rare, geographically restricted to people who have lived or visited the Horn of Africa, with the majority of the

cases from the Republic of Djibouti [225-227]. Interestingly, *M. canettii* lipid extract caused a significant decrease in LysoTracker™ intensity, which, because dye fluorescence is pH-dependent, could be explained perhaps by alkalinisation of the acidic compartment. This may be relevant because *M. canettii* is far less successful at causing disease than *Mtb*. Because there have been relatively few reports of it being responsible for clinical infections [224], it may suggest that it may employ alternative, but less successful mechanisms to achieve intracellular survival. Interestingly, the inability of *M. canettii* to inhibit Npc1 correlates with evidence of impaired infectivity.

As we have mentioned previously, NPC cannot be identified by a single phenotype alone and is characterised by the occurrence of multiple phenotypes. Therefore, it was necessary that we investigated other phenotypes in addition to lysosomal volume, but because performing each of these would have been far more time-consuming, we focused on the representative strains 281, 333, 639 and H37Rv together with *M. canettii*.

Enhanced LysoTracker™ staining intensity measured by FACS is indicative of the greater volume of the acidic compartment but cannot resolve whether this represents an increased frequency of lysosomes or if individually they are larger, or perhaps a combination of the two possibilities. We used confocal microscopy of LysoTracker™ and anti-LAMP-1 staining to demonstrate that treatment with representative *Mtb* lipid extracts affected both parameters, whereas *M. canettii* altered neither. Although microscopy images suggested greater expression of

LAMP-1, this did not correlate with western blotting or qPCR, which would imply a redistribution of the protein in the expanded lysosomes.

Intracellular redistribution of cholesterol to the endo-lysosomal system is a prominent NPC phenotype and was, for many years, the basis for clinical diagnosis [11]. All of the mycobacterial strains examined, except for *M. canettii*, caused lysosomal storage of cholesterol. Quantification of total cholesterol content established that the filipin-positive cholesterol puncta represented intracellular re-distribution of the lipid rather than enhanced level. Important associations between cholesterol and *Mtb* infection have been documented in multiple studies: cholesterol is required for entry into host cells [145], is important for enabling reactivation [146] and is a critical energy source [142]. Furthermore, the *Mtb* genome encodes proteins and enzymes that mediate its transport and catabolism [228]. The accumulation of cholesterol that results from loss of Npc1 activity is, therefore, advantageous to the pathogen.

Perturbation of sphingolipid trafficking and storage of a range of sphingolipid species are features of NPC and have been confirmed in patients, patient-derived cells and in animal and cellular models of NPC disease [11, 26, 78, 229]. In accordance with other NPC phenotypes tested, all of the representative *Mtb* clinical strains affected GM1 trafficking, which resulted in re-distribution of the ganglioside to the lysosome, but localisation of GM1 in *M. canettii* lipid-treated RAW 264.7 MΦ was not different from the vehicle control. *Mtb* produces around 30 types of glycoside hydrolysis, which can either be secreted by bacilli or function in the bacilli, involved in various degradation of nutrient molecules and

the catalysation of bacterial sugar molecules, lipids and proteins [230]. *Mtb* has been shown to interact with neutral GSL, LacCer, on the cell surface to form lipid raft for internalisation [231]. In comparison to cholesterol, it is currently unclear if and how mycobacteria might benefit from changes to the intracellular distribution of specific GSLs that result from Npc1 inhibition, but it deserves further investigation. Similarly, strain 281, 333, 639 and H37Rv caused an accumulation of GSLs in MΦ, consistent with loss of Npc1 activity, whereas incubation with *M. canettii* lipid extract uniquely resulted in a significant decrease in total and specific GSLs.

Previously, BCG infection of RAW 264.7 MΦ was shown to result in a significant increase in Npc1 protein [96], but here, only lipid extract of H37Rv had a comparable effect. We are not fully able to reconcile these data as the investigations differed in the use of live bacteria against lipid extracts as well as the nature of mycobacterial species. In addition, relatively little is currently known about the factors that regulate Npc1 expression [232].

We also reported that *Mtb* lipids significantly impaired pro-IL1β synthesis by LPS-stimulated MΦ. Reduced generation of the cytokine precursor is not currently a recognised NPC phenotype, but unpublished evidence [215] has revealed significantly lower synthesis both *in vivo* and *in vitro*. It is relevant that *Mtb* infection has been shown to limit the generation of IL-1β [233, 234].

The mycobacterial envelope is architecturally and biochemically complex. It is composed of multiple carbohydrates and lipid species [168], and functions as a

permeability barrier [235]. Intercalated within the lipid environment of the cell wall are extractable free lipid species that can influence the balance between pathogen and host by affecting pathogenesis and shaping immune responses [168, 236, 237]. In light of the findings that lipid extracts from strains representative of the four *Mtb* lineages increased the relative LE/Lys volume to differing extents, we performed lipidomic analyses of sixteen clinical isolates, plus the laboratory strain, H37Rv, to explore lipid diversity and the possibility of correlation between bioactivity and lipid composition. We focused on extractable lipids. As seen on the TLCs, qualitatively no differences were observed, whereas quantitatively, there were some differences in the levels/ratios of the respective lipids within and across lineages. MALDI analysis of the mycobacterial strains confirmed these differences: mass spectra in the negative ion mode displayed similar patterns, mainly assigned to phosphatidyl-*myo*-inositol-mannosides [238-241] and sulpholipids [242, 243]. However, mass spectra in the positive ion mode revealed a range of lipids, glycolipids and species-specific lipids, which is in accordance with the published literature [238, 244, 245]. These differences could be a factor influencing the phenotypes observed. In addition, it is known that one of the major surface exposed lipids, lipooligosaccharides (LOS), is absent in *Mtb* as opposed to *M. canettii* due to the mutation within the *pks5* locus abrogating synthesis [223]. LOS could, therefore, be an ideal candidate to explain the suppression of the phenotypes in *M. canettii* compared to *Mtb*, masking more potent surface-exposed lipids in the strains used in this study. It would be of interest in future studies to analyse the lipid extract of *M. canettii* rough morphotype variants I and K, which are deficient for LOS, and test its capacity to induce NPC1 inhibition.

From the current data, we proposed that pathogenic mycobacteria shed lipids that inhibit the activity of the NPC pathway, as shown in Fig 2.4. After phagocytosis by the host cells, pathogenic mycobacteria shed lipids that migrate into the cytosol of host cells to inhibit the NPC1 protein on the LE/Lys membrane, induce NPC cellular phenotypes, including reducing Ca^{2+} levels and therefore preventing vesicle trafficking and fusion events between phagosomes and LE/Lys to facilitate their intracellular survival. The shed lipids are endocytosed by the uninfected neighbouring cells therefore inducing NPC cellular phenotypes as a bystander cell effect.

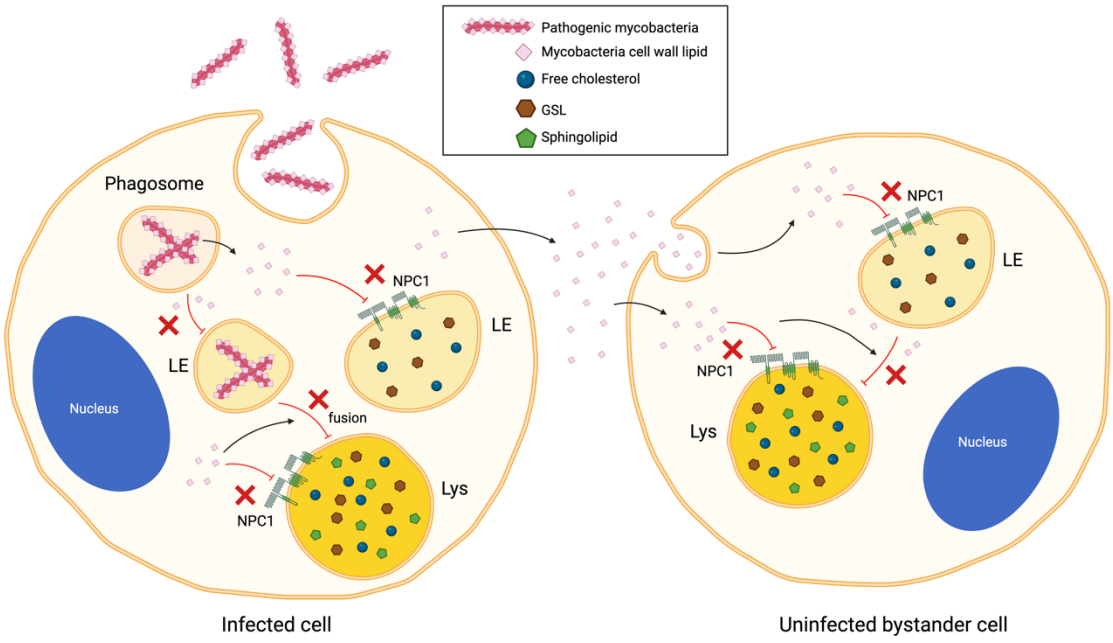


Figure 2.4. Schematic of proposed lipid-mediated inhibition of NPC pathway during pathogenic mycobacteria infection.

Pathogenic mycobacteria are phagocytosed and shed cell wall lipid(s) to the cytosol. The mycobacteria containing vacuole and the shed lipids facilitate the intracellular persistence of bacilli by inhibiting NPC1 activity. The shed lipids can be released from the infected cell and then be endocytosed and induce NPC cellular phenotypes in uninfected neighbouring cells. EE, early endosome; LE, late endosome; Lys, lysosome; GSL, glycosphingolipid.

In summary, the findings presented in this chapter indicate that the lipid-dependent capacity to trigger specific host cell phenotypes indicative of NPC1 inhibition is broadly distributed among pathogenic mycobacteria species and *Mtb* clinical strains. The lack of activity in extracts of the *M. canettii* smooth morphotype is consistent with the hypothesis that the evolution of the lipid(s) that are responsible for NPC1 inhibition occurred after the divergence of MTBC from the ancestral *M. canettii*-like species.

Chapter 3. Other Mycobacteria and the NPC pathway

3.1. Introduction

In the previous chapter, we demonstrated the ability of total lipid extracts of modern human tubercular *Mtb* strains to inhibit NPC1 protein activity in host cells. Whilst *Mtb* is the major causative agent of human TB, *M. bovis* causes comparable disease in cattle and other animals [246]. Both *Mtb* and *M. bovis* are members of MTBC [246]. *Mtb*, along with *M. leprae*, the causative agent of leprosy, are the predominant mycobacteria that infect humans [247]. However, a number of other mycobacteria species, which are collectively known as NTM, are important pathogens that can infect humans, especially immunocompromised individuals [248]. NTM are opportunistic pathogens that typically infect the airways, skin and soft tissues and are not usually transmitted from person to person but are environmentally acquired. Although a large number of NTM species have been identified, those most commonly associated with pulmonary disease are *Mycobacterium avium* (*M. avium*) *complex* (MAC), *Mycobacterium kansasii* (*M. kansasii*) and *Mycobacterium abscessus* (*M. abscessus*). Because the pathology of these pathogens involves the formation of foamy cells and they can survive in host cells, we were interested in determining whether they might also target NPC1 and induce NPC cellular phenotypes.

We selected pathogenic NTM, *M. avium* and *M. abscessus*, which are species that cause the majority of clinical NTM infection cases; *M. leprae*, which is responsible for leprosy; *M. bovis*, a tubercular mycobacterium that causes TB in domestic animals and the non-pathogenic environmental mycobacterium, *M. smegmatis*, to test their ability to inhibit the NPC pathway. We examined the ability of lipid extracts derived from these species to induce NPC cellular

phenotypes in MΦ. In order to provide greater context to these studies, we provide some details about the nature of these mycobacteria and host pathogenesis.

***Mycobacterium abscessus* (*M. abscessus*)**

The *M. chelonae-abscessus* complex is a group of rapid-growing NTM that comprises *M. abscessus* subspecies *abscessus*, *M. abscessus* subspecies *bolletti*, *M. abscessus* subspecies *massiliense*, *Mycobacterium chelonae* and *Mycobacterium fortuitum* [118]. *M. abscessus* is a water-born mycobacteria [249] that has limited human-to-human transmission [250]. The majority of cases of *M. abscessus* infection are believed to be nosocomial, but the precise route of transmission is frequently not clear [251]. *M. abscessus* is an opportunistic pathogen and the morbidity is increased by host factors, including immunodeficiency, such as in HIV infection and genetic conditions, such as cystic fibrosis and lung diseases, that include chronic obstructive pulmonary diseases (COPD) and bronchiectasis [250-253]. Healthy individuals usually resist the infection [251]. The incidence rate of *M. abscessus* infection varies between 2.6% to 13% of all mycobacterial pulmonary infections across different sites [250, 252, 254-256]. *M. abscessus* primarily persists in the lung and results in lung lesions characterised by the formation of granuloma. Cell membrane proteins and lipids play important roles during *M. abscessus* infection and pathogenicity [257]. The two variants of *M. abscessus* display differential virulence, with the rough (R) variant being more virulent in the zebrafish model of infection than the smooth (S) variant [258]. The R variant lacks the production of glycopeptidolipids (GPL), which are transported to the outer mycobacterial membrane by MmpL4 proteins

in the S variant [259]. The R variant can form a serpentine cording morphology and trigger pro-inflammatory responses and MΦ apoptosis and thereby persist extracellularly [260, 261]. Other mycolic acid-associated lipid components from *M. abscessus*, such as PIM_2, can induce activation of TLR2 to promote the production of TNF-α-mediated inflammation [262]. Similar to *Mtb*, TDM on the outer membrane of *M. abscessus* is necessary for granuloma formation [263]. Macrolide drugs, including clarithromycin, amikacin and cefoxitin, are the current antimicrobial treatments for *M. abscessus* infections, which have a success rate of approximately 45.6% [264]. Currently, no vaccine is available to prevent *M. abscessus* infection [265] and the efficacy of drug treatments is limited by the emergence of antimicrobial resistance [249, 266].

***Mycobacterium avium* (*M. avium*)**

The MAC is the most common species of NTM associated with pulmonary diseases, accounting for approximately 80% of all cases [267, 268]. The two major species of mycobacteria belonging to MAC are *M. avium* and *Mycobacterium intracellulare* [268]. *M. avium* is a heterogeneous group of four subspecies: *M. avium* subspecies *avium*, *M. avium* subspecies *silvatium*, *M. avium* subspecies *hominissuis*, and *M. avium* subspecies *paratuberculosis* [269]. *M. avium* is a slow-growing environmental mycobacterium that can be isolated from water, soil or house dust and infect humans via the respiratory or intestinal tracts [270]. No example of human-to-human transmission has been reported [271]. It is an opportunistic pathogen that is able to persist within MΦ and avoid host immune clearance mechanisms [271]. Similar to *M. abscessus*, patients with compromised immunity, such as those suffering from HIV infection, having pre-

existing pulmonary disease and under immunosuppressive regimes (such as anti-TNF-α therapy) are more susceptible to infection with *M. avium* [271]. It primarily causes pulmonary nodule lesions and bronchiectasis in patients with no underlying lung disease and also causes cavitation in patients with COPD or hypersensitivity pneumonia in immunocompetent individuals [271]. *M. avium* infection results in the formation of foamy MΦ characterised by cholesterol accumulation [272]. Similar to *M. abscessus*, the rough morphotype of *M. avium* shows greater virulence in human MΦ and murine infections [273]. *M. avium* achieves successful intracellular persistence by inhibiting phagosome-lysosome fusion [274] and preventing phagosome acidification [270, 275], which is similar to the activities of *Mtb*. The cell wall lipid component of *M. avium*, GPL, can modulate host MΦ immune responses to affect phagosome-lysosome fusion via the inactivation of TLR2 receptor and downregulation of NF-κB pathway activation [276]. Treatment of MAC infection is usually a combination of macrolide antimicrobial drugs, but the precise regime is determined at the level of the individual because of the necessary extended duration of treatment [271].

***Mycobacterium leprae* (*M. leprae*)**

M. leprae is not an NTM but is a slow-growing mycobacterium that causes leprosy. It is endemic in specific locations in the Americas, Asia and Africa, and approximately 200,000 new cases are reported each year [247]. Interestingly, leprosy can also be caused by a distinct species of mycobacterium, *Mycobacterium lepromatosis* [116]. *M. leprae* primarily infects skin MΦ and myelin-producing Schwann cells in the nervous system, resulting in skin lesions and peripheral nerve damage [247, 277]. Although precise routes of transmission

are not fully understood, there is good verification for airborne transmission of *M. leprae* between individuals living in close proximity [278]. Additional natural hosts and animal reservoirs of *M. leprae* have been identified, which are principally armadillo species (nine-banded, USA), non-human primates and unexpectedly red squirrels in the UK [278]. Although unequivocal evidence of transmission from these species to humans is not yet available, the strongest suspicions point to armadillos, primates and perhaps insects (e.g. amoebae and mosquitos) sources [247, 279, 280]. The pathology of *M. leprae* infection is seen as granulomatous local skin lesions and the formation of foamy MΦ that is consistent with localised inflammation and the absence of systemic inflammatory responses [281, 282]. Live *M. leprae* infection inhibits phagosome-lysosome fusion and the autophagic clearance of the mycobacteria [283, 284]. Specific lipid components of the *M. leprae* membrane are associated with pathogenicity. For example, LAM and PGL-I regulate the immune response in the host cells, and PGL-I is used as a biomarker for leprosy diagnosis [285, 286]. PGL-I from *M. leprae* can suppress cytokine secretion, anchor bacterium to Schwann cells and promote demyelination and mitochondrial damage, resulting in neural loss [287-289]. Both infected MΦ and Schwann cells are characterised by lipid droplet accumulation with storage of both triacylglycerol (TAG) and cholesterol, which is likely caused by mycolic acid-containing *M. leprae* cell wall lipids [290, 291]. Combined rifampicin, clofazimine, dapsone, minocycline and ofloxacin anti-microbial drugs are recognised treatments for leprosy [292]. However, the efficacy of treatments is still restricted by the development of antimicrobial resistance [293].

***Mycobacterium bovis* (*M. bovis*)**

M. bovis is primarily responsible for TB in cattle and other domesticated animals, but it can also be transmitted to humans and cause human TB [246]. Although human TB caused by *M. bovis* infection is rare (about 1% of total TB cases), it is concerning for those individuals at high risk, including those living in rural environments and have agricultural and animal-related occupations [294]. MΦ infected with *M. bovis* become foamy in appearance with lipid accumulation and alterations in lipid metabolism, thereby resembling the changes observed with *Mtb* [295, 296]. Lipid components of the cell membrane of *M. bovis*, PDIM and PGL, influence host-pathogen interactions and modulate the immune responses [297]. An attenuated strain of *M. bovis*, BCG, is used as a vaccine to prevent TB in young children [298].

***Mycobacterium smegmatis* (*M. smegmatis*)**

M. smegmatis is a non-pathogenic, fast-growing environmental mycobacterium that is commonly found in soil, water, and plants [299]. Due to its non-pathogenicity, similarities to *Mtb*, isolation of genetically traceable mc^2155 mutant, along with the subsequent development of experimental tools such as episomal plasmids that facilitate transformation, *M. smegmatis* has become an established model mycobacteria for *Mtb*-related research [300]. Unlike pathogenic mycobacteria, *M. smegmatis* cannot persist in host cells [301]. Although *M. smegmatis* is non-pathogenic, a small number of cases of skin infection and cardiomediastinal tuberculoma have been documented [302-304]. Limited research has been focused on the roles of cell wall lipid components of *M. smegmatis* during infection, but the lipid compositions (including mycolic acid-

containing lipids and mannan-containing lipids) on the cell wall are essential for the growth of *M. smegmatis* and biofilm formation [305-307].

Aims

In this chapter, we investigated whether the NPC pathway is inhibited by total cell wall lipid extract prepared from pathogenic NTM (*M. abscessus* and *M. avium*), *M. leprae*, non-human tubercular *M. bovis* and non-pathogenic *M. smegmatis*.

3.2. Material and methods

3.2.1. Cells

RAW 264.7 MΦ were obtained and cultured as described in Section 2.2.1.

3.2.2. Mycobacterial culture and cell wall lipid extraction

Mycobacteria were grown, and the cell wall lipids were extracted as described in Section 2.2.2. NTM, *Mycobacterium abscessus* (ATCC19977) and *Mycobacterium avium* subspecies *avium* (ATCC 25291) (referred to as *M. avium*), and the environmental species, *Mycobacterium smegmatis* mc2155 (ATCC 700084) were cultured and the cell wall lipid extract was prepared at Imperial College, London. *Mycobacterium bovis*, Strain AF 2122/97 (ATCC BAA-935), total lipids, NR-44100; *Mycobacterium leprae,* total lipids, NR-19332 were obtained from BEI Resources (NIH).

3.2.3. Lipid solubilisation and addition to cell culture

Lipid solubilisation was performed as described in Section 2.2.3. RAW 264.7 MΦ were treated with 100μg/ml mycobacterial lipids for 48h.

3.2.4. LysoTracker™ staining for FACS analysis

LysoTracker™ staining was performed as described in Section 2.2.4.

3.2.5. Immunofluorescence staining

LAMP-1 immunostaining of RAW 264.7 MΦ treated with mycobacterial lipids was performed as described in Section 2.2.10.

3.2.6. Filipin staining of cholesterol

Filipin staining of RAW 264.7 MΦ for free cholesterol was performed as described in Section 2.2.11.

3.2.7. Amplex Red assay determination of cholesterol

Total cholesterol level was measured with the Amplex Red assay kit as described in Section 2.2.12.

3.2.8. CtxB staining

CtxB staining to analyse GM1 trafficking in RAW 264.7 MΦ treated with mycobacterial lipids was performed as described in Section 2.2.13.

3.2.9. Analysis and quantification of GSLs by NP-HPLC

Cell lysate preparations for GSL analysis were performed as described in Section 2.2.14. GSL analysis was performed as described in Section 2.2.14.

3.2.10. Statistical analysis

Statistical analyses were performed as described in Section 2.2.16.

3.3. Results

3.3.1. TL extracts of *M. abscessus*, *M. avium* and *M. bovis*, but not *M. leprae* or *M. smegmatis*, increase LysoTracker™ staining intensity of RAW 264.7 MΦ.

In the previous chapter, we demonstrated the ability of cell wall lipids of modern clinical human *Mtb* strains to inhibit NPC1 protein and induce NPC cellular phenotypes. Here, we investigated whether TL extracts of another member of MTBC (*M. bovis*); NTM, including the pathogenic mycobacteria (*M. abscessus*, *M. avium*); leprosy-causing agent (*M. leprae*); and non-pathogenic mycobacteria (*M. smegmatis*) also inhibit NPC1 activity.

After treating RAW 264.7 MΦ with mycobacteria lipid extract as indicated above (100μg/ml for 48h), cells were stained with LysoTracker™ Green DND-26 and analysed by FACS. TL extracts of *M. abscessus*, *M. avium* and *M. bovis* induced a significant increase in LysoTracker™ staining intensity to a level comparable with *Mtb* H37Rv TL extract (Fig. 3.3.1.). TL extracts of *M. leprae* and non-pathogenic *M. smegmatis* did not significantly increase the intensity of LysoTracker™ staining (Fig. 3.3.1.).

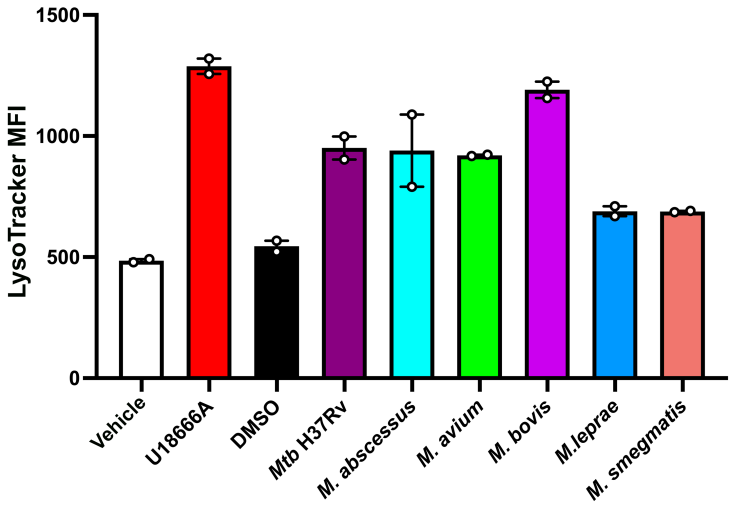


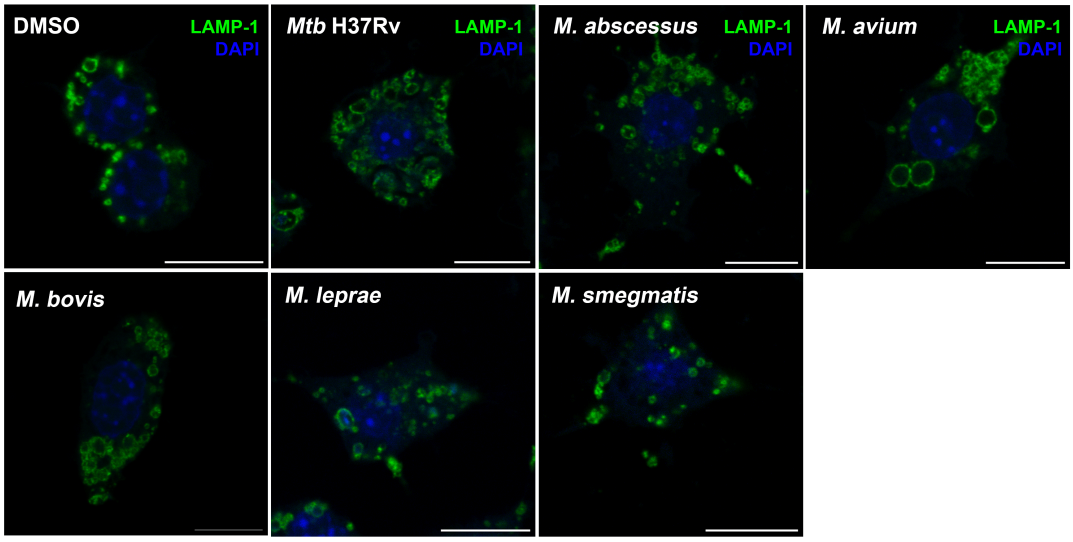
Figure 3.3.1. TL extracts of M. abscessus, M. avium and M. bovis, but not M. leprae and M. smegmatis, significantly increase LysoTracker™ staining intensity of RAW 264.7 MΦ.

RAW 264.7 MΦ were treated with TL extract of NTM, *M. bovis*, *M. leprae* and *M. bovis* (100µg/ml for 48h), stained with LysoTracker™ Green DND-26 and analysed by FACS. DMSO and U18666A (2µg/ml for 48h) treatments were vehicle and positive controls respectively. MFI, mean fluorescence intensity. Data are mean ± SEM, n=2. Data are representative of 2 independent experiments.

3.3.2. TL extracts of *M. abscessus*, *M. avium*, *M. bovis* and *M. leprae*, but not *M. smegmatis*, induce expansion of LE/Lys in RAW 264.7 MΦ.

We investigated if the size of individual LE/Lys was increased in RAW 264.7 MΦ after treatment with TL extracts of *M. abscessus*, *M. avium*, *M. bovis*, *M. leprae* and *M. smegmatis* by immunostaining for LAMP-1 protein. Lysosomal diameter was significantly increased in RAW 264.7 MΦ treated with TL extract *M. abscessus*, *M. avium*, *M. bovis* and *M. leprae* (****p<0.0001, Fig 3.3.2.A.B.), but to a lesser extent with TL extract of *M. smegmatis* (p=0.0119, Fig 3.3.2.A.B.). A histogram of lysosomal size distribution frequency confirmed a shift towards larger lysosomal diameter and increased median lysosomal diameter value with TL extracts of all of the mycobacteria with the exception of the non-pathogenic *M. smegmatis* (Fig 3.3.2.C.).

A



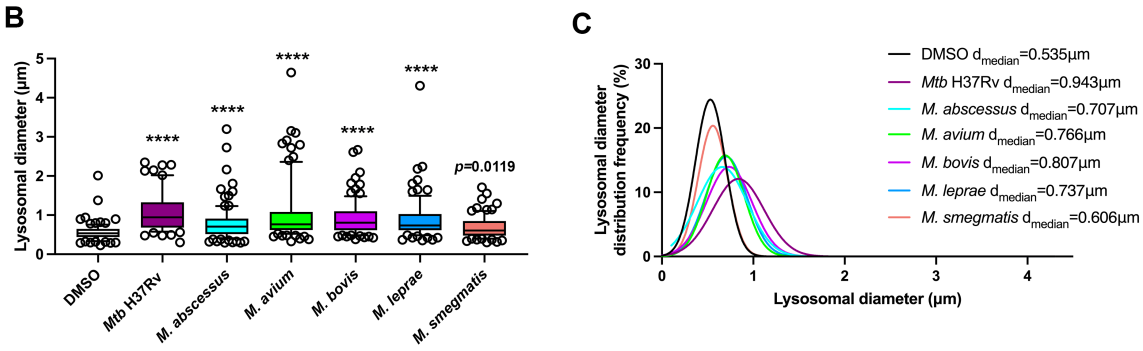


Figure 3.3.2. TL extract of M. abscessus, M. avium, M. bovis and M. leprae, but to a much lesser extent M. smegmatis, induce significant expansion of LE/Lys in RAW 264.7 MΦ visualised by LAMP-1 immunostaining.

RAW 264.7 MΦ were treated with TL extract (100µg/ml for 48h) and stained with anti-LAMP-1 antibody. DMSO represents the vehicle control. Panel A. Representative confocal microscopy images of stained RAW 264.7 MΦ. LAMP-1, green; DAPI, blue. Scale bar represents 10µm. Panel B. Mean lysosomal diameter in treated cells. n>100 for at least 3 cells from random fields. Box and whisker plot, box contains 90% of events. Statistical analysis, Kruskall-Wallis test. ****p<0.0001, other p values as indicated. Statistical comparisons of lipid treatments are relative to DMSO controls. Panel C. Histogram of lysosomal diameter distribution in treated cells. Bin width, 0.1µm. DMSO: min: 0.229µm, max: 2.01µm, centre: 0.535µm; *Mtb* H37Rv: min: 0.303µm, max: 2.35µm, centre: 0.943µm; *M. abscessus*: min: 0.292µm, max: 3.20µm, centre: 0.707µm; *M. avium*: min: 0.327µm, max: 4.64µm, centre: 0.766µm; *M. bovis*: min: 0.381µm, max: 2.67µm, centre: 0.807µm; *M. leprae*: min: 0.351µm, max: 4.31µm, centre: 0.737µm; *M. smegmatis*: min: 0.301µm, max: 1.71µm, centre: 0.606µm. Statistical analysis, Gaussian distribution.

3.3.3. TL extracts of *M. abscessus*, *M. bovis* and *M. leprae*, but not *M. avium* and *M. smegmatis,* induce cholesterol accumulation in the endo-lysosomal system of RAW 264.7 MΦ.

In Chapter 2, we showed that lipid extracts of *Mtb* strains induced lysosomal accumulation of free cholesterol, which is an NPC cellular phenotype revealed by positive filipin staining (Section 2.3.13.). We therefore tested if TL extracts of *M. abscessus*, *M. avium*, *M. bovis*, *M. leprae* and *M. smegmatis* have the same effect on RAW 264.7 MΦ. We observed a significantly increased frequency of cells with intracellular filipin-positive puncta in RAW 264.7 MΦ treated with TL extracts of the above species (red arrows, Fig 3.3.3.A.B.). The frequency of puncta-positive cells exposed to *M. bovis* and *M. leprae* was not different to that seen with *Mtb* H37Rv TL (****p<0.0001, Fig 3.3.3.B.), but the frequency of filipin-positive cells was lower in RAW 264.7 MΦ treated with TL extract of *M. abscessus* (p=0.0260, 36.11% filipin positive cells) and was further reduced for *M. avium* (p=0.0025, 20.58% filipin positive cells) and *M. smegmatis* (p=0.0096, 25.21% filipin positive cells) (Fig 3.3.3.B.). Interestingly, TL extract of *M. leprae* induced needle-like structures of free cholesterol accumulation, which was not observed with other extracts (red arrowhead, Fig 3.3.3.A.).

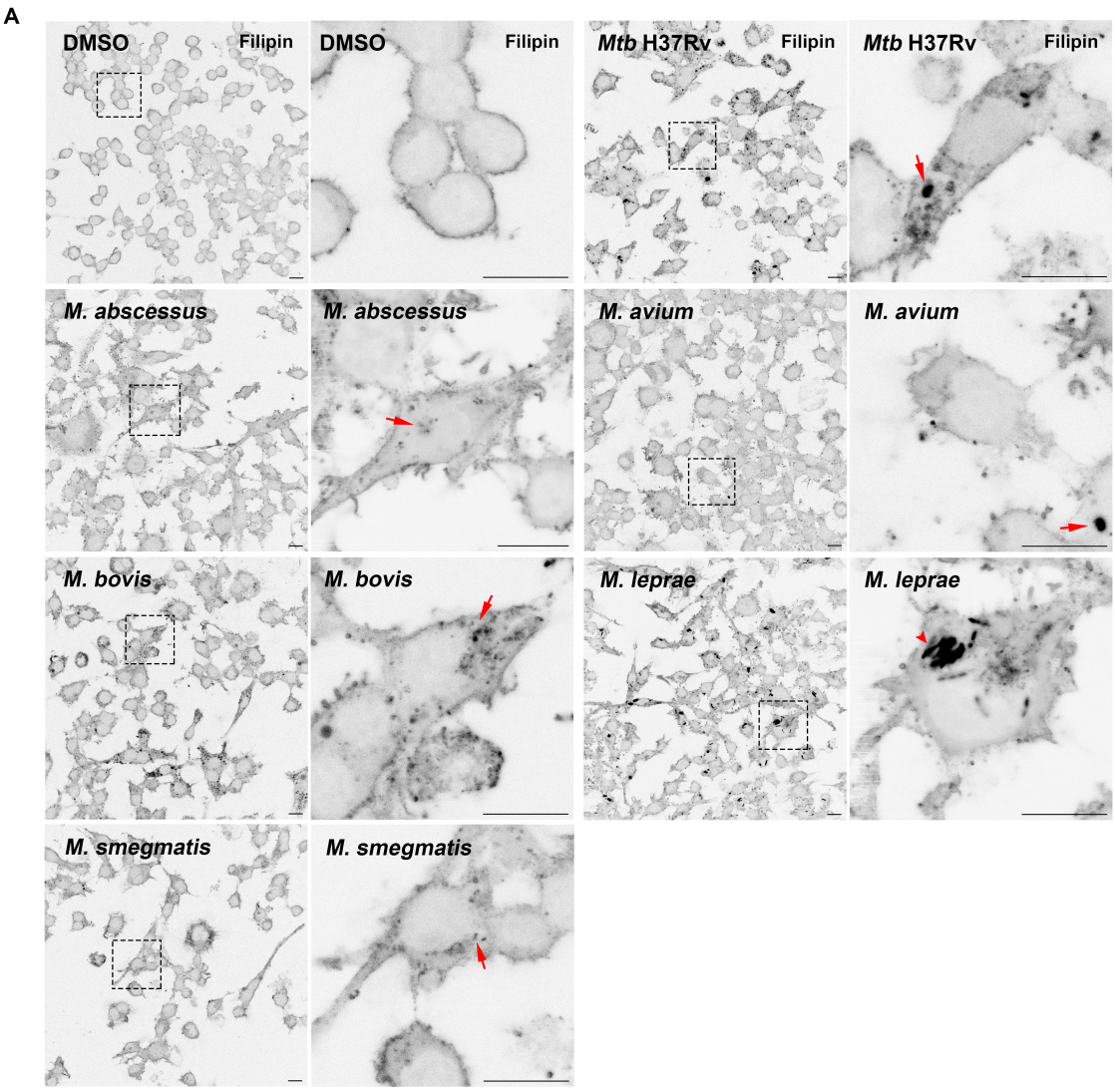

A
DMSO
Filipin
DMSO
Filipin
Mtb H37Rv
Filipin
Mtb H37Rv
Filipin
M. abscessus
M. abscessus
M. avium
M. avium
M. bovis
M. bovis
M. leprae
M. leprae
M. smegmatis
M. smegmatis
B
% Cells with Filipin positive intracellular puncta
100
80
60
40
20
0
p=0.0002
p=0.0260
p=0.0025
****
****
p=0.0096
DMSO
Mtb H37Rv
M. abscessus
M. avium
M. bovis
M. leprae
M. smegmatis

Figure 3.3.3. TL extracts of M. abscessus, M. avium, M. bovis, M. leprae and M. smegmatis induce a partial redistribution of cholesterol to intracellular puncta in RAW 264.7 MΦ.

RAW 264.7 MΦ were treated with TL extract (100μg/ml for 48h) and stained filipin for free cholesterol. DMSO is vehicle control. Panel A. Representative confocal microscopy images of treated cells. Red arrows indicate filipin puncta; red arrowheads indicate needle-like cholesterol structures. Filipin, black. Scale bar represents 10μm. For each pair, the right image is a higher magnification of the region outlined in the left image. Panel B. Frequency of cells with filipin-positive intracellular puncta. Data are mean ± SEM, n=5. Statistical analysis, Welch ANOVA test with Dunnett multiple comparisons. ****$p<0.0001$, other p values as indicated. Statistical comparisons of lipid treatments are relative to DMSO controls. Data is representative of 2 independent experiments.

3.3.4. TL extracts of *M. abscessus*, *M. bovis*, *M. leprae* or *M. avium* do not affect cholesterol content of RAW 264.7 MΦ, but significantly increased by *M. smegmatis* extract.

The cholesterol content of RAW 264.7 MΦ treated with TL extracts was measured by Amplex Red assay. There was no significant alteration to cholesterol content in cells treated with TL extracts of *M. abscessus*, *M. avium*, *M. bovis* or *M. leprae* (Fig 3.3.4.), but a significant increase was detected in cells treated with TL extract of *M. smegmatis* (*p*=0.0441, Fig 3.3.4.).

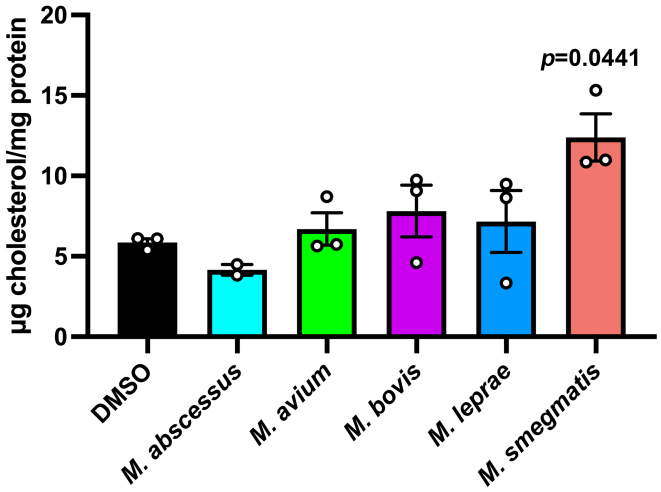


Figure 3.3.4. TL extracts of M. abscessus, M. bovis, M. leprae or M. avium do not affect cholesterol content, while M. smegmatis significantly increased it in RAW 264.7 MΦ.

RAW 264.7 MΦ were treated with TL extract (100µg/ml for 48h), and cholesterol content was measured by Amplex Red assay. DMSO served as vehicle control. Data are mean ± SEM, n=2 or 3. Statistical analysis, Welch's t-test. *p* values as indicated, otherwise not significant. Statistical comparisons of lipid treatments are relative to the DMSO control.

3.3.5. TL extracts of *M. abscessus*, *M. bovis*, *M. leprae*, *M. avium* and *M. smegmatis* perturb GM1 ganglioside intracellular trafficking in RAW 264.7 MΦ.

Miss-trafficking and lysosomal accumulation of GM1 ganglioside were assessed by incubating lipid-treated RAW 264.7 MΦ with fluorescently labelled CtxB. Imaging by confocal microscopy revealed an accumulation of fluorescent puncta in lysosomes of cells treated with TL extract of *M. abscessus*, *M. avium*, *M. leprae*, *M. bovis* and *M. smegmatis* (red arrows, Fig 3.3.5.A.). The frequency of cells with lysosomal GM1 puncta was significantly increased in RAW 264.7 MΦ treated with TL extracts of *M. abscessus* (p=0.0008), *M. avium* (p=0.0007), *M. leprae* (p=0.0002), *M. bovis* (p=0.0047) and *M. smegmatis* (p=0.0003) (Fig 3.3.5.B.). These frequencies were not significantly different from that of cells exposed to *Mtb* H37Rv TL (p=0.0005, Fig 3.3.5.B.)

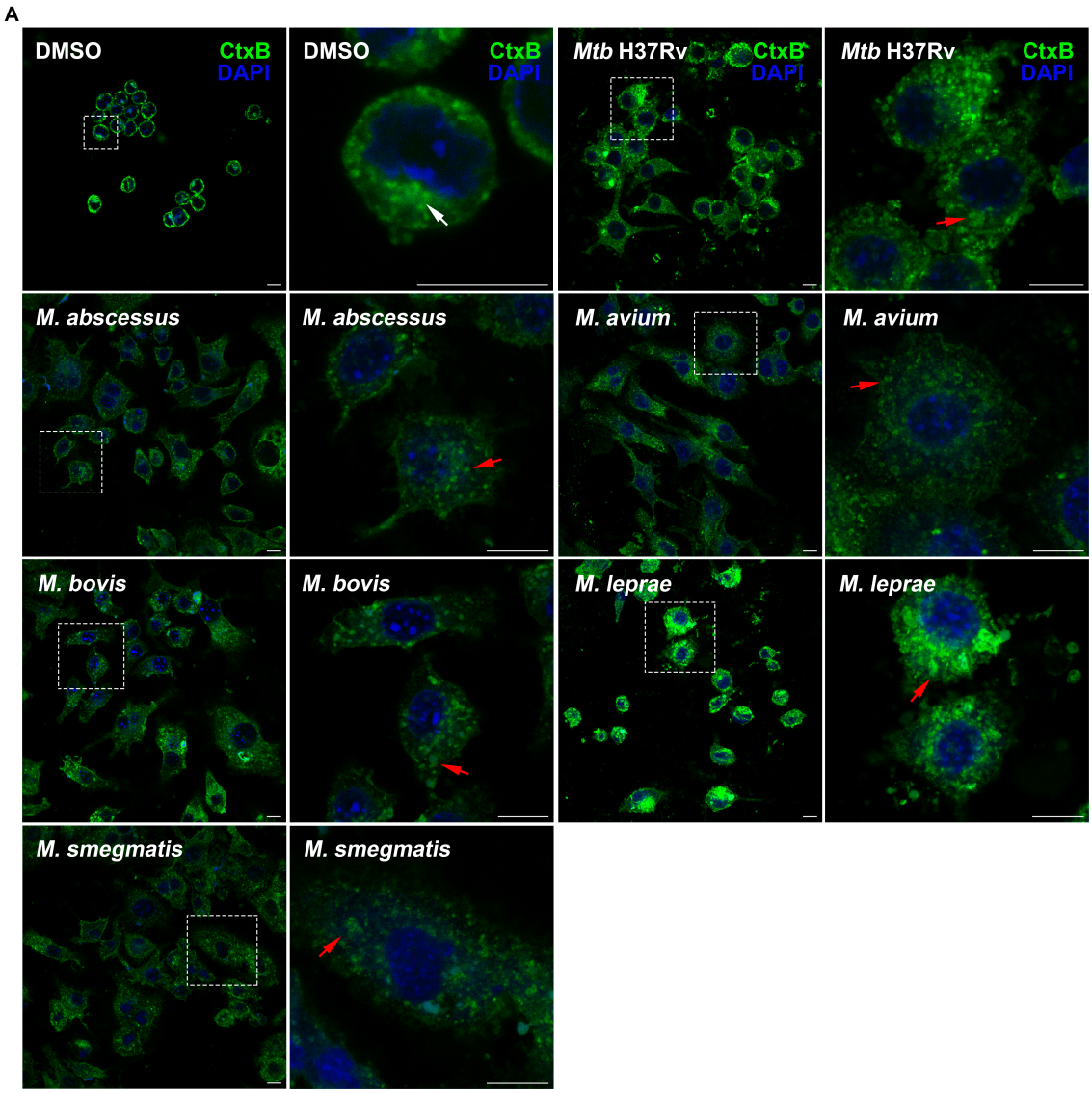

A
DMSO
CtxB
DAPI
DMSO
CtxB
DAPI
Mtb H37Rv
CtxB
DAPI
Mtb H37Rv
CtxB
DAPI
M. abscessus
M. abscessus
M. avium
M. avium
M. bovis
M. bovis
M. leprae
M. leprae
M. smegmatis
M. smegmatis
B
% Cells with lysosomal Cholera Toxin B localisation
100
50
0
p=0.0005
p=0.0008
p=0.0007
p=0.0002
p=0.0047
p=0.0003
DMSO
Mtb H37Rv
M. abscessus
M. avium
M. bovis
M. leprae
M. smegmatis

Figure 3.3.5. TL extracts of M. abscessus, M. avium, M. bovis, M. leprae and M. smegmatis perturb GM1 ganglioside intracellular trafficking in RAW 264.7 MΦ.

RAW 264.7 MΦ were treated with TL extract (100μg/ml for 48h) and pulse chased with CtxB. DMSO served as vehicle control. Panel A. Representative confocal microscopy images of GM1 distribution in cells revealed by CtxB staining. CtxB, green; DAPI, blue. Scale bar represents 10μm. White arrows indicate Golgi distribution; red arrows indicate lysosomal distribution. For each pair, the right image is a higher magnification of the region outlined in the left image. Panel B. Frequency of cells showing lysosomal GM1 distribution in treated RAW 264.7 MΦ. Data are mean ± SEM, n=3, each representing a minimum of 100 cells in randomly selected fields per sample. Statistical analysis, Welch ANOVA test with Dunnett multiple comparisons. *p* values as indicated. Statistical comparisons of lipid treatments are relative to DMSO controls. Data are representative of 2 independent experiments.

3.3.6. Levels of identified GSL species are changed significantly in RAW 264.7 MΦ treated with TL extracts of specific mycobacteria.

Incubation of RAW 264.7 MΦ with TL extracts of *Mtb* strains resulted in a statistically significant accumulation of specific GSL species (Section 2.3.17.). We therefore examined whether incubations with TL extracts of *M. abscessus*, *M. avium*, *M. bovis*, *M. leprae* and *M. smegmatis* had the same effects. GSLs were measured by NP-HPLC analysis. Total GSL in RAW 264.7 MΦ was significantly increased following treatment with TL extract of *M. avium* (p=0.0075) and *M. smegmatis* (p=0.0007), was significantly decreased by exposure to *M. abscessus* TL (p=0.0363, Fig 3.3.6.A.) and was unchanged by incubation with TL

of *M. bovis* or *M. leprae* (Fig 3.3.6.A.). The amount of GlcCer was not significantly increased by any of the mycobacterial lipid extracts tested but was significantly decreased in cells treated with TL extract of *M. abscessus* (****$p<0.0001$) and *M. bovis* ($p=0.0002$, Fig 3.3.6.B.).

With respect to individual GSL species, TL extract of *M. avium* induced a significant increase in GA2 ($p=0.0014$), Gb3 ($p=0.0439$), GM3 ($p=0.0063$), GM2 ($p=0.0022$), GA1 ($p=0.0008$), GM1a ($p=0.0018$) and GM1b ($p=0.0079$) (Fig 3.3.6.C.). TL extract of *M. abscessus* increased the amount of GA1 ($p=0.0298$) but significantly decreased the level of GM1b ($p=0.0249$) and GD1a ($p=0.0029$) (Fig 3.3.6.C.). TL extract of *M. bovis* caused a significant increase in GM3 ($p=0.0021$), GM2 ($p=0.0005$), GA1 ($p=0.0103$) and GM1a ($p=0.0460$), but a significant decrease in GD1a ($p=0.0370$) (Fig 3.3.6.C.). Only GM2 level ($p=0.0238$) was significantly increased with TL extract of *M. leprae* (Fig 3.3.6.C.). Finally, TL extract of *M. smegmatis* induced significant increases in GA2 ($p=0.0098$), GM3 ($p=0.0063$), GM2 (****$p<0.0001$), GA2 (****$p<0.0001$), GM1a (****$p<0.0001$) and GM1b ($p=0.0011$) (Fig 3.3.6.C.). These results are summarised in Table 3.3.6.

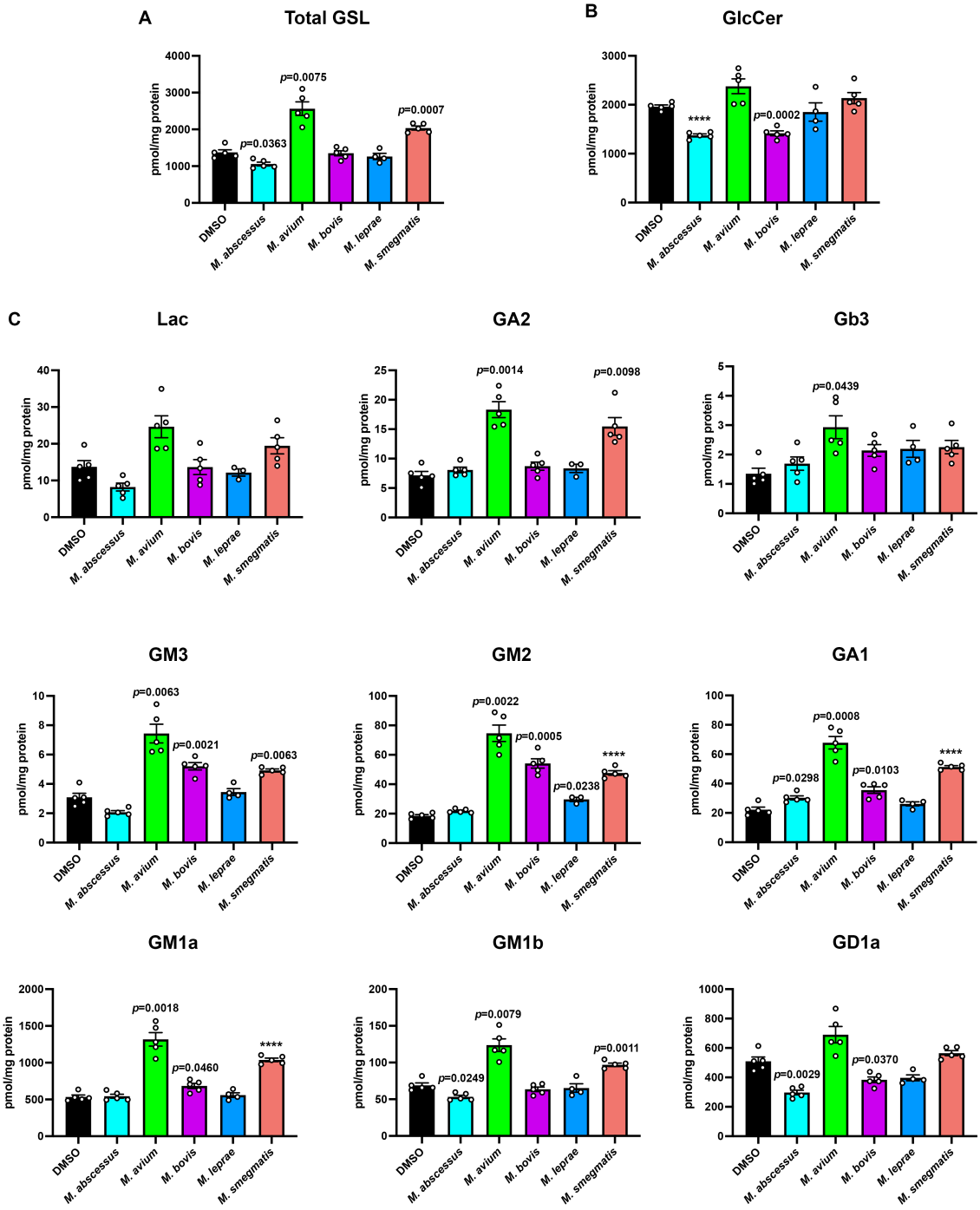

A
Total GSL
pmol/mg protein
p=0.0363
p=0.0075
p=0.0007
B
GlcCer
****
p=0.0002
C
Lac
GA2
p=0.0014
p=0.0098
Gb3
p=0.0439
GM3
p=0.0063
p=0.0021
p=0.0063
GM2
p=0.0022
p=0.0005
****
p=0.0238
GA1
p=0.0008
p=0.0298
p=0.0103
****
GM1a
p=0.0018
p=0.0460
****
GM1b
p=0.0079
p=0.0249
p=0.0011
GD1a
p=0.0029
p=0.0370
DMSO
M. abscessus
M. avium
M. bovis
M. leprae
M. smegmatis

Figure 3.3.6. Levels of identified GSL species are changed significantly in RAW 264.7 MΦ treated with TL extracts of specific mycobacteria. RAW 264.7 MΦ were treated with TL extract (100µg/ml for 48h), and GSLs analysed by NP-HPLC. DMSO served as vehicle control. Panel A, Total GSLs; Panel B, GlcCer; Panel C, individual GSL species; in mycobacterial TL extract treated cells. Data are mean ± SEM, n=5 or 4. Statistical analysis, Welch ANOVA test with Dunnett multiple comparisons. ****$p<0.0001$, other p values as indicated, otherwise not significant. Statistical comparisons of lipid treatments are relative to DMSO controls.

GSL species	*M. abscessus*	*M. avium*	*M. bovis*	*M. leprae*	*M. smegmatis*
Lac	ns 0.60±0.08	ns 1.80±0.22	ns 0.99±0.15	ns 0.89±0.07	ns 1.42±0.16
GA2	ns 1.13±0.07	*p*=0.0014 2.56±0.19	ns 1.22±0.10	ns 1.17±0.10	*p*=0.0098 2.16±0.21
Gb3	ns 1.25±0.04	*p*=0.0439 2.17±0.21	ns 1.59±0.08	ns 1.63±0.08	ns 1.67±0.03
GM3	ns 0.67±0.04	*p*=0.0063 2.41±0.21	*p*=0.0021 1.68±0.08	ns 1.12±0.08	*p*=0.0063 1.59±0.03
GM2	ns 1.18±0.03	*p*=0.0022 4.02±0.30	*p*=0.0005 2.92±0.17	*p*=0.0238 1.60±0.08	**** 2.57±0.08
GA1	*p*=0.0298 1.36±0.06	*p*=0.0008 3.05±0.19	*p*=0.0103 1.60±0.10	ns 1.18±0.06	**** 2.31±0.04
GM1a	ns 1.02±0.05	*p*=0.0018 2.47±0.17	*p*=0.0460 1.28±0.07	ns 1.05±0.06	**** 1.94±0.05
GM1b	*p*=0.0249 0.77±0.03	*p*=0.0079 1.79±0.12	ns 0.92±0.05	ns 0.95±0.09	*p*=0.0011 1.41±0.03
GD1a	*p*=0.0029 0.58±0.03	ns 1.35±0.11	*p*=0.0370 0.75±0.04	ns 0.78±0.04	ns 1.11±0.03
Total GSL	*p*=0.0363 0.77±0.04	*p*=0.0075 1.87±0.13	ns 0.98±0.05	ns 0.92±0.06	*p*=0.0007 1.48±0.04
GlcCer	**** 0.70±0.02	ns 1.21±0.08	*p*=0.0002 0.72±0.02	ns 0.94±0.10	ns 1.09±0.06

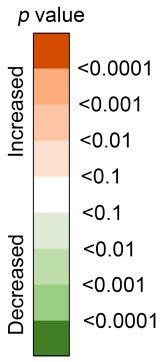


Table 3.3.6. Summary of changes to identified GSL species are changed significantly in RAW 264.7 MΦ treated with TL extracts of specific mycobacteria.

Numbers represent the mean fold change compared with DMSO control. Data are mean ± SEM, n=5. Statistical analysis, Welch's t-test. ****p<0.0001, other p values as indicated, otherwise not significant. Statistical comparisons of lipid treatments are relative to DMSO controls. Levels that significantly increased are marked red, and those that significantly decreased are marked green.

3.4. Discussion

In this chapter, we examined the induction of the NPC cellular phenotypes (expansion of lysosomal volume, lysosomal storage of free cholesterol, miss-trafficking of GM1 gangliosides and altered GSL levels) in RAW 264.7 MΦ treated with cell wall lipid extracts of the NTM, *M. abscessus* and *M. avium*; leprosy causing mycobacterium, *M. leprae*; *M. bovis* which causes TB in domesticated animals; and the non-pathogenic, environmental species, *M. smegmatis*. Our objective was to determine whether the lipid-mediated inhibition of NPC1 activity found in clinically relevant *Mtb* was present in other pathological mycobacteria. In summary, we were able to obtain evidence for lipid-mediated induction of all the NPC cellular phenotypes, but they were not all induced by lipid extracts of each of the mycobacteria that were tested, with evidence of species-specific activities (Table 3.4.).

NPC Phenotype	*M. abscessus*	*M. avium*	*M. bovis*	*M. leprae*	*M. smegmatis*	*Mtb* H37Rv
LE/Lys expansion by FACS	Yes	Yes	Yes	No	No	Yes
LE/Lys expansion by LAMP-1 immunostaining	Yes	Yes	Yes	Yes	No	Yes
Filipin-positive lysosomal puncta	Yes	Yes	Yes	Yes	Yes	Yes
Increased Total Cholesterol	No	No	No	No	Yes	No
GM1 mis-trafficking	Yes	Yes	Yes	Yes	Yes	Yes
Total GSL storage	No	Yes	No	No	Yes	Yes

Table 3.4. Summary of NPC cellular phenotypes induced by TL extracts of M. abscessus, M. avium, M. bovis, M. leprae, M. smegmatis and Mtb H37Rv in RAW 264.7 MΦ.

In the absence of a direct assay for measuring NPC1 activity, induction of multiple NPC cellular phenotypes was used to demonstrate the mechanistic convergence between NPC and infection by BCG or *Mtb* [96, 207]. These studies involved the treatment of host cells with *Mtb* lipid extracts rather than infection with the intact mycobacterium, which would have required enhanced biosafety conditions, thereby confirming the inhibitory activity was lipid-mediated. Therefore, we used the same experimental strategy to investigate whether other species of mycobacteria might also inhibit NPC1.

The observation that initiated the first investigation into the relationship between NPC and *Mtb* was that cholesterol accumulates in both [24, 146]. Because lipid-enriched foamy MΦ have been reported in infections caused by other mycobacteria species, we reasoned that these species might also target NPC1 [308-310]. *Mtb* is an obligate human pathogen responsible for TB. The mycobacterial species we chose to investigate included one that causes comparable tubercular disease in domestic animals and on occasion, in humans *(M. bovis*); NTM that also infect humans and cause diseases but usually only in individuals at increased risk (*M. abscessus* and *M. avium*); a mycobacteria responsible for a human condition distinct from TB but with overlapping pathology (*M. leprae*); and an environmental, non-pathogenic mycobacteria that has been frequently used as an experimental model (*M. smegmatis*). These studies would allow us to determine whether lipid-mediated inhibition of NPC1 is restricted to *Mtb* and is associated with its specific pathogenic mechanisms or if the lipid-mediated activity is more widespread amongst mycobacteria and may contribute to the infection and survival strategies of other species.

FACS analysis of LysoTracker™ green DND-26 staining is a relatively high throughput method that facilitated our studies of TL extracts of *Mtb* clinical strain and provided the first evidence that *M. canettii* does not apparently target NPC1 (Chapter 2, [207]). Using this approach, the activities of extracts of *M. abscessus*, *M. avium* and *M. bovis* were found to be comparable to that of *Mtb* H37Rv, but those of *M. leprae* and *M. smegmatis* were not above the baseline, suggesting the absence of bioactive lipids in these mycobacteria species. However, the fluorescent intensity of LysoTracker™ emission is known to be sensitive to changes in pH [311], meaning that an increase in lysosomal number and/or volume could be obscured by lysosomal alkalisation. Lysosomal pH in MΦ can be modulated by mycobacteria. For example, it has been shown that the acidification of phagosomes containing the R variant of *M. abscessus* is less inhibited than those infected with the S variant [312]. Therefore, we measured the lysosome size of lipid-treated cells by immunostaining for the lysosome-restricted antigen LAMP-1 which is not influenced by pH. Using this technique, we also found a significant increase in lysosome diameter in *M. abscessus*, *M. avium* and *M. bovis* but not in *M. smegmatis* TL-treated RAW 264.7 MΦ. However, in contrast to the LysoTracker™ data, there was a significant enlargement of lysosomes after *M. leprae* TL treatment. It has been reported that there is failure to acidify vesicles after the uptake of live *M. leprae* which would be compatible with our hypothesis [283]. This could be tested directly by measurement of lysosomal pH in lipid-treated cells using appropriate chemical probes, such as LysoSensor™.

As mentioned above, endo-lysosomal accumulation of cholesterol is the most prominent NPC cellular phenotype and the infection with mycobacteria is often associated with the formation of foamy MΦ [129]. We therefore examined the evidence of storage of cholesterol in cells that had been incubated with lipid extracts. The frequency of cells harbouring filipin-positive puncta treated with either *M. bovis* or *M. leprae* extract was equivalent to that for *Mtb* H37Rv, whilst for *M. abscessus*, *M. avium*, and *M. smegmatis* were significantly lower, but still greater than that of the vehicle control.

Cholesterol is a growth substrate for intracellular *M. abscessus*, and its genome encodes enzymes necessary for its catabolism, which are upregulated after the uptake of the mycobacteria by the host [313]. However, the precise changes to host cell biology after mycobacterial infection that favour survival and persistence have not been extensively explored for this species. Therefore, the relatively modest increase in the frequency of filipin-positive puncta observed after treatment with *M. abscessus* TL extract as compared to *Mtb* H37Rv treatment may be biologically important.

It has been shown that cholesterol accumulation in *M. avium* subspecies *paratuberculosis*-infected MΦ can be visualised by filipin staining within 4h of infection [272]. However, TAG accumulation, rather than cholesterol accumulation, was observed in *M. avium* subspecies *avium* infection in MΦ [310]. Therefore, investigating the activity of lipid extract of other subspecies from *M. avium* may be of relevance.

The data for *M. bovis* is consistent with previous reports that filipin-positive puncta result from BCG infection in RAW 264.7 MΦ [96]. Although there is published evidence that BCG cell wall lipid induces inflammatory responses in MΦ and the formation of granuloma in mice, as far as we are aware, there have been no published reports that include cholesterol analysis of *M. bovis* infection in animal models [314].

There is a good deal of evidence of foamy MΦ formation in *M. leprae* infection with extensive lipid droplet formation, especially those containing cholesterol, along with *de novo* host cholesterol biosynthesis and LDL uptake [290, 308]. Infected cells stain positive for Nile red, confirming lipid droplets and also for filipin [290]. In addition, cholesterol metabolism has been shown to be essential for the intracellular survival of the mycobacterium, indicating an intimate relationship between *M. leprae* and the lipid [308]. Interestingly, the structure of *M. leprae* TL-induced filipin-positive puncta was morphologically different from those puncta induced by lipid extracts of other mycobacteria. Cholesterol accumulation in *M. leprae* TL-treated MΦ appeared as a needle-like form, resembling the cholesterol crystals that have been reported in atherosclerotic plaques and specific LSDs such as Tangier disease (in which cholesterol accumulates due to the impaired ABCA1 efflux activity on the plasma membrane) and Fabry disease (which has reduced lysosomal galactosidase A activity that cause accumulation of Gb3 and lyso-Gb3) [315-319]. Cholesterol is considered to favour *M. leprae* survival in host cells because of the close contact between intracellular mycobacteria and LD containing cholesterol esters has been observed [290, 320]. However, as far as we are aware, cholesterol crystal formation has not been reported in *M. leprae*

infected MΦ. Cholesterol crystals can activate the NLRP3 inflammasomes, and overexpression of NLRP3 inflammasomes is associated with a higher risk of lepromatous leprosy [321, 322].

In contrast to our expectation, there was a relatively small but statistically significant increased frequency of filipin-positive puncta in cells treated with *M. smegmatis* TL extract. In the study that first identified the mechanism between NPC and pathogenic mycobacteria, infection with *M. smegmatis* did not induce detectable lysosomal cholesterol accumulation [96]. One possible explanation for the difference in the results from the two studies is that inhibitory lipids are not shed by live *M. smegmatis*, but preparation of the lipid extract liberates lipids that are able to inhibit NPC1 and induce NPC cellular phenotypes. Future identification of the specific lipids from mycobacteria that inhibit NPC1 will allow an unequivocal demonstration of its distribution between different species of mycobacteria and whether it is released from the cell wall. This will also be discussed in further detail in Chapter 5.

Although BCG infection significantly increased total cholesterol content [96], lipid extracts of clinical *Mtb* strains [207] or mycobacteria tested in this study did not have that effect. However, our data showed *M. smegmatis* TL treatment resulted in significantly enhanced cellular cholesterol, for which we currently have no explanation. The cholesterol data between this study and the previously published works are consistent in that the mycobacteria lipid extract redistributes cholesterol intracellularly rather than stimulates cholesterol biosynthesis. Although pharmacological inhibition of NPC1 with U18666A increases both endo-

lysosome storage and cellular levels of cholesterol, genetic loss of NPC typically results in a far more modest increase in total cholesterol [11, 207]. This would suggest that the extent of cholesterol accumulation is likely influenced by the degree and duration of inhibition of NPC1 activity.

In NPC cells, GSL trafficking is perturbed and they are targeted to the lysosome [323]. This change can be visualised by pulse-chase labelling with fluorescently tagged CtxB, which predominantly binds to GM1 ganglioside on the plasma membrane [323]. This study revealed that TL extracts of *M. abscessus*, *M. avium*, *M. bovis*, *M. leprae* and *M. smegmatis* cause GM1 ganglioside miss-trafficking. The data for *M. smegmatis* are seemingly incompatible with infection studies when no alteration was observed, but this might be explained by the presence of bioactive lipid in the TL extract that is not normally shed by *M. smegmatis* and therefore unable to inhibit NPC1 in a live infection study [96]. *M. avium* infection of murine J774 MΦ induced phagosomes containing GM1-enriched lipid rafts derived from the host cell membrane, which was likely to be induced by the high polarity lipid fractions of the *M. avium* cell wall [324].

Our investigation of the accumulation of GSL in RAW 264.7 MΦ treated with *Mtb* H37Rv TL extract demonstrated a significant increase not only in total GSLs but also all of the individual GSL species (Chapter 2). The profile of GSLs for cells treated with NTM, *M. bovis*, *M. leprae* or *M. smegmatis* was much more variable, of which only *M. avium* and *M. smegmatis* enhances total GSLs and *M. abscessus* and *M. leprae* each only increased a single GSL (GA1 and GM2 respectively). An increase in GM3 in the lymph node and liver of lepromatous

armadillos has been reported, but we were unable to measure increased storage of this ganglioside in lipid-treated RAW 264.7 MΦ [325]. It is perhaps relevant that *M. leprae* modulates expression of a modified GD3, 9-O-acetyl GD3 ganglioside in Schwann cells, which is important for attachment of the mycobacterium to the glial cells [326]. In addition, GD3 is almost undetectable in RAW 264.7 MΦ. The data obtained with treatment with *M. smegmatis* TL extract did not agree with that previously obtained for total GSLs in RAW 264.7 MΦ infected with the same mycobacterium [96]. In that study, only the total level of GSL was measured and not the individual GSL species. Again, this difference might be due to differential availability of active lipids between TL extract and live bacteria.

Our objective in making this study was to examine whether we could detect lipid-mediated inhibition of NPC1, as shown by the induction of specific cellular phenotypes indicative of loss of activity, in mycobacteria more generally. Our hypothesis was that if it is a conserved property and associated with intracellular survival, it would be present in species that can cause disease but absent from non-pathological mycobacteria. In summary, we confirmed the induction of multiple NPC cellular phenotypes by lipid extracts of each of the pathogenic mycobacteria, but also by that of environmental *M. smegmatis*. Lipid extracts of other mycobacteria infections, such as *M. marinum* and *M. fortuitum* inducing foamy cell phenotypes, can also be tested in the future [309, 327]. Data from future investigations that involve infection by each of the microbes, together with structural identification of the relevant species of mycobacterial lipid, will permit critical evaluation of the results reported here.

Chapter 4. *Mtb* cell wall lipids and sphingosine metabolism

4.1. Introduction

One of the most significant sphingolipids that is stored in NPC cellular and animal models and patient tissues is the sphingoid base, sphingosine [328]. Sphingolipids play crucial roles in multiple fundamental cellular processes including growth, proliferation, differentiation, apoptosis and cellular signalling pathways [329]. Their importance is reflected by demonstrations that perturbation of sphingolipids is linked to cancer, inflammation, diabetes, neurodegeneration and other diseases [330, 331].

Sphingolipid metabolism

The generation of sphingolipids is initiated by *de novo* synthesis of 3-ketosphinganine from palmitate and serine by serine palmitoyl transferase (SPT) in ER [332]. 3-ketosphinganine is reduced by reductases to dihydrosphingosine, also known as sphinganine (shaded in pink, Figure 4.1.2.), and then acylated to dihydroceramide via the activity of ceramide synthase (CerS). It is subsequently desaturated into ceramide (Fig 4.1.2.) [330, 333].

Ceramide synthesised in ER is transported to the *trans* Golgi by vesicular trafficking and to the *cis* Golgi by the ceramide transport protein (CERT) [334], Ceramide can be glucosylated on the cytosolic face of an early Golgi compartment by glucosylceramide synthase (GCS) to form GlcCer [335]. GlcCer can be transported from the *trans* to *cis* Golgi by four-phosphate adaptor protein 2 (FAPP2) for the biosynthesis of neutral more complex GSL [336]. *Trans* Golgi-located ceramide can also be phosphorylated by ceramide kinase (CK) to generate ceramide-1-phosphate (C1P) or converted to SM mediated by the

action of sphingomyelin synthase (SMS) [333]. GSL, SM and C1P are transported to the plasma membrane by vesicular trafficking [337, 338].

Sphingosine is mainly generated in lysosomes by the degradation of ceramide derived from GSLs and SM. Deacylation of ceramide is the only known way to generate sphingosine [330]. Sphingosine is protonated at acidic pH, and so requires a transport mechanism for it to leave the lysosome. Sphingosine efflux from lysosomes is dependent on NPC1, and recently, sphingosine has been shown to directly bind to NPC1 [40]. Sphingosine that leaves the lysosome reaches the ER at lysosome/ER membrane contact sites or can be phosphorylated by sphingosine kinase (SphK) 1 on the outer leaflet of the lysosome-limiting membranes to form the signalling lipid, sphingosine-1-phosphate (S1P) (shaded in green, Figure 4.1.2.) [339], which can be dephosphorylated by S1P phosphatase (SPPase) into sphingosine or irreversibly broken down by S1P lyase into non-sphingolipid products [333, 340]. Pathogens, cytokines and other stimuli can activate SMase and SphK1 on the plasma membrane for the generation of S1P [6], which can be exported by transporters and activate the S1P receptor for subsequent cellular signalling [330].

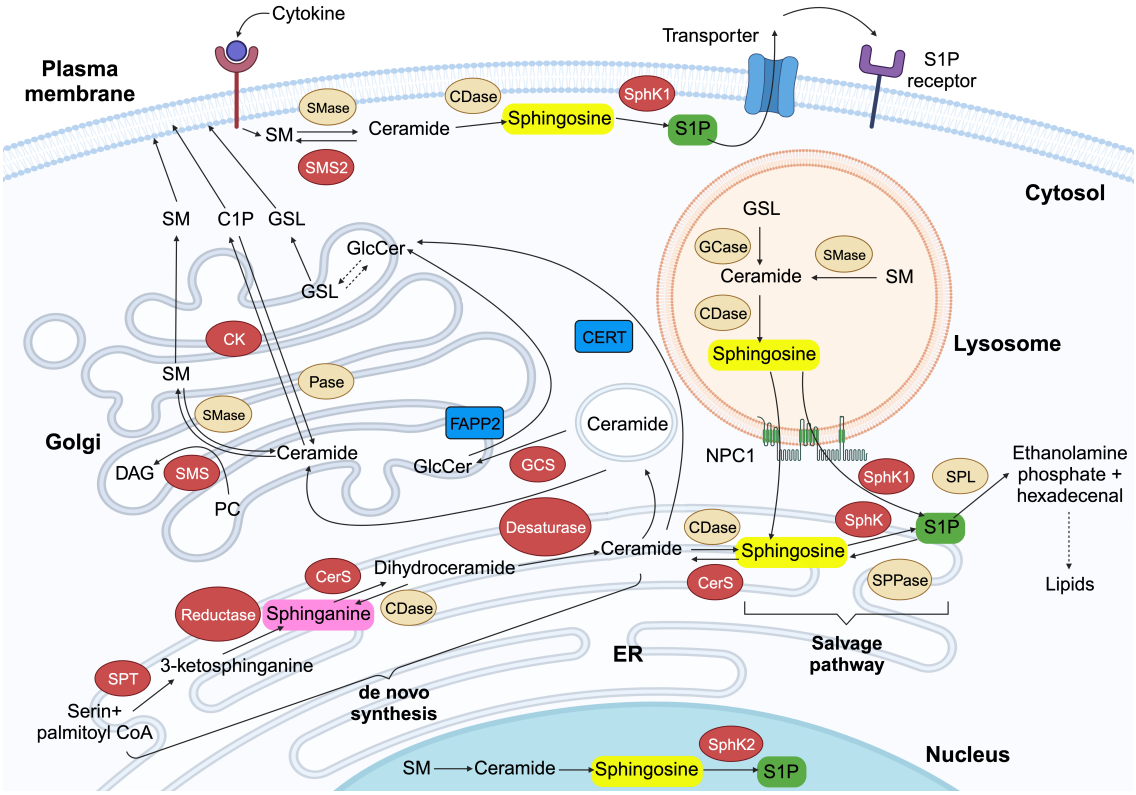


Figure 4.1.1. The sphingolipid metabolism pathway.

De novo biosynthesis of ceramide and the salvage pathway for sphingolipid biosynthesis are indicated with brackets. Sphingosine is highlighted with yellow; sphinganine is highlighted with pink; S1P is highlighted with green. Dotted arrowed lines indicate multiple steps in the biosynthetic pathway. Enzymes shaded with yellow are involved in degrative pathways; enzymes shaded with red are involved in metabolic pathways. CDase, ceramidase; SPT, serine palmitoyl transferase; CerS, ceramide synthase; SMase, sphingomyelinase; SK, sphingosine kinase; SPPase, S1P phosphate; CK, ceramide kinase; GCS, glucosylceramide synthase; GCase, glucosylceramidase; DAG, diacylglycerol; PC, phosphatidylcholine; SMS, sphingomyelin synthase. Adapted from [330, 333, 341].

Sphingosine and sphinganine

Sphingosine ((2*S*,3*R*,4*E*)-2-amino-4-octadecen-1,3-diol) is the backbone of sphingolipids, which include ceramide, SM and other GSLs (Figure 4.1.2.A.) [342]. The majority of intracellular sphingosine is located in the lysosomes (Figure 4.1.1.) [343]. Sphingosine (shaded in yellow, Figure 4.1.2.) is generated in the lysosomal lumen by the catabolic of GSLs and SM by GCase or SMase respectively into ceramide, and then deacylated by CDase to produce sphingosine [344]. Sphingosine generated from ceramide catabolism has two potential fates, to be used in the salvage pathway of sphingolipid biosynthesis or to be phosphorylated to form the signalling S1P [339].

On the other hand, sphinganine ((2*S*,3*R*)-2- amino-octadecan-1,3-diol) (Figure 4.1.2.B.) is produced during the *de novo* biosynthesis of ceramide on the ER membrane (Figure 4.1.1.) [332, 342].

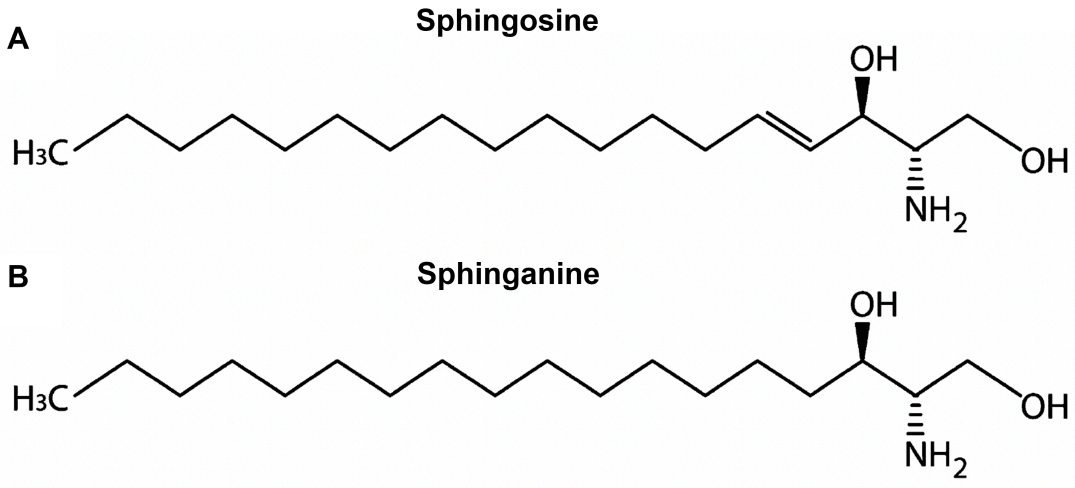


Figure 4.1.2. Structure of sphingosine and sphinganine.

Adapted from [342].

Sphingosine-1-phosphate (S1P)

S1P (Fig 4.1.3.) is generated on the inner leaflet of the plasma membrane, in the cytosol, on ER membrane and in the nucleus by SphKs [345]. SphK1 mainly resides in the cytoplasm and is transported to the plasma membrane upon cell activation [346, 347]. SphK1 is also recruited to sphingosine-enriched endocytic vesicles to facilitate the membrane trafficking [348]. SphK2, which is located in mitochondria, ER and nucleus, can also phosphorylate sphingosine to generate S1P [349]. Although SphK1 and SphK2 share the same activity, they have opposing roles during cell survival; in general, SphK1 is protective and promotes survival and proliferation, whereas phosphorylation by SphK2 mediates cell apoptosis [350]. However, the role of SphK2 is complex because it has an important role in preventing damage to the brain resulting from murine cerebral ischaemia [351].

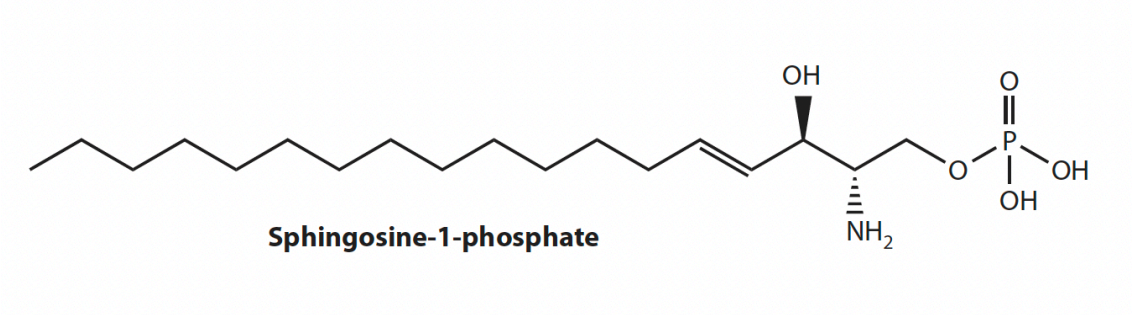


Figure 4.1.3. Structure of sphingosine-1-phosphate.

Adapted from [352].

Sphingosine and its relevance to NPC

Dysregulated sphingosine metabolism results in sphingolipid accumulation, which is a characteristic of LSDs, including Niemann-Pick diseases. NPC disease is characterised by defects in vesicle trafficking and fusion between lysosomes and ER primarily due to the loss of NPC1 activities, leading to

lysosomal lipid accumulation [26, 34]. Although the activity of SMase is intact in NPC disease, SM accumulates in NPC patient cells, which may contribute to the impaired vesicular trafficking [353]. Both sphingosine and sphinganine accumulate in NPC patient tissues and the liver of NPC1-deficient mice [354, 355]. There is a deficit in the production of S1P in the NPC1 mutant animals as compared with WT, most probably because sphingosine remains trapped in the lysosome as its phosphorylation occurs in the cytosol [354, 356]. This proposal is consistent with the differential levels of sphingosine and S1P in U18666A-treated MΦ [26], but in addition, there is evidence that NPC1-deficient patient fibroblasts have reduced SphK1 activity [37]. As described in Chapter 1, sphingosine accumulation in lysosomes is the first event in RAW 264.7 MΦ treated with U18666A to inhibit NPC1 function [26]. A direct interaction between the lysosomal membrane protein and sphingolipid has been subsequently demonstrated through the use of a lysosome-targeted cross-linkable sphingosine probe [40].

Roles of sphingolipids during *Mtb* infection

Various sphingolipid metabolites have been shown to be important during different stages of the life cycle of *Mtb* infection/progression. The generation of SM is essential for the entry and growth of *Mtb* bacilli in host MΦ [357, 358]. On the other hand, S1P has antimicrobial activity against *Mtb* infection both *in vivo* and *in vitro*; exogenous S1P treatment inhibits *Mtb* growth and viability in cultured MΦ and in the lung and spleen of infected mice [359], which is consistent with decreased S1P level in NPC mice. The trafficking of *Mtb* bacilli to lysosomes in MΦ is enhanced by S1P [359, 360]. S1P promotes antigen presentation to *Mtb*-

specific T cells, cytokine production and the differentiation of naïve MΦ, which are protective against infection [360, 361]. However, the beneficial effects of S1P are dependent upon the timing of treatment during *Mtb* infection. In infected mice, S1P inhibits the replication of *Mtb* bacilli in the lung during the early stages (within the first 28 days) but promotes replication if S1P treatment is delayed until 53 days post-infection [362]. In *Mtb*-infected MΦ, the level of S1P is enhanced, and SphK activity is inhibited, thereby attenuating the delivery of *Mtb* bacilli to the lysosomes [363]. Impairment of SphK activity also promotes intracellular survival of *M. smegmatis*, which is otherwise normally cleared from host cells [364]. Therefore, S1P and SphK are both important for the host defence against infection by *Mtb*.

Aims

- Investigate the abundance and temporal profile of sphingolipids in RAW 264.7 MΦ treated with *Mtb* H37Rv TL extract.
- Determine the levels of SphK in RAW 264.7 MΦ treated with *Mtb* H37Rv TL extract.

4.2. Material and methods

4.2.1. Cells

RAW 264.7 MΦ were obtained and cultured as described in Section 2.2.1.

4.2.2. Mycobacterial culture and cell wall lipid extraction.

Mtb H37Rv was cultured, and cell wall lipids extracted were generated as described in Section 2.2.2.

4.2.3. Lipid solubilisation and addition to cell culture.

Dried *Mtb* lipids were solublised DMSO as described in Section 2.2.3. RAW 264.7 MΦ were seeded into 12-well plates at a density of 0.25 x 10^6 cells/well for sphingolipids lipidomic analysis. *Mtb* H37Rv TL extract (100µg/ml) was added to RAW 264.7 MΦ for the period of time specified in each experiment.

4.2.4. Cell lysate preparation for sphingolipids lipidomic analysis.

After treatment, RAW 264.7 MΦ were washed with PBS and pelleted by centrifugation (377xg for 5min). Cell pellets were lysed in 50µl ddH_2O, vortexed, and freeze/thawed three times. BCA assays were performed to determine the protein concentration of samples as described in Section 2.2.15.

4.2.5. Determination of sphingosine and sphinganine by reverse-phase high-performance liquid chromatography (RP-HPLC).

The method used for extraction and fluorescent labelling of sphingosine and sphinganine was described by He *et al.* [365]. 500µl of $CHCl_3$: MeOH 1:2 (v/v) containing 0.3nmol purified C18 sphingosine (Avanti Polar Lipids, 860490), C18

sphinganine (Avanti Polar Lipids, 860498) and C20 sphingosine (Avanti Polar Lipids, 860660) were processed and labelled parallel to the cell extracts as standards to confirm the retention times of the specific sphingolipid species. 100µl of aqueous cell lysate containing 0.1mg of protein was mixed with 500µl $CHCl_3$: MeOH 1:2 (v//v) containing 0.3nmol C20 sphingosine as an internal standard. Samples were sonicated in a water bath at RT for 10min. 500µl of 1M NaCl (Fisher Scientific, S/3120/63), 500µl of $CHCl_3$ and 100µl of 3M NaOH (Fisher Scientific, S/4920/60) were added to the sample in that order, and the mixture incubated at RT for 15min with vortexing every 5min. The mixture was centrifuged at 1500xg for 10min to separate the two phases. The lower phase containing sphingosine and sphinganine was collected and loaded onto an ISOLUTE SPE NH_2 column (Biotage, 221-0010-A), which was pre-conditioned with 2x1ml of $CHCl_3$. Sphingosine and sphinganine were eluted with 900µl of acetone (Sigma, 179124). The eluates were dried under a stream of N_2 at 42^oC and labelled with phthaldialdehyde (OPA) (Sigma, 79760). OPA working solution was prepared by dissolving OPA in EtOH (20µl EtOH per 1mg OPA), and 2-mercaptoethanol (Sigma, 63689) was added (1ul per 1mg OPA) and diluted 1:2000 in 3% boric acid solution (w/v) (pH 10.5) (Sigma, B0252,). The dried lipid was then dissolved in 50µl of pre-warmed EtOH (Sigma, 34852), and 50µl of the OPA working solution was added. The labelling mixture was incubated for 20min in the dark, vortexing every 10min. Finally, 100µl of MeOH: 5mM Tris aminomethane hydrochloride (9:1, v/v) (pH 7) (Fisher Scientific, T/P631/48) was added to stop the reaction. The reaction mixture final product was centrifuged at 1500xg for 2min, and 50ul supernatant was loaded to Chromolith Performance RP-18e 100-4.6 HPLC column (Merck, 1.02129.0001) for analysis.

4.2.6. Sphingoid-base lipid analysis by liquid chromatography-mass spectrometry (LC-MS).

LC-MS analysis of sphingolipids was performed by Dr Ryan Brown in the laboratory of Professor Sarah Spiegel, Virginia Commonwealth University (VCU), Richmond, Virginia, USA. In brief, cell pellets were lysed with 100µl ddH_2O and 1ml MeOH. 250pmol of internal lipid standard was added, and samples were sonicated in a water bath until fully mixed. 500µl of $CHCl_3$ was added, vortexed for 5s, sonicated for 30s and vortexed for 10s. Samples were incubated at 48^oC overnight. After incubation, samples were centrifuged at 4200xg for 5min at 4^oC, and the supernatant transferred to a glass tube. Samples were dried under vacuum and resuspended in 600µl of MeOH: H_2O 1:1 (v/v) and sonicated for 15s. Samples were then centrifuged at 4200xg for 5min at 4^oC, and the supernatants were transferred to MS vials using glass pipettes for lipid analysis. Lipids were quantified by LC-ESI-MS/MS (5500 QTrap; AB Sciex, Framingham, MA, USA) and normalised to total protein.

4.2.7. BODIPY-LacCer trafficking by confocal microscopy

RAW 264.7 MΦ were plated onto glass coverslips in 24 well plates for *Mtb* H37Rv TL extract treatment. After treatment, cells were washed with HBSS three times and incubated in HBSS containing 100ul of 2µM BODIPY-LacCer/BSA (BODIPY^{TM} FL C5-Lactosylceramide complexed to BSA, ThermoFisher, B34402) for 30 min at 4^oC in dark. Cells were washed twice with cold HBSS and incubated in HBSS containing 5% defatted BSA (BSA fatty acid-free, Merck, A8806) for 10min at 4^oC. After blocking, BODIPY-LacCer were chased into cells by replacing the culture media and incubating at 37^oC for 2h. Cells were then washed with

PBS and fixed with 4% PFA, and nuclei were stained with DAPI. Coverslips were mounted with Prolong Gold Antifade. Imaging was carried out on a Leica-SP8 confocal microscope. Images were analysed using ImageJ Fiji 3 (NIH, USA).

4.2.8. Western blotting

Protein lysates (generated as described in Section 2.2.7.) of treated cells were diluted to 2mg/ml, mixed with SDS Blue loading buffer and DTT and heated at 100^{o}C for 5min. Sample loading, gel electrophoresis, and transfer to membranes were described in Section 2.2.8. Membranes were blocked with PBS containing 5% (v/v) skimmed milk and 0.1% Tween 20 (v/v) for 1h at room temperature or overnight at 4^{o}C, and then incubated with anti-SphK1/2 antibodies (rabbit polyclonal SphK1 (central region), 1:1000, ECM Biosciences, SP1621; rabbit polyclonal SphK2 antibody, 1:1000, Proteintech, 17096-1-AP) diluted PBS containing 2.5% (v/v) skimmed milk, 0.1% Tween 20 (v/v) and 10mM sodium azide overnight at 4^{o}C. Membranes were washed with PBS containing 0.1% Tween 20 three times (10min for each wash) and then incubated with HRP-conjugated anti-rabbit secondary antibody (mouse monoclonal, 1:5000, Sigma, A1949-1VL) diluted in PBS containing 2.5% skimmed milk with 0.1% Tween 20 for 1h at room temperature. The membrane was washed three times (30 min each) with PBS containing 0.1% Tween 20 and developed with SuperSignal^{TM} West Femto substrate or Pierce^{TM} ECL western blotting substrate. Imaging was performed using Universal Hood imager (BioRad) and ImageLab (BioRad). Membranes were re-probed with mouse peroxidase-conjugated anti-β-actin antibody, 1:10,000 (mouse monoclonal, Sigma, A3845) to evaluate the equivalence of protein loading.

4.2.9. Statistical analysis

Statistical analyses were performed as described in Section 2.2.16.

4.3. Results

4.3.1. Optimisation of RP-HPLC analysis of sphingosine and sphinganine.

Unfortunately, the conditions that had been used previously for RP-HPLC separation of other sphingolipid species were not suitable for sphingosine and sphinganine; retention times of the peaks were too close together to permit accurate integration. Therefore, the retention times were optimised by adjusting the flow rate of the mobile phase solvent to achieve good separation of the peaks representing C18 sphingosine (Panel A) and sphinganine (Panel B) (Fig 4.3.1.1.). At a flow rate of 2ml/min, the retention times for C18 sphingosine and C18 sphinganine were 5.9min and 6.8min respectively (Fig 4.3.1.1.). The retention time for C20 sphingosine was 7.8min, which was used as an internal standard for all samples (Fig 4.3.1.1.).

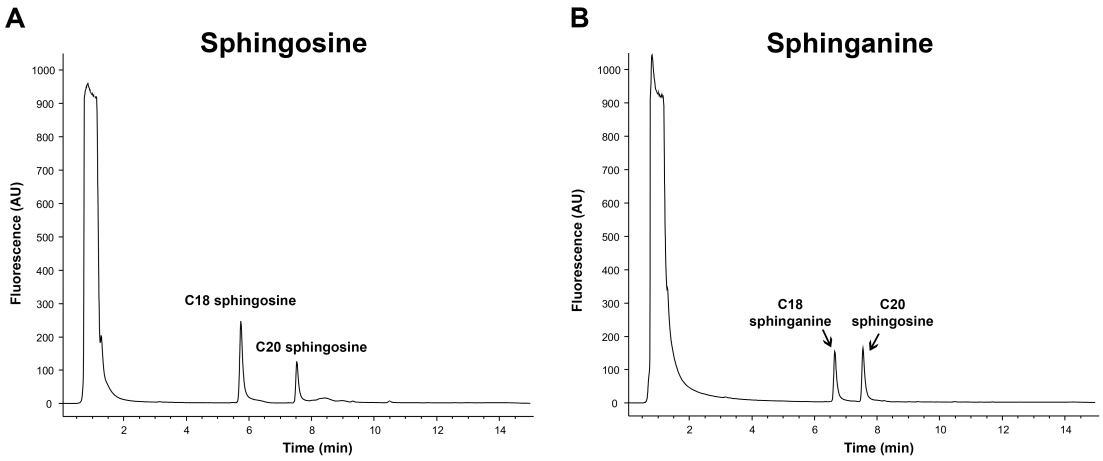


Figure 4.3.1.1. Representative RP-HPLC profiles for C18 sphingosine, C18 sphinganine and C20 sphingosine.

Lipid standards (0.3nmol) were processed and labelled with OPA, and 25% of the final product was loaded into the RP-HPLC system and separated. Panel A. Representative HPLC profile of C18 sphingosine and C20 sphingosine. Panel B. Representative HPLC profile of C18 sphinganine and C20 sphingosine.

To utilise RP-HPLC to successfully measure sphingosine and sphinganine, it was essential to confirm the sensitivity and linearity of the assay. In order to do this, lysates containing between 0.05 to 1.0mg of protein were processed and analysed. Representative RP-HPLC traces of lipid profiles of RAW 264.7 MΦ are shown in Fig 4.3.1.2.A. These data demonstrated assay sensitivity of about 0.05mg protein input and a linear correlation between the amount of sphingosine and sphinganine and protein input, with r^2 values of 0.9992 and 0.9978 respectively (Fig 4.3.1.2.B.).

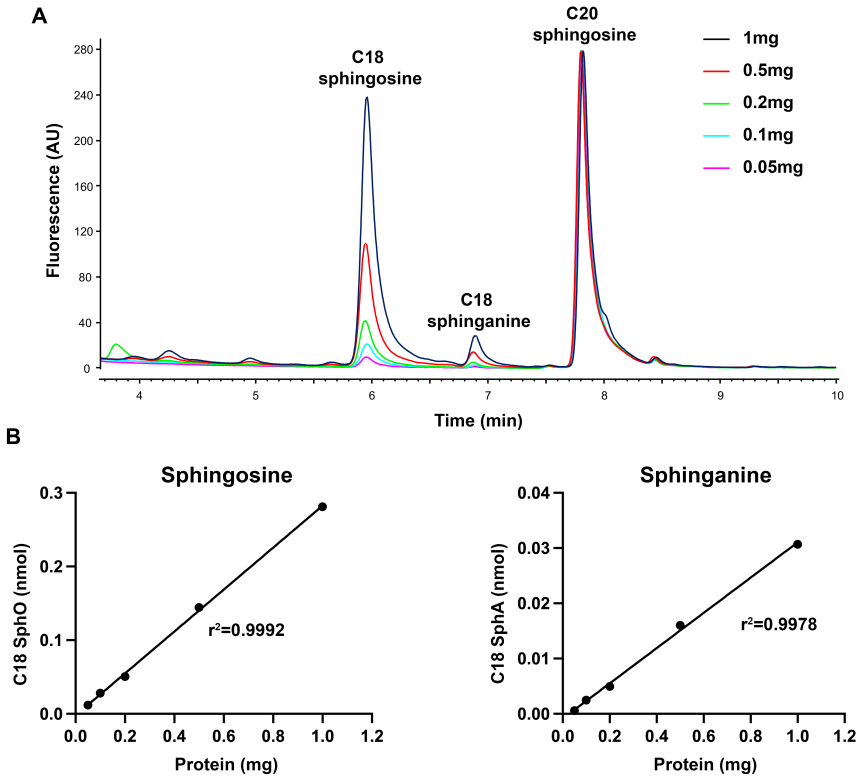


Figure 4.3.1.2. Linear correlation between the quantification of sphingosine and sphinganine in RAW 264.7 MΦ and protein input as determined by RP-HPLC.

Panel A. Representative RP-HPLC profiles of sphingosine and sphinganine of RAW 264.7 MΦ lysate containing varying amounts of protein (from 0.05mg to 1mg). Panel B. Linear correlation between sphingosine, sphinganine levels as determined by RP-HPLC and quantity of protein input of RAW 264.7 MΦ lysate.

4.3.2. Optimisation of the extraction of sphingosine and sphinganine from cell lysates.

Because of the scarcity of mycobacterial lipids available to treat RAW 264.7 MΦ, it was important to optimise the extraction protocol to ensure the highest possible yield of host cell lipids from a minimum number of cells. In order to avoid unnecessary losses due to the adhesion of lipids to different surfaces, we compared the use of glass against plastic tubes in the procedure. Although initial inspection of lipid profiles suggested higher yield from samples processed using glass (as indicated by peak height) (Fig 4.3.2.A.), normalisation to the C20 internal standard revealed a greater yield of sphingosine and sphinganine was achieved with the use of plasticware (p=0.0145, Fig 4.3.2.B.). Therefore, plasticware was used in all subsequent experiments.

We also investigated whether the composition (organic to aqueous content ratio; $CHCl_3$: MeOH: H_2O) of the extraction buffer influenced lipid yield. We compared the solvent ratio described in Section 4.2.5. ($CHCl_3$: MeOH: H_2O 2:1:2.1, v/v/v; referred to as 'Old') with Bligh and Dyer extraction mixture ($CHCl_3$: MeOH: H_2O 2:2:1.8, v/v/v; referred to as 'New'). Lysates of RAW 264.7 MΦ treated with 2µg/ml U18666A for 5min or 1h to induce sphingosine and sphinganine accumulation were used for the comparison. Analysis confirmed that a significant increase in the level of sphingosine required treatment of U18666A for 1h, whereas 5min of drug treatment was sufficient to enhance sphinganine levels (p=0.0006 and p=0.0057 for 'old' and 'new' in sphingosine levels; p=0.0017 and p=0.0010 for 'old' and 'new in sphinganine levels, Fig 4.3.2.C.). There was no significant difference between lipid yields when either of the two extraction

protocols was used (Fig 4.3.2.C.). Therefore, we used extraction buffer with the composition $CHCl_3$: MeOH: H_2O 2:1:2.1 (v/v/v) ('Old') in all subsequent experiments.

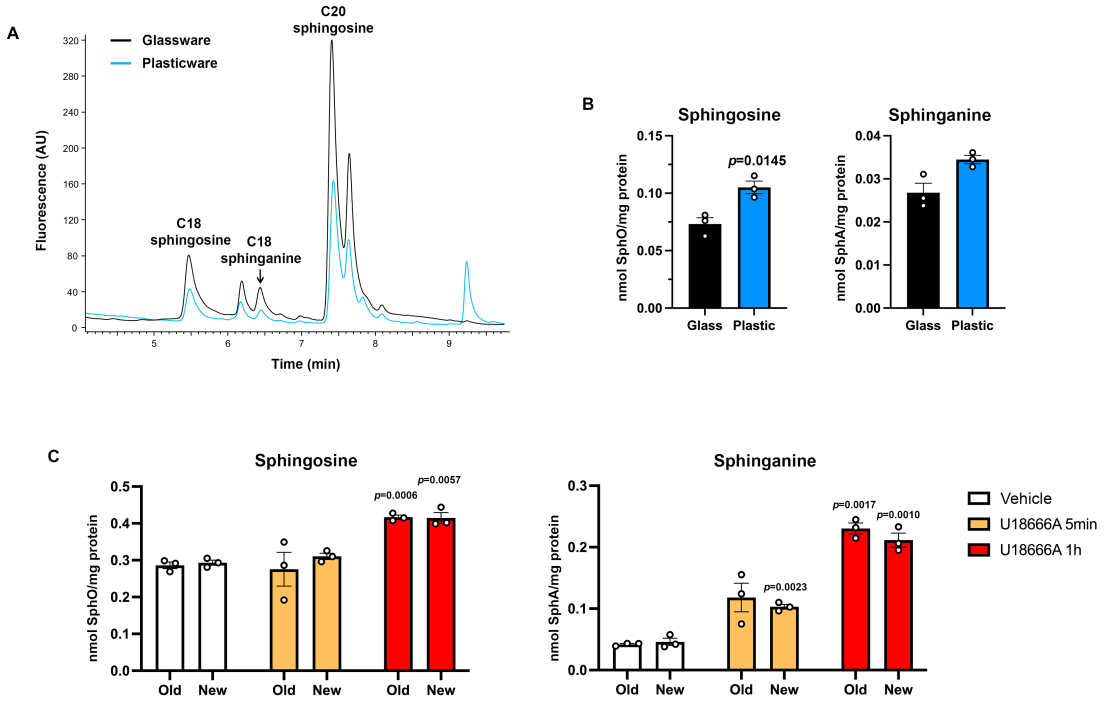


Figure 4.3.2. Optimisation of the extraction of sphingosine and sphinganine from RAW 264.7 MΦ.

RAW 264.7 MΦ were treated with U18666A (2µg/ml) for 5min or 1h to induce sphingosine and sphinganine accumulation. Panel A. Representative RP-HPLC profiles of sphingosine and sphinganine in untreated RAW 264.7 MΦ. Panel B. Quantitative analysis in treated RAW 264.7 MΦ processed in plasticware or glassware. Panel C. Comparison of sphingosine and sphinganine extracted by the 'old' and 'new' methods. Data are mean ± SEM, n=3. Statistical analysis, Welch's t-test. Statistical comparisons are relative to vehicle controls. *p* values as indicated, otherwise not significant.

4.3.3. U18666A induces a sustained increase in sphingosine but a transient increase in sphinganine, whereas *Mtb* H37Rv TL extract induces a transient increase of both sphingosine and sphinganine in RAW 264.7 MΦ.

Before investigating the effects of *Mtb* H37Rv TL extract, we undertook a temporal analysis of sphingosine and sphinganine abundance in RAW 264.7 MΦ treated with the NPC1 inhibitor, U18666A, for a period of up to 24h. All samples were extracted and analysed using the optimised protocols. We detected rapid accumulation of sphingosine within 15min of initiating drug treatment (****p<0.0001), which peaked at about 1h and subsequently declined over 24h but remained significantly greater (****p<0.0001) than the vehicle control (indicated as dotted line, Fig 4.3.3.A.(i)) at that time point. Sphinganine content was also significantly higher within 15min of exposure to U18666A (p=0.0002), remained at that level at 1h (p=0.0002), but declined significantly within 6h to a level not different to the vehicle control (indicated as dotted line, Fig 4.3.3.A.(ii)).

In light of the data obtained with U18666A treatment, we initially made a comparable time course of incubation with *Mtb* H37Rv TL extract. However, we were unable to detect significantly more sphingosine after 1h of treatment, and although there was a small increase at 6h and 24h, it was not statistically significant (Fig 4.3.3.B.(i)). In contrast, there was significantly more sphinganine within the first hour of incubation with the TL extract, which then declined but remained statistically greater at 6h and was not different at 24h (Fig 4.3.3.B.(ii)). As a result, we adjusted the period of *Mtb* H37Rv TL treatment. A significant increase in sphingosine was measured at 3h (****p<0.0001) and 6h (p=0.0395)

of treatment, which subsequently declined after 12h to 24h of treatment to a level not significantly different from the DMSO control (Fig 4.3.3.C.(i)). A similar trend was observed for sphinganine; *Mtb* H37Rv TL induced a significant increase at 3h (****p<0.0001) and 6h (p=0.0009) of treatment, which thereafter declined but remained statistically greater than vehicle control DMSO at 18h (p=0.0307) and 24h (p=0.0064) treatment (Fig 4.3.3.C.(ii)). It was noticeable that DMSO alone significantly affected sphingosine and sphinganine levels in RAW 264.7 MΦ in comparison to untreated cells (time 0h) (Fig 4.3.3.C.(i)(ii)).

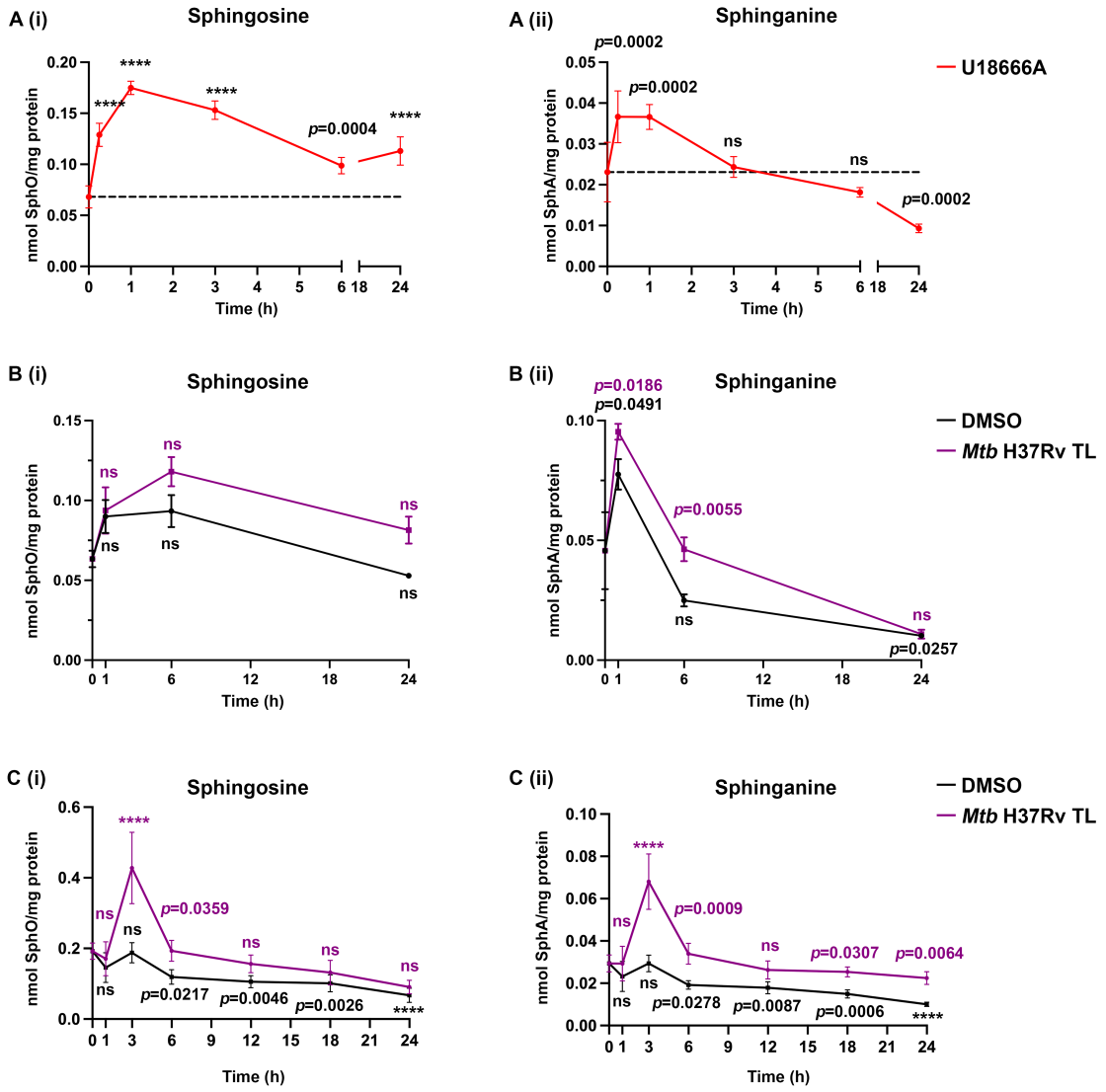


Figure 4.3.3. Mtb H37Rv TL extract induces a transient increase in sphingosine and sphinganine in RAW 264.7 MΦ.

RAW 264.7 MΦ were treated with U18666A (2μg/ml) for 15min to 24h; *Mtb* H37Rv TL extract (100μg/ml) and 0.5% DMSO (vehicle control) for 1h to 24h. Panel A. Sphingosine (i) and sphinganine (ii) levels in U18666A-treated cells. Dotted line indicates the vehicle level. Data are mean ± SEM, n=5. Statistical analysis, one-way ANOVA with Dunnett's multiple comparisons. ****p<0.0001, other p values as indicated, otherwise not significant. Statistical comparison of U18666A treatment was relative to time 0. Panel B.C. Sphingosine (i) and sphinganine (ii) levels in *Mtb* H37Rv TL extract-treated cells. Data are mean ± SEM, n=5. Statistical analysis, 2-way ANOVA with Sidak's multiple comparisons. ****p<0.0001, other p values as indicated, otherwise not significant. Statistical comparisons of lipid treatments (annotated in purple) are relative to DMSO controls at each time point. Statistical comparison of DMSO control (annotated in black) is relative to time 0. Data are representative of 2 independent experiments.

4.3.4. *Mtb* H37Rv TL extract induces S1P and dihydro-S1P (DHS1P) accumulation in RAW 264.7 MΦ.

The sphingolipid content of RAW 264.7 MΦ treated with *Mtb* H37Rv TL extract for a period of between 30 min and 24h was analysed by LC-MS by Dr Ryan Brown in the laboratory of Professor Sarah Spiegel, Virginia Commonwealth University. The profile of U18666A-dependent sphingosine and sphinganine accumulation was comparable to that determined by RP-HPLC (Fig 4.3.4.A.B.). Exposure to U18666A resulted in a significant increase in S1P at 30 min and 1h of treatment (****p<0.0001), which then declined to that of vehicle control at 3h and 6h but was significantly increased at 24h (p=0.0001, Fig 4.3.4.C.). No significant change in DHS1P was detected with U18666A treatment at all time points (Fig 4.3.4.D.).

With respect to *Mtb* H37Rv TL treatment, sphingosine was significantly higher at 30 min of treatment (p=0.0030) and remained enhanced through to 6h (****p<0.0001 for 1h, 3h and 6h treatment) but was reduced at 24h, though it was statistically greater than control (p=0.0003, Figure 4.3.5.A.). Significant accumulation of sphinganine was confirmed at 30 min of treatment, was still elevated at 6h and subsequently declined but remained statistically increased at 24h (****p<0.0001 for 30 min, 1h, 3h and 6h treatment; p=0.0011 for 24h treatment, Fig 4.3.4.B.). Accumulation of S1P was detected at 30 min, which remained elevated until 6h and declined by 24h of treatment but was statistically higher than pre-treatment levels (****p<0.0001 for 30 min, 1h, 6h and 24h treatment; p=0.0003 for 3h treatment, Fig 4.3.5.C.). DHS1P accumulated at 30 min of treatment with a peak at 1h and then declined (p=0.0148 for 30 min

treatment; ****p<0.0001 for 1h, 3h, 6h and 24h treatment, Fig 4.3.5.D.). It was noticeable that DMSO alone significantly increased S1P and DHS1P in RAW 264.7 MΦ (Fig 4.3.4.C.D.).

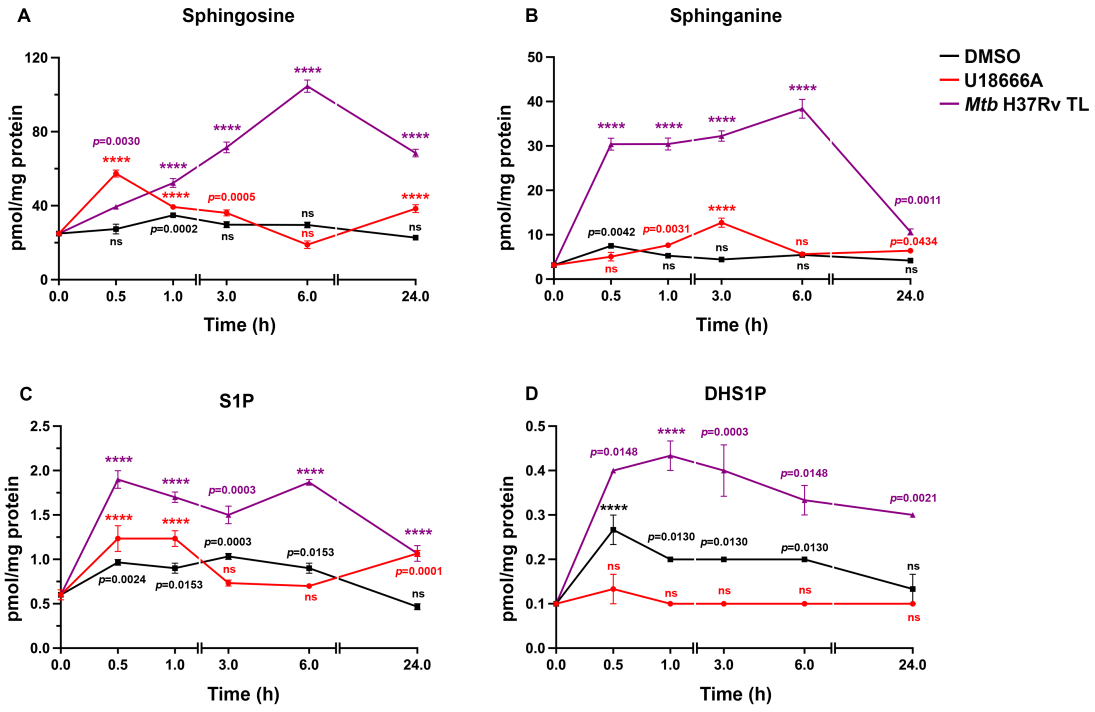
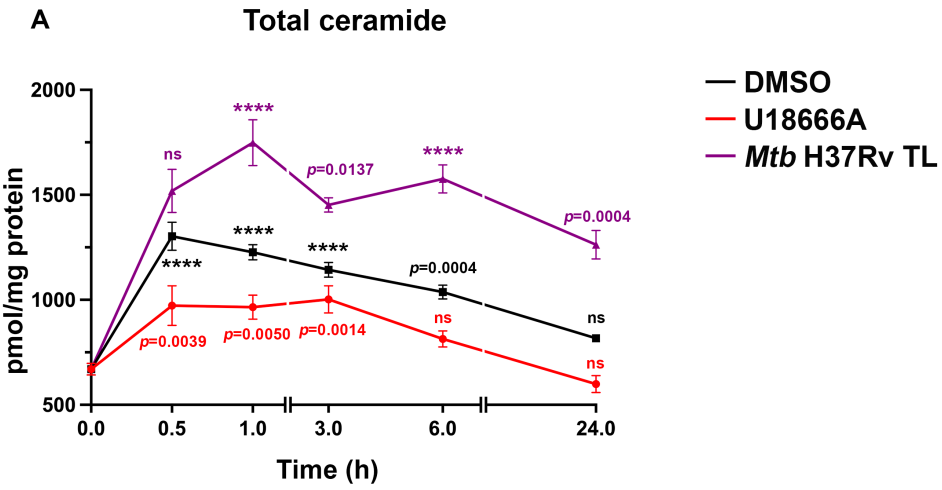


Figure 4.3.4. Mtb H37Rv TL extract induces sphingosine, sphinganine, S1P and DHS1P accumulation in RAW 264.7 MΦ.

RAW 264.7 MΦ were treated with U18666A (2μg/ml) for 30 min to 24h; *Mtb* H37Rv TL extract (100μg/ml) and 0.5% DMSO (vehicle control) for 30 min to 24h. Quantification of sphingosine (panel A), sphinganine (panel B), S1P (panel C) and DHS1P (panel D) were determined by LC-MS. Data are mean ± SEM, n=3. Statistical analysis, 2-way ANOVA with Sidak's multiple comparisons. ****p<0.0001, other p values as indicated, otherwise not significant. Statistical comparisons of U18666A treatment (annotated in red) are relative to time 0. Statistical comparisons of lipid treatments (annotated in purple) are relative to DMSO controls at each time point. Statistical comparison of DMSO control (annotated in black) is relative time 0. Data are representative of 2 independent experiments. Data were generated by Dr Ryan Brown in the laboratory of Professor Sarah Spiegel, Virginia Commonwealth University.

4.3.5. *Mtb* H37Rv TL extract induces ceramide and monohexosylceramide accumulation in RAW 264.7 MΦ.

The ceramide levels were also analysed by LC-MS by Dr Ryan Brown in the laboratory of Professor Sarah Spiegel, Virginia Commonwealth University. We measured a significant accumulation of ceramide at 30 min (p=0.0039) following the exposure to U18666A, which remained elevated at 3h (p=0.0050 for 1h; p=0.0014 for 3h) but was reduced to that of vehicle control at 6h and 24h (Fig 4.3.5.A.). When treated with *Mtb* H37Rv TL, ceramide was significantly increased at 1h and persisted through to 24h (1h and 6h, ****p<0.0001; 3h, p=0.0137; 24h, p=0.0004, Fig 4.3.5.A.). Monohexosylceramides, which represent GlcCer and GalCer since they are indistinguishable by MS analysis [366], were not altered at 30 min and 1h but were significantly increased after 3h (p=0.0166) and 6h (p=0.0017) and then returned to a level equivalent to that of DMSO-treated cells at 24h (Fig 4.3.5.B.). It is noticeable that DMSO vehicle control significantly increased total ceramide and monohexosylceramide levels in RAW 264.7 MΦ compared to untreated cells (Fig 4.3.5.A.B.).



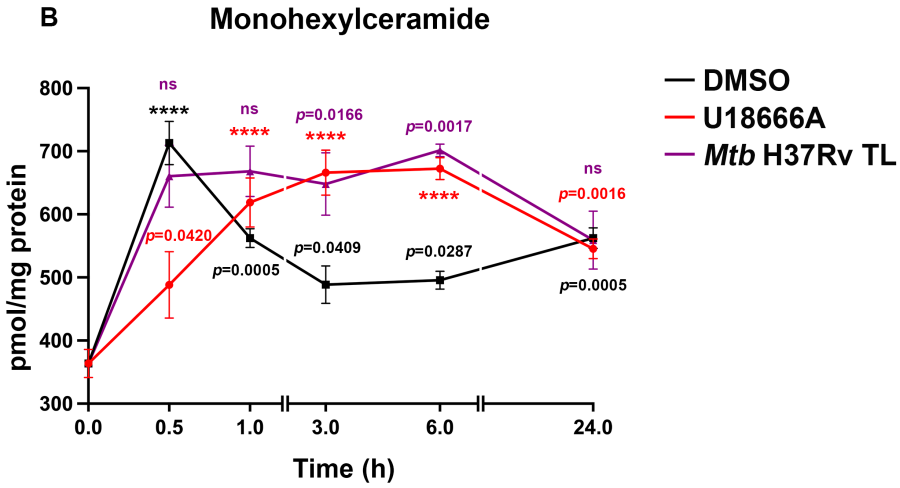


Figure 4.3.5. Mtb H37Rv TL extract treatment induces ceramide and monohexosylceramide accumulation in RAW 264.7 MΦ.

RAW 264.7 MΦ were treated with U18666A (2µg/ml) for 30 min to 24h; *Mtb* H37Rv TL extract (100µg/ml) and 0.5% DMSO (vehicle control) for 30 min to 24h. Quantification of total ceramide (panel A) and monohexosylceramide (Panel B) were analysed by LC-MS. Data are mean ± SEM, n=3. Statistical analysis, 2-way ANOVA with Sidak's multiple comparisons. ****p<0.0001, other p values as indicated, otherwise not significant. Statistical comparisons of U18666A treatment (annotated in red) are relative to time 0. Statistical comparisons of lipid treatments (annotated in purple) are relative to DMSO controls at each time point. Statistical comparison of DMSO control (annotated in black) is relative time 0. Data are representative of 2 independent experiments. Data were generated by Dr Ryan Brown in the laboratory of Professor Sarah Spiegel, Virginia Commonwealth University.

4.3.6. *Mtb* H37Rv TL extract induces SM accumulation in RAW 264.7 MΦ.

SM level was also measured by LC-MS by Dr Ryan Brown in the laboratory of Professor Sarah Spiegel, Virginia Commonwealth University. U18666A induced an increase in SM after 30 min of treatment, which was sustained through to 24h (****p<0.0001 for 30 min, 3h and 6h; p=0.0001 for 1h and 24h, Fig 4.3.6.). In contrast, *Mtb* H37Rv TL did not alter SM at 30 min and 1h of treatment but induced a significant increase at 3h and 6h (p=0.0102 and p=0.0003 respectively), which returned back to a level not different from the vehicle at 24h (Fig 4.3.6.). It is noticeable that DMSO vehicle control significantly increased SM levels in RAW 264.7 MΦ (****p<0.0001, Fig 4.3.6.).

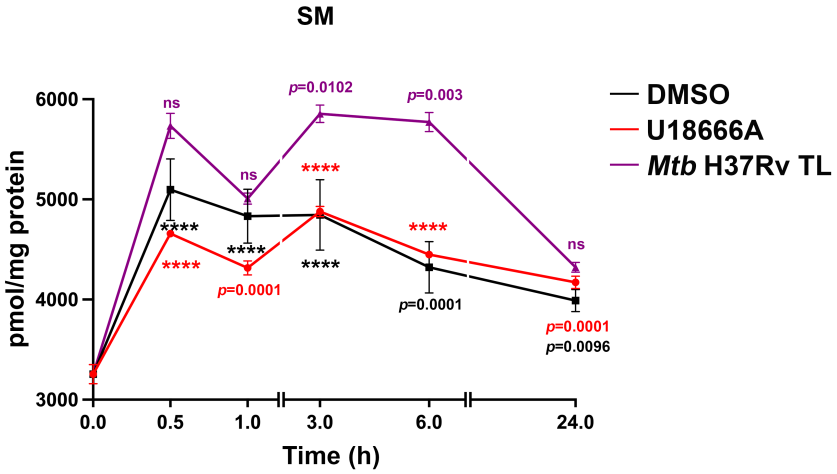


Figure 4.3.6. Mtb H37Rv TL extract induced SM accumulation in RAW 264.7 MΦ.

RAW 264.7 MΦ were treated with U18666A (2μg/ml) for 30 min to 24h; *Mtb* H37Rv TL extract (100μg/ml) and 0.5% DMSO (vehicle control) for 30 min to 24h. Quantification of SM was determined by LC-MS. Data are mean ± SEM, n=3. Statistical analysis, 2-way ANOVA with Sidak's multiple comparisons. ****p<0.0001, other p values as indicated, otherwise not significant. Statistical comparisons of U18666A treatment (annotated in red) are relative to time 0. Statistical comparisons of lipid treatments (annotated in purple) are relative to DMSO controls at each time point. Statistical comparison of DMSO control (annotated in black) is relative time 0. Data are representative of 2 independent experiments. Data were generated by Dr Ryan Brown in the laboratory of Professor Sarah Spiegel, Virginia Commonwealth University.

4.3.7. Optimisation of BODIPY-LacCer trafficking in RAW 264.7 MΦ.

In Chapter 2, lysosomal accumulation of GM1 ganglioside was observed in RAW 264.7 MΦ treated with *Mtb* H37Rv TL extract (Section 2.3.16.). We wished to determine whether the trafficking of LacCer (a precursor of complex GSLs) is also perturbed in cells treated with the *Mtb* H37Rv TL extract [367]. To investigate this, RAW 264.7 MΦ exposed to vehicle were pulsed with BODIPY-LacCer for 30 min at 4^{o}C and then incubated in fresh media for 1h or 2h and the cellular distribution of fluorescent lipids was examined by confocal microscopy. Inspection confirmed that a chase period of 2h resulted in Golgi localisation of BODIPY-LacCer, as revealed by peri-nuclear distribution (white arrows, Fig 4.3.8.), whereas in U18666A-treated RAW 264.7 MΦ, puncta were restricted to

lysosomes (red arrows, Fig 4.3.8.). Therefore, a chase period of 2h was adopted in subsequent experiments.

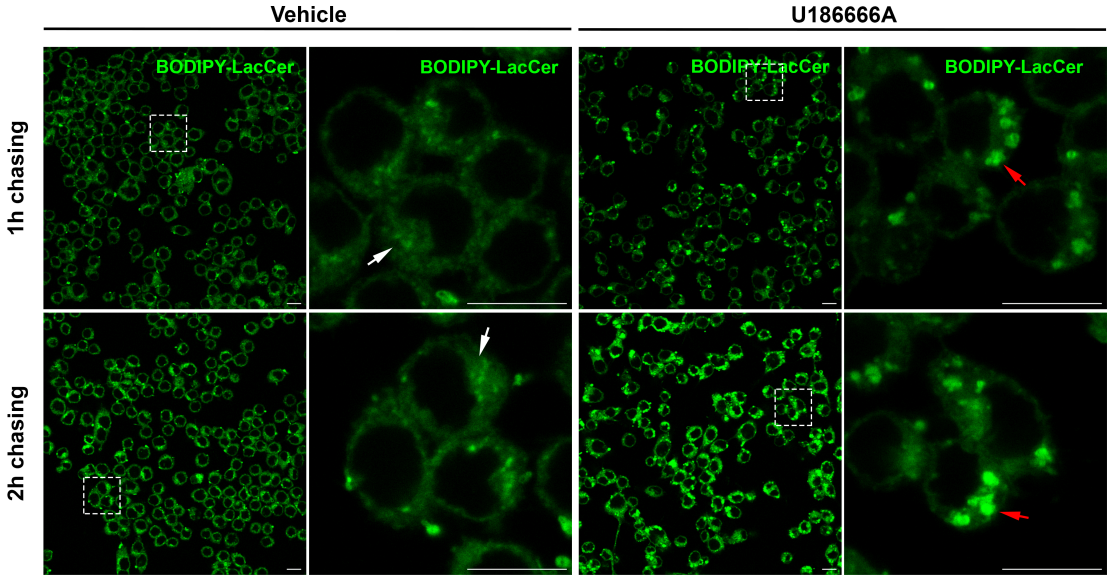


Figure 4.3.7. Optimisation of BODIPY-LacCer trafficking in RAW 264.7 MΦ.

RAW 264.7 MΦ were treated with U18666A (2μg/ml for 48h) to inhibit NPC1. 1h (top) and 2h (bottom) of chasing of BODIPY-LacCer in treated RAW 264.7 MΦ. BODIPY-LacCer, green. White arrows indicate Golgi distribution; red arrows indicate lysosomal distribution. For each pair, the right image is a higher magnification of the region outlined in the left image. Scale bar represents 10μm.

4.3.8. *Mtb* H37Rv TL extract induces BODIPY-LacCer accumulation in lysosomes in RAW 264.7 MΦ.

Pulse-labelling of *Mtb* H37Rv TL extract-treated RAW 264.7 MΦ with BODIPY-LacCer resulted in the accumulation of fluorescent puncta in lysosomes (red arrows, Fig 4.3.8.A.). The frequency of *Mtb* H37Rv TL-treated cells with lysosomal BODIPY-LacCer puncta was significantly greater than that of DMSO-treated cells (****p<0.0001, Fig 4.3.8.B.) and equivalent to that of U18666A-treated RAW 264.7 MΦ (****p<0.0001, Fig 4.3.8.B.).

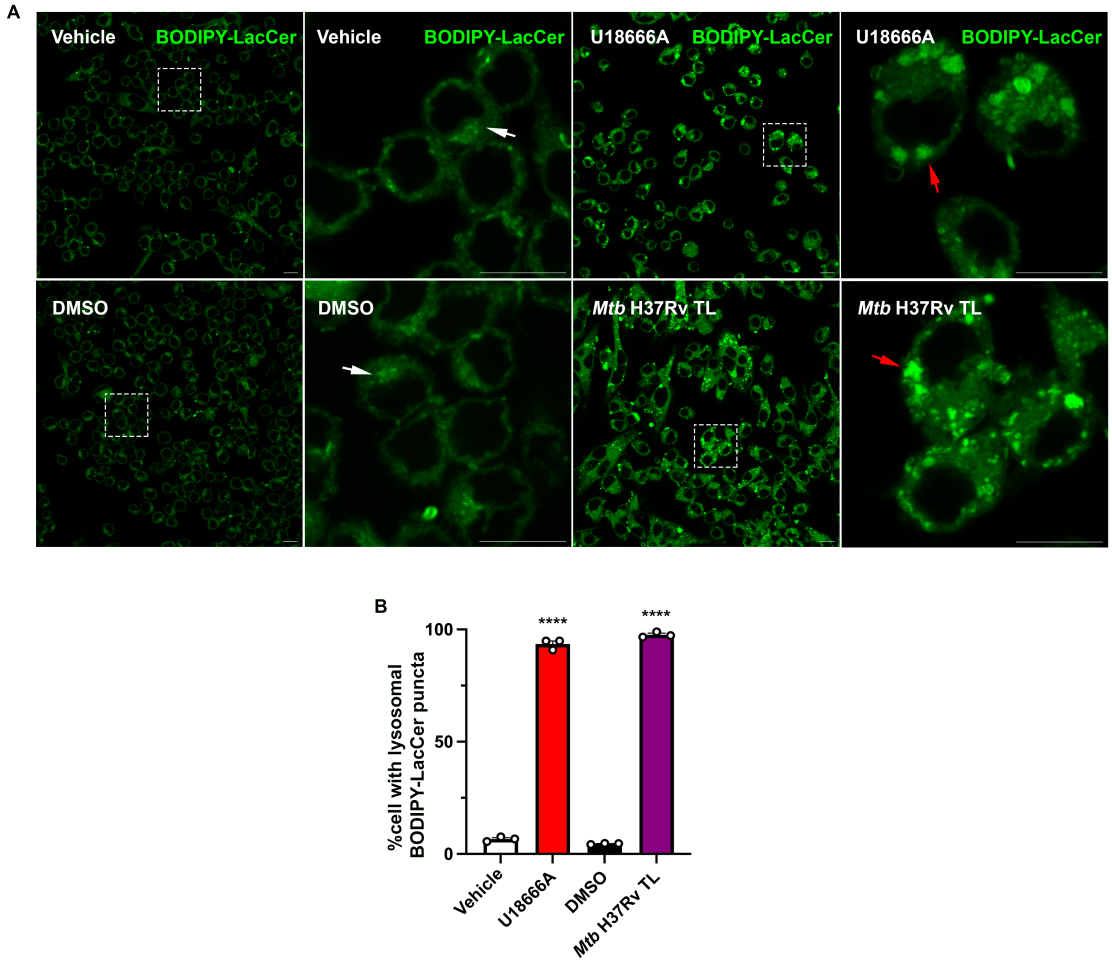


Figure 4.3.8. Mtb H37Rv TL extract induces BODIPY-LacCer lysosomal accumulation in RAW 264.7 MΦ.

Cells were treated with *Mtb* H37Rv TL (100µg/ml for 48h). DMSO and U18666A (2µg/ml for 48h) treatments were vehicle and positive controls respectively. Panel A. Representative confocal microscopy images of BODIPY-LacCer in treated cells. Panel B. Frequency of cells with lysosomal BODIPY-LacCer puncta. White arrows indicate Golgi distribution; red arrows indicate lysosomal distribution. For each pair, the right image is a higher magnification of the region outlined in the left image. BODIPY-LacCer, green. Scale bar represents 10µm. Data are mean ± SEM, n=3. Statistical analysis, Welch's t-test. ****p<0.0001. Statistical comparison of U18666A treatment is relative to vehicle control. Statistical comparisons of lipid treatment is relative to DMSO controls. Data are representative of 2 independent experiments.

4.3.9. U18666A does not alter SphK1 or SphK2 protein expression in RAW 264.7 MΦ.

SphK1 and SphK2 are enzymes that phosphorylate sphingosine to generate S1P [330]. SphK1 is composed of two isoforms, SphK1a and SphK1b [368]. In order to examine whether SphK1 and SphK2 are changed by inhibition of NPC1, we analysed RAW 264.7 MΦ treated with U18666A (2µg/ml) for up to 72h by probing western blots with specific antibodies. In cells treated with U18666A, the amount of SphK1a and SphK1b were not different from those of the DMSO vehicle control at the time points analysed (Fig 4.3.9.A.B.). Similarly, there was no significant difference in SphK2 between drug treatment and controls (Fig 4.3.9.A.C.).

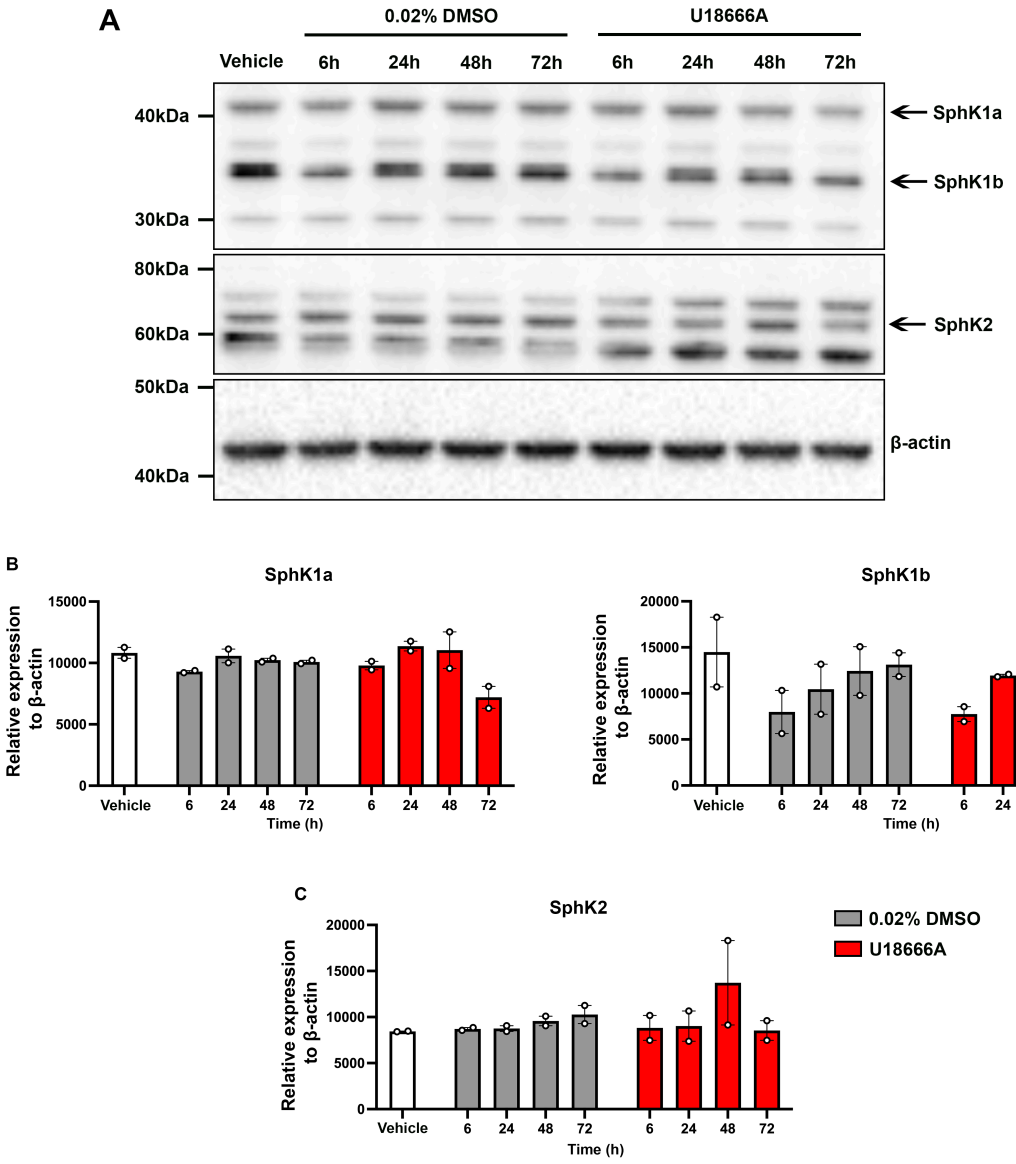
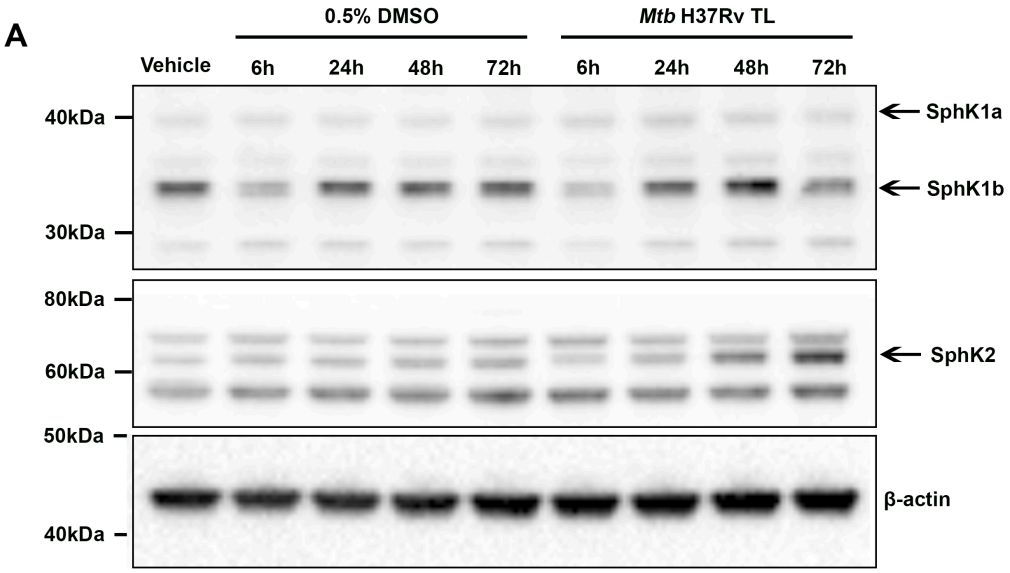


Figure 4.3.9. U18666A treatment does not alter SphK1 and SphK2 protein levels in RAW 264.7 MΦ.

RAW 264.7 MΦ were treated with U18666A (2μg/ml) for 6h to 72h. Panel A. Representative images of western blots of SphK1a, SphK1b, SphK2 and β-actin in treated cells. Expression level of SphK1a (Panel B), SphK1b (Panel B), and SphK2 (Panel C) relative to β-actin. Data are mean ± SEM, n=2. Data are representative of 2 independent experiments.

4.3.10. *Mtb* H37Rv TL increases SphK2, but not SphK1 in RAW 264.7 MΦ.

We made a comparable time course of *Mtb* H37Rv TL extract treatment of RAW 264.7 MΦ. The expression of SphK1a did not differ from the DMSO control at all time points examined, and although the expression of SphK1b was more variable, there was no difference between treatments (Fig 4.3.10.A.B.). In contrast, despite a small but significant decrease in the amount of SphK2 at 6h of treatment, by 48h and 72h, there was a significant increase in the amount of the SphK2 at later time points (Fig 4.3.10.A.C.).



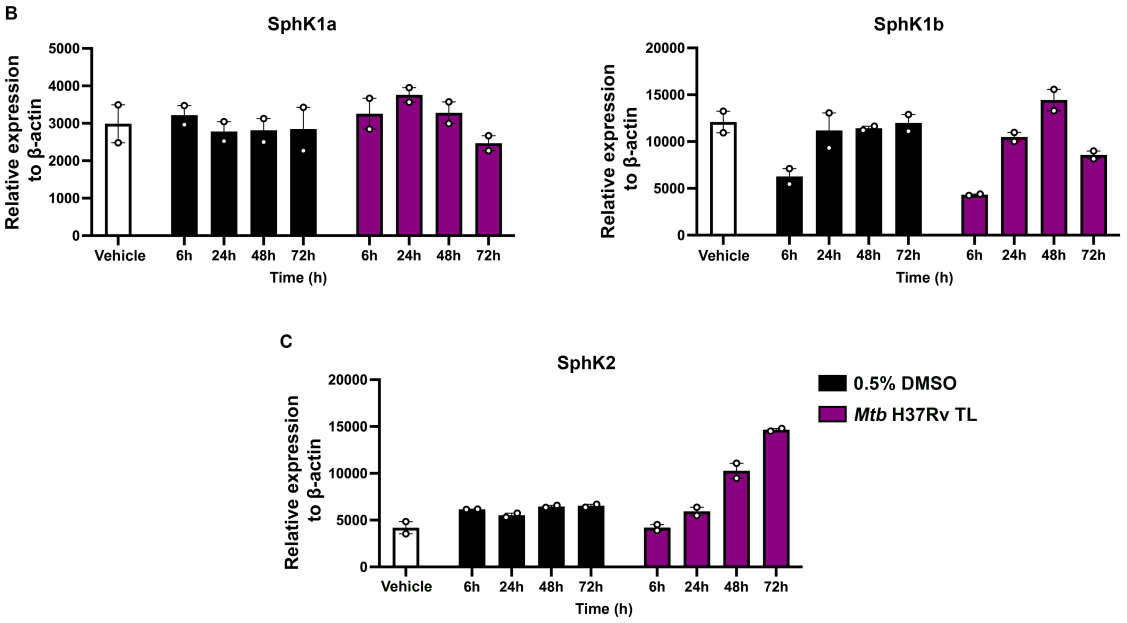


Figure 4.3.10. Mtb H37Rv TL extract does not alter SphK1 but increases SphK2 expression in RAW 264.7 MΦ.

RAW 264.7 MΦ were treated with *Mtb* H37Rv TL extract (100µg/ml) for up to 72h. Panel A. Representative images of western blots of SphK1a, SphK1b, SphK2 and β-actin in treated cells. Expression level of SphK1a (Panel B), SphK1b (Panel B) and SphK2 (Panel C) relative to β-actin in treated cells. Data are mean ± SEM, n=2. Data are representative of 2 independent experiments.

4.4. Discussion

Although NPC is frequently referred to as a disease of cholesterol metabolism because of the prominent storage of this lipid in the endo-lysosomal system, multiple sphingolipids, including GSLs and SM, also accumulate and contribute to pathology [26]. We hypothesised that the inhibition of NPC1 by pathogenic mycobacterial lipids would phenocopy the accumulation of sphingolipids that occurs in the genetic disease.

Sphingosine and sphinganine, which are formed by the condensation of serine with palmitoyl-CoA, are elevated in tissues from NPC patients, although absolute levels can vary between organs [369, 370]. Sphingosine is generated by the degradation of ceramide in the lysosome, and because it is protonated, it is unable to exit from the organelle unless actively transported [371]. The profile of sphingosine accumulation in the pathological cascade underlying NPC has been investigated and showed that sphingosine levels were rapidly elevated within 15min of pharmacological inhibition of NPC1, whereas GSLs were not significantly increased until 4h and cholesterol and SM until 8h [26]. Importantly, sphingosine was the only lipid species that was capable of inducing the lysosomal Ca^{2+} deficiency that is characteristic of NPC [26]. Fusion of *Mtb*-containing phagosomes and host lysosomes has been shown to be influenced by cytosolic Ca^{2+} level [372]. Elevated cytosolic Ca^{2+} promotes trafficking of *Mtb* bacilli to the lysosomal compartment and reduces their survival and replication, whilst the *Mtb* lipid LAM can inhibit the elevation of cytosolic Ca^{2+} [373]. Therefore, the impairment of re-filling of the lysosome with Ca^{2+} by sphingosine, which would result in insufficient release, is likely to enhance intracellular survival of *Mtb* bacilli.

We optimised an RP-HPLC assay to enable sensitive measurement of the sphingosine and sphinganine content of control and *Mtb* H37Rv lipid-treated cells. Consistent with the published data, sphingosine and sphinganine storage occurred within 15min of adding U18666A [26]. Although *Mtb* H37Rv TL did have a similar effect, significant sphingosine accumulation was delayed and was not detectable until the 3h time point. We reasoned that differences in the temporal profiles of sphingolipid abundance caused by the two treatments might be due to the relative amount of NPC inhibition achieved with each treatment (U18666A is a potent pharmacological inhibitor of NPC1 that was used at 2μg/ml, whereas the bioactive lipid is probably only a small fraction of the 100μg/ml *Mtb* H37Rv lipid extract that was added). It could also be that the physical and/or chemical properties of *Mtb* H37Rv lipid result in less uptake or reduced trafficking to the endo-lysosomal system in comparison.

Impaired transport of sphingosine out of the lysosome would be expected to result in a reduction of S1P due to the unavailability of the sphingolipid substrate in the cytosol. Following the inhibition with U18666A, this decline was only transient, which may be due to compensatory upregulation of other ceramidases that act on sphingosine generated outside of the lysosome [26]. Reports documenting S1P in NPC offer differing findings dependent upon the tissue. Fan *et al.* reported the level of S1P was not significantly altered in the liver of *Npc1*$^{-/-}$ mice as compared to wild-type animals but was significantly lower in the plasma of human NPC1 subjects [38]. Significantly reduced levels of S1P and DHS1P [37] in NPC1 mutant fibroblasts have been documented. It may be that the

metabolism of these sphingolipids is affected differentially between tissues in NPC and perhaps influenced by the duration of NPC1 inhibition [37].

S1P abundance is not only influenced by the availability of the sphingosine substrate, but also by the activity of the kinases SphK1 and SphK2 that phosphorylate the sphingolipid [374]. SphK activity has been reported to be markedly reduced in NPC neurons and patient fibroblasts [37, 375]. Cells with pharmacological inhibition or genetic loss of SphK result in the failure of ER-lysosomal membrane contact site formation and cholesterol accumulation [37, 340]. However, we did not detect a significant change in SphK1 and increased SphK2 after *Mtb* H37Rv lipid treatment, with the caveat that we examined for the amount of protein, which may not be an accurate reflection of enzymatic activity.

We found that there was a significant increase in ceramide in response to *Mtb* H37Rv TL treatment. Accumulation of ceramide species, especially Cer:16 has been confirmed in *Npc1*$^{-/-}$ mouse tissues and lysosomes isolated from *NPC1* or *NPC2* mutant HeLa cells [38, 376]. However, although *Mtb* H37Rv TL induced significant storage, we were unable to measure accumulation in U18666A-treated RAW 264.7 MΦ. It may be that ceramide storage was caused by a different lipid component of the mycobacterial extract and was, therefore, independent of NPC1 inhibition.

Accumulation of the glycosphingolipid, GlcCer, is a biomarker of NPC in both patients, and in spleens and livers in murine disease models [11, 377]. The cellular levels of GlcCer are controlled by the activity of GCS and its enzymatic

activity is enhanced in NPC [378]. Therefore, increased levels of the glycolipid (monohexosylceramide as detected by MS) in U18666A-treated cells were not unexpected and the comparable increase induced by *Mtb* H37Rv TL extract is therefore consistent with inhibition of NPC1.

SM accumulation is also a feature of NPC, and we were able to confirm a significant increase with *Mtb* H37Rv TL treatment over a period of 24h, which was comparable to U18666A treatment, indicative inhibition of NPC1. A previous study that utilised staining with fluorescent lysenin revealed the accumulation of SM and re-localisation to lysosomes after 8h of U18666A treatment [26]. Failure to deliver SMase to the lysosome or plasma membrane causes the inhibition of *Mtb*-containing phagosome maturation and promotes intracellular replication of the microbe [379].

In previous chapters, we demonstrated miss-trafficking of GM1 ganglioside in NPC1-inhibited cells or ones treated with TL extracts of *Mtb* and other mycobacteria by pulse-labelling using fluorescent-conjugated CtxB and observing the accumulation of puncta in acidic compartments (Section 2.3.16.; Section 3.3.5.). In order to examine whether there was a comparable perturbation of LacCer transport, we incubated RAW 264.7 MΦ with BODIPY/BSA-conjugated analogue and inspected for lysosomal accumulation by pause-chasing methods. Evidence of altered sphingolipid trafficking was proved by a high frequency of cells displaying lysosomal accumulation with *Mtb* H37Rv TL treatment as well as pharmacological inhibition of NPC1.

Our expectation was that analysis of sphingolipid metabolism in drug and mycobacteria lipid-treated cells would not only provide additional support for a mechanistic link between pathogenic mycobacteria and NPC but also identify sphingolipids that are altered as a result of NPC1 inhibition and affect *Mtb* pathogenesis. It is known that multiple pathogens, including *Mtb*, dysregulate sphingolipid metabolism for survival [380]. As outlined in the introduction, S1P is a particularly important bioactive lipid because of its roles in cell signalling and association with diseases, whose metabolism is regulated by SphK1 and SphK2 and is dependent on the substrate (sphingosine) [330]. Several studies have documented that *Mtb* can manipulate SphK to enhance survival. Malik *et al.* reported that the block in the maturation of *Mtb*-containing phagosome is a result of the inhibition of SK activities that are necessary for the elevation of cytosolic Ca^{2+} [363]. Translocation of SphK1 to nascent phagosomes, which is required for actin nucleation, is actively prevented by *Mtb* [381, 382]. Furthermore, SphK activity is important for the elimination of non-pathogenic mycobacteria and the generation of pro-inflammatory responses; pharmacological inhibition of SphK1 rendered MΦ susceptible to *M. smegmatis* infection, and the production of inflammatory mediators requires SphK-dependent activation of calmodulin and MAP kinase pathway [364, 383].

Bioactive host lipids, some of which are altered in NPC, are known to impact mycobacterial survival, such as by regulating phagosome biogenesis and development [188]. Signalling lipids can activate or inhibit actin assembly on phagosome membranes, a process linked to organelle maturation and the acquisition of anti-microbial activities. Studies made using an *in vivo* phagosome

assembly assay together with live cells have identified a network of host lipids. Sphingosine, S1P and ceramide could affect actin nucleation on pathogenic and non-pathogenic mycobacterial phagosomes and phagosome lysosome fusion, but with the exception of ceramide, could not stimulate the release of nitric oxide [384]. Ceramide, sphingosine and S1P can enhance the killing of mycobacteria without activating NF-κB [385]. These data would suggest that changes in the abundance of sphingolipids that occur in NPC have the potential to affect mycobacterial survival, but it is their intracellular distribution and availability, rather than absolute abundance, that is likely to be important.

In summary, we hypothesised that mechanistic convergence between NPC and *Mtb* H37Rv TL-treated RAW 264.7 MΦ would be reflected by comparable changes to sphingolipids metabolism. In general, the hypothesis held true, but there was evidence of added complexity that may be explained by the presence of multiple ligands in the mycobacterial extract that was tested.

Chapter 5. Inhibition of the NPC Pathway by Lipid Components from *Mtb*

List of *Mtb* membrane lipids abbreviation

AG	arabinogalactan
DAT	diacyltrehalose
LAM	lipoarabinomannan
LM	lipomannan
MA	mycolic acid
ManLAM	mannose-capped lipoarabinomannan
PAT	polyacyltrehalose
PDIM	phthiocerol dimycocerosate
PG	peptidoglycan
PGL	phenolic glycolipid
PI	phosphatidylinositol
PIM	phosphatidylinositol mannoside
SL	sulpholipid
TDM	trehalose di-mycolate
TMM	trehalose mono-mycolate

5.1. Introduction

In the previous chapters, we have shown that cell wall lipid extracts of multiple species of pathogenic mycobacteria were able to induce cellular phenotypes characteristic of NPC, which was consistent with inhibition of the NPC pathway. We hypothesised that particular lipid(s) were responsible for the inhibition of NPC1 activity and therefore undertook investigations to identify bioactive specific lipid(s).

The structure of the mycobacterial cell wall

Mycobacteria have an outer membrane with a complex lipid composition, which is critical for microbial physiology. It plays important roles in the regulation of membrane permeability, formation of biofilms, protection from hostile conditions and survival in host cells [168]. The mycobacterial cell wall represents the interface between the microbe and the environment. Structurally, it differs from both Gram-positive and Gram-negative bacteria. It is a lipid-rich structure, which is composed of inner membrane and outer membrane connected by peptidoglycan and arabinogalactan and a capsule of mannan-containing long-chain lipids that surround the outer membrane (Fig 5.1.1.) [168].

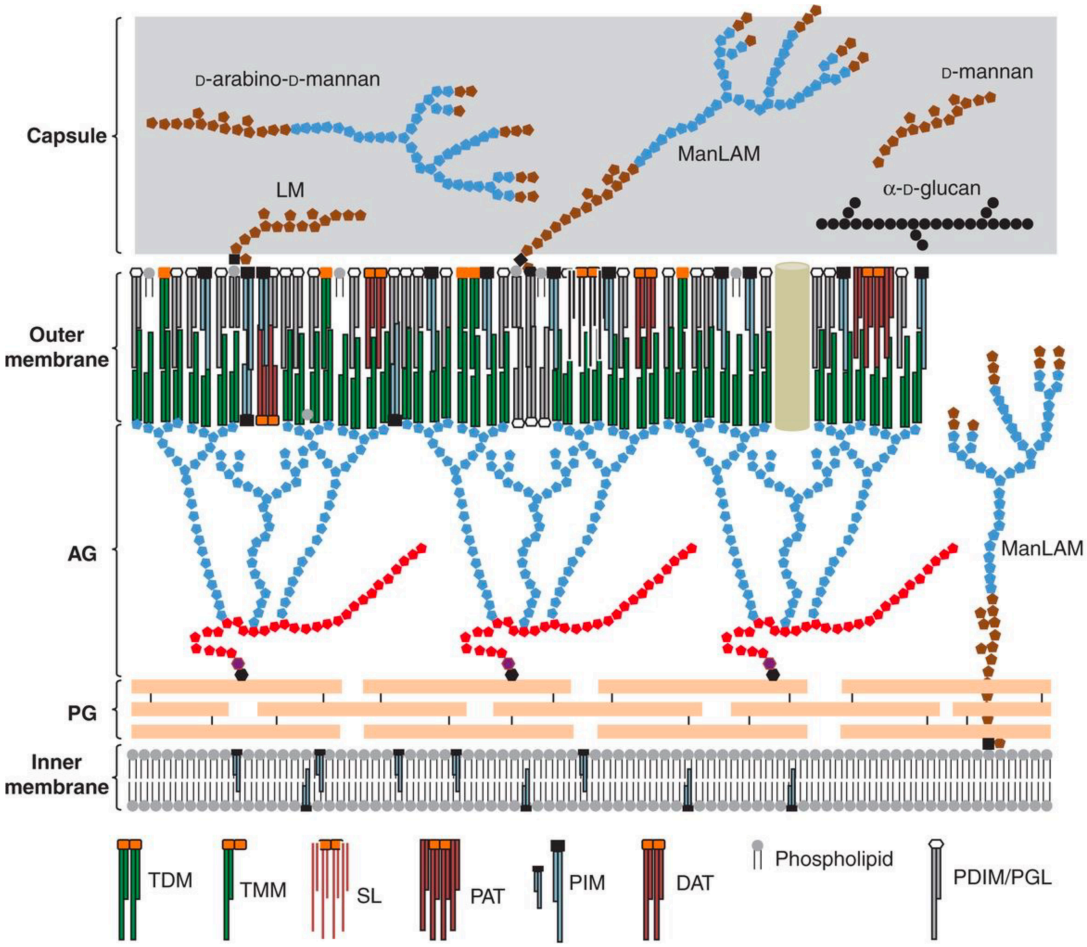


Figure 5.1.1. Schematic of the Mtb cell envelope.

The *Mtb* cell wall is composed of an inner membrane containing phospholipids and PIM that is surrounded by a layer of PG to which it is non-covalently bonded. The PG layer is covalently linked to the outer membrane by an AG layer, which is itself esterified to mycolic acids in the outer membrane. The outer membrane contains TMM, TDM, SL, PDIM, PAT and DAT. The outermost capsule contains LM and LAM. Light blue, arabinose residues; red, galactose residues; brown, mannose residues; black circles, glucose residues; dark green, mycolic acid. PIM, phosphatidylinositol mannoside; PG, peptidoglycan; AG, arabinogalactan; TMM, trehalose mono-mycolate; TDM, trehalose di-mycolate; SL, sulpholipid; PDIM, phthiocerol dimycocerosate; DAT, diacyltrehalose; PAT, polyacyltrehalose. Adapted from [168].

The inner membrane is mainly made up of phospholipid and mannosylated forms of phosphatidylinositol (PI), collectively known as PIMs [238]. About 50% of the dry weight of the outer membrane is MA [168]. MA is shuttled from the cytosol to the outer membrane as TMM and formed into TDM in the outer membrane or is covalently bound to the inner membrane [172]. PIM species are the major lipids of the outer membrane [168]. Other lipoglycans, such as LM and mannose-capped lipoarabinomannan (ManLAM), constitute the capsule surrounding the outer membrane. Some lipids in the outer membrane, such as sulpholipid-1 (SL-1), phenolic glycolipid (PGL), PDIM, diacyltrehalose (DAT) and polyacyltrehalose (PAT) are specific to particular species of mycobacteria. For example, SL-1 production is restricted to human tubercular *Mtb* strains, including H37Rv, HN878, CDC1551, Erdman and *M. canettii* [386]. PDIM, DAT and PAT are constrained to virulent *Mtb* strains [168, 387].

MA and TDM in *Mtb* pathogenesis

As the most abundant lipid in the *Mtb* outer membrane, MA and MA-containing lipid species are important during *Mtb* infection [388]. MA forms the backbone of the outer membrane and is also present in other bacterial species such as *Corynebacterium*, *Nocardia* and *Rhodoccocus* [388, 389]. It is critical for the viability, cell membrane integrity and drug resistance of *Mtb* bacilli [390]. Three classes of MA are present in *Mtb,* including α-, keto- and methoxy-mycolates, of which α-MA is the most abundant (>70%) (Fig 5.1.2.A.) [390]. Keto-MA and methoxy-MA are the most potent with respect to the induction of foamy MΦ, with keto-MA being the most active at inducing cholesterol accumulation and promoting *Mtb* proliferation within the host cells [391]. A *Mtb* mutant, which is

unable to synthesise MA, displays attenuated virulence in the mouse model [392]. For this reason, multiple studies have concluded that the inhibition of the MA biosynthetic pathway may be a promising target for the development of antimicrobial drugs [393].

TDM, widely referred to as 'cord factor', is crucial for the progression of disease pathogenesis, granuloma formation, intracellular persistence of bacilli and influences host immune responses (Fig 5.1.2.B.) [394-396]. The inhibition of phagosome-lysosomal fusion is one of the most profound effects of TDM and facilitates the survival and persistence of *Mtb* inside host cells. In the early 1990s, studies showed that both free MA and TDM inhibit fusion between phospholipid vesicles [191]. Injection of TDM in mice sensitised with low doses of *Mtb* induces caseation of lung granuloma and prolongs systemic persistence of bacilli [397]. TDM also binds to and activates the C-type lectin, Mincle, on the host cell membrane, which mediates inhibition of *Mtb*-containing phagosome maturation and acidification [184, 190, 398]. Infection with *Mtb* that has diminished TDM production results in impaired inhibition of phagosome maturation and increased co-localisation of bacilli and lysosomes [399].

SL-1

SL-1 is a sulphated glycolipid found only in cell walls of virulent *Mtb* (Fig 5.1.2.C.) [400]. Unlike MA-based lipids, which are essential for the outer membrane structure, SL-1 is not necessary for mycobacterial growth but contributes to the pathogenicity [168]. Synthesis of SL-1 in mycobacteria is regulated by the expression of the *pks2* gene [401]. In mice and guinea pig infection models, there

was no difference between WT and mutant *Mtb* lacking SL-1 with respect to systemic replication and persistence of mycobacteria [400, 402, 403]. However, *in vitro* studies have shown that SL-1 affects host responses and induces superoxide production by neutrophils [404]. SL-1 also acts as an antagonist of the effects of TDM by reducing TNF-α production and lung granuloma formation in mice [405]. The importance of SL-1 for successful infection is supported by the evidence that an *Mtb* strain mutant for MmpL8, which encodes a transporter required for release of the lipid during infection, is unable to persist in mice [406, 407].

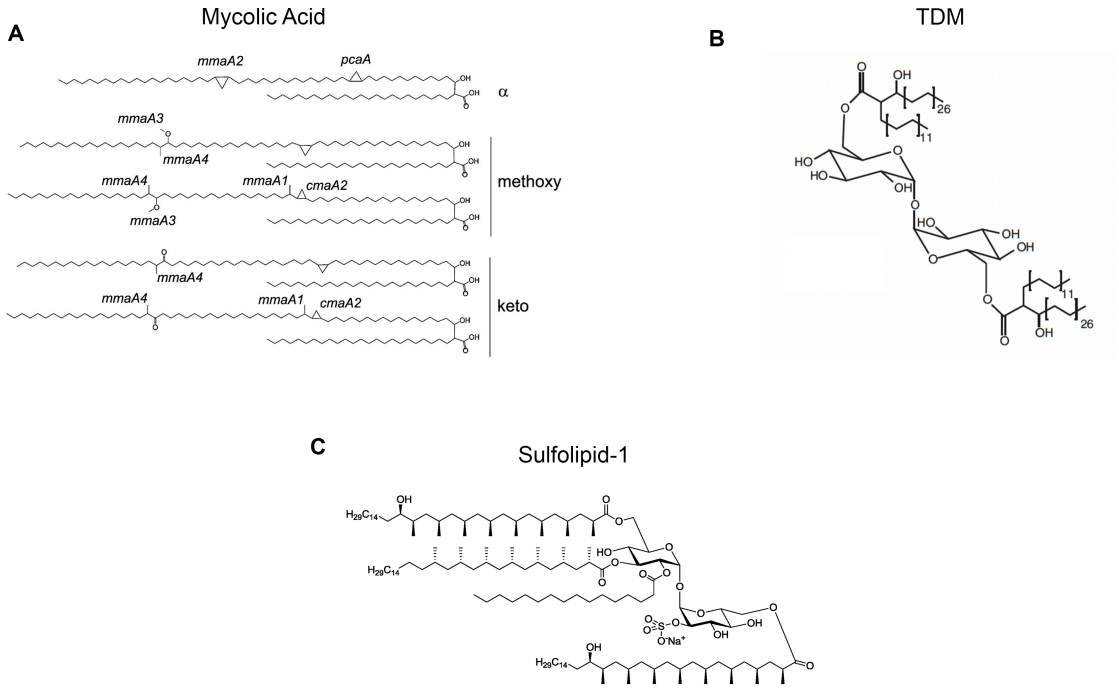


Figure 5.1.2. Structure of mycolic acid, TDM and sulfolipid-1 from Mtb cell wall.

TDM, trehalose dimycolate. Adapted from [168, 390, 408].

PIM, LM and LAM

PI acts as a shared lipid anchor for PIM, LM and LAM on the *Mtb* outer membrane. PIM accounts for ~43% of all the lipids of the outer leaflet of the outer membrane [409]. The molecular synthesis pathway of PIM species is shown in Fig 5.1.3.B. In brief, the inositol residue in PI is mannosylated to generate PIM_1 and additional mannose groups are added to produce PIM_2 through to PIM_6 [410]. PIM_1 and PIM_2 are synthesised on the inner leaflet of the *Mtb* cell membrane [170]. PIM_2 can be inositol acetylated to $AcPIM_2$ and $AcPIM_3$. $AcPIM_3$ can be flipped to the outer leaflet of the cell membrane where it is mannosylated into $AcPIM_4$ [170]. $AcPIM_4$ is the branch point between the end products of PIM synthesis and those of LM/LAM [170]. PimE elongates $AcPIM_4$ through the addition of mannoses to form $AcPIM_6$ [411]. Although not essential for mycobacteria survival, the growth rates of *M. smegmatis* and *Mtb* lacking PIM are attenuated [412]. Inositol acetylation of PIM facilitates mycobacterial membrane fluidity, which promotes resistance under extracellular stress [413]. During *Mtb* infection, PIM stimulates EE formation and inhibits endosomal acidification in murine MΦ [188]. PIM_1 and PIM_2 have also been shown to inhibit aspects of host immune responses [414]. Other PI-containing lipids, such as LM and LAM, also exhibit the ability to block phagosome maturation [415, 416].

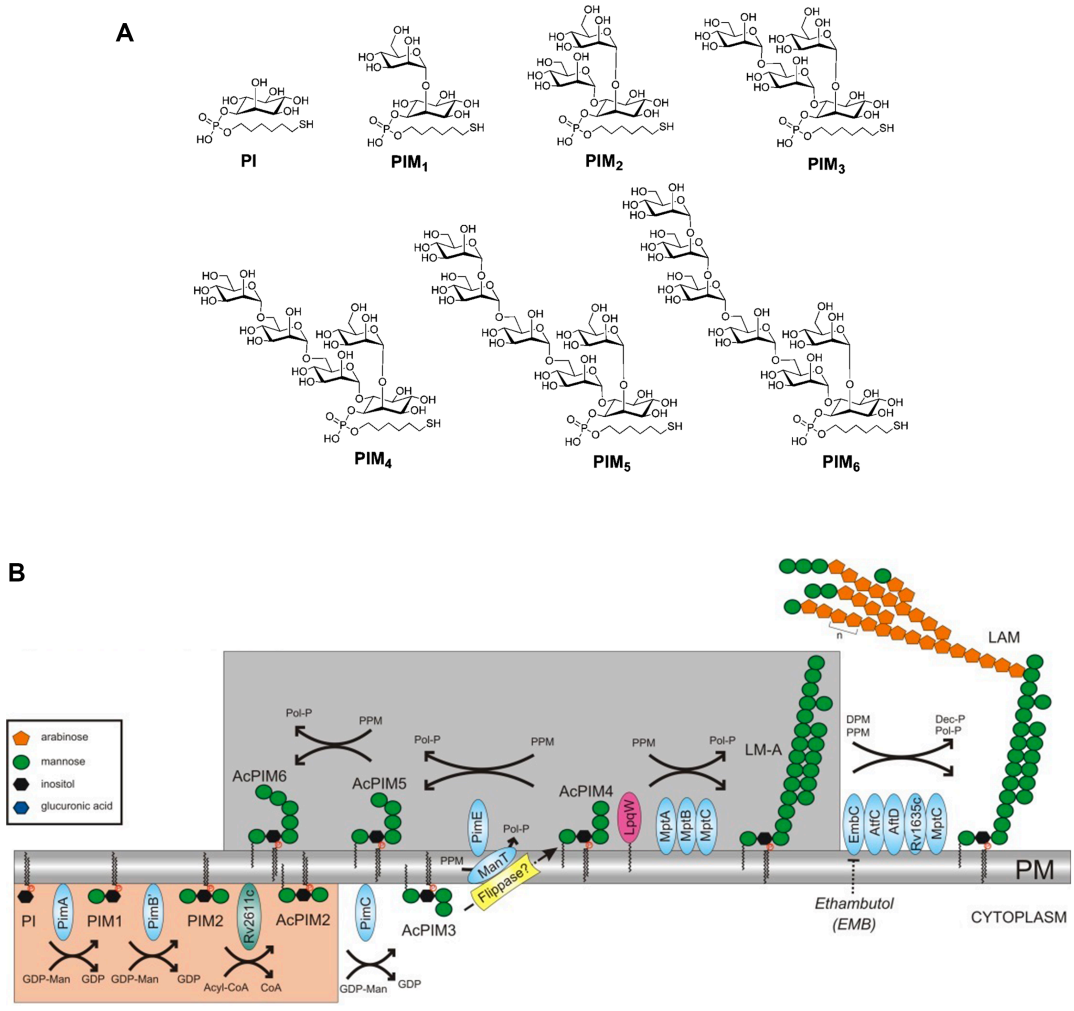


Figure 5.1.3. Structure (A) and the biosynthesis pathway (B) of PIM.

PI, phosphatidylinositol; PIM, phosphatidylinositol mannoside; LM, lipomannan; LAM, lipoarabinomannan. Adapted from [170, 410].

Although there is evidence that *Mtb* lipids facilitate intracellular survival of bacilli via activities such as inhibition of phagosome maturation and modulation of host cell immune responses, understanding of the mechanisms by which they are involved and how they are coordinated is remains incomplete [169]. Fineran *et al.* reported that TDM and MA from BCG were able to inhibit NPC1 [96]. MA treatment in both murine and human MΦ induced NPC cellular phenotypes, including cholesterol storage and lysosomal GM1 and SM accumulation [96].

Similarly, TDM treatment in both murine and human MΦ increased lysosomal volume, reduced lysosomal Ca^{2+} content and caused cholesterol storage and lysosomal sphingosine accumulation [96]. However, at the time, only selected lipid fractions were made available by a collaborator for these studies, and their lipid content and purity were unknown.

In this chapter, we therefore initiated a classical biochemical strategy involving fractionating the TL extract of *Mtb* H37Rv with the intention of determining activity to unambiguously identify the specific lipid(s). Second, we tested purified mycobacterial lipid species that were available from a biological resource centre (BEI Resources) for inhibition of the NPC pathway and provided accompanying composition data.

Aims

- Undertake biochemical fractionation of a *Mtb* H37Rv TL extract and test abilities of fractions to inhibit NPC1 with the objective of identifying the specific lipid(s).
- Screen for the ability of purified lipid components from *Mtb* H37Rv to induce NPC phenotypes in MΦ.

5.2. Material and Methods

5.2.1. Cells

RAW 264.7 MΦ were obtained and cultured as described in Section 2.2.1.

5.2.2. Mycobacterial culture and lipid extract

Mycobacteria were cultured as described in Section 2.2.2. Cultures of *Mtb* H37Rv were made by Dr Gerald Larrouy-Maumus at Imperial College, London. *Mtb* H37Rv and *ΔpimE Mtb* H37Rv were cultured, and TL extracts were prepared in the laboratory of Professor Mary Jackson at Colorado State University. Total lipids were extracted twice with $CHCl_3$: MeOH 2:1 (v/v) with continuous stirring at room temperature for 24h, dried under N_2 flow and washed in $CHCl_3$: MeOH: H_2O 4:2:1 (v/v/v). Purified lipids from *Mtb* H37Rv obtained from BEI Resources are listed in Table 5.2.2.

Lipid species	Cat No.	Solvent for solublisation
H37Rv, Purified Mycolic Acid Methyl Esters	NR-14854	$CHCl_3$
H37Rv, Purified Sulfolipid-1 (SL-1)	NR-14845	DMSO
H37Rv, Purified Trehalose Dimycolate (TDM)	NR-14844	DMSO
H37Rv, Purified Mycolylarabinogalactan-Peptidoglycan (mAGP)	NR-14851	DMSO
H37Rv, Purified Lipomannan (LM)	NR-14850	PBS
H37Rv, Purified Phosphatidylinositol Mannosides 1 & 2 ($PIM_{1,2}$)	NR-14846	DMSO
H37Rv, Purified Phosphatidylinositol Mannoside 6 (PIM_6)	NR-14847	PBS
H37Rv, Purified Lipoarabinomannan (LAM)	NR-14848	PBS
H37Rv, Mycobactin	NR-44101	DMSO
H37Rv, Purified Trehalose Monomycolate (TMM)	NR-48784	DMSO
H37Rv, Purified Arabinogalactan	NR-14852	ddH_2O
H37Rv, Purified Phthiocerol Dimycocerosate (PDIM)	NR-20328	DMSO
H37Rv, Acetone-Insoluble Lipids Mycobacterium tuberculosis	NR-14843	DMSO
H37Rv, Acetone-soluble Lipids Mycobacterium tuberculosis	NR-14842	DMSO

Table 5.2.2. Mtb H37Rv purified lipids obtained from BEI Resources and the solvents used for solubilisation.

5.2.3. *Mtb* lipid fractionation

Total lipid from *Mtb* H37Rv was extracted and fractionated using sequential $CHCl_3$, MeOH and H_2O solubility according to published methods [126]. Seventeen fractions representing the least polar to the most polar (labelled 1 to 17) were provided by Dr Gerald Larrouy-Maumus at Imperial College, London. Fractions 1 to 3 were eluted with pure $CHCl_3$; fractions 4 to 6 were eluted with $CHCl_3$: MeOH 9:1 (v/v); fractions 7 to 9 were eluted with $CHCl_3$: MeOH 8:2 (v/v); fractions 10 to 12 were eluted with $CHCl_3$: MeOH 7:3 (v/v); fractions 13 to 15 were eluted with $CHCl_3$: MeOH: H_2O 60:25:14 (v/v/v) and fractions 16 and 17 were eluted with $CHCl_3$: MeOH: H_2O 60:35:8 (v/v/v).

5.2.4. Lipid solubilisation and addition to cell culture

Total lipid extracts were dissolved in DMSO as described in Section 2.2.3. Purified lipids were solubilised in the appropriate solvent, as indicated in Table 5.2.2. RAW 264.7 MΦ were treated with individual *Mtb* lipid fractions (10μg/ml for 48h) before staining with LysoTracker™ Green DND-26 and analysed by FACS as described in Section 2.2.4. For analysis of pro-IL1β expression, RAW 264.7 MΦ were treated with *Mtb* H37Rv lipid fractions (2μg/ml for 48h) and then stimulated with LA (50ng/ml) as described in Section 2.2.5. For analysing cholesterol re-distribution, GM1 ganglioside miss-trafficking, Npc1 and Npc2 protein expression and sphingolipid content, RAW 264.7 MΦ were treated with 25μg/ml of the purified lipid for 48h. In studies comparing the activities of *Mtb* H37Rv and *ΔpimE Mtb*, RAW 264.7 MΦ were treated with 100μg/ml for 48h with TL extracts.

5.2.5. MALDI-ToF analysis of lipid composition.

The MALDI-ToF MS analysis of the lipid composition was performed by Dr Gerald Larrouy-Maumus as described in Section 2.2.15.

5.2.6. TLC for PIM profile

TLC was performed by Dr Zuzana Palcekova in the laboratory of Professor Mary Jackson at Colorado State University. Total lipids from WT and *ΔpimE Mtb* H37Rv were extracted twice with $CHCl_3$: MeOH 2:1 (v/v) while stirring at RT for 24h, dried in nitrogen and Folch washed in $CHCl_3$: MeOH: H_2O 4:2:1 (v/v/v). PIM profile was analysed by TLC on Silica gel 60 F_{254} (Merck, 1055540001).

5.2.7. LysoTracker™ staining for FACS analysis.

LysoTracker™ Green DND-26 staining was performed as described in Section 2.2.4.

5.2.8. Immunofluorescent staining

LAMP-1 immunostaining of RAW 264.7 MΦ treated with mycobacterial lipids was performed as described in Section 2.2.10.

5.2.9. Filipin staining of free cholesterol.

Filipin staining for free cholesterol was performed as described in Section 2.2.11.

5.2.10. CtxB staining

CtxB labelling analysis of GM1 trafficking in RAW 264.7 MΦ treated with mycobacterial lipids was performed as described in Section 2.2.13.

5.2.11. Sphingosine and sphinganine levels by RP-HPLC.

Preparation of cell lysates for analysis of sphingosine and sphinganine was described in Section 4.2.4. Sphingosine and sphinganine RP-HPLC analysis was performed as in Section 4.2.5.

5.2.12. GSL levels determined by NP-HPLC.

Preparation of cell lysates for GSL analysis was performed as described in Section 2.2.14. GSL analysis was as described in Section 2.2.14.

5.2.13. Statistical analysis

Statistical analyses were performed as described in Section 2.2.16.

5.3. Results

5.3.1. Fractionated *Mtb* H37Rv TL extract significantly increases LysoTracker™ staining intensity of RAW 264.7 MΦ.

In order to isolate the *Mtb* cell wall lipid(s) which inhibit the activity of NPC1, TL extract was fractionated according to polarity and the resulting fractions were assayed for their ability to enhance relative acidic compartment volume using FACS-based LysoTracker™ assay. Nine out of 17 fractions from *Mtb* H37Rv induced a small but significant increase in LysoTracker™ staining intensity. Fraction 14 was the most potent fraction and enhanced LysoTracker™ intensity to a level comparable to U18666A treatment (Fig 5.3.1.A.). Although several fractions of *M. smegmatis* (a non-pathogenic environmental mycobacteria) TL extract induced small but significant increases in LysoTracker™ staining intensity in RAW 264.7 MΦ, none were comparable to U18666A-treatment (Fig 5.3.1.B.).

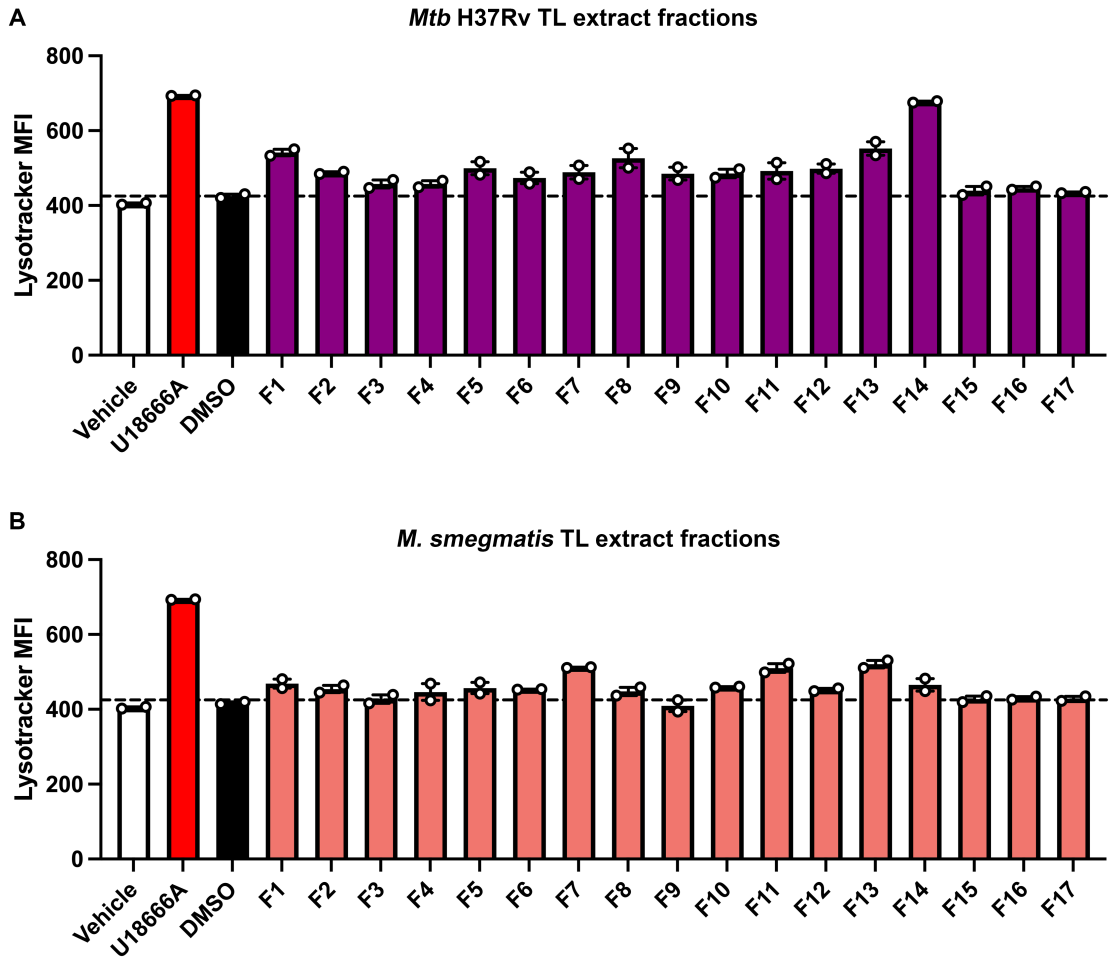


Figure 5.3.1. Fractionated Mtb H37Rv and M. smegmatis TL extracts significantly increase LysoTracker™ staining intensity of RAW264.7 MΦ.

RAW 264.7 MΦ were treated with fractionated *Mtb* H37Rv or *M. smegmatis* lipid extract (10μg/ml for 48h), stained with LysoTracker™ Green DND-26 and analysed by FACS. Panel A. Quantification of LysoTracker™ staining intensity in fractionated *Mtb* H37Rv TL treated cells. Panel B. Quantification of LysoTracker™ staining intensity in fractionated *M. smegmatis* TL-treated cells. MFI, mean fluorescence intensity. Data are mean ± SEM, n=2. Data are representative of 2 independent experiments.

5.3.2. Fractionated *Mtb* H37Rv TL extract inhibits pro-IL1β synthesis in RAW 264.7 MΦ.

We investigated the ability of *Mtb* cell wall lipid fractions to inhibit the LA-dependent pro-IL1β synthesis by RAW 264.7 MΦ (performed by Dawn Shepherd). Although inhibitory activity was found within multiple fractions of *Mtb* H37Rv TL extract, the most potent were fractions F7 and F14 (****p<0.0001, Fig 5.3.2.A.). Inhibitory activity was also widespread across *M. smegmatis* lipid fractions but none were of the extent that was observed with *Mtb* H37Rv TL extract (****p<0.0001, Fig 5.3.2.B.).

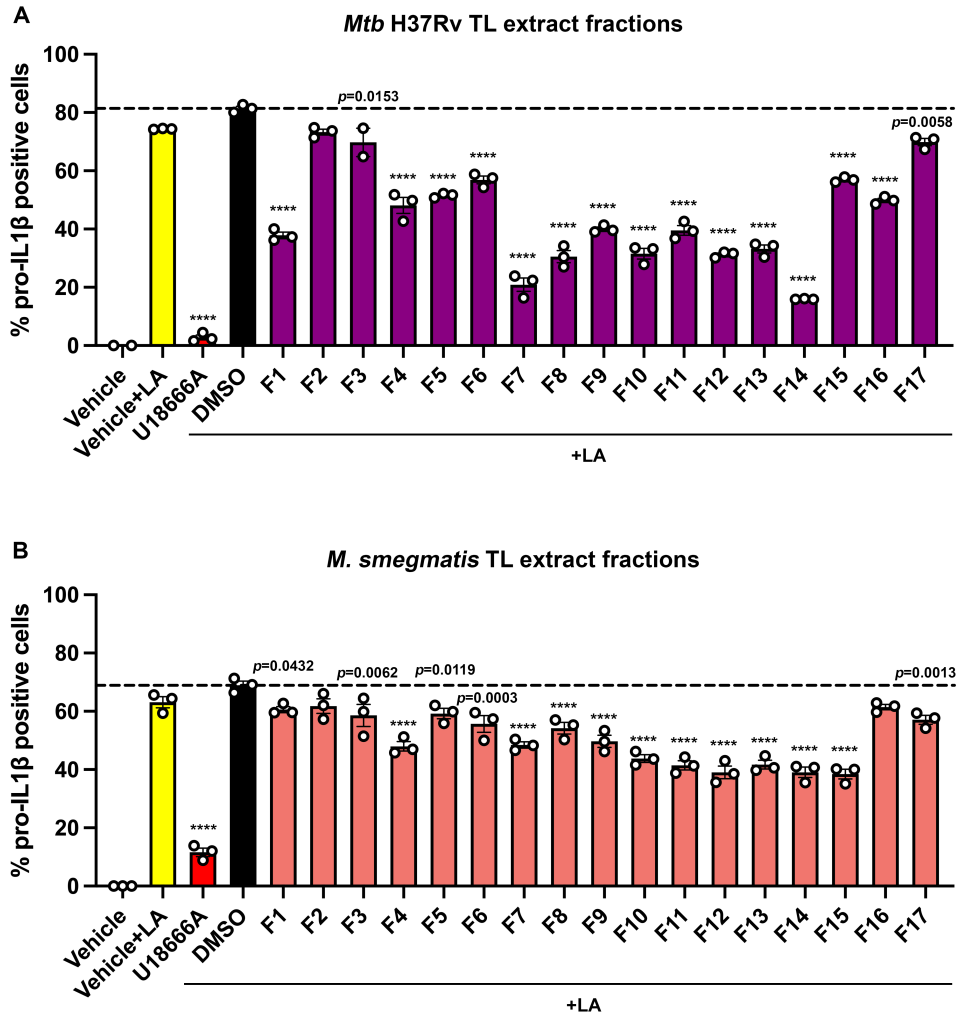


Figure 5.3.2. LA-dependent pro-IL1β synthesis in RAW 264.7 MΦ inhibited by selected Mtb H37Rv cell wall lipid fractions.

RAW 264.7 MΦ were treated with fractionated *Mtb* H37Rv or *M. smegmatis* TL extract (2μg/ml for 48h), stimulated with 50ng/ml LA for 6h and production of pro-IL1β was determined by FACS. Panel A. Frequency of pro-IL1β positive cells treated with fractionated *Mtb* H37Rv TL extract. Panel B. Frequency of pro-IL1β positive cells treated with fractionated *M. smegmatis* TL extract. Dotted lines indicate DMSO level. Data are mean ± SEM, n=2. Statistical analysis, one-way ANOVA with Dunnett's multiple comparisons. ****p<0.0001, other p values as indicated, otherwise not significant. Statistical comparison of U18666A treatment is relative to vehicle control + LA treatment. Statistical comparisons of lipid treatments are relative to the DMSO control. Data are representative of 2 independent experiments. These data were generated by Dawn Shepherd.

5.3.3. MALDI-ToF MS analysis of the lipid compositions in fractions 13, 14 and 15 of *Mtb* TL extract.

Because it was the most potent lipid fraction in terms of increasing relative lysosomal volume and inhibition of pro-IL1β synthesis, the lipid compositions of fraction 14 and adjacent fractions 13 and 15 was determined by MALDI-ToF MS by Dr Gerald Larrouy-Maumus at Imperial College, London. The resulting MS profiles (Fig 5.3.3.) indicated relative enrichment of PI lipid species in fractions 13, 14, and 15. There was a greater abundance of Ac_2PIM_2, Ac_3PIM_2 and Ac_4PIM_6 in fraction 14 as compared to fractions 13 and 15 (Fig 5.3.3.A.B.), and more Ac_4PIM_6 in fraction 15 than in fractions 13 and 14. (Fig 5.3.3.B.C.).

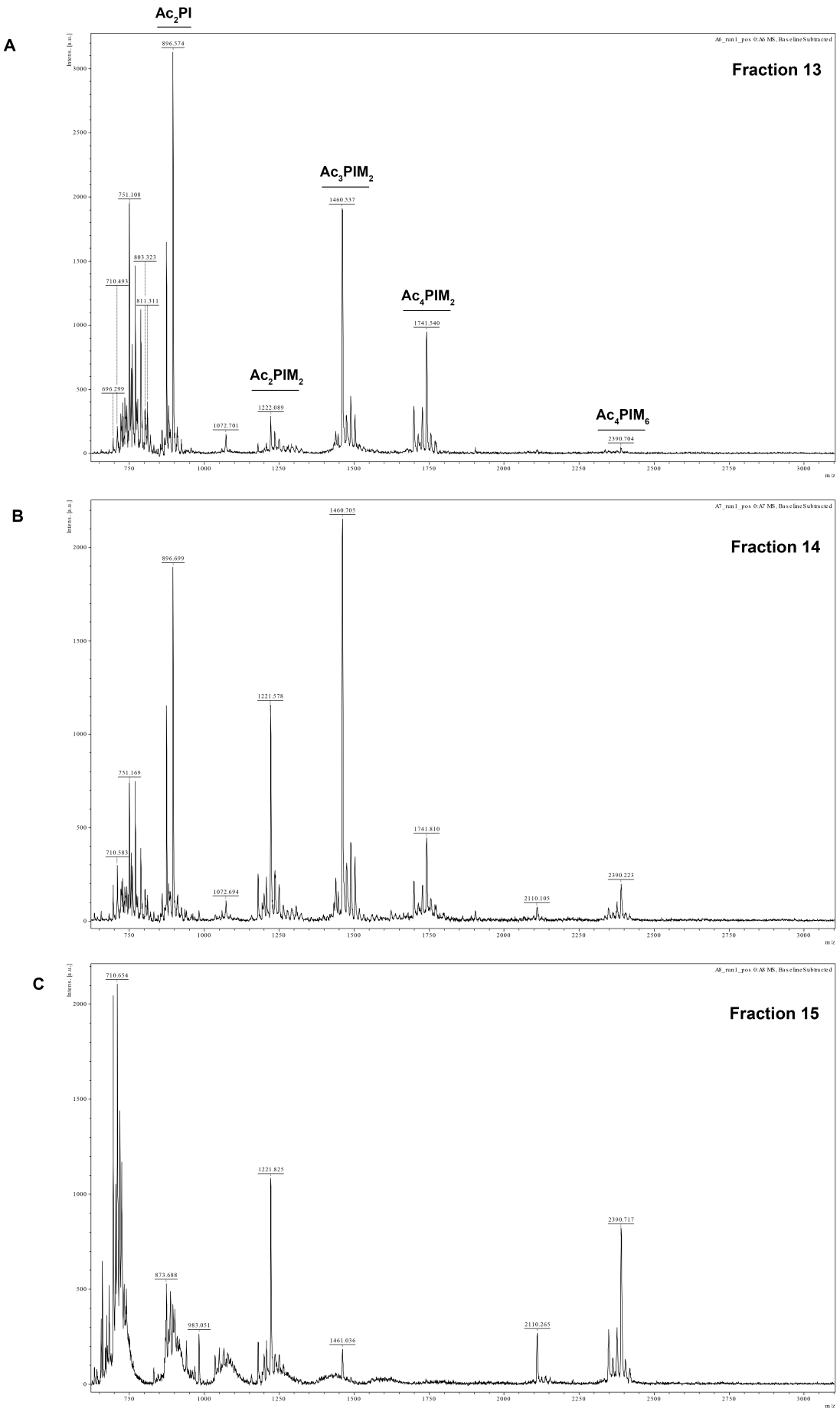

A
Ac2PI
Fraction 13
Ac3PIM2
Ac4PIM2
Ac2PIM2
Ac4PIM6
B
Fraction 14
C
Fraction 15
Intens. [a.u.]
m/z

Figure 5.3.3. MALDI-ToF MS of Mtb H37Rv lipid fractions 13, 14, and 15.

MALDI-ToF MS of fractionated *Mtb* H37Rv TL extract was analysed in positive ion mode. Ac_2PI, tretra-acy-phosphatidylinositol; Ac_2PIM_2, tetra-acyl-phosphatidyl-*myo*-inositol-dimannosides; Ac_3PIM_2, tri-acyl-phosphatidylinositol dimannosides; Ac_4PIM_2, tetra-acyl-phosphatidyl-*myo*-inositol-dimannosides; Ac_4PIM_6, tetra-acyl- phosphatidyl-*myo*-inositol-hexamannosides. These data were generated by Dr Gerald Larrouy-Maumus at Imperial College, London.

5.3.4. Lipid components of the *Mtb* cell wall increase the relative volume of the acidic compartment in RAW 264.7 MΦ.

In order to investigate whether individual components of the mycobacterial cell wall might account for the NPC1 inhibitory activity, we screened a number of *Mtb* H37Rv lipids and lipoproteins obtained from BEI Resources. Cells were incubated with lipids, stained with LysoTracker™ green DND-26, and analysed by FACS. Essentially, all of the activity of the *Mtb* H37Rv TL extract was found within the acetone-insoluble, with negligible activity present in the acetone-soluble fraction from BEI Recourses (Fig 5.3.4.). The lipids SL-1, TDM, $PIM_{1,2}$ and PIM_6 all induced a significant increase in LysoTracker™ staining intensity of RAW 264.7 MΦ (Fig 5.3.4.), indicating an increase in the relative volume of the acidic compartment. However, components including TMM, PDIM, MAME, LM and LAM had no significant effect (Fig 5.3.4.). The intensity of LysoTracker™ staining induced by $PIM_{1,2}$ and PIM_6 was comparable to that of U18666A (Fig 5.3.4.). Arabinogalactan and mAGP did not induce any increase in LysoTracker™ staining intensity in treated cells (Fig 5.3.4.).

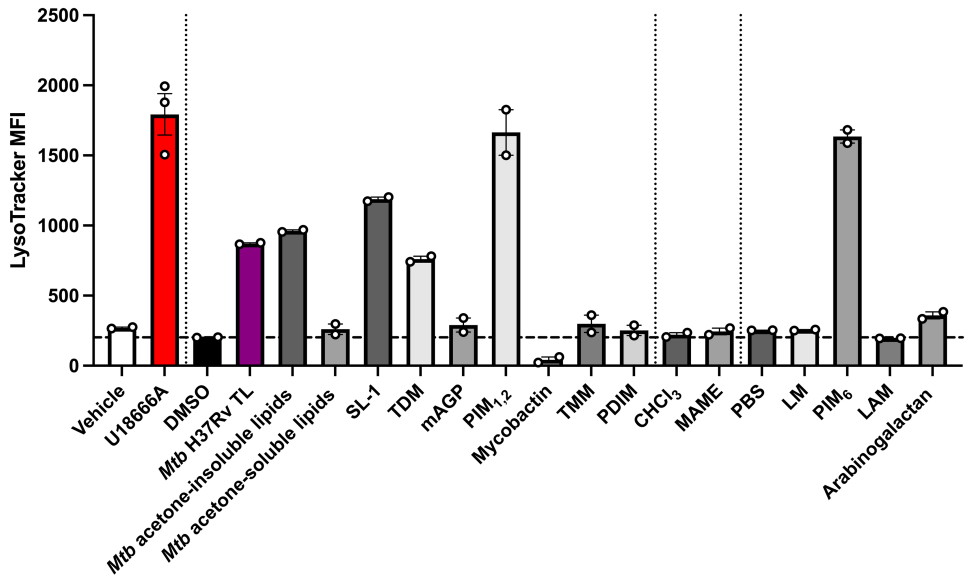
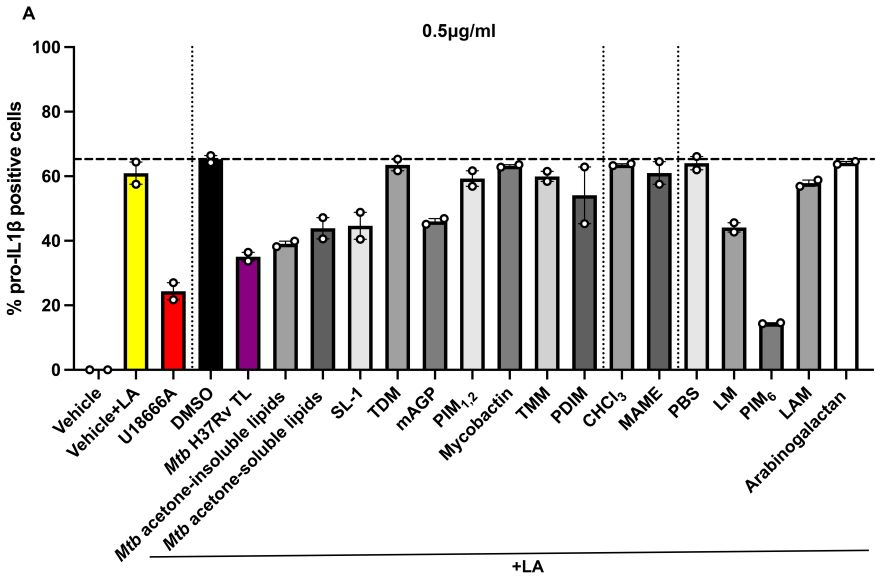


Figure 5.3.4. Lipid components from Mtb cell wall increase LysoTracker™ MFI in RAW 264.7 MΦ.

RAW 264.7 MΦ were incubated with purified components from *Mtb* H37Rv cell wall for (50µg/ml for 48h). U18666A (2µg/ml for 48h) treatment was the positive control, and DMSO (0.5%), $CHCl_3$ and PBS were vehicle controls for lipid treatments. MFI, mean fluorescence intensity. Data are mean ± SEM, n=2. Data are representative of 2 independent experiments. SL-1, sulpholipid-1; TDM, trehalose 6,6'-dimycolate; mAGP, mycolyl-arabinogalactan-peptidoglycan; PIM, phosphotidyinositol mannoside; TMM, trehalose monomycolate; PDIM, phthiocerol dimycocerates; MAME, mycolic acid methyl esters; LM, lipomannan; LAM, lipoarabinomannan.

5.3.5. Lipid components of the *Mtb* cell wall induced a reduction in the frequency of pro-IL1β positive RAW 264.7 MΦ that had been stimulated by LA.

We tested the ability of cell wall lipid components to inhibit pro-IL1β synthesis in RAW 264.7 MΦ stimulated with LA. Cells were treated with purified components (5μg/ml for 48h) as described above, stimulated with LA (50ng/ml for 6h), fixed, stained with anti-pro-IL1β antibody and analysed by FACS. *Mtb* H37Rv TL extract, acetone-soluble and acetone-insoluble fractions inhibited pro-IL1β production to near equivalence (Fig 5.3.5.A.). Other components such as SL-1, mAGP, TMM and LAM resulted in significant inhibition, and only PIM_6 and LM, inhibited pro-IL1β to a level comparable to that seen with *Mtb* H37Rv TL extract (Fig 5.3.5.A.). No significant inhibition was observed with TDM, PDIM and MAME (Fig 5.3.5.A.). Similar trends in pro-IL1β inhibition were observed when applying a lower dose (0.5μg/ml for 48h, Fig 5.3.5.A.).



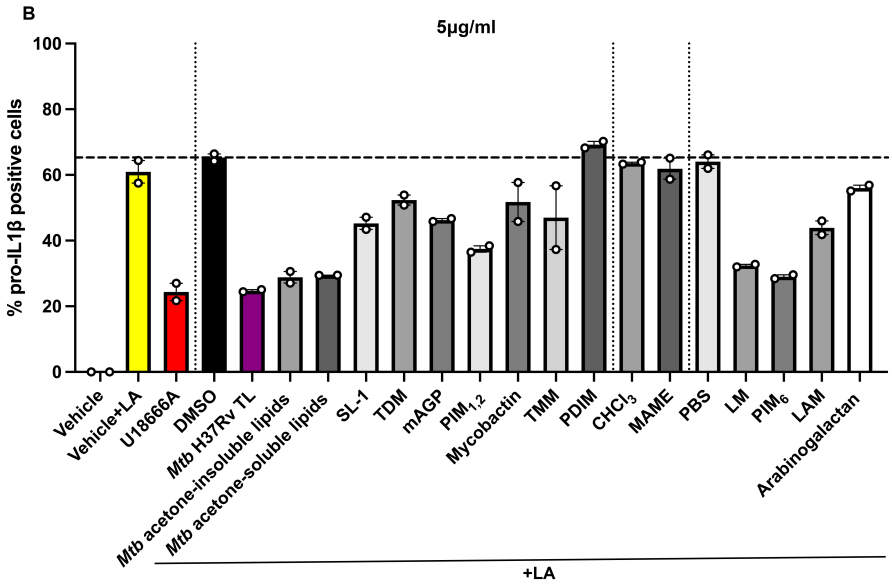


Figure 5.3.5. Lipid components from Mtb cell wall induced an reduction in the frequency of pro-IL1β positive RAW 264.7 MΦ that has been stimulated by LA.

Cells were incubated with purified components from *Mtb* H37Rv cell wall for (0.5 or 5µg/ml for 48h). U18666A (2µg/ml for 48h) treatment was the positive control, and DMSO (0.5%), $CHCl_3$ and PBS were vehicle control for lipid treatment. Panel A. Frequency of pro-IL1β positive cells treated with 0.5µg/ml lipid components and stimulated with LA. Panel B. Frequency of pro-IL1β positive cells treated with 5µg/ml lipid components and stimulated with LA. Data are mean ± SEM, n=2. SL-1, sulpholipid-1; TDM, trehalose 6,6'-dimycolate; mAGP, mycolyl-arabinogalactan-peptidoglycan; PIM, phosphotidyinositol mannoside; TMM, trehalose monomycolate; PDIM, phthiocerol dimycocerates; MAME, mycolic acid methyl esters; LM, lipomannan; LAM, lipoarabinomannan. These data were generated by Dawn Shepherd.

5.3.6. Lipid components of the *Mtb* cell wall cause dose-dependent inhibition in pro-IL1β synthesis in RAW 264.7 MΦ.

The previous experiment indicated that multiple cell wall components, when applied at the concentration of 5μg/ml, were able to inhibit pro-IL1β synthesis significantly. In order to determine the relative potency of each component, we treated RAW 264.7 MΦ with concentrations of each ranging from 0.0005 to 5μg/ml for 48h before stimulating and determining the extent of pro-IL1β production (performed by Dawn Shepherd). Importantly, *Mtb* H37Rv TL extract displayed dose-dependent inhibition, with statistically significant inhibition detected at a minimum of 0.005μg/ml (p=0.0375, Fig 5.3.6., Table 5.3.6.). PIM_6 was the most potent component, exhibiting a significant inhibition at 0.0005μg/ml (****p<0.0001, Fig 5.3.6., Table 5.3.6.). In contrast, with the exception of LM and LAM, significant inhibition was not seen at doses below 0.5μg/ml for all other cell wall components. These data are summarised in Table 5.3.6.

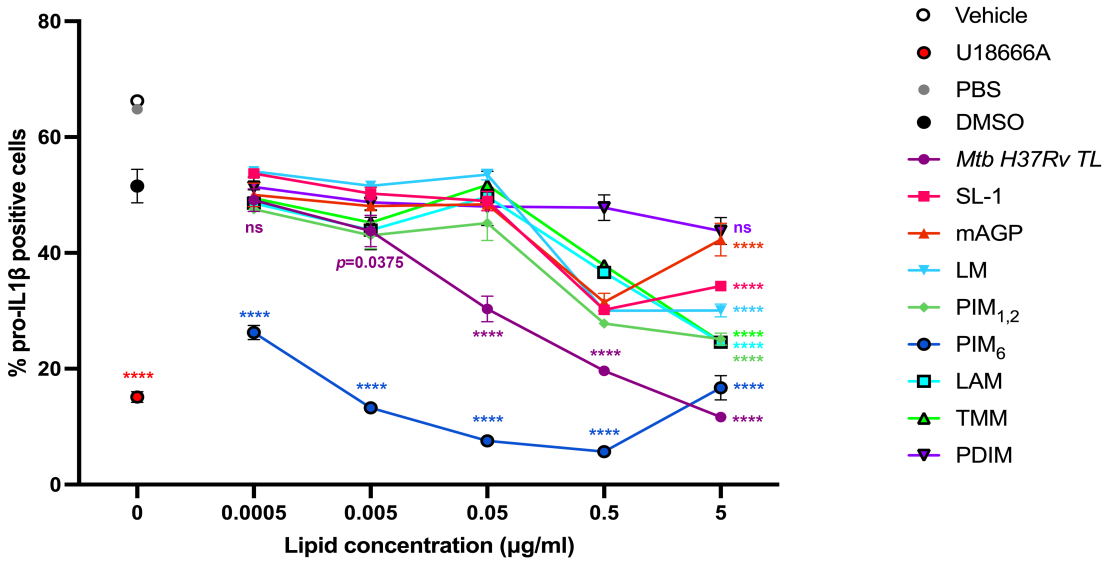


Figure 5.3.6. Lipid components of the Mtb cell wall induce dose-dependent inhibition of pro-IL1β in RAW 264.7 MΦ.

RAW 264.7 MΦ were treated with purified components for 48h with a dose from 500pg/ml to 5μg/ml, and the frequency of cells with positive pro-IL1β signals was measured by FACS. U18666A (2μg/ml for 48h) treatment was the positive control; DMSO (0.5%) and PBS were vehicle controls for lipid treatment. Data are mean ± SEM, n=3. Statistical analysis, 2-way ANOVA with Dunnett multiple comparisons. ****p<0.0001, other p values as indicated, otherwise not significant. Statistical comparison of U18666A treatment is relative to vehicle control. Statistical comparisons of lipid treatments are relative to accorded vehicle controls annotated with accorded colours.

Concentration (μg/ml)		0.0005	0.005	0.05	0.5	5
Compared to PBS	LM	54.1±0.5% ****	51.6±0.8% ****	53.5±0.9% ****	30.0±0.7% ****	30.1±1.1% ****
	PIM_6	26.3±1.2% ****	13.2±0.2% ****	7.5±0.2% ****	5.7±0.3% ****	16.7±2.0% ****
	LAM	48.6±0.6% ****	44.0±3.4% ****	50.0±0.4% ****	36.6±0.4% ****	24.6±0.5% ****
Compared to DMSO	SL-1	53.7±0.6% ns	50.2±1.1% ns	49.0±1.68% ns	30.17±0.9% ****	34.3±0.8% ****
	mAGP	50.0±2.0% ns	48.1±0.8% ns	48.4±0.5% ns	31.5±1.5% ****	42.3±2.8% p=0.0090
	$PIM_{1,2}$	47.5±0.8% ns	43.0±2.3% p=0.0188	45.2±3.0% ns	27.8±0.4% ****	25.1±1.1% ****
	TMM	49.5±1.5% ns	45.2±2.2% ns	51.7±2.4% ns	37.8±0.7% ****	24.6±0.9% ****
	PDIM	51.4±1.7% ns	48.7±2.6% ns	48.0±3.2% ns	47.8±2.2% ns	43.8±2.3% p=0.0375
	Mtb H37Rv TL	49.1±1.9% ns	43.8±2.7% p=0.0375	30.3±2.2% ****	19.6±0.7% ****	11.7±0.6% ****

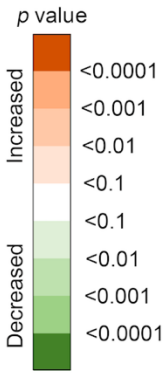


Table 5.3.6. Summary of dose-dependent inhibition of pro-IL1β synthesis by lipid components from Mtb cell wall in RAW 264.7 MΦ.

Summary of statistical significance values relative to vehicle control. Numbers indicate the frequency of pro-IL1β positive cells. Data are mean ± SEM, n=3, 2-way ANOVA with Dunnett multiple comparisons. ****p<0.0001, other p values as indicated, otherwise not significant. Statistical comparison of U18666A treatment is relative to vehicle control. Statistical comparisons of lipid treatments are relative to accorded vehicle controls. Levels significantly decreased are marked green.

5.3.7. MALDI-ToF MS analysis of the composition of *Mtb* lipids, SL-1, TDM, $PIM_{1,2}$ and PIM_6.

Before we tested the ability of SL-1, TDM, $PIM_{1,2}$ and PIM_6 from BEI Resources to induce NPC phenotypes, the purity was determined by MALDI-ToF MS by Dr Gerald Larrouy-Maumus at Imperial College, London. MS profiles revealed SL-1, TDM and $PIM_{1,2}$ each contained only the expected lipid species (Fig 5.3.7.). However, PIM_6 contained a mixture of species, with peaks corresponding to Ac_3PIM_2, Ac_4PIM_2, Ac_3PIM_6 and Ac_4PIM_6 (Fig 5.3.7.).

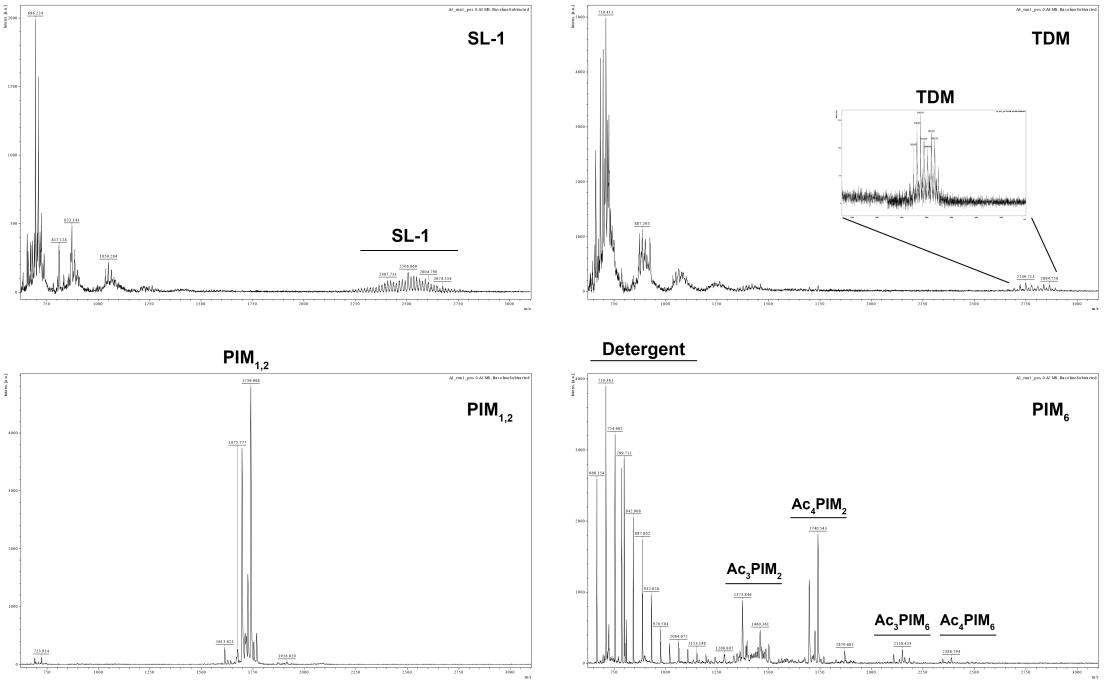


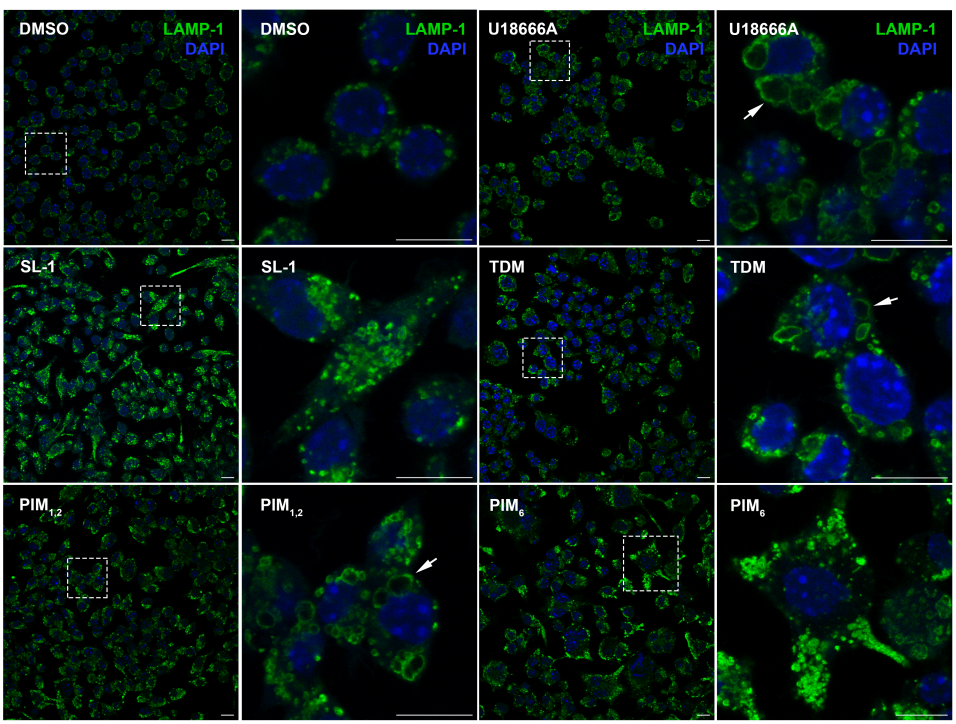
Figure 5.3.7. MS profile of SL-1, TDM, $PIM_{1,2}$, and PIM_6.

SL-1, sulpholipid-1; TDM: trehalose dimycolate; PIM, phosphatidylinositol mannoside. The lipid composition was analysed by positive mode MALDI-ToF MS by Dr Gerald Larrouy-Maumus at Imperial College, London.

5.3.8. SL-1, TDM, $PIM_{1,2}$ and PIM_6 of *Mtb* cell wall increase the size of LE/Lys in RAW 264.7 MΦ visualised by LAMP-1 immunostaining.

While studying the ability of *Mtb* TL extracts to induce NPC phenotypes, we analysed the expansion of LE/Lys with LysoTracker™ staining with FACS analysis but also by confocal microscopy of cell immunostained for the lysosomal antigen, LAMP-1 (Section 2.3.8.). We used the latter methodology to independently validate the data obtained by FACS and in addition to determine whether the frequency of lysosomes was greater than in controls, the size of lysosomes was larger than in controls, or a combination of the two. In brief, RAW 264.7 MΦ were treated with the purified lipids (25µg/ml for 48h), stained with anti-LAMP-1 antibodies, and examined by confocal microscopy (Fig 5.3.8.A.). The mean LE/Lys diameter of RAW 264.7 MΦ treated with SL-1, TDM, $PIM_{1,2}$ or PIM_6 was significantly increased (****p<0.0001, Fig 5.3.8.B.C.). LE/Lys of In RAW 264.7 MΦ treated with TDM or $PIM_{1,2}$ appeared as enlarged vacuoles similar to those observed in U18666A-treated cells (white arrows, Fig 5.3.8.A.).

A



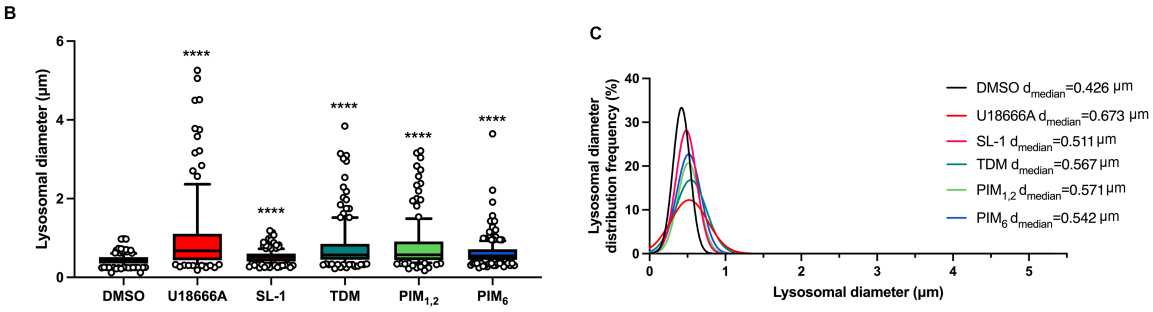


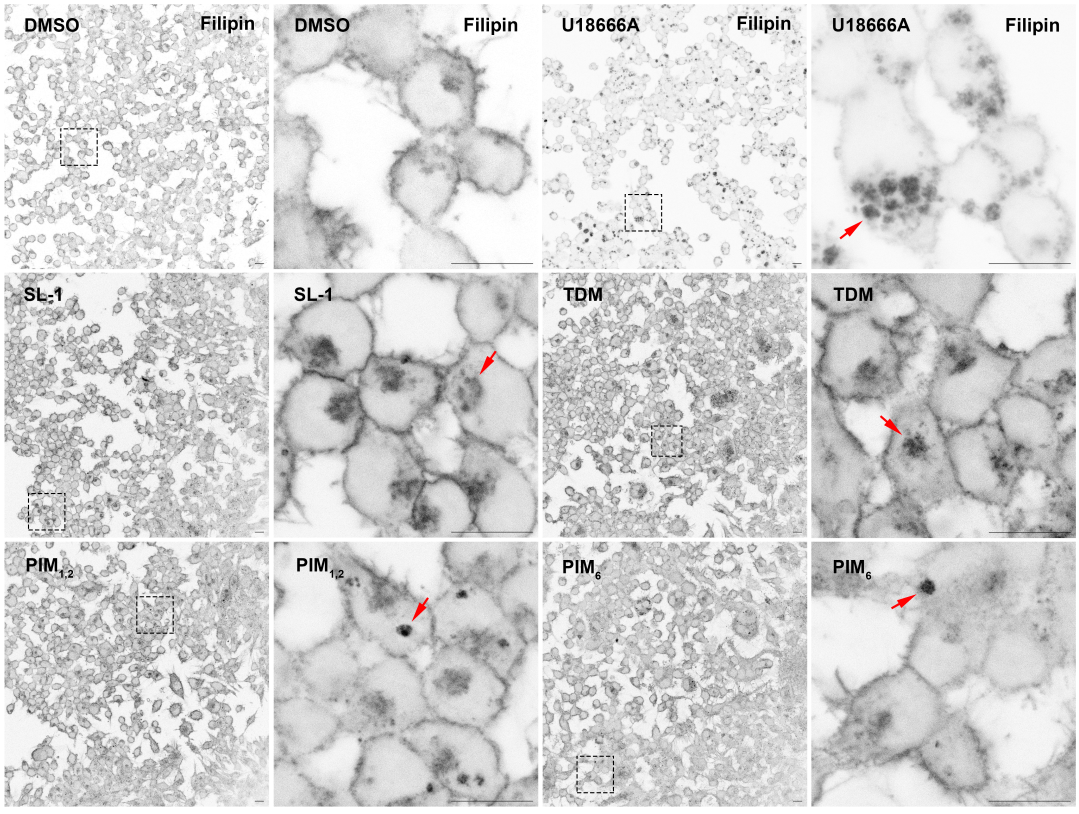
Figure 5.3.8. Expansion of lysosomal compartment in RAW 264.7 MΦ in response to SL-1, TDM, $PIM_{1,2}$ and PIM_6 visualised by anti-LAMP-1 staining.

RAW 264.7 MΦ were treated with purified lipids (25µg/ml for 48h). DMSO (0.25%) and U18666A (2µg/ml for 48h) were vehicle control and positive control respectively. Panel A. Representative confocal microscopy images of treated cells. LAMP-1, green; DAPI, blue. Scale bar represents 10µm. For each pair, the right image is a higher magnification of the region outlined in the left image. White arrows indicate enlarged LE/Lys. Panel B. Mean lysosomal diameter in treated RAW 264.7 MΦ. n>130 from at least 3 individual cells. Box and whisker plot, box contains 90% of events. Mann-Whitney test. ****p<0.0001. Statistical comparison of U18666A and lipid treatments are relative to the DMSO control. Panel C. Histogram of the statistical distribution of median lysosomal diameter in treated RAW 264.7 MΦ. Bin width, 0.2µm. DMSO: min: 0.120µm, max: 0.980µm, centre: 0.426µm; U18666A: min: 0.181µm, max: 5.255µm, centre: 0.673µm; SL-1: min: 0.241µm, max: 1.185µm, centre: 0.673µm; TDM: min: 0.223µm, max: 3.838µm, centre: 0.567µm; $PIM_{1,2}$: min: 0.170µm, max: 3.210µm, centre: 0.571µm; PIM_6: min: 0.241µm, max: 3.643µm, centre: 0.542µm. Statistical analysis, Gaussian distribution. Data are representative of 2 independent experiments.

5.3.9. SL-1, TDM, $PIM_{1,2}$ and PIM_6 induce cholesterol accumulation in RAW 264.7 MΦ.

Lysosomal storage of cholesterol is a hallmark of NPC and indicative of the inhibition of NPC1; we therefore tested the capacity of SL-1, TDM, $PIM_{1,2}$ or PIM_6 to induce intracellular cholesterol redistribution. RAW 264.7 MΦ were treated with SL-1, TDM, $PIM_{1,2}$ or PIM_6 and stained with filipin. Cholesterol accumulation, as indicated by the presence of filipin-positive lysosomal puncta, was observed (red arrows, Fig 5.3.9.1.A.). There was a significantly greater frequency of SL-1, TDM, $PIM_{1,2}$ or PIM_6 treated cells with lysosomal puncta than for the vehicle control (****p<0.0001, Fig 5.3.9.1.B.).

A



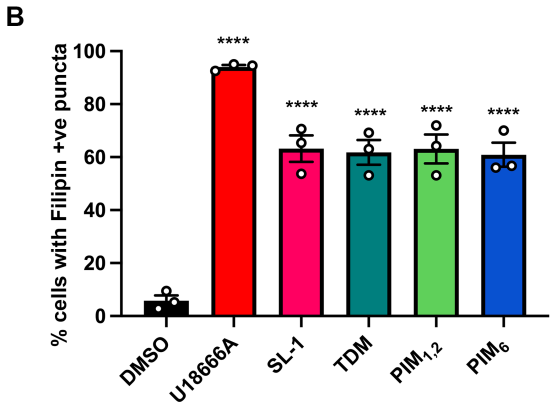
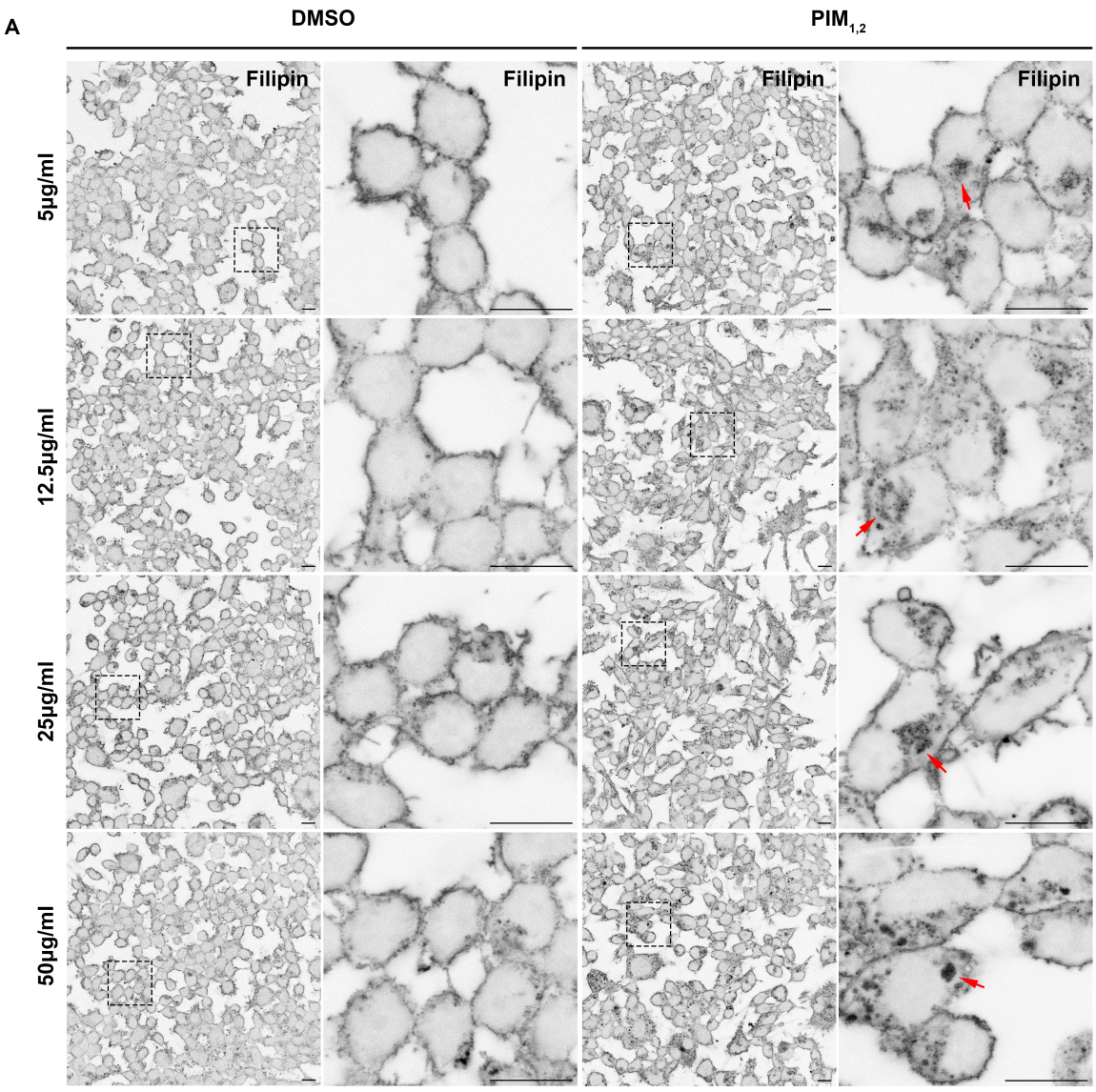


Figure 5.3.9.1. SL-1, TDM, $PIM_{1,2}$ and PIM_6 induce redistribution of cholesterol to intracellular puncta in RAW 264.7 MΦ.

RAW 264.7 MΦ were treated with purified lipid components (25μg/ml for 48h). DMSO (0.25%) and U18666A (2μg/ml for 48h) were vehicle control and positive control respectively. Panel A. Representative confocal microscopy images of treated cells. Filipin, black. Scale bar represents 10μm. Red arrows indicate filipin-positive puncta. For each pair, the right image is a higher magnification of the region outlined in the left image. U18666A images were collected under a lower gain. Panel B. Frequency of cells with filipin-positive puncta. Data are mean ± SEM, n=3, each representing a minimum of 100 cells in randomly selected fields. Statistical analysis, one-way ANOVA with Dunnett multiple comparisons. ****p<0.0001. Statistical comparisons of U18666A and lipid treatments are relative to the DMSO control. Data are representative of 2 independent experiments.

We also investigated whether the induction of filipin-positive puncta by $PIM_{1,2}$ was dose-dependent since it was the most potent lipid in the above phenotype screening. Analysis of the frequency of filipin-positive puncta confirmed a dose-dependent increase when lipid concentrations ranged from 5μg/ml to 50μg/ml (****p<0.0001, Fig 5.3.9.2., filipin-positive puncta indicated with red arrows).



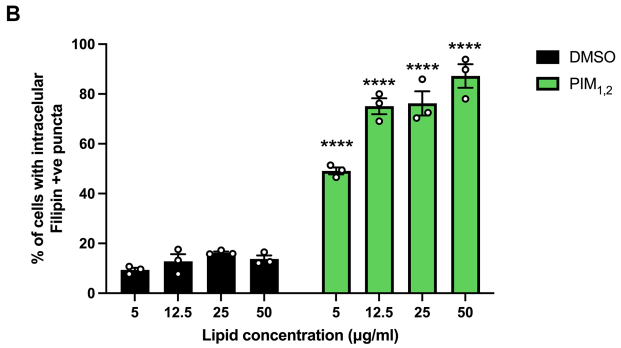
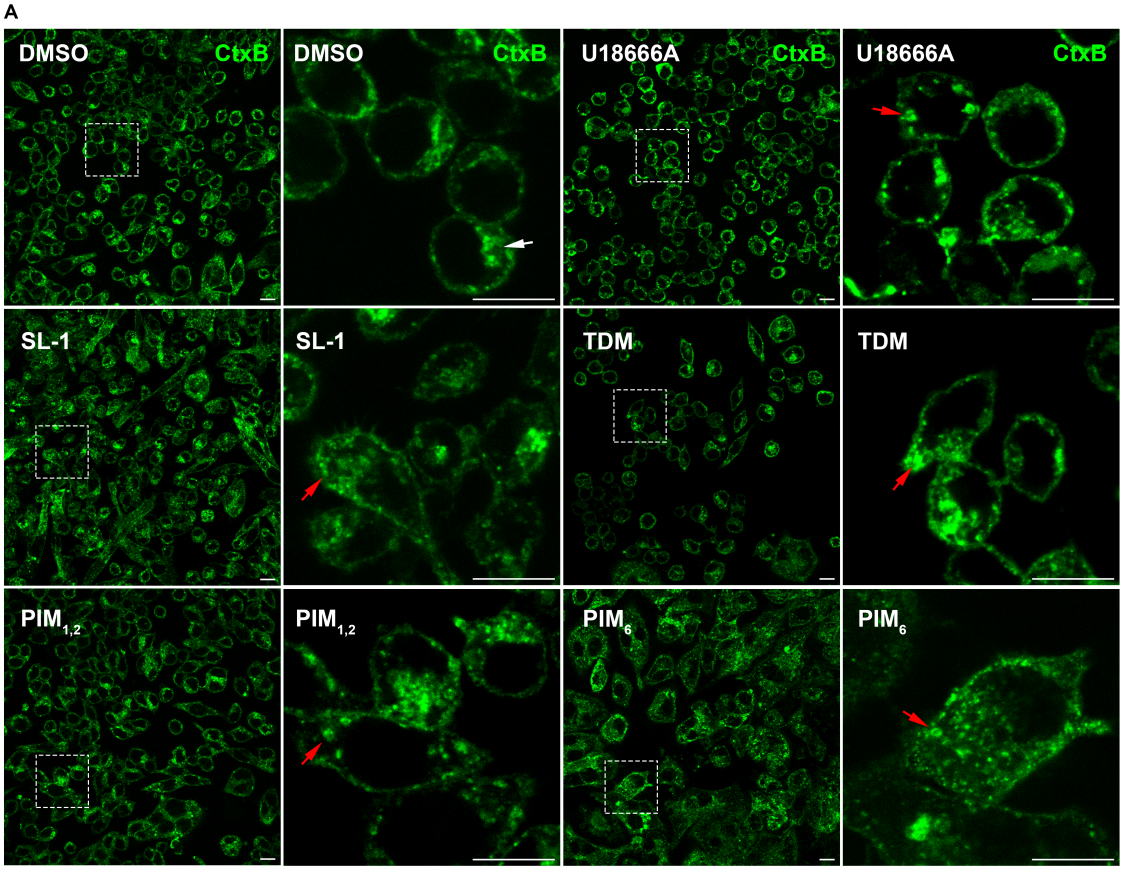


Figure 5.3.9.2. $PIM_{1,2}$ induces a dose-dependent redistribution of cholesterol to intracellular puncta in RAW 264.7 MΦ.

RAW 264.7 MΦ were treated with $PIM_{1,2}$ components (5, 12.5, 25 and 50µg/ml for 48h). DMSO (0.25%) and U18666A (2µg/ml for 48h) were vehicle control and positive control respectively. Panel A. Representative confocal microscopy images of treated cells. Filipin, black. Scale bar represents 10µm. Red arrows indicate filipin-positive puncta. For each pair, the right image is a higher magnification of the region outlined in the left image. Panel B. Frequency of cells with filipin-positive puncta. Data are mean ± SEM, n=3, each representing a minimum of 100 cells in randomly selected fields. Statistical analysis, 2-way ANOVA with Sidak multiple comparisons. ****p<0.0001. Statistical comparisons of lipid treatments are relative to the accorded DMSO controls.

5.3.10. SL-1, TDM, $PIM_{1,2}$ and PIM_6 perturb GM1 ganglioside intracellular trafficking in RAW 264.7 MΦ.

We found that exposure to *Mtb* TL extract results in the miss-trafficking of GSLs away from the Golgi recycling pathway and targets them to lysosomes (Section 2.3.16.). This perturbation is a characteristic of NPC and other sphingolipid LSDs [323]. We therefore, examined whether SL-1, TDM, $PIM_{1,2}$ and PIM_6 induced the same effect by pulse-labelling with fluorescent CtxB to label GM1 ganglioside (Section 2.3.16.). Confocal microscopy analysis showed SL-1, TDM, $PIM_{1,2}$ and PIM_6 caused redistribution of GM1 to the LE/Lys compartment (red arrows), whereas in vehicle-treated RAW 264.7 MΦ, it remained associated with the Golgi apparatus (white arrows, Fig 5.3.10.A.). The frequency of cells with lysosomal GM1 distribution was significantly increased in SL-1, TDM, $PIM_{1,2}$ or PIM_6-treated RAW 264.7 MΦ (****p<0.0001, Fig 5.3.10.B.).



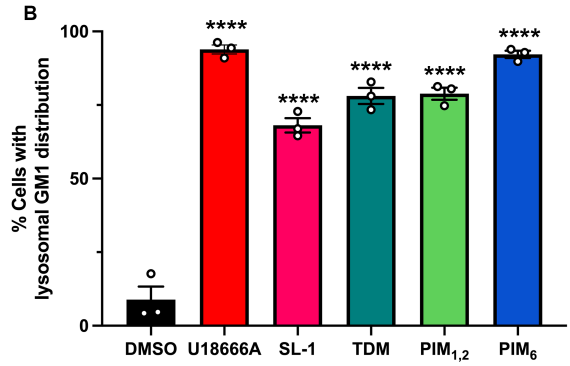
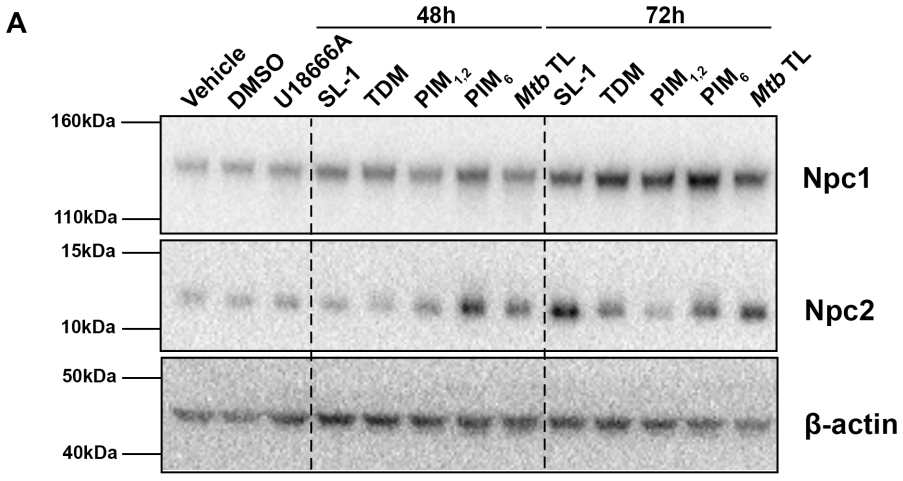


Figure 5.3.10. SL-1, TDM, $PIM_{1,2}$ and PIM_6 perturb GM1 ganglioside trafficking in RAW 264.7 MΦ.

RAW 264.7 MΦ were treated with purified lipids (25μg/ml for 48h). DMSO (0.25%) and U18666A (2μg/ml for 48h) were vehicle control and positive control respectively. Panel A. Representative confocal microscopy images of treated cells. CtxB, green. Scale bar represents 10μm. White arrows indicate Golgi distribution; red arrows indicate lysosomal distribution. For each pair, the right image is a higher magnification of the region outlined in the left image. Panel B. Frequency of cells with lysosomal GM1 distribution. Data are mean ± SEM, n=3, each representing a minimum of 100 cells in randomly selected fields. Statistical analysis, one-way ANOVA with Dunnett multiple comparisons. ****p<0.0001. Statistical comparison of U18666A and lipid treatments are relative to the DMSO control. Data are representative of 2 independent experiments.

5.3.11. Exposure to PIM_6 significantly increases Npc1 and Npc2 expression, whereas SL-1 only increases Npc2 expression in RAW 264.7 MΦ.

Previously, we demonstrated that incubation of RAW 264.7 MΦ with *Mtb* H37Rv TL extract significantly enhanced Npc1 expression (Section 2.3.11.). In order to examine whether SL-1, TDM, $PIM_{1,2}$ or PIM_6 had the same effect, cells were treated with lipids and expression was examined by western blotting. After 48h of lipid treatment, no significant change in expression was observed in SL-1, TDM, $PIM_{1,2}$ or PIM_6-treated RAW 264.7 MΦ (Fig 5.3.11.A.B.C.). However, Npc1 was significantly increased in both PIM_6 and *Mtb* H37Rv TL-treated cells at 72h (Fig 5.3.11.A.B.). Although there was a trend of increased expression with TDM and $PIM_{1,2}$, it was not statistically significant (Fig 5.3.11.A.B.). At 72h, SL-1, PIM_6 and *Mtb* H37Rv TL had induced significantly increased Npc2 expression (Fig 5.3.11.A.C.).



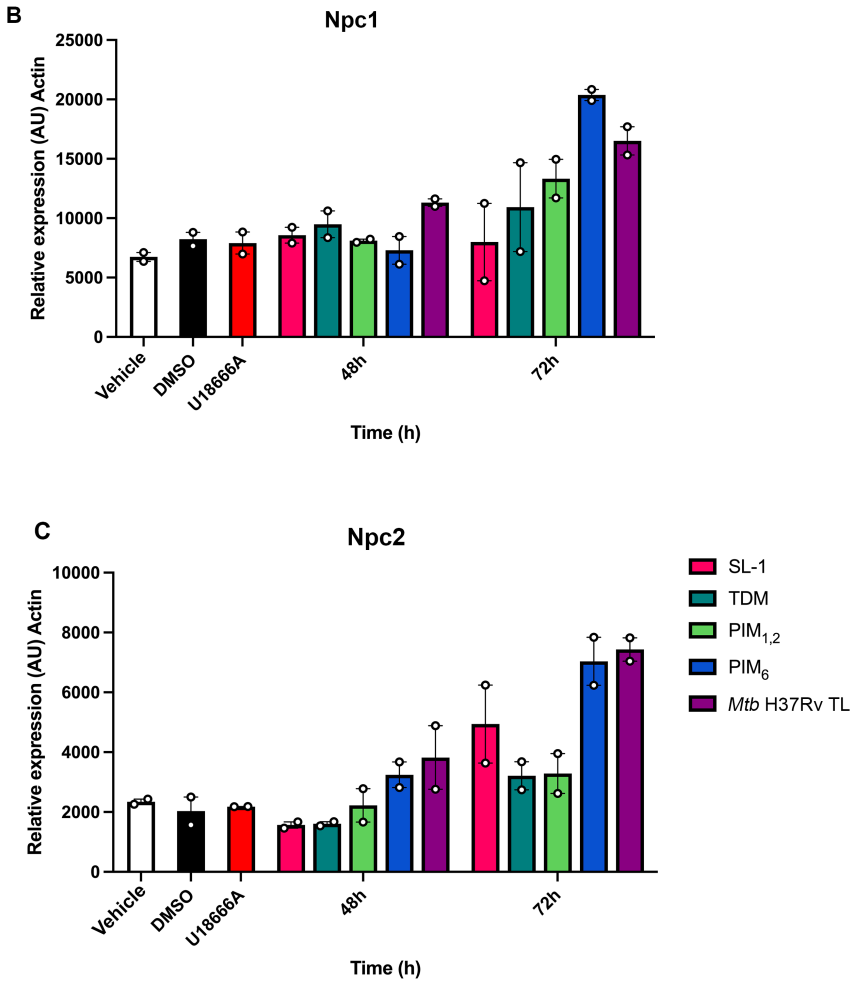


Figure 5.3.11. Exposure to PIM_6 significantly increases the expression of Npc1 and Npc2 in RAW 264.7 MΦ.

RAW 264.7 MΦ were treated with purified components (25μg/ml for 48h or 72h). DMSO (0.25%) and U18666A (2μg/ml for 48h) were vehicle and positive controls respectively. Panel A. Western blot of protein lysates of treated cells probed with anti-Npc1 or anti-Npc2 antibodies. Panel B. Quantification of Npc1 protein normalised to β-actin. Panel C. Quantification of Npc2 protein normalised to β-actin. Data are mean ± SEM, n=2. Data are representative of 2 independent experiments.

5.3.12. PIM_6 enhances transcriptions of *Npc1* and *Npc2* in RAW 264.7 MΦ.

We investigated whether lipid components of the *Mtb* cell wall could affect the transcription of *Npc1* and *Npc2* genes. Q-PCR analysis of lipid-treated cells revealed PIM_6 significantly enhanced expression of *Npc1* and *Npc2* at 48h and 72h (p=0.0493 for *Npc1* 48h; p=0.0033 for *Npc1* 72h; p=0.0202 for *Npc2* 48h; p=0.0251 for *Npc2* 72h, Fig 5.3.12.). No significant changes in *Npc1* or *Npc2* gene expression levels were observed in RAW 264.7 MΦ treated with SL-1, TDM or $PIM_{1,2}$ at 48h or 72h (Fig 5.3.12.).

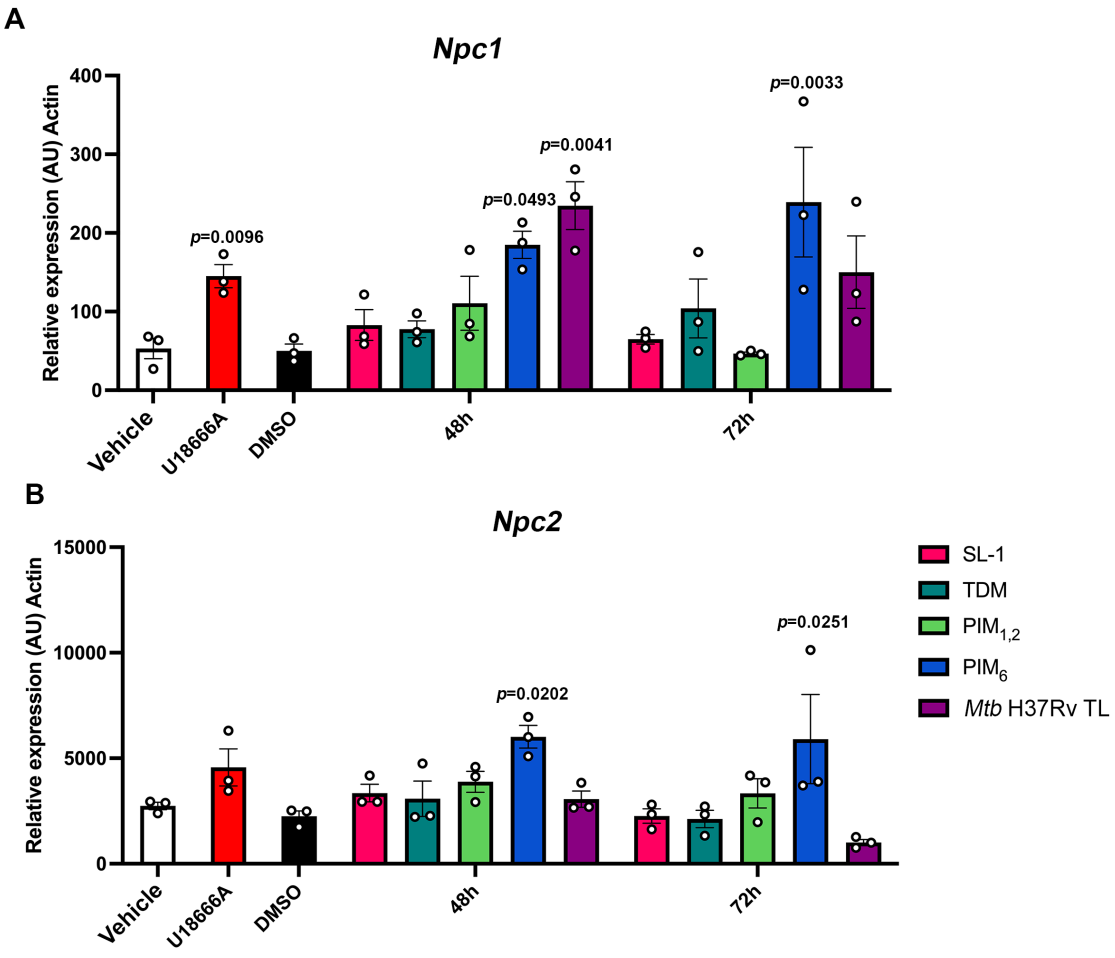


Figure 5.3.12. PIM_6 enhances the transcription of Npc1 and Npc2 in RAW 264.7 MΦ.

RAW 264.7 MΦ were treated with purified components (25μg/ml for 48h or 72h). DMSO (0.25%) and U18666A (2μg/ml for 48h) were vehicle and positive control respectively. Relative *Npc1* (panel A) and *Npc2* (panel B) expression was normalised to *β-actin* in treated cells. Data are mean ± SEM, n=3. Statistical analysis, one-way ANOVA with Dunnett multiple comparisons. *p* values as indicated, otherwise not significant. Statistical comparison of U18666A treatment is relative to vehicle control. Statistical comparisons of lipid treatments are relative to DMSO controls. Data are representative of 2 independent experiments.

5.3.13. SL-1 increases the level of sphingosine level, and PIM_6 increases the level of sphinganine level in RAW 264.7 MΦ.

As shown in Chapter 4, sphingosine peaked in RAW 264.7 MΦ at around 3h to 6h post treatment with *Mtb* H37Rv TL extract (Section 4.3.3.). Therefore, we treated RAW 264.7 MΦ with lipid components for 6h before measuring sphingosine and sphinganine levels by HPLC. Sphingosine levels were increased by SL-1 treatment in RAW 264.7 MΦ (p=0.0004) but were not altered by other lipid components (Fig 5.3.13.A.). Sphinganine was increased by PIM_6 but was not altered by other lipid components (p=0.0024, Fig 5.3.13.B.).

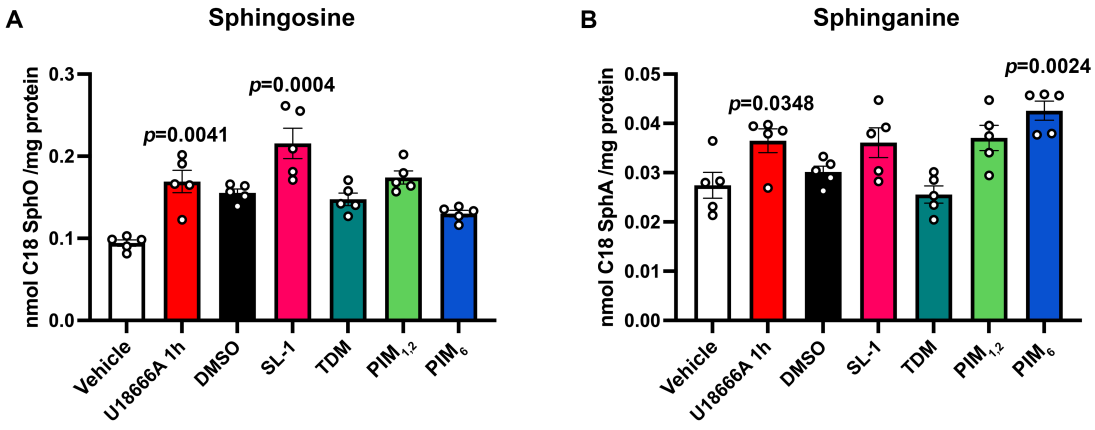


Figure 5.3.13. SL-1 increases sphingosine, and PIM_6 increases sphinganine content of RAW 264.7 MΦ.

RAW 264.7 MΦ were treated with the lipid (25μg/ml for 6h). DMSO (0.25% for 6h) and U18666A (2μg/ml for 1h) were vehicle and positive control respectively. Quantification of sphingosine (Panel A) and sphinganine (Panel B) in treated cells. Data are mean ± SEM, n=5. Statistical analysis, one-way ANOVA with Dunnett multiple comparisons. p values as indicated, otherwise not significant. Statistical comparison of U18666A treatment is relative to vehicle control. Statistical comparisons of lipid treatments are relative to the DMSO control.

5.3.14. SL-1 and $PIM_{1,2}$ induce GSL accumulation in RAW 264.7 MΦ.

GSLs accumulate in NPC and in cells exposed to *Mtb* H37Rv TL extract (Section 2.3.17.). We therefore investigated whether any of the purified cell wall lipid components could also induce GSL storage. Representative GSL profiles of RAW 264.7 MΦ treated with SL-1, TDM, $PIM_{1,2}$ and PIM_6 are shown in Fig 5.3.14.A. Exposure of RAW 264.7 MΦ to SL-1 (****p<0.0001) or $PIM_{1,2}$ (p=0.0060) resulted in a significant increase in total GSLs but to a level significantly lower than that induced by U18666A (Fig 5.3.14.B.). Of the nine individual GSL species that were resolved and quantified, SL-1 significantly increased all of them (****p<0.0001 for GM3, GM2, GA1 and GD1a; p=0.0003 for Lac; p=0.0088 for GA2; p=0.0004 for Gb3; p=0.0003 for GM1a; p=0.0011 for GM1b, Fig 5.3.14.C.). $PIM_{1,2}$ induced a significant increase in six GSL species: Gb3 (p=0.0097), GM2 (****p<0.0001), GA1 (p=0.0276), GM1a (p=0.0296) and GD1a (p=0.0019, Fig 5.3.14.C.). PIM_6 increased six species of GSLs significantly: Lac (p=0.0004), GM3 (p=0.0008), GM2 (****p<0.0001), GA1 (****p<0.0001) and GM1a (p=0.0013, Fig 5.3.14.C.). TDM treatment did not affect total GSLs or the amount of individual GSL species (Fig 5.3.14.B.C.). The fold change of total GSL and individual GSLs in RAW 264.7 MΦ treated with SL-1, TDM, $PIM_{1,2}$ and PIM_6 are summarised in Table 5.3.14.

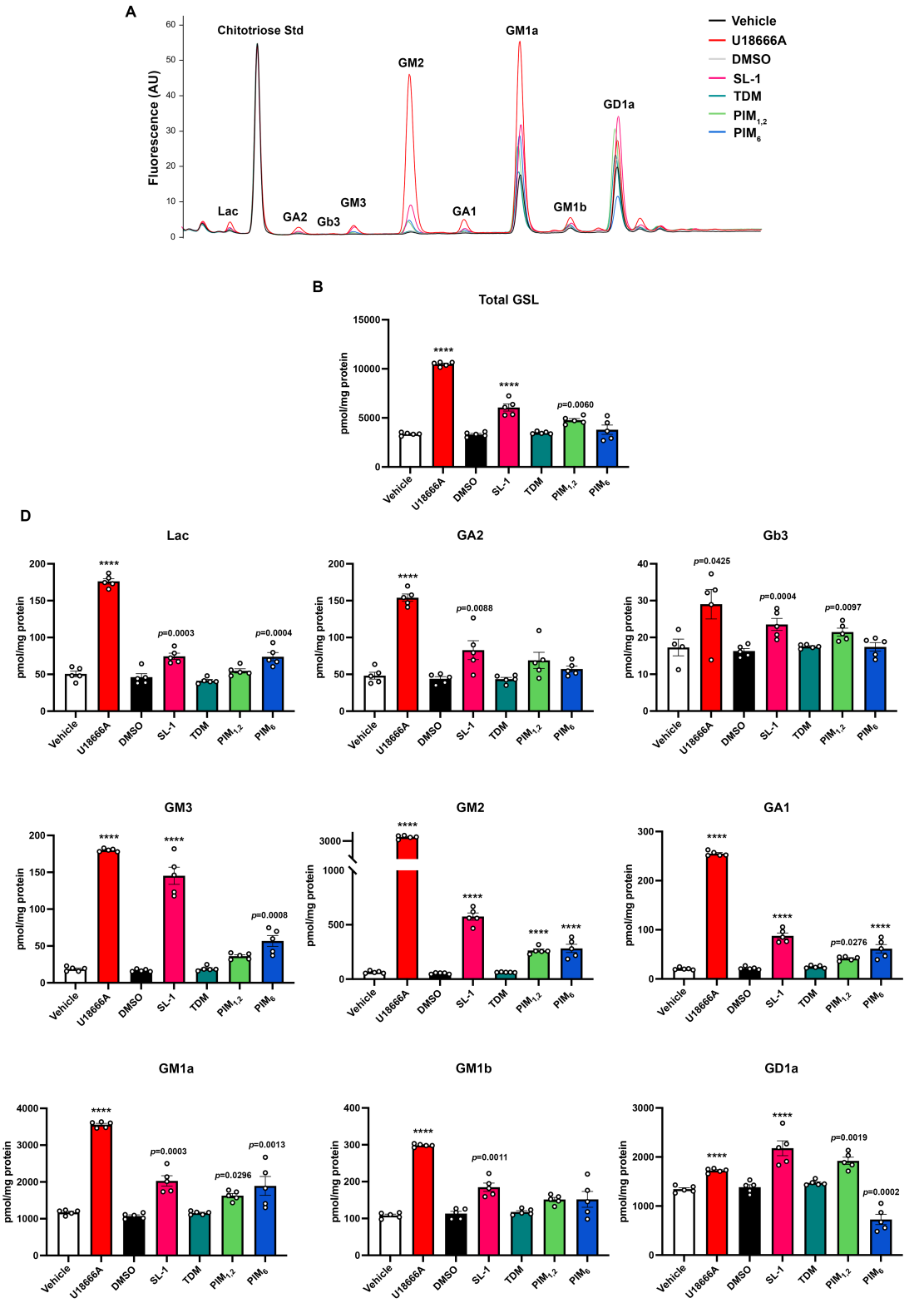

A
Chitotriose Std
Lac
GA2
Gb3
GM3
GM2
GA1
GM1a
GM1b
GD1a
Fluorescence (AU)
Vehicle
U18666A
DMSO
SL-1
TDM
PIM1,2
PIM6
B
Total GSL
pmol/mg protein
****
p=0.0060
D
Lac
GA2
Gb3
GM3
GM2
GA1
GM1a
GM1b
GD1a
p=0.0003
p=0.0004
p=0.0088
p=0.0425
p=0.0004
p=0.0097
p=0.0008
p=0.0276
p=0.0013
p=0.0296
p=0.0011
p=0.0019
p=0.0002

Figure 5.3.14. SL-1 and $PIM_{1,2}$ induce GSL accumulation in RAW 264.7 MΦ.

RAW 264.7 MΦ were treated with purified cell wall components (25μg/ml for 48h). DMSO (0.25%) and U18666A (2μg/ml, 48h) were vehicle and positive controls respectively. Panel A. Representative HPLC traces of GSL profile in treated cells. Quantification of total GSL (Panel B) and individual GSL species (Pane C) in treated cells. Data are mean ± SEM, n=5. Statistical analysis, one-way ANOVA with Dunnett multiple comparisons. ****$p<0.0001$, p values as indicated, otherwise not significant. Statistical comparison of U18666A treatment is relative to vehicle control. Statistical comparisons of lipid treatments are relative to the DMSO control.

GSL species	U18666A	SL-1	TDM	$PIM_{1,2}$	PIM_6
Lac	**** 3.49±0.07	*p*=0.0003 1.61±0.09	ns 0.90±0.04	ns 1.19±0.06	*p*=0.0004 1.60±0.12
GA2	**** 3.20±0.10	*p*=0.0088 1.89±0.29	ns 0.99±0.06	ns 1.57±0.25	ns 1.30±0.09
Gb3	*p*=0.0425 1.68±0.23	*p*=0.0004 1.44±0.10	ns 1.08±0.01	*p*=0.0097 1.32±0.07	ns 1.07±0.07
GM3	**** 9.59±0.05	**** 8.66±0.70	ns 1.14±0.09	ns 2.16±0.11	*p*=0.0008 3.39±0.44
GM2	**** 50.78±0.66	**** 11.03±0.65	ns 1.20±0.02	**** 5.04±0.28	**** 5.40±0.72
GA1	**** 12.42±0.11	**** 4.02±0.27	ns 1.12±0.06	*p*=0.0276 1.91±0.08	**** 2.82±0.39
GM1a	**** 3.03±0.03	*p*=0.0003 1.89±0.13	ns 1.08±0.019	*p*=0.0296 1.51±0.06	*p*=0.0013 1.76±0.24
GM1b	**** 2.75±0.02	*p*=0.0011 1.63±0.10	ns 1.04±0.03	ns 1.34±0.05	ns 1.34±0.19
GD1a	**** 1.28±0.01	**** 1.58±0.11	ns 1.06±0.02	*p*=0.0019 1.39±0.05	*p*=0.0002 0.53±0.08
Total GSL	**** 3.12±0.03	**** 1.83±0.11	ns 1.05±0.02	*p*=0.0060 1.44±0.05	ns 1.15±0.14
GlcCer	ns 0.95±0.11	ns 0.53±0.15	ns 1.25±0.15	ns 0.74±0.38	ns 1.27±0.15

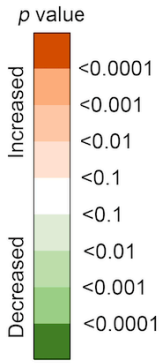


Table 5.3.14. Summary of the fold change and statistical analysis of GSLs in RAW 264.7 MΦ treated with lipid component from the Mtb cell wall.

Experiments are compared to DMSO vehicle control. Data are mean ± SEM, n=5. Statistical analysis, one-way ANOVA with Dunnett multiple comparisons. ****p<0.0001, p values as indicated, otherwise not significant. Levels that significantly increased are marked red, and those that significantly decreased are marked green.

5.3.15. MALDI-ToF MS of TL extracts of *Mtb* H37Rv and *ΔpimE Mtb* H37Rv.

The data presented in this chapter showed that PIM_6 was able to induce several NPC phenotypes. However, MS analysis of the purified PIM_6 used in those studies revealed that the preparation was not a single lipid but a mixture of species. We hypothesised that PIM_6 is one of the active molecules that is responsible for NPC1 inhibition and a mycobacterial strain genetically incapable

of synthesising the lipid should not induce NPC phenotypes. A TL extract from a deficient strain, *ΔpimE Mtb* H37Rv, was provided by Professor Mary Jackson (Colorado State University). In order to substantiate the inability of the mutant strain to synthesise PIM_6, the TL extract was analysed by MALDI-ToF MS by Dr Gerald Larrouy-Maumus at Imperial College, London and TLC for the PIMs profile by Dr Zuzana Palcekova in the laboratory of Professor Mary Jackson at Colorado State University, USA. Both MS (Fig 5.3.15.1.) and TLC (Fig 5.3.15.2.) profiles confirmed the absence of PIM_6 lipid (polar PIMs) in *ΔpimE Mtb* H37Rv TL extract.

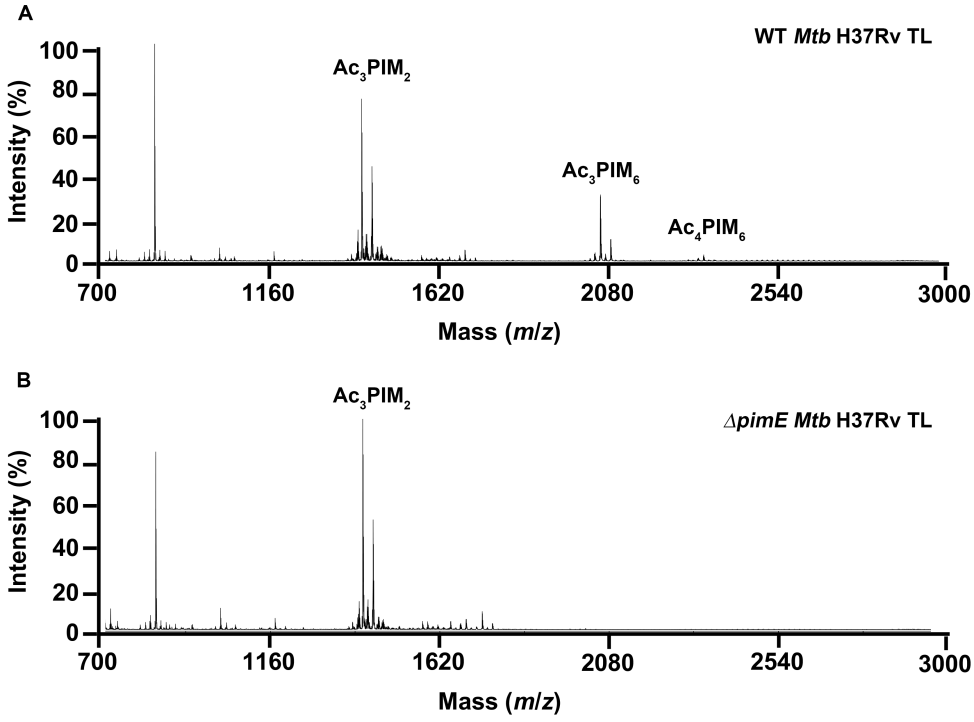


Figure 5.3.15.1. MALDI-ToF MS profile of TL extracts from H37Rv (A) and ΔpimE Mtb H37Rv (B).

The lipid composition was analysed by positive mode MALDI-ToF MS by Dr Gerald Larrouy-Maumus at Imperial College, London.

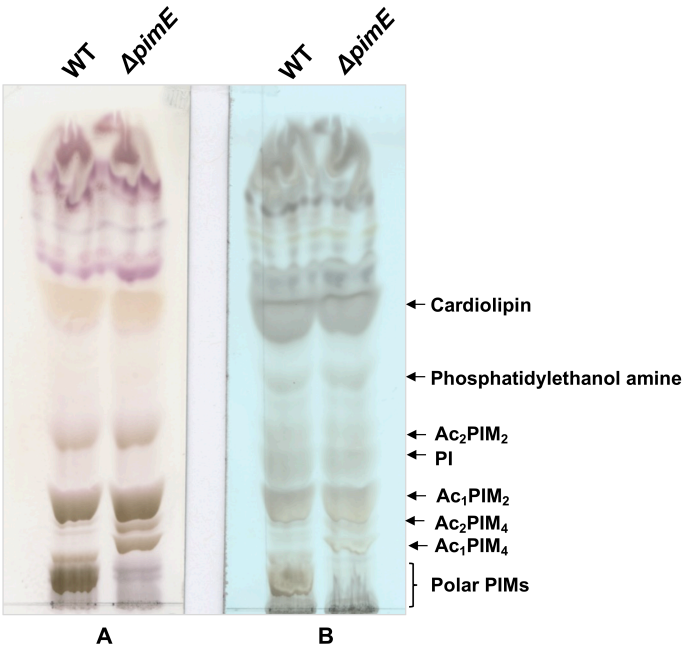


Figure 5.3.15.2. TLC profile of PIMs of WT and ΔpimE Mtb H37Rv lipid extract.

TLC were run in $CHCl_3$: MeOH: NH_4OH: H_2O 65:25:0.5:4 (v/v/v/v). Panel A. α-naphthol stain; Panel B. $CuSO_4$ in H_3PO_4 stain for PIMs in WT and *ΔpimE Mtb* H37Rv lipid extract. PIM, phosphatidylinositol mannoside; PI, phosphatidylinositol. TLC was performed by Dr Zuzana Palcekova in the laboratory of Professor Mary Jackson at Colorado State University.

5.3.16. TL extract of *Mtb* H37Rv and *ΔpimE Mtb* H37Rv increase LysoTracker™ staining intensity of RAW 264.7 MΦ.

Using LysoTracker™ staining, we measured the relative LE/Lys volume of RAW 264.7 MΦ that had been incubated with TL extracts of the two strains at lipid concentrations between 12.5μg/ml and 100μg/ml for 48h. We observed a dose-dependent increase of LysoTracker™ staining intensity of RAW 264.7 MΦ treated with TL extracts prepared from parental *Mtb* H37Rv and Δ*pimE Mtb* H37Rv

strains (****p<0.0001, Fig 5.3.16.). At two of the concentrations tested (12.5μg/ml and 100μg/ml), Δ*pimE Mtb* H37Rv induced significantly stronger LysoTracker™ staining than that for *Mtb* H37Rv (****p<0.0001, Fig 5.3.16.).

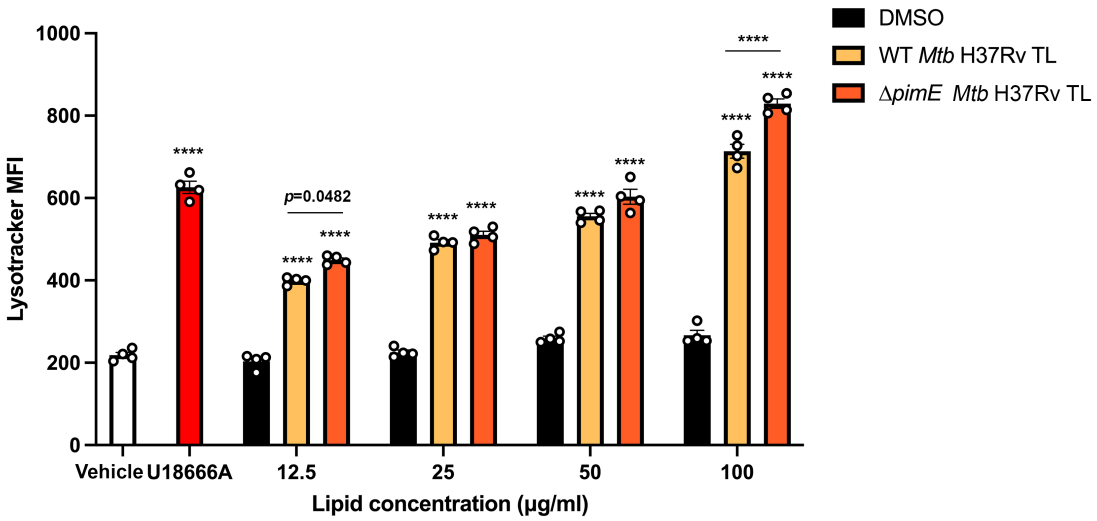


Figure 5.3.16. TL extracts of Mtb H37Rv and ΔpimE Mtb H37Rv significantly increase LysoTracker™ staining intensity of RAW 264.7 MΦ.

RAW 264.7 MΦ were treated with TL extracts (12.5, 25, 50 and 100μg/ml for 48h). DMSO and U18666A (2μg/ml, 48h) were vehicle and positive control respectively. MFI, mean fluorescence intensity. Data are mean ± SEM, n=4. Statistical analysis, one-way ANOVA with Tukey multiple comparisons. ****p<0.0001, p values as indicated. Statistical comparison of U18666A treatment is relative to vehicle control. Statistical comparisons of lipid treatments are relative to DMSO controls. Data are representative of 2 independent experiments.

5.3.17. TL extracts of *Mtb* H37Rv and *ΔpimE Mtb* H37Rv induce cholesterol re-distribution in RAW 264.7 MΦ.

We tested the ability of the TL extracts of *Mtb* H37Rv and *ΔpimE Mtb* H37Rv to cause intracellular cholesterol storage as indicated by the presence of filipin-positive intracellular puncta. We confirmed a significant accumulation of puncta in cells (indicated with red arrows) that had been treated with *Mtb* H37Rv and *ΔpimE Mtb* H37Rv TL extracts (p=0.0002, Fig 5.3.17.) and that there was no statistically significant difference in frequency between the two treatments (Fig 5.3.17.).

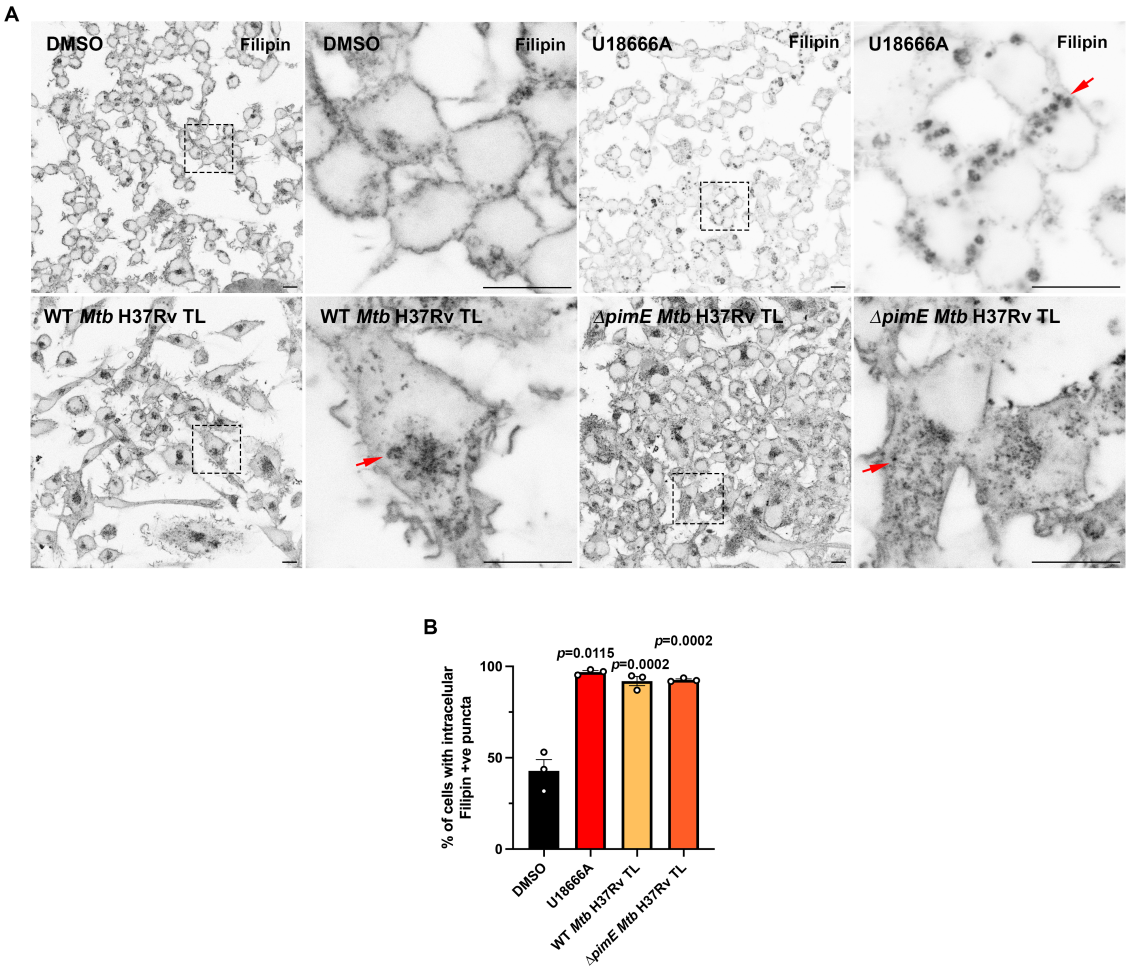


Figure 5.3.17. TL extracts of Mtb H37Rv and ΔpimE Mtb H37Rv induce re-distribution of cholesterol in RAW 264.7 MΦ.

Cells were treated with TL extract (100μg/ml for 48h). DMSO and U18666A (2μg/ml for 48h) were vehicle and positive control respectively. Panel A. Representative confocal microscopy images in treated RAW 264.7 MΦ. Filipin, black. Scale bar represents 10μm. For each pair, the right image is a higher magnification of the region outlined in the left image. Red arrows indicate filipin-positive puncta. Panel B. Frequency of cells with intracellular filipin-positive puncta. Data are mean ± SEM, n=3, each representing a minimum of 100 cells in randomly selected fields. Statistical analysis, one-way ANOVA with Dunnett multiple comparisons. *p* values as indicated. Statistical comparisons of U18666A and lipid treatments are relative to DMSO control. Data are representative of 2 independent experiments.

5.3.18. TL extracts of *Mtb* H37Rv and *ΔpimE Mtb* H37Rv significantly increase the expression of Npc1 but not Npc2 in RAW 264.7 MΦ.

Mtb H37Rv TL extract significantly enhanced the expression in Npc1 in RAW 264.7 MΦ (Section 2.3.11., [207]). In order to examine if the absence of PIM_6 affected the capacity of mycobacterial lipid extract to modulate Npc1 expression, we compared RAW 264.7 MΦ that had been incubated with either parental *Mtb* H37Rv or *ΔpimE Mtb* H37Rv extract by western blotting of cell lysates. TL extract from both *Mtb* H37Rv and *ΔpimE Mtb* H37Rv significantly increased the level of Npc1 (Fig 5.3.18.A.B.). Npc2 was not significantly altered with *Mtb* H37Rv or *ΔpimE Mtb* H37Rv TL treatment of RAW 264.7 MΦ (Fig 5.3.18.A.C.), but neither significantly changed the expression of Npc2 (Fig 5.3.18.A.C.).

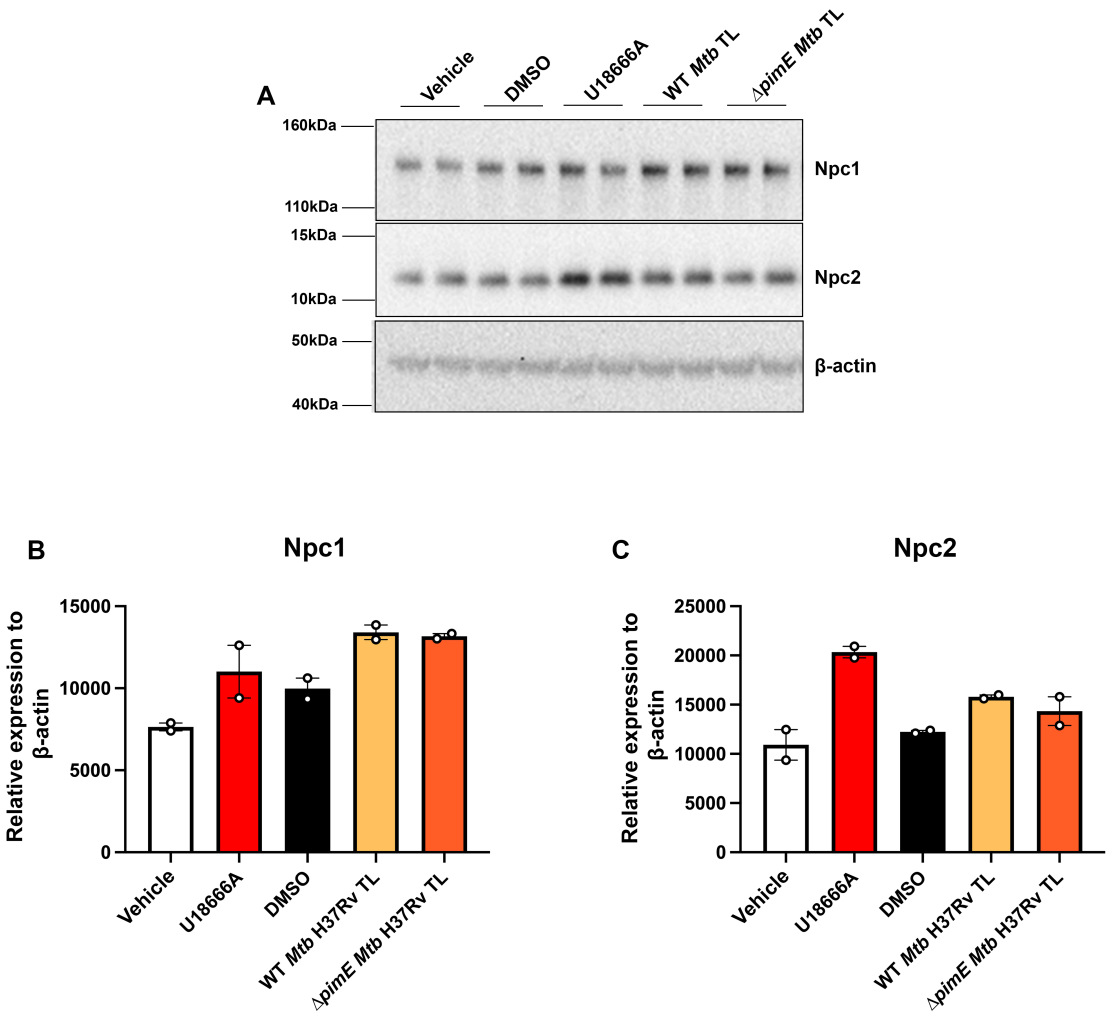


Figure 5.3.18. TL extracts of Mtb H37Rv and ΔpimE Mtb H37Rv increased the expression of Npc1, but not Npc2 in RAW 264.7 MΦ. Cells were treated with TL extract (100μg/ml for 48h). DMSO and U18666A (2μg/ml for 48h) were vehicle and positive control respectively. Panel A. Western blot of protein lysate of treated cells probed with anti-Npc1 and anti-Npc2 antibodies. Panel B. Quantification of Npc1 protein normalised to β-actin. Panel C. Quantification of Npc2 protein normalised to β-actin. Data are mean ± SEM, n=2. Data are representative of 2 independent experiments.

5.3.19. TL extracts of *Mtb* H37Rv and *ΔpimE Mtb* H37Rv significantly increase the transcription of Npc1 but not Npc2 in RAW 264.7 MΦ.

We also examined the effect of *ΔpimE Mtb* H37Rv TL extract on the transcription of *Npc1* and *Npc2* genes using Q-PCR. Analysis revealed that treatment with both *Mtb* H37Rv and *ΔpimE Mtb* H37Rv significantly increased the abundance of Npc1 transcripts in RAW 264.7 MΦ (****p<0.0001 and p=0.0005 respectively, Fig 5.3.19.A.). In fact, the effect of WT strain was, to a small but significant extent, greater than that of the mutant (p=0.0367, Fig 5.3.19.A). *Npc2* expression was also significantly increased in RAW 264.7 MΦ treated with *Mtb* H37Rv (p=0.0280) and *ΔpimE* (p=0.0352) *Mtb* H37Rv TL extracts relative to control (Fig 5.3.19.B.), but there was no significant difference between the effectiveness of the two TL extracts (Fig 5.3.19.B.).

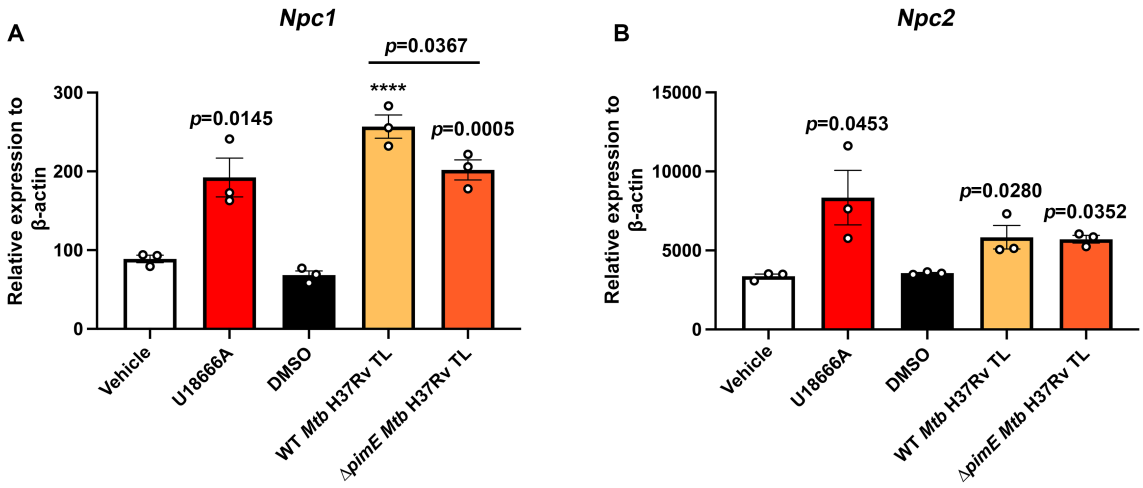


Figure 5.3.19. TL extracts of Mtb H37Rv and ΔpimE Mtb H37Rv increase Npc1 and Npc2 transcription in RAW 264.7 MΦ.

Cells were treated with TL extract (100μg/ml for 48h). DMSO and U18666A (2μg/ml for 48h) were vehicle and positive control respectively. Relative *Npc1* (A) and *Npc2* (B) transcription were determined by qPCR and normalised to *β-actin*. Data are mean ± SEM, n=3. Statistical analysis, one-way ANOVA with Tukey multiple comparisons. ****$p<0.0001$, other p values as indicated. Statistical comparison of U18666A treatment is relative to vehicle control. Statistical comparisons of lipid treatments are relative to the DMSO control. Data are representative of 2 independent experiments.

5.4. Discussion

The objective of the studies conducted in this chapter was to begin to identify the nature of the lipid(s) from *Mtb* H37Rv that inhibit the NPC pathway. We adopted two complementary approaches to address this question. First, by using a classical biochemical strategy, the TL extract of *Mtb* H37Rv was fractionated and enriched by differential solvent partitioning and silicic acid chromatography steps [417], and the resulting fractions assayed for their capacity to expand lysosomal volume and inhibit the biosynthesis of a pro-inflammatory cytokine [207, 215]. Second, candidate *Mtb* lipids obtained from BEI Resources were assessed for induction of specific NPC phenotypes. Our examination of *Mtb* lipids available from a bioresource showed that SL-1, $PIM_{1,2}$ and PIM_6, in particular, induced multiple NPC phenotypes.

We used a defined lipidomic platform [418] to test the hypothesis that pathogenic mycobacteria, such as *Mtb* H37Rv, produce specific lipid(s) which inhibit Npc1 but are absent from non-pathogenic species such as *M. smegmatis*. This strategy has been successfully exploited to identify specific mycobacterial lipids, such as those associated with virulence and remodelling of host phagosomes [187, 417]. Optimised chromatography separation resolved bioactive lipid fractions whose retention corresponded to the least polar (fraction 1 and 2) through to more polar lipids (fractions 13 and 14). MALDI-ToF MS analysis of the latter identified enrichment for PIM species. The distribution of bioactivity across chromatographic fractions of the two mycobacteria was consistent with the hypothesis, with fraction 14 from *Mtb* H37Rv having the greatest activity, which was absent from the equivalent fraction of *M. smegmatis*. Although infection with

M. smegmatis has been shown to be unable to induce NPC phenotypes [96], the identification of activity in lipid fractions prepared from the mycobacterium is in agreement with the findings that a TL extract was bioactive (Chapter 3, Section 3.3.3., Section 3.3.4., Section 3.3.5., Section 3.3.6.). Whilst an initial evaluation would suggest these data are incompatible with the hypothesis that non-pathogenic mycobacteria cannot inhibit Npc1, it may be that these lipids are present in the *M. smegmatis* cell wall so are extractable with solvent, but that they are not produced or shed in effective amounts during natural infection so do not inhibit NPC1. However, preparation of a lipid extract could solubilise specific lipid(s) and make them available to inhibit NPC1 when the lipid extract is added to wild-type cells.

We used two assays, LysoTracker™ staining as a measurement of acidic compartment volume and inhibition of pro-IL1β synthesis to screen for activity. This approach was validated by the significant overlap of active fractions using these two independent screens (fraction 14 from *Mtb* H37Rv was the most potent in both assays). Results from the two assays also indicated that inhibition of pro-IL1β production was more sensitive than lysosomal expansion measured with the LysoTracker™ assay; statistically significant inhibition of pro-IL1β synthesis was also detected in a greater number of lipid fractions as compared with the LysoTracker™ assay. Re-adjusting to lipid fraction treatment with a lower concentration may highlight a greater similarity of active fractions between the two assays. Although impaired synthesis of the cytokine is not currently established as an NPC phenotype, pre-print evidence is supportive of it being a recently discovered NPC phenotype [215], with data showing reduced production

of pro-IL1β, but not other pro-inflammatory species such as TNF-α in *Npc1*$^{-/-}$ mice both *ex vivo* and *in vivo* [419]. It is relevant that there is evidence that *Mtb* infection is known to limit IL-1β generation *in vitro* [233].

Comparing the lipid compositions of fraction 14 and adjacent fractions, we found an enrichment in PIs and mannosylated PIs. This suggests the PI and PIM species are candidate lipids that can inhibit the NPC1 protein. Definitive identification of the bioactive lipid(s) will likely require the production of scaled-up cultures of *Mtb* H37Rv that would allow for the necessary chromatography and isolation steps and structural determinations.

We took the opportunity to obtain purified *Mtb* lipids, which included surface-exposed lipids and glycolipids, membrane-anchored mannan-based lipids, and PIMs, and examined their capacity to induce NPC phenotypes in RAW 264.7 MΦ. The candidates we were able to screen were restricted to those available from BEI Resources (listed in Table 5.2.2.), which were supplied together with data documenting their purity. In this case, the provision of greater amounts of each lipid meant we were able to investigate the ability to induce multiple NPC phenotypes. Of the 14 candidate species that were initially screened by LysoTracker^{TM} assay, SL-1, TDM, $PIM_{1,2}$ and PIM_6 significantly increased the intensity of staining and were able to significantly inhibit pro-IL1β synthesis. Therefore, we focused on the capacity of these species to induce additional NPC cellular phenotypes. We found that under the conditions used, all of the lipids were able to induce the majority of NPC phenotypes (summarised in Table 5.4. with the structure of each lipid shown in Fig 5.4.).

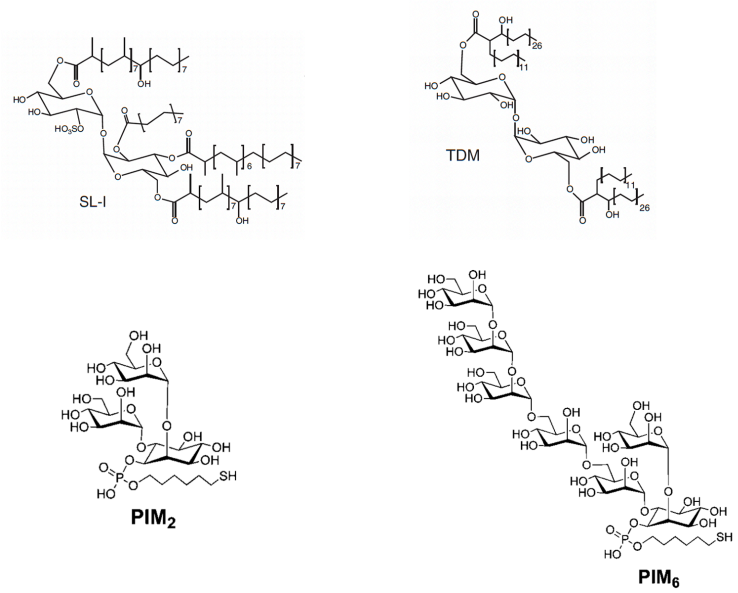


Figure 5.4. Structure of SL-1, TDM, PIM_2 and PIM_6.

SL, sulpholipid; TDM, trehalose di-mycolate; PIM, phosphatidylinositol mannoside. Adapted from [168, 410].

NPC Phenotype	U18666A	SL-1	TDM	$PIM_{1,2}$	PIM_6
LysoTracker™ MFI	↑	↑	↑	↑	↑
Pro-IL1β synthesis stimulated by LA	↓	↓	↓	↓	↓
LE/Lys size	↑	↑	↑	↑	↑
Free cholesterol accumulation	Yes	Yes	Yes	Yes	Yes
Lysosomal GM1 accumulation	Yes	Yes	Yes	Yes	Yes
Npc1 protein expression	↑	-	-	-	↑
Npc2 protein expression	↑	-	-	-	↑
Sphingosine accumulation	Yes	Yes	No	No	No
GSL accumulation	Yes	Yes	No	Yes	No

Table 5.4. Summary of NPC phenotypes induced by SL-1, TDM, $PIM_{1,2}$ and PIM_6.

↑: increased; ↓: decreased; -: not altered.

As outlined in the introduction to this chapter, as a consequence of the recognition of the abundance and diversity of lipids associated with the mycobacterial cell envelope, many studies have concentrated on the identification of individual species on their biological activities and, in particular, how they may promote pathogenesis [169]. Therefore, we will consider the results reported here in the context of published studies of mycobacterial lipids and focus on possible relevance to the NPC pathway.

Of the NPC phenotypes investigated, SL-1 was able to induce all of them with the exception of not enhancing Npc1 and Npc2 protein expression. SL-1 is an abundant cell wall lipid that has been proposed to play important roles in mycobacterial manipulation of host physiology, including triggering cough, which promotes the transmission of bacilli [386]. An initial study reported SL-1 prevented phagosome-lysosome fusion in murine peritoneal MΦ [420], but this was later shown to be an artefact [421]. Inhibition of trafficking events and lysosomal fusion is a characteristic of NPC [24]. However, the precise role of SL-1 in *Mtb* pathogenesis remains controversial. The SL-deficient strain, *msl2*, was reported to have unchanged virulence in mice and guinea pigs [402]. Disruption of the sulphotransferase, Stf0, which is required for the addition of a sulphate group in the first step of SL-1 biosynthesis, resulted in a viable mycobacterium that was less susceptible to an anti-microbial peptide and had enhanced survival in human MΦ but not in murine cells [400]. Conversely, although both the lipid transporter *mmpL8* and *pks2,* which encodes a polyketide synthase, are essential for SL-1 biosynthesis, loss of the former attenuates mycobacterial growth in mice, whereas lack of *pks2* had no effect [406]. Evidence suggests that

the absence of SL-1 may perhaps not impact virulence significantly because of functional overlap and hierarchical dominance of other lipid species [403].

Although TDM was able to induce some NPC phenotypes, there was no significant effect with respect to NPC1 and NPC2 expression or sphingoid-base lipids metabolism, and in particular, there was no accumulation of GSLs (both total and individual GSL species). It would seem that TDM is unlikely to inhibit NPC1. TDM is an outer membrane, surface exposed lipid that has been shown to be highly relevant to TB immunopathology because of its interactions with host receptors such as Mincle and DC-SIGN and is released in significant amounts by *Mtb* to modulate surrounding cells [183, 184, 422]. We acknowledged that the study by Fineran *et al.* showed that a commercial TDM (from Sigma) had NPC phenotype-inducing activity [96], but as we have indicated previously, details of the composition and purity of the lipid preparation used were unavailable at the time.

Incubation of RAW 264.7 MΦ with the phosphatidylinositol mannosides. $PIM_{1,2}$ and PIM_6, resulted in multiple NPC phenotypes. However, their effects on GSLs were less clear. PIMs are required for the viability of *Mtb*, which are released and taken up by bystander non-infected cells and mediate interactions with host cells that favour survival and immune evasion [183, 423]. Initially, the evidence that PIM_6 inhibited NPC1 was problematic because the PIM_6 preparation was not composed of a single lipid species. However, in support was the MS analysis of the active *Mtb* lipid fraction 14 that confirmed the presence of differentially acetylated forms of PIM_2 and PIM_6. Therefore, we decided to assay the activity

of a TL extract of the mutant strain, *ΔpimE Mtb* H37Rv. *PimE* is required for $AcPIM_6$ biosynthesis in mycobacteria and encodes a mannosyltransferase (ManT) responsible for the formation of $AcPIM_5/Ac_2PIM_5$ from $AcPIM_4/Ac_2PIM_4$ (Fig 5.1.3.B.) [411, 424]. We hypothesised that TL extract of *ΔpimE Mtb* H37Rv would be unable to induce NPC phenotypes. TLC and MS analysis demonstrated the absence of this specific lipid. However, we found no significant difference in the induction of NPC phenotypes by this strain as compared to the parental wild-type *Mtb* H37Rv. These data are therefore not apparently consistent with our hypothesis. However, the MS profile of *ΔpimE Mtb* H37Rv indicated not only the lack of PIM_6 but also a significant increase in the levels of Ac_3PIM_2 (in the order of about 20%), and TLC analysis showed an enrichment of Ac_1PIM_2 and Ac_2PIM_2, most likely because of the absence of PimE activity. It is relevant that $PIM_{1,2}$ was positive in several NPC1 inhibition assays and that preventing the biosynthesis of a single lipid may alter the abundance of other lipids and as a consequence, trigger compensatory mechanisms. Unfortunately, disruption of the entire PIM biosynthesis pathway by deletion of PimA, which is a ManT to produce PIM_1 from PI, is not feasible, as those lipids are essential for *Mtb* survival and growth [423].

A recent study from Sachdeva *et al.* [425] is particularly relevant to the results presented in this chapter because the authors focused upon modulation of the lysosomal system by *Mtb* surface components that included some of those that we examined. In summary, *Mtb* H37Rv infected MΦ had a higher frequency of LysoTracker™ positive vesicles that was verified by LAMP-1 immunostaining, and comparable data were obtained for *in vivo* murine infections [425]. When *Mtb* lipids, were tested, a total lipid extract, along with SL-1, PIM_6 and arabinogalactan

(all of which were sourced from BEI Resources), significantly increased the frequency of LysoTracker™-positive compartments and enhanced LAMP-1 expression [425]. Although the criteria examined were not precisely the same; Sachdeva *et al.* determined the frequency of LysoTracker™ positive vesicles [425], whereas we measured relative staining intensity, the two sets of data are in agreement, with the exception that we were not able to detect a significant effect with arabinogalactan and in our hands, TDM was effective. It is of interest that SL-1 mediated lysosome increase was indicated to be via inhibition of the mammalian target of rapamycin complex 1 (mTORC1) that enables the translocation of the transcription factor TFEB into the nucleus to drive the expression of lysosomal genes [425]. This would seemingly conflict with SL-1 inhibiting NPC1 because of a publication indicating mTORC1 hyperactivation in NPC cells, but this finding is currently controversial [426]. According to other studies, *Mtb* prefers to infect MΦ with defective lysosomal function and less TFEB production, and mycobacterial acyl carrier protein suppresses TFEB and upregulates miR0155 to inhibit host deference [427, 428]. The inconsistency of some of these data would suggest that the effects of *Mtb* infection and individual mycobacterial lipids on lysosomal biogenesis and the regulation of lysosomal genes requires further systematic investigations.

A second recent study is supportive of our proposal of the convergence of mechanisms that promote the survival of intracellular microbes, particularly *Mtb* and those underlying LSDs. 1-TbAd, the product of a virulence-associated *Mtb* enzyme [417] has been demonstrated to cause lysosomal accumulation of lipids that are characterised by specific LSDs, such as GD and Wolman's disease [429].

We adopted two independent experimental approaches that had the objective of identifying specific *Mtb* lipid(s) that can inhibit NPC1. We made, albeit on a small scale, a proof-of-principle investigation of the feasibility of isolating the bioactive species starting with a 100% lipid extract of *Mtb* using a combination of biochemical enrichment through chromatographical separation and analysis by MS. Through our research, we discovered that inhibitory activities were enriched in specific fractions, suggesting that starting with larger cultures of *Mtb* would allow for the incorporation of additional separation steps as required and should enable isolation and characterisation of the specific lipid(s). Second, we tested purified *Mtb* H37Rv lipids for their ability to induce NPC phenotypes, and although we were unable to unambiguously demonstrate the inhibition of NPC1, several have emerged as potential candidates and they should be studied further. Even if none are directly responsible for NPC1 inhibition because they clearly affect the endo-lysosomal system to some degree, they are likely of interest.

Chapter 6. *Salmonella* and the NPC pathway

6.1. Introduction

Intracellular pathogens

Microbes that have evolved the ability to enter, survive and replicate within host cells are one of the greatest causes of infectious disease. Intracellular bacteria have evolved a variety of methods to successfully enter and survive in eukaryotic cells and overcome host defence mechanisms that are often shared between different types of host cells. One of these is the need to prevent their delivery to the lysosome. We speculated that pathogens, in addition to persistent mycobacteria, may also inhibit the NPC1 pathway to enhance their survival. As described in Chapter 1, inhibition of the NPC pathway may be involved in the pathogenesis of various intracellular pathogens, one of which is *Salmonella* infection. We therefore examined the induction of NPC phenotypes by this pathogen.

Salmonella

Salmonella is a genus of Gram-negative bacteria of the Enterobacteriaceae family that is classified into two species, *Salmonella enterica* and *Salmonella bongori*, of which over 2600 serotypes of *Salmonella* have been identified [430, 431]. *Salmonella enterica* is further classified into 6 subspecies, *arizonae* (IIIa), *diarizonae* (IIIb), *houtenae* (IV), *salamae* (II), *indica* (VI) and *enterica* (I) [431].

Epidemiology, symptoms and treatments

Salmonellosis is mostly caused by *Salmonella enterica* subspecies *enterica* (responsible for about 99% of salmonellosis cases in humans) [431] and is a major public health problem worldwide. It is primarily transmitted through

ingestion of contaminated food or water, to which infants, young children, elderly people and immunocompromised individuals display increased susceptibility [432]. Based upon the clinical characteristics of salmonellosis, *Salmonella* is classified into typhoid and non-typhoidal *Salmonella* (NTS) [433]. Typhoid fever, or enteric fever, is caused by *S.* Typhi or *S.* Paratyphi infection and has an incidence of approximately 22 million cases and 220,000 deaths annually [434]. Typhoid fever is characterised by an incubation period of 10 to 14 days with abdominal pain, headache and diarrhoeal symptoms, followed by the onset of fever [435]. In contrast, symptoms of NTS infection are mainly gastrointestinal, which include non-bloody diarrhoea, vomiting, nausea and abdominal pain [433]. NTS is prevalent in sub-Saharan Africa, with higher susceptibility in children under 5 years of age as well as HIV and malaria patients [436]. The development of non-typhoid salmonellosis is more rapid, normally taking between 6 and 72h post-infection [437]. It is estimated that around 95.1 million cases are caused by NTS infection annually, resulting in around 50,000 deaths [436, 438]. Whilst self-limiting gastroenteritis is usually allowed to run its course, treatments for *Salmonella* infection involve the use of antibiotics, such as ampicillin, chloramphenicol and trimethoprim-sulfamethoxazole [433]. However, the effectiveness of these treatments is increasingly limited by multi-drug resistance (MDR).

***Salmonella enterica* Serovar Typhimurium (*S.* Typhimurium)**

Salmonella enterica Serovar Typhimurium (*S.* Typhimurium) is responsible for 25% of NTS infection cases, which is second only to those caused by *S. enterica* Serovar Enteritidis [433, 439, 440]. *S.* Typhimurium consists of an inner

membrane, a peptidoglycan layer, and an outer cell membrane containing lipopolysaccharide (LPS) (Fig 6.1.1.). Flagellin and pili facilitate the motility of *Salmonella*, which is important for adhesion to and invasion of host cells [441]. Two type 3 secretion systems (T3SSs) are encoded in the genome of *S.* Typhimurium on either *Salmonella* pathogenicity island-1(SPI) or SPI-2. This secretion apparatus, also called the injectisome, is located through the inner and outer membranes and is responsible for the secretion of effector proteins into host cells, that are important for *Salmonella* pathogenesis [442].

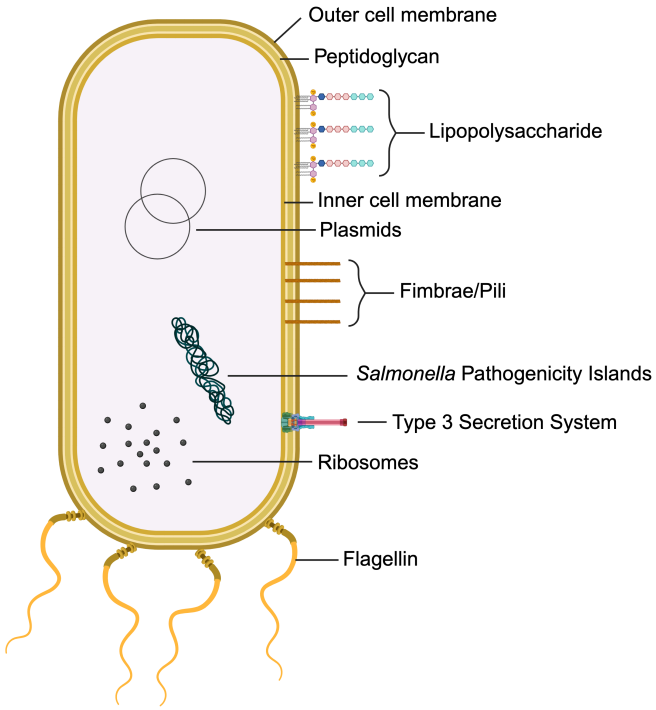


Figure 6.1.1. Schematic of the structure of S. Typhimurium.

S. Typhimurium is a Gram-negative bacterium with an inner and outer membrane linked by a peptidoglycan layer. Flagellin and fimbriae facilitate the motility of the bacteria. Type 3 secretion systems are located through the inner and outer membranes of *S.* Typhimurium. Effector molecules are secreted via the type 3 secretion system apparatus into the host cell. Lipopolysaccharide is located on the outer membrane. Adapted from [443].

Pathogenesis of *S.* Typhimurium

S. Typhimurium exhibits unique survival mechanisms to manipulate the host defence system, enabling it to survive and replicate in infected cells. After oral ingestion, *S.* Typhimurium descends through the gastric acidic environment and activates acid tolerance responses to enable the bacterium to maintain pH homeostasis [444]. Once in the large intestine, *S.* Typhimurium invades non-phagocytic cells (Microfold (M) cells in the Peyer's patches and intestinal epithelial cells) through the use of effector proteins secreted from the SPI-1 encoded T3SS (T3SS1) (Fig 6.1.2.) [445]. *S.* Typhimurium is also phagocytosed by dendritic cells in the intestinal lumen or submucosal areas. The formation of *Salmonella*-containing vacuoles (SCV) within host cells mediated by effector proteins secreted from the T3SS2 facilitates the intracellular survival of *S.* Typhimurium [446]. Production of pro-inflammatory cytokines such as IL-8, IL-1β and TNF-α recruits immune cells, including MΦ and neutrophils, to the sites of infection [447]. *S.* Typhimurium is phagocytosed by recruited MΦ, replicates inside these immune cells and is released from the cell after activating cellular apoptosis or pyroptosis [448]. *S.* Typhimurium is shed in faeces and thereby transmitted to other organisms [449].

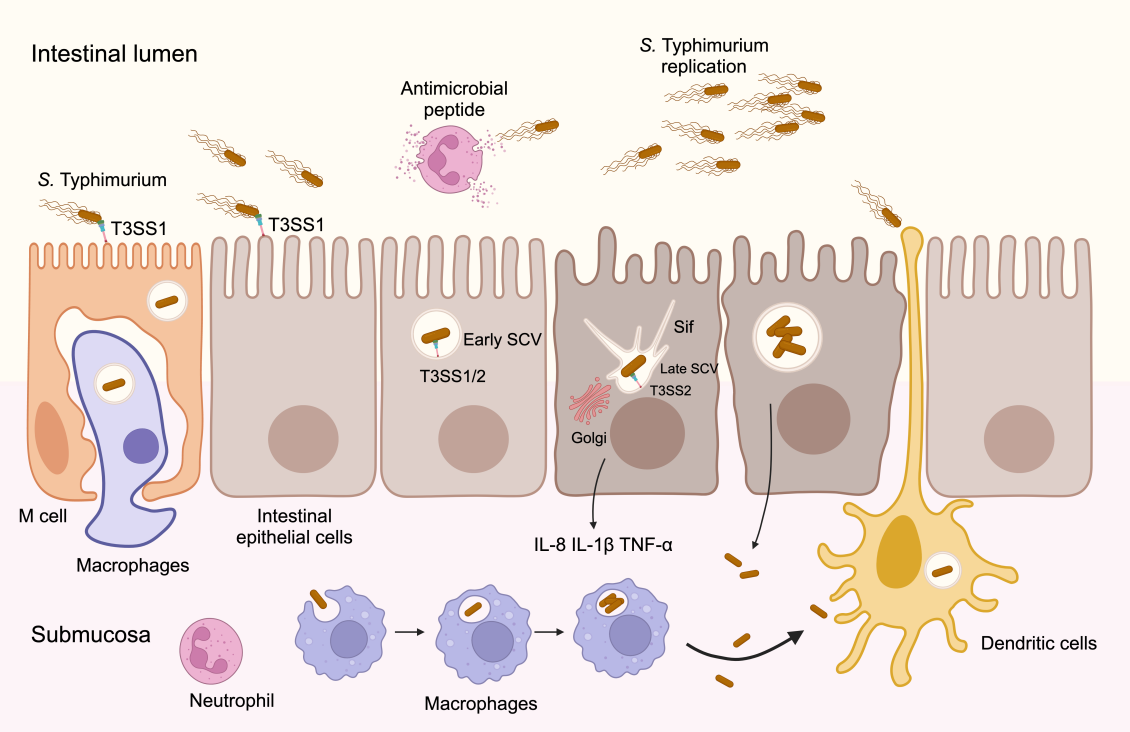


Figure 6.1.2. Pathogenesis of S. Typhimurium.

After reaching the large intestine, *S.* Typhimurium adheres to M cells in Peyer's patch or epithelial cells and enters non-phagocytic cells via effector proteins from T3SS1. The activation of T3SS1 and T3SS2 mediates the formation of early SCVs. Late SCVs are located in the perinuclear region of the host cell close to the Golgi apparatus and are characterised by the formation of *Salmonella*-induced filaments (SIF). Pro-inflammatory cytokines (IL-8, IL-1β, TNF-α) are secreted to recruit immune phagocytes such as neutrophils and MΦ. *S.* Typhimurium released by epithelial cells are phagocytosed and replicate within MΦ. *S.* Typhimurium that escape from MΦ can subsequently infect dendritic cells which migrate and release bacteria into the intestinal lumen. T3SS, type 3 secretion system; Sif, *Salmonella*-induced filament; SCV, *Salmonella*-containing vacuole; IL, interleukin; TNF, tumour necrotic factor. Adapted from [450, 451].

Intracellular survival of *S.* Typhimurium

S. Typhimurium infects both non-phagocytic and phagocytic cells, but the mechanism by which bacteria invade the two cell types differs (Fig 6.1.3.). In the case of professional phagocytes such as MΦ and dendritic cells, the primary mechanism is phagocytosis, which involves antibody and complement-mediated ingestion as well as the uptake of non-opsonised bacteria via the ligation of specific receptors [452]. In the case of non-phagocytic cells, *S.* Typhimurium injects effector proteins via T3SS1 to stimulate plasma membrane ruffling that forms macropinosomes and tight vacuoles which surround bacilli [453, 454]. The tight vacuoles containing *S.* Typhimurium fuse with macropinosomes to form the early SCV [455]. The same entry mechanism has also been observed in MΦ in addition to phagocytic uptake [456]. Early SCVs are enriched with early endosomal markers, such as Rab4, Rab5 and EEA1 [457-459]. Following SPI-1-mediated invasion, approximately 10 to 20% of vacuoles rupture and bacteria are then susceptible to degradation by the process of xenophagy [460, 461]. Xenophagy, or antibacterial autophagy, re-encloses these bacteria in a double membrane autophagosome which can subsequently fuse to lysosome [460]. Lysis of early SCVs releases *S.* Typhimurium into the cytosol, whereas some of these bacteria are restricted by xenophagy, replication in cell culture models is observed in non-phagocytic cells *in vivo* [462]. SCV maturation is mediated by effector proteins delivered by the SPI-2-encoded secretion apparatus and is characterised by the acquisition of LE/Lys markers such as LAMP-1, Rab7, Rab9 and vATPases, concurrent with acidification (pH~4.5) [463-465]. Although SCV requires access to contents in LE/Lys compartments, perhaps due to nutrient acquisition [466], it is a restricted and dynamic process [462] to avoid degradation

by the host cell lysosomes [467, 468]. With maturation, late SCVs relocate to peri-nuclear regions through dynein-mediated transport on the remodelled host cell cytoskeleton and formation of a microtubule organising centre (MTOC), which facilitates survival and replication of bacilli [469-471]. *Salmonella*-induced filament (SIF) formation occurs at late stages of SCV maturation to facilitate nutrient access between SCVs and the endocytic system, thereby facilitating formation of *Salmonella* replicative compartments [466, 472, 473].

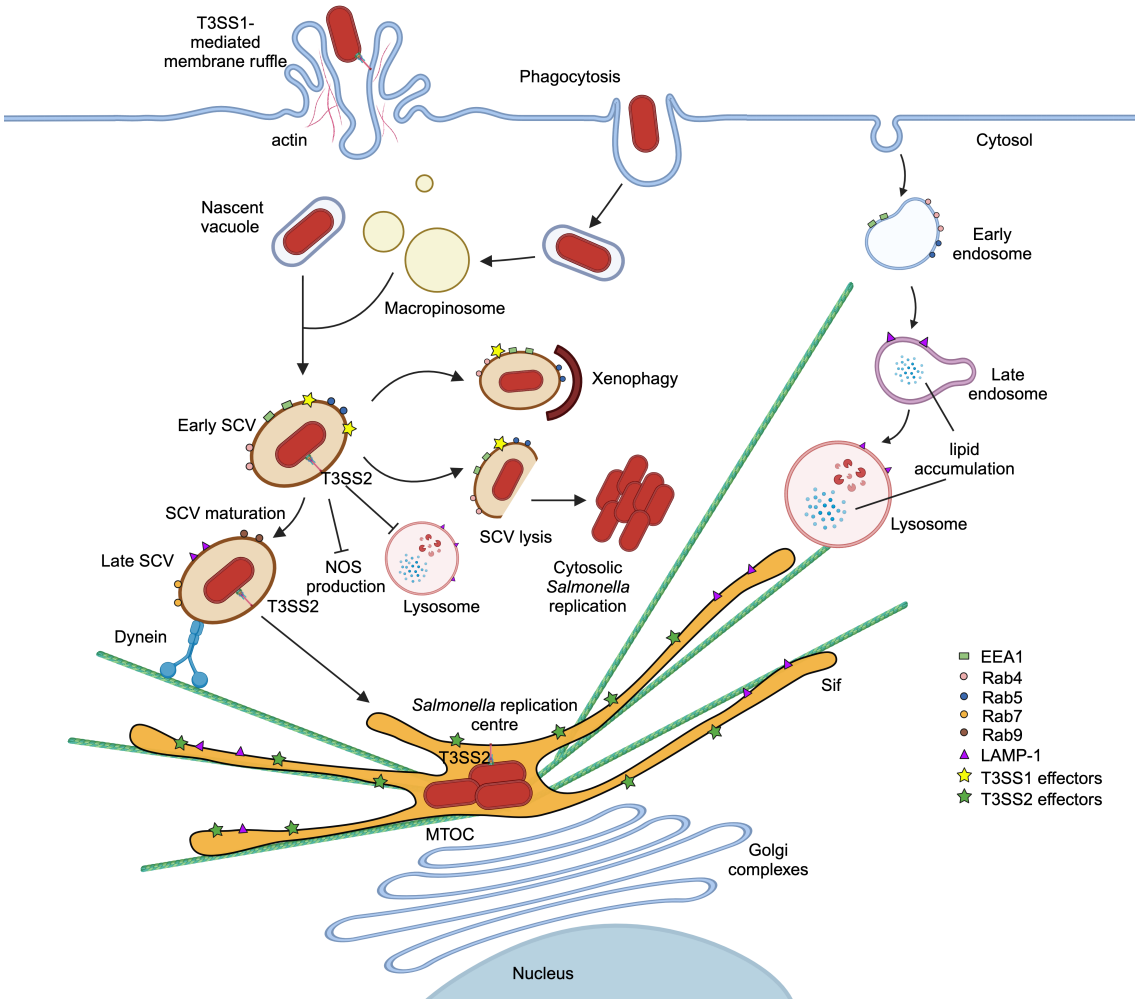


Figure 6.1.3. The intracellular life cycle of S. Typhimurium.

S. Typhimurium enters non-phagocytic cells by provoking membrane ruffling as a result of the release of effectors from T3SS1 or through phagocytosis by cells such as MΦ. Nascent vacuoles containing individual *S.* Typhimurium fuse with macropinosomes to generate early SCV, a process mediated by T3SS1 effector molecules. The early SCV acquires molecular markers characteristic of early endosomes, which include EEA1, Rab4 and Rab5. Early SCVs can either be cleared by xenophagy or lysed, which allows for bacterial escape into the cytoplasm. T3SS2 inhibits SCV-lysosome fusion and NOS production. Late SCVs procure LAMP-1, Rab7 and Rab9 and are transported by dynein on microtubules to MTOC, located in close proximity to the Golgi complexes. When at the MTOC, LAMP-1 positive SIF are formed as a result of the activity of T3SS2. Lipid accumulation is also observed. NOS, nitric oxide species; SIF, *Salmonella*-induced filament; T3SS, type 3 secretion system; MTOC, microtubule-organising centre; SCV, *Salmonella*-containing vacuole. Adapted from [474-476].

Persistence of *Salmonella*

S. Typhimurium exhibits long-term persistence during infection [477-479]. In asymptomatic BALB/c mice, *S.* Typhimurium is able to persist systemically for up to 1 year after inoculation, and bacteria can be detected in faeces, spleen and lymph nodes [480]. A separate study found such bacteria were not actively replicating and had seemingly adopted a dormant-like state, suggesting they may represent a reservoir of persistent bacteria [481, 482]. A genome-wide screen has identified a significant number of *Salmonella* genes required for long-term infection [483]. Clinical studies have confirmed that infections can extend for up to 8.3 years, and about 8.5% of all clinical cases of *S.* Typhimurium are persistent

[478]. These findings suggest that bacteria have localised to a permissive niche within the host.

At the cellular level, *S.* Typhimurium achieves intracellular survival by the secretion of effector proteins encoded in SPIs to modulate host cell immunity machinery, such as lysosomes and inflammasomes. Early studies showed that SCV inhibits phagosome-lysosome fusion in infected murine MΦ [484, 485]. *Salmonella* can also enter a dormant state regulated by effectors secreted from T3SS2, facilitating its persistence in the epithelial cells [482].

Lipid accumulation in *S.* Typhimurium infection

Foam cell phenotypes are observed in *S.* Typhimurium-infected cells, characterised by the accumulation of lipids, including cholesterol [486]. Lipid droplet formation occurs during early *S.* Typhimurium infection, which facilitates survival and replication of bacteria [133]. Neutral lipids also accumulate in *S.* Typhimurium-infected cells and are enriched around SCVs, suggesting they may serve as a nutrient source [486, 487].

***S.* Typhimurium effector proteins**

Effector proteins delivered by both the SPI-1 and SPI-2 encoded T3SSs are critical for *Salmonella* virulence and the ability of the bacterium to manipulate host cell function [488, 489]. There are five SPIs present in *Salmonella* in total, including SPI-1 to SPI-5, with SPI-1 primarily responsible for the invasion of intestinal epithelial cells, and SPI-2, 3 and 4 are required for intracellular survival and replication [490]. SPI-5 has been shown to encode effectors that mediate

inflammation in host cells [490]. Effector proteins, especially those encoded in SPI-2 and exported by T3SS2, have great importance for intracellular survival and replication of *S.* Typhimurium. More than 28 effector proteins are delivered by T3SS injectisome from SCV-enclosed bacteria and have diverse functions, including roles related to lipid biogenesis that contribute to the virulence [488].

S. Typhimurium effectors and NPC

SifA is important for SIF formation [491, 492]. SseJ and SifA exhibit complementary actions to regulate the dynamic of the SCV membrane [493]. SseJ is regarded as a cholesterol acyltransferase that esterifies cholesterol in the host cells and has been shown to inhibit the cholesterol exchange between SIF and lysosomes mediated by SifA [487, 494]. SseL is a deubiquitinase which prevents lipid accumulation *in vivo* [495]. SseL forms a stable complex with oxysterol-binding protein (OSBP)-1 to tether the Golgi and ER to facilitate cholesterol and PI(4)P transport between SCVs and these organelles [496]. During *S.* Typhimurium infection, the interaction between SCVs and endo-lysosomal compartments is necessary because acidification is required for induction of T3SS2. However, lysosomal activity is tightly regulated during *Salmonella* infection. *Salmonella* inhibits retrograde trafficking of mannose-6 phosphate (M6P) receptors from endosomes to the Golgi, which detoxify the LE/Lys by disrupting the trafficking of M6P-tagged hydrolases to LE/Lys [497]. This permits the SCV to access nutrients from LE/Lys without exposure to antimicrobial agents, such as lysosomal enzymes. *S.* Typhimurium downregulates lysosome biogenesis via the TFEB pathway and limits access to lysosomes by maintaining a low number of bacilli in SCV [460, 467, 498]. Delivery

of LE/Lys components to SCV for SIF formation is facilitated by the homotypic fusion and sorting (HOPS) complex which is enriched during the later stages of the SCV maturation [499, 500].

A recent study is particularly relevant to the investigations reported in this chapter. Walch *et al.* undertook an unbiased global mapping of interactions between *Salmonella* effector proteins and those of the host cell [501]. They found that SifA, SseJ and SseL (effector proteins secreted by T3SS2) modulate cholesterol trafficking between the SCV membrane and ER in part by interacting with NPC1 [501]. The NPC1 protein was recruited to SCVs by SifA, where it physically interacts with SseJ, which promotes cholesterol accumulation in SCV and is functionally inhibited by SseL (Fig 6.1.4.) [501].

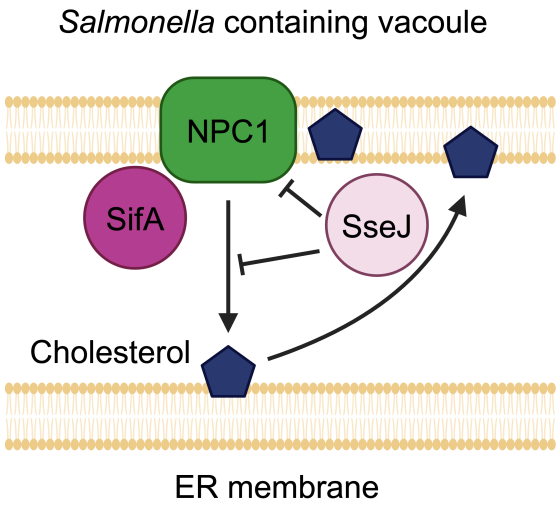


Figure 6.1.4. Proposed interaction of Salmonella effector proteins with NPC1 between Salmonella-containing vacuole and ER membrane. Adapted from [501].

In conclusion, lipid accumulation is observed during *S.* Typhimurium infection consistent with NPC1 inhibition. There is published evidence that *S.* Typhimurium effector proteins interact with the NPC1 in host cells directly consistent with NPC1

being an important host target of this pathogen. In this chapter, we have investigated whether *S.* Typhimurium also sheds lipids that target the NPC pathway in infected and bystander cells, analogous to the persistence of mycobacterial infection.

Aims

- Determine whether NPC cellular phenotypes are induced by *S.* Typhimurium infection.
- Determine if the inhibition of the NPC pathway in host cells is mediated by lipid components of *S.* Typhimurium.

6.2. Material and methods

6.2.1. Cells

RAW 264.7 MΦ were cultured as described in Section 2.2.1. WT Chinese hamster ovary (CHO) and CHO$^{Npc1-/-}$ were generated as described in the published studies [502-504] and cultured in Dulbecco's Modified Eagle's Medium with high glucose (Sigma, D5671) supplemented with 10% (v/v) Foetal Bovine Serum (FBS) (Sigma, F7524), 1% (v/v) glutamine (Gibco, 25030-024) and 1% (v/v) penicillin/streptomycin (P/S) (Sigma-Aldrich, P0781) at 37°C with 5% CO_2. Adherent cells were detached with Trypsin-EDTA solution (Sigma, T3924) and passaged routinely for no more than 10 consecutive passages to maintain viability (>90%). WT and *Tlr4*$^{-/-}$ immortalised murine bone marrow-derived MΦ (iBMDMΦ) were supplied by Dr Teresa Thurston at Imperial College, London [505]. iBMDMΦ were cultured in Dulbecco's Modified Eagle's Medium with high glucose supplemented with 10% Foetal Bovine Serum (FBS), 1mM sodium pyruvate (Gibco, 11360070), 1% glutamine, 1% P/S, and 30% (v/v) L929-conditioned media [506] at 37°C with 5% CO_2.

6.2.2. *S.* Typhimurium strains and infection assays

GFP or mCherry-tagged WT, *ΔssaV, ΔsifA, ΔsseJ* and *ΔsifAsseJ S.* Typhimurium were provided by Dr Teresa Thurston at Imperial College, London [507]. Bacteria were grown in LB media containing 50μg/ml carbenicillin at 37°C overnight until reaching stationary phase. RAW 264.7 MΦ were seeded in 6-well plates (for lipid analysis) at a density of 0.5 x 10^6 cell/well or 24-well plates (for confocal microscopy analysis) at a density of 0.2 x 10^6 cell/well and incubated overnight. *S.* Typhimurium was opsonised in R10 containing 10% (v/v) mouse serum for

20min at room temperature and diluted 3 times with R10. Opsonised *S.* Typhimurium in R10 was added to cells at ~1.3 x 10^6 bacilli/ml. In the case of *ΔssaV* mutant, this was increased to ~2.6 x 10^6 bacilli/ml. Plates were centrifuged at 110xg for 5min and incubated at 37°C for 25min. After infecting cells for 25min, the media was then removed and cells were washed twice with PBS. Cells were then incubated in R10 containing 100µg/ml gentamycin for 1h at 37°C to kill extracellular bacteria. After 1h, the media was removed and replaced with media containing 20µg/ml gentamycin and incubated for a further 24h or as indicated. Analysis indicated that using this regime, approximately 30% of the cells were infected with *S.* Typhimurium.

6.2.3. *S.* Typhimurium TL extract.

A TL extract of WT *S.* Typhimurium was prepared as described in Section 2.2.2.

6.2.4. Lipid solubilisation and addition to cells.

S. Typhimurium TL extract was solubilised in DMSO and added to cell cultures as described in Section 2.2.3. Cells were incubated with *S.* Typhimurium TL extract at 100µg/ml or as indicated for 48h and then analysed. LPS from *S.* Typhimurium (Sigma, L2262) was dissolved in water (Gibco, A1287301) at 1mg/ml by vortexing for 10min and heating for 10min at 60°C. LPS dilutions were prepared in culture medium and cells were treated for 48h.

6.2.5. Filipin staining for free cholesterol.

After *S.* Typhimurium infection or *S.* Typhimurium TL extract treatment, cells were fixed with 4% PFA and stained with filipin, as described in Section 2.2.11.

6.2.6. LAMP-1 immunostaining for confocal analysis.

Immunostaining for LAMP-1 was performed as described in Section 2.2.10.

6.2.7. AmplexRed assay determination of total cholesterol.

Cholesterol levels were determined by AmplexRed assay as described in Section 2.2.12.

6.2.8. CtxB staining for intracellular GM1 ganglioside distribution.

Plasma membrane GM1 gangliosides were labelled with Alexa Fluor™ 555 conjugated CtxB (Invitrogen, C34776) in *S.* Typhimurium-infected cells or with Alexa Fluor™ 488 conjugated CtxB was used to label GM1 gangliosides in *S.* Typhimurium TL extract-treated RAW 264.7 MΦ. Experiments were performed as described in Section 2.2.13.

6.2.9. RP-HPLC measurement of sphingosine and sphinganine levels.

Cell lysates were prepared as described in Section 4.2.4. and sphingosine and sphinganine measured by RP-HPLC as described in Section 4.2.5.

6.2.10. NP-HPLC measurement of GSL levels.

Cell lysates were prepared and GSL levels measured by NP-HPLC as described in Section 2.2.14.

6.2.11. Western blotting

Cell lysates were prepared as described in Section 2.2.8. Immunoblotting for Npc1, Npc2 and SphK2 was performed as described in Section 2.2.8. and Section 4.2.8.

6.2.12. qPCR

Quantification of *Npc1* and *Npc2* transcripts was made by qPCR as described in Section 2.2.9.

6.2.13. Immunofluorescent staining of Npc1 for confocal microscopy.

RAW 264.7 MΦ were infected with mCherry-WT or *ΔssaV S.* Typhimurium and fixed with 4% PFA. Cells were permeabilised with 0.1% saponin (w/v) in PBS for 15min at room temperature and blocked with PBS containing 10% (v/v) horse serum for 1h at room temperature. After blocking, cells were incubated with rabbit anti-Npc1 antibody (1:70, rabbit monoclonal [EPR5209], Abcam, ab134113) and rat anti-LAMP-1 (1:500, rat monoclonal, clone 1D4B, Abcam, ab25245) antibodies diluted in PBS containing 0.1% saponin and 10% horse serum at 4^{o}C overnight. Cells were washed with PBS containing 0.1% saponin three times and stained with secondary antibodies prepared in PBS containing 0.1% saponin and 5% horse serum (1:500, goat polyclonal, anti-rabbit IgG, Alexa Flour^{TM} 647, Invitrogen, A21245; 1:1000, donkey polyclonal, anti-rat IgG, Alexa Flour^{TM} 488, Invitrogen, A21208) for 45min at room temperature. Nuclei were stained with DAPI, and cells were mounted with Prolong Gold Antifade. Imaging was carried out on a Leica-SP8 confocal microscope. Images were analysed using ImageJ Fiji (NIH, USA).

6.2.14. BODIPY-LacCer trafficking

BODIPY-LacCer trafficking in treated RAW 264.7 MΦ was performed as described in Section 4.2.7.

6.2.15. Statistical analysis

Statistical analyses were performed as described in Section 2.2.16.

6.3. Results

6.3.1. Optimisation of the post-infection (pi) period of *S.* Typhimurium infection in RAW 264.7 MΦ.

To determine the optimal duration of *S.* Typhimurium infection that would allow for the development of NPC cellular phenotypes in RAW 264.7 MΦ, we examined initially for cell viability and lysosomal cholesterol accumulation. RAW 264.7 MΦ were infected with opsonised WT *S.* Typhimurium for 25 min and incubated for 17h, 24h or 48h pi before fixation and staining with filipin. Filipin-positive intracellular puncta were observed in RAW 264.7 MΦ infected with WT *S.* Typhimurium for 17h, 24h and 48h pi (red arrows, Fig 6.3.1.). Whilst RAW 264.7 MΦ incubated with WT *S.* Typhimurium for 17h and 24h pi retained an intact and healthy morphology, at 48h pi infected cells appeared apoptotic with blebbing of the plasma membrane (blue arrows, Fig 6.3.1.). Therefore, post-infection periods of between 17 and 24h were used for analysis of the induction of NPC cellular phenotypes.

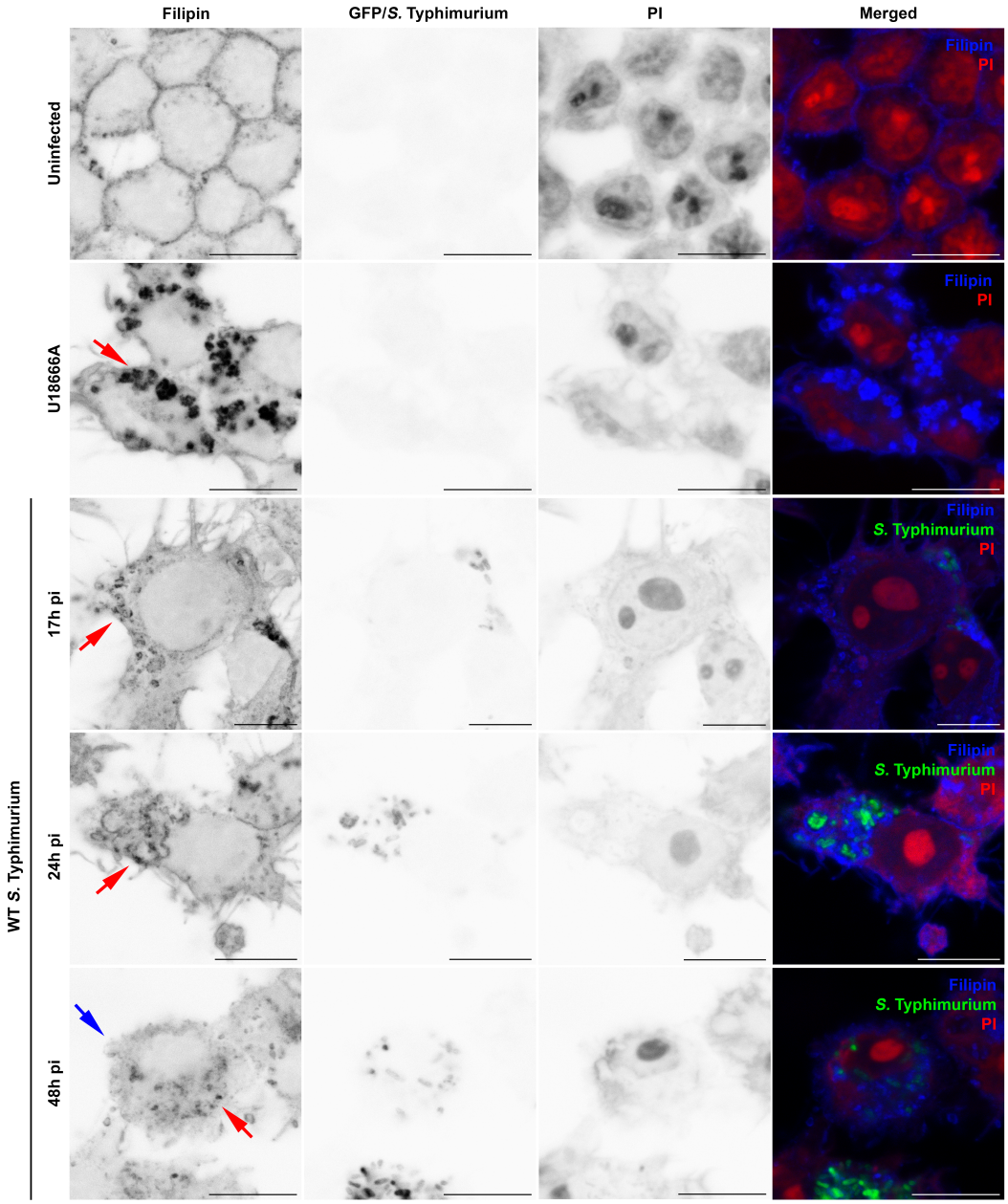
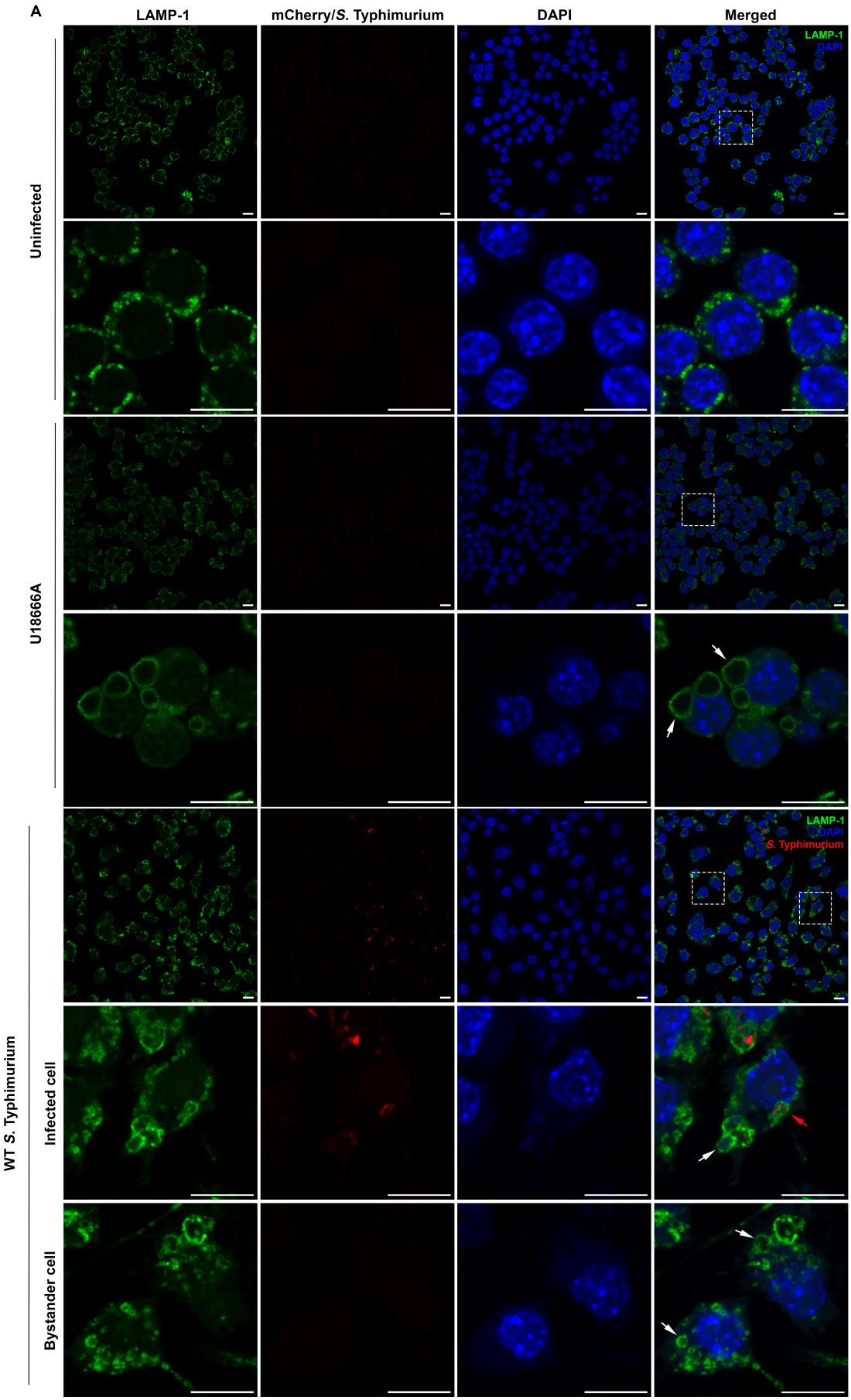


Figure 6.3.1. WT S. Typhimurium infection induces a partial redistribution of cholesterol to intracellular puncta in RAW 264.7 MΦ.

Representative confocal microscopy images of RAW 264.7 MΦ infected with WT *S.* Typhimurium and incubated for 17h, 24h or 48h pi. Uninfected and U18666A (2μg/ml for 17h) treated cells served as vehicle and positive controls respectively. Red arrows indicate filipin-positive puncta; blue arrows indicate membrane blebbing. In merged images: Filipin, blue; *S.* Typhimurium, green; PI, red. Scale bar represents 10μm. Data are representative of 2 independent experiments.

6.3.2. Infection with WT and *ΔssaV S.* Typhimurium increases the size of LAMP-1 positive compartments in RAW 264.7 MΦ.

We determined LE/Lys size in infected RAW 264.7 MΦ by confocal microscopy analysis of cells immunostained for LAMP-1. *ΔssaV* mutant *S.* Typhimurium, unable to secret effectors from the SPI-2 encoded T3SS, was used to exclude the effects of effector proteins [508]. There was a significant increase in the diameter of LAMP-1 positive compartments in RAW 264.7 MΦ infected with WT and *ΔssaV S.* Typhimurium (****p<0.0001, Fig 6.3.2.A.B.C.), with a greater than two-fold increase in median diameter (Fig 6.3.2.C). Large vacuoles containing bacteria (red arrows) or without bacteria (white arrows) were obvious in infected cells and were comparable to those seen in U18666A-treated cells (white arrows, Fig 6.3.2.A.). The diameter of LAMP-1 positive compartments was significantly greater not only in RAW 264.7 MΦ harbouring WT or *ΔssaV S.* Typhimurium but also in neighbouring uninfected cells (white arrows, ****p<0.0001, Fig 6.3.2.A.B.C.). There was no difference in the size of LAMP-1 positive compartments in RAW 264.7 MΦ infected with either WT or *ΔssaV S.* Typhimurium (Fig 6.3.2.A.B.C.).


A
LAMP-1
mCherry/S. Typhimurium
DAPI
Merged
LAMP-1
DAPI
Uninfected
U18666A
WT S. Typhimurium
LAMP-1
DAPI
S. Typhimurium
Infected cell
Bystander cell

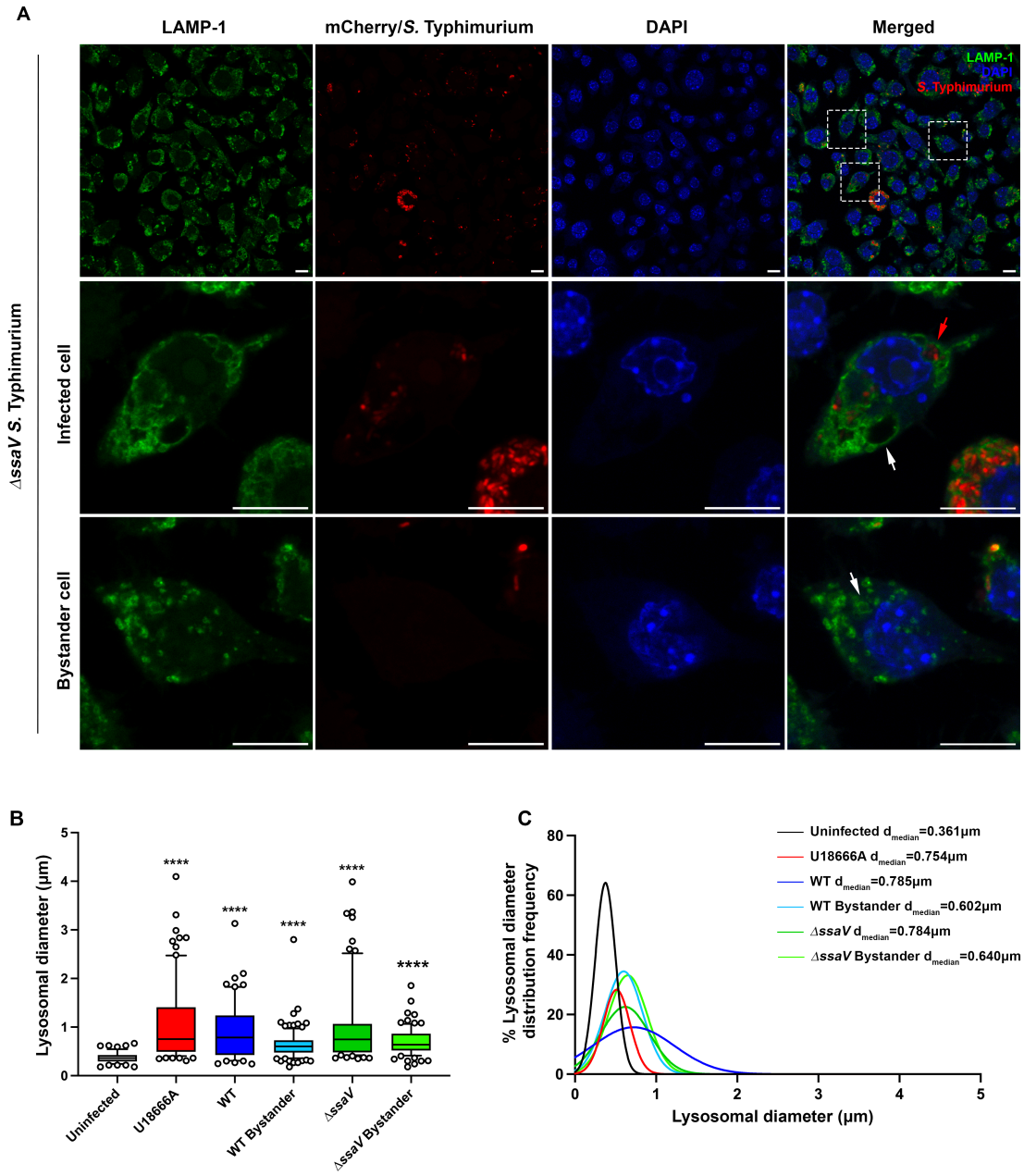
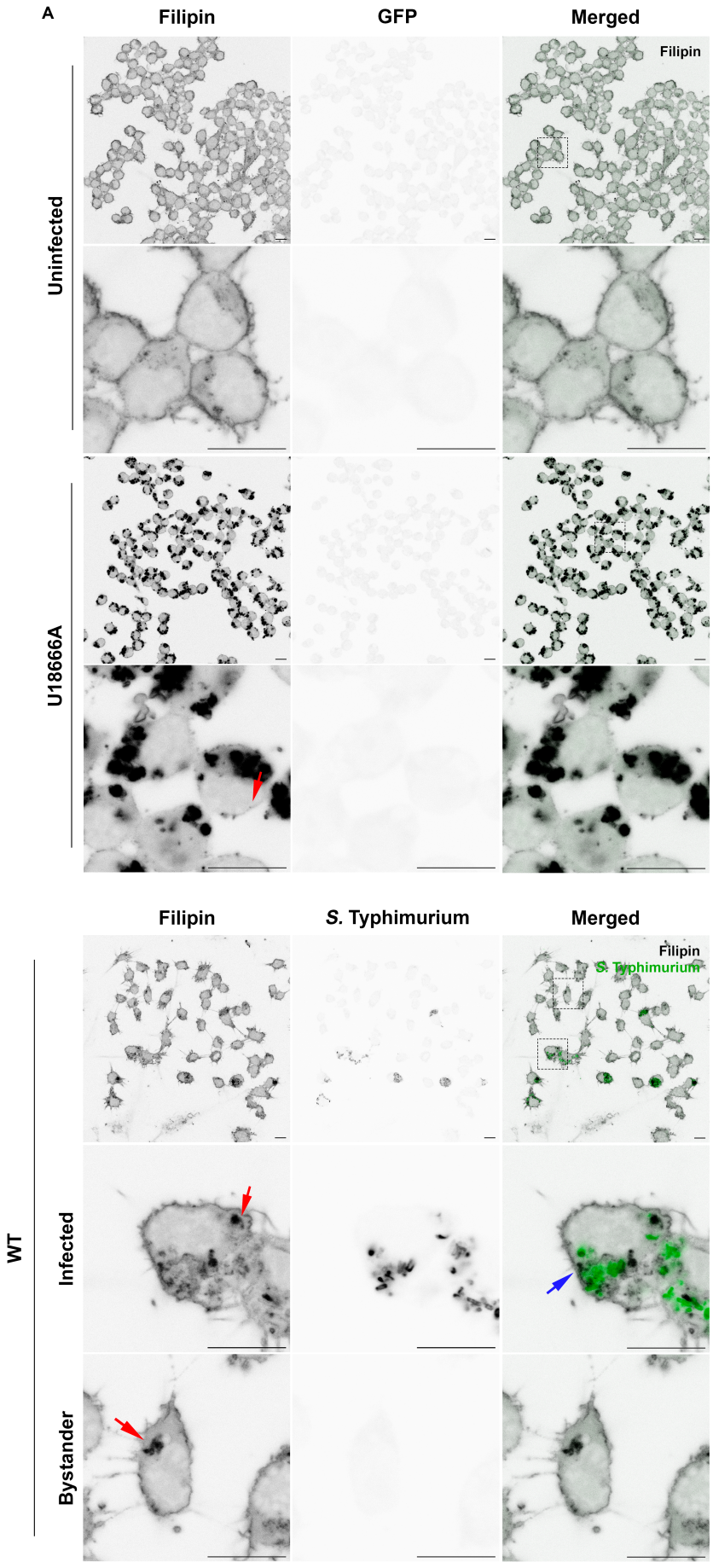

A
LAMP-1
mCherry/S. Typhimurium
DAPI
Merged
LAMP-1
DAPI
S. Typhimurium
ΔssaV S. Typhimurium
Infected cell
Bystander cell
B
Lysosomal diameter (μm)
****
Uninfected
U18666A
WT
WT Bystander
ΔssaV
ΔssaV Bystander
C
% Lysosomal diameter distribution frequency
Lysosomal diameter (μm)
Uninfected d median=0.361μm
U18666A d median=0.754μm
WT d median=0.785μm
WT Bystander d median=0.602μm
ΔssaV d median=0.784μm
ΔssaV Bystander d median=0.640μm

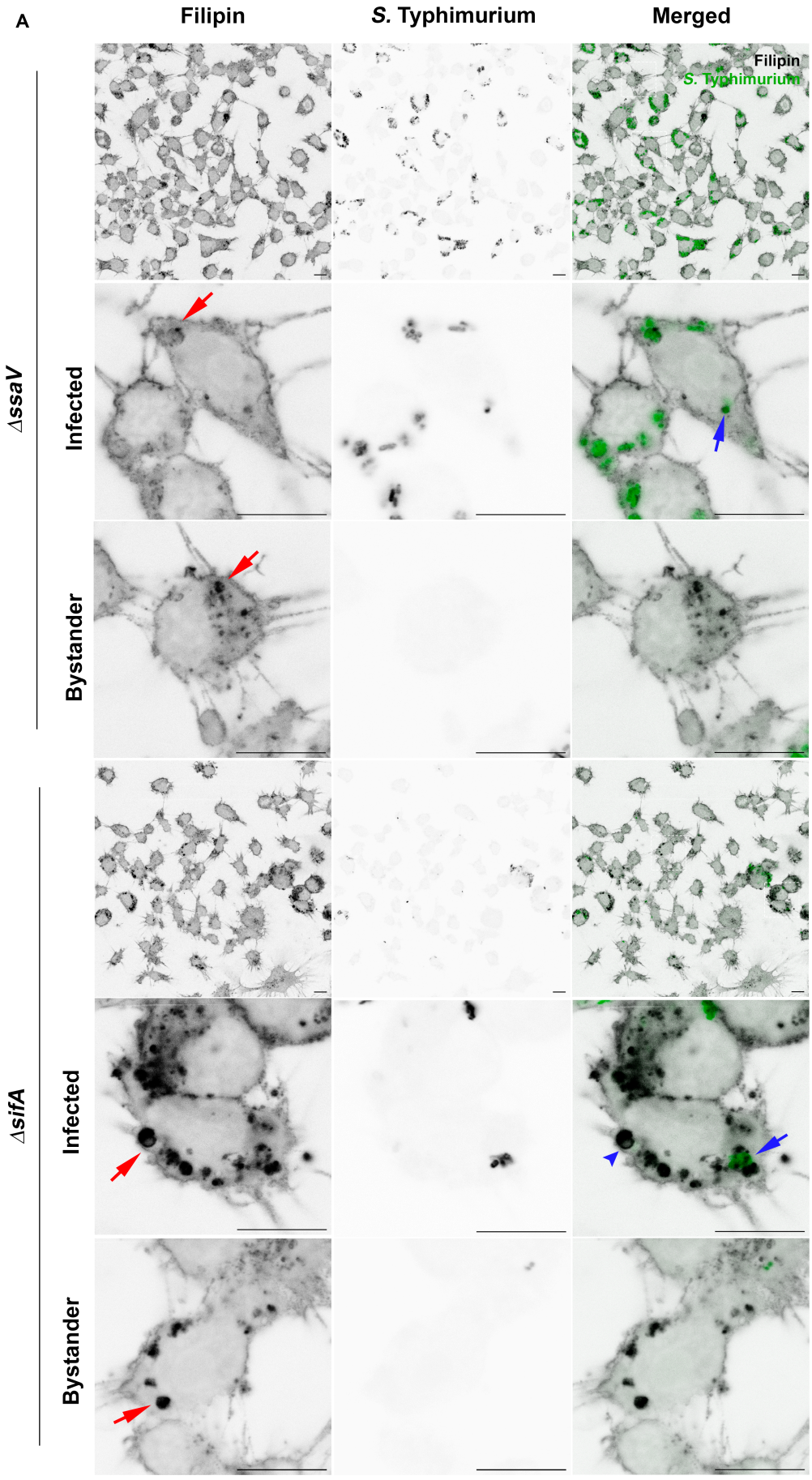
Figure 6.3.2. Expansion of LAMP-1 positive compartments in RAW 264.7 MΦ infected with WT or ΔssaV S. Typhimurium.

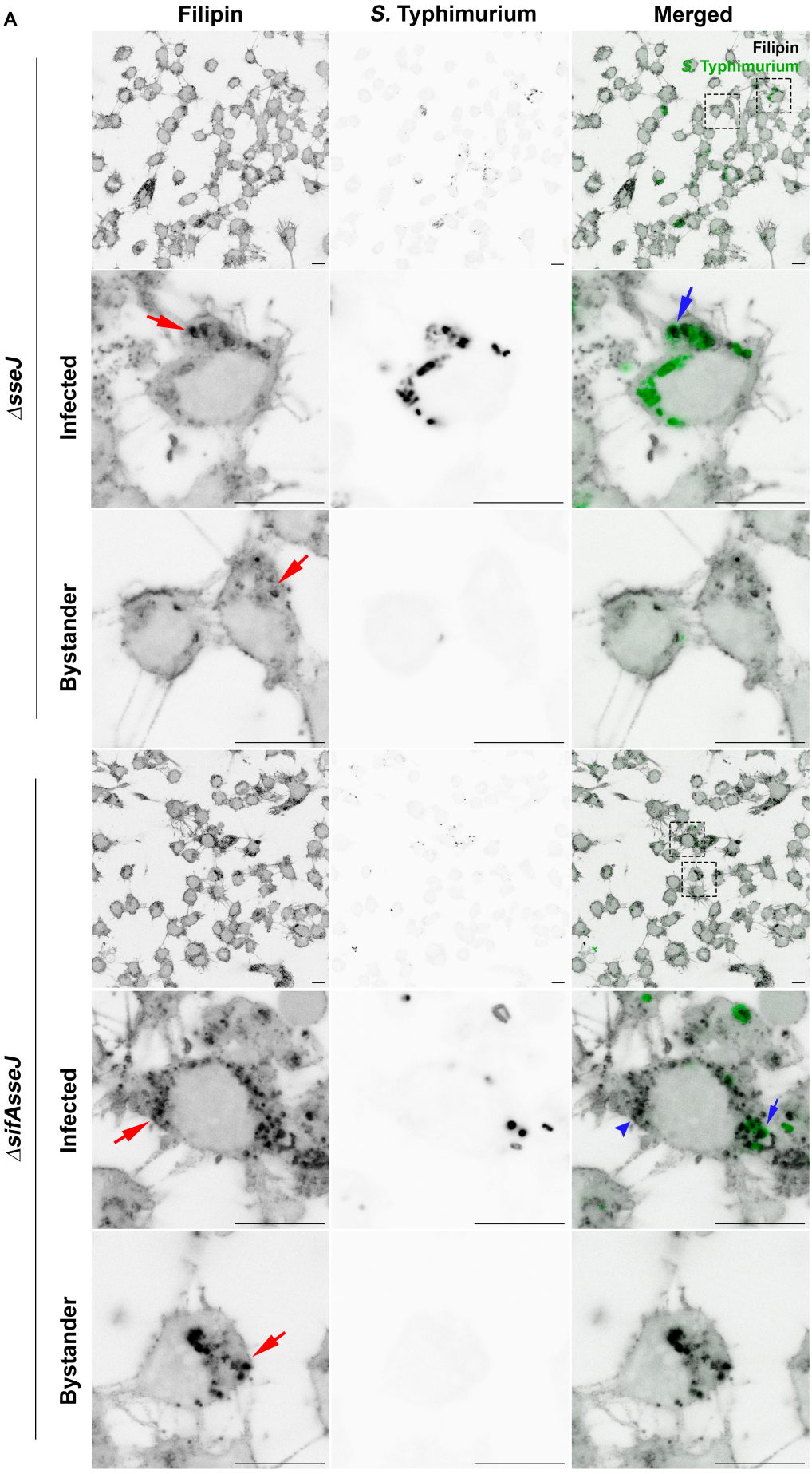
RAW 264.7 MΦ were infected with WT or *ΔssaV S.* Typhimurium and incubated for 24h pi. Uninfected and U18666A (2μg/ml for 24h) treatments represents vehicle and positive controls respectively. Panel A. Representative confocal microscopy images of LE/Lys compartments stained with anti-LAMP-1 antibody. LAMP-1, green; mCherry-tagged *S.* Typhimurium, red; DAPI, blue. White arrows indicate enlarged LE/Lys without bacteria; red arrows indicate expanded LE/Lys containing bacteria. For each pair, the lower image is a higher magnification of the region outlined in the top image. Scale bar represents 10μm. Panel B. Quantification of LAMP-1 positive compartment diameter in infected RAW 264.7 MΦ and uninfected bystander cells. Box and whisker plot, box contains 90% of all events. n>100 within 3 random fields. Statistical analysis, one-way ANOVA with Kruskal-Wallis test. ****$p<0.0001$. Statistical comparisons are relative to uninfected control. Panel C. Histogram of statistical distribution of median LAMP-1 positive compartments diameter. Bin width, 0.2μm. Uninfected: min: 0.181μm, max: 0.665μm, centre: 0.361μm; U18666A: min: 0.307μm, max: 4.096μm, centre: 0.754μm; WT: min: 0.241μm, max: 3.130μm, centre: 0.785μm; WT bystander: min: 0.181μm, max: 2.800μm, centre: 0.602μm; *ΔssaV*: min: 0.351μm, max: 3.989μm, centre: 0.748μm; *ΔssaV* bystander: min: 0.181μm, max: 1.854μm, centre: 0.640μm. Statistical distribution values indicated are median diameters. Statistical analysis, Gaussian distribution. Data are representative of 2 independent experiments.

6.3.3. Infection with WT, *ΔssaV, ΔsifA, ΔsseJ* or *ΔsifAsseJ S.* Typhimurium induces endo-lysosomal cholesterol accumulation in RAW 264.7 MΦ.

RAW 264.7 MΦ were infected with WT, *ΔssaV, ΔsifA, ΔsseJ* or *ΔsifAsseJ S.* Typhimurium for 24h pi, and the intracellular distribution of free cholesterol was examined by filipin staining. Filipin-positive puncta with a lysosomal distribution were observed in RAW 264.7 MΦ infected with WT, *ΔssaV, ΔsifA, ΔsseJ* or *ΔsifAsseJ S.* Typhimurium (red arrows, Fig 6.3.3.A.), and the frequency of cells containing cholesterol-positive puncta was significantly greater than uninfected cells (****p<0.0001, Fig 6.3.3.B.). Filipin-positive puncta were observed in both RAW 264.7 MΦ containing bacteria and cells that showed no evidence of infection ('bystander cells', red arrows, Fig 6.3.3.A.). Interestingly, the precise localisation of puncta with respect to internalised bacteria appeared to differ between cells infected with WT, *ΔssaV* or *ΔsseJ S.* Typhimurium and those infected with *ΔsifA* or *ΔsifAsseJ* mutants. In the former, filipin fluorescence was very closely associated with bacteria (blue arrows, Fig 6.3.3.A), whereas in the latter, it was more distinct from bacilli (blue arrowheads, Fig 6.3.3.A). There was no significant difference in the frequency of cells with filipin-positive puncta infected with different bacterial strains (Fig 6.3.3.B.).


A
Filipin
GFP
Merged
Filipin
Uninfected
U18666A
Filipin
S. Typhimurium
Merged
Filipin
S. Typhimurium
WT
Infected
Bystander


A
Filipin
S. Typhimurium
Merged
Filipin
S. Typhimurium
ΔssaV
Infected
Bystander
ΔsifA
Infected
Bystander


A
Filipin
S. Typhimurium
Merged
Filipin
S. Typhimurium
ΔsseJ
Infected
Bystander
ΔsifAsseJ
Infected
Bystander

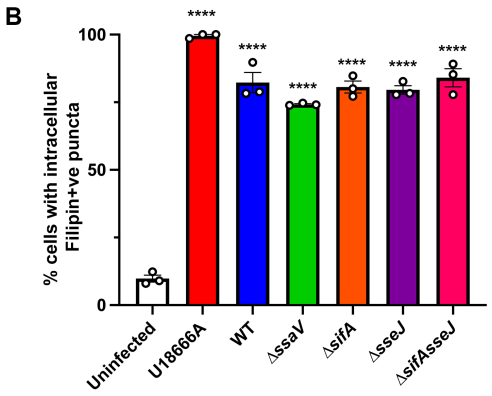


Figure 6.3.3. WT, ΔssaV, ΔsifA, ΔsseJ or ΔsifAsseJ S. Typhimurium infection induces a partial redistribution of cholesterol to intracellular puncta in RAW 264.7 MΦ.

RAW 264.7 MΦ were infected with WT, *ΔssaV, ΔsifA, ΔsseJ* or *ΔsifAsseJ S.* Typhimurium and incubated for 24h pi. Uninfected and U18666A (2μg/ml for 24h) treatments represent vehicle and positive controls respectively. Panel A. Representative confocal microscopy images of filipin staining of free cholesterol in infected cells. In the merged images, filipin, black; *S.* Typhimurium, green. For each pair, the lower image is a higher magnification of the region outlined in the top image. Red arrows indicate filipin-positive puncta; blue arrows indicate filipin-positive puncta with close proximity to bacteria; blue arrowheads indicate filipin-positive puncta distant from bacteria. Scale bar represents 10μm. Panel B. Quantification of the frequency of infected and uninfected cells with intracellular filipin-positive puncta. Data are mean ± SEM, n=3, each representing a minimum of 100 cells in randomly selected fields. Statistical analysis, one-way ANOVA with Tukey multiple comparisons. ****$p<0.0001$. Statistical comparisons are relative to uninfected control. Data are representative of 2 independent experiments.

6.3.4. Infection with WT, *ΔssaV* and *ΔsseJ*, but not in *ΔsifA* or *ΔsifAsseJ S.* Typhimurium increases the cholesterol content of RAW 264.7 MΦ.

The cholesterol content of RAW 264.7 MΦ infected with WT, *ΔssaV, ΔsifA, ΔsseJ* or *ΔsifAsseJ S.* Typhimurium was measured using the Amplex Red assay. There was a significant increase in cholesterol in RAW 264.7 MΦ infected with WT (p=0.0158), *ΔssaV* (p=0.0252) or *ΔsseJ* (p=0.0073) *S.* Typhimurium (Fig 6.3.4.). There was a trend towards increased cholesterol in cells infected with *ΔsifA* and *ΔsifAsseJ,* but values did not reach statistical significance (Fig 6.3.4.).

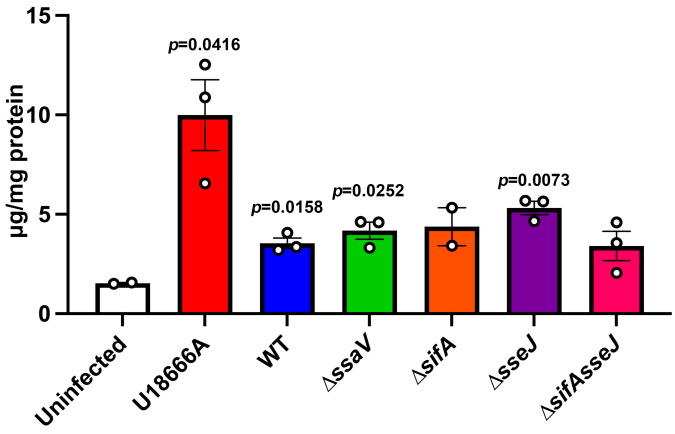
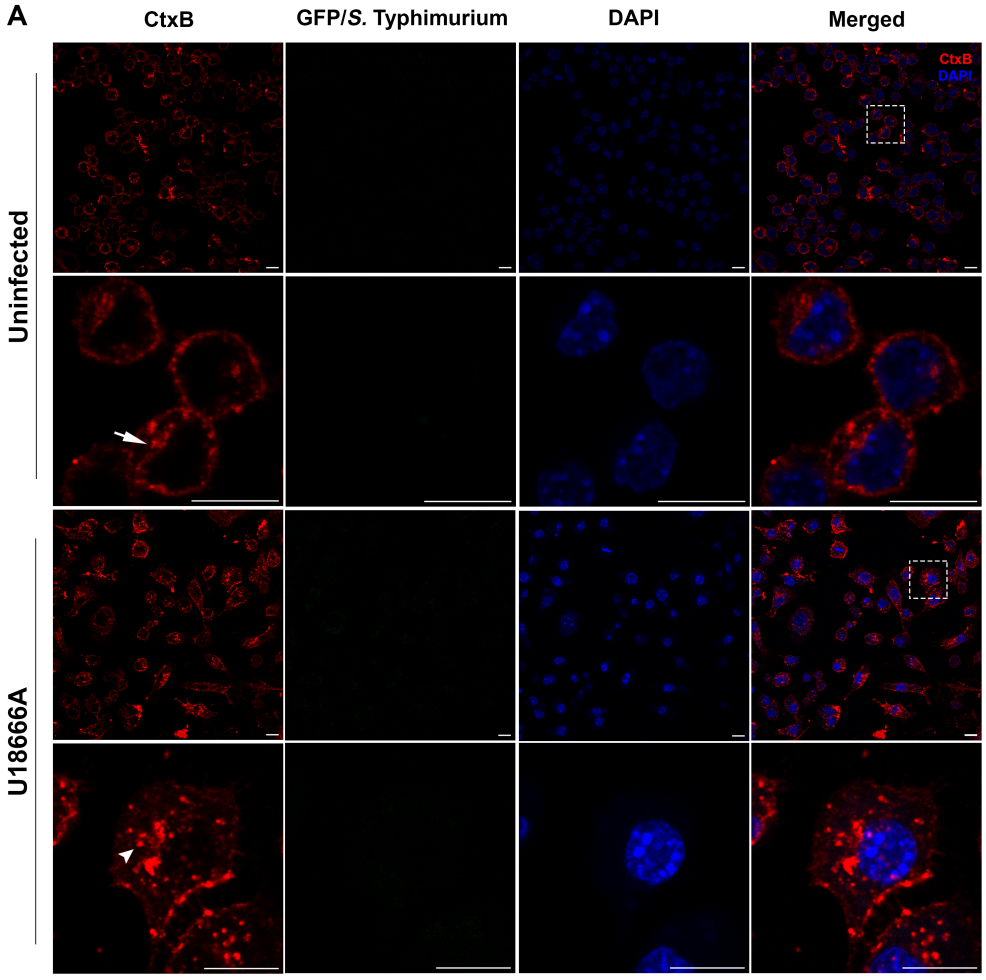
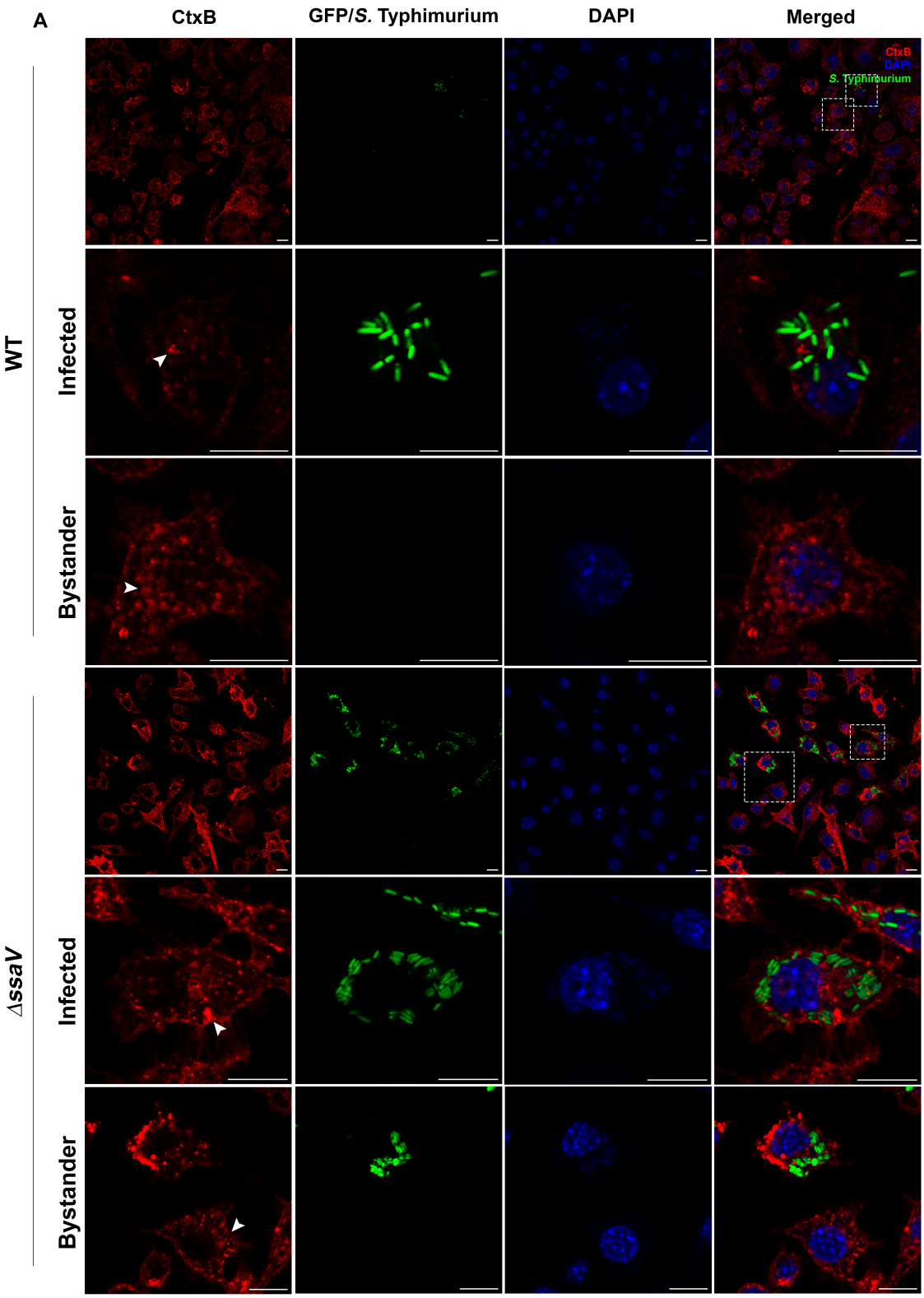


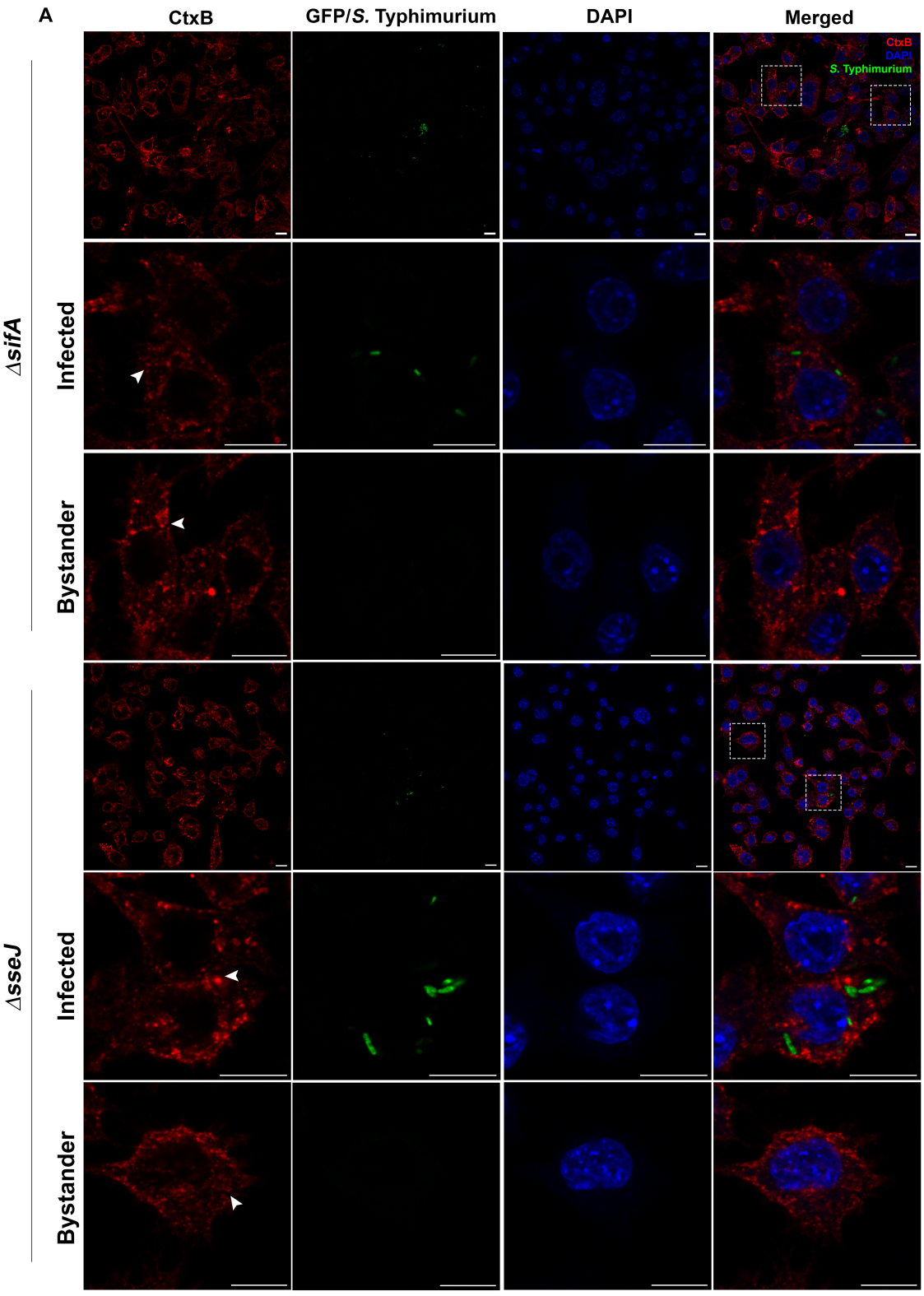
Figure 6.3.4. WT, ΔssaV and ΔsseJ, but not ΔsifA or ΔsifAsseJ S. Typhimurium infection increases cholesterol in RAW 264.7 MΦ.
RAW 264.7 MΦ were infected with WT, *ΔssaV, ΔsifA, ΔsseJ* or *ΔsifAsseJ S.* Typhimurium and incubated for 24h pi. Uninfected and U18666A (2µg/ml for 24h) treatments were vehicle and positive controls respectively. Data are mean ± SEM, n=2 or 3. Statistical analysis, Welch's t-test. p values as indicated, otherwise not significant. Statistical comparisons are relative to uninfected control. Data are presentative of 2 independent experiments.

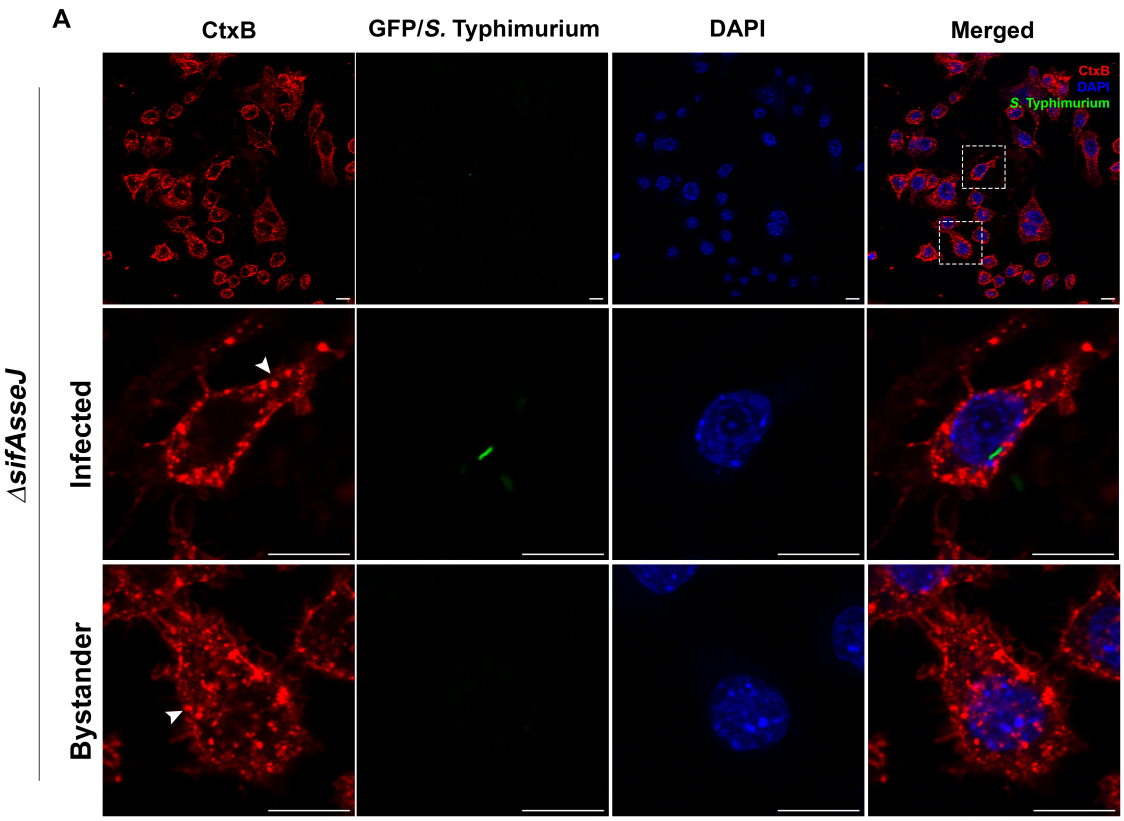
6.3.5. Perturbed intracellular trafficking of GM1 ganglioside in RAW 264.7 MΦ infected with WT, *ΔssaV, ΔsifA, ΔsseJ* or *ΔsifAsseJ S.* Typhimurium.

Intracellular trafficking of GM1 ganglioside in infected RAW 264.7 MΦ was studied by pulse-chase labelling with fluorescently-tagged CtxB. Confocal microscopy revealed the accumulation of fluorescent puncta in cells infected with WT, *ΔssaV, ΔsifA, ΔsseJ* or *ΔsifAsseJ S.* Typhimurium (white arrowheads, Fig 6.3.5.A.). The frequency of cells with lysosomal GM1 distribution was significantly increased in infected cells (****p<0.0001, Fig 6.3.5.B.). A comparable distribution was also observed in RAW 264.7 MΦ in which there was no visible indication of intracellular bacteria (white arrowheads, Fig 6.3.5.A.).




A
CtxB
GFP/S. Typhimurium
DAPI
Merged
CtxB
DAPI
S. Typhimurium
WT
Infected
Bystander
ΔssaV
Infected
Bystander


A
CtxB
GFP/S. Typhimurium
DAPI
Merged
CtxB
DAPI
S. Typhimurium
ΔsifA
Infected
Bystander
ΔsseJ
Infected
Bystander


A
CtxB
GFP/S. Typhimurium
DAPI
Merged
CtxB
DAPI
S. Typhimurium
ΔsifAsseJ
Infected
Bystander

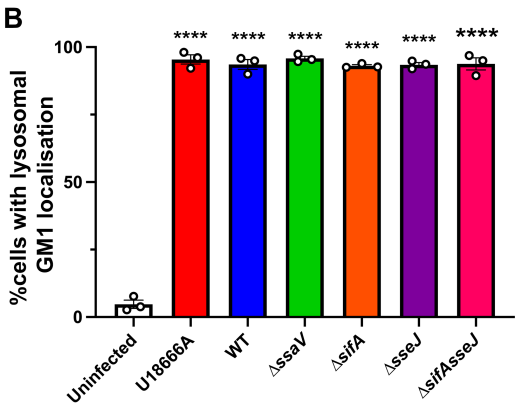

B
%cells with lysosomal GM1 localisation
100
50
0
****
Uninfected
U18666A
WT
ΔssaV
ΔsifA
ΔsseJ
ΔsifAsseJ

Figure 6.3.5. WT, ΔssaV, ΔsifA, ΔsseJ or ΔsifAsseJ S. Typhimurium infection perturb GM1 ganglioside trafficking in RAW 264.7 MΦ. RAW 264.7 MΦ were infected with WT, *ΔssaV ΔsifA, ΔsseJ* or *ΔsifAsseJ S.* Typhimurium and incubated for 24h pi. Plasma membrane GM1 ganglioside was labelled with Alexa Fluor™ 555-conjugated CtxB for 30 min and chased for 1h. Uninfected and U18666A (2μg/ml for 24h) treatments were vehicle and positive controls respectively. Panel A. Representative confocal microscopy images of GM1 ganglioside distribution in infected cells. CtxB, red; GFP-tagged *S.* Typhimurium, green; DAPI, blue. For each pair, the lower image is a higher magnification of the region outlined in the top image. Scale bar represents 10μm. White arrows indicate Golgi GM1 distribution; white arrowheads indicate lysosomal GM1 distribution. Panel B. Frequency of infected and uninfected cells with lysosomal GM1 ganglioside localisation. Data are mean ± SEM, n=3, each representing a minimum of 100 cells in randomly selected fields. Statistical analysis, one-way ANOVA with Tukey multiple comparisons. ****$p<0.0001$. Statistical comparisons are relative to uninfected control. Data are presentative of 2 independent experiments.

6.3.6. Infection with WT, *ΔssaV, ΔsifA, ΔsseJ* and *ΔsifAsseJ S.* Typhimurium causes sphingosine and sphinganine accumulation in RAW 264.7 MΦ.

The metabolism of sphingoid-bases was also analysed in WT and mutant *S.* Typhimurium-infected RAW 264.7 MΦ by RP-HPLC. In cells infected with WT ($p=0.0141$), *ΔssaV* ($p=0.0026$), *ΔsifA* ($p=0.0005$), *ΔsseJ* ($p=0.0004$) or *ΔsifAsseJ* (****$p<0.0001$) *S.* Typhimurium, sphingosine was significantly increased (Fig 6.3.6.). The increase was greater for infections with *ΔsifA* and *ΔsifAsseJ* than for the other strains (Fig 6.3.6.A.). Sphinganine was also significantly increased in

RAW 264.7 MΦ infected with WT (*p*=0.0096), *ΔssaV* (*p*=0.0084), *ΔsifA* (*p*=0.0047), *ΔsseJ* (*p*=0.0006) or *ΔsifAsseJ* (*p*=0.0008) *S.* Typhimurium (Fig 6.3.6.B.).

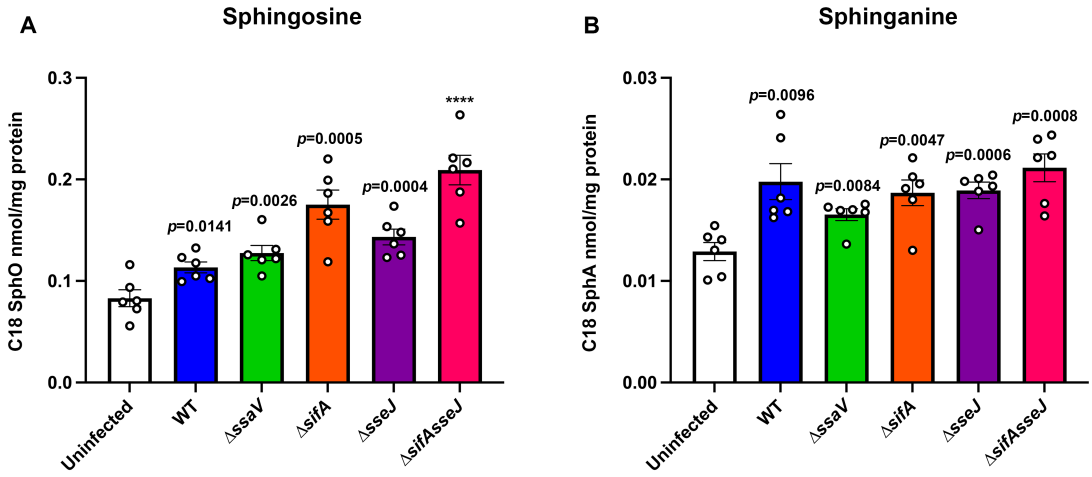
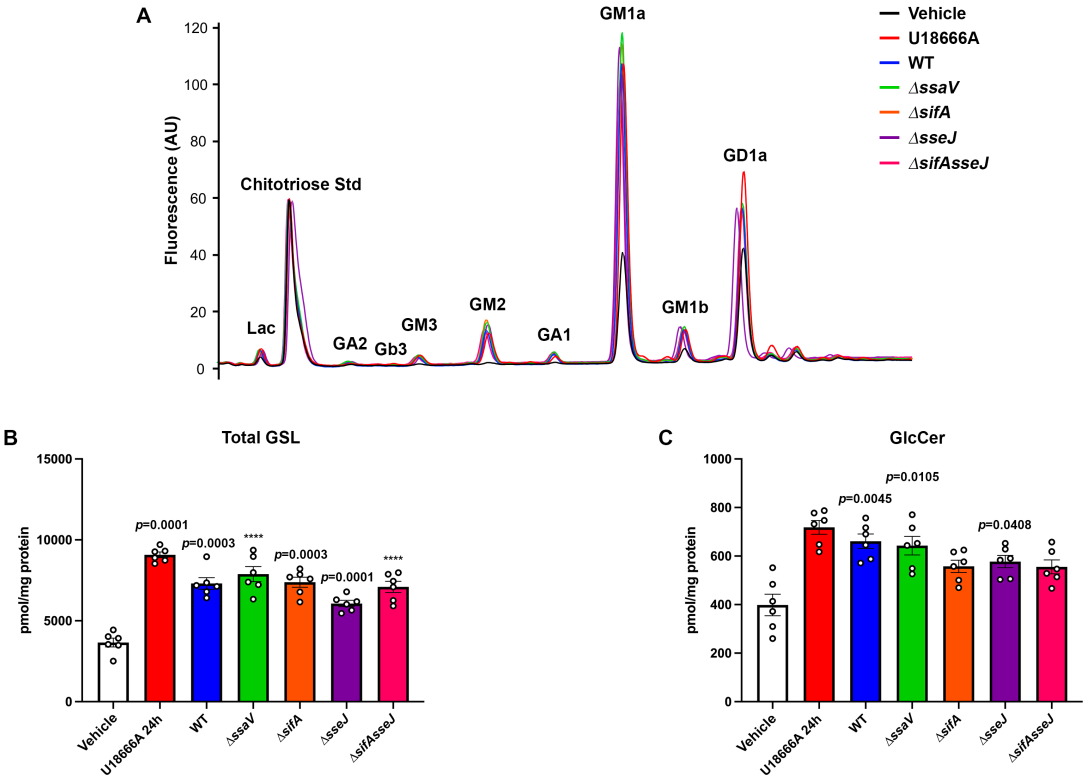


Figure 6.3.6. Infection with WT, ΔssaV, ΔsifA, ΔsseJ or ΔsifAsseJ S. Typhimurium causes sphingosine and sphinganine accumulation in RAW 264.7 MΦ.

RAW 264.7 MΦ were infected with WT, *ΔssaV ΔsifA, ΔsseJ* or *ΔsifAsseJ S.* Typhimurium incubated for 24h pi. Uninfected and U18666A (2μg/ml for 24h) treatments were vehicle and positive controls respectively. Panel A. Quantification of sphingosine. Panel B. Quantification of sphinganine in infected cultures. Data are mean ± SEM, n=6. Statistical analysis, Welch's t-test. ****p<0.0001, other p values as indicated. Statistical comparisons are relative to uninfected control. Data are representative of 3 independent experiments.

6.3.7. GSLs accumulate in RAW 264.7 MΦ infected with WT, *ΔssaV, ΔsifA, ΔsseJ* or *ΔsifAsseJ S.* Typhimurium.

GSLs in *S.* Typhimurium-infected cells were analysed by NP-HPLC; representative profiles are shown in Fig 6.3.7.A. Total GSLs were significantly increased in RAW 264.7 MΦ infected with WT (p=0.0003), *ΔssaV* (****p<0.0001), *ΔsifA* (p=0.0003), *ΔsseJ* (p=0.0001) or *ΔsifAsseJ* (****p<0.0001) *S.* Typhimurium to an extent comparable to that of U18666A-treated cells (Fig 6.3.7.B.). GlcCer was also significantly increased in WT (p=0.0045), *ΔssaV* (p=0.0105) or *ΔsseJ* (p=0.0408) *S.* Typhimurium-infected RAW 264.7 MΦ (Fig 6.3.7.C.). Levels of the two of the most abundant GSL species GM1a and GM1b were increased by all bacterial strains, as were GA1, GM2, GM3 and GA2 (Fig 6.3.7.D.). The fold changes of GSLs compared to uninfected RAW 264.7 MΦ are summarised in Table 6.3.7.



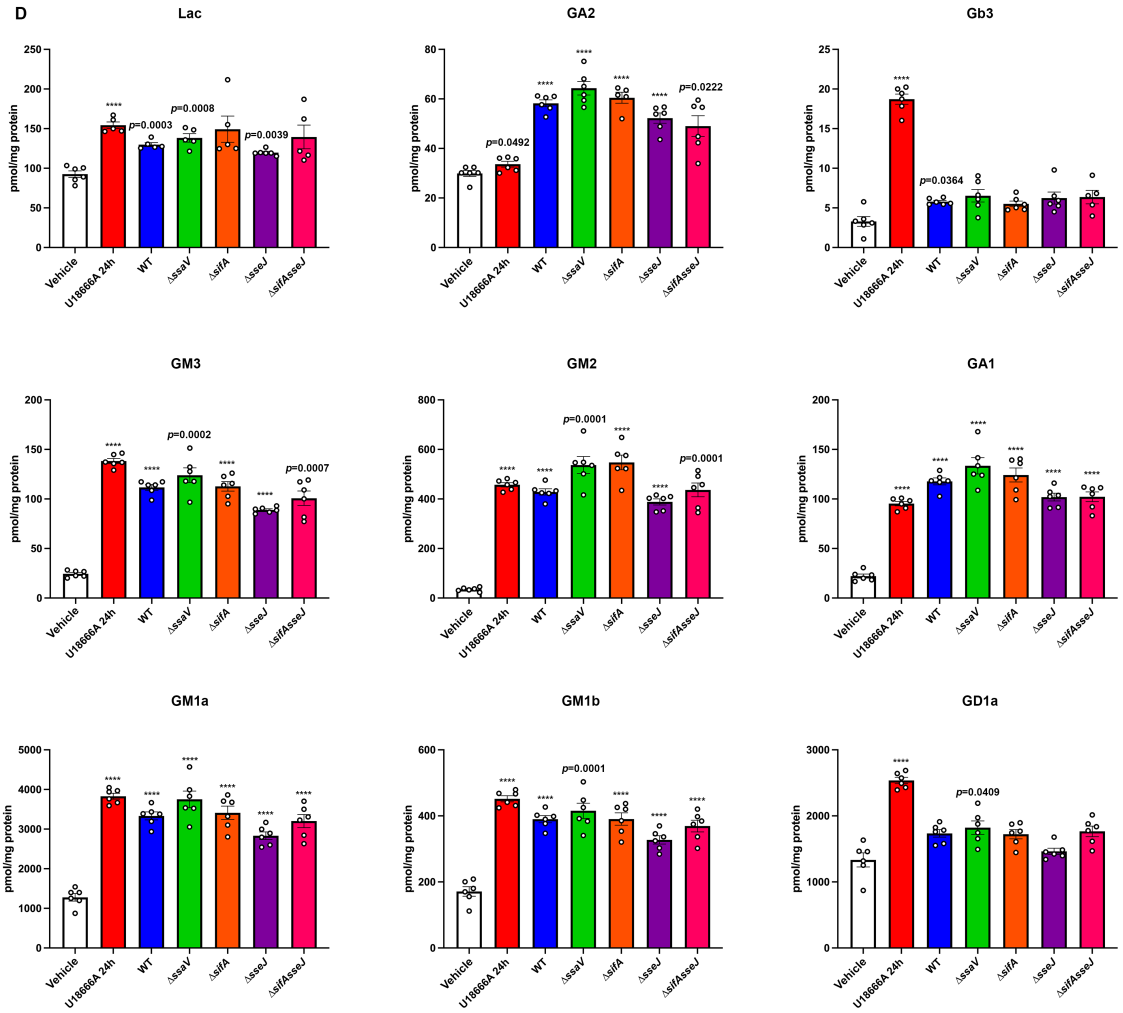


Figure 6.3.7. WT, ΔssaV, ΔsifA, ΔsseJ or ΔsifAsseJ S. Typhimurium infection cause GSL accumulation in RAW 264.7 MΦ.

RAW 264.7 MΦ were infected with WT, *ΔssaV ΔsifA, ΔsseJ,* or *ΔsifAsseJ S.* Typhimurium and incubated for 24h pi. Uninfected and U18666A (2μg/ml for 24h) treatments represent vehicle and positive controls respectively. Panel A. Representative HPLC profiles of GSLs. Panel B. Quantification of total GSL levels in infected cells. Panel C. Quantification of GlcCer levels in infected cells. D. Quantification of individual GSLs species. Data are mean ± SEM, n=6. Statistical analysis, one-way ANOVA with Dunnett multiple comparisons. ****$p<0.0001$, other p values as indicated, otherwise not significant. Statistical comparisons are relative to uninfected control. Data are representative of 3 independent experiments.

GSL species	U18666A	*S.* Typhimurium				
		WT	*ΔssaV*	*ΔsifA*	*ΔsseJ*	*ΔsifAsseJ*
Lac	**** 1.667±0.045	*p*=0.0003 1.402±0.027	*p*=0.0008 1.493±0.058	ns 1.612±0.179	*p*=0.0039 1.294±0.016	ns 1.507±0.162
GA2	*p*=0.0492 1.125±0.039	**** 1.947±0.046	**** 2.150±0.091	**** 2.022±0.074	**** 1.747±0.069	*p*=0.0222 1.639±0.140
Gb3	**** 5.69±0.196	*p*=0.0364 1.76±0.048	ns 1.99±0.241	ns 1.68±0.108	ns 1.90±0.231	ns 1.94±0.259
GM3	**** 5.65±0.106	**** 4.56±0.117	*p*=0.0002 5.06±0.303	**** 4.61±0.197	**** 3.63±0.048	*p*=0.0007 4.12±0.298
GM2	**** 13.2±0.246	**** 12.3±0.363	*p*=0.0001 15.5±0.983	**** 15.8±0.848	**** 11.2±0.355	*p*=0.0001 12.6±0.803
GA1	**** 4.30±0.101	**** 5.31±0.157	**** 6.02±0.371	**** 5.60±0.317	**** 4.59±0.176	**** 4.61±0.221
GM1a	**** 3.00±0.058	**** 2.61±0.079	**** 2.94±0.164	**** 2.67±0.131	**** 2.22±0.076	**** 2.51±0.128
GM1b	**** 2.64±0.054	**** 2.28±0.064	*p*=0.0001 2.43±0.135	**** 2.28±0.110	**** 1.91±0.073	**** 2.16±0.103
GD1a	**** 1.90±0.036	ns 1.30±0.043	*p*=0.0409 1.37±0.076	ns 1.29±0.052	ns 1.10±0.036	ns 1.32±0.060
Total GSL	*p*=0.0001 2.483±0.048	*p*=0.0003 1.999±0.098	**** 2.157±0.127	*p*=0.0003 2.020±0.085	*p*=0.0001 1.660±0.053	**** 1.941±0.095
GlcCer	ns 1.80±0.072	*p*=0.0045 1.66±0.075	*p*=0.0105 1.61±0.096	ns 1.40±0.064	*p*=0.0408 1.45±0.063	ns 1.39±0.072

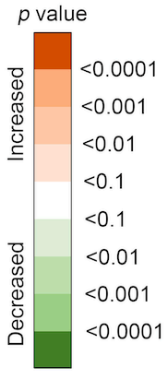
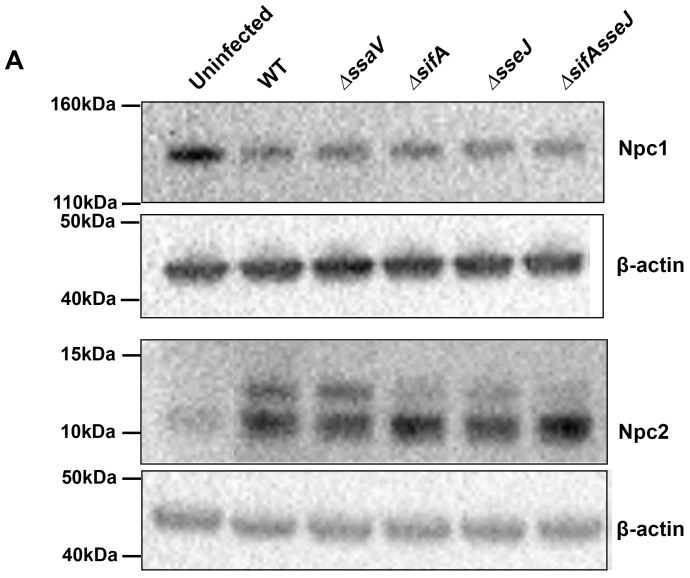


Table 6.3.7. Summary table of fold change and statistical significance of GSL content of RAW 264.7 MΦ infected with WT, ΔssaV, ΔsifA, ΔsseJ and ΔsifAsseJ S. Typhimurium.

Fold change was normalised to GSL levels in uninfected RAW 264.7 MΦ. Data are mean ± SEM, n=6. Statistical analysis, one-way ANOVA with Dunnett multiple comparisons. ****p<0.0001, other p values as indicated, otherwise not significant. Statistical comparisons are relative to uninfected control. Data are representative of 3 independent experiments. GSLs that were significantly increased are highlighted in red.

6.3.8. RAW 264.7 MΦ infection with WT, *ΔssaV, ΔsifA, ΔsseJ* or *ΔsifAsseJ S.* Typhimurium does not affect Npc1 expression but significantly increases the expression of Npc2.

We have detected NPC phenotypes in RAW 264.7 MΦ infected with mutant *S.* Typhimurium strains. We determined therefore the expression of Npc1 and Npc2 proteins in RAW 264.7 MΦ infected with WT, *ΔssaV, ΔsifA, ΔsseJ* or *ΔsifAsseJ S.* Typhimurium by western blotting. No significant difference was observed in Npc1 protein expression in *S.* Typhimurium-infected RAW 264.7 MΦ (Fig 6.3.8.A.B.). The expression of Npc2 protein was significantly increased in cells infected with WT and mutant strains of *S.* Typhimurium-infected cells (Fig 6.3.8.A.C.). It is notable that *S.* Typhimurium-infection of RAW 264.7 MΦ resulted in the detection of an additional higher MW band corresponding to a potentially secondary modified form of Npc2 (Fig 6.3.8.A.).



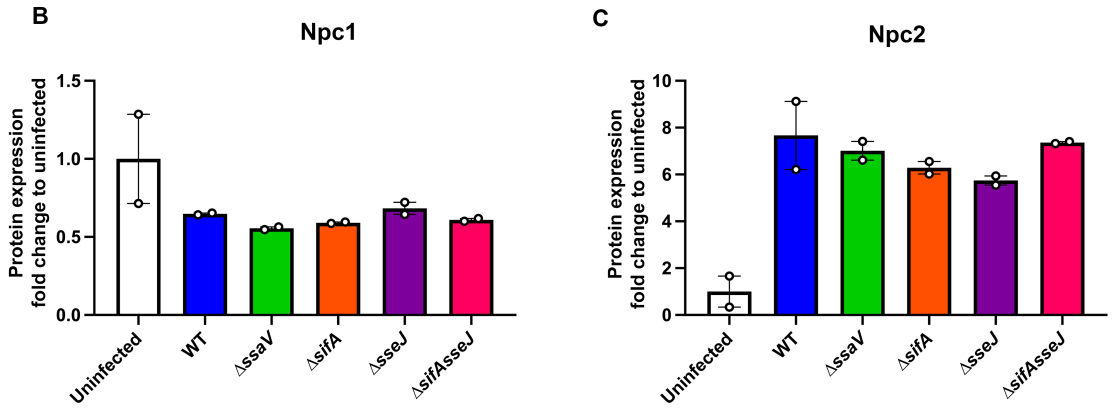


Figure 6.3.8. Infection with WT, ΔssaV, ΔsifA, ΔsseJ or ΔsifAsseJ S. Typhimurium infections do not alter Npc1 expression but increase that of Npc2 in RAW 264.7 MΦ.

RAW 264.7 MΦ were infected with WT, *ΔssaV ΔsifA, ΔsseJ* or *ΔsifAsseJ S.* Typhimurium and incubated for 24h pi. Uninfected and U18666A (2μg/ml for 24h) treatments were vehicle and positive controls respectively. Panel A. Representative western blot images of Npc1 and Npc2 protein expression. Panel B. Quantification of Npc1 protein; Panel C. Quantification of Npc2 protein normalised to β-actin level. Data are mean ± SEM, n=2. Data are representative of 2 independent experiments.

6.3.9. Expression of *Npc1* and *Npc2* genes are decreased in WT, *ΔssaV, ΔsifA* or *ΔsseJ S.* Typhimurium-infected RAW 264.7 MΦ but are increased with *ΔsifAsseJ S.* Typhimurium infection.

Npc1 and *Npc2* gene expression was analysed in RAW 264.7 MΦ infected with WT and mutant *S.* Typhimurium by qPCR. For WT (p=0.0681), *ΔssaV* (p=0.0887), *ΔsifA* (p=0.0329), *ΔsseJ* (p=0.0167) *S.* Typhimurium-infected RAW 264.7 MΦ, *Npc1* gene expression level was significantly decreased (Fig 6.3.9.A.), as was that of *Npc2* expression (p=0.0028 for WT, p=0.0014 for *ΔssaV,* p=0.0106 for *ΔsifA,* p=0.0439 for *ΔsseJ*, Fig 6.3.9.A.). In contrast, *Npc1* (p=0.0253) and *Npc2* (p=0.0103) gene expression was significantly increased in *ΔsifAsseJ S.* Typhimurium-infected RAW 264.7 MΦ to a level equal to or greater than that of U18666A-treated cells (Fig 6.3.9.A.B.).

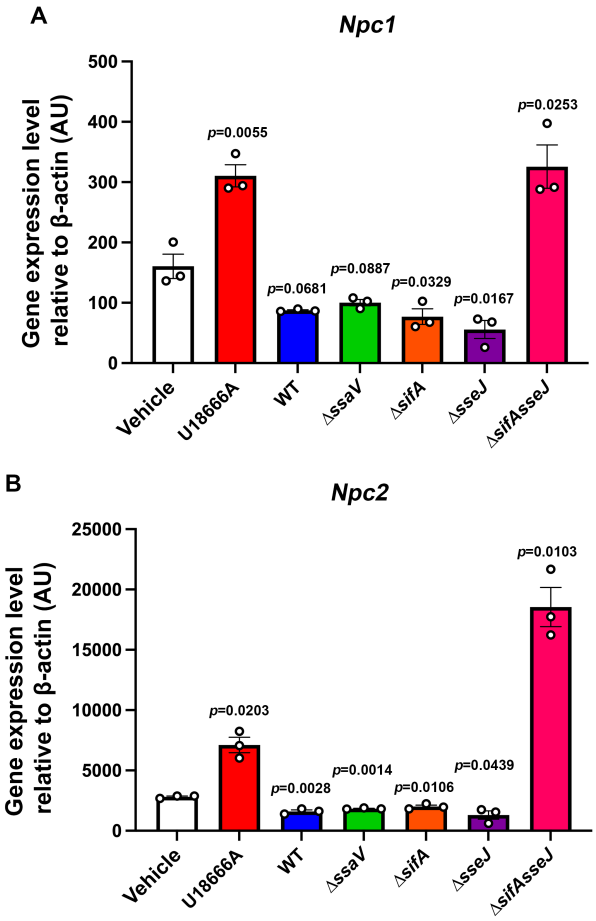
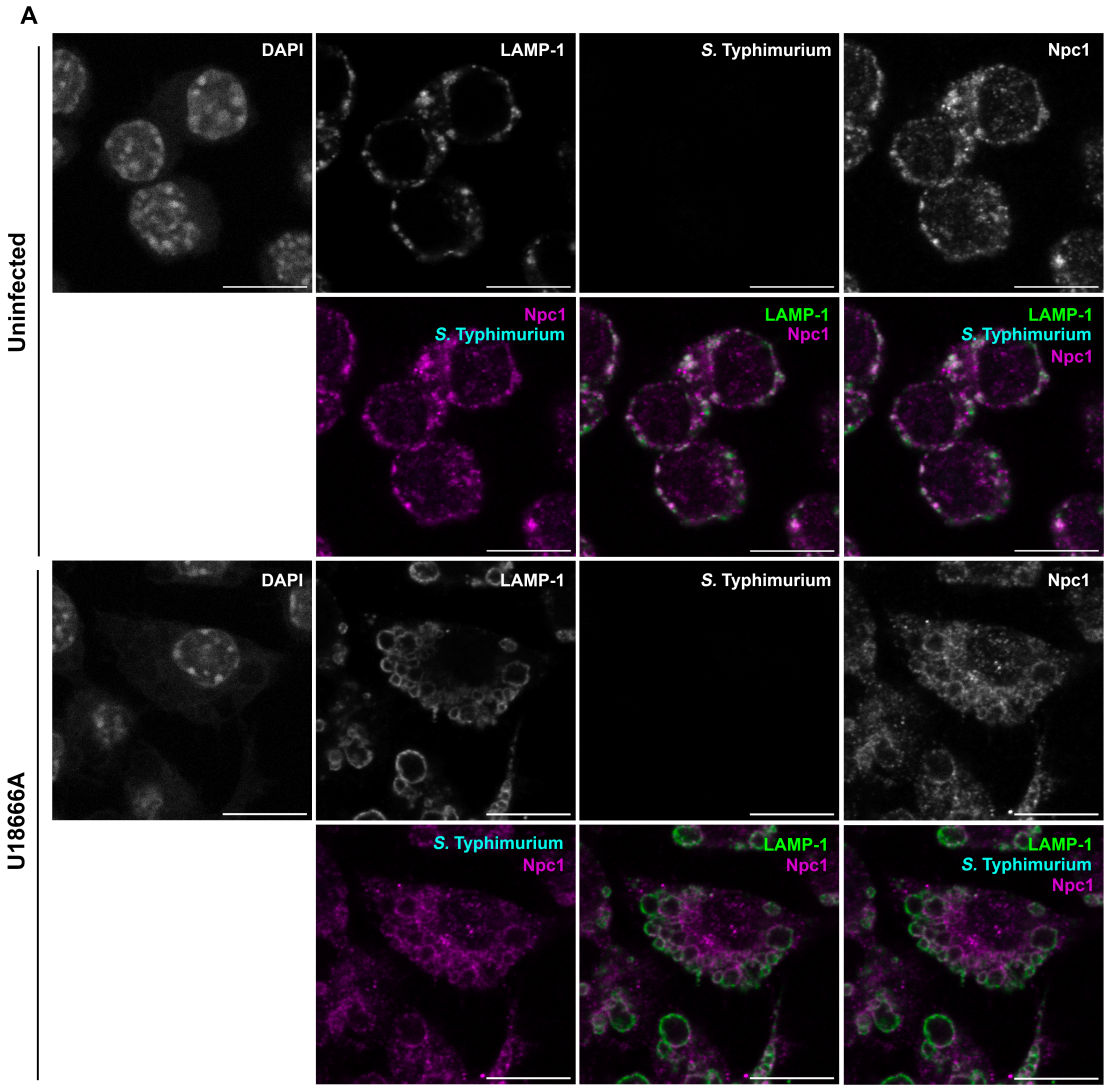


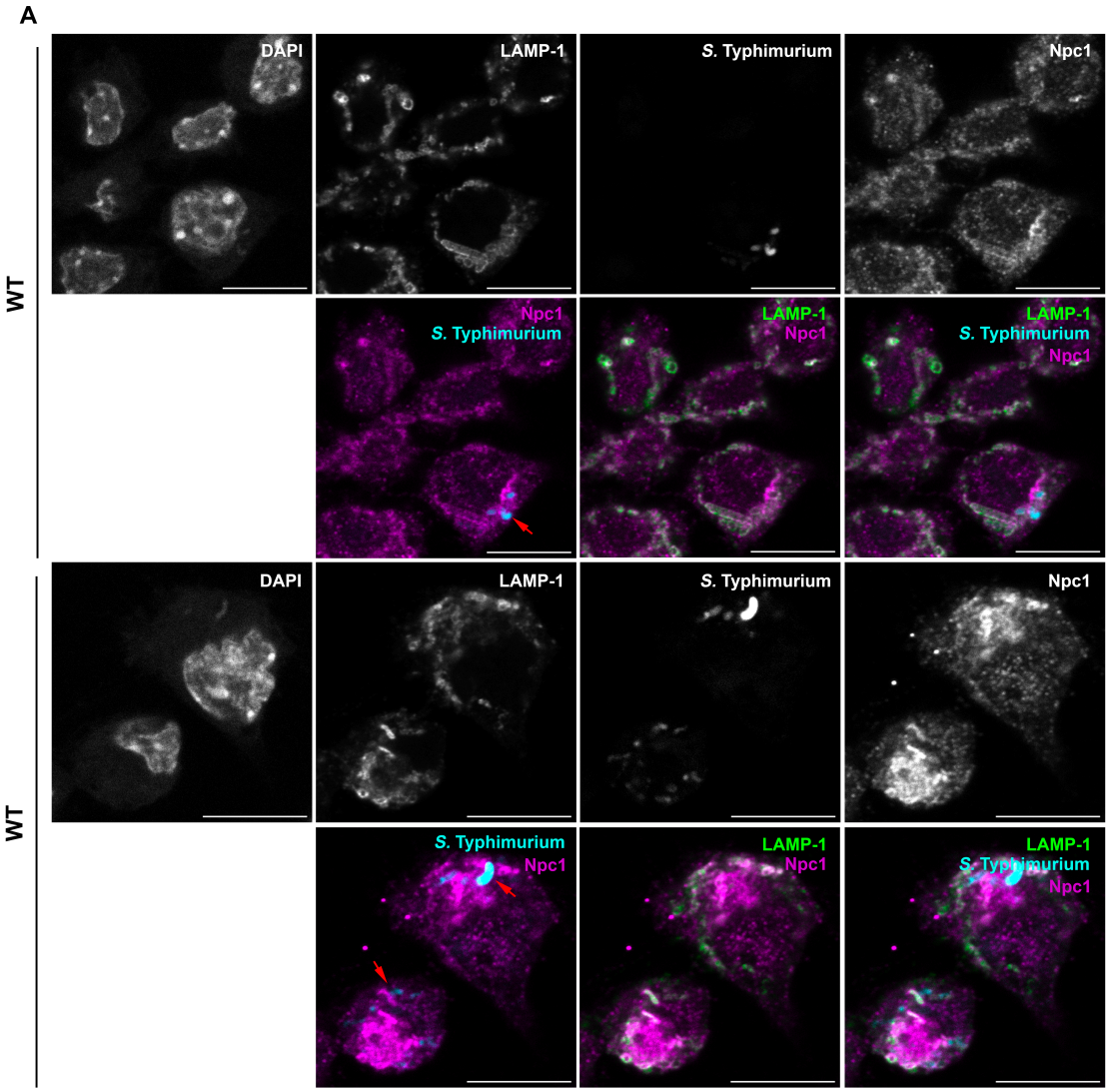
Figure 6.3.9. Gene expression of Npc1 and Npc2 in RAW 264.7 MΦ is reduced by infection with WT, ΔssaV, ΔsifA or ΔsseJ S. Typhimurium but increased by infection with ΔsifAsseJ.

RAW 264.7 MΦ were infected with WT, *ΔssaV ΔsifA, ΔsseJ* or *ΔsifAsseJ S.* Typhimurium and incubated for 24h pi. Uninfected and U18666A (2μg/ml for 24h) treatments represent vehicle and positive controls respectively. Panel A. *Npc1* gene expression relative to *β-actin* in infected cells. Panel B. *Npc2* gene expression relative to *β-actin* in infected cells. Data are mean ± SEM, n=3. Statistical analysis, Welch's t-test. *p* values as indicated. Statistical comparisons are relative to uninfected control. Data are representative of 2 independent experiments.

6.3.10. Npc1 is recruited to SCV in RAW 264.7 MΦ infected with WT or *ΔssaV S.* Typhimurium.

In the report by Walch *et al.* [501], Npc1 and *S.* Typhimurium co-localised in WT and *ΔsseJ S.* Typhimurium-infected Hela cells but did not colocalise in cells infected with *ΔsifA S.* Typhimurium. We analysed for the extent of co-localisation of Npc1, LAMP-1 and *S.* Typhimurium in RAW 264.7 MΦ infected with WT or *ΔssaV S.* Typhimurium. In uninfected and U18666A-treated RAW 264.7 MΦ, Npc1 and LAMP-1 were highly co-localised, confirming that the Npc1 protein was primarily located in lysosomes (Fig 6.3.10.A.). Inspection of RAW 264.7 MΦ infected with either WT or *ΔssaV S.* Typhimurium and immunostained for the two proteins confirmed a statistically significant level of co-localisation of bacteria and Npc1 (red arrows, Pearson's correlation coefficient value of 0.214 ± 0.034 for WT; 0.210 ± 0.017 for *ΔssaV*, Fig 6.3.10.B.), indicating recruitment of Npc1 to SCVs.


A
Uninfected
U18666A
DAPI
LAMP-1
S. Typhimurium
Npc1
Npc1
S. Typhimurium
LAMP-1
Npc1
LAMP-1
S. Typhimurium
Npc1
DAPI
LAMP-1
S. Typhimurium
Npc1
S. Typhimurium
Npc1
LAMP-1
Npc1
LAMP-1
S. Typhimurium
Npc1


A
WT
DAPI
LAMP-1
S. Typhimurium
Npc1
Npc1
S. Typhimurium
LAMP-1
Npc1
LAMP-1
S. Typhimurium
Npc1
WT
DAPI
LAMP-1
S. Typhimurium
Npc1
S. Typhimurium
Npc1
LAMP-1
Npc1
LAMP-1
S. Typhimurium
Npc1

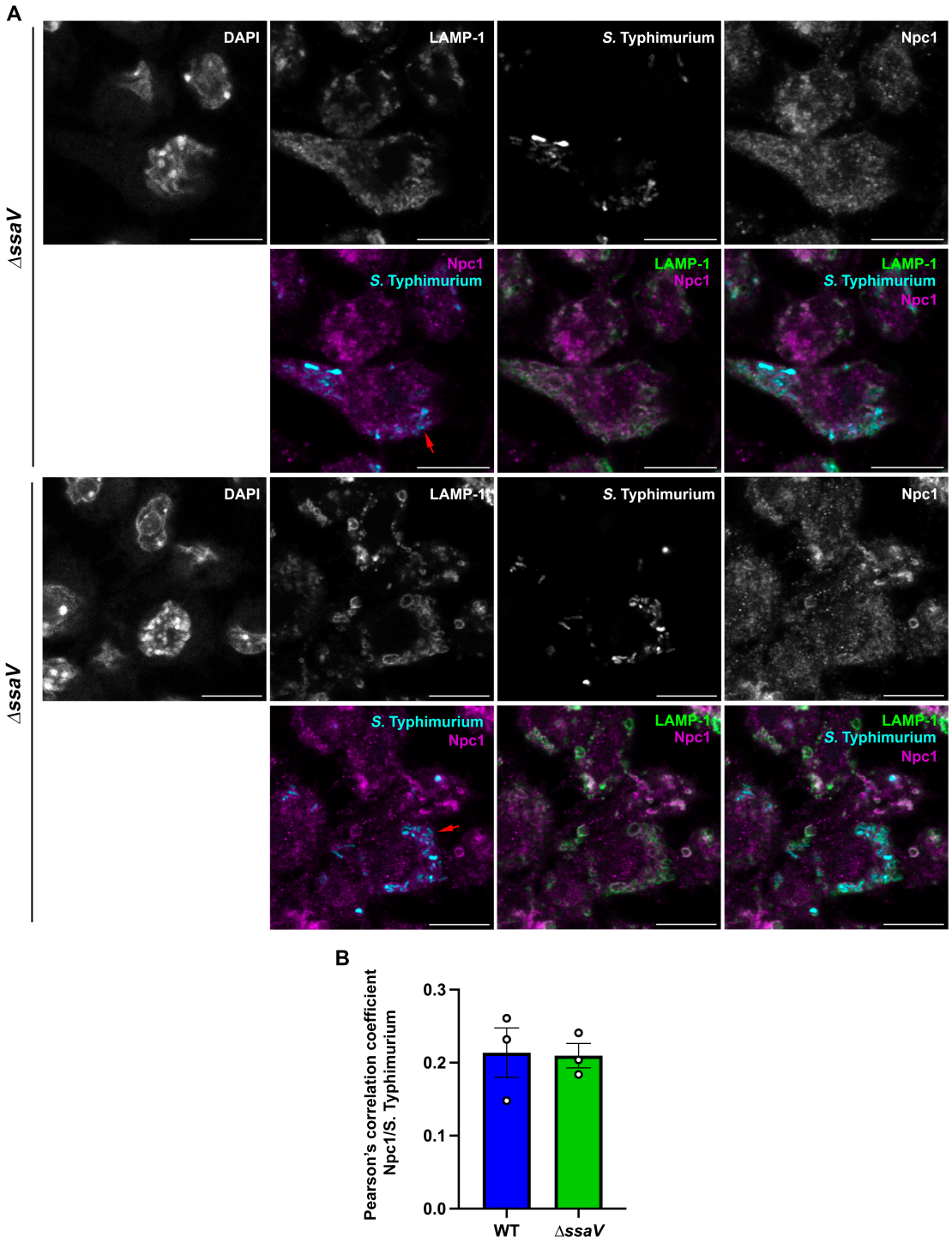

A
ΔssaV
DAPI
LAMP-1
S. Typhimurium
Npc1
Npc1
S. Typhimurium
LAMP-1
Npc1
LAMP-1
S. Typhimurium
Npc1
ΔssaV
DAPI
LAMP-1
S. Typhimurium
Npc1
S. Typhimurium
Npc1
LAMP-1
Npc1
LAMP-1
S. Typhimurium
Npc1
B
Pearson's correlation coefficient
Npc1/S. Typhimurium
0.3
0.2
0.1
0.0
WT
ΔssaV

Figure 6.3.10. Co-localisation of S. Typhimurium, Npc1 and LAMP-1 in RAW 264.7 MΦ infected with WT or ΔssaV S. Typhimurium.

RAW 264.7 MΦ were infected with WT or *ΔssaV S.* Typhimurium and incubated for 24h pi. Uninfected and U18666A (2μg/ml for 24h) treatments represent vehicle and positive controls respectively. Panel A. Representative confocal microscopy images of uninfected, U18666A-treated, WT or *ΔssaV S.* Typhimurium infected cells. Individual channels are shown in black and white. In merged images: Npc1, magenta; *S.* Typhimurium, cyan; LAMP-1, green. Scale bar represents 10μm. Red arrows indicate the contact between *S.* Typhimurium and Npc1 protein. Panel B. Quantification of co-localisation of bacteria and Npc1 in WT or *ΔssaV S.* Typhimurium-infected cells according to Pearson's correlation coefficient. Data are mean ± SEM, n=3 replicates per sample representing a minimum of 30 cells from 3 randomly selected fields. Statistical analysis, Welch's t-test. No statistically significant differences were detected.

6.3.11. *S.* Typhimurium TL extract increases LysoTracker™ staining intensity of RAW 264.7 MΦ.

The above data demonstrated that infection of RAW 264.7 MΦ with multiple *S.* Typhimurium strains, including mutants that lack specific effector proteins, were able to induce NPC cellular phenotypes. To investigate whether this was due to a lipid component inhibiting NPC1, we tested for induction of NPC phenotypes in RAW 264.7 MΦ by an *S.* Typhimurium TL extract. RAW 264.7 MΦ were treated with doses of *S.* Typhimurium TL extract, and the relative intensity of LysoTracker™ staining of live cells and the frequency of PI-positive dead cells were measured by FACS. There was a dose-dependent increase in LysoTracker™ relative intensity, with 0.05μg/ml *S.* Typhimurium TL extract inducing a significant increase in LysoTracker™ relative intensity (****p<0.0001, Fig 6.3.11.A.). Cell viability was reduced with the *S.* Typhimurium TL extract treatment but was not significantly greater than that for the positive control, U18666A (****p<0.0001, Fig 6.3.11.B.). In addition, two independent preparations of *S.* Typhimurium TL extract were tested and showed comparable activities (Fig 6.3.11.).

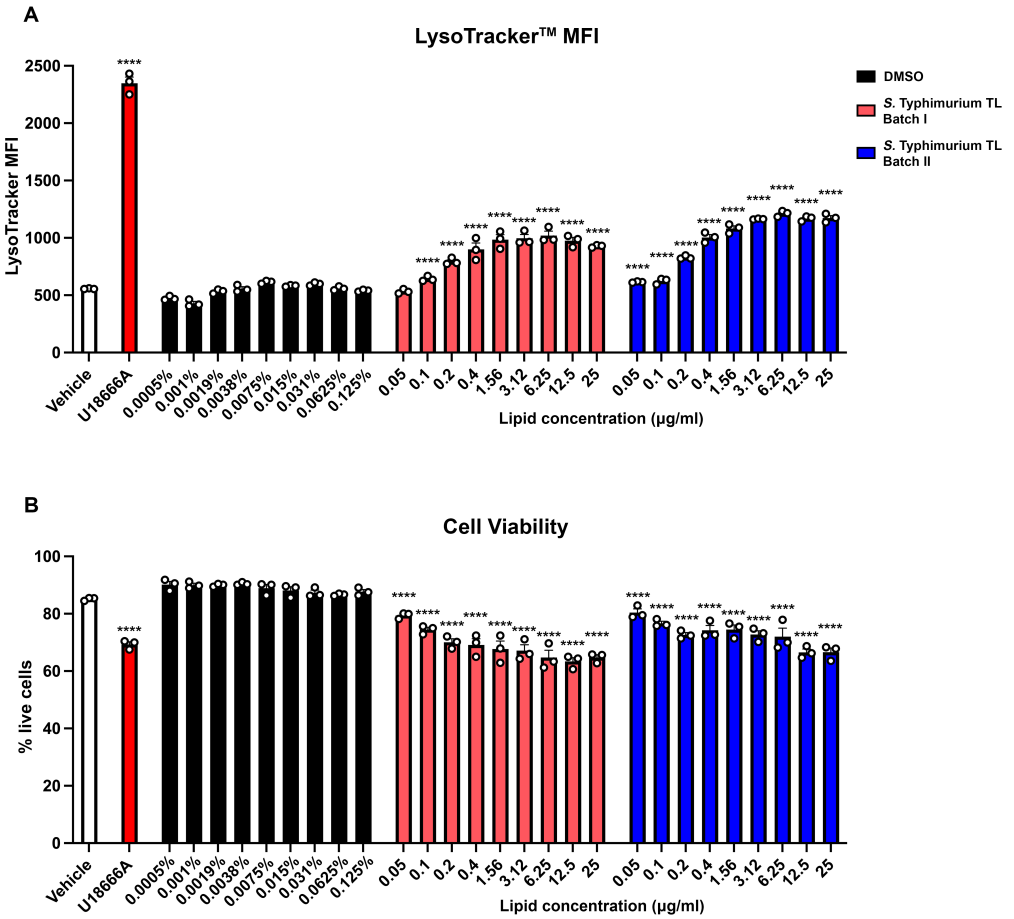


Figure 6.3.11. S. Typhimurium TL extract significantly increases LysoTracker™ staining intensity but reduces cell viability of RAW 264.7 MΦ.

RAW 264.7 MΦ were incubated with *S.* Typhimurium TL (0.05µg/ml to 25µg/ml for 48h) and relative lysosomal volume and cell viability were determined by FACS. DMSO at concentrations equivalent to diluted TL extract and U18666A (2µg/ml for 48h) were vehicle and positive controls respectively. Panel A. Quantification of LysoTracker™ staining intensity of treated cells. Panel B. Viability of treated cells. Data are mean ± SEM, n=3. Statistical ansalysis, two-way ANOVA with Tukey multiple comparisons. ****p<0.0001, otherwise not significant. Statistical comparison of U18666A treatment is relative to vehicle control. Statistical comparisons of lipid treatment are relative to DMSO control. Data are representative of 4 independent experiments.

6.3.12. Confocal microscopy of LysoTracker™ staining confirms expansion of the acidic compartment in RAW 264.7 MΦ treated with *S.* Typhimurium TL extract.

The acidic compartments marked with LysoTracker™ Green DND-26 in RAW 264.7 MΦ treated with 100μg/ml *S.* Typhimurium TL extract for 48h were also inspected by confocal microscopy. With *S.* Typhimurium TL extract treatment, enlarged LysoTracker™ positive compartments appeared as large vacuoles, with significantly increased lysosomal diameter, which was comparable to that observed with U18666A treatment (****p<0.0001, Fig 6.3.12.A.C.D.). *S.* Typhimurium TL extract also increased the frequency of lysosomes in each cell (p=0.0220, Fig 6.3.12.B).

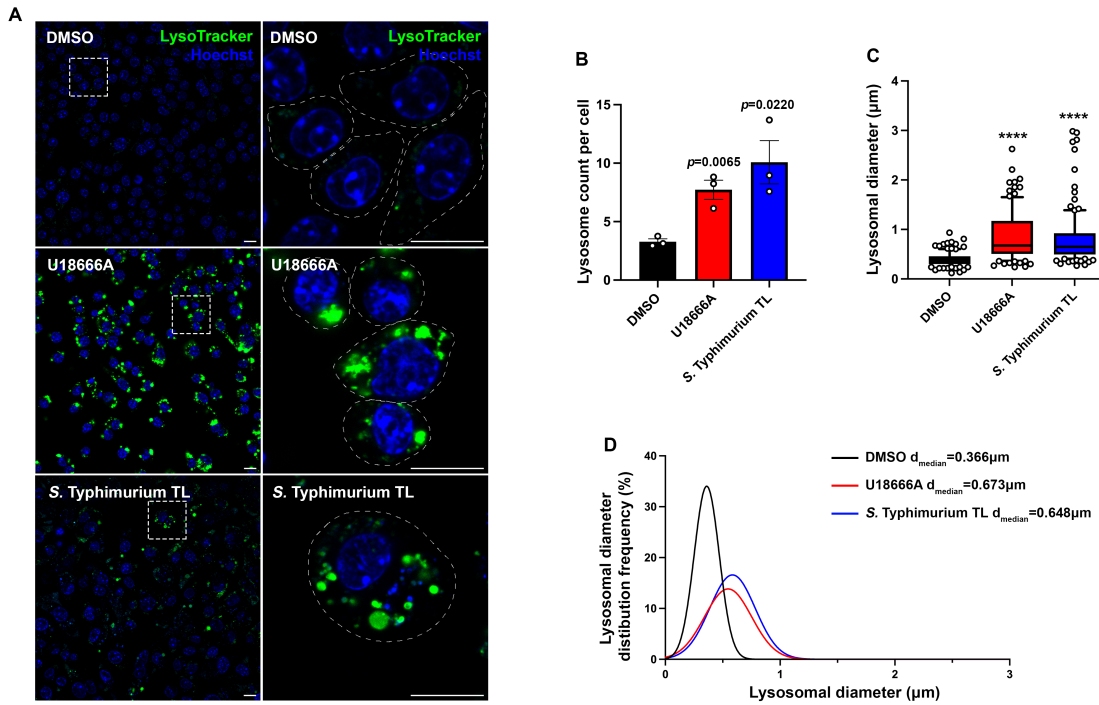


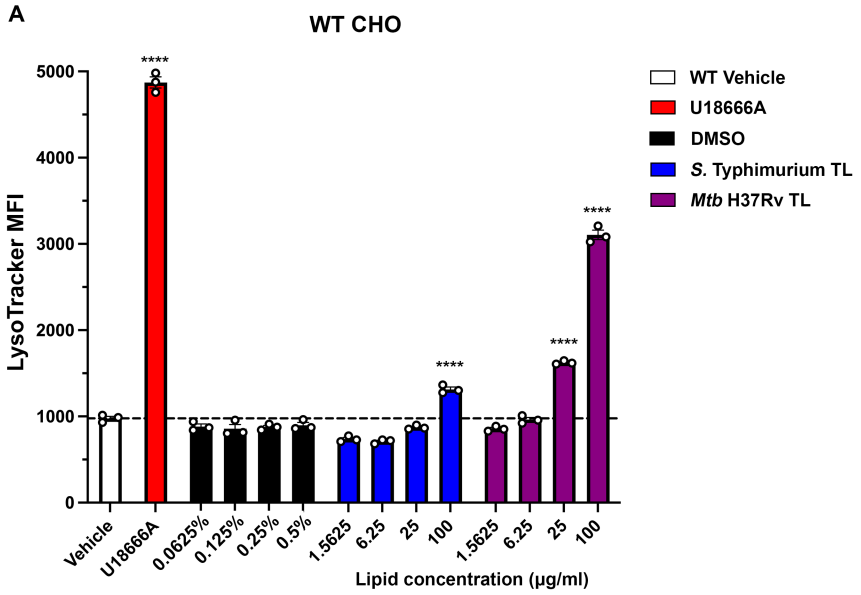
Figure 6.3.12. Increased lysosomal frequency and size in RAW 264.7 MΦ treated with S. Typhimurium TL extracts visualised with LysoTracker™ Green DND-26.

RAW 264.7 MΦ were treated with *S.* Typhimurium TL extract (100μg/ml for 48h). DMSO and U18666A (2μg/ml) were applied for 48h as vehicle and positive controls respectively. Panel A. Representative confocal microscopy images of treated cells. LysoTracker™ Green DND-26, green; Hoechst, blue. For each pair, the right image is a higher magnification of the region outlined in the left image. Scale bar represents 10μm. White dotted lines indicate the outline of individual cells. Panel B. Frequency of lysosomes per treated cell per optical plane. Data are mean ± SEM, n=3. Statistical analysis, Welch's t test. *p* values as indicated. Statistical comparisons are relative to DMSO control. Panel C. Mean lysosomal diameter in treated RAW 264.7 MΦ. Box and whisker plot, box contains 90% of all events, n>120 from at least 3 individual cells. Statistical analysis, one-way ANOVA with Kruskal-Wallis multiple comparisons. ****$p<0.0001$. Statistical comparisons are relative to DMSO control. Panel D. Statistical distribution of lysosomal diameters (μm) in treated cells. Bin width: 0.1μm. DMSO: min: 0.120μm, max: 0.934μm, centre: 0.366μm; U18666A: min: 0.241μm, max: 2.62μm, centre: 0.673μm; *S.* Typhimurium TL: min: 0.269μm, max: 2.98μm, centre: 0.648μm. Statistical analysis, Gaussian distribution. Statistical distribution values indicated are median diameters. Data are representative of 2 independent experiments.

6.3.13. *S.* Typhimurium and *Mtb* H37Rv TL extracts increase LysoTracker™ staining intensity of WT but not CHO$^{Npc1-/-}$ cells.

We were concerned that the *S.* Typhimurium TL extract could contain activity that impacts upon LysoTracker™ staining intensity independent of NPC1 inhibition. LPS is a cell wall component of *S.* Typhimurium that has multiple effects on MΦ.

We therefore tested *S.* Typhimurium TL extract on cells unable to recognise LPS; for example, CHO cells, which do not express TLR4, the major receptor for this pathogen-associated molecule [509]. We also analysed treated CHO$^{Npc1-/-}$ cells to confirm Npc1 specificity. We incubated WT and CHO$^{Npc1-/-}$ cells with *S.* Typhimurium TL extract and measured the intensity of LysoTracker™ Green DND-26 staining by FACS. As expected, untreated CHO$^{Npc1-/-}$ cells had significantly greater LysoTracker™ staining than vehicle WT cells (Fig 6.3.13.A.B.). Similarly, the staining intensity of WT CHO was significantly increased by U18666A, but that of mutant cells was not significantly changed (****p<0.0001, Fig 6.3.13.A.B.). In the case of WT CHO cells, doses of 25μg/ml and 100μg/ml of *Mtb* H37Rv TL and 100μg/ml of *S.* Typhimurium TL extract significantly enhanced staining intensity (****p<0.0001, Fig.6.3.13.A.). For CHO$^{Npc1-/-}$ cells, DMSO reduced the intensity of staining as compared to vehicle-treated conditions, and although LysoTracker™ intensities with the highest concentrations of lipid extracts were significantly greater than DMSO controls, they were not increased beyond that of vehicle CHO$^{Npc1-/-}$ cells (Fig 6.3.13.B).



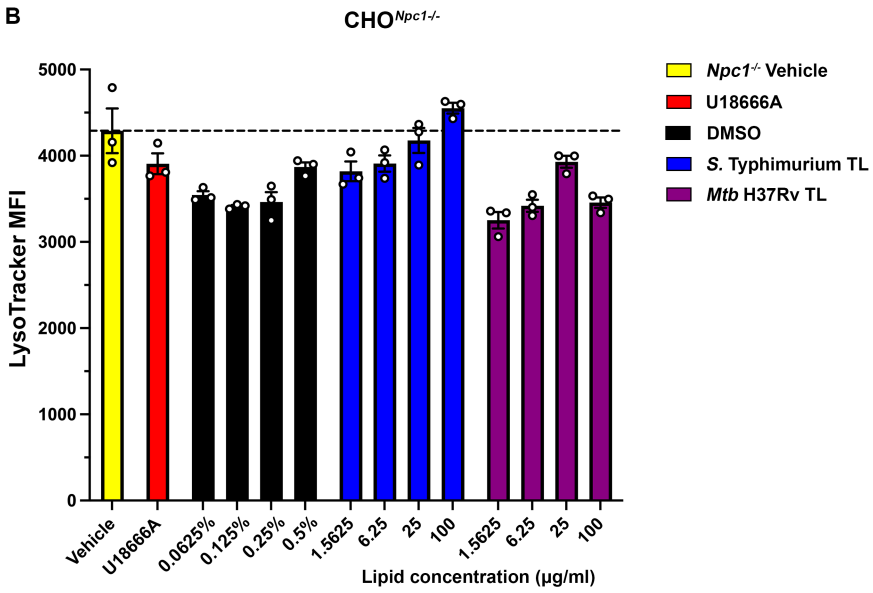


Figure 6.3.13. S. Typhimurium and Mtb H37Rv TL extracts increase LysoTracker™ staining intensity in WT but not in CHO$^{Npc1-/-}$ cells. WT and CHO$^{Npc1-/-}$ cells were treated with *S.* Typhimurium and *Mtb* H37Rv TL extract for 48h. DMSO and U18666A (2µg/ml for 48h) treatments were vehicle and positive controls respectively. Panel A. LysoTracker™ staining intensity in treated WT CHO cells. Panel B. LysoTracker™ staining intensity in treated CHO$^{Npc1-/-}$ cells. Data are mean ± SEM, n=3. Statistical analysis, two-way ANOVA with Tukey multiple comparisons. ****p<0.0001, other p values as indicated, otherwise not significant. Statistical comparison of U18666A treatment is relative to vehicle control. Statistical comparisons of lipid treatment are relative to DMSO control. Data are representative of 2 independent experiments.

6.3.14. LPS significantly increases LysoTracker™ staining intensity of RAW 264.7 MΦ but not WT CHO cells.

To examine whether the LPS content of *S.* Typhimurium could affect the volume of the acidic compartment, we treated RAW 264.7 MΦ and WT CHO cells with

purified LPS from *S.* Typhimurium and analysed the intensity of LysoTracker™ staining. At concentrations greater than 0.1ng/ml, LPS caused a significant increase in LysoTracker™ staining intensity of RAW 264.7 MΦ (****p<0.0001 for 1ng/ml and 500ng/ml, p=0.0046 for 10ng/ml, p=0.0009 for 100ng/ml, Fig 6.3.14.A.), with evidence of a dose-dependent relationship. In the case of WT CHO cells, there was no statistically significant increase in staining intensity, including at the highest concentration of LPS that was tested (Fig 6.3.14.B.)

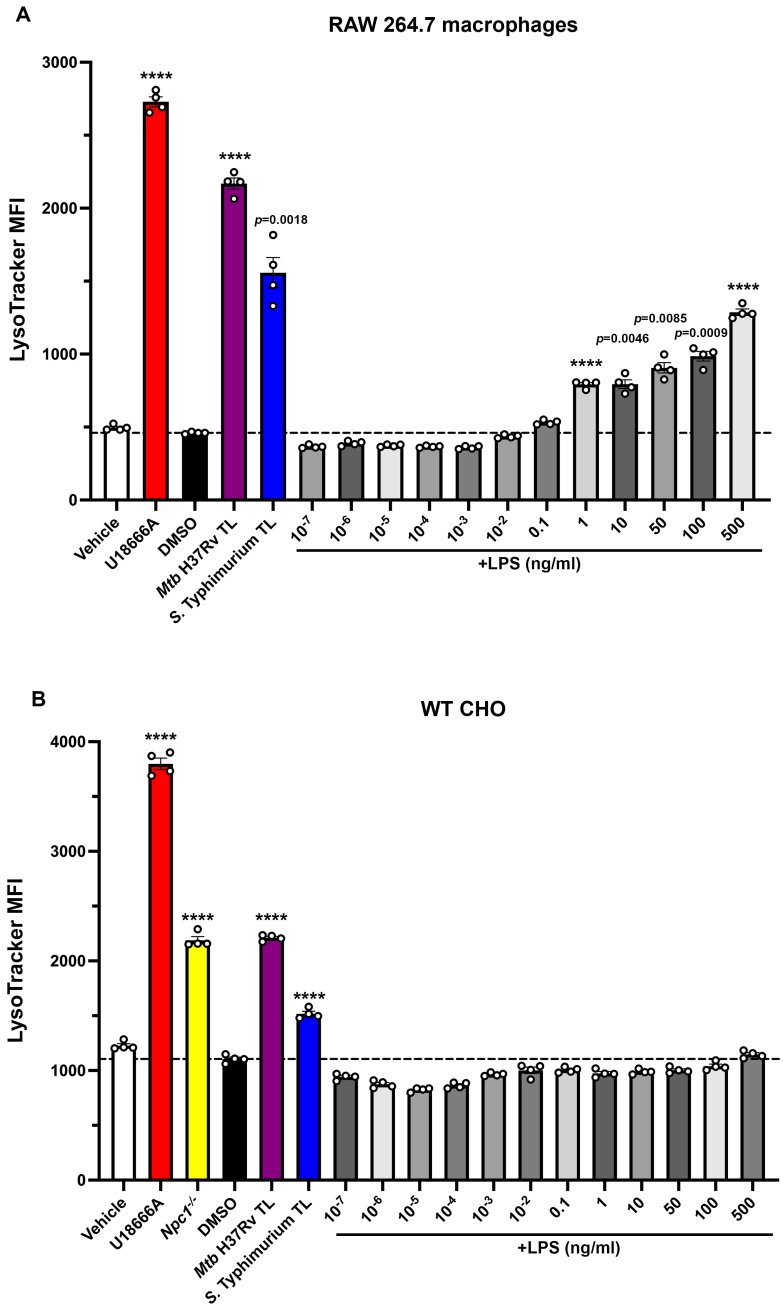
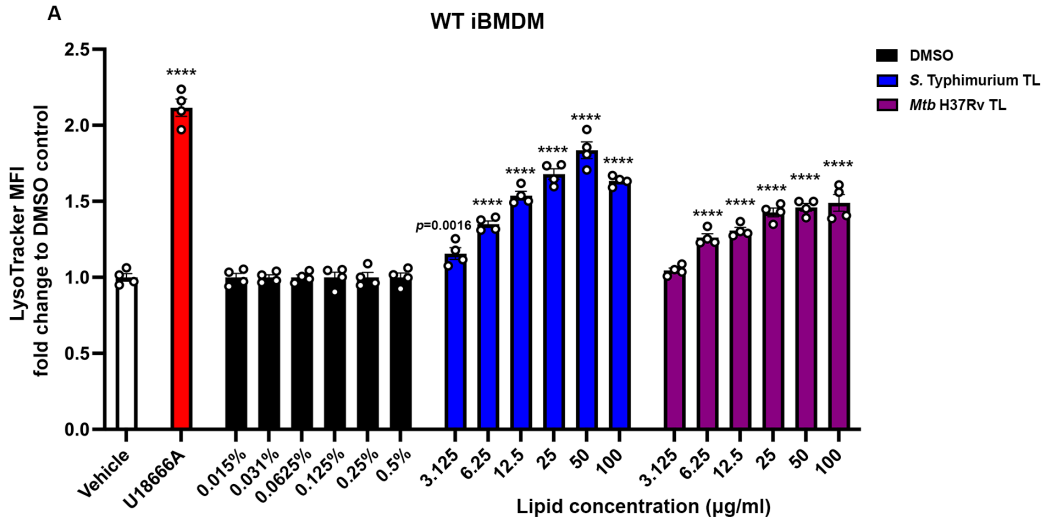


Figure 6.3.14. LPS increases LysoTracker™ staining intensity in RAW 264.7 MΦ but not in WT CHO cells.

RAW 264.7 MΦ and WT CHO cells were treated with LPS from *S.* Typhimurium from doses of 10^{-7}ng/ml to 500ng/ml for 48h. DMSO and U18666A (2µg/ml for 48h) treatments were vehicle and positive controls respectively. Panel A. Quantification of LysoTracker™ staining intensity in treated RAW 264.7 MΦ. Panel B. Quantification of LysoTracker™ staining intensity in treated WT CHO cells. Data are mean ± SEM, n=4. Statistical analysis, one-way ANOVA with Dunnett multiple comparisons. ****p<0.0001, other p values as indicated, otherwise not significant. Statistical comparisons are relative to vehicle control. Data are representative of 2 independent experiments.

6.3.15. *Mtb* H37Rv and *S.* Typhimurium TL extracts significantly increase LysoTracker™ staining intensity of WT and *Tlr4*$^{-/-}$ murine bone marrow-derived MΦ (iBMDMΦ).

To verify that LPS contamination of the *S.* Typhimurium TL extract was not responsible for the expansion of the acidic compartment, we treated WT and *Tlr4*$^{-/-}$ iBMDMΦ, which lack the receptor TLR4 that binds endotoxin, with *Mtb* H37Rv or *S.* Typhimurium TL extract and analysed for LysoTracker™ staining intensity. The baseline LysoTracker™ staining intensity of WT and *Tlr4*$^{-/-}$ iBMDMΦ varied between the genotypes; therefore LysoTracker™ staining intensity was normalised to that of vehicle control. In WT iBMDMΦ, *Mtb* H37Rv and *S.* Typhimurium TL extract induced dose-dependent increases in LysoTracker™ staining intensity (****p<0.0001, Fig 6.3.15.A.). In the case of *Tlr4*$^{-/-}$ iBMDMΦ, *Mtb* H37Rv and *S.* Typhimurium TL extract induced significant increases in LysoTracker™ staining intensity but not in a manner that was dose-dependent over the range of concentrations that were tested (****p<0.0001, Fig 6.3.15.B.).



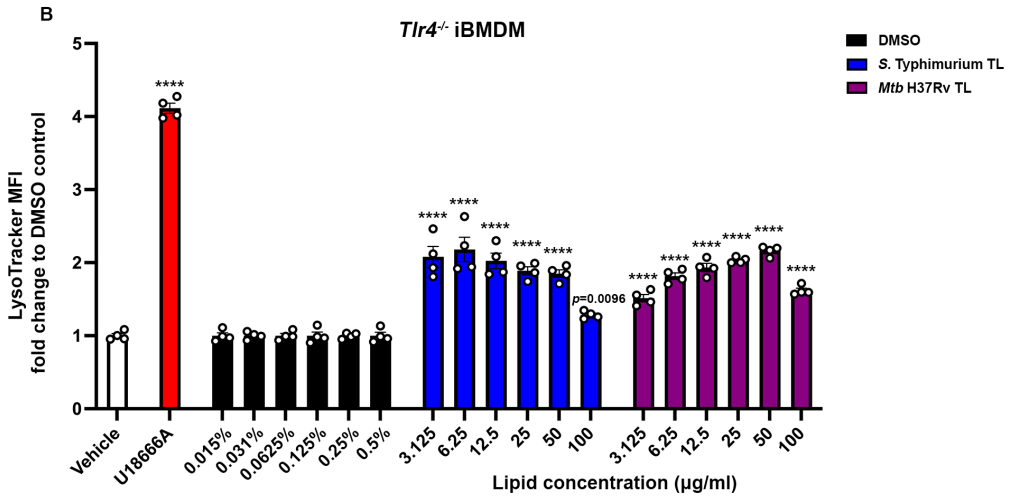


Figure 6.3.15. Mtb H37Rv and S. Typhimurium TL extracts significantly increase LysoTracker™ staining intensity in WT and Tlr4-/- murine iBMDMΦ.

WT and *Tlr4*$^{-/-}$ murine iBMDMΦ were treated with *Mtb* H37Rv and *S.* Typhimurium TL for 48h. DMSO and U18666A (2µg/ml for 48h) were vehicle and positive controls respectively. LysoTracker™ staining intensity was normalised to DMSO control. Panel A. Quantification of LysoTracker™ staining intensity in treated WT iBMDMΦ. Panel B. Quantification of LysoTracker™ staining intensity in treated *Tlr4*$^{-/-}$ iBMDMΦ. MFI, mean fluorescent intensity. Data are normalised relative to the DMSO vehicle control. Data are mean ± SEM, n=4. Statistical analysis, two-way ANOVA with Sidak multiple comparisons. ****p<0.0001, other p values as indicated, otherwise not significant. Statistical comparison of U18666A treatment is relative to vehicle control. Statistical comparisons of lipid treatment are relative to DMSO control. Data are representative of 2 independent experiments.

6.3.16. LAMP-1 immunostaining confirms expansion of LE/Lys volume in RAW 264.7 MΦ treated with *S.* Typhimurium TL extract.

To validate the expansion of the acidic compartment, we stained RAW 264.7 MΦ that had been treated with *S.* Typhimurium TL extract with anti-LAMP-1 antibody. Confocal microscopy images revealed LE/Lys were enlarged following *S.* Typhimurium TL extract treatment, with a vacuolar appearance similar to that of U18666A-treated cells (white arrows, Fig 6.3.16.A.). *S.* Typhimurium TL extract significantly increased the mean lysosomal diameter (****p<0.0001, Fig 6.3.16.B.), with a shift in distribution towards a larger diameter comparable to that of U18666A-treated cells (Fig 6.3.16.C.).

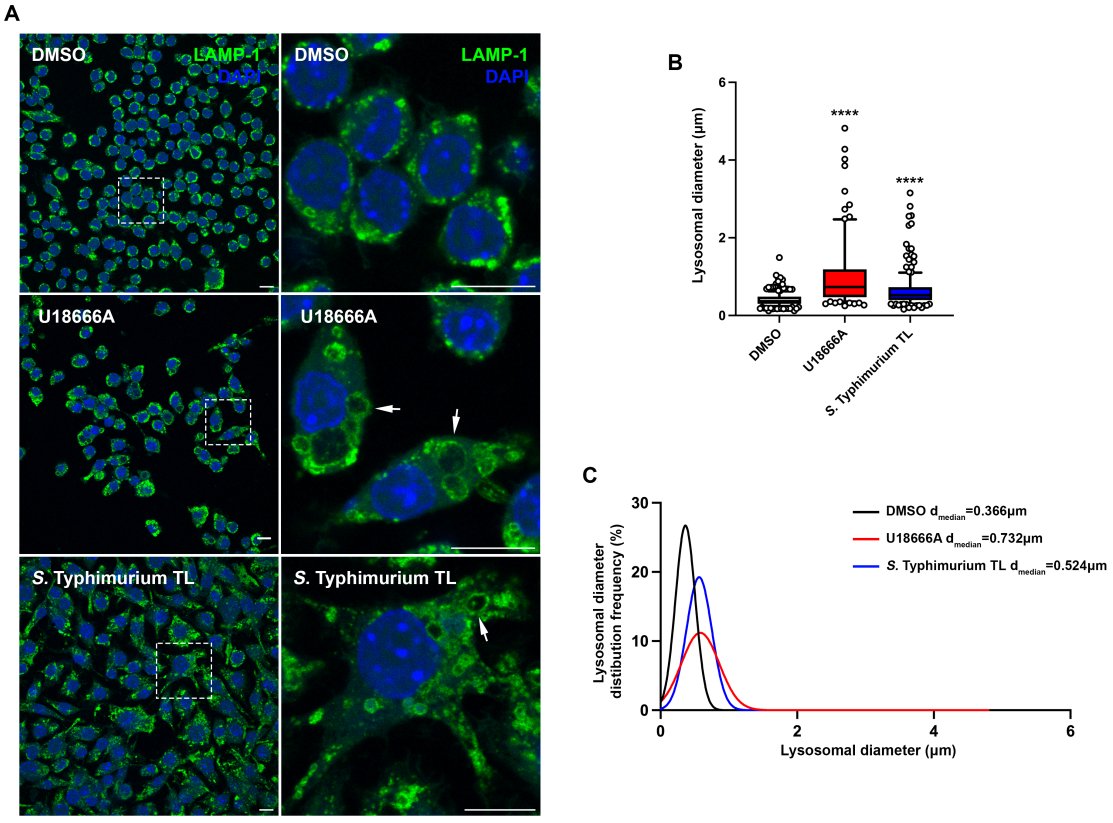
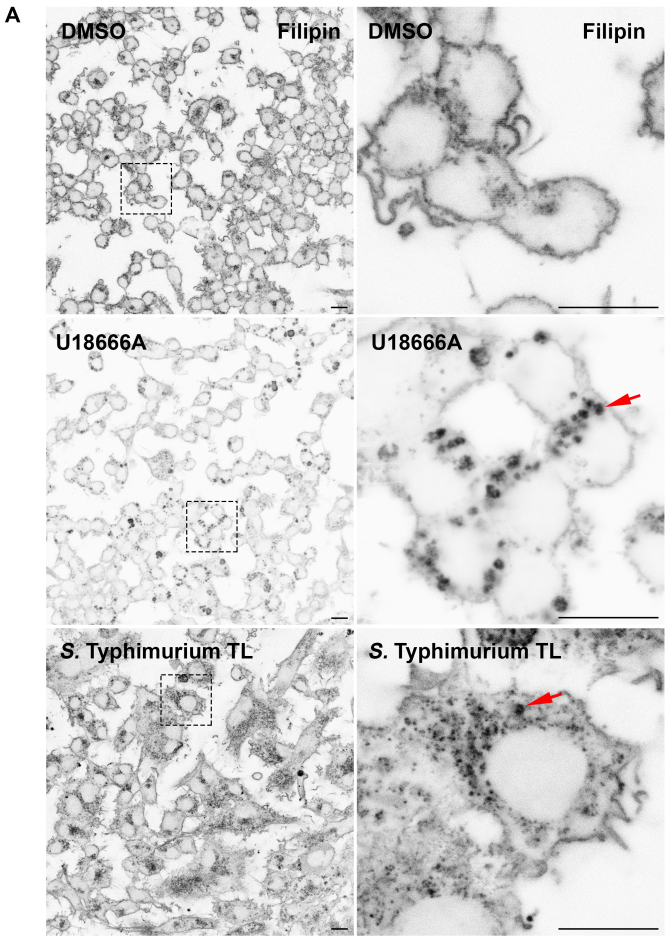


Figure 6.3.16. Expansion of the LE/Lys compartment in RAW 264.7 MΦ in response to treatment with S. Typhimurium TL extract visualised by anti-LAMP-1 immunostaining.

RAW 264.7 MΦ were treated with *S.* Typhimurium TL extract (100μg/ml for 48h). DMSO and U18666A (2μg/ml for 48h) treatment were vehicle and positive controls respectively. Panel A. Representative confocal microscopy images of treated RAW 264.7 MΦ. White arrows indicate enlarged LE/Lys. LAMP-1, green; DAPI, blue. For each pair, the right image is a higher magnification of the region outlined in the left image. Scale bar represents 10μm. Panel B. Mean lysosomal diameter in treated RAW 264.7 MΦ. Box and whisker plot, box contains 90% of all events, n>180 within 4 random fields. Statistical analysis, Man-Whitney test. ****p<0.0001. Statistical comparisons are relative to DMSO control. Panel C. Statistical distribution of lysosomal diameter (μm) in treated RAW 264.7 MΦ. Bin width, 0.1 μm. DMSO: min: 0.120μm, max: 1.490μm, centre: 0.366μm; U18666A: min: 0.248μm, max: 4.818μm, centre: 0.732μm; *S.* Typhimurium TL: min: 0.161μm, max: 3.154μm, centre: 0.524μm. Statistical distribution values indicated are median diameters. Statistical analysis, Gaussian distribution. Statistical distribution values indicated are median diameters. Data are representative of 2 independent experiments.

6.3.17. *S.* Typhimurium TL extract induces partial cholesterol redistribution to the endo-lysosomal system of RAW 264.7 MΦ.

The storage of cholesterol in the endo-lysosomal system is an NPC cellular phenotype (Section 2.3.13.). To test whether *S.* Typhimurium TL would induce this phenotype, we determined the intracellular distribution of cholesterol by filipin staining. Cholesterol accumulation was observed as intracellular filipin-positive puncta (red arrows, Fig 6.3.17.A.). The frequency of cells with intracellular filipin puncta was significantly increased in RAW 264.7 MΦ treated with *S.* Typhimurium TL extract (p=0.0076) and was comparable to that of U18666A treated RAW 264.7 MΦ (p=0.0115, Fig 6.3.17.B.).



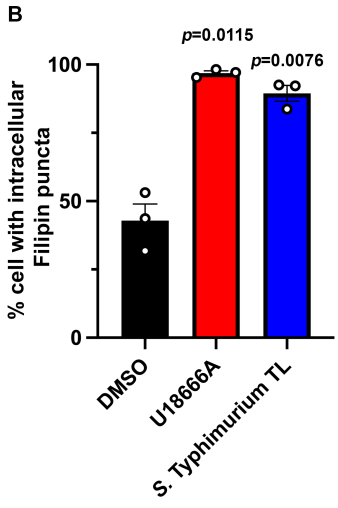


Figure 6.3.17. S. Typhimurium TL extract induces a partial redistribution of cholesterol to intracellular puncta in RAW 264.7 MΦ.

RAW 264.7 MΦ were treated with *S.* Typhimurium TL extract (100µg/ml for 48h). DMSO and U18666A (2µg/ml for 48h) treatments were vehicle and positive controls respectively. Panel A. Representative confocal microscopy images of treated cells stained with filipin. Filipin, black. Red arrows indicate filipin-positive puncta. For each pair, the right image is a higher magnification of the region outlined in the left image. Scale bar represents 10µm. Panel B. Quantification of the frequency of cells with intracellular filipin-positive puncta. Data are mean ± SEM, n=3, each representing a minimum of 100 cells in randomly selected fields. Statistical analysis, Welch's t-test. *p* values as indicated. Statistical comparisons are relative to DMSO control. Data are representative of 2 independent experiments.

6.3.18. *S.* Typhimurium TL extract does not affect the total cholesterol level content of RAW 264.7 MΦ.

To determine whether *S.* Typhimurium TL affects not only the intracellular distribution of cholesterol but also quantity, RAW 264.7 MΦ were treated with bacterial lipids and the level of cholesterol was measured by Amplex Red assay. No significant increase in total cholesterol levels were observed with any of the concentrations of *S.* Typhimurium TL extract tested (Fig 6.3.18.).

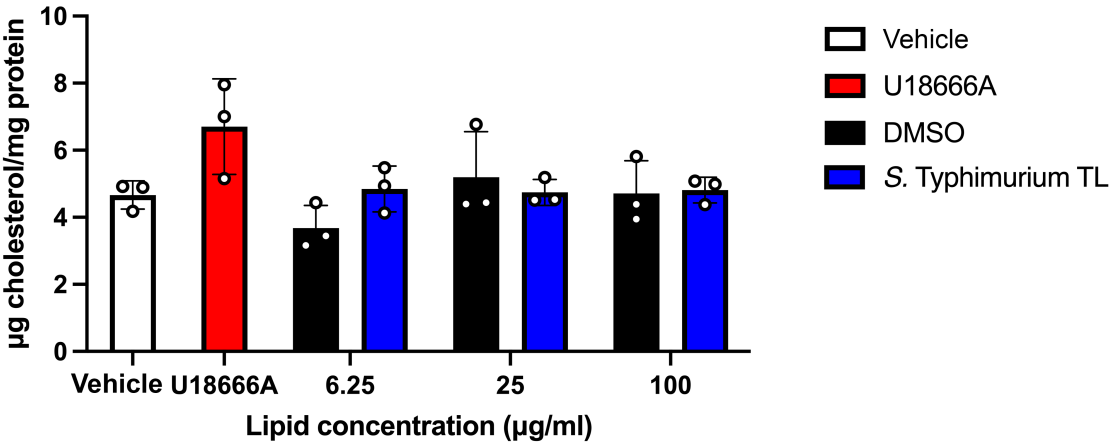


Figure 6.3.18. S. Typhimurium TL extract treatment does not change the amount of cholesterol in RAW 264.7 MΦ.

RAW 264.7 MΦ were treated with 6.25µg/ml, 25µg/ml, and 100µg/ml *S.* Typhimurium TL extract. DMSO and U18666A (2µg/ml for 48h) treatments were vehicle and positive controls. Data are mean ± SEM, n=3. Statistical analysis, two-way ANOVA with Sidak multiple comparisons. No statistically significant difference was detected. Statistical comparisons are relative to DMSO control. Data are representative of 2 independent experiments.

6.3.19. *S.* Typhimurium TL extract perturbs GM1 ganglioside trafficking in RAW 264.7 MΦ.

Perturbation of recycling and accumulation of GSLs in the lysosome is a phenotype of NPC cells [11]. To investigate whether there was a comparable defect in *S.* Typhimurium TL extract treated RAW 264.7 MΦ, cells were pulse-labelled with fluorescent CtxB, which binds to GM1 ganglioside. *S.* Typhimurium TL treatment resulted in the accumulation of intracellular CtxB positive puncta (white arrowheads, Fig 6.3.19.A.), whereas vehicle control cells displayed a perinuclear distribution (white arrows, Fig 6.3.19.A.). The frequency of cells with lysosomal GM1 ganglioside distribution was significantly greater after *S.* Typhimurium TL extract treatment (p=0.0014, Fig 6.3.19.B.).

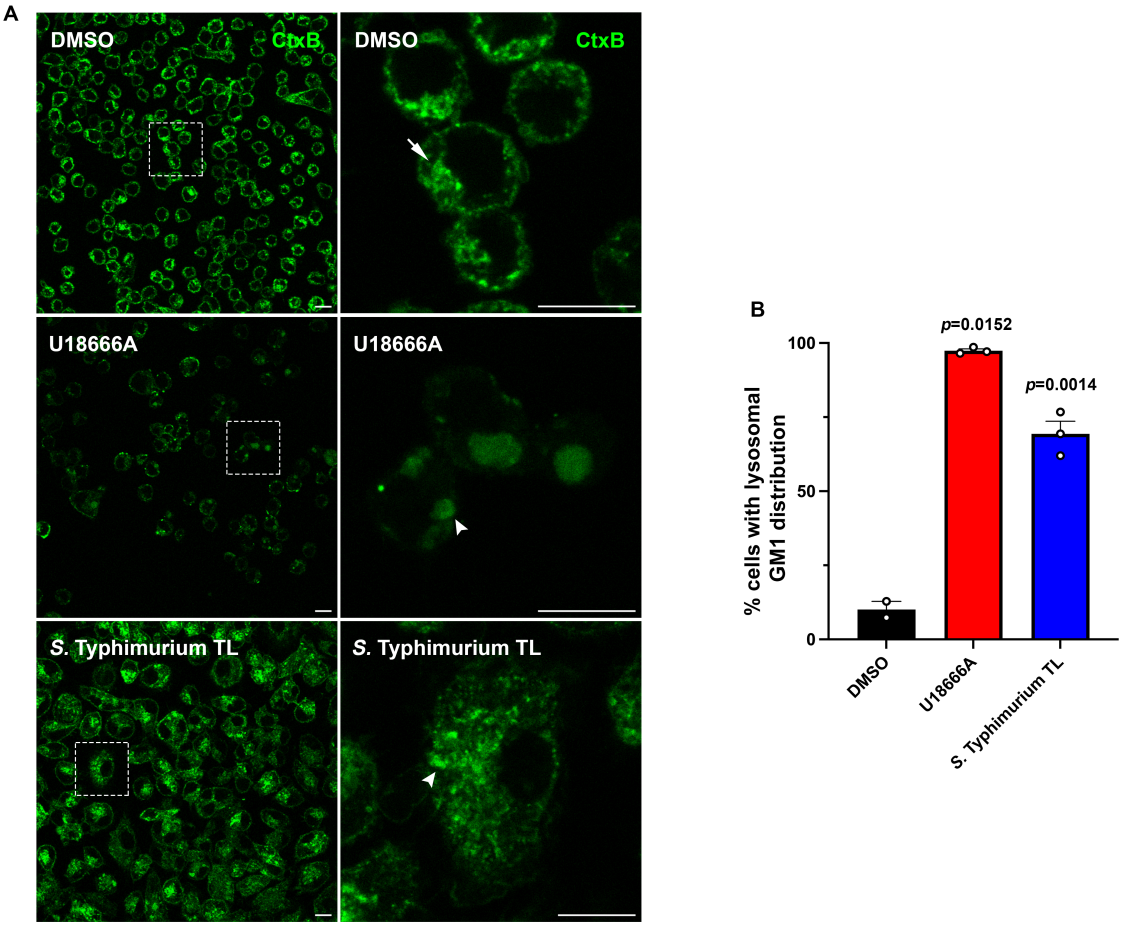


Figure 6.3.19. S. Typhimurium TL extract perturbs GM1 ganglioside trafficking in RAW 264.7 MΦ.

RAW 264.7 MΦ were treated with *S.* Typhimurium TL extract (100μg/ml for 48h) and incubated with Alexa Fluor™ 488-conjugated CtxB for 30 min and chased for 1h. DMSO and U18666A (2μg/ml for 48h) treatments were vehicle and positive controls respectively. Panel A. Representative confocal microscopy images of CtxB-labelled GM1 ganglioside in treated cells. CtxB, green. For each pair, the right image is a higher magnification of the region outlined in the left image. White arrows indicate Golgi distribution; white arrowheads indicate lysosomal distribution. Scale bar represents 10μm. Panel B. Frequency of cells with lysosomal GM1 distribution. Data are mean ± SEM, n=3, each representing a minimum of 100 cells from 3 randomly selected fields. Statistical analysis, Welch's t-test. *p* values as indicated. Statistical comparisons are relative to DMSO control. Data are representative of 2 independent experiments.

6.3.20. *S.* Typhimurium TL extract perturbs BODIPY-LacCer trafficking in RAW 264.7 MΦ.

To examine the effect of *S.* Typhimurium TL extract on sphingolipid recycling, we also analysed the trafficking of BODIPY-LacCer. RAW 264.7 MΦ were treated with *S.* Typhimurium TL for 48h, pulsed with fluorescent BODIPY-LacCer for 30 min, chased for 2h and imaged by confocal microscopy. In DMSO-treated cells, BODIPY-LacCer has a primarily peri-nuclear Golgi distribution (white arrows, Fig 6.3.20.A.). In contrast, *S.* Typhimurium TL treatment resulted in lysosomal concentration of BODIPY-LacCer, which was similar to those observed with U18666A treatment (white arrowheads, Fig 6.3.20.A.). For both treatments,

BODIPY-LacCer was associated with vacuole-like structures (Fig 6.3.20.A.). Quantitatively, there was a statistically significant increase in the frequency of RAW 264.7 MΦ with lysosomal distribution of BODIPY-LacCer after *S.* Typhimurium TL extract treatment compared to vehicle control (p=0.0004, Fig 6.3.20.B.).

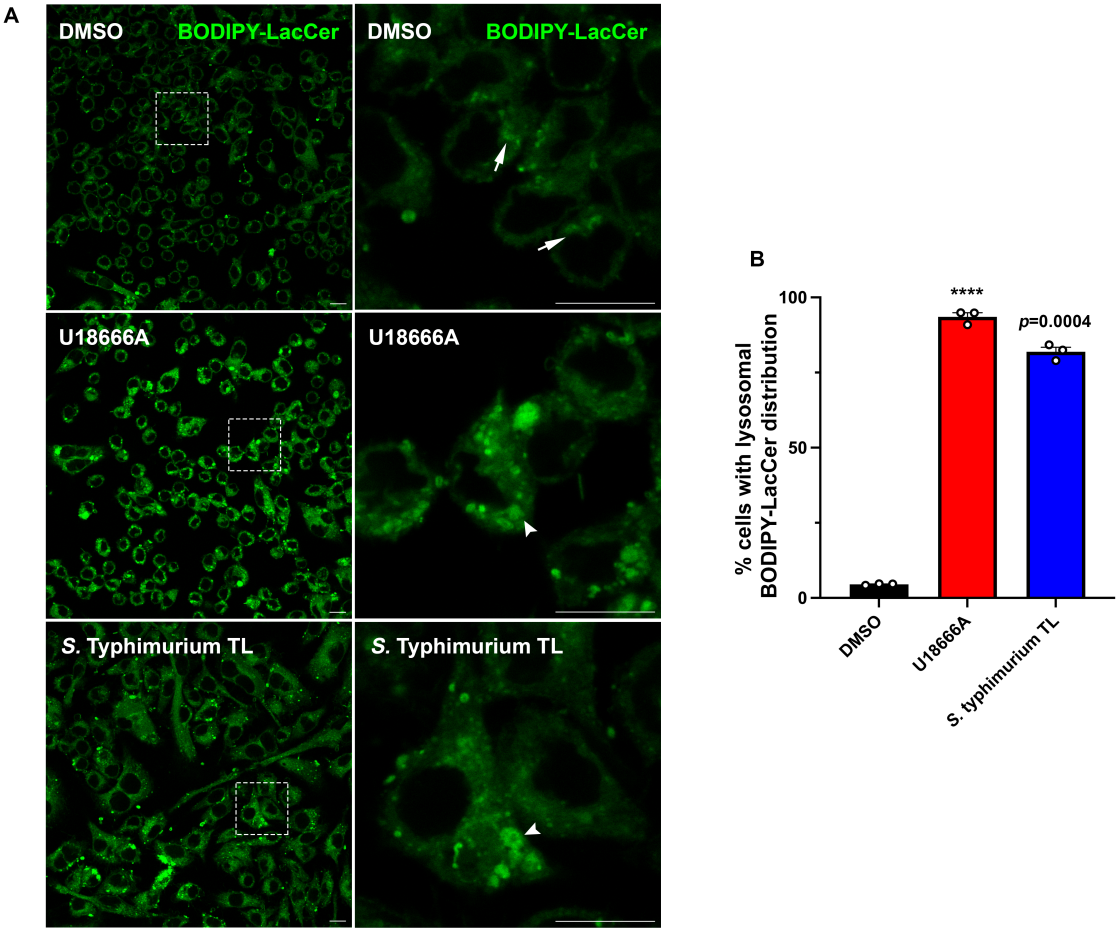
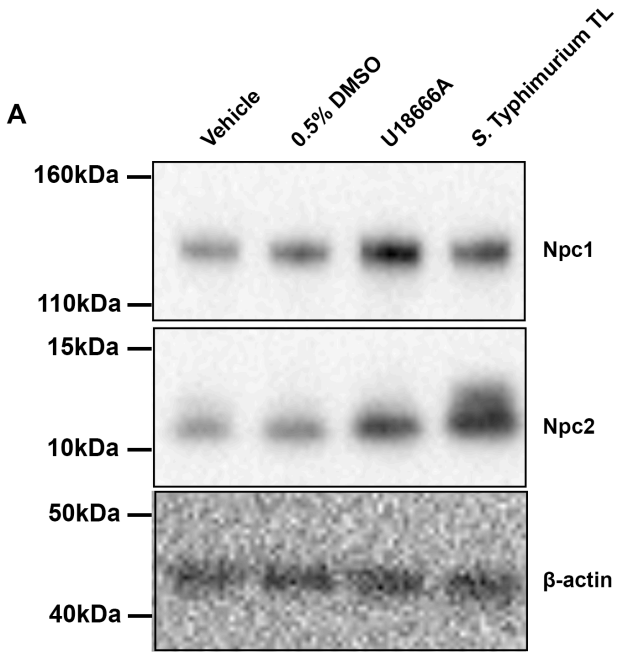


Figure 6.3.20. S. Typhimurium TL extract perturbs BODIPY-LacCer trafficking in RAW 264.7 MΦ.

RAW 264.7 MΦ were treated with *S.* Typhimurium TL extract (100μg/ml for 48h). DMSO and U18666A (2μg/ml for 48h) treatments were vehicle and positive controls respectively. Panel A. Representative confocal microscopy images of BODIPY-LacCer distribution in MΦ. BODIPY-LacCer, green. For each pair, the right image is a higher magnification of the region outlined in the left image. White arrows indicate Golgi distribution; white arrowheads indicate lysosomal distribution. Scale bar represents 10μm. Panel B. Frequency of cells with lysosomal BODIPY-LacCer distribution. Data are mean ± SEM, n=3, each representing a minimum of 100 cells randomly selected fields. Statistical analysis, Welch's t-test. ****$p<0.0001$, other p values as indicated. Statistical comparisons are relative to DMSO control. Data are representative of 2 independent experiments.

6.3.21. *S.* Typhimurium TL extract significantly increases Npc2 but not Npc1 protein levels in RAW 264.7 MΦ.

We investigated whether *S.* Typhimurium TL extract could alter the abundance of Npc1 and Npc2 proteins by western blotting of RAW 264.7 MΦ lysates. U18666A significantly increased both Npc1 (p=0.0219) and Npc2 (p=0.0147, Fig 6.3.21.). The amount of Npc2 but not Npc1 protein level was significantly higher following *S.* Typhimurium TL extract treatment (100μg/ml for 48h) (Fig 6.3.21.A.B.C.). Although there was a trend towards Npc1 being increased, it did not reach statistical significance (Fig 6.3.21.B.). In addition, we observed a second band detected by the anti-Npc2 antibody, of a greater molecular mass in *S.* Typhimurium TL extract-treated cells, which was not detected in the U18666A-treated lysate (Fig 6.3.21.A).



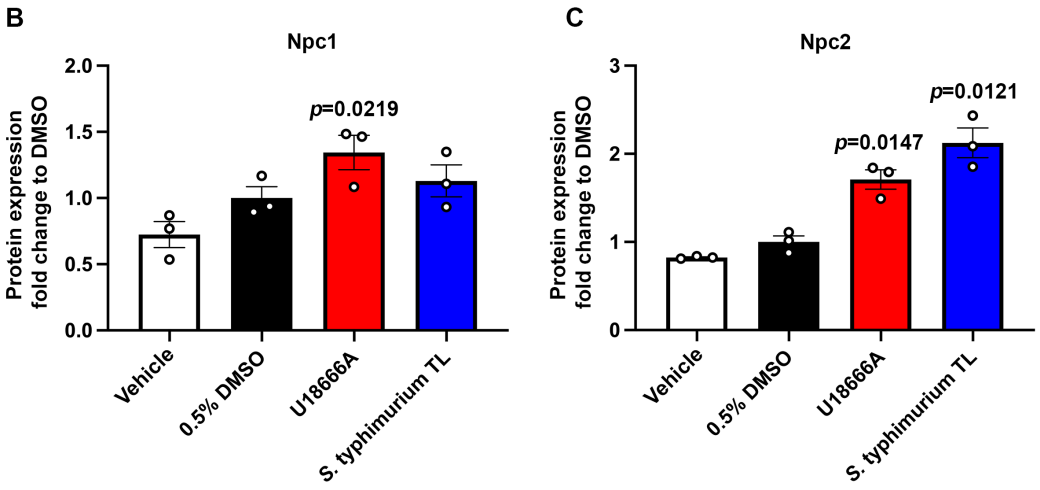


Figure 6.3.21. S. Typhimurium TL extract increases the amount of Npc2 but not Npc1 protein in RAW 264.7 MΦ.

RAW 264.7 MΦ were treated with *S.* Typhimurium TL extract (100µg/ml for 48h). DMSO and U18666A (2µg/ml for 48h) treatments were vehicle and positive controls respectively. Specific protein expression level was normalised to β-actin. Panel A. Representative western blot images of lysate probed for Npc1, Npc2 and β-actin. Panel B. Quantification of Npc1 protein bands normalised to β-actin; Panel C. Quantification of Npc2 protein bands normalised to β-actin. Data are mean ± SEM, n=3. Statistical analysis, Welch's t-test. *p* values as indicated, otherwise not significant. Statistical comparison of U18666A treatment is relative to vehicle control. Statistical comparison of lipid treatment is relative to 0.5% DMSO control. Data are representative of 2 independent experiments.

6.3.22. *S.* Typhimurium TL extract enhances expression of *Npc1* and *Npc2* genes in RAW 264.7 MΦ.

We investigated whether transcription of *Npc1* and *Npc2* in RAW 264.7 MΦ were affected by exposure to *S.* Typhimurium TL extract. *S.* Typhimurium treatment significantly increased *Npc1* and *Npc2* gene expression in RAW 264.7 MΦ (p=0.0172 and p=0.0059 respectively, Fig 6.3.22.A.B.). The increase was significantly greater than that seen for U18666A treatment (Fig 6.3.22.A.B.).

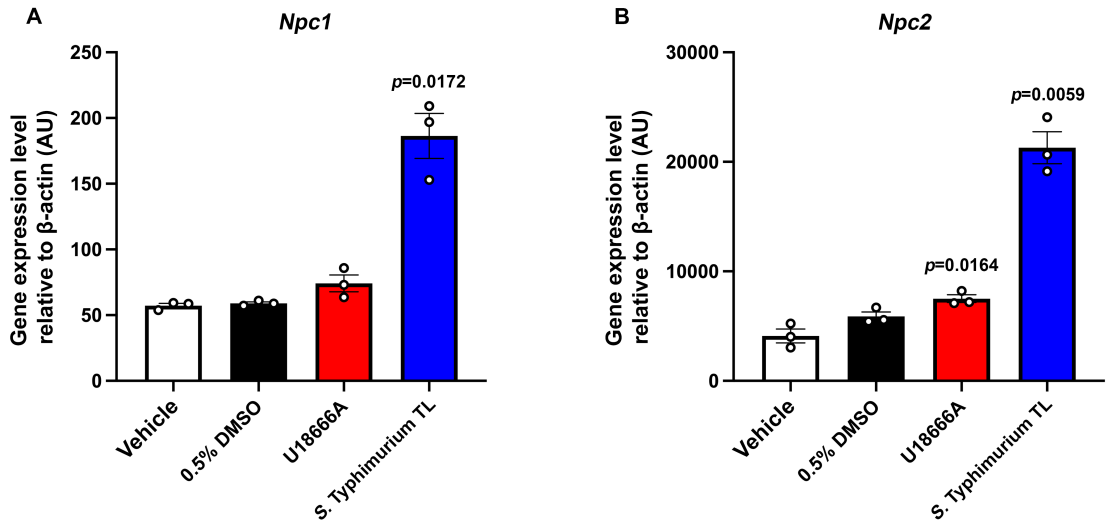


Figure 6.3.22. S. Typhimurium TL extract enhances the expression of Npc1 and Npc2 genes in RAW 264.7 MΦ.

RAW 264.7 MΦ were treated with *S.* Typhimurium TL extract (100µg/ml for 48h). DMSO and U18666A (2µg/ml for 48h) served as vehicle and positive controls. Npc1 and Npc2 transcripts were quantified by qPCR. Panel A. Quantification of relative gene expression of *Npc1* normalised to β-actin. Panel B. Quantification of relative gene expression of *Npc2* normalised to β-actin. Data are mean ± SEM, n=3. Statistical analysis, Welch's t-test. p values as indicated, otherwise not significant. Significant values are indicated. Statistical comparison of U18666A treatment is relative to vehicle control. Statistical comparison of lipid treatment is relative to 0.5% DMSO control. Data are representative of 2 independent experiments.

6.3.23. *S.* Typhimurium TL extract induces transient sphingosine and sphinganine accumulation in RAW 264.7 MΦ.

We next tested the effect of *S.* Typhimurium TL on the level of sphingoid bases. The sphingosine and sphinganine content of cells was measured by RP-HPLC. A significant increase in sphingosine following *S.* Typhimurium TL extract treatment was confirmed at 3h (p=0.0280), which remained significantly higher at 6h (p=0.0008) and declined to a non-significant level at 24h (Fig 6.3.23.A.). The level of sphinganine was significantly greater at 1h (****p<0.0001), 3h (p=0.0011) and 6h (p=0.0003) but was not significant at 24h (Fig 6.3.23.B.).

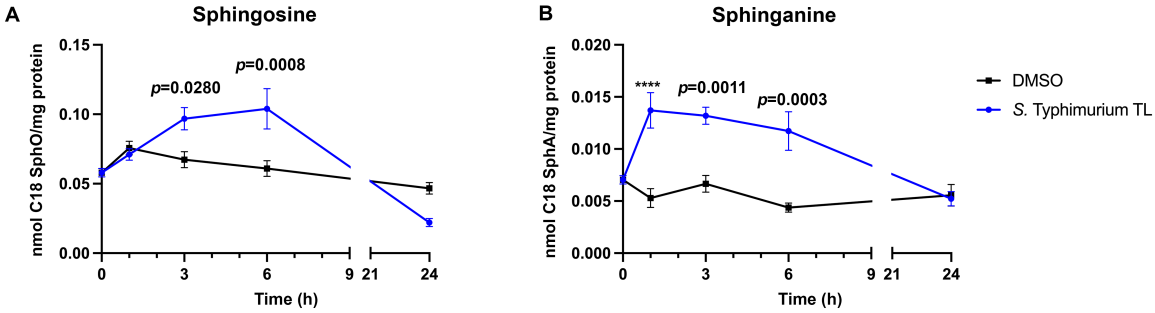


Figure 6.3.23. S. Typhimurium TL extract induces transient sphingosine and sphinganine accumulation in RAW 264.7 MΦ. RAW 264.7 MΦ were treated with DMSO as vehicle control and 100µg/ml *S.* Typhimurium TL extract for between 1h and 24h. Panel A. Temporal profile of sphingosine content. Panel B. Temporal profile of sphinganine content. Data are mean ± SEM, n=5. Statistical analysis, two-way ANOVA with Sidak Multiple comparisons. ****p<0.0001, other p values as indicated, otherwise not significant. Statistical comparisons are relative to DMSO control at each time point. Data are representative of 2 independent experiments.

6.3.24. *S.* Typhimurium TL extract enhances SphK2 protein in RAW 264.7 MΦ.

As part of our analysis of sphingoid base metabolism in mycobacterial lipid-treated cells, we analysed the expression of the kinase, SphK2. We made a comparable study of *S.* Typhimurium TL treated RAW 264.7 MΦ. Western blotting revealed that 48h of exposure to the bacterial lipid extract resulted in a significant increase in SphK2 protein (p=0.0213, Fig 6.3.24.A.B.).

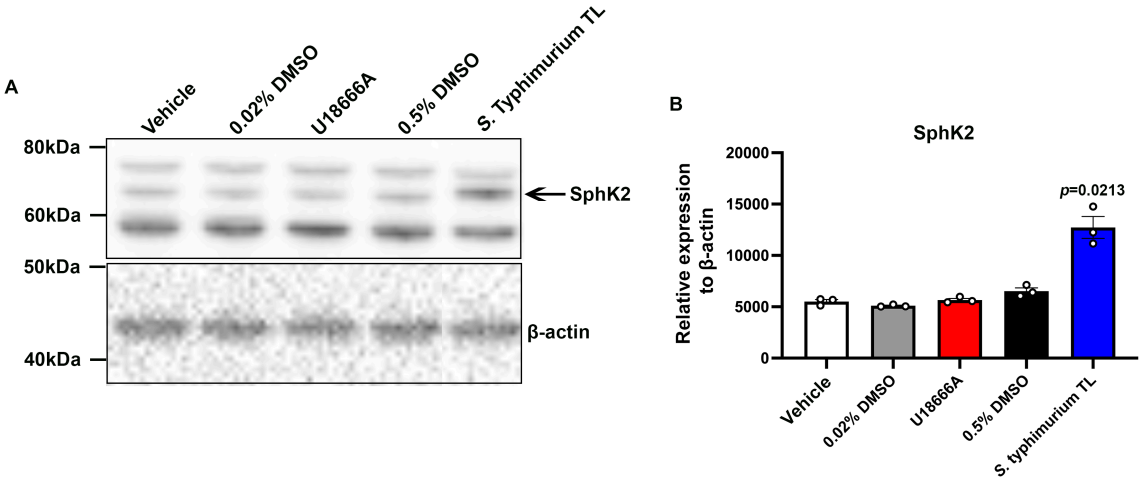
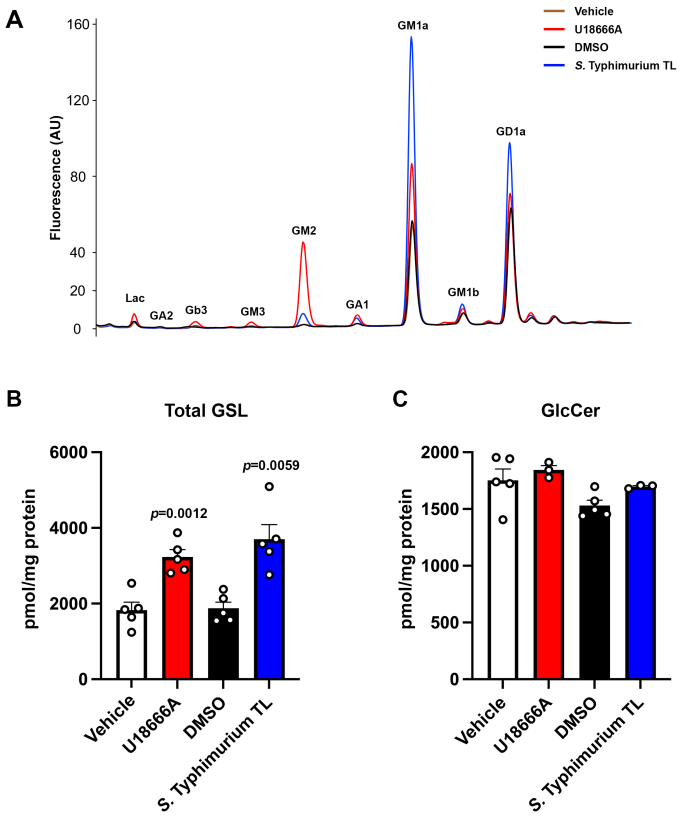


Figure 6.3.24. S. Typhimurium TL increases SphK2 in RAW 264.7 MΦ. RAW 264.7 MΦ were treated with *S.* Typhimurium TL extract (100µg/ml for 48h), DMSO and U18666A (2µg/ml for 48h) treatments were vehicle and positive controls. Panel A. Representative western blot images of SphK2 and β-actin bands. Panel B. Quantification of SphK2 normalised to β-actin. Data are mean ± SEM, n=3. Statistical analysis, Welch's t-test. p values as indicated, otherwise not significant. Statistical comparison of U18666A treatment is relative to vehicle control. Statistical comparison of lipid treatment is relative to 0.5% DMSO control.

6.3.25. *S.* Typhimurium TL extract induces GSL accumulation in RAW 264.7 MΦ.

The GSL content of RAW 264.7 MΦ treated with *S.* Typhimurium TL extract was analysed by NP-HPLC. Representative profiles of GSLs are shown in Fig 6.3.25.A. Total GSL levels were significantly increased with *S.* Typhimurium TL extract treatment (p=0.0059) and exceeded that of U18666A treatment (2µg/ml for 48h) (p=0.0012, Fig 6.3.25.B.). All individual GSL species were also significantly increased by *S.* Typhimurium TL extract treatment (p=0.0366 for Lac, p=0.0196 for GA2, p=0.0076 for Gb3, p=0.0025 for GM3, p=0.0010 for GM2, ****p<0.0001 for GA1, p=0.0024 for GM1a, p=0.0081 for GM1b, p=0.0211 for GD1a, Fig 6.3.25.D.) and mirrored the increases caused by U18666A with the exception of GD1a. No significant changes to GlcCer were detected after U18666A or *S.* Typhimurium TL treatment (Fig 6.3.25.C.). Fold changes of each GSL species with significance values are summarised in Table 6.3.25.



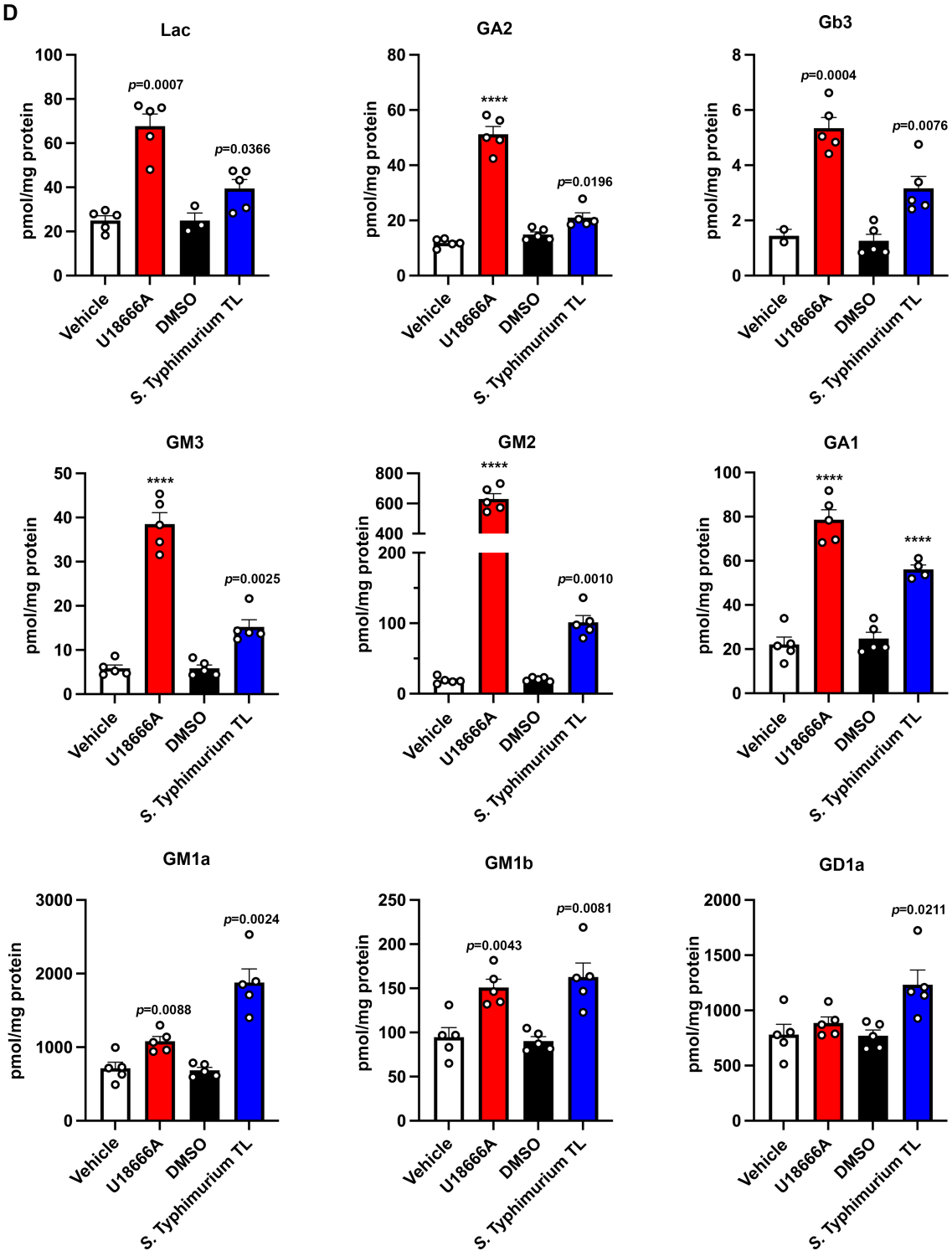

D
Lac
GA2
Gb3
GM3
GM2
GA1
GM1a
GM1b
GD1a
pmol/mg protein
p=0.0007
p=0.0366
****
p=0.0196
p=0.0004
p=0.0076
p=0.0025
p=0.0010
p=0.0088
p=0.0024
p=0.0043
p=0.0081
p=0.0211
Vehicle
U18666A
DMSO
S. Typhimurium TL

Figure 6.3.25. S. Typhimurium TL causes GSL accumulation in RAW 264.7 MΦ.

RAW 264.7 MΦ were treated with *S.* Typhimurium TL extract (100µg/ml for 48h). DMSO and U18666A (2µg/ml for 48h) treatments were vehicle and positive controls respectively. Panel A. Representative HPLC profiles of GSLs in treated cells. Panel B. Quantification of total GSLs. Panel C. Quantification of GlcCer. Panel D. Quantification of individual GSL species in treated cells. Data are mean ± SEM, n=5. Statistical analysis, Welch's t-test. ****$p<0.0001$, other p values as indicated, otherwise not significant. Statistical comparison of U18666A treatment is relative to vehicle control. Statistical comparison of lipid treatment is relative to 0.5% DMSO control. Data are representative of 2 independent experiments.

GSL species	U18666A	*S.* Typhimurium TL
Lac	*p*=0.0007 2.71±0.221	*p*=0.0366 1.58±0.166
GA2	**** 4.32±0.236	*p*=0.0196 1.41±0.155
Gb3	*p*=0.0004 3.70±0.270	*p*=0.0076 2.51±0.342
GM3	**** 6.61±0.440	*p*=0.0025 2.60±0.280
GM2	**** 33.2±1.880	*p*=0.0010 4.98±0.471
GA1	**** 3.55±0.204	**** 2.27±0.083
GM1a	*p*=0.0088 1.52±0.092	*p*=0.0024 2.75±0.270
GM1b	*p*=0.0043 1.60±0.097	*p*=0.0081 1.80±0.175
GD1a	ns 1.13±0.071	*p*=0.0211 1.60±0.171
Total GSL	*p*=0.0012 1.77±0.105	*p*=0.0059 1.97±0.204
GlcCer	ns 1.05±0.022	ns 1.11±0.006

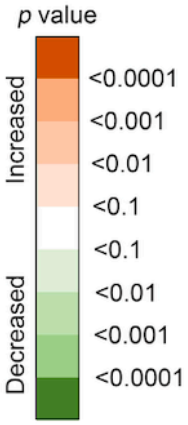


Table 6.3.25. Summary of the fold change and statistical analysis of GSLs in RAW 264.7 MΦ treated with S. Typhimurium TL extract.

Data were normalised to vehicle controls. Data are mean ± SEM, n=5. Statistical analysis, Welch's t-test. ****p<0.0001, other p values as indicated, otherwise not significant. Statistical comparison of U18666A treatment is relative to vehicle control. Statistical comparison of lipid treatment is relative to 0.5% DMSO control. Data are representative of 2 independent experiments. GSLs that are significantly increased are highlighted in red.

6.4. Discussion

In this chapter, we explored whether *S.* Typhimurium inhibits the NPC pathway as a mechanism to establish a protective intracellular niche. We found that the bacterium does indeed induce multiple phenotypes consistent with NPC inhibition. These included; lysosomal expansion, GSL miss-trafficking, sphingoid base and GSL accumulation and cholesterol redistribution. Importantly, the changes did not require specific effector proteins since infection with mutants unable to synthesise or deliver those proteins induced comparable phenotypes to WT *S.* Typhimurium. We also demonstrated that a lipid extract of *S.* Typhimurium was able to induce identical phenotypes. These data are supportive of the hypothesis that *Salmonella* inhibits Npc1 via a microbial lipid component and this, in conjugation with our findings with persistent mycobacterial pathogens, strongly suggests that multiple pathogens may have evolved to target the NPC pathway.

The investigation of *S.* Typhimurium as a candidate intracellular microbe that potentially inhibits the NPC pathway was based upon three lines of evidence in the literature. First, *S.* Typhimurium affects host sterol biosynthesis and induces the accumulation of cholesterol early in infection, which is required for the replication of intracellular bacteria [486, 487]. Bacteria within the SCV are intimately associated with cholesterol and typically are surrounded by the lipid [486]. Second, cholesterol transport and esterification are influenced by the activities of specific effector proteins. Effector proteins are injected by the microbe T3SS into host cells where they interfere with host defence processes to promote survival and replication and have been shown to be critical for

virulence [488, 489]. In a global mapping study of effector protein-host protein interactions, Walch *et al.* demonstrated that NPC1 is recruited to SCV by the effector SifA, interacts with SseJ and is antagonised by SseL [501]. These findings therefore demonstrated a potential link between NPC1 and cholesterol metabolism during *S.* Typhimurium infection but left unresolved whether there is a direct interaction between the lysosomal membrane protein NPC1 and SifA or SseJ and the impact on its function. Finally, a genome-wide screen in human MΦ to identify host factors that modulate *Salmonella* infection pinpointed *NPC1* as one of 183 candidate genes [510].

The experimental approaches undertaken to investigate whether *S.* Typhimurium inhibits Npc1 were those used previously to interrogate *Mtb*. In the absence of a direct assay for Npc1 activity, we examined infected or *S.* Typhimurium lipid-treated MΦ for the induction of a combination of cellular phenotypes downstream of Npc1 inhibition [207].

In order to exclude contributions by effectors that may interact directly or indirectly with Npc1 and therefore complicate the interpretation of data, we made infections with *S.* Typhimurium mutant strains in which the proteins are absent or disabled (Table 6.4.1.). SsaV is a component of SPI-2 that controls the secretion of T3SS effectors [508, 511, 512]. SifA maintains the integrity of the SCV, forming SIFs, and the interaction between SCVs and LE/Lys compartments [491, 513] and has been shown to recruit NPC1 to the vacuole [501]. SseJ is responsible for the esterification of the host cell cholesterol [487, 514] and physically interacts with NPC1 [501]. It should be noted that the activities of effectors encoded with

SPI-1, which are known to include ones that affect the cholesterol [515], did not have to be excluded because they are not required for infection of MΦ [445] and are downregulated during the stationary phase of *S.* Typhimurium growth [516, 517], which was the status of the bacterial cultures used for the infection studies.

Effector	SPI-1	SPI-2	Biochemical Activities	Functions
SsaV	-	+	Structural configuration of T3SS	• Maintain functional T3SS structure
SifA	ND	+	ND	• SIF formation; • Vacuolar membrane partitioning
SseJ	-	+	Acyltransferase	• Cholesterol esterification
SseL	ND	+	Deubiquitinase	• Prevents accumulation of lipid droplets; • Inhibits autophagic clearance of cytosolic aggregates; • Induces late macrophage cell death

Table 6.4.1. Summary of functions of effector proteins from SPI-2.

SPI, *Salmonella* pathogenicity island; T3SS, type 3 secretion system; SIF, *Salmonella*-induced filament; ND, not determined; -, not present; +, present. Adapted from [488, 512].

In summary, infection with each of the mutant strains phenocopied NPC1-deficient cells (Table 6.4.2.).

NPC phenotype	S. Typhimurium infection					S. Typhimurium TL extract
	WT	Δ*ssaV*	Δ*sifA*	Δ*sseJ*	Δ*sifA sseJ*	
LE/Lys expansion by FACS	Not evaluated	Not evaluated	Not evaluated	Not evaluated	Not evaluated	Yes
LE/Lys expansion by LAMP-1 immunostaining	Yes	Yes	Yes	Yes	Yes	Yes
Filipin-positive lysosomal puncta	Yes	Yes	Yes	Yes	Yes	Yes
Total cholesterol level	↑	↑	Not altered	↑	Not altered	Not altered
GM1 mis-trafficking	Yes	Yes	Yes	Yes	Yes	Yes
BODIPY-LacCer mis-trafficking	Not evaluated	Not evaluated	Not evaluated	Not evaluated	Not evaluated	Yes
SphO and SphA level	↑	↑	↑	↑	↑	↑
Total GSL level	↑	↑	↑	↑	↑	↑
NPC1 protein level	Not altered	Not altered	Not altered	Not altered	Not altered	Not altered
NPC1 gene expression	↓	↓	↓	↓	↑	↑
NPC2 protein level	↑	↑	↑	↑	↑	↑
NPC2 gene expression	↓	↓	↓	↓	↑	↑

Table 6.4.2. Summary of NPC cellular phenotypes induced by S. Typhimurium infection and TL extract of S. Typhimurium in RAW 264.7 MΦ.

We demonstrated that *S.* Typhimurium infection resulted in shared phenotypic similarities with NPC1-deficient cells, suggesting inhibition of the NPC pathway. The phenotypes included changes to host cell biology, such as the expansion of the endo-lysosomal system, intracellular cholesterol redistribution and deficits in GSL recycling, together with biochemical changes, including sphingolipid metabolism and GSL accumulation (Table 6.4.2.). At this time, we were unable to examine all of the known NPC phenotypes; for example, the loss of lysosomal Ca^{2+} homeostasis, which could be undertaken in a future confirmatory study [26].

The intracellular re-distribution of cholesterol within infected cell cultures with *S.* Typhimurium highlighted a significant finding in common with *Mtb*-mediated inhibition of the NPC pathway. Intracellular cholesterol re-distribution, as identified by filipin staining, was not restricted to *S.* Typhimurium-infected MΦ but was also present in uninfected bystander cells, as had been observed with pathogenic mycobacteria [96]. We suggested previously that this very likely reflects the inhibition of NPC1 in non-infected cells by the endocytosis of *Mtb* cell wall lipid(s) that are actively trafficked out of infected cells [96, 175]. Although we currently know far less about the potential for the release or shedding of lipids by *S.* Typhimurium, such a mechanism is compatible with the observations. The re-distribution of intracellular cholesterol into puncta occurred when infections were made with both WT and effector protein mutant strains, indicating that they were not essential for the induction of the phenotype.

Interactions between *S.* Typhimurium and the host cell with respect to cholesterol homeostasis are complex and have important roles in pathogenesis. The

bacterium is unable to synthesise the lipids; therefore, host precursor molecules are necessary for optimal survival and manipulation of cholesterol transport enhances bacterial replication [486, 492]. The effector SseJ localised to the SCV is responsible for the esterification of cholesterol stored in lipid droplets [487], as well as interacting with NPC1 [501]. Strains deficient in SseJ are attenuated [493]. It is pertinent that SseJ also manipulates cholesterol by inhibiting the transport protein ABCA1 [494], and the reduction in ABCA1 activity due to mutations is the cause of Tangier disease, in which there is secondary inhibition of NPC1 [518].

Accumulation of cholesterol at SCVs has been visualised in both MΦ and epithelial cells as soon as 2h post-infection, with a significant increase in the amount of cholesterol and the 3β-hydroxysteroid lanosterol at 16h [486]. However, cholesterol accumulation at sites in the infected cell other than at SCV has not been a focus in published studies. We suggested that the expansion of LE/Lys results from the inhibition of Npc1 rather than as a direct effect of effector proteins at LE/Lys.

Inspection of the spatial intimacy between cholesterol and internalised bacteria revealed that for WT, *ΔssaV* and *ΔsseJ* strains, the lipid was enriched in close proximity to internalised *S.* Typhimurium but was not the case for *ΔsifA* or *ΔsifAsseJ* mutants, which has a distribution more compatible with limited accessibility to bacteria. These observations are in agreement with reports that SifA is important for the vacuole stability [488] and that it recruits NPC1 [501]. The level of total cholesterol was also increased following WT, *ΔssaV* and *ΔsseJ* strains, arguing that effectors are not required, and for *ΔsifA* and *ΔsifAsseJ*, there

was a trend to an increase that was not statistically significant, perhaps due to the small sample size. However, we were unable to measure a significant increase in cholesterol content of cells treated with *S.* Typhimurium TL extract, which suggests that infection with bacteria is necessary to induce this phenotype, perhaps because of the requirement for sustained inhibition of NPC1.

Expansion of the acidic compartment in RAW 264.7 MΦ infected with *S.* Typhimurium was revealed by anti-LAMP-1 staining. In uninfected cells, LAMP-1 immunoreactivity is restricted to LE/Lys. But in infected cells, *Salmonella*-containing phagosomes acquire LAMP-1 from Golgi-associated vesicles without fusing with lysosomes, which then matures into late SCVs [464]. We were able to discriminate LAMP-1 positive LE/Lys from LAMP-1 positive SCVs by the absence of co-localised fluorescent bacteria and confirmed that both populations of vacuoles were significantly larger. The size of LE/Lys in uninfected neighbouring cells was also increased, as were those in MΦ infected with *ΔssaV* mutant, demonstrating that expansion is independent of effector proteins.

Consistent with the inhibition of NPC1, infection with all mutants caused miss-localisation of GM1 ganglioside. This ganglioside has been reported to be associated with SCV as evidenced by the recruitment of multiple raft components to bacterial vacuoles [486]. As far as we are aware, there have been few, if any reports of the effect of *Salmonella* on sphingolipid trafficking.

Various lipids are stored in NPC cells, but sphingosine accumulation is the first that is changed and happens within 10min of pharmacological inhibition of Npc1

in RAW 264.7 MΦ [26]. We reasoned that if *S.* Typhimurium also inhibits Npc1, there would be a similar profile of sphingosine accumulation. Analyses confirmed that infection with all *S.* Typhimurium mutant strains resulted in significant increases in sphingosine and sphinganine content, consistent with the hypothesis. Studies have shown that defective *de novo* synthesis of sphingosine increases the intracellular survival of *S.* Typhimurium [519], and the activity of SMase in host cells is antimicrobial [520]. As a result of impaired transport and catabolism, multiple GSL species accumulate in NPC and in *Mtb*-infected cells [6, 96], and infections with WT and effector mutant *S.* Typhimurium strains had equivalent effects.

Although Walch and colleagues found that NPC1 is a target of specific effectors [501], our data showed that bacterial mutants lacking the proteins were still able to induce phenotypes consistent with loss of NPC1 activity. This implies that there are other bacterial components that can inhibit NPC1. Analogous to *Mtb* lipid-mediated inhibition, together with the 'bystander cell effect' observed with *S.* Typhimurium infection, which is lipid-mediated during *Mtb* infection, we investigated whether the same might be true for *S.* Typhimurium. Therefore, a total lipid extract from *S.* Typhimurium was prepared using the same protocol as for mycobacteria and was tested for capacity to promote NPC phenotypes.

Significantly, *S.* Typhimurium TL extract expanded the relative volume of the acidic compartment in RAW 264.7 MΦ and WT CHO cells but not in CHO$^{Npc1-/-}$ cells, which is consistent with the inhibition of Npc1. However, it could not be excluded that another component of the lipid extract might stimulate LE/Lys

enlargement via an NPC1-independent mechanism. LPS is a biologically important constituent of the cell membrane of Gram-negative bacteria such as *S.* Typhimurium and causes endosomal and lysosomal accumulation of cholesterol as a consequence of TLR4 activation [521]. In agreement with this, we measured a dose-dependent increase in LysoTracker™ intensity in RAW 264.7 MΦ after LPS stimulation but not in CHO cells, which are unresponsive [509]. However, *S.* Typhimurium lipid treatment increased LysoTracker™ staining intensity of CHO cells and murine *Tlr4*$^{-/-}$ iBMDMΦ which are unable to respond to endotoxin, demonstrating that LPS was not responsible for the observed lipid extract activity.

A major aim of this study was to determine whether TL extract of *S.* Typhimurium was able to phenocopy infection with *S.* Typhimurium and induce NPC phenotypes, hence providing support for lipid-mediated inhibition of NPC1 in host cells. In summary, our investigations endorsed this proposal because NPC cellular phenotypes, such as the expansion of acidic compartment volume, intracellular cholesterol re-distribution, altered GSL trafficking and sphingoid base and GSL accumulation, were induced (Table 6.4.2.). Importantly, they were frequently induced of a magnitude comparable to those seen with *Mtb* H37Rv lipid extract. The induction of certain NPC phenotypes, such as increased cellular cholesterol content and Npc1 protein, were not obvious. As we reported previously for *Mtb*, infection with the pathogen enhanced cholesterol levels, but a lipid extract did not [96, 207], and the results for *S.* Typhimurium were comparable. *Mtb* H37Rv lipid stimulated Npc1 expression, whereas Npc1 was unchanged and Npc2 increased in response to *S.* Typhimurium TL extract. Interestingly, a higher molecular mass band of Npc2 was observed with both

infection and *S.* Typhimurium TL extract, which could indicate differential glycosylation of Npc2 [497, 522]. But at this point, we are unable to offer a detailed explanation for these findings.

In comparison to mycobacteria, the importance of lipids in *Salmonella* pathogenicity and the actual lipid composition of the bacterium have been poorly explored, which may reflect the predominant interests in LPS and effectors in host-pathogen interactions. Gram-negative cell envelopes compose an inner membrane, which is predominantly composed of phospholipids, a layer of peptidoglycan, and an outer layer membrane of more complex lipids, in which LPS resides (Fig 6.1.1.). Phosphatidylethanolamine (PE), phosphatidylglycerol (PG), and cardiolipin (CL) were also identified on the outer membrane of *S.* Typhimurium [523, 524]. Recently, lipidomic analysis of *Salmonella* serovars has been instigated with the intention of determining molecular diversity and identifying lipid species that may be of particular biological interest [245]. Although at this stage we can only speculate as to the nature of the inhibitory lipid(s), the study by Reink *et al.* provided evidence of functional convergence of lipid species in *Salmonella* and *Mtb* [245]. In a screen to reveal pathogen-specific cell wall components, they identified phosphatidyl trehalose (PT) from *S.* Typhi, which can activate Mincle, an MΦ pattern recognition receptor that also recognises mycobacterial cord factor (6,6'-TDM) [184, 245]. Therefore, it is possible that there could be a comparable convergence of Npc1 inhibitory activities between the two pathogens.

The data presented here and that of Walch *et al.* indicate that *Salmonella* has two distinct mechanisms with which to target the NPC1 protein, which are via effector proteins and lipids. Significantly, there is precedence because of the evidence that NPC1 can recognise both lipids and proteins: binding of cholesterol by Npc1 has been proposed based on structural studies and modelling of interactions with the lipid [525]. NPC1 has also been shown to be an intracellular receptor for the Ebola virus through recognition of the viral glycoprotein that facilitates the escape of the pathogen from the lysosome [526] and forms a tethering complex with the ER-resident lipid transfer protein Gramd1b [34]. Furthermore, the existence of two systems through which *Salmonella* can modulate Npc1 activity would imply that it is a very important host target for the bacterium. It may be that they offer redundancy or that effector or lipid-mediated inhibition operates at specific points during the intracellular survival and replication.

In summary, we have generated evidence consistent with *S.* Typhimurium inhibiting the NPC pathway suggesting that this capacity of *S.* Typhimurium is important for the establishment of its intracellular niche/survival and merits further investigation. Taken together with our findings in *Mtb*, this chapter also reinforces the concept that the NPC pathway may be a common target in host-pathogen interactions.

Chapter 7. Conclusion and Future Studies

The primary objective of the studies described in this thesis was to investigate the targeting of the host NPC pathway by pathogens as a mechanism to promote their intracellular survival. Fineran and colleagues provided the foundation to this work by showing that pathogenic mycobacteria shed lipid(s) that inhibit NPC1 activity [96]. Induction of NPC phenotypes, such as defective trafficking in the endo-lysosomal system, provides an intracellular environment favourable to microbe survival and replication. In this thesis, we observed that mycobacterial lipid(s) components that can block NPC1 activity are widely distributed amongst clinically relevant *Mtb* strains and are present in other tubercular and non-tubercular species that cause diseases. Furthermore, the NPC1 inhibitory activity was absent from *M. canettii*, a species that infrequently causes infection and resembles a progenitor from which the *Mtb* complex evolved, indicating that the evolution of the inhibitory lipid was likely concurrent with the transition to pathogenicity. These studies have been published in the journal Nature Communications [207] (see Appendix 1).

As inhibition of the NPC pathway could also be beneficial for other intracellular pathogens, we confirmed that *S.* Typhimurium was also capable of lipid-mediated induction of NPC phenotypes in host cells. Interestingly, *S.* Typhimurium ostensibly has two distinct mechanisms that inhibit NPC1: one is through specific effector proteins, and the second is lipid-dependent [501], implying that affecting the NPC pathway is important. Furthermore, the range of micro-organisms that may target the pathway has now been extended further to include *Burkholderia pseudomallei* (*B. pseudomallei*) because recent studies in the laboratory have shown that bacterial lipid extracts increase acidic compartment volume in treated

RAW 264.7 MΦ (see Appendix 2). Therefore, including mycobacteria, we have found three genetically distinct microbes (Fig 7.) that could target the NPC pathway, indicating the importance of NPC pathway in host-pathogen interaction.

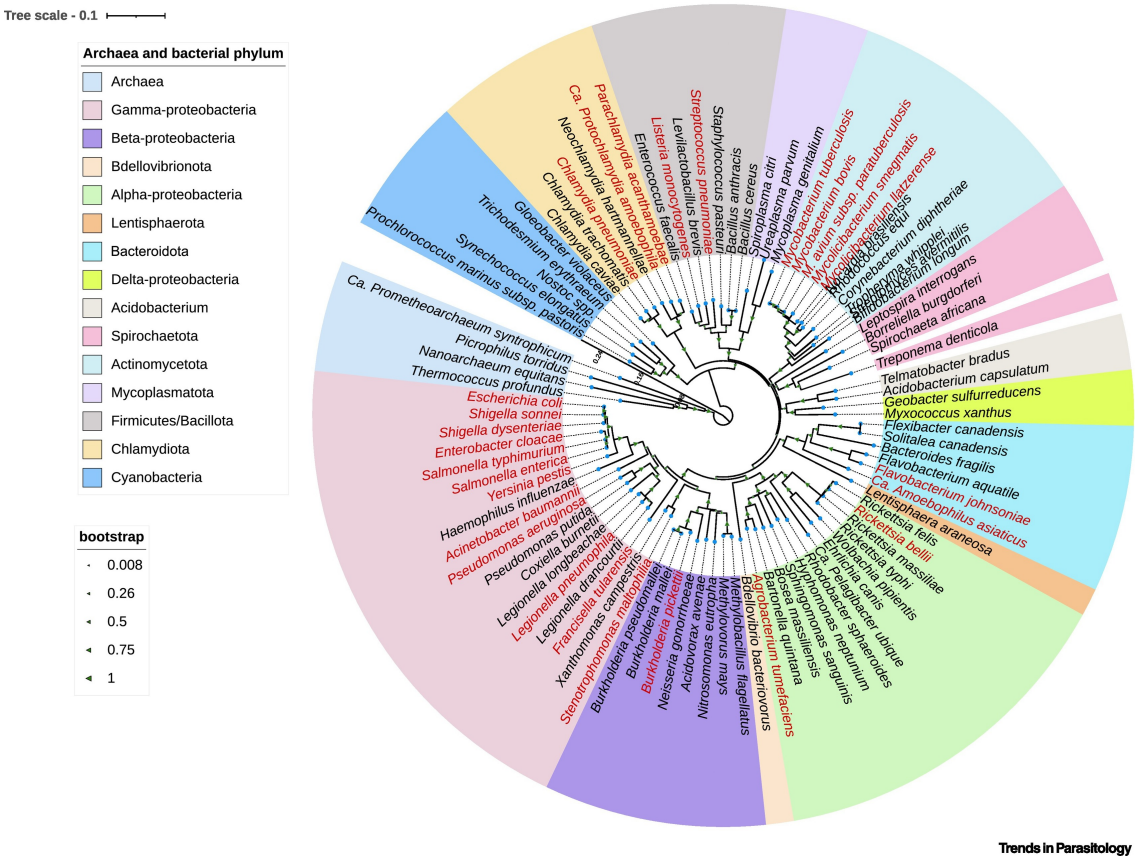


Figure 7. Some selected human pathogens able to resist Acanthamoeba phagocytosis in the phylogenetic tree of prokaryotes.

The 16S rRNA nucleotide sequences of published amoeba-resisting bacteria (ARBs) and four archaea were retrieved from the NCBI GenBank database, aligned using CLUSTALW and the phylogenetic tree was reconstructed using Kimura parameter with 1000 bootstraps using MEGAX. The phylogenetic tree was rooted between bacteria and archaea and visualised using iTOLv6. *Acanthamoeba* digestion-resistant bacteria (shown in red) do not belong to a specific phylum but are dispersed to different phylogenetic clades in the prokaryotic tree. Adapted from [527].

Our experimental approach of examining for phenotypes that result from loss of NPC1 function as a proxy for inhibition was necessary because of the absence of a direct functional assay for NPC1/NPC pathway. As we have discussed previously in this thesis, NPC cannot be confirmed unambiguously by the presentation of a single phenotype but requires measuring multiple phenotypes that in combination are unique to NPC disease. A crucial NPC cellular phenotype is the reduced Ca^{2+} content of the lysosome, which results in insufficient release and, as a consequence, impaired intracellular trafficking and other defects. In the original study that verified loss of lysosomal Ca^{2+} homeostasis in NPC, a commercial low-affinity Rhod-dextran Ca^{2+} probe facilitated ion determination in a relatively high-throughput manner [26]. Unfortunately, this reagent was discontinued and measuring lysosomal Ca^{2+} homeostasis using other methodologies is not straightforward [528]. In the subsequent investigation that revealed the mechanistic link between the genetic disease and pathogenic mycobacteria, acidic store Ca^{2+} analysis was made collaboratively and required loading of cells with fluorescent dye (fura 2-AM) and assessing release by imaging individual cells using dedicated equipment and software [96]. Hence, we reasoned that it was not practical to perform these measurements as part of our studies. However, because the deficit in lysosomal Ca^{2+} is important evidence of NPC1 inhibition, we suggest that corroboration of the Ca^{2+} phenotype should be undertaken in future studies and if a suitable chemical probe becomes available, it could even become a primary screen for identifying other microbial candidates that target the NPC pathway.

We were able to extend the analysis of some NPC cellular phenotypes that result from microbial lipid inhibition beyond those in previous reports. For example, we interrogated changes in the abundance of individual GSLs in addition to total GSLs and made more detailed studies of sphingolipid metabolism. Because lipids, such as S1P, are signalling molecules, they have the potential to impact host responses more broadly and, therefore, provide useful leads for further investigations.

Another goal for our studies was to identify the lipid(s) species from the *Mtb* cell wall that inhibits the host cell NPC pathway. This was perhaps over-ambitious given the amount of starting material required and the time available and the impact of the pandemic, but at a minimum we were able to undertake a proof-of-principle study that established a protocol that could be the basis for future in depth studies. It is probable that the inclusion of additional separation steps will be necessary to provide sufficiently pure lipids, and this will require starting with an *Mtb* culture that is much larger in volume, e.g. 10 litres. Testing commercially available “purified” lipid components identified several active lipid species, such as SL-1 and PIMs that could induce at least some NPC phenotypes. Some of these enriched fractions were pure single components, which is a challenge for data interpretation. It would be of interest to delineate how these lipids contribute to pathogenicity in addition to the mechanism responsible for Npc1 inhibition. Both NPC1 and NPC2 protein levels are increased by lipids or infection with different pathogens, which may indicate that the activities of both proteins are affected, implicating the importance of the NPC pathway during infection (Table 7.).

	NPC1	NPC2
Mtb H37Rv TL extract	↑	↑ ns
SL-1	-	↑
TDM	-	-
$PIM_{1,2}$	-	-
PIM_6	↑	↑
WT *S.* Typhimurium infection	-	↑
WT *S.* Typhimurium TL extract	-	↑

Table 7. Summary of alteration in NPC1 and NPC2 levels in RAW 264.7 MΦ treated with bacterial lipid(s) or bacterial infection.

NPC1 and NPC2 protein levels summarised based on the quantification by western blotting. ↑, increase; -, not altered; ns, not statistically significant; TL, total lipid; SL-1, sulpholipid-1; TDM, trehalose di-mycolate; PIM, phosphatidylinositol mannose.

Independent confirmation of active lipid(s) using approaches such as the generation of mutant strains and chemical synthesis will be essential. We will also collaborate with Professor Carol Robinson's group in the Department of Chemistry at the University of Oxford to perform native MS of NPC1, expressing the protein in mammalian cells with and without exposure to microbial lipid extracts to determine which lipids bind and where they bind. When this has been achieved, it should be more straightforward to determine the distribution of the lipid across mycobacterial species and strains. In particular, it will facilitate detailed investigations of host-pathogen interactions that involve inhibition of NPC1 as well as the structural basis for lipid-NPC1 binding.

Our focus was to obtain evidence of microbial inhibition of NPC1 by documenting the induction of NPC cellular phenotypes. A complementary approach that will address the broader consequences will be to investigate whether inhibition of NPC1 is responsible for the multiple changes in host cells that characterise *Mtb* infection. Pathogenic mycobacteria manipulate other MΦ activities, such as lysosome biogenesis, generation of reactive oxygen and nitrogen intermediates, autophagy and antigen presentation to establish a protective environment [529]. These could be investigated by examining for the capacity of lipid extracts or specific lipids to mimic the effects of the microbe and also whether comparable phenotypes occur in *Npc1*-deficient cells. We hypothesise that inhibition of Npc1 may be upstream of multiple pathogen-induced phenotypes.

The relevance of the findings presented here would be further reinforced by *in vivo* studies. Indeed, there are a wide range of investigations that could be made. For example, mycobacterial lipids can be delivered via injection of lipid-coated beads or gel matrix, and the induction of NPC phenotypes and host responses can be analysed. Strains deficient in lipids that inhibit NPC1 would be predicted to display impaired pathogenicity. In the reverse situation, the prediction would be that *Npc1*$^{-/-}$ mice will be unable to clear strains of bacteria that do not normally persist, such as *M. smegmatis*. Ultimately, it will be important to conduct investigations in human TB disease to corroborate the importance of NPC1 as one of the most upregulated genes in a study of the human granuloma [178].

An unbiased experimental scheme with respect to the inhibition of NPC1 would have the potential to complement the experimental approaches used in this

thesis and reveal unexpected consequences. Recently, RNA-sequencing of RAW 264.7 MΦ treated with *Mtb* lipid extract or U18666A was performed in the laboratory (Shepherd *et al.*, unpublished). Initial analysis has confirmed a greater than 80% overlap in genes whose expression was significantly changed by both treatments (see Appendix 3), strongly suggesting that NPC1 is the target of U18666A and *Mtb* lipid(s). Deeper analysis of this data set has the potential to identify novel pathways that are affected.

An exciting prospect that may be realised as a result of the studies initiated in this thesis is the potential of exploring the NPC pathway as an anti-microbial strategy. It would be a host-directed approach and, therefore, not subject to the evolution of microbial resistance, which is a reason why with time, drugs directly against microbes lose their effectiveness. We hypothesise that compounds that could relieve microbial inhibition of NPC1 would restore the normal function of the endo-lysosomal system and promote the destruction of the pathogen. Importantly, because our data implicate multiple pathogens in the inhibition of the NPC pathway, the approach could target multiple infectious agents. The Platt laboratory has pioneered therapies for NPC; the GSL biosynthesis inhibitor, miglustat, is clinically approved [530], and curcumin has been confirmed to provide benefit in a mouse model of NPC [26], with curcumin being a potential therapeutic approach for TB treatment indicated in several published studies [195, 531, 532]. Curcumin is a weak SERCA antagonist and can therefore transiently elevate cytosolic Ca^{2+}, compensating for the attenuated release of Ca^{2+} from the lysosome in NPC. Indeed, curcumin is beneficial in a mouse model of NPC1 deficiency for this reason [26].

In conclusion, in this thesis, we have provided evidence that the NPC pathway is a target of several intracellular pathogens that impact significantly upon global health and, as a result, highlighted the potential to exploit existing NPC therapeutics as host-directed anti-microbial treatments.

Bibliography

1. Trivedi, P.C., J.J. Bartlett, and T. Pulinilkunnil, *Lysosomal Biology and Function: Modern View of Cellular Debris Bin.* Cells, 2020. **9**(5).
2. Ballabio, A. and J.S. Bonifacino, *Lysosomes as dynamic regulators of cell and organismal homeostasis.* Nat Rev Mol Cell Biol, 2020. **21**(2): p. 101-118.
3. Settembre, C., et al., *Signals from the lysosome: a control centre for cellular clearance and energy metabolism.* Nat Rev Mol Cell Biol, 2013. **14**(5): p. 283-96.
4. Morgan, A.J., et al., *Molecular mechanisms of endolysosomal Ca2+ signalling in health and disease.* Biochem J, 2011. **439**(3): p. 349-74.
5. Sachdeva, K. and V. Sundaramurthy, *The Interplay of Host Lysosomes and Intracellular Pathogens.* Front Cell Infect Microbiol, 2020. **10**: p. 595502.
6. Platt, F.M., et al., *Lysosomal storage diseases.* Nat Rev Dis Primers, 2018. **4**(1): p. 27.
7. Parenti, G., D.L. Medina, and A. Ballabio, *The rapidly evolving view of lysosomal storage diseases.* EMBO Mol Med, 2021. **13**(2): p. e12836.
8. Rajkumar, V. and V. Dumpa, *Lysosomal Storage Disease*, in *StatPearls*. 2023: Treasure Island (FL).
9. Castillon, G., S.C. Chang, and Y. Moride, *Global Incidence and Prevalence of Gaucher Disease: A Targeted Literature Review.* J Clin Med, 2022. **12**(1).
10. Mehta, A., *Epidemiology and natural history of Gaucher's disease.* Eur J Intern Med, 2006. **17 Suppl**: p. S2-5.
11. Vanier, M.T., *Niemann-Pick disease type C.* Orphanet J Rare Dis, 2010. **5**: p. 16.
12. Winsor, E.J. and J.P. Welch, *Genetic and demographic aspects of Nova Scotia Niemann-Pick disease (type D).* Am J Hum Genet, 1978. **30**(5): p. 530-8.

13. Greer, W.L., et al., *The Nova Scotia (type D) form of Niemann-Pick disease is caused by a G3097-->T transversion in NPC1.* Am J Hum Genet, 1998. **63**(1): p. 52-4.
14. Schuchman, E.H., et al., *Structural organization and complete nucleotide sequence of the gene encoding human acid sphingomyelinase (SMPD1).* Genomics, 1992. **12**(2): p. 197-205.
15. Schuchman, E.H. and R.J. Desnick, *Types A and B Niemann-Pick disease.* Mol Genet Metab, 2017. **120**(1-2): p. 27-33.
16. McGovern, M.M., et al., *Morbidity and mortality in type B Niemann-Pick disease.* Genet Med, 2013. **15**(8): p. 618-23.
17. McGovern, M.M., et al., *Disease manifestations and burden of illness in patients with acid sphingomyelinase deficiency (ASMD).* Orphanet J Rare Dis, 2017. **12**(1): p. 41.
18. McGovern, M.M., et al., *Prospective study of the natural history of chronic acid sphingomyelinase deficiency in children and adults: eleven years of observation.* Orphanet J Rare Dis, 2021. **16**(1): p. 212.
19. Qureshi, K., et al., *Niemann-Pick Disease Type A: A Rare Disease With a Fatal Outcome.* Cureus, 2022. **14**(2): p. e21955.
20. Raddadi, A.A. and A.A. Al Twaim, *Type A Niemann-Pick disease.* J Eur Acad Dermatol Venereol, 2000. **14**(4): p. 301-3.
21. Wasserstein, M.P., et al., *Olipudase alfa for treatment of acid sphingomyelinase deficiency (ASMD): safety and efficacy in adults treated for 30 months.* J Inherit Metab Dis, 2018. **41**(5): p. 829-838.
22. Patterson, M., *Niemann-Pick Disease Type C.*, G. [Internet], Editor. 2000 Jan 26: Seattle (WA): University of Washington, Seattle.
23. Patterson, M.C., et al., *Long-term survival outcomes of patients with Niemann-Pick disease type C receiving miglustat treatment: A large retrospective observational study.* J Inherit Metab Dis, 2020. **43**(5): p. 1060-1069.
24. Vanier, M.T., *Complex lipid trafficking in Niemann-Pick disease type C.* J Inherit Metab Dis, 2015. **38**(1): p. 187-99.
25. Vanier, M.T. and P. Latour, *Laboratory diagnosis of Niemann-Pick disease type C: the filipin staining test.* Methods Cell Biol, 2015. **126**: p. 357-75.

26. Lloyd-Evans, E., et al., *Niemann-Pick disease type C1 is a sphingosine storage disease that causes deregulation of lysosomal calcium.* Nat Med, 2008. **14**(11): p. 1247-55.
27. Watari, H., et al., *Niemann-Pick C1 protein: obligatory roles for N-terminal domains and lysosomal targeting in cholesterol mobilization.* Proc Natl Acad Sci U S A, 1999. **96**(3): p. 805-10.
28. Xu, S., et al., *Structural basis of sterol binding by NPC2, a lysosomal protein deficient in Niemann-Pick type C2 disease.* J Biol Chem, 2007. **282**(32): p. 23525-31.
29. Scott, C. and Y.A. Ioannou, *The NPC1 protein: structure implies function.* Biochim Biophys Acta, 2004. **1685**(1-3): p. 8-13.
30. Pfeffer, S.R., *NPC intracellular cholesterol transporter 1 (NPC1)-mediated cholesterol export from lysosomes.* J Biol Chem, 2019. **294**(5): p. 1706-1709.
31. Qian, H., et al., *Structural Basis of Low-pH-Dependent Lysosomal Cholesterol Egress by NPC1 and NPC2.* Cell, 2020. **182**(1): p. 98-111 e18.
32. Hodoscek, M. and N. Elghobashi-Meinhardt, *Simulations of NPC1(NTD):NPC2 Protein Complex Reveal Cholesterol Transfer Pathways.* Int J Mol Sci, 2018. **19**(9).
33. Kwon, H.J., et al., *Structure of N-terminal domain of NPC1 reveals distinct subdomains for binding and transfer of cholesterol.* Cell, 2009. **137**(7): p. 1213-24.
34. Hoglinger, D., et al., *NPC1 regulates ER contacts with endocytic organelles to mediate cholesterol egress.* Nat Commun, 2019. **10**(1): p. 4276.
35. Lu, F., et al., *Identification of NPC1 as the target of U18666A, an inhibitor of lysosomal cholesterol export and Ebola infection.* Elife, 2015. **4**.
36. Platt, F.M., *The expanding boundaries of sphingolipid lysosomal storage diseases; insights from Niemann-Pick disease type C.* Biochem Soc Trans, 2023. **51**(5): p. 1777-1787.
37. Newton, J., et al., *Targeting defective sphingosine kinase 1 in Niemann-Pick type C disease with an activator mitigates cholesterol accumulation.* J Biol Chem, 2020. **295**(27): p. 9121-9133.

38. Fan, M., et al., *Identification of Niemann-Pick C1 disease biomarkers through sphingolipid profiling.* J Lipid Res, 2013. **54**(10): p. 2800-14.
39. Wheeler, S., R. Schmid, and D.J. Sillence, *Lipid(-)Protein Interactions in Niemann(-)Pick Type C Disease: Insights from Molecular Modeling.* Int J Mol Sci, 2019. **20**(3).
40. Altuzar, J., et al., *Lysosome-targeted multifunctional lipid probes reveal the sterol transporter NPC1 as a sphingosine interactor.* Proc Natl Acad Sci U S A, 2023. **120**(11): p. e2213886120.
41. Christensen, K.A., J.T. Myers, and J.A. Swanson, *pH-dependent regulation of lysosomal calcium in macrophages.* J Cell Sci, 2002. **115**(Pt 3): p. 599-607.
42. Gerasimenko, J.V., et al., *Calcium uptake via endocytosis with rapid release from acidifying endosomes.* Curr Biol, 1998. **8**(24): p. 1335-8.
43. Raffaello, A., et al., *Calcium at the Center of Cell Signaling: Interplay between Endoplasmic Reticulum, Mitochondria, and Lysosomes.* Trends Biochem Sci, 2016. **41**(12): p. 1035-1049.
44. Garrity, A.G., et al., *The endoplasmic reticulum, not the pH gradient, drives calcium refilling of lysosomes.* Elife, 2016. **5**.
45. Lloyd-Evans, E. and H. Waller-Evans, *Lysosomal Ca(2+) Homeostasis and Signaling in Health and Disease.* Cold Spring Harb Perspect Biol, 2020. **12**(6).
46. Churchill, G.C., et al., *NAADP mobilizes Ca(2+) from reserve granules, lysosome-related organelles, in sea urchin eggs.* Cell, 2002. **111**(5): p. 703-8.
47. Galione, A., et al., *NAADP as an intracellular messenger regulating lysosomal calcium-release channels.* Biochem Soc Trans, 2010. **38**(6): p. 1424-31.
48. Calcraft, P.J., et al., *NAADP mobilizes calcium from acidic organelles through two-pore channels.* Nature, 2009. **459**(7246): p. 596-600.
49. Ruas, M., et al., *Purified TPC isoforms form NAADP receptors with distinct roles for Ca(2+) signaling and endolysosomal trafficking.* Curr Biol, 2010. **20**(8): p. 703-9.
50. Cheng, X., et al., *Mucolipins: Intracellular TRPML1-3 channels.* FEBS Lett, 2010. **584**(10): p. 2013-21.

51. Pitt, S.J., et al., *TPC2 is a novel NAADP-sensitive Ca2+ release channel, operating as a dual sensor of luminal pH and Ca2+.* J Biol Chem, 2010. **285**(45): p. 35039-46.
52. Luzio, J.P., P.R. Pryor, and N.A. Bright, *Lysosomes: fusion and function.* Nat Rev Mol Cell Biol, 2007. **8**(8): p. 622-32.
53. Morgan, A.J., L.C. Davis, and A. Galione, *Choreographing endo-lysosomal Ca(2+) throughout the life of a phagosome.* Biochim Biophys Acta Mol Cell Res, 2021. **1868**(7): p. 119040.
54. Elkin, S.R., A.M. Lakoduk, and S.L. Schmid, *Endocytic pathways and endosomal trafficking: a primer.* Wien Med Wochenschr, 2016. **166**(7-8): p. 196-204.
55. Gruenberg, J., *The endocytic pathway: a mosaic of domains.* Nat Rev Mol Cell Biol, 2001. **2**(10): p. 721-30.
56. Pfeffer, S.R., *Rab GTPase regulation of membrane identity.* Curr Opin Cell Biol, 2013. **25**(4): p. 414-9.
57. Wilson, J.M., et al., *EEA1, a tethering protein of the early sorting endosome, shows a polarized distribution in hippocampal neurons, epithelial cells, and fibroblasts.* Mol Biol Cell, 2000. **11**(8): p. 2657-71.
58. Scott, C.C., F. Vacca, and J. Gruenberg, *Endosome maturation, transport and functions.* Semin Cell Dev Biol, 2014. **31**: p. 2-10.
59. Han, J., K. Pluhackova, and R.A. Bockmann, *The Multifaceted Role of SNARE Proteins in Membrane Fusion.* Front Physiol, 2017. **8**: p. 5.
60. Pryor, P.R., et al., *The role of intraorganellar Ca(2+) in late endosome-lysosome heterotypic fusion and in the reformation of lysosomes from hybrid organelles.* J Cell Biol, 2000. **149**(5): p. 1053-62.
61. Raiborg, C. and H. Stenmark, *The ESCRT machinery in endosomal sorting of ubiquitylated membrane proteins.* Nature, 2009. **458**(7237): p. 445-52.
62. Bright, N.A., M.J. Gratian, and J.P. Luzio, *Endocytic delivery to lysosomes mediated by concurrent fusion and kissing events in living cells.* Curr Biol, 2005. **15**(4): p. 360-5.
63. Blom, T.S., et al., *Defective endocytic trafficking of NPC1 and NPC2 underlying infantile Niemann-Pick type C disease.* Hum Mol Genet, 2003. **12**(3): p. 257-72.

64. Zhang, M., et al., *Cessation of rapid late endosomal tubulovesicular trafficking in Niemann-Pick type C1 disease.* Proc Natl Acad Sci U S A, 2001. **98**(8): p. 4466-71.
65. Huynh, K.K., E. Gershenzon, and S. Grinstein, *Cholesterol accumulation by macrophages impairs phagosome maturation.* J Biol Chem, 2008. **283**(51): p. 35745-55.
66. Ko, D.C., et al., *Dynamic movements of organelles containing Niemann-Pick C1 protein: NPC1 involvement in late endocytic events.* Mol Biol Cell, 2001. **12**(3): p. 601-14.
67. Ikonen, E., *Cellular cholesterol trafficking and compartmentalization.* Nat Rev Mol Cell Biol, 2008. **9**(2): p. 125-38.
68. Brown, M.S. and J.L. Goldstein, *A receptor-mediated pathway for cholesterol homeostasis.* Science, 1986. **232**(4746): p. 34-47.
69. Cerqueira, N.M., et al., *Cholesterol Biosynthesis: A Mechanistic Overview.* Biochemistry, 2016. **55**(39): p. 5483-5506.
70. Chen, L., et al., *Molecular mechanisms for ABCA1-mediated cholesterol efflux.* Cell Cycle, 2022. **21**(11): p. 1121-1139.
71. Pfisterer, S.G., J. Peranen, and E. Ikonen, *LDL-cholesterol transport to the endoplasmic reticulum: current concepts.* Curr Opin Lipidol, 2016. **27**(3): p. 282-7.
72. Chang, T.Y., et al., *Acyl-coenzyme A:cholesterol acyltransferases.* Am J Physiol Endocrinol Metab, 2009. **297**(1): p. E1-9.
73. Boadu, E., R.C. Nelson, and G.A. Francis, *ABCA1-dependent mobilization of lysosomal cholesterol requires functional Niemann-Pick C2 but not Niemann-Pick C1 protein.* Biochim Biophys Acta, 2012. **1821**(3): p. 396-404.
74. Wang, M.D., et al., *Differential regulation of ATP binding cassette protein A1 expression and ApoA-I lipidation by Niemann-Pick type C1 in murine hepatocytes and macrophages.* J Biol Chem, 2007. **282**(31): p. 22525-33.
75. Wilhelm, L.P., et al., *STARD3 mediates endoplasmic reticulum-to-endosome cholesterol transport at membrane contact sites.* EMBO J, 2017. **36**(10): p. 1412-1433.

76. Zhao, K. and N.D. Ridgway, *Oxysterol-Binding Protein-Related Protein 1L Regulates Cholesterol Egress from the Endo-Lysosomal System.* Cell Rep, 2017. **19**(9): p. 1807-1818.
77. Kennedy, B.E., M. Charman, and B. Karten, *Niemann-Pick Type C2 protein contributes to the transport of endosomal cholesterol to mitochondria without interacting with NPC1.* J Lipid Res, 2012. **53**(12): p. 2632-42.
78. te Vruchte, D., et al., *Accumulation of glycosphingolipids in Niemann-Pick C disease disrupts endosomal transport.* J Biol Chem, 2004. **279**(25): p. 26167-75.
79. Schnaar, R.L., Sandhoff, R., Tiemeyer, M., and Kinoshita, T, *Essentials of Glycobiology*, in *Essentials of Glycobiology*, A. Varki, et al., Editors. 2022: Cold Spring Harbor (NY).
80. Ryckman, A.E., I. Brockhausen, and J.S. Walia, *Metabolism of Glycosphingolipids and Their Role in the Pathophysiology of Lysosomal Storage Disorders.* Int J Mol Sci, 2020. **21**(18).
81. Platt, F.M., *Sphingolipid lysosomal storage disorders.* Nature, 2014. **510**(7503): p. 68-75.
82. Salvioli, R., et al., *Glucosylceramidase mass and subcellular localization are modulated by cholesterol in Niemann-Pick disease type C.* J Biol Chem, 2004. **279**(17): p. 17674-80.
83. Puri, V., et al., *Cholesterol modulates membrane traffic along the endocytic pathway in sphingolipid-storage diseases.* Nat Cell Biol, 1999. **1**(6): p. 386-8.
84. Wallom, K.L., et al., *Glycosphingolipid metabolism and its role in ageing and Parkinson's disease.* Glycoconj J, 2022. **39**(1): p. 39-53.
85. Platt, F.M. and M. Jeyakumar, *Substrate reduction therapy.* Acta Paediatr, 2008. **97**(457): p. 88-93.
86. Lachmann, R.H. and F.M. Platt, *Substrate reduction therapy for glycosphingolipid storage disorders.* Expert Opin Investig Drugs, 2001. **10**(3): p. 455-66.
87. Patterson, M.C., et al., *Treatment outcomes following continuous miglustat therapy in patients with Niemann-Pick disease Type C: a final report of the NPC Registry.* Orphanet J Rare Dis, 2020. **15**(1): p. 104.

88. Mengel, E., et al., *Efficacy and safety of arimoclomol in Niemann-Pick disease type C: Results from a double-blind, randomised, placebo-controlled, multinational phase 2/3 trial of a novel treatment.* J Inherit Metab Dis, 2021. **44**(6): p. 1463-1480.
89. Sitarska, D., A. Tylki-Szymanska, and A. Lugowska, *Treatment trials in Niemann-Pick type C disease.* Metab Brain Dis, 2021. **36**(8): p. 2215-2221.
90. Carette, J.E., et al., *Ebola virus entry requires the cholesterol transporter Niemann-Pick C1.* Nature, 2011. **477**(7364): p. 340-3.
91. Herbert, A.S., et al., *Niemann-pick C1 is essential for ebolavirus replication and pathogenesis in vivo.* mBio, 2015. **6**(3): p. e00565-15.
92. Ng, M., et al., *Filovirus receptor NPC1 contributes to species-specific patterns of ebolavirus susceptibility in bats.* Elife, 2015. **4**.
93. John, L., et al., *Redirecting Imipramine against Bluetongue Virus Infection: Insights from a Genome-wide Haploid Screening Study.* Pathogens, 2022. **11**(5).
94. Garcia-Dorival, I., et al., *Identification of Niemann-Pick C1 protein as a potential novel SARS-CoV-2 intracellular target.* Antiviral Res, 2021. **194**: p. 105167.
95. Coleman, E.M., T.N. Walker, and J.E. Hildreth, *Loss of Niemann Pick type C proteins 1 and 2 greatly enhances HIV infectivity and is associated with accumulation of HIV Gag and cholesterol in late endosomes/lysosomes.* Virol J, 2012. **9**: p. 31.
96. Fineran, P., et al., *Pathogenic mycobacteria achieve cellular persistence by inhibiting the Niemann-Pick Type C disease cellular pathway.* Wellcome Open Res, 2016. **1**: p. 18.
97. Bagcchi, S., *WHO's Global Tuberculosis Report 2022.* Lancet Microbe, 2023. **4**(1): p. e20.
98. Glaziou, P., et al., *Global epidemiology of tuberculosis.* Cold Spring Harb Perspect Med, 2014. **5**(2): p. a017798.
99. Lei, Y., et al., *Geographical evolutionary pathway of global tuberculosis incidence trends.* BMC Public Health, 2023. **23**(1): p. 755.
100. Pai, M., et al., *Tuberculosis.* Nat Rev Dis Primers, 2016. **2**: p. 16076.
101. Dheda, K., C.E. Barry, 3rd, and G. Maartens, *Tuberculosis.* Lancet, 2016. **387**(10024): p. 1211-26.

102. Suarez, I., et al., *The Diagnosis and Treatment of Tuberculosis.* Dtsch Arztebl Int, 2019. **116**(43): p. 729-735.
103. Andrews, J.R., et al., *Risk of progression to active tuberculosis following reinfection with Mycobacterium tuberculosis.* Clin Infect Dis, 2012. **54**(6): p. 784-91.
104. Getahun, H., et al., *Management of latent Mycobacterium tuberculosis infection: WHO guidelines for low tuberculosis burden countries.* Eur Respir J, 2015. **46**(6): p. 1563-76.
105. Kiazyk, S. and T.B. Ball, *Latent tuberculosis infection: An overview.* Can Commun Dis Rep, 2017. **43**(3-4): p. 62-66.
106. den Boon, S., *Guidelines on the Management of Latent Tuberculosis Infection*, in *Guidelines on the Management of Latent Tuberculosis Infection*. 2015: Geneva.
107. Drain, P.K., et al., *Incipient and Subclinical Tuberculosis: a Clinical Review of Early Stages and Progression of Infection.* Clin Microbiol Rev, 2018. **31**(4).
108. Okafor, C.N., A. Rewane, and Momodu, II, *Bacillus Calmette Guerin*, in *StatPearls*. 2023: Treasure Island (FL).
109. Abubakar, I., et al., *Systematic review and meta-analysis of the current evidence on the duration of protection by bacillus Calmette-Guerin vaccination against tuberculosis.* Health Technol Assess, 2013. **17**(37): p. 1-372, v-vi.
110. Mangtani, P., et al., *Protection by BCG vaccine against tuberculosis: a systematic review of randomized controlled trials.* Clin Infect Dis, 2014. **58**(4): p. 470-80.
111. Tran, V., J. Liu, and M.A. Behr, *BCG Vaccines.* Microbiol Spectr, 2014. **2**(1): p. MGM2-0028-2013.
112. Furin, J., H. Cox, and M. Pai, *Tuberculosis.* Lancet, 2019. **393**(10181): p. 1642-1656.
113. Perrin, C., et al., *Recently developed drugs for the treatment of drug-resistant tuberculosis: a research and development case study.* BMJ Glob Health, 2022. **7**(4).
114. Gutierrez, M.C., et al., *Ancient origin and gene mosaicism of the progenitor of Mycobacterium tuberculosis.* PLoS Pathog, 2005. **1**(1): p. e5.

115. Barberis, I., et al., *The history of tuberculosis: from the first historical records to the isolation of Koch's bacillus.* J Prev Med Hyg, 2017. **58**(1): p. E9-E12.
116. Han, X.Y., et al., *A new Mycobacterium species causing diffuse lepromatous leprosy.* Am J Clin Pathol, 2008. **130**(6): p. 856-64.
117. Kim, C.J., et al., *Differentiating rapid- and slow-growing mycobacteria by difference in time to growth detection in liquid media.* Diagn Microbiol Infect Dis, 2013. **75**(1): p. 73-6.
118. Johansen, M.D., J.L. Herrmann, and L. Kremer, *Non-tuberculous mycobacteria and the rise of Mycobacterium abscessus.* Nat Rev Microbiol, 2020. **18**(7): p. 392-407.
119. Sharma, S.K. and V. Upadhyay, *Epidemiology, diagnosis & treatment of non-tuberculous mycobacterial diseases.* Indian J Med Res, 2020. **152**(3): p. 185-226.
120. Prasanna, A.N.a.M., S. , *Comprehensive Phylogenetic Analysis of Mycobacteria.* IFAC Proceedings Volumes, 2013. **46**(31): p. 101-106.
121. Prasanna, A.N. and S. Mehra, *Comparative phylogenomics of pathogenic and non-pathogenic mycobacterium.* PLoS One, 2013. **8**(8): p. e71248.
122. Gupta, R.S., B. Lo, and J. Son, *Phylogenomics and Comparative Genomic Studies Robustly Support Division of the Genus Mycobacterium into an Emended Genus Mycobacterium and Four Novel Genera.* Front Microbiol, 2018. **9**: p. 67.
123. Pandey, S.D., et al., *Iron-regulated protein HupB of Mycobacterium tuberculosis positively regulates siderophore biosynthesis and is essential for growth in macrophages.* J Bacteriol, 2014. **196**(10): p. 1853-65.
124. Singh, N., et al., *HupB, a nucleoid-associated protein, is critical for survival of Mycobacterium tuberculosis under host-mediated stresses and for enhanced tolerance to key first-line antibiotics.* Front Microbiol, 2022. **13**: p. 937970.
125. Filliol, I., et al., *Global phylogeny of Mycobacterium tuberculosis based on single nucleotide polymorphism (SNP) analysis: insights into tuberculosis evolution, phylogenetic accuracy of other DNA fingerprinting systems, and recommendations for a minimal standard SNP set.* J Bacteriol, 2006. **188**(2): p. 759-72.

126. Bottai, D., et al., *TbD1 deletion as a driver of the evolutionary success of modern epidemic Mycobacterium tuberculosis lineages.* Nat Commun, 2020. **11**(1): p. 684.
127. Brites, D. and S. Gagneux, *Co-evolution of Mycobacterium tuberculosis and Homo sapiens.* Immunol Rev, 2015. **264**(1): p. 6-24.
128. Orgeur, M. and R. Brosch, *Evolution of virulence in the Mycobacterium tuberculosis complex.* Curr Opin Microbiol, 2018. **41**: p. 68-75.
129. Russell, D.G., et al., *Foamy macrophages and the progression of the human tuberculosis granuloma.* Nat Immunol, 2009. **10**(9): p. 943-8.
130. van Crevel, R., T.H. Ottenhoff, and J.W. van der Meer, *Innate immunity to Mycobacterium tuberculosis.* Clin Microbiol Rev, 2002. **15**(2): p. 294-309.
131. Ramakrishnan, L., *Revisiting the role of the granuloma in tuberculosis.* Nat Rev Immunol, 2012. **12**(5): p. 352-66.
132. Peyron, P., et al., *Foamy macrophages from tuberculous patients' granulomas constitute a nutrient-rich reservoir for M. tuberculosis persistence.* PLoS Pathog, 2008. **4**(11): p. e1000204.
133. Kiarely Souza, E., et al., *Lipid droplet accumulation occurs early following Salmonella infection and contributes to intracellular bacterial survival and replication.* Mol Microbiol, 2022. **117**(2): p. 293-306.
134. Meester, I., A.G. Rosas-Taraco, and M.C. Salinas-Carmona, *Nocardia brasiliensis induces formation of foamy macrophages and dendritic cells in vitro and in vivo.* PLoS One, 2014. **9**(6): p. e100064.
135. Boven, L.A., et al., *Myelin-laden macrophages are anti-inflammatory, consistent with foam cells in multiple sclerosis.* Brain, 2006. **129**(Pt 2): p. 517-26.
136. Pryma, C.S., et al., *Pathways of smooth muscle foam cell formation in atherosclerosis.* Curr Opin Lipidol, 2019. **30**(2): p. 117-124.
137. Chistiakov, D.A., et al., *Mechanisms of foam cell formation in atherosclerosis.* J Mol Med (Berl), 2017. **95**(11): p. 1153-1165.
138. Agarwal, P., S. Gordon, and F.O. Martinez, *Foam Cell Macrophages in Tuberculosis.* Front Immunol, 2021. **12**: p. 775326.
139. Mahajan, S., et al., *Mycobacterium tuberculosis modulates macrophage lipid-sensing nuclear receptors PPARgamma and TR4 for survival.* J Immunol, 2012. **188**(11): p. 5593-603.

140. Parthasarathy, S., et al., *Oxidized low-density lipoprotein.* Methods Mol Biol, 2010. **610**: p. 403-17.
141. Vrieling, F., et al., *Oxidized low-density lipoprotein (oxLDL) supports Mycobacterium tuberculosis survival in macrophages by inducing lysosomal dysfunction.* PLoS Pathog, 2019. **15**(4): p. e1007724.
142. Brzostek, A., et al., *Mycobacterium tuberculosis is able to accumulate and utilize cholesterol.* J Bacteriol, 2009. **191**(21): p. 6584-91.
143. Wilburn, K.M., et al., *Pharmacological and genetic activation of cAMP synthesis disrupts cholesterol utilization in Mycobacterium tuberculosis.* PLoS Pathog, 2022. **18**(2): p. e1009862.
144. Gibson, S.E.R., et al., *Cholesterol-dependent activity of dapsone against non-replicating persistent mycobacteria.* Microbiology (Reading), 2022. **168**(12).
145. Gatfield, J. and J. Pieters, *Essential role for cholesterol in entry of mycobacteria into macrophages.* Science, 2000. **288**(5471): p. 1647-50.
146. Soto-Ramirez, M.D., et al., *Cholesterol plays a larger role during Mycobacterium tuberculosis in vitro dormancy and reactivation than previously suspected.* Tuberculosis (Edinb), 2017. **103**: p. 1-9.
147. Rivera-Calzada, A., et al., *Type VII secretion systems: structure, functions and transport models.* Nat Rev Microbiol, 2021. **19**(9): p. 567-584.
148. Bunduc, C.M., W. Bitter, and E.N.G. Houben, *Structure and Function of the Mycobacterial Type VII Secretion Systems.* Annu Rev Microbiol, 2020. **74**: p. 315-335.
149. Daugelat, S., et al., *The RD1 proteins of Mycobacterium tuberculosis: expression in Mycobacterium smegmatis and biochemical characterization.* Microbes Infect, 2003. **5**(12): p. 1082-95.
150. Hsu, T., et al., *The primary mechanism of attenuation of bacillus Calmette-Guerin is a loss of secreted lytic function required for invasion of lung interstitial tissue.* Proc Natl Acad Sci U S A, 2003. **100**(21): p. 12420-5.
151. Renshaw, P.S., et al., *Structure and function of the complex formed by the tuberculosis virulence factors CFP-10 and ESAT-6.* EMBO J, 2005. **24**(14): p. 2491-8.

152. Conrad, W.H., et al., *Mycobacterial ESX-1 secretion system mediates host cell lysis through bacterium contact-dependent gross membrane disruptions.* Proc Natl Acad Sci U S A, 2017. **114**(6): p. 1371-1376.
153. Guo, S., et al., *The CFP10/ESAT6 complex of Mycobacterium tuberculosis may function as a regulator of macrophage cell death at different stages of tuberculosis infection.* Med Hypotheses, 2012. **78**(3): p. 389-92.
154. Abebe, F., et al., *Association of ESAT-6/CFP-10-induced IFN-gamma, TNF-alpha and IL-10 with clinical tuberculosis: evidence from cohorts of pulmonary tuberculosis patients, household contacts and community controls in an endemic setting.* Clin Exp Immunol, 2017. **189**(2): p. 241-249.
155. Sreejit, G., et al., *The ESAT-6 protein of Mycobacterium tuberculosis interacts with beta-2-microglobulin (beta2M) affecting antigen presentation function of macrophage.* PLoS Pathog, 2014. **10**(10): p. e1004446.
156. Marei, A., et al., *Superior T cell activation by ESAT-6 as compared with the ESAT-6-CFP-10 complex.* Int Immunol, 2005. **17**(11): p. 1439-46.
157. Cohen, S.B., et al., *Alveolar Macrophages Provide an Early Mycobacterium tuberculosis Niche and Initiate Dissemination.* Cell Host Microbe, 2018. **24**(3): p. 439-446 e4.
158. Zhang, L., et al., *Effects of Mycobacterium tuberculosis ESAT-6/CFP-10 fusion protein on the autophagy function of mouse macrophages.* DNA Cell Biol, 2012. **31**(2): p. 171-9.
159. Tan, T., et al., *The ESAT-6/CFP-10 secretion system of Mycobacterium marinum modulates phagosome maturation.* Cell Microbiol, 2006. **8**(9): p. 1417-29.
160. Serafini, A., et al., *The ESX-3 secretion system is necessary for iron and zinc homeostasis in Mycobacterium tuberculosis.* PLoS One, 2013. **8**(10): p. e78351.
161. Ilghari, D., et al., *Solution structure of the Mycobacterium tuberculosis EsxG.EsxH complex: functional implications and comparisons with other M. tuberculosis Esx family complexes.* J Biol Chem, 2011. **286**(34): p. 29993-30002.

162. Mehra, A., et al., *Mycobacterium tuberculosis type VII secreted effector EsxH targets host ESCRT to impair trafficking.* PLoS Pathog, 2013. **9**(10): p. e1003734.
163. Sayes, F., et al., *Strong immunogenicity and cross-reactivity of Mycobacterium tuberculosis ESX-5 type VII secretion: encoded PE-PPE proteins predicts vaccine potential.* Cell Host Microbe, 2012. **11**(4): p. 352-63.
164. Yang, Y., et al., *Mycobacterial PPE13 activates inflammasome by interacting with the NATCH and LRR domains of NLRP3.* FASEB J, 2020. **34**(9): p. 12820-12833.
165. Mayer-Barber, K.D., et al., *Caspase-1 independent IL-1beta production is critical for host resistance to mycobacterium tuberculosis and does not require TLR signaling in vivo.* J Immunol, 2010. **184**(7): p. 3326-30.
166. Novikov, A., et al., *Mycobacterium tuberculosis triggers host type I IFN signaling to regulate IL-1beta production in human macrophages.* J Immunol, 2011. **187**(5): p. 2540-7.
167. Master, S.S., et al., *Mycobacterium tuberculosis prevents inflammasome activation.* Cell Host Microbe, 2008. **3**(4): p. 224-32.
168. Jackson, M., *The mycobacterial cell envelope-lipids.* Cold Spring Harb Perspect Med, 2014. **4**(10).
169. Gago, G., L. Diacovich, and H. Gramajo, *Lipid metabolism and its implication in mycobacteria-host interaction.* Curr Opin Microbiol, 2018. **41**: p. 36-42.
170. Crellin, P.K., Luo, C., Morita, Y.S., *Metabolism of Plasma Membrane Lipids in Mycobacteria and Corynebacteria*, in *Lipid Metabolism*, R.V. Baez, Editor. 2013, IntechOpen.
171. Takayama, K., C. Wang, and G.S. Besra, *Pathway to synthesis and processing of mycolic acids in Mycobacterium tuberculosis.* Clin Microbiol Rev, 2005. **18**(1): p. 81-101.
172. Su, C.C., et al., *Structures of the mycobacterial membrane protein MmpL3 reveal its mechanism of lipid transport.* PLoS Biol, 2021. **19**(8): p. e3001370.

173. Su, C.C., et al., *MmpL3 is a lipid transporter that binds trehalose monomycolate and phosphatidylethanolamine.* Proc Natl Acad Sci U S A, 2019. **116**(23): p. 11241-11246.
174. de Chastellier, C., et al., *Mycobacterium requires an all-around closely apposing phagosome membrane to maintain the maturation block and this apposition is re-established when it rescues itself from phagolysosomes.* Cell Microbiol, 2009. **11**(8): p. 1190-207.
175. Beatty, W.L., et al., *Trafficking and release of mycobacterial lipids from infected macrophages.* Traffic, 2000. **1**(3): p. 235-47.
176. Prados-Rosales, R., et al., *Mycobacteria release active membrane vesicles that modulate immune responses in a TLR2-dependent manner in mice.* J Clin Invest, 2011. **121**(4): p. 1471-83.
177. Wojtas, B., et al., *Mannosylated lipoarabinomannan balances apoptosis and inflammatory state in mycobacteria-infected and uninfected bystander macrophages.* Microb Pathog, 2011. **51**(1-2): p. 9-21.
178. Kim, M.J., et al., *Caseation of human tuberculosis granulomas correlates with elevated host lipid metabolism.* EMBO Mol Med, 2010. **2**(7): p. 258-74.
179. Queiroz, A. and L.W. Riley, *Bacterial immunostat: Mycobacterium tuberculosis lipids and their role in the host immune response.* Rev Soc Bras Med Trop, 2017. **50**(1): p. 9-18.
180. Astarie-Dequeker, C., et al., *Phthiocerol dimycocerosates of M. tuberculosis participate in macrophage invasion by inducing changes in the organization of plasma membrane lipids.* PLoS Pathog, 2009. **5**(2): p. e1000289.
181. Alonso, H., et al., *Protein O-mannosylation deficiency increases LprG-associated lipoarabinomannan release by Mycobacterium tuberculosis and enhances the TLR2-associated inflammatory response.* Sci Rep, 2017. **7**(1): p. 7913.
182. Puissegur, M.P., et al., *Mycobacterial lipomannan induces granuloma macrophage fusion via a TLR2-dependent, ADAM9- and beta1 integrin-mediated pathway.* J Immunol, 2007. **178**(5): p. 3161-9.

183. Rhoades, E., et al., *Identification and macrophage-activating activity of glycolipids released from intracellular Mycobacterium bovis BCG.* Mol Microbiol, 2003. **48**(4): p. 875-88.
184. Ishikawa, E., et al., *Direct recognition of the mycobacterial glycolipid, trehalose dimycolate, by C-type lectin Mincle.* J Exp Med, 2009. **206**(13): p. 2879-88.
185. Kan-Sutton, C., C. Jagannath, and R.L. Hunter, Jr., *Trehalose 6,6'-dimycolate on the surface of Mycobacterium tuberculosis modulates surface marker expression for antigen presentation and costimulation in murine macrophages.* Microbes Infect, 2009. **11**(1): p. 40-8.
186. Rousseau, C., et al., *Production of phthiocerol dimycocerosates protects Mycobacterium tuberculosis from the cidal activity of reactive nitrogen intermediates produced by macrophages and modulates the early immune response to infection.* Cell Microbiol, 2004. **6**(3): p. 277-87.
187. Buter, J., et al., *Mycobacterium tuberculosis releases an antacid that remodels phagosomes.* Nat Chem Biol, 2019. **15**(9): p. 889-899.
188. Vergne, I., et al., *Mycobacterium tuberculosis phagosome maturation arrest: mycobacterial phosphatidylinositol analog phosphatidylinositol mannoside stimulates early endosomal fusion.* Mol Biol Cell, 2004. **15**(2): p. 751-60.
189. Hayakawa, E., et al., *A Mycobacterium tuberculosis-derived lipid inhibits membrane fusion by modulating lipid membrane domains.* Biophys J, 2007. **93**(11): p. 4018-30.
190. Axelrod, S., et al., *Delay of phagosome maturation by a mycobacterial lipid is reversed by nitric oxide.* Cell Microbiol, 2008. **10**(7): p. 1530-45.
191. Spargo, B.J., et al., *Cord factor (alpha,alpha-trehalose 6,6'-dimycolate) inhibits fusion between phospholipid vesicles.* Proc Natl Acad Sci U S A, 1991. **88**(3): p. 737-40.
192. Lerner, T.R., et al., *Phthiocerol dimycocerosates promote access to the cytosol and intracellular burden of Mycobacterium tuberculosis in lymphatic endothelial cells.* BMC Biol, 2018. **16**(1): p. 1.
193. Lin, J.J., et al., *A Niemann-pick C1 disease child with BCG-itis: a case report and analysis.* BMC Pediatr, 2021. **21**(1): p. 218.

194. Dong, W., et al., *MiR-25 blunts autophagy and promotes the survival of Mycobacterium tuberculosis by regulating NPC1.* iScience, 2022. **25**(5): p. 104279.
195. de Araujo, L.S., et al., *Transcriptomic Biomarkers for Tuberculosis: Validation of NPC2 as a Single mRNA Biomarker to Diagnose TB, Predict Disease Progression, and Monitor Treatment Response.* Cells, 2021. **10**(10).
196. Wheelwright, M., et al., *All-trans retinoic acid-triggered antimicrobial activity against Mycobacterium tuberculosis is dependent on NPC2.* J Immunol, 2014. **192**(5): p. 2280-2290.
197. Frieden, T.R., et al., *Tuberculosis.* Lancet, 2003. **362**(9387): p. 887-99.
198. Athman, J.J., et al., *Bacterial Membrane Vesicles Mediate the Release of Mycobacterium tuberculosis Lipoglycans and Lipoproteins from Infected Macrophages.* J Immunol, 2015. **195**(3): p. 1044-53.
199. Augenstreich, J. and V. Briken, *Host Cell Targets of Released Lipid and Secreted Protein Effectors of Mycobacterium tuberculosis.* Front Cell Infect Microbiol, 2020. **10**: p. 595029.
200. O'Toole, R.F. and S.S. Gautam, *Limitations of the Mycobacterium tuberculosis reference genome H37Rv in the detection of virulence-related loci.* Genomics, 2017. **109**(5-6): p. 471-474.
201. Ioerger, T.R., et al., *Variation among genome sequences of H37Rv strains of Mycobacterium tuberculosis from multiple laboratories.* J Bacteriol, 2010. **192**(14): p. 3645-53.
202. Bifani, P., et al., *Molecular characterization of Mycobacterium tuberculosis H37Rv/Ra variants: distinguishing the mycobacterial laboratory strain.* J Clin Microbiol, 2000. **38**(9): p. 3200-4.
203. Chitale, P., et al., *A comprehensive update to the Mycobacterium tuberculosis H37Rv reference genome.* Nat Commun, 2022. **13**(1): p. 7068.
204. Al Shammari, B., et al., *The Extracellular Matrix Regulates Granuloma Necrosis in Tuberculosis.* J Infect Dis, 2015. **212**(3): p. 463-73.
205. Zhang, M., et al., *Growth of virulent and avirulent Mycobacterium tuberculosis strains in human macrophages.* Infect Immun, 1998. **66**(2): p. 794-9.

206. Marquina-Castillo, B., et al., *Virulence, immunopathology and transmissibility of selected strains of Mycobacterium tuberculosis in a murine model.* Immunology, 2009. **128**(1): p. 123-33.
207. Weng, Y., et al., *Inhibition of the Niemann-Pick C1 protein is a conserved feature of multiple strains of pathogenic mycobacteria.* Nat Commun, 2022. **13**(1): p. 5320.
208. Weischenfeldt, J. and B. Porse, *Bone Marrow-Derived Macrophages (BMM): Isolation and Applications.* CSH Protoc, 2008. **2008**: p. pdb prot5080.
209. Brudey, K., et al., *Mycobacterium tuberculosis complex genetic diversity: mining the fourth international spoligotyping database (SpolDB4) for classification, population genetics and epidemiology.* BMC Microbiol, 2006. **6**: p. 23.
210. Comas, I., et al., *Out-of-Africa migration and Neolithic coexpansion of Mycobacterium tuberculosis with modern humans.* Nat Genet, 2013. **45**(10): p. 1176-82.
211. Krishnan, N., et al., *Mycobacterium tuberculosis lineage influences innate immune response and virulence and is associated with distinct cell envelope lipid profiles.* PLoS One, 2011. **6**(9): p. e23870.
212. Neville, D.C., et al., *Analysis of fluorescently labeled glycosphingolipid-derived oligosaccharides following ceramide glycanase digestion and anthranilic acid labeling.* Anal Biochem, 2004. **331**(2): p. 275-82.
213. David A Priestman, D.t.V., Kerri-Lee Wallom, María E Fernández-Suárez, Maria Leondaraki, Carissa Drake , Frances M Platt, *Analysis of glycosphingolipids from human plasma.* protocols.io, 2021.
214. te Vruchte, D., et al., *Relative acidic compartment volume as a lysosomal storage disorder-associated biomarker.* J Clin Invest, 2014. **124**(3): p. 1320-8.
215. Platt, N., et al., *Release of acidic store calcium is required for effective priming of the NLRP3 inflammasome.* bioRxiv, 2022: p. 2022.01.06.475262.
216. Vanier, M.T., *Niemann-Pick diseases.* Handb Clin Neurol, 2013. **113**: p. 1717-21.

217. Sugimoto, Y., et al., *Accumulation of cholera toxin and GM1 ganglioside in the early endosome of Niemann-Pick C1-deficient cells.* Proc Natl Acad Sci U S A, 2001. **98**(22): p. 12391-6.
218. Pagano, R.E., *Endocytic trafficking of glycosphingolipids in sphingolipid storage diseases.* Philos Trans R Soc Lond B Biol Sci, 2003. **358**(1433): p. 885-91.
219. Gagneux, S. and P.M. Small, *Global phylogeography of Mycobacterium tuberculosis and implications for tuberculosis product development.* Lancet Infect Dis, 2007. **7**(5): p. 328-37.
220. Gagneux, S., *Host-pathogen coevolution in human tuberculosis.* Philos Trans R Soc Lond B Biol Sci, 2012. **367**(1590): p. 850-9.
221. Coscolla, M. and S. Gagneux, *Consequences of genomic diversity in Mycobacterium tuberculosis.* Semin Immunol, 2014. **26**(6): p. 431-44.
222. Coscolla, M. and S. Gagneux, *Does M. tuberculosis genomic diversity explain disease diversity?* Drug Discov Today Dis Mech, 2010. **7**(1): p. e43-e59.
223. Boritsch, E.C., et al., *pks5-recombination-mediated surface remodelling in Mycobacterium tuberculosis emergence.* Nat Microbiol, 2016. **1**: p. 15019.
224. Supply, P. and R. Brosch, *The Biology and Epidemiology of Mycobacterium canettii.* Adv Exp Med Biol, 2017. **1019**: p. 27-41.
225. Fabre, M., et al., *Molecular characteristics of "Mycobacterium canettii" the smooth Mycobacterium tuberculosis bacilli.* Infect Genet Evol, 2010. **10**(8): p. 1165-73.
226. Koeck, J.L., et al., *Clinical characteristics of the smooth tubercle bacilli 'Mycobacterium canettii' infection suggest the existence of an environmental reservoir.* Clin Microbiol Infect, 2011. **17**(7): p. 1013-9.
227. van Soolingen, D., et al., *A novel pathogenic taxon of the Mycobacterium tuberculosis complex, Canetti: characterization of an exceptional isolate from Africa.* Int J Syst Bacteriol, 1997. **47**(4): p. 1236-45.
228. Cole, S.T., et al., *Deciphering the biology of Mycobacterium tuberculosis from the complete genome sequence.* Nature, 1998. **393**(6685): p. 537-44.

229. Fog, C.K. and T. Kirkegaard, *Animal models for Niemann-Pick type C: implications for drug discovery & development.* Expert Opin Drug Discov, 2019. **14**(5): p. 499-509.
230. van Wyk, N., et al., *Current perspectives on the families of glycoside hydrolases of Mycobacterium tuberculosis: their importance and prospects for assigning function to unknowns.* Glycobiology, 2017. **27**(2): p. 112-122.
231. Nakayama, H., et al., *The regulatory roles of glycosphingolipid-enriched lipid rafts in immune systems.* FEBS Lett, 2018. **592**(23): p. 3921-3942.
232. Hughes, M.P., et al., *A Novel Small NPC1 Promoter Enhances AAV-Mediated Gene Therapy in Mouse Models of Niemann-Pick Type C1 Disease.* Cells, 2023. **12**(12).
233. Hackett, E.E., et al., *Mycobacterium tuberculosis Limits Host Glycolysis and IL-1beta by Restriction of PFK-M via MicroRNA-21.* Cell Rep, 2020. **30**(1): p. 124-136 e4.
234. Llibre, A., et al., *Tuberculosis alters immune-metabolic pathways resulting in perturbed IL-1 responses.* Front Immunol, 2022. **13**: p. 897193.
235. Brennan, P.J., *Structure, function, and biogenesis of the cell wall of Mycobacterium tuberculosis.* Tuberculosis (Edinb), 2003. **83**(1-3): p. 91-7.
236. Hingley-Wilson, S.M., V.K. Sambandamurthy, and W.R. Jacobs, Jr., *Survival perspectives from the world's most successful pathogen, Mycobacterium tuberculosis.* Nat Immunol, 2003. **4**(10): p. 949-55.
237. Reed, M.B., et al., *A glycolipid of hypervirulent tuberculosis strains that inhibits the innate immune response.* Nature, 2004. **431**(7004): p. 84-7.
238. Larrouy-Maumus, G. and G. Puzo, *Mycobacterial envelope lipids fingerprint from direct MALDI-TOF MS analysis of intact bacilli.* Tuberculosis (Edinb), 2015. **95**(1): p. 75-85.
239. Gilleron, M., B. Lindner, and G. Puzo, *MS/MS approach for characterization of the fatty acid distribution on mycobacterial phosphatidyl-myo-inositol mannosides.* Anal Chem, 2006. **78**(24): p. 8543-8.
240. Kordulakova, J., et al., *Identification of the required acyltransferase step in the biosynthesis of the phosphatidylinositol mannosides of mycobacterium species.* J Biol Chem, 2003. **278**(38): p. 36285-95.

241. Guerin, M.E., et al., *Molecular basis of phosphatidyl-myo-inositol mannoside biosynthesis and regulation in mycobacteria.* J Biol Chem, 2010. **285**(44): p. 33577-83.
242. Layre, E., et al., *Deciphering sulfoglycolipids of Mycobacterium tuberculosis.* J Lipid Res, 2011. **52**(6): p. 1098-1110.
243. Goren, M.B., *Sulfolipid I of Mycobacterium tuberculosis, strain H37Rv. I. Purification and properties.* Biochim Biophys Acta, 1970. **210**(1): p. 116-26.
244. Jia Khor, M., et al., *An Improved Method for Rapid Detection of Mycobacterium abscessus Complex Based on Species-Specific Lipid Fingerprint by Routine MALDI-TOF.* Front Chem, 2021. **9**: p. 715890.
245. Reinink, P., et al., *Discovery of Salmonella trehalose phospholipids reveals functional convergence with mycobacteria.* J Exp Med, 2019. **216**(4): p. 757-771.
246. Neill, S.D., et al., *Pathogenesis of Mycobacterium bovis infection in cattle.* Vet Microbiol, 1994. **40**(1-2): p. 41-52.
247. Sugawara-Mikami, M., et al., *Pathogenicity and virulence of Mycobacterium leprae.* Virulence, 2022. **13**(1): p. 1985-2011.
248. Piersimoni, C. and C. Scarparo, *Pulmonary infections associated with non-tuberculous mycobacteria in immunocompetent patients.* Lancet Infect Dis, 2008. **8**(5): p. 323-34.
249. Benwill, J.L. and R.J. Wallace, Jr., *Mycobacterium abscessus: challenges in diagnosis and treatment.* Curr Opin Infect Dis, 2014. **27**(6): p. 506-10.
250. Lipworth, S., et al., *Epidemiology of Mycobacterium abscessus in England: an observational study.* Lancet Microbe, 2021. **2**(10): p. e498-e507.
251. Abdelaal, H.F.M., et al., *Mycobacterium abscessus: It's Complex.* Microorganisms, 2022. **10**(7).
252. Wetzstein, N., et al., *Molecular Epidemiology of Mycobacterium abscessus Isolates Recovered from German Cystic Fibrosis Patients.* Microbiol Spectr, 2022. **10**(4): p. e0171422.
253. Degiacomi, G., et al., *Mycobacterium abscessus, an Emerging and Worrisome Pathogen among Cystic Fibrosis Patients.* Int J Mol Sci, 2019. **20**(23).

254. Yoshida, M., et al., *Molecular Epidemiological Characteristics of Mycobacterium abscessus Complex Derived from Non-Cystic Fibrosis Patients in Japan and Taiwan.* Microbiol Spectr, 2022. **10**(3): p. e0057122.
255. Huang, J.J., et al., *Prevalence of nontuberculous mycobacteria in a tertiary hospital in Beijing, China, January 2013 to December 2018.* BMC Microbiol, 2020. **20**(1): p. 158.
256. Ayoubi, S., et al., *Prevalence of Mycobacterium abscessus among the Patients with Nontuberculous Mycobacteria.* Arch Iran Med, 2020. **23**(3): p. 163-168.
257. Parmar, S. and E.I. Tocheva, *The cell envelope of Mycobacterium abscessus and its role in pathogenesis.* PLoS Pathog, 2023. **19**(5): p. e1011318.
258. Kam, J.Y., et al., *Rough and smooth variants of Mycobacterium abscessus are differentially controlled by host immunity during chronic infection of adult zebrafish.* Nat Commun, 2022. **13**(1): p. 952.
259. Pawlik, A., et al., *Identification and characterization of the genetic changes responsible for the characteristic smooth-to-rough morphotype alterations of clinically persistent Mycobacterium abscessus.* Mol Microbiol, 2013. **90**(3): p. 612-29.
260. Bernut, A., et al., *Mycobacterium abscessus cording prevents phagocytosis and promotes abscess formation.* Proc Natl Acad Sci U S A, 2014. **111**(10): p. E943-52.
261. Bernut, A., et al., *Mycobacterium abscessus-Induced Granuloma Formation Is Strictly Dependent on TNF Signaling and Neutrophil Trafficking.* PLoS Pathog, 2016. **12**(11): p. e1005986.
262. Rhoades, E.R., et al., *Mycobacterium abscessus Glycopeptidolipids mask underlying cell wall phosphatidyl-myo-inositol mannosides blocking induction of human macrophage TNF-alpha by preventing interaction with TLR2.* J Immunol, 2009. **183**(3): p. 1997-2007.
263. Llorens-Fons, M., et al., *Trehalose Polyphleates, External Cell Wall Lipids in Mycobacterium abscessus, Are Associated with the Formation of Clumps with Cording Morphology, Which Have Been Associated with Virulence.* Front Microbiol, 2017. **8**: p. 1402.

264. Kwak, N., et al., *M ycobacterium abscessus pulmonary disease: individual patient data meta-analysis.* Eur Respir J, 2019. **54**(1).
265. Ferrell, K.C., et al., *Virulence Mechanisms of Mycobacterium abscessus: Current Knowledge and Implications for Vaccine Design.* Front Microbiol, 2022. **13**: p. 842017.
266. Broda, A., et al., *Comparative drug resistance of Mycobacterium abscessus and M. chelonae isolates from patients with and without cystic fibrosis in the United Kingdom.* J Clin Microbiol, 2013. **51**(1): p. 217-23.
267. Cassidy, P.M., et al., *Nontuberculous mycobacterial disease prevalence and risk factors: a changing epidemiology.* Clin Infect Dis, 2009. **49**(12): p. e124-9.
268. Busatto, C., et al., *Mycobacterium avium: an overview.* Tuberculosis (Edinb), 2019. **114**: p. 127-134.
269. Mizzi, R., et al., *Global Phylogeny of Mycobacterium avium and Identification of Mutation Hotspots During Niche Adaptation.* Front Microbiol, 2022. **13**: p. 892333.
270. To, K., et al., *General Overview of Nontuberculous Mycobacteria Opportunistic Pathogens: Mycobacterium avium and Mycobacterium abscessus.* J Clin Med, 2020. **9**(8).
271. Daley, C.L., *Mycobacterium avium Complex Disease.* Microbiol Spectr, 2017. **5**(2).
272. Johansen, M.D., et al., *Mycobacterium avium subspecies paratuberculosis is able to manipulate host lipid metabolism and accumulate cholesterol within macrophages.* Microb Pathog, 2019. **130**: p. 44-53.
273. Nishimura, T., et al., *The rough colony morphotype of Mycobacterium avium exhibits high virulence in human macrophages and mice.* J Med Microbiol, 2020. **69**(7): p. 1020-1033.
274. Frehel, C., et al., *Evidence for inhibition of fusion of lysosomal and prelysosomal compartments with phagosomes in macrophages infected with pathogenic Mycobacterium avium.* Infect Immun, 1986. **52**(1): p. 252-62.
275. Oh, Y.K. and R.M. Straubinger, *Intracellular fate of Mycobacterium avium: use of dual-label spectrofluorometry to investigate the influence of*

bacterial viability and opsonization on phagosomal pH and phagosome-lysosome interaction. Infect Immun, 1996. **64**(1): p. 319-25.

276. Rocco, J.M. and V.R. Irani, *Mycobacterium avium and modulation of the host macrophage immune mechanisms.* Int J Tuberc Lung Dis, 2011. **15**(4): p. 447-52.
277. Scollard, D.M., *The biology of nerve injury in leprosy.* Lepr Rev, 2008. **79**(3): p. 242-53.
278. Ploemacher, T., et al., *Reservoirs and transmission routes of leprosy; A systematic review.* PLoS Negl Trop Dis, 2020. **14**(4): p. e0008276.
279. Araujo, S., et al., *Molecular Evidence for the Aerial Route of Infection of Mycobacterium leprae and the Role of Asymptomatic Carriers in the Persistence of Leprosy.* Clin Infect Dis, 2016. **63**(11): p. 1412-1420.
280. Chokkakula, S., et al., *Genotyping of Mycobacterium leprae for understanding the distribution and transmission of leprosy in endemic provinces of China.* Int J Infect Dis, 2020. **98**: p. 6-13.
281. Moura, D.F., et al., *CD163 favors Mycobacterium leprae survival and persistence by promoting anti-inflammatory pathways in lepromatous macrophages.* Eur J Immunol, 2012. **42**(11): p. 2925-36.
282. Wheat, W.H., et al., *Long-term survival and virulence of Mycobacterium leprae in amoebal cysts.* PLoS Negl Trop Dis, 2014. **8**(12): p. e3405.
283. Alves, L., et al., *Mycobacterium leprae infection of human Schwann cells depends on selective host kinases and pathogen-modulated endocytic pathways.* FEMS Microbiol Lett, 2004. **238**(2): p. 429-37.
284. Silva, B.J., et al., *Autophagy Is an Innate Mechanism Associated with Leprosy Polarization.* PLoS Pathog, 2017. **13**(1): p. e1006103.
285. Wang, H., et al., *Detection of antibodies to both M. leprae PGL-I and MMP-II to recognize leprosy patients at an early stage of disease progression.* Diagn Microbiol Infect Dis, 2015. **83**(3): p. 274-7.
286. Penna, M.L., et al., *Anti-PGL-1 Positivity as a Risk Marker for the Development of Leprosy among Contacts of Leprosy Cases: Systematic Review and Meta-analysis.* PLoS Negl Trop Dis, 2016. **10**(5): p. e0004703.
287. Rambukkana, A., et al., *Contact-dependent demyelination by Mycobacterium leprae in the absence of immune cells.* Science, 2002. **296**(5569): p. 927-31.

288. Mietto, B.S., et al., *Myelin breakdown favours Mycobacterium leprae survival in Schwann cells.* Cell Microbiol, 2020. **22**(1): p. e13128.
289. Oliveira, M.F., et al., *Reduction of host cell mitochondrial activity as Mycobacterium leprae's strategy to evade host innate immunity.* Immunol Rev, 2021. **301**(1): p. 193-208.
290. Mattos, K.A., et al., *Mycobacterium leprae intracellular survival relies on cholesterol accumulation in infected macrophages: a potential target for new drugs for leprosy treatment.* Cell Microbiol, 2014. **16**(6): p. 797-815.
291. Girardi, K., et al., *Phenolic glycolipid-1 of Mycobacterium leprae is involved in human Schwann cell line ST8814 neurotoxic phenotype.* J Neurochem, 2023. **164**(2): p. 158-171.
292. Mungroo, M.R., N.A. Khan, and R. Siddiqui, *Mycobacterium leprae: Pathogenesis, diagnosis, and treatment options.* Microb Pathog, 2020. **149**: p. 104475.
293. Williams, D.L., et al., *Drug resistance in patients with leprosy in the United States.* Clin Infect Dis, 2014. **58**(1): p. 72-3.
294. Davidson, J.A., et al., *Epidemiology of Mycobacterium bovis Disease in Humans in England, Wales, and Northern Ireland, 2002-2014.* Emerg Infect Dis, 2017. **23**(3): p. 377-386.
295. Gao, W., et al., *Lipidomics revealed the global lipid responses of primary bovine alveolar macrophages to infections of Mycobacterium tuberculosis and Mycobacterium bovis.* Int Immunopharmacol, 2022. **104**: p. 108407.
296. D'Avila, H., et al., *Mycobacterium bovis bacillus Calmette-Guerin induces TLR2-mediated formation of lipid bodies: intracellular domains for eicosanoid synthesis in vivo.* J Immunol, 2006. **176**(5): p. 3087-97.
297. Hotter, G.S. and D.M. Collins, *Mycobacterium bovis lipids: virulence and vaccines.* Vet Microbiol, 2011. **151**(1-2): p. 91-8.
298. Li, J., L. Zhan, and C. Qin, *The double-sided effects of Mycobacterium Bovis bacillus Calmette-Guerin vaccine.* NPJ Vaccines, 2021. **6**(1): p. 14.
299. T, J.A.S., et al., *Features of the biochemistry of Mycobacterium smegmatis, as a possible model for Mycobacterium tuberculosis.* J Infect Public Health, 2020. **13**(9): p. 1255-1264.
300. Sparks, I.L., et al., *Mycobacterium smegmatis: The Vanguard of Mycobacterial Research.* J Bacteriol, 2023. **205**(1): p. e0033722.

301. Sousa, S., et al., *Nontuberculous Mycobacteria Persistence in a Cell Model Mimicking Alveolar Macrophages.* Microorganisms, 2019. **7**(5).
302. Alqurashi, M.M., et al., *Mycobacterium smegmatis causing a granulomatous cardiomediastinal mass.* IDCases, 2019. **18**: p. e00608.
303. Wang, C.J., et al., *Mycobacterium smegmatis Skin Infection Following Cosmetic Procedures: Report of Two Cases.* Clin Cosmet Investig Dermatol, 2022. **15**: p. 535-540.
304. Newton, J.A., Jr., et al., *Soft-tissue infection due to Mycobacterium smegmatis: report of two cases.* Clin Infect Dis, 1993. **16**(4): p. 531-3.
305. Dhiman, R.K., et al., *Lipoarabinomannan localization and abundance during growth of Mycobacterium smegmatis.* J Bacteriol, 2011. **193**(20): p. 5802-9.
306. Mahapa, A., et al., *Mannopyranoside Glycolipids Inhibit Mycobacterial and Biofilm Growth and Potentiate Isoniazid Inhibition Activities in M. smegmatis.* Chembiochem, 2019. **20**(15): p. 1966-1976.
307. Pacheco, S.A., et al., *MmpL11 protein transports mycolic acid-containing lipids to the mycobacterial cell wall and contributes to biofilm formation in Mycobacterium smegmatis.* J Biol Chem, 2013. **288**(33): p. 24213-22.
308. Marques, M.A., et al., *The Essential Role of Cholesterol Metabolism in the Intracellular Survival of Mycobacterium leprae Is Not Coupled to Central Carbon Metabolism and Energy Production.* J Bacteriol, 2015. **197**(23): p. 3698-707.
309. Johansen, M.D., et al., *Mycobacterium marinum infection drives foam cell differentiation in zebrafish infection models.* Dev Comp Immunol, 2018. **88**: p. 169-172.
310. Caire-Brandli, I., et al., *Reversible lipid accumulation and associated division arrest of Mycobacterium avium in lipoprotein-induced foamy macrophages may resemble key events during latency and reactivation of tuberculosis.* Infect Immun, 2014. **82**(2): p. 476-90.
311. Guha, S., et al., *Approaches for detecting lysosomal alkalinization and impaired degradation in fresh and cultured RPE cells: evidence for a role in retinal degenerations.* Exp Eye Res, 2014. **126**: p. 68-76.

312. Viljoen, A., et al., *Controlling Extra- and Intramacrophagic Mycobacterium abscessus by Targeting Mycolic Acid Transport.* Front Cell Infect Microbiol, 2017. **7**: p. 388.
313. Crowe, A.M., et al., *The unusual convergence of steroid catabolic pathways in Mycobacterium abscessus.* Proc Natl Acad Sci U S A, 2022. **119**(40): p. e2207505119.
314. Rhoades, E.R., et al., *Cell wall lipids from Mycobacterium bovis BCG are inflammatory when inoculated within a gel matrix: characterization of a new model of the granulomatous response to mycobacterial components.* Tuberculosis (Edinb), 2005. **85**(3): p. 159-76.
315. Shirai, T., et al., *Atypical Fabry's disease presenting with cholesterol crystal embolization.* Intern Med, 2000. **39**(8): p. 646-9.
316. Schmitz, G., et al., *Interaction of Tangier lipoproteins with cholesteryl ester-laden mouse peritoneal macrophages.* J Lipid Res, 1987. **28**(1): p. 87-99.
317. Herbert, P.N., et al., *Tangier disease: one explanation of lipid storage.* N Engl J Med, 1978. **299**(10): p. 519-21.
318. Yazd, H.S., et al., *LC-MS lipidomics of renal biopsies for the diagnosis of Fabry disease.* J Mass Spectrom Adv Clin Lab, 2021. **22**: p. 71-78.
319. Baumer, Y., S.G. McCurdy, and W.A. Boisvert, *Formation and Cellular Impact of Cholesterol Crystals in Health and Disease.* Adv Biol (Weinh), 2021. **5**(11): p. e2100638.
320. Rosa, T., et al., *Reductive Power Generated by Mycobacterium leprae Through Cholesterol Oxidation Contributes to Lipid and ATP Synthesis.* Front Cell Infect Microbiol, 2021. **11**: p. 709972.
321. Mendes, A.L.G., et al., *Expression of NLRP3 inflammasome in leprosy indicates immune evasion of Mycobacterium leprae.* Mem Inst Oswaldo Cruz, 2020. **115**: p. e190324.
322. Duewell, P., et al., *NLRP3 inflammasomes are required for atherogenesis and activated by cholesterol crystals.* Nature, 2010. **464**(7293): p. 1357-61.
323. Chen, C.S., et al., *Broad screening test for sphingolipid-storage diseases.* Lancet, 1999. **354**(9182): p. 901-5.

324. Maldonado-Garcia, G., et al., *High-polarity Mycobacterium avium-derived lipids interact with murine macrophage lipid rafts.* Scand J Immunol, 2004. **60**(5): p. 463-70.
325. Harris, E.B., Y.T. Li, and S.C. Li, *Ganglioside patterns in normal and lepromatous armadillo tissues.* Int J Lepr Other Mycobact Dis, 1986. **54**(2): p. 289-93.
326. Ribeiro-Resende, V.T., et al., *Involvement of 9-O-Acetyl GD3 ganglioside in Mycobacterium leprae infection of Schwann cells.* J Biol Chem, 2010. **285**(44): p. 34086-96.
327. Okamori, S., et al., *Natural history of Mycobacterium fortuitum pulmonary infection presenting with migratory infiltrates: a case report with microbiological analysis.* BMC Infect Dis, 2018. **18**(1): p. 1.
328. Newton, J., S. Milstien, and S. Spiegel, *Niemann-Pick type C disease: The atypical sphingolipidosis.* Adv Biol Regul, 2018. **70**: p. 82-88.
329. Iessi, E., et al., *On the role of sphingolipids in cell survival and death.* Int Rev Cell Mol Biol, 2020. **351**: p. 149-195.
330. Maceyka, M. and S. Spiegel, *Sphingolipid metabolites in inflammatory disease.* Nature, 2014. **510**(7503): p. 58-67.
331. Lee, M., S.Y. Lee, and Y.S. Bae, *Functional roles of sphingolipids in immunity and their implication in disease.* Exp Mol Med, 2023. **55**(6): p. 1110-1130.
332. Merrill, A.H., Jr., *De novo sphingolipid biosynthesis: a necessary, but dangerous, pathway.* J Biol Chem, 2002. **277**(29): p. 25843-6.
333. Hannun, Y.A. and L.M. Obeid, *Principles of bioactive lipid signalling: lessons from sphingolipids.* Nat Rev Mol Cell Biol, 2008. **9**(2): p. 139-50.
334. Hanada, K., et al., *Molecular machinery for non-vesicular trafficking of ceramide.* Nature, 2003. **426**(6968): p. 803-9.
335. Ichikawa, S. and Y. Hirabayashi, *Glucosylceramide synthase and glycosphingolipid synthesis.* Trends Cell Biol, 1998. **8**(5): p. 198-202.
336. D'Angelo, G., L.R. Rega, and M.A. De Matteis, *Connecting vesicular transport with lipid synthesis: FAPP2.* Biochim Biophys Acta, 2012. **1821**(8): p. 1089-95.

337. Deng, Y., et al., *Sphingomyelin is sorted at the trans Golgi network into a distinct class of secretory vesicle.* Proc Natl Acad Sci U S A, 2016. **113**(24): p. 6677-82.
338. Halter, D., et al., *Pre- and post-Golgi translocation of glucosylceramide in glycosphingolipid synthesis.* J Cell Biol, 2007. **179**(1): p. 101-15.
339. Kitatani, K., J. Idkowiak-Baldys, and Y.A. Hannun, *The sphingolipid salvage pathway in ceramide metabolism and signaling.* Cell Signal, 2008. **20**(6): p. 1010-8.
340. Palladino, E.N.D., et al., *Sphingosine kinases regulate ER contacts with late endocytic organelles and cholesterol trafficking.* Proc Natl Acad Sci U S A, 2022. **119**(39): p. e2204396119.
341. Gault, C.R., L.M. Obeid, and Y.A. Hannun, *An overview of sphingolipid metabolism: from synthesis to breakdown.* Adv Exp Med Biol, 2010. **688**: p. 1-23.
342. Rechberger, G.N., *Sphingoid Bases*, in *Encyclopedia of Lipidomics*, M.R. Wenk, Editor. 2016, Springer Netherlands: Dordrecht. p. 1-2.
343. Feng, S., et al., *Lysosome-targeted photoactivation reveals local sphingosine metabolism signatures.* Chem Sci, 2019. **10**(8): p. 2253-2258.
344. Hannun, Y.A. and R.M. Bell, *Functions of sphingolipids and sphingolipid breakdown products in cellular regulation.* Science, 1989. **243**(4890): p. 500-7.
345. Kohama, T., et al., *Molecular cloning and functional characterization of murine sphingosine kinase.* J Biol Chem, 1998. **273**(37): p. 23722-8.
346. Pitson, S.M., et al., *Activation of sphingosine kinase 1 by ERK1/2-mediated phosphorylation.* EMBO J, 2003. **22**(20): p. 5491-500.
347. Wattenberg, B.W., *Role of sphingosine kinase localization in sphingolipid signaling.* World J Biol Chem, 2010. **1**(12): p. 362-8.
348. Young, M.M., et al., *Sphingosine Kinase 1 Cooperates with Autophagy to Maintain Endocytic Membrane Trafficking.* Cell Rep, 2016. **17**(6): p. 1532-1545.
349. Diaz Escarcega, R., L.D. McCullough, and A.S. Tsvetkov, *The Functional Role of Sphingosine Kinase 2.* Front Mol Biosci, 2021. **8**: p. 683767.

350. Cannavo, A., et al., *Sphingosine Kinases and Sphingosine 1-Phosphate Receptors: Signaling and Actions in the Cardiovascular System.* Front Pharmacol, 2017. **8**: p. 556.
351. Pfeilschifter, W., et al., *Activation of sphingosine kinase 2 is an endogenous protective mechanism in cerebral ischemia.* Biochem Biophys Res Commun, 2011. **413**(2): p. 212-7.
352. Rosen, H., et al., *Sphingosine-1-phosphate and its receptors: structure, signaling, and influence.* Annu Rev Biochem, 2013. **82**: p. 637-62.
353. Wanikawa, M., et al., *Accumulation of sphingomyelin in Niemann-Pick disease type C cells disrupts Rab9-dependent vesicular trafficking of cholesterol.* J Cell Physiol, 2020. **235**(3): p. 2300-2309.
354. Goldin, E., et al., *Type C Niemann-Pick disease: a murine model of the lysosomal cholesterol lipidosis accumulates sphingosine and sphinganine in liver.* Biochim Biophys Acta, 1992. **1127**(3): p. 303-11.
355. Rodriguez-Lafrasse, C., et al., *Free sphingoid bases in tissues from patients with type C Niemann-Pick disease and other lysosomal storage disorders.* Biochim Biophys Acta, 1994. **1226**(2): p. 138-44.
356. Proia, R.L. and T. Hla, *Emerging biology of sphingosine-1-phosphate: its role in pathogenesis and therapy.* J Clin Invest, 2015. **125**(4): p. 1379-87.
357. Niekamp, P., et al., *Sphingomyelin Biosynthesis Is Essential for Phagocytic Signaling during Mycobacterium tuberculosis Host Cell Entry.* mBio, 2021. **12**(1).
358. Dubos, R.J., *The effect of sphingomyelin on the growth of tubercle bacilli.* J Exp Med, 1948. **88**(1): p. 73-9.
359. Garg, S.K., et al., *Sphingosine 1-phosphate induces antimicrobial activity both in vitro and in vivo.* J Infect Dis, 2004. **189**(11): p. 2129-38.
360. Santucci, M.B., et al., *Sphingosine 1-phosphate promotes antigen processing and presentation to CD4+ T cells in Mycobacterium tuberculosis-infected monocytes.* Biochem Biophys Res Commun, 2007. **361**(3): p. 687-93.
361. Nadella, V., et al., *Sphingosine-1-Phosphate (S-1P) Promotes Differentiation of Naive Macrophages and Enhances Protective Immunity Against Mycobacterium tuberculosis.* Front Immunol, 2019. **10**: p. 3085.

362. Sali, M., et al., *Exploiting immunotherapy in Mycobacterium tuberculosis-infected mice: sphingosine 1-phosphate treatment results in a protective or detrimental effect depending on the stage of infection.* Int J Immunopathol Pharmacol, 2009. **22**(1): p. 175-81.
363. Malik, Z.A., et al., *Cutting edge: Mycobacterium tuberculosis blocks Ca2+ signaling and phagosome maturation in human macrophages via specific inhibition of sphingosine kinase.* J Immunol, 2003. **170**(6): p. 2811-5.
364. Prakash, H., et al., *Sphingosine kinase-1 (SphK-1) regulates Mycobacterium smegmatis infection in macrophages.* PLoS One, 2010. **5**(5): p. e10657.
365. He, X., et al., *Simultaneous quantitative analysis of ceramide and sphingosine in mouse blood by naphthalene-2,3-dicarboxyaldehyde derivatization after hydrolysis with ceramidase.* Anal Biochem, 2005. **340**(1): p. 113-22.
366. Reza, S., M. Ugorski, and J. Suchanski, *Glucosylceramide and galactosylceramide, small glycosphingolipids with significant impact on health and disease.* Glycobiology, 2021. **31**(11): p. 1416-1434.
367. Quinville, B.M., et al., *A Comprehensive Review: Sphingolipid Metabolism and Implications of Disruption in Sphingolipid Homeostasis.* Int J Mol Sci, 2021. **22**(11).
368. Kihara, A., Y. Anada, and Y. Igarashi, *Mouse sphingosine kinase isoforms SPHK1a and SPHK1b differ in enzymatic traits including stability, localization, modification, and oligomerization.* J Biol Chem, 2006. **281**(7): p. 4532-9.
369. Vanier, M.T., *Lipid changes in Niemann-Pick disease type C brain: personal experience and review of the literature.* Neurochem Res, 1999. **24**(4): p. 481-9.
370. Walkley, S.U. and M.T. Vanier, *Secondary lipid accumulation in lysosomal disease.* Biochim Biophys Acta, 2009. **1793**(4): p. 726-36.
371. Kagedal, K., et al., *Sphingosine-induced apoptosis is dependent on lysosomal proteases.* Biochem J, 2001. **359**(Pt 2): p. 335-43.
372. Trimble, W.S. and S. Grinstein, *TB or not TB: calcium regulation in mycobacterial survival.* Cell, 2007. **130**(1): p. 12-4.

373. Malik, Z.A., G.M. Denning, and D.J. Kusner, *Inhibition of Ca(2+) signaling by Mycobacterium tuberculosis is associated with reduced phagosome-lysosome fusion and increased survival within human macrophages.* J Exp Med, 2000. **191**(2): p. 287-302.
374. Spiegel, S. and S. Milstien, *Sphingosine-1-phosphate: an enigmatic signalling lipid.* Nat Rev Mol Cell Biol, 2003. **4**(5): p. 397-407.
375. Lee, H., et al., *Pathological roles of the VEGF/SphK pathway in Niemann-Pick type C neurons.* Nat Commun, 2014. **5**: p. 5514.
376. Tharkeshwar, A.K., et al., *A novel approach to analyze lysosomal dysfunctions through subcellular proteomics and lipidomics: the case of NPC1 deficiency.* Sci Rep, 2017. **7**: p. 41408.
377. van der Lienden, M.J.C., et al., *GCase and LIMP2 Abnormalities in the Liver of Niemann Pick Type C Mice.* Int J Mol Sci, 2021. **22**(5).
378. Hashimoto, N., et al., *Cholesterol-dependent increases in glucosylceramide synthase activity in Niemann-Pick disease type C model cells: Abnormal trafficking of endogenously formed ceramide metabolites by inhibition of the enzyme.* Neuropharmacology, 2016. **110**(Pt A): p. 458-469.
379. Vazquez, C.L., et al., *The proneurotrophin receptor sortilin is required for Mycobacterium tuberculosis control by macrophages.* Sci Rep, 2016. **6**: p. 29332.
380. Sharma, L. and H. Prakash, *Sphingolipids Are Dual Specific Drug Targets for the Management of Pulmonary Infections: Perspective.* Front Immunol, 2017. **8**: p. 378.
381. Thompson, C.R., et al., *Sphingosine kinase 1 (SK1) is recruited to nascent phagosomes in human macrophages: inhibition of SK1 translocation by Mycobacterium tuberculosis.* J Immunol, 2005. **174**(6): p. 3551-61.
382. Kusner, D.J., et al., *The localization and activity of sphingosine kinase 1 are coordinately regulated with actin cytoskeletal dynamics in macrophages.* J Biol Chem, 2007. **282**(32): p. 23147-62.
383. Yadav, M., L. Clark, and J.S. Schorey, *Macrophage's proinflammatory response to a mycobacterial infection is dependent on sphingosine kinase-mediated activation of phosphatidylinositol phospholipase C,*

protein kinase C, ERK1/2, and phosphatidylinositol 3-kinase. J Immunol, 2006. **176**(9): p. 5494-503.

384. Anes, E., et al., *Selected lipids activate phagosome actin assembly and maturation resulting in killing of pathogenic mycobacteria.* Nat Cell Biol, 2003. **5**(9): p. 793-802.
385. Gutierrez, M.G., et al., *Role of lipids in killing mycobacteria by macrophages: evidence for NF-kappaB-dependent and -independent killing induced by different lipids.* Cell Microbiol, 2009. **11**(3): p. 406-20.
386. Ruhl, C.R., et al., *Mycobacterium tuberculosis Sulfolipid-1 Activates Nociceptive Neurons and Induces Cough.* Cell, 2020. **181**(2): p. 293-305 e11.
387. Daffe, M. and M.A. Laneelle, *Distribution of phthiocerol diester, phenolic mycosides and related compounds in mycobacteria.* J Gen Microbiol, 1988. **134**(7): p. 2049-55.
388. Marrakchi, H., M.A. Laneelle, and M. Daffe, *Mycolic acids: structures, biosynthesis, and beyond.* Chem Biol, 2014. **21**(1): p. 67-85.
389. Batt, S.M., D.E. Minnikin, and G.S. Besra, *The thick waxy coat of mycobacteria, a protective layer against antibiotics and the host's immune system.* Biochem J, 2020. **477**(10): p. 1983-2006.
390. Barkan, D., et al., *Mycolic acid cyclopropanation is essential for viability, drug resistance, and cell wall integrity of Mycobacterium tuberculosis.* Chem Biol, 2009. **16**(5): p. 499-509.
391. Vermeulen, I., et al., *Mycolates of Mycobacterium tuberculosis modulate the flow of cholesterol for bacillary proliferation in murine macrophages.* J Lipid Res, 2017. **58**(4): p. 709-718.
392. Barkan, D., et al., *Mycobacterium tuberculosis lacking all mycolic acid cyclopropanation is viable but highly attenuated and hyperinflammatory in mice.* Infect Immun, 2012. **80**(6): p. 1958-68.
393. Nataraj, V., et al., *Mycolic acids: deciphering and targeting the Achilles' heel of the tubercle bacillus.* Mol Microbiol, 2015. **98**(1): p. 7-16.
394. Yarkoni, E., L. Wang, and A. Bekierkunst, *Stimulation of macrophages by cord factor and by heat-killed and living BCG.* Infect Immun, 1977. **16**(1): p. 1-8.

395. Ryll, R., Y. Kumazawa, and I. Yano, *Immunological properties of trehalose dimycolate (cord factor) and other mycolic acid-containing glycolipids--a review.* Microbiol Immunol, 2001. **45**(12): p. 801-11.

396. Hunter, R.L., et al., *Multiple roles of cord factor in the pathogenesis of primary, secondary, and cavitary tuberculosis, including a revised description of the pathology of secondary disease.* Ann Clin Lab Sci, 2006. **36**(4): p. 371-86.

397. Hunter, R.L., et al., *Trehalose 6,6'-dimycolate and lipid in the pathogenesis of caseating granulomas of tuberculosis in mice.* Am J Pathol, 2006. **168**(4): p. 1249-61.

398. Patin, E.C., et al., *Trehalose dimycolate interferes with FcgammaR-mediated phagosome maturation through Mincle, SHP-1 and FcgammaRIIB signalling.* PLoS One, 2017. **12**(4): p. e0174973.

399. Katti, M.K., et al., *The Delta fbpA mutant derived from Mycobacterium tuberculosis H37Rv has an enhanced susceptibility to intracellular antimicrobial oxidative mechanisms, undergoes limited phagosome maturation and activates macrophages and dendritic cells.* Cell Microbiol, 2008. **10**(6): p. 1286-303.

400. Gilmore, S.A., et al., *Sulfolipid-1 biosynthesis restricts Mycobacterium tuberculosis growth in human macrophages.* ACS Chem Biol, 2012. **7**(5): p. 863-70.

401. Sirakova, T.D., et al., *The Mycobacterium tuberculosis pks2 gene encodes the synthase for the hepta- and octamethyl-branched fatty acids required for sulfolipid synthesis.* J Biol Chem, 2001. **276**(20): p. 16833-9.

402. Rousseau, C., et al., *Sulfolipid deficiency does not affect the virulence of Mycobacterium tuberculosis H37Rv in mice and guinea pigs.* Infect Immun, 2003. **71**(8): p. 4684-90.

403. Passemar, C., et al., *Multiple deletions in the polyketide synthase gene repertoire of Mycobacterium tuberculosis reveal functional overlap of cell envelope lipids in host-pathogen interactions.* Cell Microbiol, 2014. **16**(2): p. 195-213.

404. Zhang, L., et al., *Effect of Mycobacterium tuberculosis-derived sulfolipid I on human phagocytic cells.* Infect Immun, 1988. **56**(11): p. 2876-83.

405. Okamoto, Y., et al., *Mycobacterial sulfolipid shows a virulence by inhibiting cord factor induced granuloma formation and TNF-alpha release.* Microb Pathog, 2006. **40**(6): p. 245-53.
406. Converse, S.E., et al., *MmpL8 is required for sulfolipid-1 biosynthesis and Mycobacterium tuberculosis virulence.* Proc Natl Acad Sci U S A, 2003. **100**(10): p. 6121-6.
407. Rodriguez, J.E., et al., *Transcription of genes involved in sulfolipid and polyacyltrehalose biosynthesis of Mycobacterium tuberculosis in experimental latent tuberculosis infection.* PLoS One, 2013. **8**(3): p. e58378.
408. Geerdink, D. and A.J. Minnaard, *Total synthesis of sulfolipid-1.* Chem Commun (Camb), 2014. **50**(18): p. 2286-8.
409. Brown, C.M., et al., *Supramolecular organization and dynamics of mannosylated phosphatidylinositol lipids in the mycobacterial plasma membrane.* Proc Natl Acad Sci U S A, 2023. **120**(5): p. e2212755120.
410. Boonyarattanakalin, S., et al., *Chemical synthesis of all phosphatidylinositol mannoside (PIM) glycans from Mycobacterium tuberculosis.* J Am Chem Soc, 2008. **130**(49): p. 16791-9.
411. Morita, Y.S., et al., *PimE is a polyprenol-phosphate-mannose-dependent mannosyltransferase that transfers the fifth mannose of phosphatidylinositol mannoside in mycobacteria.* J Biol Chem, 2006. **281**(35): p. 25143-55.
412. Haites, R.E., et al., *Function of phosphatidylinositol in mycobacteria.* J Biol Chem, 2005. **280**(12): p. 10981-7.
413. Nguyen, P.P., et al., *Inositol acylation of phosphatidylinositol mannosides: a rapid mass response to membrane fluidization in mycobacteria.* J Lipid Res, 2022. **63**(9): p. 100262.
414. Court, N., et al., *Mycobacterial PIMs inhibit host inflammatory responses through CD14-dependent and CD14-independent mechanisms.* PLoS One, 2011. **6**(9): p. e24631.
415. Vergne, I., J. Chua, and V. Deretic, *Tuberculosis toxin blocking phagosome maturation inhibits a novel Ca2+/calmodulin-PI3K hVPS34 cascade.* J Exp Med, 2003. **198**(4): p. 653-9.

416. Fratti, R.A., et al., *Mycobacterium tuberculosis glycosylated phosphatidylinositol causes phagosome maturation arrest.* Proc Natl Acad Sci U S A, 2003. **100**(9): p. 5437-42.
417. Layre, E., et al., *Molecular profiling of Mycobacterium tuberculosis identifies tuberculosinyl nucleoside products of the virulence-associated enzyme Rv3378c.* Proc Natl Acad Sci U S A, 2014. **111**(8): p. 2978-83.
418. Layre, E., et al., *A comparative lipidomics platform for chemotaxonomic analysis of Mycobacterium tuberculosis.* Chem Biol, 2011. **18**(12): p. 1537-49.
419. Platt, N., et al., *Release of acidic store calcium is required for effective priming of the NLRP3 inflammasome.* bioRxiv, 2022: p. 2022.01.06.475262.
420. Goren, M.B., et al., *Prevention of phagosome-lysosome fusion in cultured macrophages by sulfatides of Mycobacterium tuberculosis.* Proc Natl Acad Sci U S A, 1976. **73**(7): p. 2510-4.
421. Goren, M.B., A.E. Vatter, and J. Fiscus, *Polyanionic agents as inhibitors of phagosome-lysosome fusion in cultured macrophages: evolution of an alternative interpretation.* J Leukoc Biol, 1987. **41**(2): p. 111-21.
422. Russell, D.G., *Mycobacterium tuberculosis and the intimate discourse of a chronic infection.* Immunol Rev, 2011. **240**(1): p. 252-68.
423. Boldrin, F., et al., *The phosphatidyl-myo-inositol mannosyltransferase PimA is essential for Mycobacterium tuberculosis growth in vitro and in vivo.* J Bacteriol, 2014. **196**(19): p. 3441-51.
424. Angala, S.K., et al., *The cell envelope glycoconjugates of Mycobacterium tuberculosis.* Crit Rev Biochem Mol Biol, 2014. **49**(5): p. 361-99.
425. Sachdeva, K., et al., *Mycobacterium tuberculosis (Mtb) lipid mediated lysosomal rewiring in infected macrophages modulates intracellular Mtb trafficking and survival.* J Biol Chem, 2020. **295**(27): p. 9192-9210.
426. Davis, O.B., et al., *NPC1-mTORC1 Signaling Couples Cholesterol Sensing to Organelle Homeostasis and Is a Targetable Pathway in Niemann-Pick Type C.* Dev Cell, 2021. **56**(3): p. 260-276 e7.
427. Paik, S., et al., *Mycobacterial acyl carrier protein suppresses TFEB activation and upregulates miR-155 to inhibit host defense.* Front Immunol, 2022. **13**: p. 946929.

428. Zheng, W., et al., *Mycobacterium tuberculosis resides in lysosome-poor monocyte-derived lung cells during chronic infection.* bioRxiv, 2023.
429. Bedard, M., et al., *A terpene nucleoside from M. tuberculosis induces lysosomal lipid storage in foamy macrophages.* J Clin Invest, 2023. **133**(6).
430. Lamas, A., et al., *A comprehensive review of non-enterica subspecies of Salmonella enterica.* Microbiol Res, 2018. **206**: p. 60-73.
431. Desai, P.T., et al., *Evolutionary Genomics of Salmonella enterica Subspecies.* mBio, 2013. **4**(2).
432. Gordon, M.A., *Salmonella infections in immunocompromised adults.* J Infect, 2008. **56**(6): p. 413-22.
433. Eng, S., Pusparajah, P, Mutalib, N.A., Ser, H., Chan, H., Lee, L., *Salmonella: A review on pathogenesis, epidemiology and antibiotic resistance.* Frontiers in Life Science, 2015. **8**(3): p. 284-293.
434. Sanchez-Vargas, F.M., M.A. Abu-El-Haija, and O.G. Gomez-Duarte, *Salmonella infections: an update on epidemiology, management, and prevention.* Travel Med Infect Dis, 2011. **9**(6): p. 263-77.
435. Bhan, M.K., R. Bahl, and S. Bhatnagar, *Typhoid and paratyphoid fever.* Lancet, 2005. **366**(9487): p. 749-62.
436. Collaborators, G.B.D.N.-T.S.I.D., *The global burden of non-typhoidal salmonella invasive disease: a systematic analysis for the Global Burden of Disease Study 2017.* Lancet Infect Dis, 2019. **19**(12): p. 1312-1324.
437. Hohmann, E.L., *Nontyphoidal salmonellosis.* Clin Infect Dis, 2001. **32**(2): p. 263-9.
438. Gong, B., et al., *Prevalence, Serotype Distribution and Antimicrobial Resistance of Non-Typhoidal Salmonella in Hospitalized Patients in Conghua District of Guangzhou, China.* Front Cell Infect Microbiol, 2022. **12**: p. 805384.
439. Branchu, P., M. Bawn, and R.A. Kingsley, *Genome Variation and Molecular Epidemiology of Salmonella enterica Serovar Typhimurium Pathovariants.* Infect Immun, 2018. **86**(8).
440. Rabsch, W., H. Tschape, and A.J. Baumler, *Non-typhoidal salmonellosis: emerging problems.* Microbes Infect, 2001. **3**(3): p. 237-47.

441. Horstmann, J.A., et al., *Methylation of Salmonella Typhimurium flagella promotes bacterial adhesion and host cell invasion.* Nat Commun, 2020. **11**(1): p. 2013.
442. Coburn, B., I. Sekirov, and B.B. Finlay, *Type III secretion systems and disease.* Clin Microbiol Rev, 2007. **20**(4): p. 535-49.
443. de Jong, H.K., et al., *Host-pathogen interaction in invasive Salmonellosis.* PLoS Pathog, 2012. **8**(10): p. e1002933.
444. Foster, J.W. and H.K. Hall, *Inducible pH homeostasis and the acid tolerance response of Salmonella typhimurium.* J Bacteriol, 1991. **173**(16): p. 5129-35.
445. Raffatellu, M., et al., *SipA, SopA, SopB, SopD, and SopE2 contribute to Salmonella enterica serotype typhimurium invasion of epithelial cells.* Infect Immun, 2005. **73**(1): p. 146-54.
446. Steele-Mortimer, O., *The Salmonella-containing vacuole: moving with the times.* Curr Opin Microbiol, 2008. **11**(1): p. 38-45.
447. Eckmann, L. and M.F. Kagnoff, *Cytokines in host defense against Salmonella.* Microbes Infect, 2001. **3**(14-15): p. 1191-200.
448. Fink, S.L. and B.T. Cookson, *Pyroptosis and host cell death responses during Salmonella infection.* Cell Microbiol, 2007. **9**(11): p. 2562-70.
449. Silva, C., E. Calva, and S. Maloy, *One Health and Food-Borne Disease: Salmonella Transmission between Humans, Animals, and Plants.* Microbiol Spectr, 2014. **2**(1): p. OH-0020-2013.
450. Fabrega, A. and J. Vila, *Salmonella enterica serovar Typhimurium skills to succeed in the host: virulence and regulation.* Clin Microbiol Rev, 2013. **26**(2): p. 308-41.
451. Galan, J.E., *Salmonella Typhimurium and inflammation: a pathogen-centric affair.* Nat Rev Microbiol, 2021. **19**(11): p. 716-725.
452. Sansonetti, P., *Phagocytosis of bacterial pathogens: implications in the host response.* Semin Immunol, 2001. **13**(6): p. 381-90.
453. Jepson, M.A., et al., *Rapid disruption of epithelial barrier function by Salmonella typhimurium is associated with structural modification of intercellular junctions.* Infect Immun, 1995. **63**(1): p. 356-9.

454. Bueno, S.M., et al., *Salmonella pathogenicity island 1 differentially modulates bacterial entry to dendritic and non-phagocytic cells.* Immunology, 2010. **130**(2): p. 273-87.
455. Fredlund, J., et al., *The entry of Salmonella in a distinct tight compartment revealed at high temporal and ultrastructural resolution.* Cell Microbiol, 2018. **20**(4).
456. Alpuche-Aranda, C.M., et al., *Salmonella stimulate macrophage macropinocytosis and persist within spacious phagosomes.* J Exp Med, 1994. **179**(2): p. 601-8.
457. Steele-Mortimer, O., et al., *Biogenesis of Salmonella typhimurium-containing vacuoles in epithelial cells involves interactions with the early endocytic pathway.* Cell Microbiol, 1999. **1**(1): p. 33-49.
458. Smith, A.C., et al., *Interaction of the Salmonella-containing vacuole with the endocytic recycling system.* J Biol Chem, 2005. **280**(26): p. 24634-41.
459. Gog, J.R., et al., *Dynamics of Salmonella infection of macrophages at the single cell level.* J R Soc Interface, 2012. **9**(75): p. 2696-707.
460. Ammanathan, V., et al., *Restriction of intracellular Salmonella replication by restoring TFEB-mediated xenophagy.* Autophagy, 2020. **16**(9): p. 1584-1597.
461. Birmingham, C.L., et al., *Autophagy controls Salmonella infection in response to damage to the Salmonella-containing vacuole.* J Biol Chem, 2006. **281**(16): p. 11374-83.
462. Malik-Kale, P., S. Winfree, and O. Steele-Mortimer, *The bimodal lifestyle of intracellular Salmonella in epithelial cells: replication in the cytosol obscures defects in vacuolar replication.* PLoS One, 2012. **7**(6): p. e38732.
463. Drecktrah, D., et al., *Salmonella trafficking is defined by continuous dynamic interactions with the endolysosomal system.* Traffic, 2007. **8**(3): p. 212-25.
464. Madan, R., et al., *Salmonella acquires lysosome-associated membrane protein 1 (LAMP1) on phagosomes from Golgi via SipC protein-mediated recruitment of host Syntaxin6.* J Biol Chem, 2012. **287**(8): p. 5574-87.
465. Smith, A.C., et al., *A network of Rab GTPases controls phagosome maturation and is modulated by Salmonella enterica serovar Typhimurium.* J Cell Biol, 2007. **176**(3): p. 263-8.

466. Liss, V., et al., *Salmonella enterica Remodels the Host Cell Endosomal System for Efficient Intravacuolar Nutrition.* Cell Host Microbe, 2017. **21**(3): p. 390-402.
467. Eswarappa, S.M., et al., *Division of the Salmonella-containing vacuole and depletion of acidic lysosomes in Salmonella-infected host cells are novel strategies of Salmonella enterica to avoid lysosomes.* Infect Immun, 2010. **78**(1): p. 68-79.
468. Drecktrah, D., et al., *Dynamic behavior of Salmonella-induced membrane tubules in epithelial cells.* Traffic, 2008. **9**(12): p. 2117-29.
469. Salcedo, S.P. and D.W. Holden, *SseG, a virulence protein that targets Salmonella to the Golgi network.* EMBO J, 2003. **22**(19): p. 5003-14.
470. Meresse, S., et al., *Remodelling of the actin cytoskeleton is essential for replication of intravacuolar Salmonella.* Cell Microbiol, 2001. **3**(8): p. 567-77.
471. Muller, P., D. Chikkaballi, and M. Hensel, *Functional dissection of SseF, a membrane-integral effector protein of intracellular Salmonella enterica.* PLoS One, 2012. **7**(4): p. e35004.
472. Stein, M.A., et al., *Identification of a Salmonella virulence gene required for formation of filamentous structures containing lysosomal membrane glycoproteins within epithelial cells.* Mol Microbiol, 1996. **20**(1): p. 151-64.
473. Knuff, K. and B.B. Finlay, *What the SIF Is Happening-The Role of Intracellular Salmonella-Induced Filaments.* Front Cell Infect Microbiol, 2017. **7**: p. 335.
474. Fang, Z. and S. Meresse, *Endomembrane remodeling and dynamics in Salmonella infection.* Microb Cell, 2022. **9**(2): p. 24-41.
475. Bakowski, M.A., V. Braun, and J.H. Brumell, *Salmonella-containing vacuoles: directing traffic and nesting to grow.* Traffic, 2008. **9**(12): p. 2022-31.
476. Malik-Kale, P., et al., *Salmonella - at home in the host cell.* Front Microbiol, 2011. **2**: p. 125.
477. Gal-Mor, O., *Persistent Infection and Long-Term Carriage of Typhoidal and Nontyphoidal Salmonellae.* Clin Microbiol Rev, 2019. **32**(1).

478. Marzel, A., et al., *Persistent Infections by Nontyphoidal Salmonella in Humans: Epidemiology and Genetics.* Clin Infect Dis, 2016. **62**(7): p. 879-886.
479. Monack, D.M., *Salmonella persistence and transmission strategies.* Curr Opin Microbiol, 2012. **15**(1): p. 100-7.
480. Monack, D.M., D.M. Bouley, and S. Falkow, *Salmonella typhimurium persists within macrophages in the mesenteric lymph nodes of chronically infected Nramp1+/+ mice and can be reactivated by IFNgamma neutralization.* J Exp Med, 2004. **199**(2): p. 231-41.
481. Helaine, S., et al., *Dynamics of intracellular bacterial replication at the single cell level.* Proc Natl Acad Sci U S A, 2010. **107**(8): p. 3746-51.
482. Luk, C.H., et al., *Salmonella enters a dormant state within human epithelial cells for persistent infection.* PLoS Pathog, 2021. **17**(4): p. e1009550.
483. Lawley, T.D., et al., *Genome-wide screen for Salmonella genes required for long-term systemic infection of the mouse.* PLoS Pathog, 2006. **2**(2): p. e11.
484. Ishibashi, Y. and T. Arai, *Specific inhibition of phagosome-lysosome fusion in murine macrophages mediated by Salmonella typhimurium infection.* FEMS Microbiol Immunol, 1990. **2**(1): p. 35-43.
485. Buchmeier, N.A. and F. Heffron, *Inhibition of macrophage phagosome-lysosome fusion by Salmonella typhimurium.* Infect Immun, 1991. **59**(7): p. 2232-8.
486. Catron, D.M., et al., *The Salmonella-containing vacuole is a major site of intracellular cholesterol accumulation and recruits the GPI-anchored protein CD55.* Cell Microbiol, 2002. **4**(6): p. 315-28.
487. Nawabi, P., D.M. Catron, and K. Haldar, *Esterification of cholesterol by a type III secretion effector during intracellular Salmonella infection.* Mol Microbiol, 2008. **68**(1): p. 173-85.
488. Jennings, E., T.L.M. Thurston, and D.W. Holden, *Salmonella SPI-2 Type III Secretion System Effectors: Molecular Mechanisms And Physiological Consequences.* Cell Host Microbe, 2017. **22**(2): p. 217-231.
489. Agbor, T.A. and B.A. McCormick, *Salmonella effectors: important players modulating host cell function during infection.* Cell Microbiol, 2011. **13**(12): p. 1858-69.

490. Marcus, S.L., et al., *Salmonella pathogenicity islands: big virulence in small packages.* Microbes Infect, 2000. **2**(2): p. 145-56.
491. Brumell, J.H., D.L. Goosney, and B.B. Finlay, *SifA, a type III secreted effector of Salmonella typhimurium, directs Salmonella-induced filament (Sif) formation along microtubules.* Traffic, 2002. **3**(6): p. 407-15.
492. Brumell, J.H., et al., *SifA permits survival and replication of Salmonella typhimurium in murine macrophages.* Cell Microbiol, 2001. **3**(2): p. 75-84.
493. Ruiz-Albert, J., et al., *Complementary activities of SseJ and SifA regulate dynamics of the Salmonella typhimurium vacuolar membrane.* Mol Microbiol, 2002. **44**(3): p. 645-61.
494. Greene, A.R., K.A. Owen, and J.E. Casanova, *Salmonella Typhimurium manipulates macrophage cholesterol homeostasis through the SseJ-mediated suppression of the host cholesterol transport protein ABCA1.* Cell Microbiol, 2021. **23**(8): p. e13329.
495. Arena, E.T., et al., *The deubiquitinase activity of the Salmonella pathogenicity island 2 effector, SseL, prevents accumulation of cellular lipid droplets.* Infect Immun, 2011. **79**(11): p. 4392-400.
496. Mesmin, B., et al., *A four-step cycle driven by PI(4)P hydrolysis directs sterol/PI(4)P exchange by the ER-Golgi tether OSBP.* Cell, 2013. **155**(4): p. 830-43.
497. McGourty, K., et al., *Salmonella inhibits retrograde trafficking of mannose-6-phosphate receptors and lysosome function.* Science, 2012. **338**(6109): p. 963-7.
498. Schuster, E.M., et al., *TFEB induces mitochondrial itaconate synthesis to suppress bacterial growth in macrophages.* Nat Metab, 2022. **4**(7): p. 856-866.
499. McEwan, D.G., et al., *PLEKHM1 regulates Salmonella-containing vacuole biogenesis and infection.* Cell Host Microbe, 2015. **17**(1): p. 58-71.
500. Sindhwani, A., et al., *Salmonella exploits the host endolysosomal tethering factor HOPS complex to promote its intravacuolar replication.* PLoS Pathog, 2017. **13**(10): p. e1006700.
501. Walch, P., et al., *Global mapping of Salmonella enterica-host protein-protein interactions during infection.* Cell Host Microbe, 2021. **29**(8): p. 1316-1332 e12.

502. Higaki, K., et al., *Isolation of NPC1-deficient Chinese hamster ovary cell mutants by gene trap mutagenesis.* J Biochem, 2001. **129**(6): p. 875-80.
503. Dahl, N.K., et al., *Isolation and characterization of Chinese hamster ovary cells defective in the intracellular metabolism of low density lipoprotein-derived cholesterol.* J Biol Chem, 1992. **267**(7): p. 4889-96.
504. Cadigan, K.M., D.M. Spillane, and T.Y. Chang, *Isolation and characterization of Chinese hamster ovary cell mutants defective in intracellular low density lipoprotein-cholesterol trafficking.* J Cell Biol, 1990. **110**(2): p. 295-308.
505. Rolhion, N., et al., *Inhibition of Nuclear Transport of NF-kB p65 by the Salmonella Type III Secretion System Effector SpvD.* PLoS Pathog, 2016. **12**(5): p. e1005653.
506. Chen, R., *Isolation and Culture of Mouse Bone Marrow-derived Macrophages (BMM'phi').* Bio-protocol, 2012. **2**(3): p. e68.
507. Figueira, R., et al., *Identification of salmonella pathogenicity island-2 type III secretion system effectors involved in intramacrophage replication of S. enterica serovar typhimurium: implications for rational vaccine design.* mBio, 2013. **4**(2): p. e00065.
508. Yu, X.J., et al., *SsaV Interacts with SsaL to Control the Translocon-to-Effector Switch in the Salmonella SPI-2 Type Three Secretion System.* mBio, 2018. **9**(5).
509. Hamann, L., et al., *Binding of lipopolysaccharide (LPS) to CHO cells does not correlate with LPS-induced NF-kappaB activation.* Eur J Immunol, 2000. **30**(1): p. 211-6.
510. Yeung, A.T.Y., et al., *A Genome-Wide Knockout Screen in Human Macrophages Identified Host Factors Modulating Salmonella Infection.* mBio, 2019. **10**(5).
511. Xu, J., et al., *Structural and Functional Analysis of SsaV Cytoplasmic Domain and Variable Linker States in the Context of the InvA-SsaV Chimeric Protein.* Microbiol Spectr, 2021. **9**(3): p. e0125121.
512. Ramos-Morales, F., *Impact of Salmonella enterica Type III Secretion System Effectors on the Eukaryotic Host Cell.* ISRN Cell Biology, 2012. **2012**: p. 787934.

513. Beuzon, C.R., et al., *Salmonella maintains the integrity of its intracellular vacuole through the action of SifA.* EMBO J, 2000. **19**(13): p. 3235-49.
514. Kolodziejek, A.M. and S.I. Miller, *Salmonella modulation of the phagosome membrane, role of SseJ.* Cell Microbiol, 2015. **17**(3): p. 333-41.
515. Garner, M.J., R.D. Hayward, and V. Koronakis, *The Salmonella pathogenicity island 1 secretion system directs cellular cholesterol redistribution during mammalian cell entry and intracellular trafficking.* Cell Microbiol, 2002. **4**(3): p. 153-65.
516. Worrall, L.J., M. Vuckovic, and N.C. Strynadka, *Crystal structure of the C-terminal domain of the Salmonella type III secretion system export apparatus protein InvA.* Protein Sci, 2010. **19**(5): p. 1091-6.
517. Ramachandran, V.K., N. Shearer, and A. Thompson, *The primary transcriptome of Salmonella enterica Serovar Typhimurium and its dependence on ppGpp during late stationary phase.* PLoS One, 2014. **9**(3): p. e92690.
518. Colaco, A., et al., *Mechanistic convergence and shared therapeutic targets in Niemann-Pick disease.* J Inherit Metab Dis, 2020. **43**(3): p. 574-585.
519. Huang, F.C., *De Novo sphingolipid synthesis is essential for Salmonella-induced autophagy and human beta-defensin 2 expression in intestinal epithelial cells.* Gut Pathog, 2016. **8**: p. 5.
520. McCollister, B.D., et al., *Constitutive acid sphingomyelinase enhances early and late macrophage killing of Salmonella enterica serovar Typhimurium.* Infect Immun, 2007. **75**(11): p. 5346-52.
521. Hayakawa, S., et al., *Activated cholesterol metabolism is integral for innate macrophage responses by amplifying Myd88 signaling.* JCI Insight, 2022. **7**(22).
522. Liou, H.L., et al., *NPC2, the protein deficient in Niemann-Pick C2 disease, consists of multiple glycoforms that bind a variety of sterols.* J Biol Chem, 2006. **281**(48): p. 36710-23.
523. Rana, F.R., Sultany, C.M., Blazyk, J., *Determination of the lipid composition of Salmonella typhimurium outer membranes by 31P NMR.* Journal of Microbiological Methods, 1991. **14**(1): p. 41-51.

524. Ames, G.F., *Lipids of Salmonella typhimurium and Escherichia coli: structure and metabolism.* J Bacteriol, 1968. **95**(3): p. 833-43.
525. Winkler, M.B.L., et al., *Structural Insight into Eukaryotic Sterol Transport through Niemann-Pick Type C Proteins.* Cell, 2019. **179**(2): p. 485-497 e18.
526. Miller, E.H., et al., *Ebola virus entry requires the host-programmed recognition of an intracellular receptor.* EMBO J, 2012. **31**(8): p. 1947-60.
527. Rayamajhee, B., et al., *Acanthamoeba, an environmental phagocyte enhancing survival and transmission of human pathogens.* Trends Parasitol, 2022. **38**(11): p. 975-990.
528. Zajac, M., S. Modi, and Y. Krishnan, *The evolution of organellar calcium mapping technologies.* Cell Calcium, 2022. **108**: p. 102658.
529. Upadhyay, S., E. Mittal, and J.A. Philips, *Tuberculosis and the art of macrophage manipulation.* Pathog Dis, 2018. **76**(4).
530. Pineda, M., M. Walterfang, and M.C. Patterson, *Miglustat in Niemann-Pick disease type C patients: a review.* Orphanet J Rare Dis, 2018. **13**(1): p. 140.
531. Baldwin, P.R., et al., *Monocarbonyl analogs of curcumin inhibit growth of antibiotic sensitive and resistant strains of Mycobacterium tuberculosis.* Eur J Med Chem, 2015. **92**: p. 693-9.
532. Gupta, P.K., et al., *Macrophage targeted polymeric curcumin nanoparticles limit intracellular survival of Mycobacterium tuberculosis through induction of autophagy and augment anti-TB activity of isoniazid in RAW 264.7 macrophages.* Front Immunol, 2023. **14**: p. 1233630.

Appendix 1.

Inhibition of the Niemann-Pick C1 protein is a conserved feature of multiple strains of pathogenic mycobacteria

nature communications

Article

https://doi.org/10.1038/s41467-022-32553-0

Inhibition of the Niemann-Pick C1 protein is a conserved feature of multiple strains of pathogenic mycobacteria

Received: 15 December 2021

Accepted: 4 August 2022

Published online: 09 September 2022

Check for updates

Yuzhe Weng[1,4], Dawn Shepherd[1,4], Yi Liu[2], Nitya Krishnan[3], Brian D. Robertson[3], Nick Platt[1,5], Gerald Larrouy-Maumus[2,5] & Frances M. Platt[1,5]

Mycobacterium tuberculosis (*Mtb*) survives and replicates within host macrophages (MΦ) and subverts multiple antimicrobial defense mechanisms. Previously, we reported that lipids shed by pathogenic mycobacteria inhibit NPC1, the lysosomal membrane protein deficient in the lysosomal storage disorder Niemann-Pick disease type C (NPC). Inhibition of NPC1 leads to a drop in lysosomal calcium levels, blocking phagosome-lysosome fusion leading to mycobacterial survival. We speculated that the production of specific cell wall lipid(s) that inhibit NPC1 could have been a critical step in the evolution of pathogenicity. We therefore investigated whether lipid extracts from clinical *Mtb* strains from multiple *Mtb* lineages, *Mtb* complex (MTBC) members and non-tubercular mycobacteria (NTM) inhibit the NPC pathway. We report that inhibition of the NPC pathway was present in all clinical isolates from *Mtb* lineages 1, 2, 3 and 4, *Mycobacterium bovis* and the NTM, *Mycobacterium abscessus* and *Mycobacterium avium*. However, lipid extract from *Mycobacterium canettii*, which is considered to resemble the common ancestor of the MTBC did not inhibit the NPC1 pathway. We conclude that the evolution of NPC1 inhibitory mycobacterial cell wall lipids evolved early and post divergence from *Mycobacterium canettii*-related mycobacteria and that this activity contributes significantly to the promotion of disease.

Mycobacterium tuberculosis (Mtb), the causative agent of tuberculosis (TB) is a major human pathogen[1,2]. While the emergence of multi-drug-resistant strains has added to the challenges of treatment, the ability of Mtb to survive and replicate intracellularly in host macrophages (MΦ) is key to its success[3,4]. Typically, bacilli within aerosol droplets are inhaled into the lower pulmonary environment and initially infect resident alveolar macrophages (MΦ), which induces the recruitment of additional myeloid cells, leading to the formation of granulomas. Granulomas facilitate infection of other cell types and promote mycobacterial growth[3,5]. Long-term intracellular persistence is the basis for TB latency, which provides a pathogen reservoir that can subsequently become reactivated and promote transmission to a new host[6]. Mycobacteria are phagocytosed following an initial interaction with MΦ plasma membrane receptors[7,8]. However, in contrast to the fate of other ingested particles, which involves phagosome formation and subsequent phagosome-lysosome fusion, Mtb and other pathogenic mycobacteria actively block this process facilitating their long-term survival within the MΦ[5,9]. Although multiple mechanisms have

[1]Department of Pharmacology, University of Oxford, Mansfield Road, Oxford OX1 3QT, UK. [2]MRC Centre for Molecular Bacteriology and Infection, Department of Life Sciences, Faculty of Natural Sciences, Imperial College London, London, UK. [3]MRC Centre for Molecular Bacteriology and Infection, Department of Infectious Disease, Imperial College London, Flowers Building, London SW7 2AZ, UK. [4]These authors contributed equally: Yuzhe Weng, Dawn Shepherd. [5]These authors jointly supervised this work: Nick Platt, Gerald Larrouy-Maumus, Frances M. Platt. e-mail: frances.platt@pharm.ox.ac.uk

been proposed to explain the ability of Mtb to inhibit the fusion of the lysosome with the phagosomes[10,11] current understanding remains incomplete. The possibility of interfering with the Mtb-mediated block in phagosome-lysosome fusion is an attractive target for host-directed Mtb therapy.

As well as the block in phagosome–lysosome fusion, cells harboring intracellular mycobacteria display several additional characteristics[5] and we have previously reported the unexpected similarity between the cellular phenotypes of Mtb-infected MΦ and those of the rare, inherited lysosomal storage disease, Niemann-Pick disease type C (NPC)[12]. NPC is caused by mutations in either of two genes, *NPC1* (95% of clinical cases) or *NPC2*. They work cooperatively in a pathway that is involved in lipid trafficking and lysosome: ER contact site formation[13,14]. The precise function of NPC1 is incompletely understood and a direct assay to measure its function is therefore not available. We therefore demonstrated that cells harboring specific mycobacteria display the unique combination of cellular phenotypes that result from loss of NPC1 activity[12]. In brief, all of the cellular phenotypes that define NPC, including a reduction in the calcium content of lysosomes, prevention of phagosome-lysosome fusion, accumulation of specific lipid species (including cholesterol, sphingomyelin, and glycosphingolipids (GSLs)) within the endo-lysosomal system were induced in cells infected with mycobacteria that survive within host cells (Mtb and *Mycobacterium bovis Bacillus* Calmette-Guerin (BCG)), but not the environmental non-pathogenic mycobacterium *Mycobacterium smegmatis*. Very significantly, it was the lipid fraction of the cell wall from the pathogenic mycobacteria that inhibited the NPC pathway. Critically, all of the NPC cellular phenotypes were induced not only in infected and lipid-treated murine RAW 264.7 MΦ but also in human, monocyte-derived MΦ, thereby confirming relevance to human disease[12]. Additionally, we observed induction of the NPC cellular phenotypes in neighboring cells that did not contain internalized mycobacteria. These data are consistent with the proposal that pathogenic mycobacteria shed lipids that inhibit the activity of NPC1, and thereby prevent normal phagosome–lysosome maturation[12].

We hypothesized that the evolution of lipids that inhibit NPC1 would correlate with the acquisition of the ability to survive intracellularly and cause disease. In this study, we have therefore assayed the capacity of cell wall lipid extracts to induce NPC cellular phenotypes in RAW 264.7 MΦ. We report that extracts from diverse pathogenic mycobacterial species representing the main Mtb lineages differentially induce NPC phenotypes with the notable exception of *Mycobacterium canettii*, which is believed to resemble the putative common ancestor. These findings suggest that the evolution of lipids capable of inhibiting NPC1 evolved early, post-divergence from *M. canettii* and correlates with virulence and intracellular survival and therefore represents a new target for therapy.

Table 1 | Genotypes of the selected Mtb clinical isolates strains used in this study

Strain	Spoligotype[I]	ST number[II]	Lineage category[III]	Lineage number[IV]	Lineage geographical location[V]
232	EA14_VNM	ST139	Ancient	1	IO
346	EA14_VNM	ST140	Ancient	1	IO
372	EA14_VNM	ST141	Ancient	1	IO
281	ZERO	ST405	Ancient	1	IO
374	BEIJING	ST1	Modern	2	BJ
212	BEIJING	ST2	Modern	2	BJ
333	BEIJING	ST3	Modern	2	BJ
119	BEIJING	ST4	Modern	2	BJ
345	BEIJING LIKE	Unclassified	Modern	2	BJ
649	BEIJING LIKE	ST269	Modern	2	BJ
318	T1	ST53	Modern	4	EA
173	H1	ST62	Modern	4	EA
367	ZERO	ST405	Ancient	1	IO
440	H3	ST946	Modern	4	EA
639	H3	ST50	Modern	4	EA
293	T1	ST53	Modern	4	EA

I and II Classified in accordance with the international Spoligotyping database[78]. III Classified based on evolutionary phylogenetic tree[79]. IV Classified in accordance with sequence alignment[36]. V. *BJ*. East Asian/Beijing; *IO*. Indo-Oceanic; *EA*. Euro-American.

Results

Cell wall lipid fractions from Mtb clinical isolates, specific NTM, and *M. bovis Bacillus* but not *M. canettii* increase LysoTracker™ staining intensity of RAW 264.7 MΦ

We have reported previously that the volume of the acidic compartment (late endosome/lysosome (LE/Lys)) is significantly expanded in genetic NPC1-deficient cells[15] and in RAW 264.7 MΦ treated with the cationic amphiphile U18666A, which binds to NPC1 and inhibits its activities[16] as well as in cells infected with BCG[12]. Using the fluorescent probe LysoTracker™, which selectively accumulates in the acidic compartment, we measured by FACS the relative LE/Lys volume in cells that had been incubated with lipids at a concentration of 100 µg/ml for 48 h. We assayed lipids extracts prepared from mycobacterial clinical strains representative of the major Mtb lineages (Table 1) and other mycobacterial species (Supplementary Fig. 1). Their activities were compared with vehicle-treated (negative control) and U18666A-incubated (positive control) RAW 264.7 MΦ (FACS gating strategy; Supplementary Fig. 2). All of the other strains tested induced a statistically significant increase in LE/Lys volume as shown by greater LysoTracker™ staining (Fig. 1a) except for strains 232 and 346 from lineage 1 and 212 and 374 from lineage 2, which showed a similar trend. Strains 119, 173, 293, 367, 440, 369, and H37RV increased LysoTracker™ staining to a level that was not significantly lower than that of cells treated with the NPC1 pharmacological inhibitor, U18666A. Analysis of the data for each Mtb lineage confirmed there was a significant increase in LysoTracker™ staining of RAW 264.7 MΦ incubated with lipid extracts of all lineages (Fig. 1b).

Analysis of lipids from other mycobacterial species revealed that the MTBC member *M. bovis Bacillus* and NTM species *M. abscessus* and *M. avium* also significantly increased LysoTracker™ staining, while extracts from *M. smegmatis*, the non-pathogenic model organism did not achieve significance and *M. canettii* diminished reduced LysoTracker™ staining relative to control cells (Fig. 1a).

At a concentration of 100 µg/ml, we were unable to measure a significant increase in LysoTracker™ staining of RAW 264.7 cells following exposure to lipid extracts from two Mtb strains within lineage 1 (isolates 232 and 346) and two strains from lineage 2 (isolates 212 and 374). We reasoned that this could perhaps be due to lower concentrations of the active lipid species in these extracts. We therefore performed repeat assays but increased the concentration of lipid extracts to 200 µg/ml with which we observed a statistically significant increase in LysoTracker™ with all four strains (Fig. 1c).

Furthermore, even at the higher lipid concentration of 200 µg/ml *M. canettii* had no effect, whereas the Mtb strain, 91_0079, a representative of lineage 3 tested at the same concentration significantly enhanced staining, thereby demonstrating the presence of activity within this lineage (Fig. 1c).

Mycobacterial lipid extracts isolated at two separate laboratories were also assayed; one from Imperial College, London (ICL) and the second from Colorado State University, supplied through BEI Resources, Virginia. In order to exclude the possibility of significant variation in activity due to methodological differences in their isolation or bacterial growth conditions, we compared lipid extracts of H37Rv from each source within the same experimental assay. The two

https://doi.org/10.1038/s41467-022-32553-0

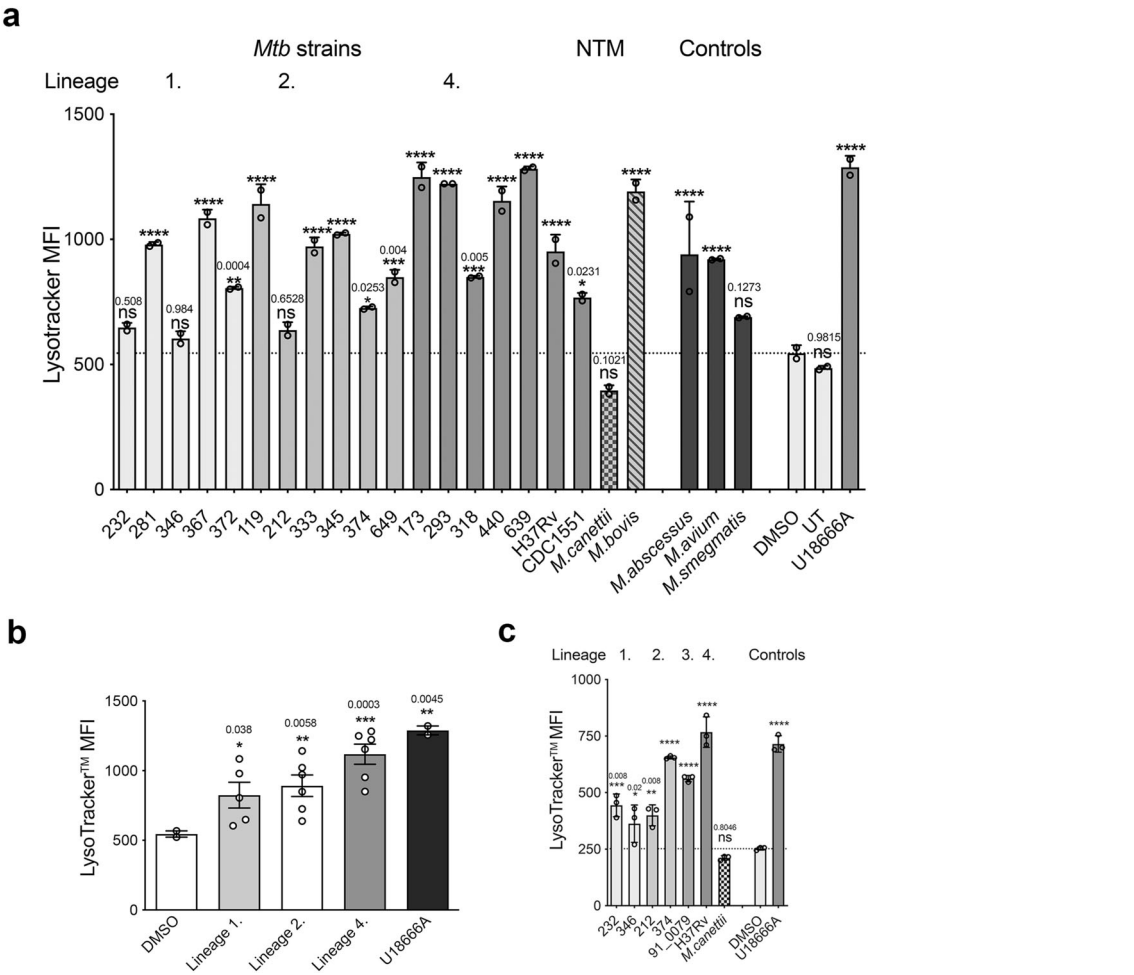


Fig. 1 | Mycobacterial lipids that can significantly increase LysoTracker™ staining of RAW 264.7 MΦ are widely distributed across Mtb clinical strains, members of the Mtb complex (MTBC) and non-tuberculous mycobacteria. **a** LysoTracker™ staining intensity of RAW 264.7 MΦ treated with 100 µg/ml lipid extract of clinical Mtb strains representative of Mtb lineages, 1, 2, and 4, Mtb complex species and non-tuberculous mycobacteria for 48 h. Data are mean ± SEM, N = minimum of 2 replicates per sample. Statistical analysis, 1-way ANOVA, ****p <0.0001, other significance values as indicated. Data are representative of three independent experiments. **b** Mean LysoTracker™ staining intensity of RAW 264.7 MΦ treated with lipid from Mtb lineages, 1, 2, and 4. Data are mean ± SEM, N = 5–7 strains tested per lineage. Statistical analysis, 1-way ANOVA, ****$p < 0.0001$, other p values as indicated. Data are representative of three independent experiments. **c** LysoTracker™ staining of RAW 264.7 MΦ treated with 200 µg/ml lipid extract of clinical Mtb strains from lineages 1, 2, 3, and 4 and *M. canettii*. Data are mean ± SEM, N = minimum of 3 replicates per sample. Statistical analysis, 1-way ANOVA, ****$p < 0.0001$, other p values as indicated. Data are representative of two independent experiments. Source data are provided as a Source data file.

extracts significantly increased LysoTracker™ staining to the same extent, which was equal to or greater than that of U18666A-treated MΦ (Supplementary Fig. 3a). Furthermore, we confirmed dose-dependent responses for both H37Rv samples (Supplementary Fig. 3a) and for lipid extracts of several of the positive Mtb clinical strains (Supplementary Fig. 3b). We also tested the ability of specific non-lipid components of Mtb to increase LysoTracker™ staining and found that mycolylarabinogalactan-peptidoglycan (mAGP), lipomannan (LM) lipoarabinomannan (LAM) and arabinogalactan (all from BEI) did not have a significant effect on staining intensity (Supplementary Fig. 3c).

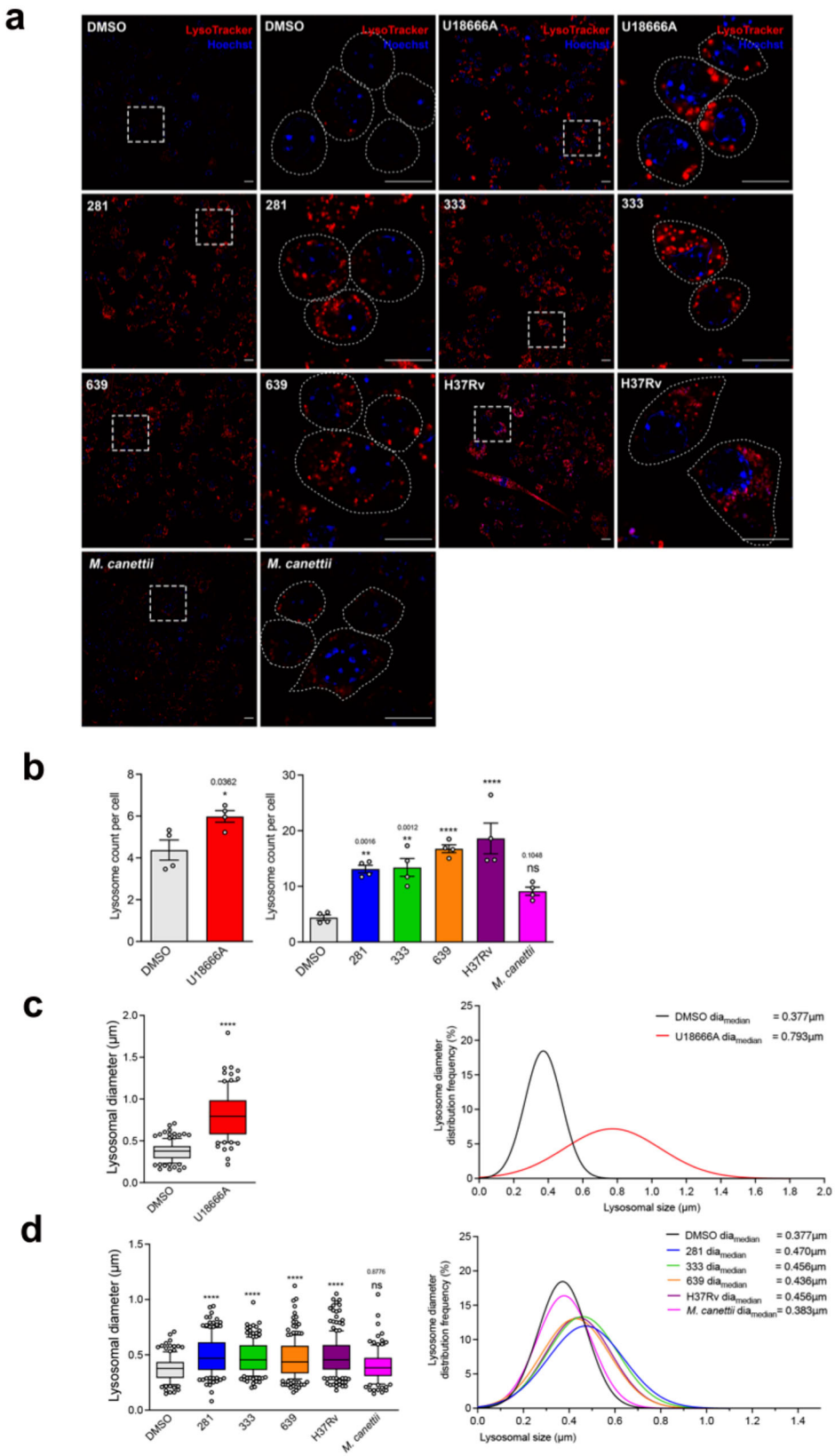
Cell wall lipid fractions from representative Mtb clinical isolates but not *M. canettii* increase lysosome number and size in treated RAW 264.7 MΦ

The intensity of LysoTracker™ staining when measured by FACS provides a measure of the relative acidic compartment volume in the cell[15]. This could represent an increase in the number and/or size of lysosomes per cell. We therefore stained cells that had been incubated with lipid extracts of Mtb clinical stains representative of three lineages (lineage 1, strain 281; lineage 2, strain 333; lineage 4, strains 639 and H37Rv) and *M. canettii*, which did not induce an increase in LysoTracker™ intensity for examination by confocal microscopy (Fig. 2a). Analyses of the frequency of lysosomes, as indicated by the distribution of fluorescence confirmed that there was a statistically significant greater number of LysoTracker™ stained organelles in cells treated with U18666A and the lipid extracts of each of the Mtb strains, but not in RAW 264.7 MΦ exposed to *M. canettii* lipid (Fig. 2b). We measured the diameter of the fluorescent puncta and determined that there was a significant increase in the mean size and size distribution with U18666A (Fig. 2c) and Mtb lipid (Fig. 2d) treatment, but not with *M. canettii* (Fig. 2d). These data indicate that Mtb lipids increase both the number and size of lysosomes but *M. canettii* does not affect either parameter.

LAMP-1 staining confirms expansion of late endosome/lysosomal volume following incubation with lipids from representative Mtb strains but not *M. canettii*, but its level of expression is not significantly increased

In order to further validate the expansion of the acidic compartment (LE/Lys), we imaged RAW 264.7 MΦ that had been treated with

https://doi.org/10.1038/s41467-022-32553-0



U18666A or lipid from the specific Mtb strains and stained for the protein LAMP-1 (Fig. 3a, b). Quantification of LAMP-1 positive compartments confirmed a significant increase in the mean size (diameter) and size distribution of LAMP-1 positive compartments of cells treated with U18666A (Fig. 3c) and Mtb lipids, but not *M. canettii* (Fig. 3d). However, Q-PCR analysis (Fig. 3e) and western blotting (Fig. 3f) did not confirm significant increases in either LAMP-1 transcription or protein abundance in Mtb H37Rv lipid treated cells, implying that differences in confocal images likely reflect a change to protein distribution affecting immunoreactivity.

Fig. 2 | Expansion of the lysosomal compartment in RAW 264.7 MΦ in response to treatment with mycobacterial lipid (100 µg/ml for 48 h) visualized with LysoTracker™-Red staining. a Representative confocal microscopy images of RAW 264.7 MΦ either untreated, DMSO or U18666A treated or incubated with lipid extracts of Mtb clinical strains 281, 333, 639 or H37Rv or *M. canettii* stained with LysoTracker™-Red. The right image of each pair is a higher magnification of the region indicated in the left image. Nucleus is stained with Hoechst 33342 (blue). Scale bar represents 10 µm. Exposure times for all images was equivalent, except for DMSO indicated as a longer exposure. **b** Quantification of lysosome frequency per cell in vehicle or U18666A (left histogram) or DMSO and Mtb lipid or *M. canettii* lipid treated cells (right histogram). Data are means ± SEM, $N = 4$ replicates per sample comprising a minimum of 50 cells per random field. Statistical analysis, unpaired *t* test with Welch's correction for DMSO and U18666A, two-tailed; 1-way ANOVA with Dunnett test, $F = 1.945$ for DMSO or lipid treated. ****$p < 0.0001$, other *p* values as indicated. Data are representative of two independent experiments. **c** Box-and-whisker plot of lysosome diameters (µm) and statistical distribution of lysosome diameters in vehicle or U18666A treated RAW 264.7 MΦ. Left histogram, data are means ± SEM, N = minimum of 100 lysosomes within four random fields. DMSO: min: 0.149 µm, max: 0.709 µm, center: 0.377 µm; U18666A: min: 0.216 µm, max:1.791 µm, center: 0.793 µm. Box contains 90% of all events. Statistical analysis, unpaired *t* test with Welch's correction, two-tailed. ****$p < 0.0001$. Statistical distribution values indicated are median diameter (µm). **d** Box-and-whisker plot of lysosome diameter (µm) and statistical distribution of lysosome diameters in DMSO or lipid treated RAW 264.7 MΦ. Data are means ± SEM, N = minimum of 100 lysosomes within four random fields. DMSO: min: 0.149 µm, max: 0.709 µm, center: 0.377 µm; 281: min: 0.081 µm, max: 0.941 µm, center: 0.470 µm; 333: min: 0.204 µµm, max: 0.975 µm, center: 0.456 µm; 639: min: 0.161 µm, max: 1.124 µm, center: 0.436 µm; H37Rv: min: 0.180 µm, max: 1.052 µm, center: 0.456 µm; *M. canettii*: min: 0.149 µm, max: 1.047 µm, center: 0.383 µm. Box contains 90% of all events. Statistical analysis, 1-way ANOVA with Kruskal–Wallis test, Kruskal–Wallis statistics: 79.61. ****$p < 0.0001$, other *p* values as indicated. Statistical distribution values indicated are median diameter (µm). Data are representative of two independent experiments. Source data are provided as a Source data file.

H37Rv lipid extract significantly increases Npc1 expression in treated RAW 264.7 MΦ

In our previous study demonstrating the induction of NPC cellular phenotypes in RAW 264.7 MΦ infected with pathogenic mycobacteria, we observed a significant increase in the expression of NPC1[12]. We examined whether treatment with mycobacterial lipids might have the same effect. While U18666A (Fig. 4a) and H37Rv lipid significantly increased the level of NPC1 protein, we were unable to detect an increase with the other Mtb lipids that were tested (Fig. 4b).

Cell wall lipid extracts from representative Mtb clinical strains and H37Rv but not *M. canettii* induce cholesterol accumulation in the endo-lysosomal system of RAW 264.7 MΦ

Lysosomal storage of cholesterol is a hallmark of NPC and has historically been used for clinical diagnosis[14]. Mtb is a pathogen that manipulates host cell lipid metabolism and transforms infected cells into lipid-laden, foamy MΦ that are enriched in cholesterol and indeed cholesterol is important for the formation of granulomas[5,17,18]. Cholesterol has also been shown to be a critical energy source for Mtb and is essential for survival[19]. We therefore investigated the capacity of mycobacterial lipid extracts to cause cholesterol accumulation. Evidence of cholesterol accumulation was investigated by filipin staining of fixed cells and biochemical measurement of cell extracts using an Amplex Red assay. As expected, imaging of cells that had been treated with the NPC1 inhibitor U18666A confirmed significant lysosomal accumulation of filipin-positive puncta (Fig. 5a), which were seen in almost all MΦ (Fig. 5b). Comparable analysis of cells that had been treated with lipid extracts of the clinical strains 281, 333, 639, and H37Rv also revealed lysosomal puncta (Fig. 5c), the frequency of which were statistically greater than control (Fig. 5d). In contrast, relatively few puncta were detected in RAW 264.7 cells treated with an extract of *M. canettii* (Fig. 5a) and were not significantly greater in number than control RAW 264.7 cells (Fig. 5d). We measured the total cholesterol content of treated cells. Cells treated with U18666A had a statistically greater cholesterol content than control (approximately 1.7-fold greater than vehicle) (Fig. 5e) but although there was a trend of increased cholesterol levels with Mtb lipid treatment, it did not reach statistical significance for any of the strains (Fig. 5f).

Exposure to lipids from representative Mtb strains but not *M. canettii* perturb GM1 ganglioside intracellular trafficking

The recycling of glycosphingolipids (GSLs) is perturbed in lysosomal storage diseases, including NPC, resulting in the miss-trafficking of GSLs away from recycling through the Golgi apparatus and instead targets them to the lysosome[20]. This change in lipid trafficking can be visualized by pulse-chase labeling with fluorescently tagged cholera toxin subunit B that binds to GM1 ganglioside at the cell surface[20]. We used this methodology to assess the extent of altered GM1 trafficking in RAW 264.7 MΦ treated with the different mycobacterial lipids. Confocal microscopy of cells labeled with fluorescently tagged cholera toxin B subunit to monitor trafficking of GM1 ganglioside showed that in wild-type cells GM1 recycles through the Golgi apparatus whereas exposure to U18666A as predicted resulted in GM1 redistribution to the endo-lysosomal compartment (Fig. 6a, b). Similarly, cells treated with lipid extracts from each of the four Mtb strains also had a significant redistribution of the GM1 to the lysosome (Fig. 6a, b), whereas the lysosomal localization of GM1 in MΦ that been exposed to lipids from *M. canettii* was not significantly different from control cells that have a Golgi recycling pattern of staining (Fig. 6a, b).

GSL species accumulate in RAW 264.7 MΦ incubated with lipid extracts of strains representative of different Mtb lineages but not with *M. canettii* lipid

Impaired lipid transport and catabolism cause the accumulation of multiple different GSLs in NPC cells[21,22]. We therefore extracted GSLs from RAW 264.7 MΦ that had been incubated with cell wall lipid extracts from representative Mtb strains and *M. canettii* and determined their abundance by normal phase HPLC[23]. HPLC profiles representative of U18666A-treated and DMSO are shown in Fig. 7a. As predicted, U18666A significantly increased total GSL content (Fig. 7a, b). Representative HPLC profiles of GSLs from lipid-incubated MΦ extracts and DMSO control are shown in Fig. 7c. Lipid extracts from all four Mtb strains also significantly increased total GSL levels in treated MΦ, but in contrast, total GSLs were significantly lower in cells incubated with *M. canettii* lipids (Fig. 7d). Levels of the most abundant lipid species GM1a, GM1b, and GD1a were significantly increased by lipid extracts from all Mtb strains but in the case of *M. canettii* were either not significantly changed (GM1a) or were significantly reduced (GM1b and GD1a). Strain 281 from Mtb lineage 1 significantly increased eight of the individual lipid species, lineage 2 strain 333 increased five lipid species, and lineage 4 strains 639 and H37Rv increased four and seven distinct lipid species respectively (Fig. 7d and Table 2). *M. canettii* cell wall lipid extract only significantly enhanced the amounts of two minor lipid species (GM2 and GA1), albeit to a relatively small extent (both GSLs were increased by ~1.2-fold by *M. canettii* extract whereas GM2 was increased >2.0-fold and GA1 >1.8-fold by Mtb lipids), did not alter the level of three individual lipids (GA2, Gb3, and GM1a) but significantly reduced the level of four lipids (Lac, GM3, GM1b and GD1a (Table 2), which was not observed with any of the Mtb strains.

Lipid composition of clinical strains representative of different Mtb lineages

Using a combination of different solvent conditions and thin layer chromatography (TLC), together with matrix-assisted laser

https://doi.org/10.1038/s41467-022-32553-0

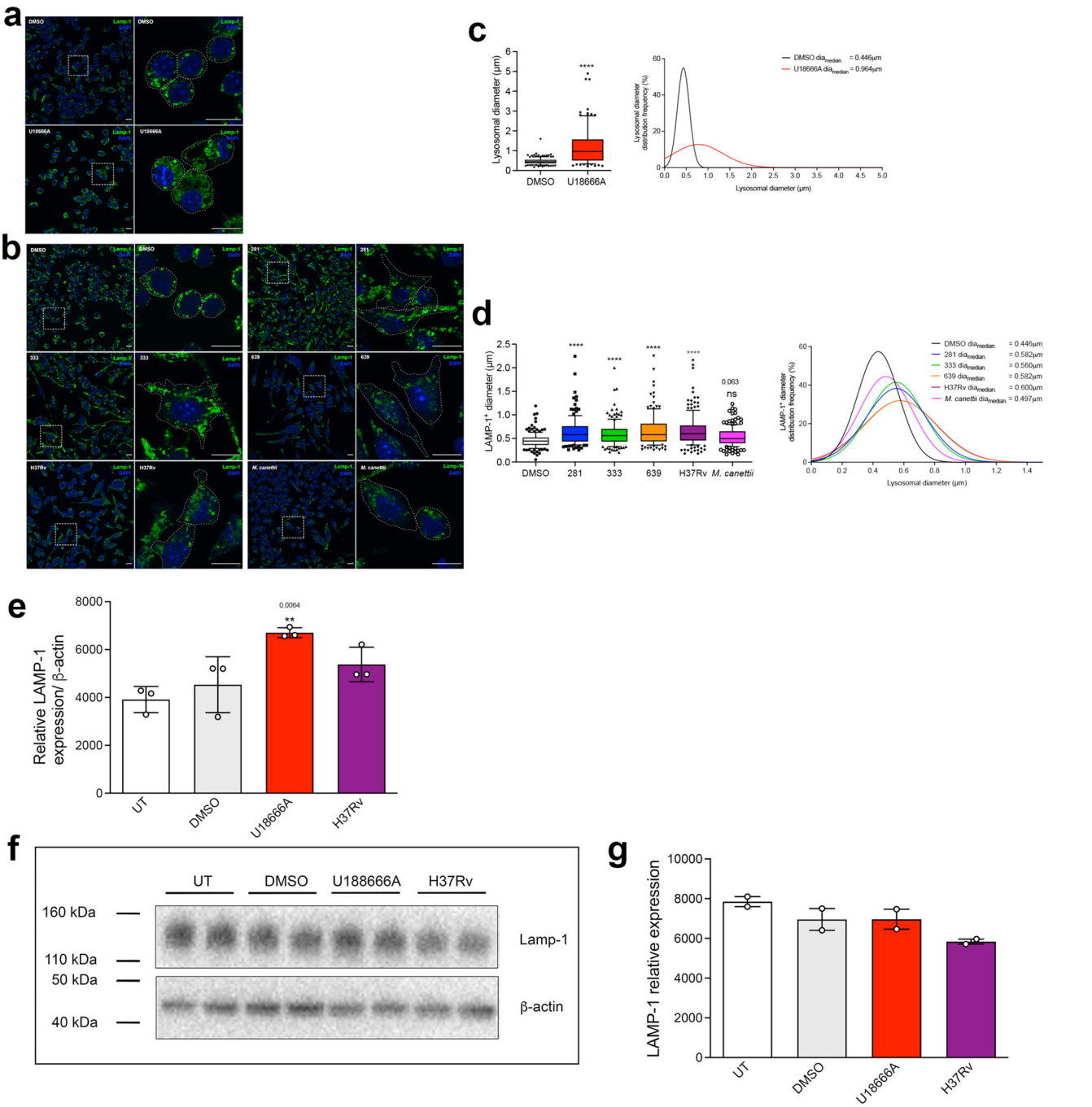


Fig. 3 | Expansion of the lysosomal compartment in RAW 264.7 MΦ in response to treatment with mycobacterial lipid (100 µg/ml for 48 h) visualized with anti-LAMP-1 staining. a Confocal microscopy images of RAW 264.7 MΦ treated with vehicle or U18666A and stained with anti-LAMP-1 antibody (green). **b** Images of RAW 264.7 MΦ treated with DMSO or Mtb lipids or *M. canettii* lipid. The right image for each pair is a higher magnification of the region indicated in the left image. Nucleus is stained with DAPI (blue). Scale bar represents 10 µm. **c** Box-and-whisker plot of LAMP-1 positive compartment diameters (µm) and statistical distribution of LAMP-1 positive compartment diameters in vehicle or U18666A treated RAW 264.7 MΦ. Left histogram, data are means ± SEM, N = minimum of 100 lysosomes within four random fields. DMSO: min: 0.051 µm, max: 1.190 µm, center: 0.446 µm; U18666A: min: 0.216 µm, max:4.894 µm, center: 0.964 µm. Box contains 90% of all events. Statistical analysis, Mann-Whitney test, two-tailed, $^{****}p < 0.0001$. Indicated statistical distribution, values are median diameter (µm). **d** Box-and-whisker plot of LAMP-1 positive compartment diameters (µm) and statistical distribution of LAMP-1 positive compartment diameters in DMSO or lipid treated RAW 264.7 MΦ. Data are means ± SEM, N = minimum of 100 lysosomes within four random fields. DMSO: min: 0.051 µm, max: 1.190 µm, center: 0.446 µm; 281: min: 0.255 µm, max: 2.243 µm, center: 0.582 µm; 333: min: 0.204 µm, max: 2.000 µm, center: 0.560 µm; 639: min: 0.253 µm, max: 2.247 µm, center: 0.582 µm; H37Rv: min: 0.180 µm, max: 2.166 µm, center: 0.600 µm; *M. canettii*: min: 0.161 µm, max: 1.232 µm, center: 0.497 µm. Box contains 90% of all events. Statistical analysis, 1-way ANOVA with Kruskal–Wallis test, Kruskal–Wallis statistics: 87.02. $^{****}p < 0.0001$. MΦ statistical distribution, values indicated are median diameter (µm). Data are representative of two independent experiments. **e** Q-PCR of relative LAMP-1 transcript expression in RAW 264.7 MΦ, normalized to β-actin. Data are mean ± SEM, $N = 5$ replicates per sample. Statistical analysis, t test with Welch's correction, two tailed; and Mann–Whitney test, two-tailed. significance value as indicated. **f** Left, Western blot of LAMP-1 and β-actin protein expression in untreated, vehicle, U18666A and H37Rv lipid treated RAW 264.7 MΦ. **g** Quantification of LAMP-1 protein expression relative to β-actin Data are mean ± SEM, $N = 2$ replicates per sample. Statistical analysis, t test with Welch's correction No statistically significant differences, two-tailed. Data shown are representative of two independent experiments. Source data are provided as a Source data file.

https://doi.org/10.1038/s41467-022-32553-0

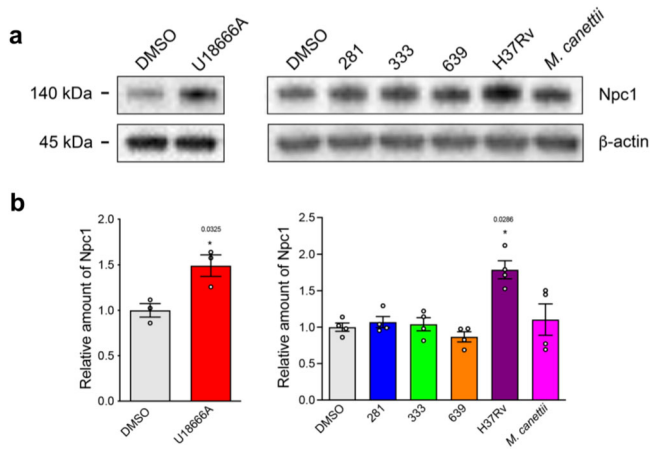


Fig. 4 | Exposure to lipid extract of strain H37Rv significantly increases the expression of NPC1 in RAW 264.7 MΦ. a Western blot of protein lysates of RAW 264.7 MΦ that had been incubated with vehicle or mycobacterial lipid extracts for 48 h. Upper band, blot probed for Npc1 and lower band, blot re-probed for β-actin. **b** Quantification of Npc1 protein bands normalized to β-actin, relative to vehicle treatment. Data are mean ± SEM, $N = 2$ or 3. Statistical analysis, t test with Welch's correction, two-tailed. p values as indicated, otherwise not significant. The blot is representative of three independent experiments. Source data are provided as a Source data file.

desorption/ionization-time of flight (MALDI-ToF mass spectrometry (MS)) in the positive and negative ion mode, lipid preparations from each of the Mtb clinical strains were analyzed. As shown in Supplementary Fig. 4a–d, TLC of extractible lipids from the strains produced qualitatively comparable profiles, but no clear differences in composition were apparent. Similarly, in the analysis by MALDI in the negative ion mode, the mass spectra of the mycobacterial strains displayed similar patterns mainly assigned to phosphatidyl-*myo*-inositol-mannosides[24–27] and sulfolipids[28,29] in the *M. tuberculosis* strains (Supplementary Fig. 4e–i). Analysis by MALDI in the positive ion mode revealed a range of lipids, glycolipids, and species-specific lipids (Supplementary Fig. 4e–i).

Discussion

TB is caused by closely related members of the MTBC family, which have evolved to become facultative intracellular pathogens. Although individual MTBC species have different host preferences, all have adopted a strategy of intracellular survival. The mechanism through which pathogenic mycobacteria survive within host cells following their ingestion is incompletely understood but is important, as it is a major factor contributing to virulence and is a potential clinical intervention point for host-targeted anti-microbial strategies.

In this study, we analyzed the ability of lipid extracts from distinct Mtb strains, other MTBC species, and NTM to inhibit the NPC pathway in host cells. We have found that the ability to increase acidic compartment volume is widespread among the pathogenic mycobacteria examined but was notably absent from *M. canettii*, a smooth bacillus that belongs to a lineage of progenitor species from which it is believed that the MTBC evolved[30–32]. Furthermore, we confirmed that lipid extracts of strains representative of Mtb lineages 1, 2, and 4 but not *M. canettii* induced multiple cellular phenotypes that characterize NPC. We hypothesized that the ability of mycobacteria to inhibit NPC1 will correlate with their ability to establish an intracellular niche and be an important event during the evolution of pathogenicity.

We have previously reported the unexpected phenocopying of the complex cellular phenotypes that occur in the rare lysosomal storage disorder NPC (genetically deficient in *NPC1*) by MΦ infected with pathogenic mycobacteria[12]. Furthermore, infected cell cultures demonstrated that induction of NPC cellular phenotypes occurred not only in cells harboring mycobacteria but also in bystander non-infected MΦ, indicating that cell wall-derived lipids released from infected cells and endocytosed by neighboring MΦ have identical effects to infection with the live mycobacterium[12].

Whole genome phylogenic studies encompassing the co-evolution of Mtb and humans have identified seven prominent lineages of human-adapted mycobacteria that correlate with spread and geographical distribution[33]. We sampled multiple strains representative of three of the major human geographical lineages[34]: lineage 1, East Africa, Philippines and the rim of Indian Ocean; lineage 2, East Asia; lineage 4, modern MTBC of Europe, America, and Africa and a single strain representative of lineage 3, East African Indian. Lineage 1 is considered representative of ancient human-adapted species, whereas lineages 2 and 4 fall within the classification of modern lineages, based upon the presence or absence of the TbD1 genomic region[35]. Cell wall-derived lipids from 20 strains were chosen to reflect genetic diversity within each lineage[36] and 16 lipid extracts significantly increased lysosomal volume when tested at a concentration of 100 µg/ml, which is consistent with NPC1 inhibition. Of the four strains that were negative, two each were from lineages 1 and 2 and none were from lineage 4, but all were positive when a higher concentration of the lipid extracts was used. The data revealed differential potencies between the strains that could significantly enhance LysoTracker™ staining. It was notable that six strains (119, 173, 293, 367, 440, and the laboratory H37Rv) were capable of increasing acidic compartment volume to a level not significantly different from that induced by the pharmacological NPC1 inhibitor U18666A, which is known to bind to and inhibit NPC1[16] and of these strains, four were from lineage 4 and one each from lineages 1 and 2. Collectively, all lineages induced a significant increase in LysoTracker™ staining. However, we cannot at this point absolutely exclude the possibility that the relative effectiveness between cell wall extracts is a result of the differential recovery of the active lipid species during the extraction process, rather than the inherent bioactive lipid content of each strain. This issue is likely to be resolved when the identity of the active lipid(s) has been determined and fractionation studies are in progress.

One aim of this study was to determine whether the lipid activity in tuberculous mycobacteria that can induce NPC cellular phenotypes is also present in NTM species and may also be involved in promoting their intracellular survival. *M. abscessus* and *M. avium* are opportunistic pathogens that do not cause TB but can be responsible for severe human infections of the respiratory system, skin and mucosa[37–40]. We therefore analyzed lipids prepared from other members of the MTBC (*M. bovis Bacillus* and *M. canettii*) and the atypical or non-tuberculous mycobacteria (NTM), *M. avium* and *M. abscessus*, as well as the environmental non-pathogenic species, *M. smegmatis* (Supplementary Fig. S1). The lack of activity of the lipid extract of the environmental non-pathogenic species *M. smegmatis* was not unexpected as we have previously shown that infection with live *M. smegmatis* did not cause cholesterol accumulation, GSL miss-trafficking, or expansion of lysosomal volume in RAW 264.7 MΦ[12]. Significant expansion of LE/Lys was observed in RAW 264.7 MΦ exposed to lipid extracts of *M. abscessus* and *M. avium*, indicating that the capacity to induce NPC phenotypes is present within the NTB group of mycobacteria. The expanded volume of the acidic compartment following incubation with lipids from specific mycobacteria was confirmed by staining for LysoTracker™ and LAMP-1. Interestingly, we were unable to measure a significant increase in the amount of the LAMP-1 protein, suggesting the pattern of immunoreactivity reflects a redistribution of the protein within enlarged organelles.

The origin and evolutionary history of Mtb and the seven other organisms that comprise the MTBC is of particular interest because of the differences in host specificities and pathogenicity, despite their

https://doi.org/10.1038/s41467-022-32553-0

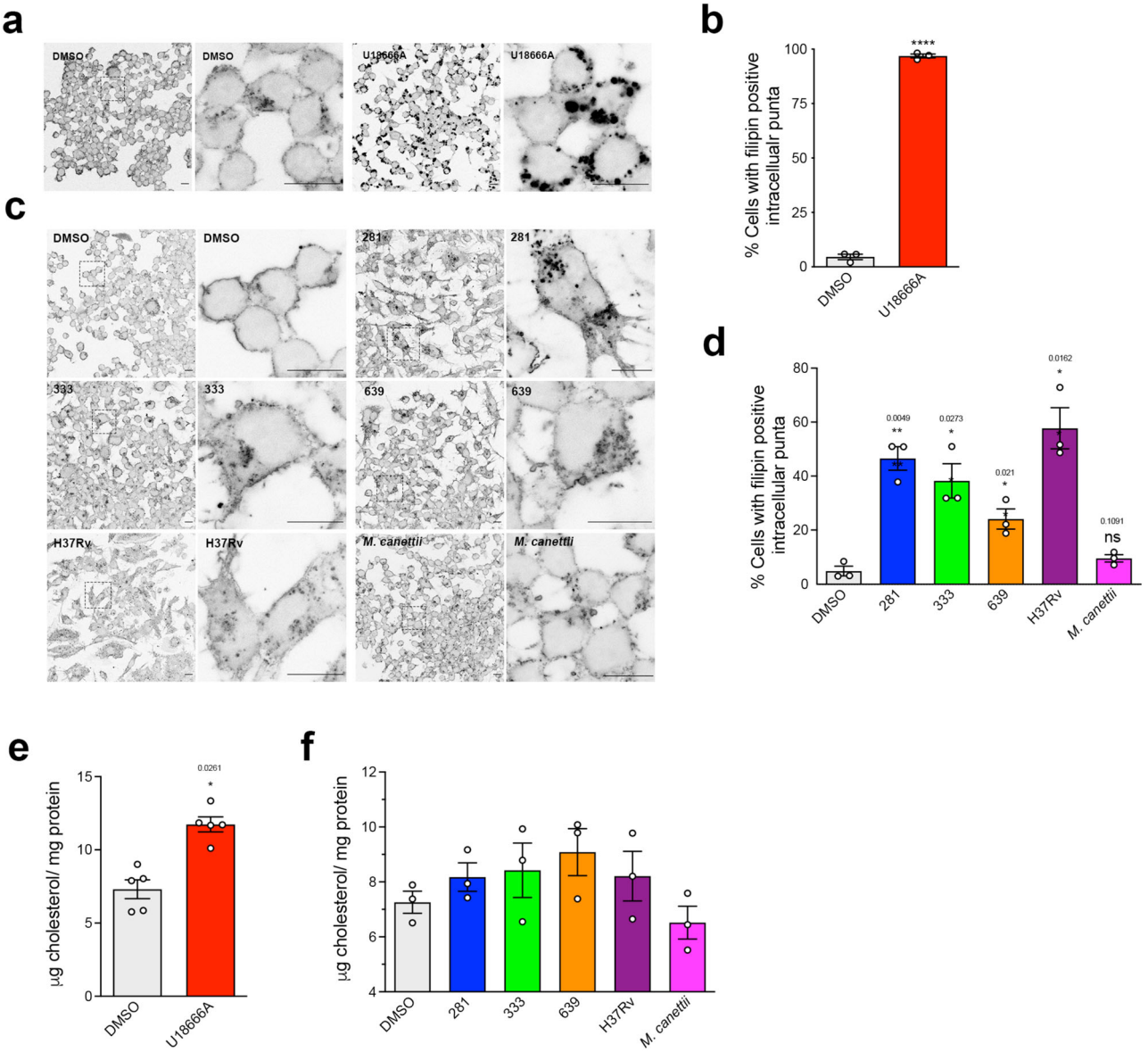


Fig. 5 | Mtb lipids induce a partial redistribution of cholesterol to intracellular puncta in RAW 264.7 MΦ. a Confocal microscopy images of vehicle (DMSO) or U18666A treated RAW 264.7 MΦ stained with filipin. For each pair, the right image is a higher magnification of the region outlined in the left image. Scale bar represents 5 µm. **b** Quantitation of the frequency of vehicle or U18666A treated cells with filipin positive intracellular puncta. Data are mean ± SEM, $N = 3$, each representing a minimum of 100 cells in randomly selected fields. Statistical analysis, unpaired t test with Welch's correction, two-tailed. ****$p < 0.0001$. **c** Confocal microscopy images of RAW 264.7 MΦ treated with vehicle (DMSO), Mtb strains or *M. canettii* lipids stained with filipin. For each pair, the right image is a higher magnification of the region outlined in the left image. Scale bar represents 5 µm. **d** Quantitation of the frequency of DMSO, Mtb lipids, or *M. canettii* lipid treated cells with filipin positive intracellular puncta. Data are mean ± SEM, $N = 3$, each representing a minimum of 100 cells in randomly selected fields. Statistical analysis, unpaired t test with Welch's correction, two-tailed. p values as indicated. **e** Amplex red quantitation of cholesterol content of RAW 264.7 MΦ treated with vehicle (DMSO) or U18666A. Data are mean ± SEM, $N = 3$ replicates per sample. Statistical analysis, unpaired t test with Welch's correction, two-tailed. Significance value as indicated. **f** Amplex red quantitation of cholesterol content of RAW 264.7 MΦ treated with vehicle (DMSO) or mycobacterial lipids. Data are mean ± SEM, $N = 5$. Statistical analysis, unpaired t test with Welch's correction, two-tailed. No statistically significant differences. Data are representative of three independent experiments. Source data are provided as a Source data file.

remarkable level of sequence similarity at the nucleotide level[30,41]. The seven human-adapted lineages are not considered monophyletic. The consensus from multiple genetic studies is that members of the MTBC emerged from progenitor species that likely resembled the smooth tubercule *M. canettii*, which itself diverged prior to the MTBC[42]. It was therefore of significant interest that incubation of RAW 264.7 MΦ with the lipid extract from *M. canettii* did not induce any NPC cellular phenotypes, suggesting that the bioactive lipid(s) is either lacking or is of very low abundance in this mycobacterium. Biochemical analysis of mycobacterial cell wall lipids has revealed a discontinuous distribution, consistent with the evolutionary emergence of Mtb from an environmental species resembling *Mycobacterium kansasii* via intermediate smooth tubercle bacilli[43]. The diversity of *M. canettii* lipids includes some that are unique, such as the phenolic glycolipids phenolphthiocerol dimycocerosates that have been lost during the subsequent emergence of MTBC[44,45]. Molecular and phenotypic studies of the smooth tubercle *M. canettii* have provided evidence for delineating the evolution of Mtb, elucidating the underlying mechanisms that were responsible and the development of pathogenicity/intracellular survival and virulence[46,47]. *M. canettii* strains display

https://doi.org/10.1038/s41467-022-32553-0

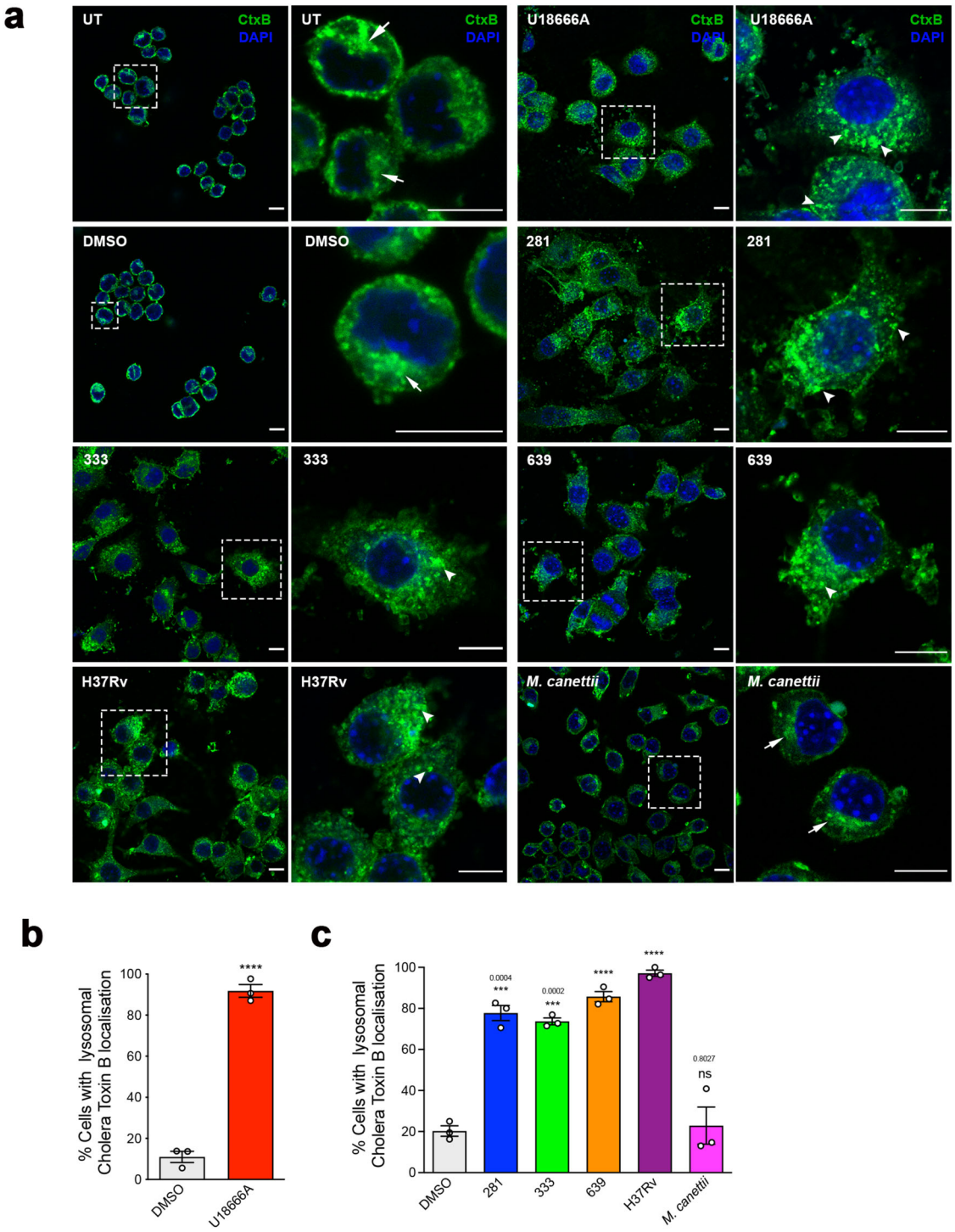
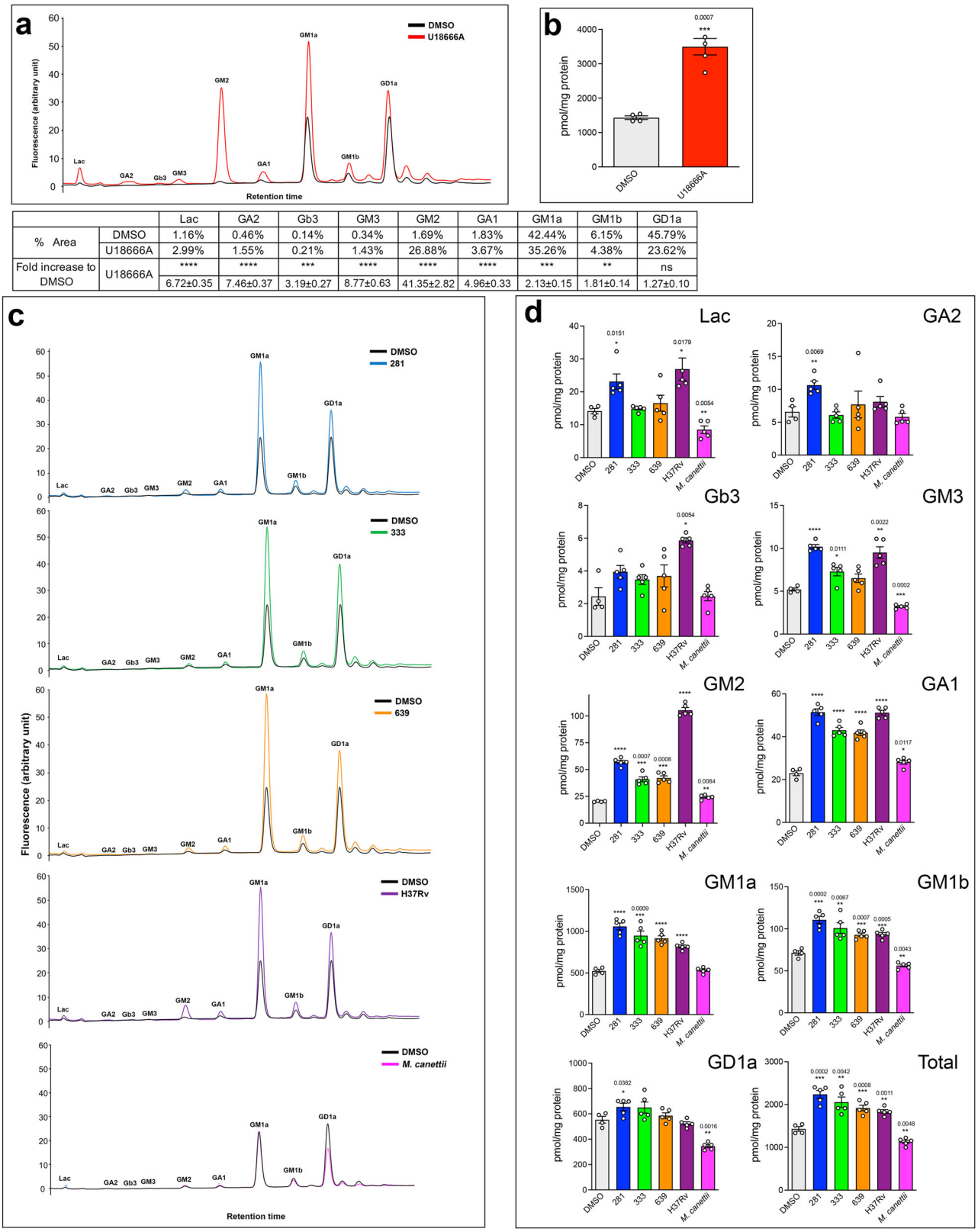


Fig. 6 | Mtb lipids affect GM1 trafficking in RAW 264.7 MΦ. a Confocal microscopy images of RAW 264.7 MΦ treated with vehicle (DMSO), U18666A, or mycobacterial lipids and pulse-chased with cholera toxin B subunit (green). Nucleus is stained with DAPI (blue). For each pair, right image is a higher magnification of the region outlined in the left image. Untreated, vehicle and *M. canettii* lipid treated cells show a predominantly Golgi pattern of staining, indicated by the white arrows. U18666A and lipids from Mtb strains induce a punctate pattern, consistent with lysosomal distribution (white arrowheads). Scale bar represents 10 µm. **b** Percentage of vehicle and U18666A treated cells with lysosomal cholera toxin B localization. Data are mean ± SEM, $N = 3$, each representing a minimum of 100 cells in randomly selected fields. Statistical analysis, unpaired t test with Welch's correction, two-tailed. $^{****}p < 0.0001$. **c** Percentage of the vehicle and mycobacterial lipid-treated cells with lysosomal cholera toxin B localization. Data are mean ± SEM, $N = 3$, each representing a minimum of 100 cells in randomly selected fields per sample. Statistical analysis, unpaired t test with Welch's correction, two-tailed. $^{****}p < 0.0001$, other p values as indicated. Data are representative of two independent experiments. Source data are provided as a Source data file.

https://doi.org/10.1038/s41467-022-32553-0



		Lac	GA2	Gb3	GM3	GM2	GA1	GM1a	GM1b	GD1a
% Area	DMSO	1.16%	0.46%	0.14%	0.34%	1.69%	1.83%	42.44%	6.15%	45.79%
	U18666A	2.99%	1.55%	0.21%	1.43%	26.88%	3.67%	35.26%	4.38%	23.62%
Fold increase to DMSO	U18666A	****	****	***	****	****	****	***	**	ns
		6.72±0.35	7.46±0.37	3.19±0.27	8.77±0.63	41.35±2.82	4.96±0.33	2.13±0.15	1.81±0.14	1.27±0.10

Fig. 7 | Mtb lipids, but not *M. canettii* lipids cause GSL accumulation in RAW 264.7 MΦ. a Representative HPLC trace of GSLs from vehicle (DMSO) and U18666A treated cells are overlaid with individual GSL peaks annotated. The table summarizes the percent area of each peak and the fold increase induced by U18666A. **b** Quantitation of total GSLs in DMSO or U18666A treated cells. Data are mean ± SEM, *N* = replicates per sample. Statistical analysis, unpaired *t* test with Welch's correction, two-tailed. ***$p < 0.0007$. **c** Overlays of representative HPLC traces of extracts of RAW 264.7 cells treated with vehicle (DMSO) and lipid extracts of Mtb strains or *M. canettii*. **d** Quantitation of individual GSL species and total GSLs in DMSO or mycobacterial lipid treated cells. Data are mean ± SEM, *N* = 4–5 replicates per sample. Statistical analysis, unpaired *t* test with Welch's correction, two-tailed ****$p < 0.0001$, other *p* values as indicated. Source data are provided as a Source data file.

Table 2 | Summary of relative accumulation of total and specific GSL species in RAW 264.7 MΦ treated with U18666A or lipid extracts from different Mtb clinical strains and *M. canettii*

	U18666A	281	333	639	H37Rv	*M. canettii*
Lac	**** 6.72 ± 0.35	*0.0151 1.64 ± 0.16	ns 1.05 ± 0.03	ns 1.17 ± 0.17	*0.0179 1.90 ± 0.24	**0.0054 0.60 ± 0.08
GA2	**** 7.46 ± 0.37	**0.0069 1.62 ± 0.10	ns 0.93 ± 0.07	ns 1.17 ± 0.31	ns 1.23 ± 0.12	ns 0.88 ± 0.08
Gb3	***0.004 3.19 ± 0.27	ns 1.62 ± 0.16	ns 1.42 ± 0.12	ns 1.51 ± 0.28	*0.0054 2.40 ± 0.07	ns 1.01 ± 0.12
GM3	**** 8.77 ± 0.63	**** 1.96 ± 0.05	*0.0111 1.40 ± 0.10	ns 1.52 ± 0.10	**0.0022 1.83 ± 0.13	***0.002 0.62 ± 0.02
GM2	**** 41.35 ± 2.82	**** 2.82 ± 0.08	***0.0007 2.02 ± 0.11	***0.008 2.08 ± 0.10	**** 5.21 ± 0.12	**0.0084 1.20 ± 0.04
GA1	**** 4.96 ± 0.33	**** 2.24 ± 0.07	**** 1.88 ± 0.06	**** 1.82 ± 0.06	**** 2.23 ± 0.05	*0.0117 1.23 ± 0.04
GM1a	***0.0006 2.13 ± 0.15	**** 2.02 ± 0.08	***0.0009 1.81 ± 0.11	**** 1.75 ± 0.06	**** 1.56 ± 0.03	ns 1.02 ± 0.03
GM1b	**0.0071 1.81 ± 0.14	***0.0002 1.55 ± 0.06	**0.0067 1.41 ± 0.09	***0.0007 1.30 ± 0.03	***0.0005 1.31 ± 0.03	**0.0043 0.79 ± 0.02
GD1a	ns 1.27 ± 0.10	*0.0382 1.18 ± 0.05	ns 1.17 ± 0.08	ns 1.06 ± 0.04	ns 0.95 ± 0.03	**0.0016 0.62 ± 0.02
Total GSL	***0.0003 2.44 ± 0.17	***0.0002 1.56 ± 0.06	**0.0042 1.44 ± 0.09	***0.0008 1.34 ± 0.05	**0.0011 1.28 ± 0.03	**0.0048 0.79 ± 0.03

Summary of relative abundance of total GSL content and individual lipid species of RAW 264.7 MΦ treated with lipid extract from different *Mtb* strains or *M. canettii*. Data represent mean ± SEM fold change in lipid abundance relative to DMSO-treated control cells. Statistical analysis, 2-way ANOVA, *N* = minimum of 4-5 samples per treatment. ****$p < 0.0001$, other p values as indicated, *ns* not significant. Data are representative of two independent experiments. Source data are provided as a Source data file.

significant genome variation[48,49], which sets them apart from other MTBC. Clinical infection with *M. canettii* is rare and geographically restricted, while variants show differential virulence, all of which indicate that it is far less successful at causing human disease in comparison to Mtb[46,50]. It is therefore possible that the failure of *M. canettii* lipids to inhibit NPC1 indicates the use of an alternative mechanism to facilitate infection and intracellular survival that is overtly less effective than the NPC1 inhibition strategy exploited by Mtb and other mycobacterial species such as *M. bovis Bacillus* and *M. avium*.

The expansion of the acidic compartment, both in terms of lysosome number and size of individual lysosomes following lipid treatment was also confirmed by confocal microscopy using LysoTracker™ and anti-LAMP-1 staining. Although microscopy images of cells stained for the lysosomal protein, LAMP-1were suggestive of greater expression, analyses of both mRNA levels and protein expression did not confirm an increase, implying that over the time course that was used, it was more likely that there was a re-distribution of the protein in the expanded lysosomes.

Previously, we have reported that infection of RAW 264.7 MΦ with BCG causes a significant upregulation of NPC1 protein[12]. When we investigated the capacity of mycobacterial lipids to induce the same effect, only the lipid extract of H37Rv significantly enhanced NPC1 expression. Currently, we are unable to fully explain the differences between these data, but one possibility is that infection with live mycobacteria achieves greater inhibition of NPC1 activity, and as a consequence protein abundance is increased in an attempt to compensate for the loss of NPC1 function.

We also investigated the capacity of mycobacterial lipid extracts to cause lysosomal accumulation of cholesterol in RAW 264.7 MΦ, which is a prominent cellular NPC phenotype[14]. The association between cholesterol and Mtb infection has been recognized in multiple studies. It is essential for the entry of mycobacteria into MΦ[51], its utilization is required for survival[19] and it is important for maintaining dormancy and enabling reactivation[52]. Cholesterol is also used as a critical energy source illustrated by the presence within the mycobacterial genome of genes encoding transport proteins that mediate its import and enzymes necessary for its metabolism[53,54]. We detected between a five and ten-fold increase in the frequency of cells that had intracellular filipin-positive punta with Mtb lipid treatment. To our knowledge, the comparative ability of different Mtb strains and members of MTBC to manipulate host cell cholesterol has not been explored previously.

Consistent with inhibition of NPC1, lipid extracts from the mycobacteria that affected cholesterol accumulation also caused miss-localization of GM1 ganglioside, which did not occur when RAW 264.7 cells were treated with lipids from *M. canettii*. At this point, it is not obvious if pathogenic mycobacteria directly benefit from biochemical changes in the intracellular distribution of host GSLs that result from blocking NPC1-dependent activities and this merits further investigation.

The mycobacterial envelope is architecturally and biochemically complex, is composed of multiple carbohydrates and lipid species[55,56], and functions as a permeability barrier[56,57]. Intercalated within the lipid environment of the cell wall are extractable free lipid species that can influence the balance between pathogen and host by affecting pathogenesis and shaping immune responses[55,58,59]. In light of the findings that lipid extracts from strains representative of the three Mtb lineages increased the relative LE/Lys volume to differing extents, we performed lipidomic analyses of sixteen clinical isolates, plus the laboratory strain, H37Rv, to explore lipid diversity and the possibility of correlation between bioactivity and lipid composition. We focused on extractable lipids. As seen on the TLCs, qualitatively no differences were observed, whereas quantitatively, there were some differences in the levels/ratios of the respective lipids within and across lineages. MALDI analysis of the mycobacterial strains confirmed these differences: mass spectra in the negative ion mode displayed similar patterns, mainly assigned to phosphatidyl-*myo*-inositol-mannosides[24–27] and sulfolipids[28,29]. However, mass spectra in the positive ion mode revealed a range of lipid, glycolipids, and species-specific lipids, which is in accordance with the published literature[24,60,61]. These differences could be a factor influencing the phenotypes observed. In addition, it is known that one of the major surface exposed lipids, lipooligosaccharides (LOS), are absent in Mtb as opposed to *M. canettii* due to

the mutation within the *pks5* locus abrogating synthesis[42]. LOS could therefore be an ideal candidate to explain the suppression of the phenotypes in *M. canettii* compared to Mtb, masking more potent surface-exposed lipids in the strains used in this study. The lack of activity of the *M. smegmatis* lipid extract could perhaps be explained by an inadequate quantity of specific lipid(s) or the presence of a significant level of exposed glycopeptidolipids[62,63]. It would be of interest in future studies to analyze the lipid extract of *M. canettii* rough morphotype variants I and K, which are deficient for LOS, and test for its capacity to induce NPC1 inhibition.

More specifically, based on the evolution of MTBC due to genetic deletions or rearrangement of regions of the genome that contains enzymes involved in the synthesis of surface exposed lipids and glycolipids, some lipids found in *M. canettii* cannot be produced by Mtb H37Rv[35,46,55,64,65]. Indeed, through evolution, Mtb has lost the ability to produce lipooligosaccharides because of pks5 locus recombination[42,66]. With respect to the biochemical differences between Mtb H37Rv and NTM, diglycosylated glycopeptidolipids and triglycosylated glycopeptidolipids make up more than 70% of the surface-exposed mycobacterial lipids in *M. abscessus* are not found in Mtb H37Rv[67–71]. In addition, mycolic acids, such as ones bound to trehalose in TMM and TDM, and particularly their decorations can differ between mycobacterial species[72,73]. Indeed, mycolic acids display high structural diversity with variations observed in chain length (60 to 90 carbon atoms), the extent of unsaturation, and chemical groups, such as ketones and methoxys[73]. This high level of diversity provides mycolic acids with species-specific characteristics[74]. In addition to mycolic acids, other lipids are also specific to particular species of mycobacteria. For example, sulfolipid 1 and polyacyltrehalose are found exclusively in *M. tuberculosis*, while trehalose polyphleate is present in NTM species[28,75,76]. Layre et al.[77] using an HPLC–MS-based lipidomics platform screened for lipids that were present in *M. tuberculosis* but not in *M. bovis* BCG and identified 1-tuberculosinyladenosine (1-TbAd), an amphipathic diterpene nucleoside. However, its presence or absence in NTM has not as yet been reported.

In summary, the findings presented here indicate that the lipid-dependent capacity to trigger specific host cell phenotypes indicative of NPC1 inhibition is broadly distributed among pathogenic mycobacteria species and Mtb clinical strains. The lack of activity in extracts of *M. canettii* smooth morphotype is consistent with the hypothesis that the evolution of the lipid(s) that is responsible for NPC1 inhibition occurred after the divergence of MTBC from the ancestral *M. canettii*-like species. Future identification and characterization of the lipid will facilitate a greater mechanistic understanding of how pathogenic strains establish infection and maintain intracellular survival.

Methods

Mammalian cell culture

The murine macrophage (MΦ) cell line RAW 264.7 was obtained from the ATCC and maintained in RPMI 1640 containing 10% (v/v) fetal bovine serum, 1% L-glutamine, and 1% penicillin–streptomycin (all Sigma-Aldrich) at 37 °C in 5% CO_2. Cells were passaged routinely to maintain viability (>90%).

Bacterial strains and culture conditions

M. tuberculosis strains were cultured in Sauton's medium as cell surface pellicle and prepared at Imperial College, University of London: Mtb clinical strains consisted of 16 clinical strains of Mtb collected in Vietnam[36]: 4 Indo-Oceanic (Lineages 1 or named Group I), 6 Beijing (Lineage 2 named Group II) and 6 Euro-American (Lineage 4 or named Group III) to reflect the genotypic diversity found within each lineage in the study Group I (232, 281, 346, 372); Group II (119, 212, 333, 345, 374, 639); Group IIII (173, 293, 318, 367, 440, 639) and Mtb H37Rv: non-tuberculous mycobacteria: *Mycobacterium abscessus* (ATCC19977) and *Mycobacterium avium* (ATCC 25291) and the environmental species *Mycobacterium smegmatis* mc^2155 (ATCC 700084). The following reagents were obtained through BEI Resources, NIAID, NIH: Mtb, Strain, CDC1551, total lipids, NR-14838, Mtb, Strain East African Indian 91_0079, NR-44098, Mtb Strain H37Rv, total lipids, NR-14837, *Mycobacterium canettii* total lipids, NR-40334 and *Mycobacterium bovis*, Strain AF 2122/97 (ATCC BAA-935), total lipids, NR-44100, Mtb Strain H37Rv, Purified Mycolylarabinogalactan-Peptidoglycan, NR-14851, Mtb Strain H37Rv, Purified Lipomannan, NR-14850, Mtb Strain H37Rv, Purified Lipoarabinomannan, NR-14848 and Mtb Strain H37Rv, Purified Arabinogalactan, NR-14852.

Lipid solubilization and addition to RAW 264.7 MΦ

Dried lipid extracts were re-constituted at a concentration of 20 mg/ml in DMSO by sonicating for 2 min at 60 °C in an ultrasonic water bath. DMSO stocks were diluted to the final concentration in pre-warmed culture medium, sonicated for 2 min at 60 °C, allowed to cool, and immediately added to cells. RAW 264.7 cells were plated at a density of 5×10^4 cells/well in 96-well culture plates in a complete medium and allowed to adhere overnight. Lipid extracts, 2 µg/ml U18666A (Merck) or vehicle (DMSO only) were added and plates were incubated at 37 °C, 5% CO_2 for 48 h before analysis.

LysoTracker™ staining: FACS analysis

LysoTracker™ staining was performed as described previously[15]. In brief, MΦ were harvested, washed twice with PBS, and stained with 200 nM LysoTracker™ Green DND-26 (ThermoFisher) for 10 min in the dark. Cells were washed with PBS and re-suspended in buffer containing 5 µg/ml Propidium iodide (Sigma) to allow for the exclusion of dead cells and immediately analyzed on a BD FACS-Canto II (Beckton Dickinson). A minimum of 10,000 events were collected for each sample using DIVA software v*.0.1 (Beckton Dickinson) and relative fluorescence values calculated using the FlowJo software (Version 10, FlowJo, LLC). The experimental design of each independent investigation ensured that all samples could be analyzed within 45 min of LysoTracker™ staining to ensure consistency of fluorescent signal[15].

LysoTracker™ staining: confocal microscopy

LysoTracker™ live cell imaging was performed using Cellview cell culture slides (Greiner). After vehicle, U18666A or lipid treatments, cells were washed with PBS and stained with 200 nM LysoTracker™ Red DND-99 (ThermoFisher) for 10 min in the dark. Cells were washed with PBS, stained with 200 nM Hoechst 33342 nuclear stain (ThermoFisher) for 5 min, and washed again. Cells were kept in PBS and imaged within 1 h of staining on a Leica-SP8 confocal microscope.

Western blotting

Cells were harvested and lysed with RIPA buffer (ThermoFisher) containing cOmplete™ EDTA-free protease inhibitor cocktail (Merck), centrifuged and the supernatant collected. The protein concentration of the supernatant was determined by BCA assay (Sigma). Volumes of cell lysate containing 20 µg protein were mixed with SDS Blue loading buffer (BioLabs) and dithiothreitol (DTT, BioLabs), and heated at 50 °C for 10 min. Samples were loaded onto NuPAGE™ 4–12% Bis-Tris Gels (ThermoFisher) and run in NuPAGE™ MOPS SDS running buffer (ThermoFisher). Novex Sharp Pre-stained protein standard (ThermoFisher) was used to indicate the extent of protein migration. Gels were transferred onto Immuno-Blot® PVDF membrane (Bio-Rad) using BIORAD transblot turbo transfer system (Bio-Rad). Membranes were blocked with 5% skimmed milk in PBS with 0.1% Tween 20 (Sigma) for 1 h at room temperature and then incubated with primary antibody (monoclonal rabbit anti-LAMP-1 antibody EPR21026, 1:1000, Abcam ab208943, polyclonal rabbit anti-NPC1 antibody NB400–148, 1:1000, Novus) diluted in PBS containing 2.5% skimmed milk with 0.1% Tween 20 and sodium azide overnight at 4 °C. Membranes were washed with PBS containing 0.1%

Tween 20 three times for 20 min each and then incubated with HRP-conjugated anti-rabbit secondary antibody (1:5000, Sigma A0545) diluted in PBS containing 2.5% skimmed milk and 0.1% Tween 20 for 1 h at room temperature. Membranes were washed as before and then developed with SuperSignal™ West Femto substrate (ThermoFisher) or Pierce™ ECL western blotting substrate (ThermoFisher). Membranes were re-probed with peroxidase-conjugated anti-β-actin antibody AC-15, 1:10,000 (Sigma A3845) to evaluate equivalent protein loading. Images were obtained using a ChemiDoc XRS system (BioRad) and processed and analyzed with ImageLab software (BioRad) with BioRad Universal Hood.

Immunofluorescence staining

After lipid treatment, cells were washed with PBS and fixed with 4% paraformaldehyde (PFA) for 15 min at room temperature. Cells were then permeabilized with 0.1% saponin in PBS for 15 min at room temperature and washed with PBS and blocked with 5% goat serum in PBS for 45 min at room temperature. Cells were incubated with a primary anti-LAMP-1 antibody with 10% goat serum and 0.1% saponin in PBS (rat monoclonal, clone 1D4B 1:500, Abcam ab25245) overnight at 4 °C and then with anti-rat IgG secondary antibody (1:1000, ThermoFisher A21208) for 45 min at room temperature. Cells were stained with DAPI (4′,6-diamidino-2-phenylindole, ThermoFisher) to visualize nuclei and mounted with Prolong Gold Antifade (ThermoFisher). Imaging was carried out on a Leica-SP8 confocal microscope.

Filipin Staining for free cholesterol

For labeling of free cholesterol, cells were fixed with 4% PFA for 15 min at room temperature and washed with PBS, then incubated with 1.5 mg/ml glycine (Sigma) in PBS for 10 min to quench aldehyde groups. Cells were then stained with a Filipin working solution composed of 0.05 mg/ml filipin complex from *Streptomyces filipinensis* (Sigma), 10% FBS (Sigma), and 0.2% Triton x100 (Sigma) in PBS for 2 h at room temperature. Cells were washed with PBS and stained with propidium iodide (PI, 1:3000, Sigma) to visualize nuclei and mounted with Prolong Gold Antifade (ThermoFisher). Imaging was carried out on a Leica-SP8 confocal microscope.

Amplex red measurement of cholesterol

Cells were lysed in glass tubes in 0.5 ml of ddH_2O and freeze/thawed three times. 2 ml chloroform: methanol (2:1, v/v, Sigma) was added, samples homogenized for 5 min and then mixed at room temperature for 2 h on a roller. 0.4 ml methanol was then added and samples were centrifuged for 10 min at 1500 × *g* and supernatant recovered. 0.8 ml chloroform and 0.73 ml ddH_2O were added to a final composition of CH_3Cl: MeOH: ddH_2O (8:4:3, v/v/v). Lysates were mixed and centrifuged, the upper phase removed, and the lower phase washed with CH_3Cl: MeOH: ddH_2O (3:48:47, v/v/v) 3 times and then dried under N_2. Total cholesterol in the samples was determined using Amplex Red Cholesterol Assay Kit (Sigma) according to the manufacturer's protocol.

Cholera toxin subunit B (CtxB) staining

After treatment with lipid or drug, cells were washed with PBS and incubated with 0.5ug/ml CtxB in PBS for 30 min on ice. Cells were washed with PBS and labeled GM1 was chased for 1 h with fresh media. Cells were washed with PBS containing 1% normal goat serum and fixed with 4% PFA for 15 min at room temperature. Nuclei were stained with DAPI and mounted with Prolong Gold Antifade. Imaging was carried out on a Leica-SP8 confocal microscope.

Analysis and quantification of GSLs by normal phase high-performance liquid chromatography (NP-HPLC)

GSLs were analyzed essentially as described previously[23]. Aqueous extracts of frozen pellets of control and lipid-treated RAW 264.7 MΦ were prepared by three cycles of freeze/thawing. Protein concentration was determined by BCA assay (Sigma). Lipids were extracted from aqueous cell homogenates (approximately 0.2 mg in 0.2 ml) with chloroform and methanol overnight at 4 °C. GSLs were further purified using solid-phase C18 columns (Telios, Kinesis) and eluted. Fractions were dried down under a stream of nitrogen at 42 °C and treated with recombinant ceramide glycanase (rEGCase; GenScript) to release ceramide-linked glucosylceramide-derived GSL oligosaccharides. The liberated free glycans were fluorescently labeled at 80 °C for 60 min with anthranilic acid (2AA) and sodium cyanoborohydride. Purification of labeled glycans and removal of excess 2AA was achieved by passing reaction mixes over DPA-6S SPE columns (Supelco). 2AA-labeled oligosaccharides were separated and quantified by normal-phase HPLC as described by the authors in ref. 23. The NP-HPLC equipment consisted of a Waters Alliance 2695 separation module and an in-line Waters 2475 multi λ-fluorescence detector set at Ex λ 1360 nm and Em λ 1425 nm. The solid phase was a 4.6 × 250 mm TSK gel-Amide 80 column (Anachem). Glucose unit values (GUs) were determined using a 2AA-labeled glucose homopolymer ladder (Ludger). To calculate molar quantities from integrated peaks in the chromatogram, 2.5 pmol 2AA-labeled chitotriose (Ludger) was injected as a calibration standard with each sample set.

qPCR

RNA from RAW 264.7 MΦ was isolated using Monarch total RNA MiniPrep kit (BioLabs) according to the manufacturer's protocol. cDNA was synthesized using iScript cDNA synthesis kit (BIO-RAD). Reaction mixes containing cDNA template, PowerUp SYBER Green (ThermoFisher), and primers specific for LAMP-1 gene expression level were run on a CFX96 Real-Time PCR system (BIO-RAD). Assays specific for relative expression of murine β-actin was used to normalize for input.

TLC of extractible lipids and MALDI lipid fingerprinting

Heat-killed mycobacteria were first washed 3 times with PBS. The pellets were then submitted to $CHCl_3$/MeOH 1:2 (v/v) extraction for 12 h at room temperature followed by one $CHCl_3$/MeOH 1:1 (v/v) extraction and one $CHCl_3$/MeOH 2:1 (v/v) extraction for 3 h at room temperature. Pooled extracts were concentrated and evaporated to dryness. Total lipids extracted were normalized to the dried weight of the lipid extract. The dried lipid extracts were resuspended in $CHCl_3$ at a final concentration of 20 mg/ml. Five microliters, equivalent to 100 µg, were loaded on TLC.TLCs were run in four different solvent systems: Petroleum Ether/Diethyl Ether 95:5 (v/v); $CHCl_3$/MeOH 9:1 (v/v); $CHCl_3$/MeOH 8:2 (v/v) and $CHCl_3$/MeOH/H_2O 60:25:4 (v/v/v). Then, TLCs were sprayed with a solution of 5% phosphomolybdic acid in 100% ethanol and heated at 200 °C for 2 min in order to reveal the lipids. All experiments were performed in triplicate for statistical confidence.

For lipid fingerprinting, 0.5 µg of total lipid extract was loaded onto the target and immediately overlaid with 0.5 µl of a 2,5-dihydroxybenzoic acid (DHB) matrix used at a final concentration of 10 mg/ml in chloroform/methanol ($CHCl_3$/MeOH) 90:10 v/v. Bacterial total lipid extracts and matrix were mixed directly on the target by pipetting and the mix was dried gently under a stream of air. MALDI-TOF MS analysis was performed on a 4800 Proteomics Analyzer (Applied Biosystems) using the reflectron mode. Samples were analyzed by operating at 20 kV in the positive and negative ion mode using an extraction delay time set at 20 ns. Data were obtained using Data Explorer version 4.9 (build 115) Applied Biosystems.

Image acquisition and processing

Confocal images were acquired using Leica TPC SP8 confocal microscope and LAS X software. Images for LysoTracker™ Red DND-99, Lamp-1, and GM1 trafficking were captured using a ×60

oil-immersion (Type F immersion oil, Leica) objective with the 488 nm laser for excitation and 690 nm laser for emission (LysoTracker™ Red setting for LysoTracker™ Red DND-99 LFITC for Lamp-1; Alexa 488 for GM1). Lysosomal GM1 was identified as fluorescent Cholera Toxin subunit B positive vesicles (puncta) in the endo-lysosome, whereas Golgi distributed GM1 was identified by a perinuclear pattern of CtxB staining. Counts were made from a minimum of 100 cells across three random fields. Filipin images for cholesterol distribution were obtained using x40 oil-immersion objective with 405 nm laser for excitation and 727 nm laser for emission with 0.75% UV. Data for intracellular cholesterol accumulation were determined as the percentage of cells with lysosome distributed puncta. For each sample, at least 3 random fields were examined, and counts were made of a minimum of 100 cells in each. Nuclear staining was captured using 405 nm laser for excitation, 480 nm laser for emission for DAPI and Hoechst 33342 staining, or 552 nm laser for excitation, 786 nm laser for emission for PI staining. Lysosomal diameter was determined by analysis of LysoTracker™ Red DND-99 and LAMP-1 staining of treated cells. Punctate lysosomes in RAW 264.7 MΦ were defined from 0 to 0.6μm, and enlarged lysosomes were defined by having diameters from 0.6 to 5 μm. A minimum of 100 lysosomes were measured in at least three random fields and analyzed. Confocal images were analyzed using ImageJ Fiji (NIH, USA).

Statistical analysis

Normality of data was determined before performing statistical analyses. Analysis and statistical significance of all data sets were determined using GraphPad Prism 9.

Reporting summary

Further information on research design is available in the Nature Research Reporting Summary linked to this article.

Data availability

Source data are provided with this paper.

References

1. Gagneux, S. Ecology and evolution of *Mycobacterium tuberculosis*. *Nat. Rev. Microbiol* **16**, 202–213 (2018).
2. Frieden, T. R., Sterling, T. R., Munsiff, S. S., Watt, C. J. & Dye, C. Tuberculosis. *Lancet* **362**, 887–899 (2003).
3. Cambier, C. J., Falkow, S. & Ramakrishnan, L. Host evasion and exploitation schemes of *Mycobacterium tuberculosis*. *Cell* **159**, 1497–1509 (2014).
4. Stewart, G. R., Robertson, B. D. & Young, D. B. Tuberculosis: a problem with persistence. *Nat. Rev. Microbiol.* **1**, 97–105 (2003).
5. Russell, D. G., Cardona, P. J., Kim, M. J., Allain, S. & Altare, F. Foamy macrophages and the progression of the human tuberculosis granuloma. *Nat. Immunol.* **10**, 943–948 (2009).
6. Barry, C. E. 3rd et al. The spectrum of latent tuberculosis: rethinking the biology and intervention strategies. *Nat. Rev. Microbiol.* **7**, 845–855 (2009).
7. Schlesinger, L. S., Bellinger-Kawahara, C. G., Payne, N. R. & Horwitz, M. A. Phagocytosis of *Mycobacterium tuberculosis* is mediated by human monocyte complement receptors and complement component C3. *J. Immunol.* **144**, 2771–2780 (1990).
8. Schlesinger, L. S. Macrophage phagocytosis of virulent but not attenuated strains of *Mycobacterium tuberculosis* is mediated by mannose receptors in addition to complement receptors. *J. Immunol.* **150**, 2920–2930 (1993).
9. Pieters, J. *Mycobacterium tuberculosis* and the macrophage: maintaining a balance. *Cell Host Microbe* **3**, 399–407 (2008).
10. Jayachandran, R. et al. Survival of mycobacteria in macrophages is mediated by coronin 1-dependent activation of calcineurin. *Cell* **130**, 37–50 (2007).
11. de Chastellier, C. The many niches and strategies used by pathogenic mycobacteria for survival within host macrophages. *Immunobiology* **214**, 526–542 (2009).
12. Fineran, P. et al. Pathogenic mycobacteria achieve cellular persistence by inhibiting the Niemann-Pick Type C disease cellular pathway. *Wellcome Open Res.* **1**, 18 (2016).
13. Hoglinger, D. et al. NPC1 regulates ER contacts with endocytic organelles to mediate cholesterol egress. *Nat. Commun.* **10**, 4276 (2019).
14. Vanier, M. T. Niemann-Pick disease type C. *Orphanet J. Rare Dis.* **5**, 16 (2010).
15. te Vruchte, D. et al. Relative acidic compartment volume as a lysosomal storage disorder-associated biomarker. *J. Clin. Investig.* **124**, 1320–1328 (2014).
16. Lu, F. et al. Identification of NPC1 as the target of U18666A, an inhibitor of lysosomal cholesterol export and Ebola infection. *Elife* **4**, e12177 (2015).
17. Russell, D. G., Mwandumba, H. C. & Rhoades, E. E. Mycobacterium and the coat of many lipids. *J. Cell Biol.* **158**, 421–426 (2002).
18. Guerrini, V. et al. Storage lipid studies in tuberculosis reveal that foam cell biogenesis is disease-specific. *PLoS Pathog.* **14**, e1007223 (2018).
19. Pandey, A. K. & Sassetti, C. M. Mycobacterial persistence requires the utilization of host cholesterol. *Proc. Natl Acad. Sci. USA* **105**, 4376–4380 (2008).
20. Chen, C. S., Patterson, M. C., Wheatley, C. L., O'Brien, J. F. & Pagano, R. E. Broad screening test for sphingolipid-storage diseases. *Lancet* **354**, 901–905 (1999).
21. Platt, F. M. Sphingolipid lysosomal storage disorders. *Nature* **510**, 68–75 (2014).
22. Platt, F. M., d'Azzo, A., Davidson, B. L., Neufeld, E. F. & Tifft, C. J. Lysosomal storage diseases. *Nat. Rev. Dis. Prim.* **4**, 27 (2018).
23. Neville, D. C. et al. Analysis of fluorescently labeled glycosphingolipid-derived oligosaccharides following ceramide glycanase digestion and anthranilic acid labeling. *Anal. Biochem.* **331**, 275–282 (2004).
24. Larrouy-Maumus, G. & Puzo, G. Mycobacterial envelope lipids fingerprint from direct MALDI-TOF MS analysis of intact bacilli. *Tuberculosis* **95**, 75–85 (2015).
25. Gilleron, M., Lindner, B. & Puzo, G. MS/MS approach for characterization of the fatty acid distribution on mycobacterial phosphatidyl-myo-inositol mannosides. *Anal. Chem.* **78**, 8543–8548 (2006).
26. Kordulakova, J. et al. Identification of the required acyltransferase step in the biosynthesis of the phosphatidylinositol mannosides of mycobacterium species. *J. Biol. Chem.* **278**, 36285–36295 (2003).
27. Guerin, M. E., Kordulakova, J., Alzari, P. M., Brennan, P. J. & Jackson, M. Molecular basis of phosphatidyl-myo-inositol mannoside biosynthesis and regulation in mycobacteria. *J. Biol. Chem.* **285**, 33577–33583 (2010).
28. Layre, E. et al. Deciphering sulfoglycolipids of *Mycobacterium tuberculosis*. *J. Lipid Res.* **52**, 1098–1110 (2011).
29. Goren, M. B. Sulfolipid I of *Mycobacterium tuberculosis*, strain H37Rv. I. Purification and properties. *Biochim. Biophys. Acta* **210**, 116–126 (1970).
30. Brosch, R. et al. A new evolutionary scenario for the *Mycobacterium tuberculosis* complex. *Proc. Natl Acad. Sci. USA* **99**, 3684–3689 (2002).
31. Gutierrez, M. C. et al. Ancient origin and gene mosaicism of the progenitor of *Mycobacterium tuberculosis*. *PLoS Pathog.* **1**, e5 (2005).
32. Smith, N. H., Hewinson, R. G., Kremer, K., Brosch, R. & Gordon, S. V. Myths and misconceptions: the origin and evolution of *Mycobacterium tuberculosis*. *Nat. Rev. Microbiol.* **7**, 537–544 (2009).

33. Brites, D. & Gagneux, S. Co-evolution of *Mycobacterium tuberculosis* and *Homo sapiens*. *Immunol. Rev.* **264**, 6–24 (2015).
34. Gagneux, S. & Small, P. M. Global phylogeography of *Mycobacterium tuberculosis* and implications for tuberculosis product development. *Lancet Infect. Dis.* **7**, 328–337 (2007).
35. Bottai, D. et al. TbD1 deletion as a driver of the evolutionary success of modern epidemic *Mycobacterium tuberculosis* lineages. *Nat. Commun.* **11**, 684 (2020).
36. Krishnan, N. et al. *Mycobacterium tuberculosis* lineage influences innate immune response and virulence and is associated with distinct cell envelope lipid profiles. *PLoS ONE* **6**, e23870 (2011).
37. Lee, M. R. et al. *Mycobacterium abscessus* complex infections in humans. *Emerg. Infect. Dis.* **21**, 1638–1646 (2015).
38. Loebinger, M. R. *Mycobacterium avium* complex infection: phenotypes and outcomes. *Eur. Respir. J.* **50**, 1701380 (2017).
39. Inderlied, C. B., Kemper, C. A. & Bermudez, L. E. The *Mycobacterium avium* complex. *Clin. Microbiol. Rev.* **6**, 266–310 (1993).
40. Johansen, M. D., Herrmann, J. L. & Kremer, L. Non-tuberculous mycobacteria and the rise of *Mycobacterium abscessus*. *Nat. Rev. Microbiol.* **18**, 392–407 (2020).
41. Namouchi, A., Didelot, X., Schock, U., Gicquel, B. & Rocha, E. P. After the bottleneck: genome-wide diversification of the *Mycobacterium tuberculosis* complex by mutation, recombination, and natural selection. *Genome Res.* **22**, 721–734 (2012).
42. Boritsch, E. C. & Brosch, R. Evolution of *Mycobacterium tuberculosis*: new insights into pathogenicity and drug resistance. *Microbiol. Spectr*. https://doi.org/10.1128/microbiolspec.TBTB2-0020-2016 (2016).
43. Minnikin, D. E. et al. Ancient mycobacterial lipids: key reference biomarkers in charting the evolution of tuberculosis. *Tuberculosis* **95**, S133–S139 (2015).
44. Garcia-Vilanova, A., Chan, J. & Torrelles, J. B. Underestimated manipulative roles of mycobacterium tuberculosis cell envelope glycolipids during infection. *Front. Immunol.* **10**, 2909 (2019).
45. Jankute, M. et al. The role of hydrophobicity in tuberculosis evolution and pathogenicity. *Sci. Rep.* **7**, 1315 (2017).
46. Supply, P. & Brosch, R. The biology and epidemiology of *Mycobacterium canettii*. *Adv. Exp. Med. Biol.* **1019**, 27–41 (2017).
47. Supply, P. et al. Genomic analysis of smooth tubercle bacilli provides insights into ancestry and pathoadaptation of *Mycobacterium tuberculosis*. *Nat. Genet.* **45**, 172–179 (2013).
48. Fabre, M. et al. High genetic diversity revealed by variable-number tandem repeat genotyping and analysis of hsp65 gene polymorphism in a large collection of "*Mycobacterium canettii*" strains indicates that the *M. tuberculosis* complex is a recently emerged clone of "*M. canettii*". *J. Clin. Microbiol.* **42**, 3248–3255 (2004).
49. Fabre, M. et al. Molecular characteristics of "*Mycobacterium canettii*" the smooth *Mycobacterium tuberculosis* bacilli. *Infect. Genet. Evol.* **10**, 1165–1173 (2010).
50. Briquet, A. et al. Clinical features of *Mycobacterium canettii* infection: a retrospective study of 20 cases among french soldiers and relatives. *Clin. Infect. Dis.* **69**, 2003–2010 (2019).
51. Gatfield, J. & Pieters, J. Essential role for cholesterol in entry of mycobacteria into macrophages. *Science* **288**, 1647–1650 (2000).
52. Soto-Ramirez, M. D. et al. Cholesterol plays a larger role during *Mycobacterium tuberculosis* in vitro dormancy and reactivation than previously suspected. *Tuberculosis* **103**, 1–9 (2017).
53. Cole, S. T. et al. Deciphering the biology of *Mycobacterium tuberculosis* from the complete genome sequence. *Nature* **393**, 537–544 (1998).
54. Brzostek, A., Pawelczyk, J., Rumijowska-Galewicz, A., Dziadek, B. & Dziadek, J. *Mycobacterium tuberculosis* is able to accumulate and utilize cholesterol. *J. Bacteriol.* **191**, 6584–6591 (2009).
55. Jackson, M. The mycobacterial cell envelope-lipids. *Cold Spring Harb. Perspect. Med.* **4**, a021105 (2014).
56. Jankute, M., Cox, J. A., Harrison, J. & Besra, G. S. Assembly of the mycobacterial cell wall. *Annu. Rev. Microbiol.* **69**, 405–423 (2015).
57. Brennan, P. J. Structure, function, and biogenesis of the cell wall of *Mycobacterium tuberculosis*. *Tuberculosis* **83**, 91–97 (2003).
58. Hingley-Wilson, S. M., Sambandamurthy, V. K. & Jacobs, W. R. Jr Survival perspectives from the world's most successful pathogen, *Mycobacterium tuberculosis*. *Nat. Immunol.* **4**, 949–955 (2003).
59. Reed, M. B. et al. A glycolipid of hypervirulent tuberculosis strains that inhibits the innate immune response. *Nature* **431**, 84–87 (2004).
60. Jia Khor, M., Broda, A., Kostrzewa, M., Drobniewski, F. & Larrouy-Maumus, G. An improved method for rapid detection of mycobacterium abscessus complex based on species-specific lipid fingerprint by routine MALDI-TOF. *Front. Chem.* **9**, 715890 (2021).
61. Reinink, P. et al. Discovery of *Salmonella trehalose* phospholipids reveals functional convergence with mycobacteria. *J. Exp. Med.* **216**, 757–771 (2019).
62. Villeneuve, C. et al. Surface-exposed glycopeptidolipids of *Mycobacterium smegmatis* specifically inhibit the phagocytosis of mycobacteria by human macrophages. Identification of a novel family of glycopeptidolipids. *J. Biol. Chem.* **278**, 51291–51300 (2003).
63. Villeneuve, C. et al. Mycobacteria use their surface-exposed glycolipids to infect human macrophages through a receptor-dependent process. *J. Lipid Res.* **46**, 475–483 (2005).
64. Ernst, J. D., Trevejo-Nunez, G. & Banaiee, N. Genomics and the evolution, pathogenesis, and diagnosis of tuberculosis. *J. Clin. Investig.* **117**, 1738–1745 (2007).
65. Orgeur, M. & Brosch, R. Evolution of virulence in the *Mycobacterium tuberculosis* complex. *Curr. Opin. Microbiol.* **41**, 68–75 (2018).
66. Boritsch, E. C. et al. pks5-recombination-mediated surface remodelling in *Mycobacterium tuberculosis* emergence. *Nat. Microbiol.* **1**, 15019 (2016).
67. Howard, S. T. et al. Spontaneous reversion of *Mycobacterium abscessus* from a smooth to a rough morphotype is associated with reduced expression of glycopeptidolipid and reacquisition of an invasive phenotype. *Microbiology* **152**, 1581–1590 (2006).
68. Byrd, T. F. & Lyons, C. R. Preliminary characterization of a *Mycobacterium abscessus* mutant in human and murine models of infection. *Infect. Immun.* **67**, 4700–4707 (1999).
69. Ripoll, F. et al. Genomics of glycopeptidolipid biosynthesis in *Mycobacterium abscessus* and *M. chelonae*. *BMC Genomics* **8**, 114 (2007).
70. Catherinot, E. et al. Hypervirulence of a rough variant of the *Mycobacterium abscessus* type strain. *Infect. Immun.* **75**, 1055–1058 (2007).
71. Jackson, M., Stevens, C. M., Zhang, L., Zgurskaya, H. I. & Niederweis, M. Transporters involved in the biogenesis and functionalization of the mycobacterial cell envelope. *Chem. Rev.* **121**, 5124–5157 (2021).
72. Szewczyk, R., Kowalski, K., Janiszewska-Drobinska, B. & Druszczynska, M. Rapid method for *Mycobacterium tuberculosis* identification using electrospray ionization tandem mass spectrometry analysis of mycolic acids. *Diagn. Microbiol. Infect. Dis.* **76**, 298–305 (2013).
73. Marrakchi, H., Laneelle, M. A. & Daffe, M. Mycolic acids: structures, biosynthesis, and beyond. *Chem. Biol.* **21**, 67–85 (2014).
74. Song, S. H. et al. Electrospray ionization-tandem mass spectrometry analysis of the mycolic acid profiles for the identification of common clinical isolates of mycobacterial species. *J. Microbiol. Methods* **77**, 165–177 (2009).

75. Hatzios, S. K. et al. PapA3 is an acyltransferase required for polyacyltrehalose biosynthesis in *Mycobacterium tuberculosis*. *J. Biol. Chem.* **284**, 12745–12751 (2009).
76. Burbaud, S. et al. Trehalose polyphleates are produced by a glycolipid biosynthetic pathway conserved across phylogenetically distant mycobacteria. *Cell Chem. Biol.* **23**, 278–289 (2016).
77. Layre, E. et al. Molecular profiling of *Mycobacterium tuberculosis* identifies tuberculosinyl nucleoside products of the virulence-associated enzyme Rv3378c. *Proc. Natl Acad. Sci. USA* **111**, 2978–2983 (2014).
78. Brudey, K. et al. *Mycobacterium tuberculosis* complex genetic diversity: mining the fourth international spoligotyping database (SpolDB4) for classification, population genetics and epidemiology. *BMC Microbiol.* **6**, 23 (2006).
79. Comas, I. et al. Out-of-Africa migration and Neolithic coexpansion of *Mycobacterium tuberculosis* with modern humans. *Nat. Genet.* **45**, 1176–1182 (2013).

Acknowledgements

We thank Jiayun Zhu for her preliminary data on mycobacterial lipid analysis. This study was funded by an Investigator in Science Award from The Wellcome Trust to F.M.P. (202834/Z/16/Z).

Author contributions

Conceptualization F.M.P., G.L.-M., N.P., B.D.R.; methodology Y.W., D.S., Y.L.; validation Y.W., D.S., Y.L., N.P.; investigation Y.W., D.S., Y.L.; data curation Y.W., D.S., Y.L., N.K.; visualization Y.W., D.S., N.P., Y.L., G.L.-M.; writing—original draft N.P.; writing—review and editing Y.W., D.S., Y.L., N.K., B.D.R., N.P., G.L.-M., and F.M.P.; supervision F.M.P., G.L.-M., and N.P.; funding acquisition F.M.P. and G.L.-M.

Competing interests

F.M.P. is a consultant to and co-founder of IntraBio. The other authors declare no competing interests.

Additional information

Supplementary information The online version contains supplementary material available at https://doi.org/10.1038/s41467-022-32553-0.

Correspondence and requests for materials should be addressed to Frances M. Platt.

Peer review information *Nature Communications* thanks Stéphane Canaan and the other anonymous reviewer(s) for their contribution to the peer review of this work. Peer review reports are available.

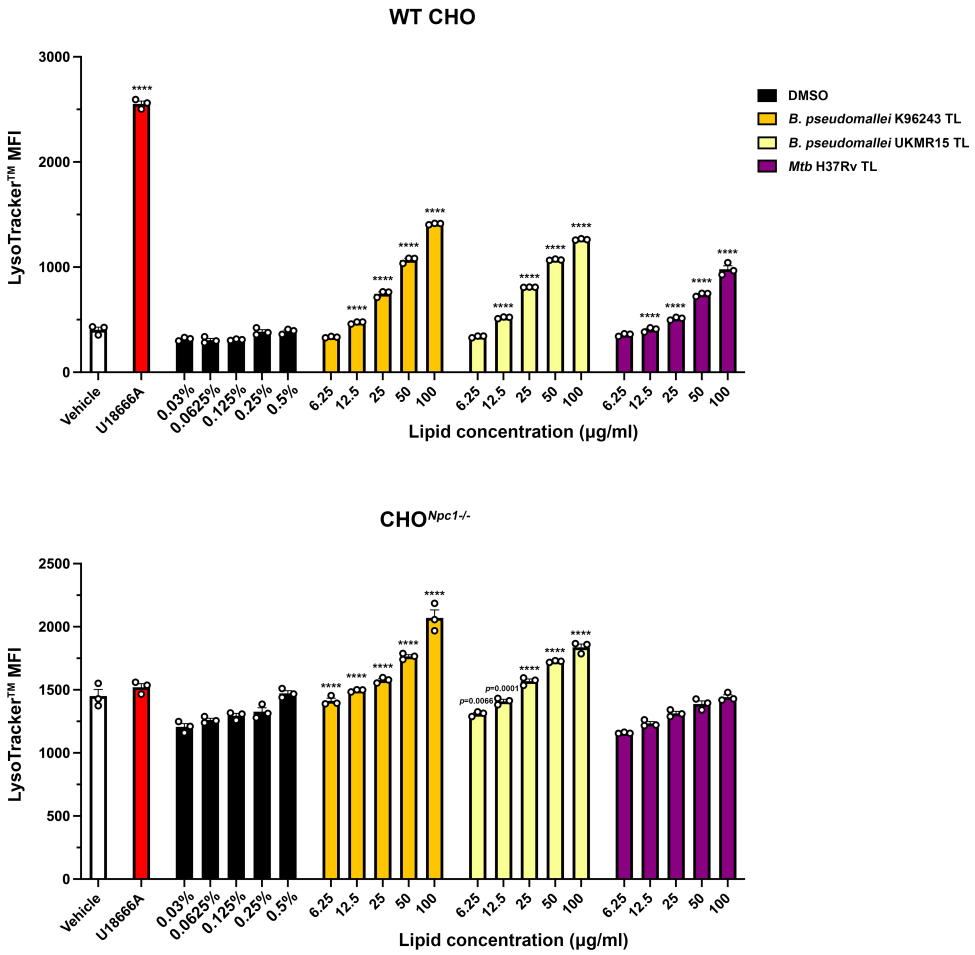
Reprints and permission information is available at http://www.nature.com/reprints

Publisher's note Springer Nature remains neutral with regard to jurisdictional claims in published maps and institutional affiliations.

Open Access This article is licensed under a Creative Commons Attribution 4.0 International License, which permits use, sharing, adaptation, distribution and reproduction in any medium or format, as long as you give appropriate credit to the original author(s) and the source, provide a link to the Creative Commons license, and indicate if changes were made. The images or other third party material in this article are included in the article's Creative Commons license, unless indicated otherwise in a credit line to the material. If material is not included in the article's Creative Commons license and your intended use is not permitted by statutory regulation or exceeds the permitted use, you will need to obtain permission directly from the copyright holder. To view a copy of this license, visit http://creativecommons.org/licenses/by/4.0/.

© The Author(s) 2022

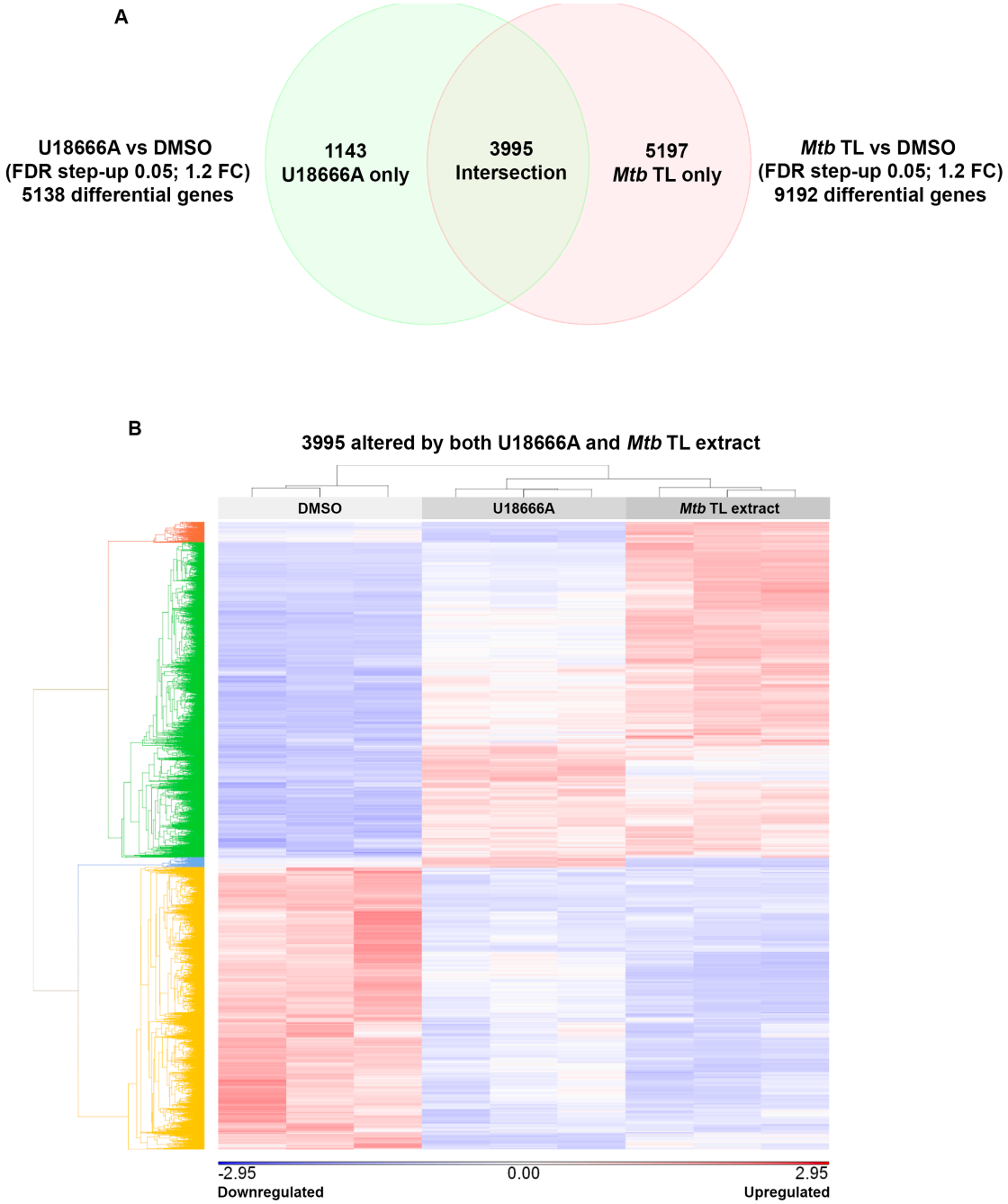
Appendix 2.



Appendix figure 1. TL extract of B. pseudomallei increases LysoTracker™ staining intensity of WT and CHO$^{Npc1-/-}$ cells.

Cells were treated with TL extract from *B. pseudomallei* (strain K96243 or strain UKMR15) or *Mtb* H37Rv (6.25, 12.5, 25, 50 and 100µg/ml for 48h). DMSO and U18666A (2µg/ml for 48h) treatments were vehicle and positive controls. Panel A. Quantification of LysoTracker™ staining intensity in treated WT CHO cells. Panel B. Quantification of LysoTracker™ staining intensity in treated CHO$^{Npc1-/-}$ cells. Data are mean ± SEM, n=3. Statistical analysis, 2-way ANOVA with Dunnett multiple comparisons. Statistical comparison of U18666A treatment is relative to vehicle control. Statistical comparisons of lipid treatments are relative to DMSO controls. ****p<0.0001, other p values as indicated, otherwise not significant. The data were generated by Dawn Shepherd.

Appendix 3.



Appendix figure 2. Gene expression levels in U18666A or Mtb H37Rv TL-treated RAW 264.7 MΦ.

RAW 264.7 MΦ were treated with *Mtb* H37Rv TL (100µg/ml for 48h). DMSO (0.5%) and U18666A (2µg/ml for 48h) were vehicle and positive controls respectively. Panel A. Venn diagram of differently expressed genes (>2-fold) in U18666A or *Mtb* TL extract-treated cells. Panel B. Heat map of differentially expressed genes in U18666A and *Mtb* H37Rv TL extract-treated RAW 264.7 MΦ. The data were generated in collaboration with Dr Dawn Watkins-Chow, NIH, USA.